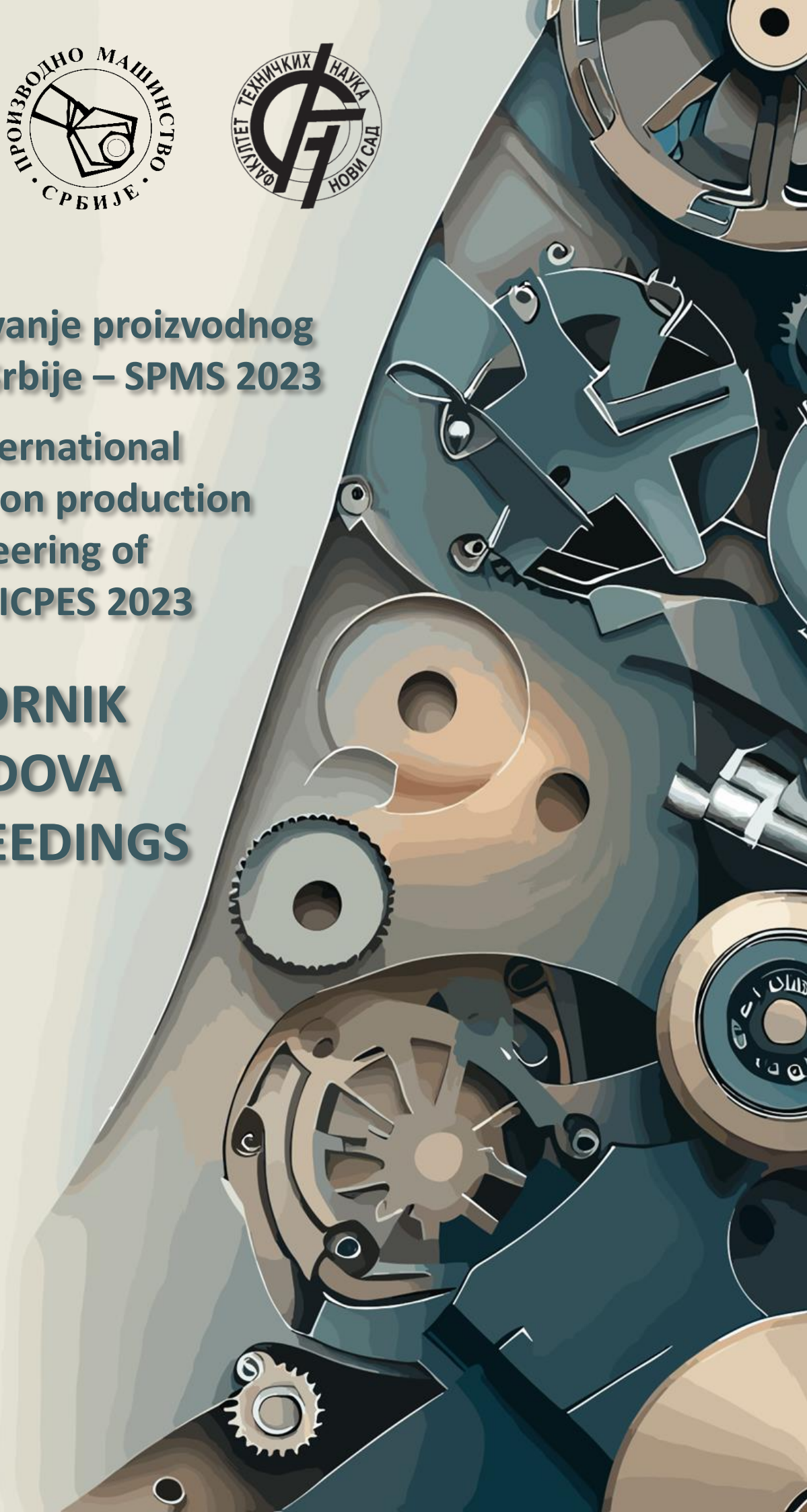




39. Savetovanje proizvodnog mašinstva Srbije – SPMS 2023

**39th International
Conference on production
Engineering of
Serbia – ICPES 2023**

**ZBORNİK
RADOVA
PROCEEDINGS**





University of Novi Sad
Faculty of Technical Sciences



**39. SAVETOVANJE PROIZVODNOG MAŠINSTVA SRBIJE
- SPMS 2023 -**

**39th INTERNATIONAL CONFERENCE ON PRODUCTION
ENGINEERING OF SERBIA
- ICPEP 2023 -**

ZBORNİK RADOVA PROCEEDINGS



Novi Sad, 26-27 October 2023

PROCEEDINGS OF THE INTERNATIONAL CONFERENCE ON PRODUCTION ENGINEERING OF
SERBIA - ICPES 2023
Novi Sad 2023

Publisher: **UNIVERSITY OF NOVI SAD, FACULTY OF TECHNICAL SCIENCES
DEPARTMENT OF PRODUCTION ENGINEERING
DEPARTMENT OF INDUSTRIAL ENGINEERING AND ENGINEERING
MANAGEMENT
21000 NOVI SAD, Trg Dositeja Obradovica 6, SERBIA**

Organization of this Conference was approved by Educational-scientific Council of Faculty of Technical Sciences in Novi Sad

Technical treatment and design: Milana ILIĆ MIĆUNOVIĆ
Miloš RANISAVLJEV
Branko ŠTRBAC
Miodrag HADŽISTEVIĆ

Printing by: FTN, Graphic Centre
GRID, Novi Sad

CIP classification:

CIP - Каталогизacija у публикацији
Библиотека Матице српске, Нови Сад

621.7/.9(082)

САВЕТОВАЊЕ производног машинства Србије (39 ; 2023 ; Нови Сад)
Zbornik radova = Proceedings / 39. Savetovanje proizvodnog mašinstva Srbije,
SPMS 2023 - 39th International Conference of Production Engineering, ICPES 2023,
26-27. October 2023, Novi Sad. - Novi Sad : Faculty of Technical Sciences, 2023
(Novi Sad : GRID). - XXV, 391 str. : ilustr. ; 24 cm
Dostupno i na: <http://spms.fink.rs/abstract.html> . - Radovi na srp. i engl. jeziku. -
Tekst štampan dvostubačno. - Tiraž 60. - Str. X-XI: Predgovor ; Foreword / Miodrag
Hadžistević. - Bibliografija uz svaki rad.

ISBN 978-86-6022-610-7

а) Производно машинство – Зборници

COBISS.SR-ID 127854345

Financing of the Proceedings was sponsored by the Ministry of Education, Science and Technological Development of the Republic of Serbia.

ACKNOWLEDGEMENT

Organisation of International Conference on Production Engineering of Serbia was made possible with understanding and financial help of following sponsors:

- **MINISTRY OF EDUCATION, SCIENCE AND TECHNOLOGICAL DEVELOPMENT OF THE REPUBLIC OF SERBIA – BELGRADE**
- **FACULTY OF TECHNICAL SCIENCES – NOVI SAD**
- **DEPARTMENT OF PRODUCTION ENGINEERING AT THE FACULTY OF TECHNICAL SCIENCES – NOVI SAD**
- **DEPARTMENT OF INDUSTRIAL ENGINEERING AND ENGINEERING MENAGEMENT AT THE FACULTY OF TECHNICAL SCIENCES – NOVI SAD**
- **ASIP PREVENT D.O.O. – NOVI SAD**
- **GM-CNC D.O.O. – INĐIJA**
- **TERMOVENT SC D.O.O. – TEMERIN**
- **ALING-CONEL D.O.O. – GAJDOBRA**
- **MAJEVICA-SERVIS D.O.O. – BAČKA PALANKA**
- **MIREN D.O.O. – SUBOTICA**
- **ESCO ELIOS D.O.O. – NOVI SAD**
- **TERMOMETAL D.O.O. – ADA**
- **ČELIK D.O.O. – BAČKI JARAK**
- **FKL D.O.O. – TEMERIN**
- **LIVNICA PRECIZNIH ODLIVAKA D.O.O. – ADA**
- **TEHNOALAT D.O.O. – NOVI SAD**
- **INGNS-INŽENJERING – NOVI SAD**
- **MECAFOR PRODUCTS D.O.O. – KIKINDA**
- **UNIMET D.O.O. – KAĆ**
- **LOLA INSTITUT D.O.O. – BEOGRAD**
- **VECOM D.O.O. – BEZDAN**

ORGANIZING INSTITUTIONS:

Community of Scientific Research Institutions of Production Engineering of Serbia:

- Faculty of Mechanical Engineering, Department for Production Engineering, Belgrade
- Faculty of Technical Sciences, Department of Production Engineering, Novi Sad
- Faculty of Technical Sciences, Department of Industrial Engineering and Engineering Management, Novi Sad
- Faculty of Mechanical Engineering, Department of Production Information Technologies, Niš
- Faculty of Technical Sciences, Department of Mechatronics, Čačak
- Faculty of Engineering University of Kragujevac, Department for Production Engineering, Kragujevac
- Faculty of Mechanical Engineering and Civil Engineering in Kraljevo, Department of Production Technologies, Kraljevo
- Faculty of Technical Sciences, Department of Production Engineering, Kosovska Mitrovica
- LOLA institute, Belgrade

CONFERENCE ORGANIZERS:

UNIVERSITY OF NOVI SAD
FACULTY OF TECHNICAL SCIENCES
Department of Production Engineering
Department of Industrial Engineering and Engineering Management
Trg Dositeja Obradovića 6
21000 Novi Sad

SCIENTIFIC COMMITTEE

Dr Ilija Ćosić, University of Novi Sad, President of the Scientific Committee

*Bojan Babić[†], University of Belgrade, Serbia
Aco Antić, University of Novi Sad, Serbia
Petar Petrović, University of Belgrade, Serbia
Zoran Miljković, University of Belgrade, Serbia
Dejan Lukić, University of Novi Sad, Serbia
Radovan Puzović, University of Belgrade, Serbia
Sebastian Baloš, University of Novi Sad, Serbia
Milenko Sekulić, University of Novi Sad, Serbia
Slobodan Tabaković, University of Novi Sad, Serbia
Branko Škorić, University of Novi Sad, Serbia
Miodrag Hadžistević, University of Novi Sad, Serbia
Đorđe Vukelić, University of Novi Sad, Serbia
Igor Budak, University of Novi Sad, Serbia
Marin Gostimirović, University of Novi Sad, Serbia
Bojan Lalić, University of Novi Sad, Serbia
Mijodrag Milošević, University of Novi Sad, Serbia
Miodrag Manić, University of Nis, Serbia
Predrag Janković, University of Nis, Serbia
Dragan Adamović, University of Kragujevac, Serbia*

*Goran Devedžić, University of Kragujevac, Serbia
Milan Erić, University of Kragujevac, Serbia
Bogdan Nedić, University of Kragujevac, Serbia
Milan Kolarević, University of Kragujevac, Serbia
Mirko Đapić, University of Kragujevac, Serbia
Snežana Dragičević, University of Kragujevac, Serbia
Jasmina Vesić-Vasović, University of Kragujevac, Serbia
Miladin Stefanović, University of Kragujevac, Serbia
Srećko Manasijević, LOLA Institute, Serbia
Nenad Simeunović, University of Novi Sad, Serbia
Ivan Milićević, University of Kragujevac, Serbia
Ognjan Lužanin, University of Novi Sad, Serbia
Saša Živanović, University of Belgrade, Serbia
Slobodan Mitrović, University of Kragujevac, Serbia
Srećko Čurčić, University of Kragujevac, Serbia
Živana Jakovljević, University of Belgrade, Serbia
Zoran Dimić, LOLA Institute, Serbia*

HONORARY COMMITTEE

*Pavao Bojanić, University of Belgrade, Serbia
Milenko Jovičić, University of Belgrade, Serbia
Milisav Kalajdžić, University of Belgrade, Serbia
Dragan Milutinović, University of Belgrade, Serbia
Miroslav Pilipović, University of Belgrade, Serbia
Miloš Glavonjić, University of Belgrade, Serbia
Sava Sekulić[†], University of Novi Sad, Serbia
Velimir Todić, University of Novi Sad, Serbia
Dragoje Milikić, University of Novi Sad, Serbia
Bogdan Sovilj, University of Novi Sad, Serbia
Jelena Stankov, University of Novi Sad, Serbia
Dragiša Vilotić, University of Novi Sad, Serbia
Miroslav Plančak, University of Novi Sad, Serbia
Miodrag Lazić, University of Kragujevac, Serbia
Milentije Stefanović, University of Kragujevac, Serbia
Ratko Mitrović, University of Kragujevac, Serbia
Slavko Arsovski, University of Kragujevac, Serbia
Branislav Jeremić, University of Kragujevac, Serbia*

*Milorad Jovanović, University of Kragujevac, Serbia
Ljubodrag Tanović, University of Belgrade, Serbia
Tihomir Pantelić, University of Kragujevac, Serbia
Ratomir Ječmenica, University of Kragujevac, Serbia
Snežana Radonjić, University of Kragujevac, Serbia
Miomir Vukićević, University of Kragujevac, Serbia
Ljubomir Lukić, University of Kragujevac, Serbia
Velibor Marinković, University of Niš, Serbia
Vojislav Stoiljković, University of Niš, Serbia
Dragan Domazet, University of Niš, Serbia
Dragan Temeljkovski, University of Niš, Serbia
Miroslav Trajanović, University of Niš, Serbia
Miroslav Radovanović, University of Niš, Serbia
Vidosav Majstorović, University of Belgrade, Serbia
Pavel Kovač, University of Novi Sad, Serbia
Svetislav Dekić, University of Priština, Serbia
Vid Jovišević, University of Banja Luka, Serbia
Milan Zeljković, University of Novi Sad, Serbia*

ORGANIZING COMMITTEE

Dr Miodrag Hadžistević, University of Novi Sad, President of the Organizing Committee

*Igor Budak, University of Novi Sad, Serbia
Đorđe Vukelić, University of Novi Sad, Serbia
Ivan Matin, University of Novi Sad, Serbia
Boris Agarski, University of Novi Sad, Serbia
Branko Štrbac, University of Novi Sad, Serbia*

*Milana Ilić Mićunović, University of Novi Sad, Serbia
Mario Šokac, University of Novi Sad, Serbia
Željko Santoši, University of Novi Sad, Serbia
Miloš Ranisavljev, University of Novi Sad, Serbia
Aleksandar Milošević, University of Novi Sad, Serbia*

**ORGANIZER OF CONFERENCE ON PRODUCTION ENGINEERING OF JUGOSLAVIJA/SERBIA
AND MONTENEGRO/SERBIA 1965 - 2021.**

I Beograd, 1965.	XXI Opatija, 1987
II Zagreb, 1966.	XXII Ohrid, 1989.
III Ljubljana, 1967.	XXIII Zagreb (nije održana), 1991.
IV Sarajevo, 1968.	XXIV Novi Sad, 1992.
V Kragujevac, 1969.	XXV Beograd, 1994.
VI Opatija, 1970.	XXVI Podgorica, 1996.
VII Novi Sad, 1971.	XXVII Niš, 1998.
VIII Ljubljana, 1973.	XXVIII Kraljevo, 2000.
IX Niš, 1974.	XXIX Beograd, 2002.
X Beograd, 1975.	XXX Čačak, 2005.
XI Ohrid, 1977.	XXXI Kragujevac, 2006.
XII Maribor, 1978.	XXXII Novi Sad, 2008.
XIII Banja Luka, 1979.	XXXIII Beograd, 2009.
XIV Čačak, 1980.	XXXIV Niš, 2011.
XV Novi Sad, 1981.	XXXV Kraljevo, 2013.
XVI Mostar, 1982.	XXXVI Beograd, 2015.
XVII Budva, 1983.	XXXVII Kragujevac, 2018.
XVIII Niš, 1984.	XXXVIII Čačak, 2021.
XIX Kragujevac, 1985.	XXXIX Novi Sad, 2023.
XX Beograd, 1986.	

DOSADAŠNJI DOBITNICI POVELJE I PLAKETE "PROF. DR PAVLE STANKOVIĆ"

za 1983. godinu

Prof. dr Rudolf Zdenkovic, dipl. ing, Strojarski fakultet, Zagreb
Prof. dr Vladimir Šolaja, dipl. ing, Mašinski fakultet, Beograd
Prof. dr Julije Kremer, dipl. ing, Fakultet tehničkih nauka, Beograd

za 1984. godinu

Prof. dr Janez Peklenik, dipl. ing, Fakultet, Ljubljana
Prof. dr Binko Musafija, dipl. ing, Mašinski fakultet, Sarajevo

za 1985. godinu

Prof. dr Predrag Popović, dipl. ing, Mašinski fakultet, Niš
Prof. dr Vladimir Milačić, dipl. ing, Mašinski fakultet, Beograd

za 1986. godinu

Prof. dr Branko Ivković, dipl. ing, Mašinski fakultet, Kragujevac

Prof. dr Strezo Trajkovski, dipl. ing, Mašinski fakultet, Skoplje

za 1987. godinu

Prof. dr Svetislav Zarić, dipl. ing, Mašinski fakultet, Beograd

Prof. dr Josip Hribar, dipl. ing, Mašinski fakultet

za 1988. godinu

Prof. dr Branislav Devedžić, dipl. ing, Mašinski fakultet, Kragujevac

Prof. dr Elso Kuljanid, dipl. ing, Mašinski fakultet, Rijeka

Prof. dr Zoran Seljak, dipl. ing, Mašinski fakultet, Ljubljana

za 1992. godinu

Prof. dr Jožef Rekecki, dipl. ing, Fakultet tehničkih nauka, Novi Sad

Prof. dr Sava Sekulić, dipl. ing, Fakultet tehničkih nauka, Novi Sad

Prof. dr Joko Stanić, dipl. ing, Mašinski fakultet, Beograd

Prof. dr Vlado Vujović, dipl. ing, Fakultet tehničkih nauka, Novi Sad

za 1994. godinu

Mile Benedetić, dipl. ing, LOLA Institut, Beograd

Prof. dr Vuko Domazetović, dipl. ing, Mašinski fakultet, Podgorica

Prof. dr Milenko Jovičić, dipl. ing, Mašinski fakultet, Beograd

za 1996. godinu

Prof. dr Milisav Kalajdžić, dipl. ing, Mašinski fakultet, Beograd

Prof. dr Dragutin Zelenović, dipl. ing, Fakultet tehničkih nauka, Novi Sad

za 1998. godinu

Prof. dr Ratko Gatalo, dipl. ing, Fakultet tehničkih nauka, Novi Sad

Prof. dr Vučko Mečanin, dipl. ing, Mašinski fakultet, Kraljevo

za 2000. godinu

Prof. dr Mihailo Milojević, dipl. ing, Mašinski fakultet, Kraljevo

Prof. dr Dragoje Milikić, Fakultet tehničkih nauka, Novi Sad

za 2002. godinu

Prof. dr Vojislav Stojiljković, dipl. ing, Mašinski fakultet, Niš

Prof. dr Ilija Ćosić, Fakultet tehničkih nauka, Novi Sad

za 2005. godinu

Prof. dr Dragan Domazet, Mašinski fakultet, Niš

Prof. dr Pavao Bojanić, Mašinski fakultet, Beograd

za 2006. godinu

Prof. dr Miroslav Plančak, dipl. ing., Fakultet tehničkih nauka, Novi Sad

Prof. dr Ratomir Ječmenica, dipl. ing., Tehnički fakultet, Čačak

za 2008. godinu

Prof. dr Dragan Milutinović, dipl. ing., Mašinski fakultet, Beograd

Prof. dr Milentije Stefanović, dipl. ing., Mašinski fakultet, Kragujevac

za 2009. godinu

Prof. dr Velimir Todić, dipl. ing., Fakultet tehničkih nauka, Novi Sad

Prof. dr Velibor Marinković, dipl. ing., Mašinski fakultet, Niš

Проф. др Сергею А. Клименко, Институт сверхтвердых материалов, НАН Украины

za 2011. godinu

Prof. dr Miodrag Lazić, dipl. inž., Mašinski fakultet, Kragujevac

Prof. dr Ljubodrag Tanović, dipl. inž., Mašinski fakultet, Beograd

za 2013. godinu

Prof. dr Bogdan Sovilj, dipl. inž., Fakultet tehničkih nauka, Novi Sad

Prof. dr Miroslav Trajanović, dipl. inž., Mašinski fakultet, Niš

za 2015. godinu

Prof. dr Janko Hodolič, Fakultet tehničkih nauka, Novi Sad

Prof. dr Bogdan Nedić, Fakultet inženjerskih nauka, Kragujevac

za 2018. godinu

Prof. dr Vidosav Majstorović, Mašinski fakultet, Beograd

Prof. dr Miroslav Radovanović, Mašinski fakultet, Niš

za 2021. godinu

Prof. dr Ljubomir Lukić, Fakultet za mašinstvo i gradjevinarstvo, Kraljevo

Prof. dr Milan Zeljković, Fakultet tehničkih nauka, Novi Sad

Prof. dr Miodrag Manić, Mašinski fakultet, Niš

Predgovor

Prvo Savetovanje proizvodnog mašinstva 7. oktobra 1965. godine su organizovali Institut za alatne mašine i alate – IAMA Beograd, Mašinski fakultet u Beogradu i Institut za alatne strojeve iz Zagreba. Tada je osnovana jugoslovenska zajednica naučno-istraživačkih institucija proizvodnog mašinstva. Prvi predsednik i nosilac inicijative za osnivanje ove Zajednice bio je prof. dr Vladimir Šolaja, redovni profesor mašinskog fakulteta u Beogradu i direktor Instituta IAMA. Zajednica je osnovana sa ciljevima:

- *Upoznavanja šire stručne javnosti sa istraživačkim i razvojnim rezultatima naših stručnjaka u oblasti proizvodnog mašinstva,*
- *razmene mišljenja među stručnjacima iz instituta i industrije i*
- *isticanja značaja proizvodnog mašinstva za razvoj privrede u celini.*

Posle prvog Savetovanja proizvodnog mašinstva, a u skladu sa ciljevima zbog kojih je osnovana organizaciju savetovanja preuzima Zajednica. Zajednica naučno-istraživačkih institucija proizvodnog mašinstva organizuje savetovanje sa tradicijom dugom blizu 60 godina.

Proizvodno mašinstvo u Srbiji ima dugu i uspešnu tradiju čiji je razvoj prekinut u vreme nesretnih dešavanja devedesetih godina na ovim prostorima i periodu tranzicije. Potencijal za razvoj proizvodnih delatnosti u Republici Srbiji, a posebno proizvodnog mašinstva prepoznali su domaći i strani investitori. Može se konstatovati da se Savetovanje proizvodnog mašinstva Srbije održava u vreme intenzivnog obnavljanja industrije u Srbiji.

Pored radova iz Republike Srbije na ovoj konferenciji će biti izložen i određen broj radova iz inostranstva u cilju razmene naučnih saznanja. Pored redovnog rada po sekcijama u sklopu konferencije će biti organizovan i panel na temu obrazovanje i industrija 4.0. Želja je da se obrazovanje do određenog nivoa usmeri u pravcu primene informaciono-komunikacionih tehnologija kao preduslova za brz razvoj proizvodnog mašinstva, privrede i društva u celini.

Nadamo se da će rezultati istraživanja koji će biti saopšteni na konferenciji i diskusija na okruglom stolu, doprineti razvoju proizvodnog mašinstva u celini i njegovom daljem povezivanju sa srodnim oblastima u ovom dobu interdisciplinarnosti.

Zavaljujemo se svim domaćim i stranim autorima, članovima recenzentskog tima, kao i institucijama i pojedincima koji su doprineli realizaciji 39. Savetovanja proizvodnog mašinstva Srbije.

*Novi Sad,
20.10.2023. godine*

*U ime organizacionog odbora 39. SPMS
Predsednik izvršnog odbora Zajednice
dr Miodrag Hadžistević, red. prof.*

Foreword

On October 7, 1965, the first Conference on Production Engineering was organized by the Institute for Machine Tools and Cutting Tools in Belgrade, the Faculty of Mechanical Engineering in Belgrade, and the Institute for Machine Tools from Zagreb. It was then that the Yugoslav Community of Scientific and Research Institutions of Production Engineering was founded. The first president and bearer of the initiative to establish this Community was Prof. Dr. Vladimir Šolaja, full professor at the Faculty of Mechanical Engineering in Belgrade and director of the mentioned Institute. The community was founded with the following goals:

*Introducing the wider professional public to the research and development results of our experts in the field of production engineering,
exchange of thoughts among experts from institutes and industry and
highlighting the importance of production engineering for the development of the economy as a whole.*

After the first Conference of Production Engineering, and by the goals for which it was founded, the organization of the Conference was taken over by the Association (Community). The community of scientific and research institutions of production engineering organizes the Conference of Production Engineering with a tradition of nearly 60 years.

Production engineering in Serbia has a long and successful tradition, the development of which was interrupted during the unfortunate events of the 1990s in the Balkans and the period of transition. Domestic and foreign investors have recognized the potential for the development of mechanical engineering in the Republic of Serbia, especially production engineering. It can be stated that the Conference on Production Engineering of Serbia is held at a time of intensive renewal of the industry in Serbia.

In addition to the scientific papers from the Republic of Serbia, a certain number of papers from abroad will be exhibited at this Conference to exchange scientific knowledge. In addition to regular assignments across the multiple sections, a panel on education and Industry 4.0 will be organized as part of the Conference. The desire is to direct education to a certain level in the direction of the application of information and communication technologies as a prerequisite for the rapid development of production engineering, the economy, and society as a whole.

We hope that the results of the research that will be announced at the Conference and the discussion at the round table will contribute to the development of production engineering as a whole and its further connection with related fields in this age of interdisciplinarity.

We are grateful to all domestic and foreign authors, members of the review team, as well as institutions and individuals who contributed to the realization of the 39th International Conference on Production Engineering of Serbia – ICPEs 2023.

*Novi Sad,
20.10.2023. godine*

*On behalf of the organizing committee of 39.ICPEs
President of the Organizing Committee
dr Miodrag Hadžistević, red. prof.*

“POVELJA I PLAKETA PROF. DR PAVLE STANKOVIĆ” ZA 2023. GODINU



prof. dr Mirko ĐAPIĆ

Mirko Đapić je rođen 11.08.1956. godine u Biteliću, opština Sinj, Republika Hrvatska. Osnovnu i srednju školu je završio u Rumi. Mašinski fakultet Univerziteta u Beogradu je upisao 1975. godine a diplomirao je na grupi za Proizvodno mašinstvo 1980. godine. Na Mašinskom fakultetu u Beogradu je magistrirao 1993. godine a na istom fakultetu je odbranio doktorsku disertaciju pod nazivom „Razvoj sistema za konceptualno projektovanje proizvoda i tehnologija upravljanog paradigama totalnog kvaliteta“ pod mentorstvom prof. dr Vladimira Milačića 2000. godine. Tokom stručnog usavršavanja u periodu od 1980. do 2021. godine pohađao je preko 30 raznih međunarodnih kurseva iz oblasti CAD/CAM, standardizovanih sistema menadžmenta, ocenjivanja usaglašenosti proizvoda, akreditacije tela za ocenjivanje usaglašenosti i novog koncepta kvaliteta, od kojih je većina sertifikovana od strane IRCA (International Registrar Certificated Auditors), Velika Britanija.

Profesionalno angažovanje Mirko Đapić je započeo odmah posle diplomiranja kao projektant u Industriji poljoprivrednih mašina “Zmaj” u Zemunu. Posle četiri godine rada u industriji posvetio se naučno-istraživačkom radu u Institutu „Kriilo Savić“ u Beogradu, gde je radio kao rukovodilac više projekata u oblasti industrijskog inženjerstva, od kojih je najznačajniji Glavni tehnološki projekat za fabriku hidrauličnih komponenti LIFAM u Staroj Pazovi. U LOLA Institutu se zaposlio 1987. godine i ostvario vrhunske naučno-istraživačke rezultate. Među prvima je na prostorima bivše Jugoslavije radio na uvođenju novih računarskih tehnologija u proces projektovanja mašina alatki. Kada je 1989. godine LOLA Institut potpisao ugovor sa IBM RACE (Austrija) za razvoj IBM CIM Centra kompetencije za Istočnu Evropu, Mirko Đapić je bio rukovodilac razvojnog IBM CAD/CAM programa (Professional CADAM, CATIA, CAEDS). Kada su sankcije prema Jugoslaviji prekinule saradnju sa IBM-om, Mirko Đapić je stupio na dužnost pomoćnika direktora LOLA Instituta za CIM sisteme i TQM. U najteže vreme inflacije, međunarodnih sankcija, ratnih sukoba, NATO bombardovanja bio je direktno odgovoran za kvalitet u LOLA Institutu što je obuhvatalo: (1) Razvoj i implementaciju QMS (Menadžment sistem za kvalitet) po zahtevima standarda ISO 9001 u LOLA Institutu, (2) Razvoj i izvođenje seminara i kurseva iz oblasti kvaliteta i primene novih računarskih tehnologija kao što su CAD, CAM, CAE itd, (3) Pružanje konsultantskih usluga u oblasti razvoja i implementacije standardizovanih sistema menadžmenta po zahtevima standarda ISO 9001, 14001, 18001, ISO/IEC 17025, 17020 itd. u drugim organizacijama, (4) Učestvovanje u realizaciji i vođenje istraživačko razvojnih projekata u oblasti kvaliteta koje finansira Ministarstvo za nauku Republike Srbije. U periodu od 2003-2008. godine, dr Mirko Đapić je veoma uspešno obavljao dužnost direktora LOLA Instituta. Organizovao je 24. Savetovanje proizvodnog mašinstva 2002. godine u Beogradu.

Kao istaknuti i međunarodno priznati naučni radnik i ekspert, dr Mirko Đapić je bio angažovan u periodu 2000-2005. godine od strane Akreditacionog tela Srbije (ATS bivši JUAT) kao vođa tima za ocenjivanje laboratorija i kontrolnih tela u postupku njihove akreditacije. Ostvario je izuzetne rezultate radeći na značajnim međunarodnim projektima. U periodu 2004-2006. godine radio je za Danski Tehnološki Institut kao lokalni ekspert EAR (Evropska Agencija za Rekonstrukciju) za oblast akreditacije i ocenjivanja usaglašenosti proizvoda na projektu „Strengthening Quality Management, Capabilities and Infrastructures in SCG“ koji je finansiran od strane EU preko EAR-a. Kao glavni ekspert, prof. dr Mirko Đapić je radio u periodu 2012-2014. godine za italijansku kompaniju RINA iz Đenove na projektu „EU Support to Introduction of Quality Management Systems in the Bosnia and Hercegovina“ koji je implementiran iz EU fonda IPA 2009 za Bosnu i Hercegovinu. Za nemačku konsultantsku kompaniju GFA iz Hamburga je radio od 2019. do 2022. godine kao glavni ekspert za ocenjivanje usaglašenost proizvoda povezanih sa energijom na projektu „Establishing and strengthening of capacities of the conformity assessment bodies for the implementation of Energy Labelling and Eco-design Directives“ koji je finansiran iz EU fonda IPA 2016 za Srbiju. Za francusko sertifikaciono telo AFNOR dr Đapić je radio kao vođa tima za ocenjivanje menadžment sistema za kvalitet, QMS-a prema zahtevima ISO 9001:2015 i menadžment sistema za zaštitu okoline po zahtevima standarda ISO 14001:2015 u Srbiji i Slovačkoj.

Profesor dr Mirko Đapić je pored izuzetnih naučno-istraživačkih ostvarenja imao i veoma uspešnu univerzitetsku karijeru. Od 2010. godine je radio kao univerzitetski nastavnik na Fakultetu za mašinstvo i građevinarstvo Kraljevo, Univerzitet u Kragujevcu sve do penzionisanja 2021. godine. Kao profesor na Katedri za proizvodno mašinstvo razvio je i izvodio nastavu na kursovima osnovnog i master studijskog programa za mašinstvo: (1) Sistemi sertifikacije proizvoda, (2) Menadžment proizvodnje i tehnička logistika, (3) CIM sistemi, (4) Menadžment i inženjerstvo kvaliteta, (5) Lineativna proizvodnja i (6) Integrisan razvoj proizvoda i procesa. Na studijskom programu doktorskih studija razvio je i izvodio nastavu na kursovima: (1) Modeliranje i merenje neodređenosti, (2) Merenje i modeliranje rizika, (3) Moderne metode unapređenja kvaliteta. Nekoliko godina je izvodio nastavu u oblasti proizvodnog mašinstva i na Mašinskom fakulteta Univerziteta u Istočnom Sarajevu.

Prof. dr Mirko Đapić je objavio oko dve stotine naučnih i stručnih radova svih kategorija, jednu monografiju nacionalnog značaja i više poglavlja u monografijama nacionalnog i međunarodnog značaja. Bavio se primenom Depster-Shaferove teorije funkcija uverenja u unapređenju projektovanja proizvoda i procesa i menadžmentu i inženjerstvu kvaliteta. Dr Đapić je u svojoj doktorskoj disertaciji prvi na našim prostorima primenio ovu teoriju u modeliranju neodređenosti u rešavanju inženjerskih problema u projektovanju proizvoda i procesa. Učestvovao je u realizaciji preko sedamdeset projekata svih kategorija od toga šest velikih projekata međunarodnog značaja od kojih pet iz IPA programa Evropske Unije. Na dva projekta iz IPA EU programa vrednosti preko tri i po miliona evra radio kao glavni ekspert za QMS, Ocenjivanje usaglašenosti proizvoda i Eko-dizajn i Energetsko označavanje proizvoda. Radio je na međunarodnim projektima u Siriji, Crnoj Gori, Bosni i Hercegovini, Slovačkoj i Srbiji.

Prof. dr Mirko Đapić je član vodećih međunarodnih organizacija u oblasti kvaliteta i provere standardizovanih sistema menadžmenta kao što su: (1) International Register of Certificated Auditors (IRCA) u zvanju „QMS Lead Auditor“, (2) Chartered Quality Institute (CQI), UK, kao sertifikovan „Chartered Quality Professional“ (CQP MCQI), (3) American Society for Quality (ASQ) kao „Senior Member“, od 2002. do 2018. bio „ASQ Country Counsellor“ za Srbiju i Crnu Goru.

U 2021. godine dr Mirko Đapić je izabran za redovnog člana Inženjerske Akademije Srbije.



Prof. dr Srećko ĆURČIĆ

Prof. dr Srećko Ćurčić, redovni profesor Fakulteta tehničkih nauka u Čačku Univerziteta u Kragujevcu, rođen je 14. 10. 1962. u selu Preseka, opština Ivanjica. Osnovnu školu je završio u rodnom mestu, a tehničku školu u Čačku. Mašinski fakultet – proizvodno mašinstvo završio je u Beogradu (1982-1987), sa prosečnom ocenom 9,00.

Magistrirao na Tehničkom fakultetu u Čačku 1996. god., iz oblasti Proizvodnih tehnologija na temu "Istraživanje metoda kalibracije visokootpornih rudarskih lanaca". Doktorsku disertaciju je odbranio na Mašinskom fakultetu u Kragujevcu 2001. god., na temu: "Reinženjering automatskih proizvodnih linija u industriji prerade metala sa aspekta produktivnosti, fleksibilnosti i kvaliteta proizvoda".

Po završetku studija zapošljava se u FRA-Čačak, gde radi na konstrukciji i tehnologiji specijalnih alata, kao i na održavanju proizvodne opreme.

Na Tehnički fakultet u Čačku prelazi školske 1989. god., gde je izabran za asistenta-pripravnika za grupu predmeta Proizvodnog mašinstva. Prof. dr Srećko Ćurčić, ima bogato tridesetčetvorogodišnje iskustvo stečeno kroz formalno i neformalno učenje, kao i izvođenje vežbi i predavanja iz nastavnih predmeta: Mašine i procesi sa NU, Mašine alatke, Inženjersko-ekonomske analize, Proizvodni sistemi i procesi, Proizvodne tehnologije, Logistički sistemi, Automatske proizvodne linije i Nove proizvodne tehnologije. Poslednjih desetak godina izvodi nastavu iz predmeta: Logistika, Logistički sistemi, Proizvodna logistika, Automatske proizvodne linije, Automatizovani tehnički sistemi, Reinženjering proizvodnih sistema.

Prof. Dr Srećko Ćurčić se intenzivno bavi naučnoistraživačkim radom iz oblasti logistike i proizvodnih tehnologija. U dosadašnjem radu objavio je preko 200 naučnih i stručnih radova kao autor ili koautor, koji su publikovani u zbornicima radova i časopisima (od toga je 40 radova u međunarodnim časopisima). Koautor je tri monografije, a autor je dva univerzitetska udžbenika. Na kraju, autor je ili koautor 7 tehničkih rešenja.

Prof. dr Srećko Ćurčić poseduje izuzetan smisao za saradnju sa privredom u iznalaženju i rešavanju svakodnevnih, rutinskih, razvojnih i strateških problema. Prof. Dr Srećko Ćurčić, učestvovao u realizaciji 20 projekata koji su finansirani od strane Ministarstava Republike Srbije i privrednih subjekata, a rukovodio jednim projektom i izradom četiri studije tehnoloških projekata koji je finansiran od strane Ministarstva nauke i tehnološkog razvoja Republike Srbije i privrednih subjekata. Trenutno je angažovan na dva projekta koje finansira Ministarstvo prosvete i nauke Republike Srbije. U toku 2018. god., rukovodio je projektom koji je finansiran od strane lokalne samouprave grada Čačka. U toku 2019. i 2020 god., rukovodio je realizacijom dva projekata koji su finansirani od strane EBRD u okviru programa BASPLATNI ZELENI VAUČERI. U periodu 2020-2023 rukovodio je pri realizaciji dva projekata u okviru programa prekogranične saradnje SMART4ALL

koji su finansirani iz evropskih fondova, a pored njih učestvovao je u realizaciji još tri projekta iz istog programa.

Prof. Dr Srećko Ćurčić je jedan od osnivača Laboratorije za mehatroniku, a od 2018 god., nalazi se na funkciji Šefa Katedre za mehatroniku. U dva mandata je bio predsednik Sindikalne organizacije fakulteta, kao i član Saveta fakulteta u tri mandata. Na kraju, član je drugih stručnih tela i komisija, a posebna njegova angažovanost i stručan rad je evidentiran u Metal klasteru Srbije.



Prof. dr Bojan BABIĆ †

Prof. dr Bojan R. Babić (1959-2023) rođen je 14. novembra 1959. godine u Čupriji. Gimnaziju je završio u Beogradu 1978. godine. Diplomirao je na Mašinskom fakultetu Univerziteta u Beogradu 1983. godine, gde je i magistrirao 1990. godine, i to na Katedri za proizvodno mašinstvo. Doktorirao je 1993.g. iz multidisciplinarnе naučne oblasti proizvodnog mašinstva, pod mentorstvom Prof. dr Vladimira Milačića. Na Mašinskom fakultetu Univerziteta u Beogradu bio je zaposlen od 1983.g. prvo kao asistent-pripravnik, zatim kao asistent 1990.g., potom kao docent 1997.g., vanredni profesor od 2002.g., a redovni profesor postao je 2007. godine. Iznenada, upokojio se u Gospodu 20. aprila 2023. godine.

Održavao je nastavu iz 8 predmeta na dodiplomskim i 7 predmeta na posle diplomskim studijama, na srpskom i engleskom jeziku. Posebno se ističu: Računarski integrisani sistemi i tehnologije, Fleksibilni i rekonfigurabilni tehnološki sistemi, Kompjuterska simulacija i veštačka inteligencija, Tehnologija mašinske obrade, Manufacturing technology, Planning, performing and controlling projects itd. Bio je gostujući profesor na Malti, gde je uveo i predavao više predmeta na MCAST (Malta College of Arts, Science and Technology). U bogatom nastavno-naučnom radu bio je angažovan na nizu fakulteta, i to na Univerzitetima u Beogradu, Novom Sadu, Minho - Braga & Guimaraes, Malta College of Arts, Science and Technology itd. Držao je seminare i radionice na univerzitetima, fakultetima i institutima u SAD, Rusiji, Portugaliji, Malti, Italiji, Španiji, Egiptu, Srbiji i regionu, kao i predavanja po pozivu na međunarodnim kongresima, konferencijama i simpozijumima održanim u nizu država, prevashodno u Evropi, ali i u SAD, kao i u Africi.

Objavio je četiri knjige, i to istaknutu monografiju nacionalnog značaja (M41) i tri zapažena udžbenika (neki su imali do devet izdanja), ima 12 naučnih radova publikovanih u najprestižnijim međunarodnim časopisima (Science Citation Index-Web of Science® - kategorije: M21a, M21, M22, M23), kao i četiri naučna rada objavljena u tematskim zbornicima kategorije M13 i M14 (uz 595 citata_izvor SCOPUS, h-index: 8), šest poglavlja objavljenih u istaknutim naučnim monografijama svetski priznatih vodećih izdavača, preko 120 radova predstavljenih na međunarodnim i nacionalnim konferencijama, a objavljenih u zbornicima radova u Srbiji, regionu i širom sveta – od SAD, Evrope, do Azije i Afrike. Citiran je u preko 550 radova publikovanih u međunarodnim i nacionalnim časopisima i zbornicima radova autora iz: SAD, Rusije, Kine, Nemačke, Japana, Švajcarske, Portugalije, Italije, Španije, Bosne i Hercegovine, Slovenije, kao i u vodećim referentnim časopisima SCI-Web of Science®, sa visokim impakt faktorima.

Naučno-istraživačka delatnost Profesora Babića obuhvatala je: projektovanje proizvodnih tehnologija – sistema i procesa, računarski integrisane tehnologije, diskretnu simulaciju tehnoloških procesa, inteligentne tehnološke sisteme i procese, veštačku inteligenciju, razvoj i primenu softvera širokog spektra aplikativnosti i aksiomatsku teoriju projektovanja fleksibilnih tehnoloških sistema. Rukovodio je brojnim naučnim i stručnim projektima finansiranim od strane ministarstava Vlade Republike Srbije i privrede, kao i jednim EUREKA projektom, a bio je učesnik

i u aktivnostima više TEMPUS projekata. Tokom četrdesetogodišnjeg neprekidnog rada na Mašinskom fakultetu Univerziteta u Beogradu, koristio je, kao vrsan programer, mnogobrojne programske jezike (FORTRAN, Pascal, Clipper, Prolog, Basic, Visual Basic, PHP), a takođe je bio veoma dobro prepoznat po sistemima za upravljanje bazama podataka (SQL, MS Access), simulacionim sistemima (GPSS, WITNESS, SimFactory, AnyLogic itd.), široko zastupljenim softverskim paketima za projektovanje (ProEngineer, CATIA, AutoCAD), po razvoju brojnih softverskih aplikacija koje su u praktičnoj primeni (baze podataka, simulacioni paketi, WEB aplikacije, programski paketi za projektovanje tehnoloških procesa itd). U naučnoj i stručnoj javnosti biće zapamćen po izvanrednom poznavanju i kontinuiranom razvoju i primeni softverskih paketa gde se posebno ističe originalni softver FLEXY sopstvenog razvoja, svetski priznat i verifikovan.

Profesor Babić bio je dopisni član Akademije inženjerskih nauka Srbije (AINS) od 2021. godine. Šef katedre za proizvodno mašinstvo bio je u periodu od 2012. do 2023. g. i rukovodilac Centra za nove tehnologije od 2003. do 2004. godine. Bio je član Veća grupacije tehničko-tehnoloških nauka na Univerzitetu u Beogradu od 2004. do 2015. godine. Bio je prodekan za finansije Mašinskog fakulteta Univerziteta u Beogradu od 2004. do 2012. godine i predsednik Saveta Mašinskog fakulteta Univerziteta u Beogradu od 2012. do 2015. godine. Bio je član Komisije za sticanje naučnih zvanja Ministarstva prosvete, nauke i tehnološkog razvoja od 2012. do 2018. godine. Bio je član više naučnih i stručnih organizacija, poput Izvršnog odbora Zajednice naučno-istraživačkih institucija proizvodnog mašinstva Srbije, JUPITER - asocijacije univerziteta, instituta i industrije u oblasti proizvodnog mašinstva (Srbija) i AMSE - Association for the Advancement of Modelling and Simulation Techniques in Enterprises (France-Spain). Bio je licencirani projektant – inženjer i član Inženjerske komore Srbije (IKS) od 2010. godine, a od 2014. godine je bio tehnički ekspert Akreditacionog tela Srbije (ATS). Kao izvestilac Revizione komisije Republike Srbije, od 2015. godine učestvovao je u reviziji dva državna projekta. Posebno su važne ekspertske aktivnosti Profesora Babića tokom petnaestogodišnje evaluacije preko 300 predloga projekata i kasnije, tokom praćenja realizacije odobrenih projekata pod jurisdikcijom Evropske komisije, pre svega u okviru FP7, H2020 i Horizon Europe poziva. Bio je dugogodišnji član žirija Privredne komore Srbije (PKS) za dodelu prestižne nagrade za najbolje doktorske disertacije.

Sa velikom tugom, ova nagrada se Prof. dr Bojanu Babiću dodeljuje posthumno.

**U ZNAK SEĆANJA
IN MEMORIAM**

**PROF. DR SAVA SEKULIĆ
(1931-2023)**



Prof. dr Sava Sekulić rođen je 28. decembra 1931. godine u Futogu kod Novog Sada. Otac Stevan je bio crkveni pojac i crkvenjak u Crkvi „Sveti Vrači“ u Futogu, a majka Jelica bila je pomoćna radnica u Osnovnoj školi i domaćica. Roditelji su došli iz Mađarske i posle dve godine provedene u Makedoniji nastanili su se u Futogu i tu zasnovali porodicu sa četvoro dece gde je Sava bio najmlađe dete. Osnovnu školu je pohađao u mestu rođenja. Nižu gimnaziju završio je 1946. godine i Tehničku srednju školu, mašinski odsek, 1949. godine, u Novom Sadu, sa odličnim uspehom.

Na Mašinski fakultet Univerziteta u Beogradu upisao se školske 1949/50. godine, i diplomirao na vazduhoplovnom odseku početkom 1956. godine. Doktorsku disertaciju odbranio je na Fakultetu tehničkih nauka Univerziteta u Novom Sadu, 1977. godine.

Posle diplomiranja zaposlio se u Fabrici automobilskih i traktorskih delova “27 Mart” u Novom Sadu, sa prekidom od godinu dana zbog odlaska na odsluženje vojnog roka, radeći kao tehnolog mašinske obrade, glavni konstruktor, tehnolog i konstruktor alata za čelične proizvode. Sredinom 1959. godine prelazi u Industriju alata i pribora za mašine “Jugoalat” u Novom Sadu, gde radi kao šef tehnološkog biroa i inženjer za ispitivanje režima rada pri rezanju. Na Mašinski fakultet Univerziteta u Novom Sadu biran je krajem 1961, a postavljen početkom 1962. godine za asistenta na predmetu Mašinska obrada. Za nastavnika Mašinskog fakulteta Univerziteta u Novom Sadu habilitovan je krajem 1965. godine a postavljen za docenta na predmet Mašinska obrada početkom 1966. godine i ponovo biran u isto zvanje 1970. godine. Za vanrednog profesora na predmetu Mašinska obrada rezanjem biran je krajem 1971. godine a za redovnog profesora 1978. godine.

Profesor doktor Sava Sekulić je držao nastavu na velikom broju predmeta na institutu za Proizvodno mašinstvo a od oktobra 1981. godine kada je prešao na institut za industrijske sisteme na poziv profesora Dragutina Zelenovića, držao je nastavu na predmetima iz oblasti Industrijskog inženjerstva. Držao je nastavu i na posdiplomskim studijama na FTN u Novom Sadu i Mašinskim fakultetima u Kragujevcu i Mostaru.

Profesor Sekulić je napisao i objavio šest knjiga i preko 300 naučnih i stručnih radova koji su objavljeni u naučnim časopisima i konferencijama u zemlji i inostranstvu. Bio je nosilac većeg broja naučno istraživačkih projekata i projekata primene naučnih rezultata u praksi. Boravio je na specijalizaciji u SAD, 2 meseca, 1960. godine, a u SSSR-u 10 meseci na MOSSTANKIN-u u Moskvi, na Katedri obrade materijala, kod prof. I.P. Tretjakova.

Bio je član redakcija međunarodnih časopisa, predsednik i član organizacionih, naučnih i programskih odbora mnogih naučnih konferencija u zemlji i inostranstvu. Bio je član izvršnog odbora zajednice Proizvodnog mašinstva Jugoslavije/Srbije, počasni podpredsednik društva alatničara Jugoslavije i podpredsednik Jugoslovenskog komiteta za tribologiju.

Profesor doktor Sava Sekulić je imao zapažene funkcije na Mašinskom odnosno FTN u Novom Sadu. Bio je član saveta, nastavno-naučnog veća, pomoćnik direktora Mašinskog instituta, prodekan za nastavu fakulteta, šef katedre za proizvodno mašinstvo i katedre za obradu materijala skidanjem strugotine, direktor instituta za industrijske sisteme. Bio je predsednik komisije za mašinske nauke nastavno-naučnog veća Univerziteta u Novom Sadu i bio je delegat u Veću udruženog rada skupštine SR Srbije.

Za svoj predani i dugogodišnji rad u oblasti obrazovanja, nauke i privrede profesor Sekulić

je dobio veliki broj povelja, priznanja i zahvalnica od Fakulteta, Univerziteta i drugih strukovnih i društvenih organizacija u zemlji. Posebno se ističu: Nagrada Boris Kidrič – srebrna plaketa za osobite zasluge u širenju tehničke kulture, povelja Mašinskog fakulteta u Kragujevcu, plaketa Fakulteta tehničkih nauka u Novom Sadu, Zlatna plaketa udruženja univerzitetskih profesora i naučnika Srbije, plaketa „Dr Pavle Stanković“ za značajni doprinos razvoju proizvodnog mašinstva (1992) kao i zlatna plaketa Inženjerske akademije Srbije.

Profesor Sekulić je bio pravi inženjer i vrstan univerzitetski profesor. Podjednako su mu bili važni i nastava, nauka i privreda. Iza njega su ostali brojni diplomirani mašinski inženjeri, magistri i doktori nauka. Ostale su napisane knjige, monografije, naučni i stručni radovi, originalna tehnička rešenja, naučni i razvojni projekti i studije. Nije bilo ozbiljnijeg skupa iz oblasti Proizvodnog mašinstva i Industrijskog inženjerstva a da profesor Sekulić nije aktivno učestvovao. Poseban doprinos je dao organizovanju naučnih skupova:

- Savetovanje proizvodnog mašinstva Jugoslavije
- Mašinska obrada, mašine alatke i alati MMA.

koji se u kontinuitetu organizuju dugi niz godina.

Nema sumnje da je profesor Sava Sekulić ostavio neizbrisiv trag u razvoju Mašinskog odnosno FTN u Novom Sadu i u naučnim oblastima PROIZVODNO MAŠINSTVO i INDUSTRIJSKO INŽENJERSTVO. Teorija rezanja, mašinska obrada, dinamika rezanja, nekonvencionalni i specijalni postupci obrade, tribologija i pouzdanost alata bili su predmet njegovih istraživanja u kojima je ostvario nesporne rezultate.

Sećaćemo ga se sa ponosom i pominjati sa pijetetom kao istaknutog člana našeg kolektiva i čoveka visokih moralnih i ljudskih vrednosti.

Prof. dr Ilija Ćosić

CONTENTS

SESSION 1:

PROCESS PLANNING, OPTIMIZATION, LOGISTICS AND INTERNET
TECHNOLOGIES IN PRODUCTION ENGINEERING

Srecko CURCIC, Aleksandar PEULIC, Vladimir MLADENOVIC: NVIDIA JETSON NANO REAL TIME MACHINE LEARNING APPLICATION IN AGRICULTURE	3
Aleksandar JOKIĆ, Milica PETROVIĆ, Zoran MILJKOVIĆ: THE ARITHMETIC OPTIMIZATION ALGORITHM FOR MULTI-OBJECTIVE MOBILE ROBOT SCHEDULING	9
Bogdan MOMCILOVIC, Nikola SLAVKOVIC: DEVELOPMENT OF THE DELTA ROBOT SIMULATION SYSTEM	16
Dušan NEDELJKOVIĆ, Živana JAKOVLJEVIĆ: GENERATION OF LIGHTWEIGHT MODELS FOR CYBER-ATTACKS DETECTION ALGORITHMS USING KNOWLEDGE DISTILLATION	24
Isak KARABEGOVIĆ, Mehmed MAHMIĆ, Edina KARABEGOVIĆ, Ermin HUSAK: IMPLEMENTATION OF INDUSTRY 4.0 IN THE METAL INDUSTRY TO ACHIEVE SMART PRODUCTION PROCESSES	32
Nikola VORKAPIC, Branko KOKOTOVIC, Sasa ZIVANOVIC: COMPARISON OF SIGNAL FEATURES FROM TIME AND FREQUENCY DOMAIN FOR CHATTER DETECTION	42
Vidoje KASALICA, Slavenko STOJADINOVIĆ: DATA INTEROPERABILITY IN COMMUNICATION BETWEEN REAL AND DIGITAL MEASURING TWIN	48
Ernad KAHROVIĆ: PRODUCTION MODELS OF DIGITAL GOODS.....	55

SESSION 2:

MATERIALS, METAL FORMING, CASTING AND WELDING

Božica BOJOVIĆ, Zorana GOLUBOVIĆ, Ivana JEFTIĆ, Žarko MIŠKOVIĆ, Aleksandar SEDMAK: MECHANICAL PROPERTIES VARIATION DUE TO BUILDING ORIENTATION OF ABS RESIN MATERIAL.....	67
Petar JANJATOVIĆ, Dragan RAJNOVIĆ, Sebastian BALOS, Miroslav DRAMICANIN, Olivera ERIC CEKIC, Milan PEĆANAC, Danka LABUS ZLATANOVIC, Leposava SIDJANIN: THE EFFECT OF CRITICAL WATER CONCENTRATION ON THE EMBRITTLEMENT OF AUSTEMPERED DUCTILE IRONS.....	72
Plavka SKAKUN, Dragan RAJNOVIĆ, Petar JANJATOVIĆ, Miroslav DRAMIĆANIN.: AN EXPERIMENTAL METHOD FOR STRAIN STATE DETERMINATION IN BULK METAL FORMING	77
Vladimir TEREK, Lazar KOVAČEVIĆ, Zoran BOBIĆ, Branko ŠKORIĆ, Aljaž DRNOVŠEK, Miha ČEKADA, Peter PANJAN, Pal TEREK: HIGH TEMPERATURE TRIBOLOGICAL EVALUATION OF NANOLAYER TiAIN/TISIN COATING DEPOSITED ON TOOL STEEL	81
Milan PEĆANAC, Danka LABUS ZLATANOVIC, Nenad KULUNDZIC, Miroslav DRAMICANIN, Petar JANJATOVIĆ, Mirjana TRIVKOVIĆ, Dragan RAJNOVIĆ, Sebastian BALOS, Leposava SIDJANIN: INFLUENCE OF SHOULDER PINCHING GAP ON MECHANICAL PROPERTIES OF THE BOBBIN TOOL FSW WELDED JOINTS.....	88
Stanko SPASOJEVIĆ, Katarina ILIĆ, Ana BRDAR, Miroslav DRAMIĆANIN, Milan PEĆANAC, Petar JANJATOVIĆ, Mirjana TRIVKOVIĆ, Dragan RAJNOVIĆ, Sebastian BALOŠ, Leposava ŠIĐANIN: ISPITIVANJE BALISTIČKE OTPORNOSTI ŠLJEMA OJAČANOG ARAMIDNIM VLAKNIMA	94

Katarina ILIC, Albert HAUCK, Ana BRDAR, Stanko SPASOJEVIC, Miroslav DRAMICANIN, Milan PECANAC, Petar JANJATOVIĆ, Mirjana TRIVKOVIĆ, Dragan RAJNOVIĆ, Sebastian BALOS, Lepasava SIDJANIN: INFLUENCE OF WAAM TECHNOLOGY PARAMETERS ON PROPERTIES OF STRUCTURAL STEEL WALLS.....	99
Danka LABUS ZLATANOVIĆ, Jean PIERRE BERGMANN, Sebastian BALOS, Petar JANJATOVIĆ, Dragan RAJNOVIĆ, Lepasava SIDJANIN: INFLUENCE OF STRAIN RATE ON METALLURGICAL AND MECHANICAL PROPERTIES OF FRICTION STIR SPOT WELDED ALUMINIUM JOINTS	105
Ana BRDAR, Katarina ILIC, Stanko SPASOJEVIC, Danka LABUS-ZLATANOVIĆ, Petar JANJATOVIĆ, I. ZABUNOV, Miroslav DRAMICANIN, Milan PECANAC, Mirjana TRIVKOVIĆ, Dragan RAJNOVIĆ, Sebastian BALOS, Lepasava SIDJANIN: ULTRASONIC WELDING OF COPPER CONDUCTORS.....	113
Saša RANĐELOVIĆ, Nikola VITKOVIĆ, Marina TRAJKOVIĆ MILENKOVIĆ, Andrija ZORIĆ: FEM ANALYSIS FORWARD EXTRUSION PROCES OF HOLOW ELEMENTS	118
Anđelija MITROVIĆ, Jelena BARALIĆ, Aleksandar JOVIČIĆ: IZRADA KALUPA ZA LIVENJE U SOLIDWORKSU.....	124
Dragan DzUNIC, Vladimir KOCOVIĆ, Suzana PETROVIĆ SAVIC, Aleksandar DjORDJEVIĆ, Aleksandra KOKIĆ ARSIĆ, Slobodan MITROVIĆ: INFLUENCE OF SURFACE ROUGHNESS ON MATERIAL TRANSFER OCCURRING IN ALUMINIUM DRY SLIDING APPLICATION	129
Ivan MATIN, Branko ŠTRBAC, Miloš RANISAVLJEV, Miodrag HADŽISTEVIĆ, Zorana LANC: NUMERICAL AND EXPERIMENTAL RESEARCH OF SHRINKAGE AND SINK MARKS ON INJECTION MOLDED PLASTIC PARTS	134
Zoran BOBIĆ, Lazar KOVAČEVIĆ, Atilla CSIK, Peter RODIĆ, Branko ŠKORIĆ, Vladimir TEREK, Pal TEREK: UTICAJ PVD GREŠAKA RASTA NA KOROZIONU OTPORNOST EN X2CrNiMo18-14-3 HIRURŠKOG ČELIKA SA TIN PREVLAKOM	140
Vladimir GAŠIĆ, Nemanja DAČEVIĆ, Pal TEREK, Zoran BOBIĆ, Marko VILOTIĆ: THE INFLUENCE OF STRAIN ON FREE SURFACE ROUGHNESS AT UNIAXIAL UPSETTING	145

SESSION 3:

MATERIAL REMOVAL TECHNOLOGIES

Dragan RODIĆ, Marin GOSTIMIROVIĆ, Milenko SEKULIĆ, Borislav SAVKOVIĆ, Andjelko ALEKSIĆ: MATERIAL REMOVAL RATE DURING ELECTRICAL DISCHARGE MACHINING OF ZIRCONIUM OXIDE	153
Milan TRIFUNOVIĆ, Miloš MADIĆ, Predrag JANKOVIĆ: MODELLING AND ANALYSIS OF CHIP COMPRESSION RATIO IN TURNING OF POM-C	158
Pavel KOVAČ, Vladimir PUCOVSKI, Borislav SAVKOVIĆ, Dušan JEŠIĆ, Branislav DUDIĆ: THE TOOL LIFE MODEL BY THE USE OF GENETIC ALGORITHM.....	165
Predrag MITIĆ, Aleksandar ĐORĐEVIĆ, Suzana PETROVIĆ SAVIĆ, Dragan DŽUNIĆ, Vladimir KOČOVIĆ: INTEGRATED OPTIMIZATION OF TOOL PATH AND CUTTING PARAMETERS IN CONTOUR MILLING USING GENETIC ALGORITHM	169
Djordje IVKOVIĆ, Dragan ADAMOVIĆ, Dušan ARSIĆ, Nada RATKOVIĆ, Ružica NIKOLIĆ: REVIEW OF THE FIRST GENERATION OF THE ADVANCED HIGH-STRENGTH STEELS (AHSS) AND THEIR MANUFACTURING PROCEDURES.....	181
Borislav SAVKOVIĆ, Milenko SEKULIĆ, Aleksandar KOŠARAC, Dragan RODIĆ, Anđelko ALEKSIĆ, Slaviša MOLJEVIĆ, Jelica ANIĆ: EFFECTS OF APPLYING A HYBRID MILLING PROCESS ASSISTED BY ULTRASONIC VIBRATIONS.....	189
Bogdan NEDIĆ, Gordana GLOBOČKI LAKIĆ: TRANSFORMING MANUFACTURING AND INDUSTRY 5.0	195
Vladimir TODIĆ, Milan DELIĆ: BASICS OF DEVELOPMENT OF AN EXPERT SYSTEM FOR THE SELECTION OF GRINDING TOOLS	201
Goran VASILIĆ, Saša ŽIVANOVIĆ, Milan MILUTINOVIĆ, Zoran DIMIĆ: KINEMATIKA PROCESA OBRADE SEČENJA ŽICOM	206
Milan IVKOVIĆ, Bogdan NEDIĆ, Suzana PETROVIĆ SAVIĆ: THERMOCOUPLE AND INFRARED SENSOR-BASED MEASUREMENT OF TEMPERATURE IN METAL CUTTING	212

Anđelko ALEKSIĆ, Marin GOSTIMIROVIĆ, Milenko SEKULIĆ, Borislav SAVKOVIĆ, Dragan RODIĆ: OPTIMIZATION OF SURFACE ROUGHNESS IN TURNING OF ALUMINUM ALLOY 2024-T3 USING TAGUCHI METHOD219

SESSION 4:

MACHINE TOOLS AND AUTOMATIC FLEXIBLE TECHNOLOGICAL SYSTEMS, CAX AND CIM PROCEDURES AND SYSTEMS

Goran MLADENOVIC, Radovan PUZOVIC, Jagos STOJANOVIC, Ivana JEVTIC, Mihajlo POPOVIC, Milos PJEVIC.: AN APPROACH FOR AUTOMATIC FREE FORM SURFACE MILLING MACHINING TECHNOLOGY DESIGN227
Jovana PERIĆ, Milovan LAZAREVIĆ, Dragić TOMIĆ, Branko RADIČEVIĆ, Vladan GRKOVIĆ: OPTIMIZACIJA PRIPREME MAŠINE ZA OBRADU DRVETA PRIMENOM SMED METODE231
Julija MALETIĆ, Saša ŽIVANOVIĆ: DEVELOPMENT OF A POSTPROCESSOR FOR MILLING WITH A ROTARY AXIS AND VERIFICATION ASSISTED BY VIRTUAL MACHINING ENVIRONMENT240
Ljubomir NEŠOVANOVIĆ, Saša ŽIVANOVIĆ: VERIFICATION OF KINEMATIC JOINTS ON A PHYSICAL PROTOTYPE OF A NOVEL PARALLEL MECHANISM BASED ON CHEBYSHEV'S LINKAGE246
Mihajlo POPOVIĆ, Marko FURTULA, Miloš PJEVIĆ, Goran MLADENOVIC: SIMULATION, ANALYSIS AND OPTIMIZATION OF FORGING PROCESS FOR AXISYMMETRIC PART252
Miloš MILOVANČEVIĆ, Srećno ĆURČIĆ: ANFIS PLASMA ARC CUTTING SYSTEM OPTIMUM PARAMETERS ESTIMATION259
Miloš MILOVANČEVIĆ, Srećno ĆURČIĆ: ANFIS CHIP-TOOL INTERFACE TEMPERATURE EVALUATION267
Sasa ZIVANOVIC, Slobodan TABAKOVIC, Zoran DIMIC, Milan ZELJKOVIC: VARIANTS OF HYBRID KINEMATICS MACHINE TOOLS BASED ON O-X GLIDE MECHANISM WITH ADDITIONAL ROTARY AXES278
Dejan MARINKOVIĆ, Miloš KNEŽEV, Aleksandar ŽIVKOVIĆ, Cvijetin MLAĐENOVIĆ, Luka MEJIĆ: ANALIZA DINAMIČKIH KARAKTERISTIKA DRŽAČA ALATA ZA OBRADU STRUGANJEM284
Jelena BARALIĆ, Bogdan NEDIĆ, Anđelija MITROVIĆ: THE INFLUENCE OF TRAVERSE SPEED ON THE APPEARANCE OF INCOMPLETE CUT288

SESSION 5:

ADDITIVE MANUFACTURING TECHNOLOGIES

Ljiljana STEFANOVIĆ, Dejan MOVRIN, Mladomir MILUTINOVIĆ, Mihajlo POPOVIĆ, Miloš PJEVIĆ: INFLUENCE OF INJECTION MOLDING PROCESS PARAMETERS ON THE MECHANICAL PROPERTIES OF POLYPROPYLENE AND POLYETHYLENE PARTS295
Miloš PJEVIĆ, Mihajlo POPOVIĆ, Mladomir MILUTINOVIĆ, Dejan MOVRIN, Ljiljana STEFANOVIĆ: IMPACT OF POLYMER TYPES ON APPLICABILITY IN RAPID TOOLING301
Slobodan MALBAŠIĆ, Bogdan NEDIĆ, Aleksandar ĐORĐEVIĆ, Srdjan ŽIVKOVIĆ, Aleksa GRUBIĆ: APPLICATIONS AND ECONOMICS OF ADDITIVE METAL PRODUCTION TECHNOLOGIES307
Rajko TURUDIJA, Jelena R. STOJKOVIĆ, Miloš STOJKOVIĆ, Jovan ARANĐELOVIĆ, Nikola KORUNOVIĆ: A MULTI-CRITERIA DECISION-MAKING APPROACH FOR ENHANCING MECHANICAL PROPERTIES OF FDM 3D-PRINTED PARTS315
Igor DRSTVENŠEK, Rembert DHONDT, Snehashis PAL, Tomaž BRAJLIH: EFFECTS OF AGING AND REFRESHMENT RATIO ON THE STRENGTH PROPERTIES OF SELECTIVELY LASER SINTERED POLYAMIDE 12324
Snehashis PAL, Matjaž FINŠGAR, Janez GOTLIH, Tomaž BRAJLIH, Prabas BANERJEE, Özkan YAPAR, Gorazd LOJEN, Tonica BONČINA, Igor DRSTVENŠEK: CHARACTERISTICS OF PARTIALLY MELTED POWDER PARTICLES IN LASER POWDER BED FUSION332
Milan KOLAREVIĆ, Stefan PAJOVIĆ, Vladan GRKOVIĆ, Boško NIKOLIĆ, Milan PEROVIĆ: RAZVOJ 3D ŠTAMPAČA TIPA FGF339

SESSION 6:
METROLOGY, QUALITY, FIXTURES, CUTTING TOOLS AND TRIBOLOGY

Borut KOSEC, Blaž KARPE, Mirko GOJIĆ, Zorana TANASIĆ, Gorazd KOSEC, Aco ANTIĆ, Aleš NAGODE: INDUCTIVE HEATING AND QUENCHING OF PLANETARY SHAFTS FOR DIESEL ENGINE STARTERS.....	353
Predrag JANKOVIĆ, Miloš MADIĆ, Miodrag HADŽISTEVIĆ, Branko ŠTRBAC: APPLICATION OF CONTROL CHARTS IN THE ANALYSIS OF MEASUREMENT SYSTEMS.....	360
Vladimir ANTIĆ, Dragan MIŠIĆ, Miodrag MANIĆ, Milan MITKOVIĆ: SMART ORTHOPEDIC IMPLANT: CONCEPTUAL SOLUTION	366
Tijana LAZENDIĆ, Slobodan TABAKOVIĆ, Miodrag HADŽISTEVIĆ: ANALYSIS OF THE IMPACT OF INDUSTRY 4.0 TECHNOLOGIES ON OCCUPATIONAL SAFETY AND HEALTH	371
Zeljko SANTOSI, Milos RANISAVLJEV, Mario SOKAC, Djordje VUKELIC: ANALYSIS OF THE SCANNING SPRAY LAYER THICKNESS USING THE FOCUS VARIATION METHOD.....	377
Saša TEŠIĆ, Goran JOTIĆ, Đorđe ČIČA, Branislav SREDANOVIĆ, Branko ŠTRBAC, Miloš RANISAVLJEV: ANALYSIS OF THE POSSIBILITY OF USING DIFFERENT MEASURING SYSTEMS FOR TESTING THE ACCURACY OF MACHINE TOOLS.....	382
Dejan BOŽIĆ, Miloš RANISAVLJEV, Mijodrag MILOŠEVIĆ, Borislav SAVKOVIĆ, Dejan LUKIĆ: THE INFLUENCE OF THE TECHNOLOGICAL PARAMETERS OF THE PRODUCTION PROCESS AND THE MATERIAL QUALITY ON THE MICROGEOMETRIC PRODUCT SPECIFICATIONS.....	388
SPONZORI	395

SPMS/ICPES 2023

**39TH INTERNATIONAL CONFERENCE ON
PRODUCTION ENGINEERING OF SERBIA**

SESSION 1

**PROCESS PLANNING, OPTIMIZATION, LOGISTICS AND INTERNET
TECHNOLOGIES IN PRODUCTION ENGINEERING**

Novi Sad, 26 – 27 October 2023



Society of Production
Engineering

SPMS 2023
39. Savetovanje proizvodnog mašinstva Srbije

ICPES 2023

39th International Conference on Production Engineering
of Serbia



Faculty of Technical
Sciences
University of Novi Sad

Novi Sad, Serbia, 26. – 27. October 2023

NVIDIA JETSON NANO REAL TIME MACHINE LEARNING APPLICATION IN AGRICULTURE

Srecko CURCIC¹, Aleksandar PEULIC^{2,3} *, Vladimir MLADENOVIC¹

¹University of Kragujevac, Faculty of Technical Science, Cacak, Serbia

²University of Belgrade, Faculty of Geography, Belgrade, Serbia

³University of Kragujevac, Faculty of Science, Kragujevac, Serbia

*Corresponding author: aleksandar.peulic@pmf.kg.ac.rs

Abstract: The use of machine learning applications (ML) is becoming more common, and their daily use requires more capacity to process information in real time. Many devices deploy their infrastructure in cloud computing environments where latency and network partitioning are the main challenges. This paper demonstrates the use of the Nvidia Jetson Nano platform with an application to process and predict the parameters of soil planted with blueberries. Temperature, Ph, moisture, and air temperature were measured and their influence on blueberry yield was determined. Used different regression models to model data sets on the Jetson Nano. We obtain results for linear regression, Ridge, Lasso, Random Forrest, GBDT, Support Vector Regression, XgBoost, Elastic Net.

Keywords: Jetson Nano; machine learning; data processing.

1. INTRODUCTION

The tremendous increase in computing capacity and the improvement in the performance of telecommunications networks have enabled the consolidation of paradigms that allow the delivery of computing services remotely. Currently, there are three environments in which data is processed and distributed remotely [1]: Cloud computing, with large computing capacity and power; Fog computing, with less computing power but with processing closer to the data source; and Dev computing, where information is processed directly in end devices. The main goal of dew computing is to fully exploit the potential of local computers and cloud services [2], minimize the impact caused by the loss of Internet connectivity, and ensure the

security and privacy of the processed data [3]. Energy consumption during the execution of processes in integrated systems is very important because the energy supply of these systems is low. In peripheral devices, resources are so limited that processing cannot be performed [1].

The use of machine learning applications (ML) is becoming more widespread, and their daily use requires more processing capacity information in real time. In 2019, Nvidia launched a device called the Jetson Nano, which focuses on solving ML tasks and enables fast and powerful implementation using the dew computing approach. The Jetson Nano has low power consumption at an affordable price and is compatible with many AI frameworks, making it easy for developers to integrate their models into the product [4]. The advantage of

wireless data transmission in agriculture is the significant reduction and simplification of wire lines in gauges. Additional savings in overall costs could be achieved by more effective control equipment through more effective environmental control. Wireless sensors in some cases enable the impossible use of sensors, such as monitoring hazardous, risky, inaccessible, and remote areas and locations. This one technology provides virtually unlimited flexibility in sensor installation and increased network reliability. Wireless technologies also reduce the cost and complexity of maintenance. Wireless sensor networks enable faster deployment and installation of different types of sensors because many of these networks offer self-organizing capabilities, can configure, diagnose and troubleshoot sensor nodes. Some of them also allow for flexible network expansion. Wireless sensor technology makes it possible to connect MEMS sensors with signal amplifiers and radio units to form sensor nodes with very low cost, small size, and low power requirements. MEMS Sensors for statics, pressure, temperature, humidity, deformation and various other measurement sensors for distances, positions, velocities and vibrations are integrated in wireless sensor nodes and available on the market. Another advantage of wireless sensors is their mobility. These sensors can be mounted in transportation vehicles to monitor the environment while the vehicle is in motion. They can also be attached to rotating equipment, such as a shaft, to measure some important parameters. Most wireless sensors have amplifiers and signal processors installed on site where the sensors themselves are located, and the signal is output in digital form. This makes the occurrence of forests less of a problem. And, of course, the reliability of the signal is increased because cables are no longer required for data transmission. Manual data collection, as the selected factors can be sporadic and cause deviations from an incorrect measurement; this can lead to complications in controlling all important factors. Wireless sensor nodes can reduce the effort and time required to

monitor an individual and the environment. Data logging can reduce the likelihood of data being misplaced or lost. Sensor nodes can be placed in critical locations without putting personnel in dangerous situations. Use of the technology would allow remote measurement of factors such as temperature, humidity, moisture, and soil acidity. It appears that the move toward wireless solutions is increasing compared to wired systems. One particular reason for this is that sensors often need to be repositioned, and traditional cable laying costs a lot of energy and time. The system aims to reduce installation costs and wiring, and also to increase the flexibility and mobility of sensor points [5]. Since the early 2000s, the development of artificial intelligence has gained new momentum. A number of extremely important problems that were thought to remain out of reach for a long time have been solved. In some areas where computers had previously been unable to match humans in terms of success, superior results are being achieved compared to those achieved by human experts. At the heart of this new momentum is machine learning. Although just the two thousand in the forefront, this field has a long history of development. Conceived in the works of Allen Turing, in the forties of the last century, has been actively developing since the fifties, when the perceptron was constructed, the first system to teach simple laws and is a distant precursor of modern neural networks, which evolve until nineties with ups and downs, when the support vector method and other kernel-based methods took precedence. However, the recent rise of machine learning is due to a renaissance neural networks, which led to today's artificial intelligence, and machine learning are often equated in the general perception. This must be kept in mind when considering that these fields are incomparably broader. There are many common machine learning algorithms, and a detailed introduction to them could take an entire book. Linear regression is a statistical analysis method that uses regression analysis in mathematical statistics to determine the

quantitative relationship between two or more variables. It belongs to supervised learning [6].

The main contributions are in this paper:

- new approach in the development of machine learning algorithms in agriculture,
- application of new IoT devices to obtain responses in real time.

This paper is organized as follow. The session II describes methods of machine learning and dataset description. Results and graphic plurals are shown and described in session 2.

2. MATERIALS ANS METHODS

The method is based on the measurement dataset, which contains 77 records. Each dataset contains detailed information about temperature, moisture and pH. The framework provides functions for segmentation, standardization and analysis of air temperature datasets and integrates several common machine learning algorithms using Python 3. In addition, XGboost is used, an optimized version of GBDT in the integration algorithm and an ML algorithm was executed on Jetson Nano. The Jetson Nano is a device of compact size (69 mm 45 mm) with Maxwell 128-core GPU, Quad-core ARM A57 CPU, 4 USB 3.0 ports; for storage it has a MicroSD card slot, connections are via Gigabit Ethernet and M.2 Key E and a 2.0 Micro-B port for connecting the power source [7]. The Jetson Nano platform does not have an embedded camera, but in this work, the Nvidia Jetson Nano HD AI model IMX219-77 was used to capture video in real time. The OS used was GNU /Linux Ubuntu 18.04.

Linear regression is usually the first algorithm learned for machine learning and data science. Linear regression is a linear model that assumes a linear relationship between the input variables (X) and the single output variable (y). In general, two cases are distinguished, linear regression with a single variable. It models the relationship between a single input variable (a single characteristic variable) and a single output variable.

Multivariable linear regression, it models the relationship between multiple input and a single output variable. This algorithm is so widely used

that Scikit-learn has built in this functionality with *Linear Regression*.

Polynomial regression is one of the most popular choices when we want to build a model for non-linearly separable data. It's similar to linear regression, but uses the relationship between the variables X and y to find the best way to draw a curve that fits the data points.

In polynomial regression, the power of some independent variables is greater than 1. Scikit-learn has incorporated this method with *Polynomial Features*.

Support Vector Machines are well known in classification problems. The use of SVM in regression is known as Support Vector Regression (SVR).

Scikit-learn has this method built in with *SVR*. Before fitting an SVR model, it's generally best to do feature scaling so that each feature has a similar meaning.

Decision Trees (DTs) are a non-parametric supervised learning method used for classification and regression. The goal is to build a model that predicts the value of a target variable by deriving simple decision rules from data features. A tree can be viewed as a piecewise constant approximation. Decision tree regression is also so widely used that Scikit-learn has incorporated it with *Decision Tree Regressor*. A *Decision Tree Regressor* object can be created without feature scaling.

Random forest regression is very similar to decision tree regression. It's a meta-estimator that fits a series of decision trees to different subsamples of the data set and uses averaging to improve predictive accuracy and control for overfitting.

A random forest repressor may perform better or worse than a decision tree in regression (while it usually performs better in classification), due to the delicate trade-off between overfitting and under fitting that is inherent in tree construction algorithms.

Random Forest Regression is so widely used that Scikit-learn has incorporated it with *Random Forest Regressor*. First, we need to create a *Random Forest*

Regressor object with a certain number of estimators [8].

LASSO regression is a variant of linear regression that uses shrinkage. Shrinkage is a process in which data values are shrunk to a central point as the mean. This type of regression is well suited for models with strong multicollinearity (strong correlation among characteristics). Scikit-Learn has built it in with *Lasso*.

Ridge regression is quite similar to LASSO regression in that both methods use shrinkage. Both ridge and LASSO -regression are well suited for models with strong multicollinearity (strong correlation among characteristics). The main difference is that ridge regression uses L2 regularization, which means that none of the coefficients become zero as they do in LASSO regression (instead they become almost zero). Scikit-learn has built in this feature with *Ridge CV*.

Elastic Net is another linear regression model trained with both L1 and L2 regularization. It's a mixture of lasso and ridge regression techniques and is therefore well suited for models with strong multicollinearity (strong correlation among features).

A practical advantage of the compromise between Lasso and Ridge is that it allows Elastic-Net to inherit some of Ridge's stability under rotation [9]. Scikit-learn has built this into *Elastic Net CV*.

Extreme Gradient Boosting (XGBoost) is an efficient and effective implementation of the gradient boosting algorithm. Gradient boosting refers to a class of ensemble machine learning algorithms that can be used for classification or regression problems.

XGBoost is an open-source library originally developed by Tianqi Chen [10]. The algorithm is designed to be both computationally efficient and highly effective.

3. RESULTS

Measuring devices were placed on the blueberry plantation. Sensors were installed to measure temperature, humidity, soil acidity, and air

temperature. Wireless communication was established and data was sent to the Jetson Nano for processing. The purpose of this experiment is to demonstrate the application of the Jetson Nano in data analysis and processing in agriculture.

After loading the data set, the first step is to analyze the measurement data for a specific blueberry plant. Figure 1 shows the percent value of air temperature in the data set, and Figure 2 shows the percent value of soil acidity in the data set.

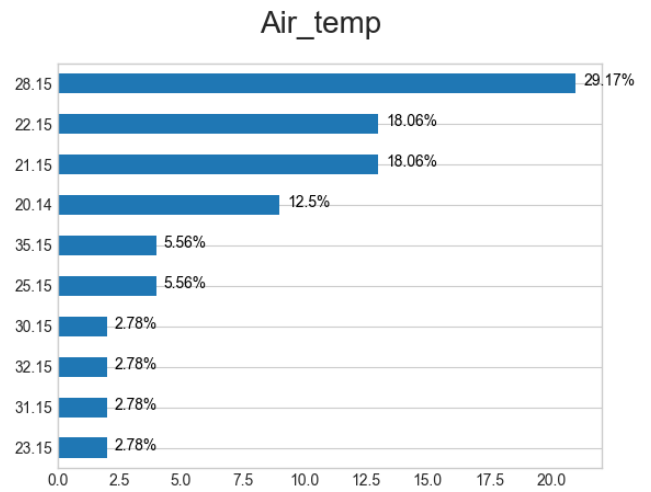


Figure 1. Percent value of air temperature in the data set

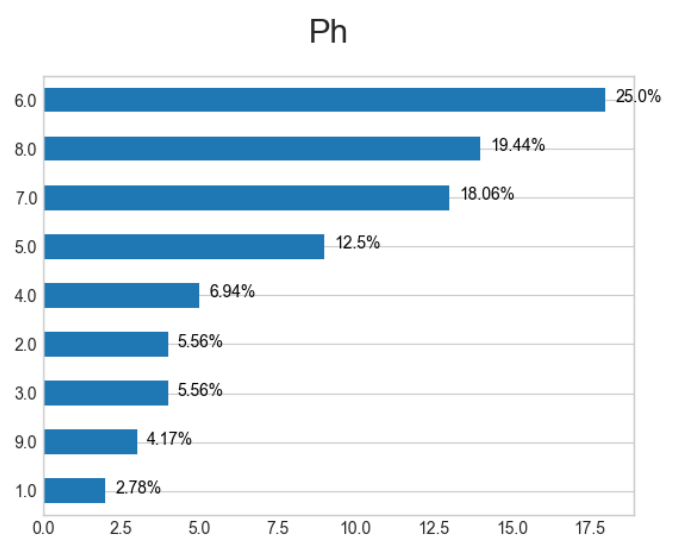


Figure 2. Percent value of soil acidity in the data set

The data set was then statistically processed on Jetson Nano, so that Figure 3 shows the data distribution of moisture, Figure 4 shows the data

distribution of blueberries, Figure 5 shows the data distribution of blueberries relative relative to moisture and Figure 6 data distribution of blueberries relative to air temperature.

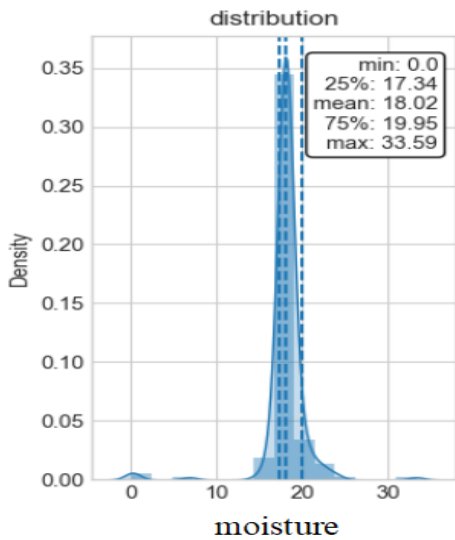


Figure 3. Data distribution of moisture

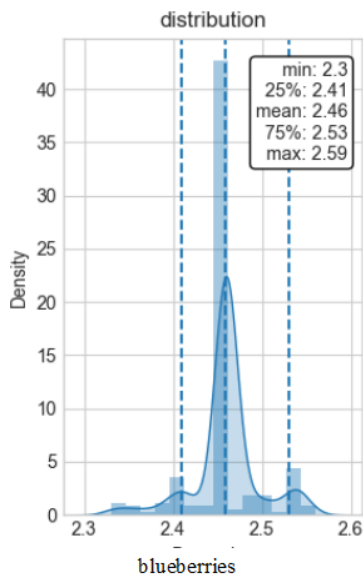


Figure 4. Data distribution of blueberries

Blueberries vs moisture

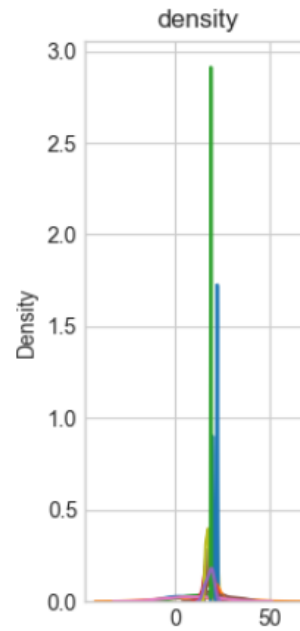


Figure 5. Data distribution of blueberries relative to moisture

Blueberries vs air temp

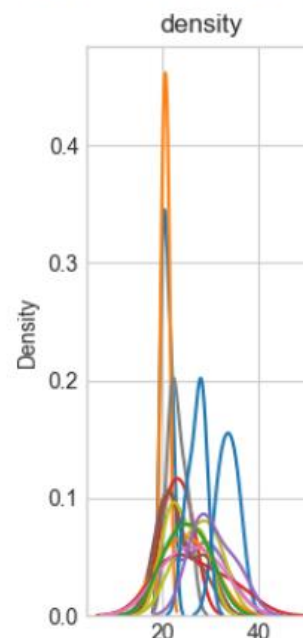


Figure 6. Data distribution of blueberries relative to air temperature

After statistical data processing and visualization using various regression models to model data sets, Liner Regression, Ridge, Lasso, Random Forrest,

GBDT, Support Vector Regression, XgBoost and Elastic Net, on Jetson Nano, using Python 3, we obtain results:

Liner Regression: -0.367705

Ridge: -0,36334

Lasso: -0.36738

Random Forest: 0.504319

GBDT: 0.158149

Support Vector: 0.066564

XgBoost: 0.025325

Elastic Net: 0.976238

By adjusting the hyper parameters using the grid search, we obtain optimal parameters.

Optimal parameter list: {'C': 1, 'gamma': 1, 'kernel': 'rbf'} Optimal model: SVR (C=1, gamma=1) and Optimal R2 value: 0.1349723643733485.

For example, we made a prediction of the Jetson Nano's ambient temperature using the trained dataset, which is visually represented in Figure 7.

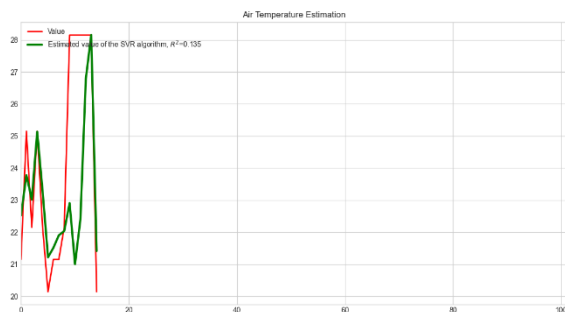


Figure 7. Air temperature estimated value

CONCLUSION

The objective of this work was to demonstrate the possibility of using Jetson Nano under real conditions in agriculture. Specifically, an experiment was conducted on a blueberry plantation. The processing of the measured data on the Jetson Nano was carried out, from analysis to statistics and the most common ML algorithms. It has been shown that the Jetson Nano is a very acceptable solution for data processing in the field. The speed of processing is acceptable, and the accuracy of

processing depends on the accuracy of the data and interdependence. The disadvantage of the Jetson Nano that can be highlighted is the increased heating when processing a larger data set. We used a small data set as a demonstration case. From the analysis of the data and the results obtained with the Jetson Nano, we can conclude for a particular case that the estimates of the outdoor temperature are independent of the influence of the elements in the soil and that the estimates of the parameters in the soil depend on the elements added to the soil, so we cannot predict certain parameters with certainty.

ACKNOWLEDGMENT

This paper is supported by the Ministry of education, science and technological development of the Republic of Serbia, and these results are part of the grant no. 451-03-68/2022-14/200132 with University of Kragujevac-Faculty of technical sciences in Čačak.

REFERENCES

- [1] Kotlar, M., Bojic, D., Punt, M., Milutinovic, V.: A survey of deep neural networks: deployment location and underlying hardware. In: Symposium Neural Networks Application NEUREL 2018, pp. 1–6 (2018)
- [2] Wang, Y.: Definition and categorization of dew computing. *Open J. Cloud Comput.* 3(1) (2016).
- [3] Wang, Y., Karolj, S., Rindos, A., Gusev, M., Yang, S., Pan, Y.: Dew computing and transition of internet computing paradigms. *ZTE Commun.* 15, 133–136 (2017).
- [4] Cass, S.: Nvidia makes it easy to embed AI: the Jetson nano packs a lot of machine-learning power into DIY projects-[Hands on]. *IEEE Spectr.* 57(7), 14–16 (2020)
- [5] Crossbow Technology Inc., Smart Dust/Mote Training Seminar, Crossbow Technology, Inc., San Francisco, California (2004) July 22–23. Huawei Technology, Artificial Intelligence Technology, Springer, Open Access Book, 2022 Nvidia Jetson Nano Developer Kit. <https://developer.nvidia.com/embedded/jetson-nanodeveloper-kit> Scikit-Learn Decision Tree docs: <https://scikitlearn.org/stable/modules/tree.html#tree>
- [9] Scikit-Learn ElasticNet docs: https://scikitlearn.org/stable/modules/linear_model.html#elastic-net
- [10] Tianqi Chen, XGBoost: A Scalable Tree Boosting System, Cornell University, 2016



Society of Production
Engineering

SPMS 2023

39. Savetovanje proizvodnog mašinstva Srbije

ICPES 2023

39th International Conference on Production Engineering of
Serbia



Faculty of Technical
Sciences
University of Novi Sad

Novi Sad, Serbia, 26. – 27. October 2023

THE ARITHMETIC OPTIMIZATION ALGORITHM FOR MULTI-OBJECTIVE MOBILE ROBOT SCHEDULING

Aleksandar JOKIĆ^{1*}, Milica PETROVIĆ¹, Zoran MILJKOVIĆ¹

¹University of Belgrade – Faculty of Mechanical Engineering,
Department of Production Engineering, Belgrade, Serbia;

ajokic@mas.bg.ac.rs; mmpetrovic@mas.bg.ac.rs; zmiljkovic@mas.bg.ac.rs

Abstract: In recent years, metaheuristic algorithms have become increasingly advantageous for solving many real-world optimization-based engineering tasks. Integrated process planning and scheduling of machine tools and mobile robots utilized for transportation tasks in a manufacturing environment represents one such task. Since the number of solutions increases exponentially with the addition of either parts, machines, or robots, this task belongs to a group of NP-hard problems. Therefore, for its successful resolution, it is essential to use efficient algorithms that are able to explore vast solution space and provide optimal solutions. In this paper, we propose an algorithm for solving integrated scheduling of machine tools and mobile robots based on a novel arithmetic metaheuristic optimization. The arithmetic optimization algorithm belongs to a group of stochastic population-based algorithms inspired by arithmetic mathematical operations. The main advantage of the proposed algorithm is in a well-suited balance between exploration and exploitation phases that are appropriate for extremely hard multi-objective optimization. A multi-objective metric is utilized to evaluate obtained Pareto front solutions in terms of the exploration capabilities in the solution space. The proposed algorithm is compared with two other state-of-the-art metaheuristic algorithms. The experimental evaluation is carried out on 20 benchmark problems, and the results show the advantages of the proposed algorithm.

Keywords: multi-objective optimization, metaheuristic algorithms, mobile robots, machine tools, scheduling

1. INTRODUCTION

Contemporary manufacturing systems, inspired by the Industry 4.0 paradigm, tend to maximize the flexibility of the production process, all while maintaining high levels of efficiency. These conflicting criteria need to be balanced to satisfy the highly diversified customer needs while meeting all necessary time requirements. For these reasons, we propose methodology for integrated process

planning and scheduling of both machine tools and transportation vehicles utilized for part manipulation. Multi-objective scheduling enables decision-makers in top management level to select a manufacturing schedule with the optimal ratio of different optimization criteria that best fit current manufacturing needs. The result of the optimization process is a set of optimal schedules represented as a Pareto front that can be directly utilized for tactical planning.

The metaheuristic population-based algorithms provide efficiency in exploring the search space, straightforward implementation, and low probability of local optima entrapment. Therefore, they have become extensively used to solve real-world mechanical engineering optimization problems [1]. Since integrated process planning and scheduling with mobile robot-related constraints represent the discrete high dimensional optimization problem (shown to be NP-hard), the optimal solution cannot be obtained using standard optimization algorithms. Therefore, this paper proposes metrology for multi-objective scheduling of manufacturing entities based on metaheuristic Arithmetic Optimization Algorithm (AOA) [2]. The initial exploration-exploitation ratio of the AOA algorithm is heavily tilted on the exploitation side. However, for the problem at hand, the exploration is a more significant phase; therefore, we propose an improvement to the AOA algorithm that enhances the exploration phase. Moreover, implementing the AOA algorithm enables fast rescheduling with different multi-objective criteria if a new part enters the manufacturing system or some other disturbance occurs.

2. IMPLEMENTATIONS OF AOA ALGORITHM – A STATE-OF-THE-ART REVIEW

Since its emergence in 2021, AOA [2] has become increasingly popular for solving many engineering problems [3]. Therefore, many authors have proposed different AOA improvements based on the problem at hand. AOA [4] was implemented for solving discrete structural problems, where the solution update strategy was improved to search around the current position of each individual in the search space instead of around the leader. Moreover, the parameter MOP_i that defines the distance each individual moves in the search space has also been modified, and a stochastic element has been added. The hybrid AOA algorithm used for many engineering optimization problems is presented in [5]. The authors utilized a specific initialization strategy to spread the initial solutions in the search space

and, therefore, improved AOA's exploration capability. Moreover, the convergence is improved by incorporating an optimal neighborhood strategy. Lastly, the AOA is hybridized with a crossover algorithm, which boosts optimization accuracy for complex problems. The development of multi-objective AOA algorithm utilized for solving real-world optimization problems is proposed in [6]. The algorithm is implemented with non-dominance sorting crowding distance, and the evaluation is performed based on five multi-objective metrics and non-parametric statistical significance testing. The experimental results show the advantages of AOA compared to the other four metaheuristic algorithms. Another interesting approach for improving the AOA algorithm is with chaotic maps [7]. Different chaotic maps were implemented to generate random numbers for two AOA parameters. The novel improved AOA was tested on benchmark function, as well as on four engineering design problems. The AOA with Circle and Piecewise maps have shown the best overall results for engineering design problems. Improving AOA exploration by integrating a forced switching mechanism is proposed in [8]. The proposed mechanism forces the solutions to significantly change their position in the search space if the fitness function value has not changed for a predefined number of iterations. The improved AOA was tested on different problems such as training of multi-layer perceptron, including various benchmark functions and real-world engineering applications.

Different from these approaches, we improve AOA algorithm by extending the range of the MOA_i parameter, providing 100% exploration in the beginning of optimization, and ensuring that only exploitation occurs in the last few iterations.

3. ARITHMETIC OPTIMIZATION ALGORITHM

Arithmetic Optimization Algorithm (AOA) represents the newly proposed metaheuristic algorithm that is often utilized in engineering optimization problems. AOA is classified as a nature-inspired metaheuristic algorithm

belonging to a physics-based group. Its main optimization principle is based on four arithmetic mathematical operations: addition, subtraction, multiplication, and division. AOA also belongs to a group of population-based algorithms in which the candidate solutions interact in a certain way to obtain the optimal solution to an optimization problem.

The entire population of candidate solutions is defined with a matrix \mathbf{X} (Eq. 1), where the rows represent individual solutions, while the columns contain different solution parameters:

$$\mathbf{X} = \begin{bmatrix} x_{1,1} & \cdots & x_{1,n} \\ \vdots & \ddots & \vdots \\ x_{N,1} & \cdots & x_{N,n} \end{bmatrix}, \quad (1)$$

where N represents the number of individual solutions, and n is the number of solution parameters. There are two distinct phases in the AOA algorithm: exploration and exploitation. In the exploration phase which is present in the early stages of the optimization process, the algorithm explores the vast solution spaces, trying to find suitable candidate solutions. Within the exploitation phase, already found suitable solutions are utilized to find even better solutions, which are close by in the search space. The exploration phase of AOA algorithm is defined with multiplication and division, while exploitation is defined with addition and subtraction. The hyper-parameter that defines if each individual solution parameter will undergo exploration or exploitation is MOA_i (Eq. 2):

$$MOA_i = M_{min} + i \left(\frac{M_{max} - M_{min}}{G} \right), \quad (2)$$

where $i=1, \dots, G$ is the current iteration number, G is the maximal number of iterations, M_{min} and M_{max} are the minimal and maximal values for parameter MOA_i . Moreover, two additional random numbers (r_1 and r_2 ranging between 0 and 1 with uniform distribution) are utilized to determine which phase is selected and which arithmetic operation is performed, which is defined with the algorithm shown in Figure 1. Initial values for the M_{max} and M_{min} , are 1.0 and 0.2.

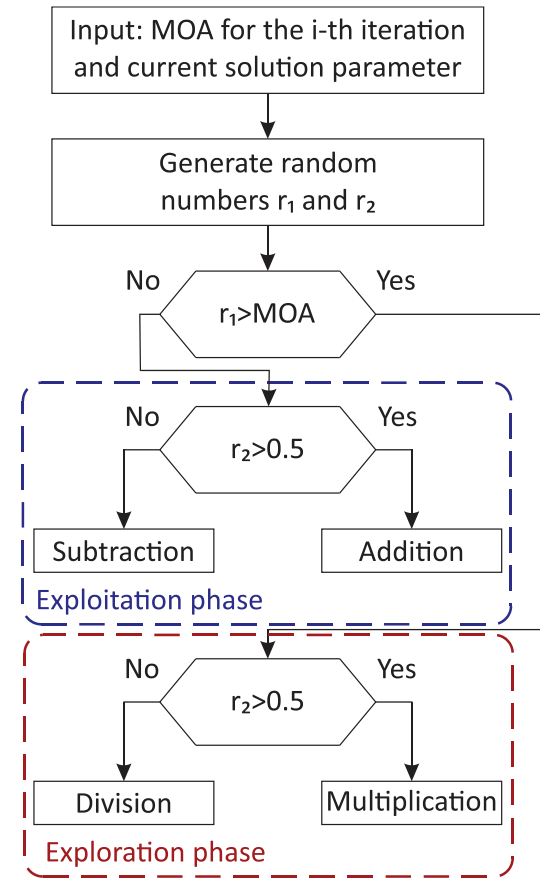


Figure 1. Algorithm for exploration/exploitation selection.

Therefore, the exploration and exploitation phases can occur at any time during optimization. However, it is not desirable that the best solution can change its position in the last few iterations based on stochastic nature. Consequently, the first improvement to the AOA algorithm is the change in the value of M_{max} from 1 to 1.2, enabling only the exploitation to be performed for the last 14% of iterations, and changing the value of M_{min} from 0.2 to -0.2, enabling only exploration in the first 14% of the iterations.

The parameter MOP_i (Eq. 3) is used to define the distance each solution moves from the leader throughout the optimization:

$$MOP_i = 1 - \frac{i^{1/\alpha}}{G^{1/\alpha}}, \quad i = 1, \dots, G, \quad (3)$$

where $\alpha=5$ represents the sensitivity parameter. Finally, each solution parameter in the population is updated according to one of the following Eqs. (4)-(7):

$$x_{k,j}(i+1) = \frac{x_{best_j}}{(MOP_i + \varepsilon)(ub_j - lb_j)\mu + lb_j}, \quad (4)$$

$$x_{k,j}(i+1) = xbest_j \cdot (MOP_i(ub_j - lb_j)\mu + lb_j), \quad (5)$$

$$x_{k,j}(i+1) = xbest_j - (MOP_i(ub_j - lb_j)\mu + lb_j), \quad (6)$$

$$x_{k,j}(i+1) = xbest_j + (MOP_i(ub_j - lb_j)\mu + lb_j), \quad (7)$$

where $xbest$ is a leader or the best individual, and $xbest_j$ is leader's j -th solution parameter, ub and lb represent the upper and lower bound of solution parameter space, ε is a small number, and $\mu=0.499$. Specific mechanisms need to be added in order to employ the AOA algorithm in multi-objective optimization. Firstly, the non-dominance sorting is employed to determine the optimal solutions in a population. Afterwards, these solutions are added to the Pareto front, and all of them are considered leaders. The method for the leader selection in Eqs. (4)-(7) is a random strategy proposed in [9]. Four strings, including process plan, schedule, machine, and tool, represent one individual solution adopted from [10]. The entire algorithm for AOA in integrated process planning and scheduling of machine tools and mobile robot is presented in Table 1.

EXPERIMENTAL RESULTS

Experiments were performed on the dataset containing 20 problems with different number of jobs and operations [10]. All the jobs have process, sequence, machine, and tool flexibility. Two multi-objective fitness functions are selected for evaluation of the proposed algorithm. The first is focused on the mobile robot performance, with robot finishing and waiting time being the criteria for optimization. Meanwhile, the second multi-objective fitness function is designed with total flow time and transportation time. Mathematical formulation for all single-objective fitness functions can be found in [9].

The metric used to differentiate between the convergence properties of the analyzed algorithms is Inverted Generational Distance (IGD) [11]. All three algorithms, Whale optimization algorithm (WOA), AOA, and Particle Swarm Optimization (PSO), have been run ten times on each problem with precisely the same initial populations.

Table 1. Multi-objective AOA algorithm.

1:	Input: μ ; α ; $G=300$; $N=300$ (population size); dataset for manufacturing system
2:	Initialize random initial solutions for the entire population
3:	while $i \leq G$ ($i++$)
4:	Calculate fitness function for each individual
5:	Perform Pareto dominance sorting, leader selection
6:	Calculate value for MOA_i (Eq. 2) and MOP_i (Eq. 3)
7:	for #1 every individual
8:	for #2 every solution parameter
9:	generate random numbers r_1 and r_2
10:	if #3 $r_1 > MOA_i$
11:	if #4 $r_2 > 0.5$
12:	Update parameter according to (Eq. 5)
13:	else #4
14:	Update parameter according to (Eq. 4)
15:	end #4
16:	else #3
17:	if #5 $r_2 > 0.5$
18:	Update parameter according to (Eq. 7)
19:	else #5
20:	Update parameter according to (Eq. 6)
21:	end #5
22:	end #3
23:	end #2
24:	end #1

Table 2. The best and mean achieved results for each problem, IGD metric, fitness function #1.

Pr.	Best			Mean		
	WOA	AOA	PSO	WOA	AOA	PSO
1.	0.175	0.182	0.388	0.403	0.365	0.552
2.	0.228	0.009	0.475	0.514	0.432	0.803
3.	0.175	0.127	0.195	0.215	0.180	0.291
4.	0.401	0.011	0.442	0.560	0.386	0.587
5.	0.035	0.093	0.166	0.191	0.180	0.285
6.	0.221	0.121	0.303	0.386	0.226	0.439
7.	0.500	0.159	0.382	0.571	0.443	0.578
8.	0.356	0.106	0.525	0.589	0.362	0.738
9.	0.008	0.188	0.472	0.499	0.466	0.641
10.	0.218	0.118	0.325	0.478	0.311	0.679
11.	0.155	0.101	0.451	0.358	0.292	0.610
12.	0.221	0.176	0.492	0.423	0.476	0.733
13.	0	0.229	0.419	0.415	0.357	0.610
14.	0	0.385	0.945	0.513	0.686	1.263
15.	0.080	0.219	0.414	0.332	0.347	0.712
16.	0.231	0.064	0.562	0.506	0.424	0.855
17.	0.063	0	0.609	0.571	0.235	0.902
18.	0	0.133	0.326	0.293	0.348	0.546
19.	0	0.295	0.434	0.451	0.531	0.684
20.	0.165	0.134	0.402	0.362	0.253	0.526

The quantitative results for multi-objective fitness function #1 can be seen in Table 2. The AOA algorithm achieves 15/20 mean best results and 12/20 best results on the 20-problem benchmark, making it the best algorithm overall.

Furthermore, to evaluate how many times algorithms achieved the best result compared on each individual run (since the initial populations are the same), for all problems and two fitness functions, the histogram in Figure 2 is shown. With this comparison, the stochastic elements are negated since randomly generated elements can be beneficial to some algorithms.

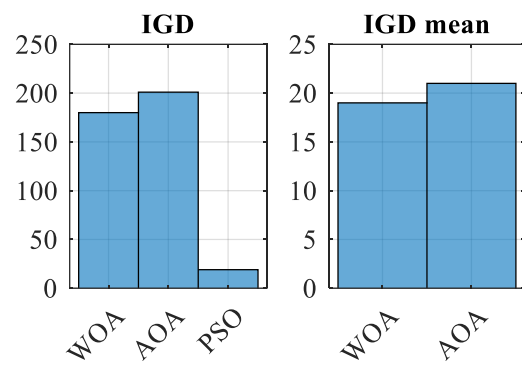
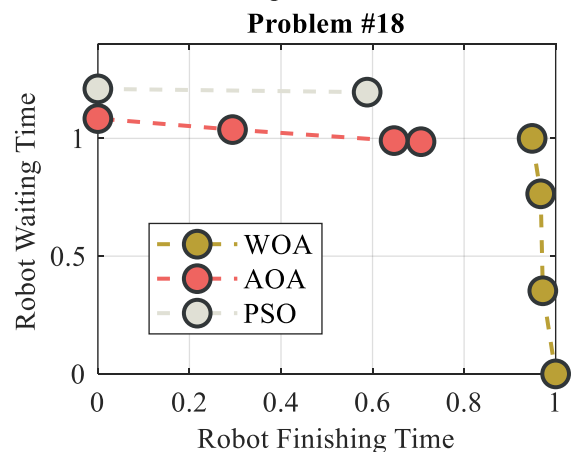
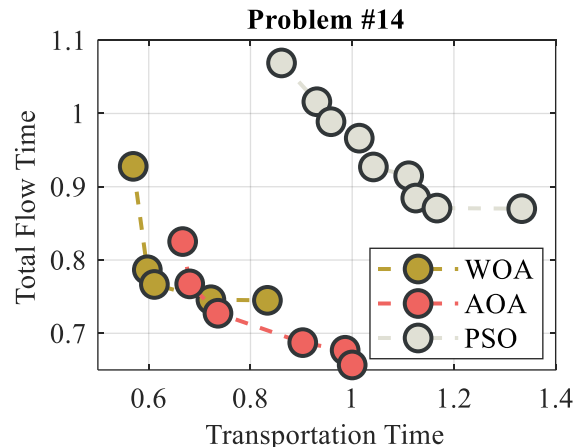
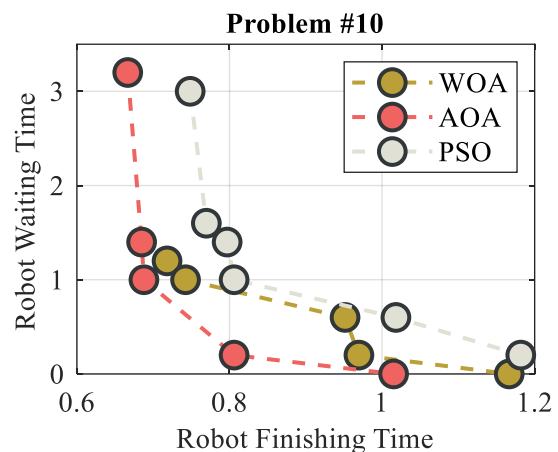


Figure 2. Histogram of results for all runs.



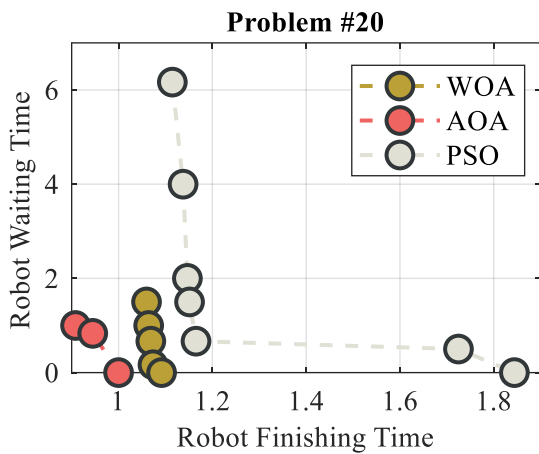


Figure 3. Pareto fronts for selected problems.

As it can be seen from Figure 3, AOA achieves the best Pareto fronts, which shows its advantages even in qualitative evaluation. Moreover, the diagram for problem #18 in Figure 3 shows that AOA focuses significantly on robot finishing time, while WOA optimizes primarily for the robot waiting time fitness function.

CONCLUSION

In this paper, we presented the methodology for multi-objective optimization of the manufacturing schedules with mobile robot utilized for the transportation tasks. The optimal schedule is obtained by employing a metaheuristic Arithmetic Optimization Algorithm (AOA). AOA is compared to two state-of-the-art optimization algorithms on a benchmark with 20 problems and two multi-objective fitness functions. Experimental results show that AOA achieves better results, both in quantitative and qualitative analysis. Future research directions include the further analysis of methodologies capable of improving the AOA algorithm.

ACKNOWLEDGEMENT

This research has been financially supported by the Ministry of Science, Technological Development and Innovation of the Serbian Government, through the project "Integrated research in macro, micro, and nano mechanical engineering – Deep learning of intelligent

manufacturing systems in production engineering" (contract No. 451-03-47/2023-01/200105).

REFERENCES

- [1] L. Abualigah, M. Elaziz, A. Khasawneh, M. Alshinwan, R. Ibrahim, M. Al-Qaness, S. Mirjalili, P. Sumari, A. Gandomi: Meta-heuristic optimization algorithms for solving real-world mechanical engineering design problems: a comprehensive survey, applications, comparative analysis, and results, *Neural Computing and Applications*, vol. 34, pp. 4081–4110, 2022.
- [2] L. Abualigah, A. Diabat, S. Mirjalili, M. Abd Elaziz, A. H. Gandomi: The arithmetic optimization algorithm, *Computer methods in applied mechanics and engineering*, vol. 376, p. 113609, 2021.
- [3] K. G. Dhal, B. Sasmal, A. Das, S. Ray, R. Rai: A comprehensive survey on arithmetic optimization algorithm, *Archives of Computational Methods in Engineering*, vol. 30, no. 5, pp. 3379–3404, 2023.
- [4] A. Kaveh, K. B. Hamedani: Improved arithmetic optimization algorithm and its application to discrete structural optimization, *Structures*, vol. 35, pp. 748–764, 2022.
- [5] G. Hu, J. Zhong, B. Du, G. Wei: An enhanced hybrid arithmetic optimization algorithm for engineering applications, *Computer Methods in Applied Mechanics and Engineering*, vol. 394, p. 114901, 2022.
- [6] M. Premkumar, P. Jangir, B. S. Kumar, R. Sowmya, H. H. Alhelou, L. Abualigah, A. R. Yildiz, S. Mirjalili: A new arithmetic optimization algorithm for solving real-world multiobjective CEC-2021 constrained optimization problems: diversity analysis and validations, *IEEE Access*, vol. 9, pp. 84263–84295, 2021.
- [7] X.-D. Li, J.-S. Wang, W.-K. Hao, M. Zhang, M. Wang: Chaotic arithmetic optimization algorithm, *Applied Intelligence*, vol. 52, no. 14, pp. 16718–16757, 2022.
- [8] R. Zheng, H. Jia, L. Abualigah, Q. Liu, S. Wang: An improved arithmetic optimization algorithm with forced switching mechanism for global optimization problems, *Math. Biosci. Eng.*, vol. 19, no. 1, pp. 473–512, 2022.
- [9] M. Petrović, A. Jokić, Z. Miljković, Z. Kulesza: Multi-objective scheduling of a single mobile robot based on the grey wolf optimization

- algorithm, *Applied Soft Computing*, vol. 131, p. 109784, 2022.
- [10]M. Petrović, Z. Miljković, A. Jokić: A novel methodology for optimal single mobile robot scheduling using whale optimization algorithm, *Applied Soft Computing*, vol. 81, p. 105520, 2019.
- [11]H. Ishibuchi, H. Masuda, Y. Tanigaki, Y. Nojima: Modified distance calculation in generational distance and inverted generational distance, in *Evolutionary Multi-Criterion Optimization. EMO 2015. Lecture Notes in Computer Science*, vol. 9019, A. Gaspar-Cunha, C. Henggeler Antunes, and C. Coello, Eds. Springer, Cham., 2015, pp. 110–125.



Society of Production
Engineering

SPMS 2023

39. Savetovanje proizvodnog mašinstva Srbije

ICPES 2023

39th International Conference on Production Engineering of
Serbia



Faculty of Technical
Sciences
University of Novi Sad

Novi Sad, Serbia, 26. – 27. October 2023

DEVELOPMENT OF THE DELTA ROBOT SIMULATION SYSTEM

Bogdan MOMCILOVIC^{1, *}, Nikola SLAVKOVIC¹

¹University of Belgrade, Faculty of Mechanical Engineering, Belgrade, Serbia

*Corresponding author: bmomcilovic@mas.bg.ac.rs

Abstract: *In the last few decades, alongside the development of serial industrial robots, parallel robots have attracted the attention of many industries and researchers. The DELTA robot is one of the most famous parallel kinematic robots. This paper presents the DELTA robot's complete kinematic modelling and simulation system development. The developed kinematic model includes the solution of the inverse and direct kinematic problem and the determination of the Jacobian matrix. Determining the robot's kinematic parameters in the iterative procedure enabled the analysis of the workspace and singular configurations. The kinematic model and both, the direct and inverse kinematic problems are included in the simulation model to realize the motion of the virtual (wireframe) robot. The virtual robot is developed in a MatLab environment. Using the direct kinematic problem, the positions of all actuated and non-actuated joints are calculated. The simulation system, besides others, includes two developed functions for G-code interpretation and Cartesian space linear interpolation. The developed simulation model can provide information about possible collisions of robot elements. In addition, the calculated joint coordinate vector provides information on whether all movements of the robot's end-effector can be executed according to the joint limits and the given G-code program. Verification of the developed robot simulation system and kinematic model was performed through several examples of the end-effector movement according to the program generated in a CAD/CAM environment.*

Keywords: *industrial robot, DELTA, kinematics, virtual model, simulations*

1. INTRODUCTION

In the last few decades, the development of robots with parallel kinematics has attracted the attention of many industries and researchers. This is because of their higher precision, rigidity, dynamic performance, and loading than the serial robots. To reduce or eliminate the disadvantages of serial kinematics machine tools or robots, parallel kinematic mechanisms are developed and

produced by companies and used in many applications [1].

One of the most famous robots with parallel kinematics is the DELTA robot. The DELTA robot is usually a 3 DoF translational manipulator that consists of a fixed base linked to a mobile platform by three arms. The first model of the DELTA robot was invented in 1987 by Reymond Clavel as a suitable structure for high-speed and high-acceleration tasks. It is used for pick and place operations, packaging, sorting, precision positioning, and

other applications [2, 3]. The parallel mechanism of the DELTA robot was the base of development for many other robots with parallel kinematics.

This paper presents the DELTA robot's simulation system development in the MatLab environment. The main advantages of using simulation systems (virtual environments) of machine tools and robots in programming tasks are (1) the ability to check the movement of the tool along the programmed path, taking into account limitations in joint ranges (joint coordinate) and axis movement speed, (2) visual detection of collisions between segments, as well as tools with workpiece and fixture, and (3) checking whether the workpiece is correctly positioned within the workspace. The existing robot off-line simulation and programming software includes almost all robotic arms with serial and parallel kinematics on the market. Using such software, it could be easy to implement an available robot structure in a simulation environment. To resolve the issues for low-cost robots, i.e., simulation and programming of a new laboratory prototype of robots, many researchers developed a system that integrated kinematics and motion control simulation using the MatLab/Simulink environments [4 - 6].

The simulation system presented in this paper is developed according to the complete robot kinematics model. The direct and inverse kinematic problems are included in the simulation model to realize the motion of the virtual (wireframe) robot. Direct kinematics allows the calculation of the positions of all actuated and non-actuated joints. The simulation system also includes two developed functions for G-code interpretation and Cartesian space linear interpolation. Verification of the developed robot simulation system and kinematic model was performed through several examples of the end-effector movement according to the program generated in a CAD/CAM environment.

2. KINEMATIC MODELING OF DELTA ROBOT

To realize the virtual robot, this Section presents the well-known DELTA robot kinematic modelling based on a minimal number of parameters [7]. The kinematic model of the DELTA robot with rotary actuated joints is shown in Figure 1. Joint parallelograms of the mechanism are represented as a unique rod.

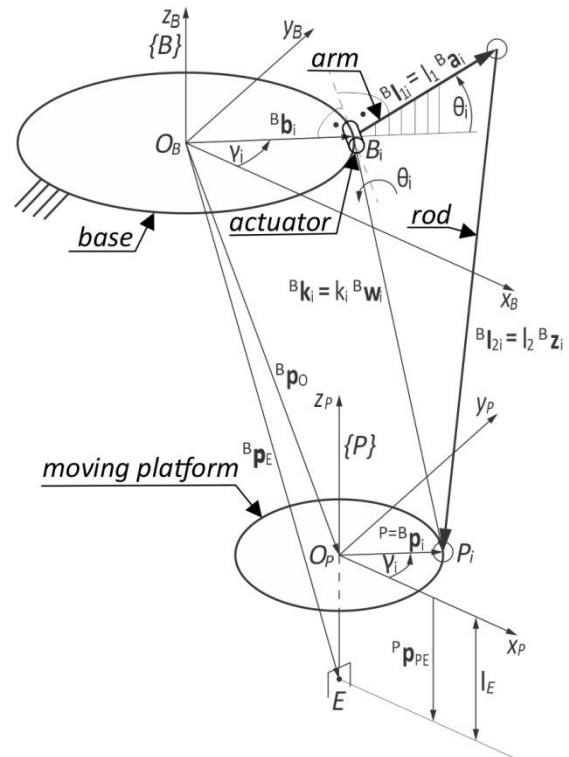


Figure 1. Kinematic model of the DELTA robot

The previously shown kinematic model can be described with the following parameters: radius of the base R , radius of the moving platform r , length of the arm l_1 , length of the rod l_2 , and length of the end-effector l_E .

To derive the DELTA robot's kinematic equations, some vectors are necessary. Position vectors, defined in frame $\{P\}$, of spherical joint centres (midpoints P_i) located on the moving platform on the circle of radius r are:

$${}^P \mathbf{p}_i = [r \cdot \cos \gamma_i \quad r \cdot \sin \gamma_i \quad 0]^T, i=1,2,3 \quad (1)$$

where joints angular positions are defined by $\gamma_i = 2\pi \cdot (i-1)/3$.

Position vector of the end-effector tip defined in coordinate frame $\{P\}$ is:

$${}^P \mathbf{p}_{PE} = [0 \quad 0 \quad -l_E]^T \quad (2)$$

Position vectors of midpoints of rotary actuated joints B_i , defined in coordinate frame $\{B\}$ are:

$${}^B \mathbf{b}_i = [R \cdot c\gamma_i \quad R \cdot s\gamma_i \quad 0]^T, i=1,2,3 \quad (3)$$

World coordinate vector \mathbf{x} that represents only the position of the moving platform in the base frame $\{B\}$ and which will be further considered is:

$$\mathbf{x} = {}^B \mathbf{p}_{OP} = \begin{bmatrix} p_x \\ p_y \\ p_z \end{bmatrix} = \begin{bmatrix} x_E \\ y_E \\ z_E - l_E \end{bmatrix} \quad (4)$$

The joint coordinate vector for the considered 3 DoF DELTA robot model is defined by:

$$\mathbf{q} = [\theta_1 \quad \theta_2 \quad \theta_3]^T \quad (5)$$

Unit vectors ${}^B \mathbf{a}_i$ that define vectors ${}^B \mathbf{l}_{1i}$ as ${}^B \mathbf{l}_{1i} = l_{1i} \cdot {}^B \mathbf{a}_i$ are consisted of joint coordinates and defined by:

$${}^B \mathbf{a}_i = [c\gamma_i \cdot c\theta_i \quad s\gamma_i \cdot c\theta_i \quad s\theta_i]^T, i=1,2,3 \quad (6)$$

Other vectors and parameters are defined as shown in Figure 1.

Based on the relations shown in Figure 1, the following equations can be derived:

$$k_i \cdot {}^B \mathbf{w}_i = {}^B \mathbf{p}_{OP} + {}^B \mathbf{p}_i - {}^B \mathbf{b}_i \quad (7)$$

$$k_i \cdot {}^B \mathbf{w}_i = l_1 \cdot {}^B \mathbf{a}_i + l_2 \cdot {}^B \mathbf{z}_i \quad (8)$$

By taking the square of both sides of equation (8), equation (9) is derived:

$$l_2^2 = k_i^2 - 2 \cdot l_1 \cdot ({}^B \mathbf{a}_i \cdot k_i \cdot {}^B \mathbf{w}_i) + l_1^2 \quad (9)$$

Using equations (1), (3), and (4) vectors $k_i \cdot {}^B \mathbf{w}_i$ can be obtained as:

$$k_i \cdot {}^B \mathbf{w}_i = \begin{bmatrix} k_{wx_i} \\ k_{wy_i} \\ k_{wz_i} \end{bmatrix} = \begin{bmatrix} p_x - a \cdot c\gamma_i \\ p_y - a \cdot s\gamma_i \\ p_z \end{bmatrix} \quad (10)$$

where $a = R - r$. Now, from equation (9) inverse and direct kinematics for the DELTA robot can be solved.

2.1 Inverse and direct kinematics

By substituting expressions (6) and (10) into equation (9) the well-known type of trigonometric equation can be obtained as:

$$c\theta_i \cdot (c\gamma_i \cdot k_{wx_i} + s\gamma_i \cdot k_{wy_i}) + s\theta_i \cdot k_{wz_i} = \frac{l_1^2 - l_2^2 + k_i^2}{2 \cdot l_1}, i=1,2,3 \quad (11)$$

From equation (11) joint coordinates θ_1 , θ_2 , and θ_3 are obtained and inverse kinematics is solved. There are two solutions of inverse kinematics, but one of the solutions has to be chosen because of singularities, Figure 2a.

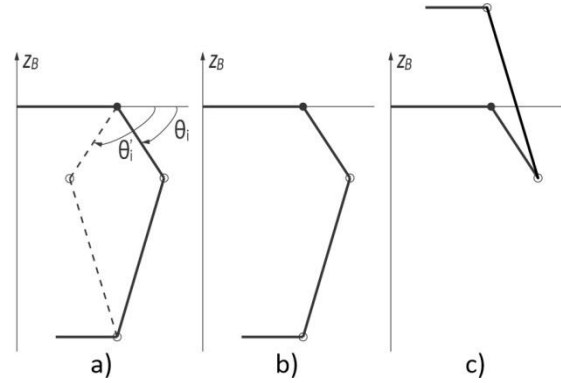


Figure 2. Solutions for inverse and direct kinematics

For direct kinematics, world coordinates p_x , p_y , and p_z can be obtained from equations (11). Substituting the corresponding vectors in equations (11), the system of three equations is derived to solve the direct kinematic problem. Two solutions of direct kinematics are presented in Figures 2b and 2c, but only one is physically possible, Figure 2b.

2.2 Jacobian matrix

The workspace analysis and analysis of the singularities needs the Jacobian matrix. The Jacobian matrix is obtained as a derivative of implicit joint and world coordinate function $f(\mathbf{x}, \mathbf{q}) = 0$ concerning time:

$$J_x \cdot \dot{\mathbf{x}} = J_q \cdot \dot{\mathbf{q}} \quad (12)$$

where $J_x = \frac{\partial(\mathbf{x}, \mathbf{q})}{\partial \mathbf{x}}$ is the Jacobian matrix of

direct kinematics, and $J_q = -\frac{\partial(\mathbf{x}, \mathbf{q})}{\partial \mathbf{q}}$ is the

Jacobian matrix of inverse kinematics. The Jacobian matrix of DELTA mechanism is derived by:

$$J = J_q^{-1} \cdot J_x \quad (13)$$

The Jacobian matrix of parallel mechanisms maps the velocities of joints with the end-effector velocities.

2.3 Workspace analysis

Using the solved direct kinematics equations and joint limits, the workspace of the DELTA robot can be obtained. The position of the rotary actuated joints is divided within the range of limits with defined increments. According to joint incremental value combinations, end-effector positions are calculated using direct kinematics. Figure 3 shows the DELTA robot's obtained workspace by this method.

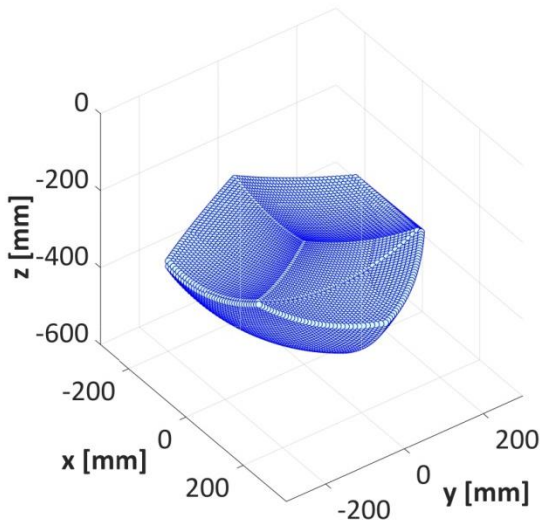


Figure 3. DELTA robot's workspace

Within the obtained workspace, workspaces with regular geometric shapes are selected, Figure 4. This is useful for programmers and operators of the robot.

Using a described method for workspace determination, the robot parameters are

adopted in an iterative procedure according to the desired workspace dimensions.

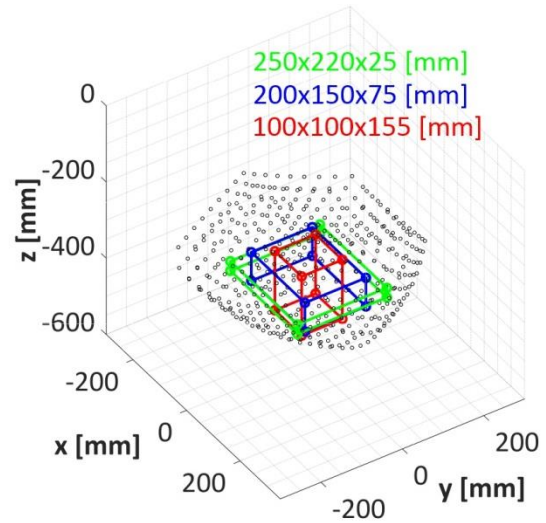


Figure 4. Selected portion of workspace

Adopted parameters of the considered DELTA mechanism are: radius of the base and moving platform $R = 100$ mm and $r = 40$ mm, respectively, arm length $l_1 = 175$ mm, rod (joint parallelogram) length $l_2 = 475$ mm, and length of the end-effector $l_E = 100$ mm.

Also, for the selected portion of the workspace, the distribution of determinants of the Jacobian matrix is calculated, Figure 5.

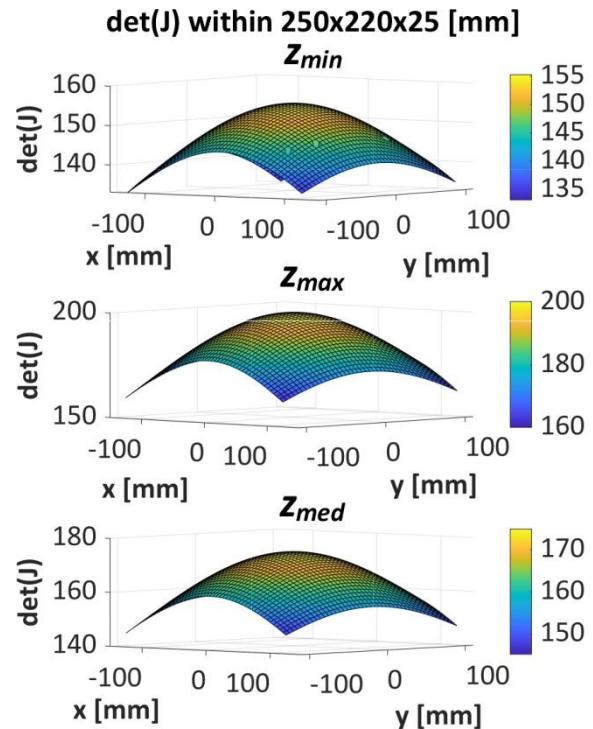


Figure 5. Distribution of determinants of the Jacobian matrix

The selected workspace's x and y coordinates are varied within the limits, while z coordinates have three values (minimum, medium, and maximum). By using that combination of the end-effector's positions, joint coordinates are calculated with the solved inverse kinematics. With known joint and world coordinates, the determinant of the Jacobian matrix can be obtained. Determinants of the Jacobian matrix for one of the selected workspaces are shown in Figure 5. Similar results are obtained for the other portions of the workspaces.

According to Figure 5, the values of the determinants aren't equal to 0 or infinity, and there are no singular positions within the selected workspaces.

3. SIMULATION SYSTEM

The developed DELTA robot simulation system consists of two modules: (1) the module for generating joint space trajectory based on the given G-code, and (2) the configured virtual (wireframe) robot in the MatLab environment, Figure 6.

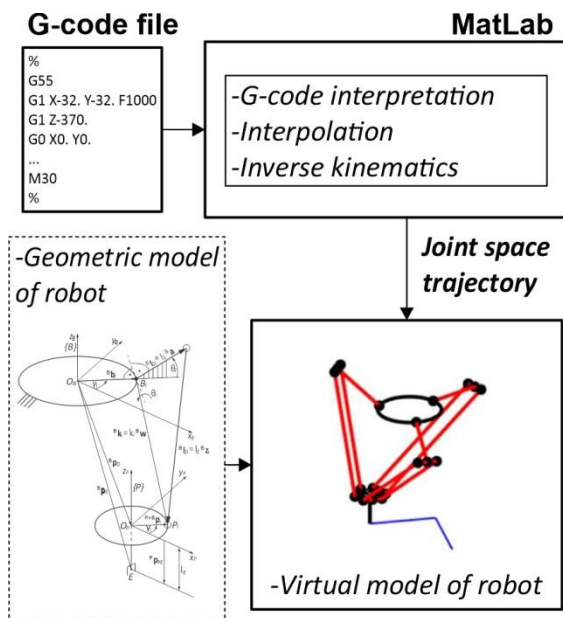


Figure 6. Developed simulation system

The first module consists of developed functions in MatLab for joint space trajectory generation based on the solved inverse kinematics of the DELTA robot. World coordinate vectors for the inverse kinematic

problem are obtained from the G-code program. The second module includes the configured virtual DELTA robot using its geometric model. Based on a joint coordinate vector, parameters of the mechanism, and the solved direct kinematic problem, the positions of all actuated and non-actuated joints can be calculated.

3.1 Joint space trajectory generation module

This module is developed to simulate the various tasks on a virtual robot, such as picking and placing objects or laser engraving. The input for this module is a previously generated G-code program with limitations referring to only linear programmed movements of the end-effector. The module consists of three parts: (1) G-code interpreter, (2) interpolation, and (3) generating joint space trajectory, Figure 7. All of these three parts are realized as functions in the MatLab environment.

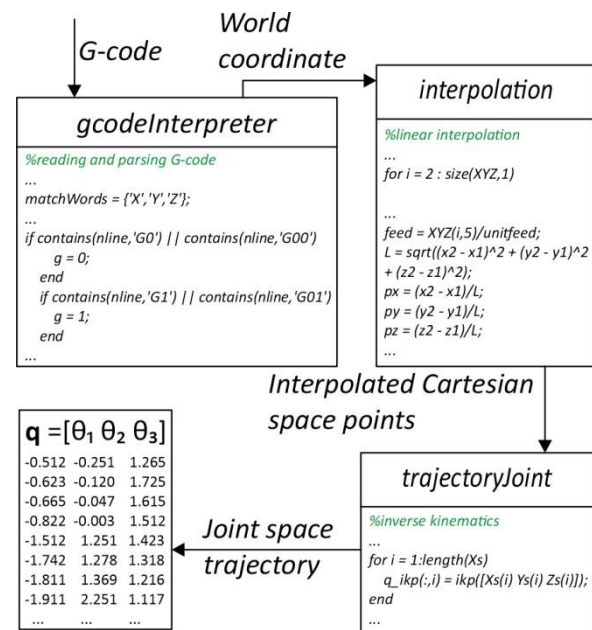


Figure 7. The joint space trajectory generation

The first part of the module reads and parses one by one line of the given G-code program. The output of this part defines the segments of the programmed trajectory and the feed rate of the end-effector on those segments.

Then, the second part divides all trajectory segments using the rule of linear interpolation in Cartesian space. The output is a series of

positions the end-effector must pass to achieve its programmed trajectory. The interpolation rule is programmed according to trajectory segment length and programmed speed.

After obtaining the series of end-effector positions, the third part of the module generates a joint space trajectory using the inverse kinematic solution.

3.2 Configuring the virtual robot

The DELTA robot's geometric model, the mechanism's parameters, and the obtained joint space trajectory are inputs for configuring the virtual DELTA robot, Figure 8. First, the positions of all actuated and non-actuated joints have to be calculated on the robot's desired joint space trajectory. For those calculations besides the joint coordinate vector, the world coordinate vector has to be calculated using the direct kinematic solution.

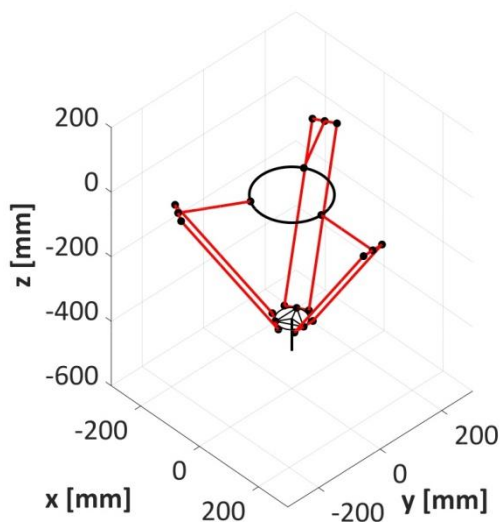


Figure 8. Virtual DELTA robot

Actuated joints on the mechanism's base are located on the circle of radius R , where angular positions are defined by $\gamma_i = 2\pi \cdot (i-1) / 3$. Positions of the spherical joint centres on the mechanism's moving platform are calculated by using the geometric relations and obtained world coordinate vector. Positions of the joint parallelograms' spherical joint centres are calculated using the joint coordinate vector (the connection between arms and parallelograms) and the

world coordinate vector (the connection between parallelograms and the moving platform).

All of the joints are represented as points with the known coordinates. It is possible to connect them, resulting in the configured virtual DELTA robot.

4. SYSTEM VERIFICATION

The developed DELTA robot simulation system has been verified through several examples of performing the technological task of laser engraving contours that are composed of linear parts, Figure 9. Testing programs were previously prepared in a CAD/CAM environment.

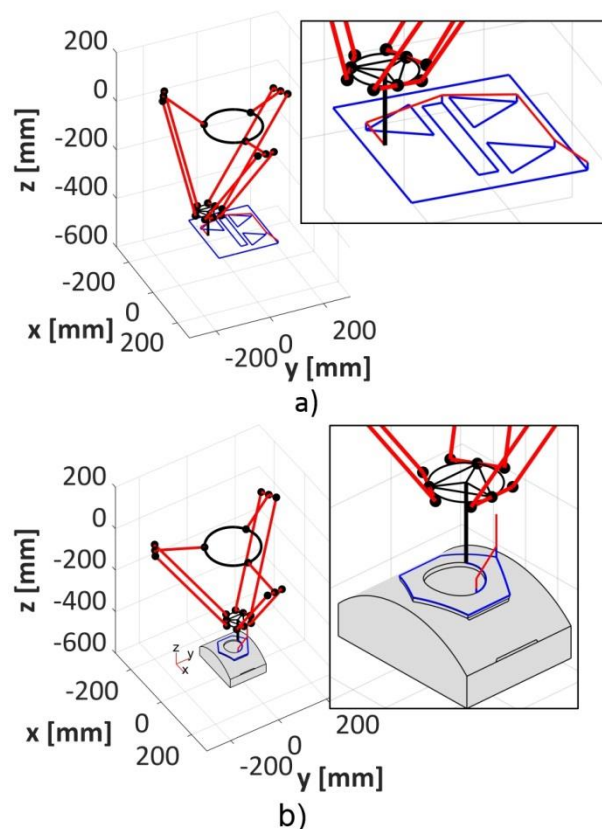


Figure 9. The examples of the system verification

One of the examples, Figure 9a, is the 2-axis laser engraving simple contours. The simulation system draws the trajectory of the end-effector tip (the blue colour is for the feed rate and the red colour is for the rapid move). In the simulation, the end-effector tip passes through all the positions that are obtained by the joint space trajectory generator. During the simulation, it can be visually checked if

some of the robot elements are close to each other or if there's a possibility of collision. After the simulation is done, all the trajectory positions can be checked with the pointer.

The second example is a 3-axis laser engraving complex contour on a calotte, Figure 9b. This example shows the simulation system's possibility to work with 3-axis programs. Also, a CAD model of the workpiece is imported into the simulation. In this case, the end-effector tip has to follow a contour on the imported CAD model.

After completing the graphic view of the simulations, calculations are checked such as values in the actuated joints. Also, the inverse and direct kinematics solutions are checked through the simulation. Based on the obtained results, it can be concluded that the configured virtual robot works correctly according to the generated G-code program.

Such the developed virtual robot can be used for checking the inverse and direct kinematics equations before their implementation in some of the open architecture control systems such as LinuxCNC [8].

5. CONCLUSION

This paper presents an approach for developing the simulation system of a 3-axis DELTA robot in the MatLab environment. The developed simulation system can check programs for various robots' tasks.

The simulation system includes solved inverse and direct kinematics as the real robot does. The system can be used for checking the inverse and direct kinematics equations before their implementation in some of the open architecture control systems. For the adopted mechanisms' parameters, the workspace of the robot is checked with determinants of the Jacobian matrix and proved that there are no singular positions in the selected workspaces. Developed module for the joint space trajectory generation and its parts can be easily reconfigured to work with machines with different kinematics. The developed simulation system has been verified through

several examples of performing the technological task of laser engraving, but it also can be used for 2-axis or 3-axis milling, 3D printing, etc.

The main advantage of using this type of virtual robot, i.e., the presented procedure for configuring such a virtual robot, is to develop a virtual robot for own developed low-cost robots and simulation and programming of a new laboratory prototype of robots with specific kinematics. The further research direction will cover the kinematic modelling of the 5-axis DELTA robot with hybrid kinematics and the development and implementation of the MatLab function for circular interpolation in the simulation system. This will enable the development of a complete methodology in the MatLab environment for the virtual robot laboratory prototype system realization with only changes in kinematics equations.

ACKNOWLEDGEMENT

This work has been financially supported by the Ministry of Education, Science and Technological Development of the Serbian Government through the project Integrated research in macro, micro, and nano mechanical engineering (contract No. 451-03-47/2023-01/200105).

REFERENCES

- [1] M. Ratiu, D. M. Anton: A brief overview of parallel robots and parallel kinematic machines, in: *IOP Conference Series: Materials Science and Engineering*, Vol. 898, No. 1, pp. 012007, IOP Publishing, 2020.
- [2] N. Cretescu, M. Neagoe, R. Saulescu: Dynamic Analysis of a Delta Parallel Robot with Flexible Links and Joint Clearances, *Applied Sciences*, Vol. 13, No. 11, pp. 6693, 2023.
- [3] R. Clavel: Dispositif Pour le Déplacement et le Positionnement d'un Elément dans L'espace, Google Patents WO1987003528A1, 18 June 1987.
- [4] H.M. Alwan, R.A. Sarhan: Kinematics Simulation of Gough-Stewart Parallel Manipulator by Using Simulink Package in MatLab Software, *Journal of University of*

- Babylon for Engineering Sciences, Vol. 27, No, 2, pp. 10-20, 2019.
- [5] M. Li, D. Bi, Z. Xiao: Mechanism simulation and experiment of 3-DOF parallel robot based on MATLAB, in: *Proceedings of the 2015 International Power, Electronics and Materials Engineering Conference*, Atlantis Press, pp. 489-494, 2015.
- [6] N. Slavković, S. Živanović, N. Vorkapić, Z. Dimić: Development of the programming and simulation system of 4-axis robot with hybrid kinematic, *FME Transactions*, Vol. 50, No. 3, pp. 403-411, 2022.
- [7] D. Milutinović, N. Slavković, B. Kokotović, M. Milutinović, S. Živanović, Z. Dimić: Kinematic modeling of reconfigurable parallel robots based on DELTA concept, in: *Proceedings of the 11th International Scientific Conference MMA 2012*, Novi Sad, Serbia, pp. 259-262, 2012.
- [8] N. Slavković, N. Vorkapić, S. Živanović, Z. Dimić, B. Kokotović: Virtual BiSCARA robot integrated with open-architecture control system, in *Proceedings of the 14th International Scientific Conference MMA 2021*, Novi Sad, Serbia, pp. 63-66, 2021.



Society of Production
Engineering

SPMS 2023

39. Savetovanje proizvodnog mašinstva Srbije

ICPES 2023

39th International Conference on Production Engineering of
Serbia



Faculty of Technical
Sciences
University of Novi Sad

Novi Sad, Serbia, 26. – 27. October 2023

GENERATION OF LIGHTWEIGHT MODELS FOR CYBER-ATTACKS DETECTION ALGORITHMS USING KNOWLEDGE DISTILLATION

Dušan NEDELJKOVIĆ^{1,*}, Živana JAKOVLEVIĆ¹

¹University of Belgrade - Faculty of Mechanical Engineering, Belgrade, Serbia

*Corresponding author: dnedeljkovic@mas.bg.ac.rs

Abstract: Industry 4.0 paradigm has brought about the changes in the way we manufacture. The integration of Cyber-Physical Systems into the Industrial Internet of Things represents the basis for the transition from traditionally centralized to distributed control systems where the overall control task is achieved through the cooperation of different devices which implies their mutual communication and constant information exchange. However, ubiquitous communication between devices with communication and computation capabilities opens up space for various cyber-attacks which can lead to catastrophic damage to equipment and also can endanger the environment and human lives. Therefore, the development and implementation of cyber-attacks detection mechanisms are necessary to prevent negative effects. Deep learning (DL) techniques are successfully applied to generate models on which cyber-attacks detection algorithms are based. However, the size of the DL models is often unsuitable for implementation on industrial control devices that usually have significant computational constraints. The use of complex DL models may disrupt the operation of control systems and introduce unacceptable delays in real-time cyber-attacks detection algorithms. This paper explores the possibilities for application of knowledge distillation technique to generate lightweight DL models. These models are designed to align with the limitations of the devices on which they are deployed. The paper evaluates the performance of lightweight models in cyber-attacks detection algorithms, and compares them to algorithms based on DL models before distillation.

Keywords: Cyber-Physical Systems, Industrial Internet of Things, Cybersecurity, Cyber-attacks detection, Machine learning, Knowledge distillation.

1. INTRODUCTION

In the context of Industry 4.0 [1], manufacturing and in particular Industrial Control Systems (ICS) have undergone a significant transformation primarily driven by the integration of Cyber-Physical Systems (CPS) into the Industrial Internet of Things (IIoT). This integration signifies a shift from centralized to distributed control systems, where diverse

devices cooperate through constant communication and information exchange.

The widespread communication between devices equipped with communication and computational modules opens up a broad area for cyber-attacks that could have catastrophic consequences. Cyber-attacks can cause damage to equipment, disrupt manufacturing processes, and even pose significant hazards to the environment and human lives. Hence, it is

essential to create and deploy mechanisms such as Intrusion Detection Systems (IDS) for timely detection of cyber-attacks and prevention of their negative outcomes.

There are two main approaches for cyber-attacks detection: design-driven and data-driven [2]. In continuously controlled systems both approaches model the signal that is communicated between devices and detect the attack as a discrepancy between modelled (estimated) and signal values received through communication link. Design-driven methods rely on predefined rules and mathematically formalized models of processes that usually require stringent assumptions and unacceptable simplifications leading to IDS that are hardly applicable in the real-world, especially for the non-linear continuously controlled systems. On the other hand, data-driven techniques can automatically obtain process models that in most cases provide high accuracy and good generalization properties. The drawback of the latter methods is that a large amount of data from process is required for model generation. Nevertheless, the data-driven approaches represent a technique of choice for designing IDS in continuously controlled processes.

The use of deep learning (DL) techniques has been successful in creating models for cyber-attacks detection algorithms [3]. However, DL models tend to be large, which can be unsuitable for their implementation on industrial control devices with limited computational capabilities. This can cause disruptions to the control system and lead to delays in real-time cyber-attacks detection algorithms.

Several techniques, such as pruning, parameter sharing, and quantization can be employed to adapt DL model size and ensure transfer of knowledge to resource-constrained environments [4]. Regardless of the chosen technique, the objective is to uphold the accuracy while minimizing the computational complexity involved.

For example, pruning is a technique that reduces neural network complexity by removing less important weights (setting them

to zero). The high sparsity level (e.g., 75% in [5]) with negligible accuracy loss and simplicity of application make pruning a widely used technique. On the other hand, parameter sharing considers using the same set of weights and biases for multiple neurons within or across layers of a neural network. Another technique - the weight-sharing algorithm proposed in [6] compresses neural networks by assigning optimized weights from a pre-trained network to a particular cluster in a Gaussian mixture prior. Quantization refers to reducing the precision or representation of numerical values, typically the weights and activations, from a high-precision format to a lower-precision format.

Although presented techniques have been proven useful in many applications, they have some significant limitations. Pruning can introduce additional hyperparameters, such as the pruning ratio (the proportion of weights to prune) or optimal threshold value, which need to be tuned to achieve desired results. Parameter sharing can reduce model size but may not work well for complex network architecture requiring distinct information in different layers. Finally, the implementation of quantization has been observed to substantially impact the accuracy loss in the case of larger neural networks [7].

To overcome these limitations, in this paper we opted to utilize knowledge distillation [8] techniques and to transfer knowledge from a larger, well-trained model (teacher) to a smaller model (student). In particular, this paper investigates the use of knowledge distillation techniques to create lightweight DL models that are customized to fit industrial control devices limitations. We evaluate the performance of models obtained using knowledge distillation in detecting cyber-attacks and compare it to the performance of DL-based IDS algorithms before distillation.

The remainder of the paper is structured as follows. In Section 2 we give a brief overview of the knowledge distillation technique, whereas Section 3 refers to the method used in this paper to develop IDS for ICS. The performance of IDS based on the distilled model and its

comparison with IDS based on the model before distillation is presented in Section 4. Finally, in Section 5 we provide conclusions and future work guidelines.

2. KNOWLEDGE DISTILLATION

As mentioned in Introduction, knowledge distillation techniques [8] transfer knowledge from a larger, well-trained model known as teacher to a smaller model referred to as student. Depending on the knowledge used for student learning, we can identify three basic categories of this technique [9]: 1) response-based, 2) feature-based, and 3) relation-based knowledge distillation. In response-based knowledge distillation, the student primarily tries to imitate the teacher model's final prediction by focusing on the response of its output layer. On the other side, the training of the student model in feature-based knowledge distillation is guided by employing both the final layer's output and the feature maps from intermediate layers. Finally, relation-based knowledge distillation thoroughly examines the connections and relationships between different layers of the teacher network.

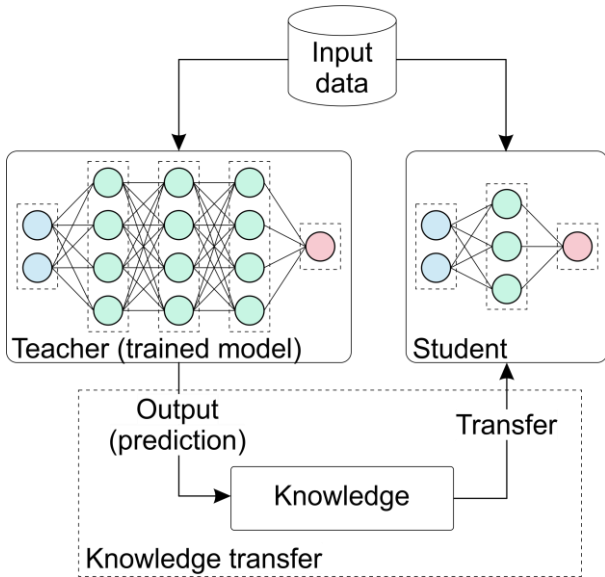


Figure 1. Response-based knowledge distillation

Since in our work the teacher model is previously chosen [10] using only its predictive performance, we opted for the response-based learning category to generate the distilled model. A schematic representation of the

response-based knowledge distillation is shown in Fig. 1.

The process starts with input data fed into a larger, more complex teacher model and a smaller student model. The input data could be time series (1D), images (2D), or any data the models are designed to work with. The teacher model is already created based on the same input data, and a prediction is obtained at its output. On the other hand, the student model for training uses ordered pairs that are composed of input data and corresponding (desired) output data obtained from the teacher. In this way, the student tries to imitate the teacher and achieve the same prediction at output.

3. METHOD FOR THE DEVELOPMENT OF IDS IN ICS

Before developing the student model, it is essential to explain the process involved in creating the teacher model. In our previous research [10], we have developed a methodology for creating IDS in ICS utilizing a CNN-based approach. This method belongs to the class of self-supervised data-driven techniques and involves offline and online phases. During the offline phase, the method generates a CNN-based model of signals transmitted between IIoT devices. This model relies on the auto-regression of transmitted signal, estimating the current output y_i using a buffer of v previously received values x_i , which can be written in the following way:

$$(\mathbf{x}_i, y_i) \in [([x_1, \dots, x_v], x_{v+1}), ([x_2, \dots, x_{v+1}], x_{v+2}), \dots, ([x_{i-v}, \dots, x_{i-1}], x_i), \dots, ([x_{n-v}, \dots, x_{n-1}], x_n)]. \quad (1)$$

With this approach, using the set criteria, it is possible to automatically select the appropriate model that represents the basis of IDS with good attack detection performance. In the offline phase, the hyperparameters of CNN-based model architecture are varied in such a way that they start from the model with the smallest number of parameters to obtain the least complex model that meets predefined criteria.

Offline IDS development involves three steps. The first part represents signal preprocessing and includes normalization by its maximum value, signal filtering (using FIR filters), creating the ordered pairs for training, and data shuffling. The second step implies the creation of unique Machine Learning (ML) model through the variation of hyperparameter values from previously defined sets. In the third step, the model is selected out based on two criteria:

1. Statistical characteristics (mean value and standard deviation) of the discrepancy between the real and estimated values must be similar for the training data and data for model selection.
2. The IDS should be robust to false positives; the robustness is tested on data received during normal conditions (without attacks), and the criterion is met if IDS does not detect any attack on this data.

If the model meets both criteria, it is selected as appropriate and the offline phase stops. IDS based on the selected model is used in the online phase for cyber-attacks detection through comparison of estimated and values received through communication links. An attack is detected if the difference between received and estimated values exceeds the threshold for z consecutive samples.

Since IDSs based on the created models have shown good detection capabilities [10], the question is whether it is feasible to create significantly smaller models that can provide equivalent detection performance.

4. LIGHTWEIGHT MODELS GENERATION USING KNOWLEDGE DISTILLATION

In this paper, we will utilize five different signals from two publicly available datasets to develop the ML models and test their performance. The following datasets are employed: 1) Secure Water Treatment (SWaT) and 2) Electro-pneumatic positioning system (DisEPP).

SWaT testbed [11] represents a fully operational scaled-down water treatment plant capable of producing 5 gallons of purified water per minute. The whole process is divided into 6 sequentially placed stages, each controlled by an independent Programmable Logic Controller (PLC). The data acquisition from 51 devices (25 sensors and 26 actuators) lasted 11 days. For the first 7 days, the system was operated under normal conditions (without attacks), and during the last 4 days, a total of 41 (5 without any physical impact on the system) attacks of various duration and intensity have been launched.

Sensors are divided into four different classes depending on the quantity they measure: flow (FIT), liquid level (LIT), pressure (PIT), and chemical properties (AIT). In this paper we will consider 4 out of 25 sensory signals. Two signals (LIT301 and PIT501) were chosen to include as many attacks as possible that affected their work directly or through adjacent devices. The other signals (FIT101 and AIT401) were chosen based on the most complex ML models obtained in [10] to demonstrate the advantages of the application of the knowledge distillation (possible higher reduction rate between original and distilled model). In addition, each chosen sensor belongs to a unique sensor class and stage.

The DisEPP, on the other hand, was created in the Laboratory for Manufacturing Automation at the University of Belgrade - Faculty of Mechanical Engineering. The main goal of DisEPP is to achieve the desired position of the pneumatic cylinder piston. The system is comprised of a smart actuator (rodless pneumatic cylinder with electro-pneumatic pressure regulator and local controller 1) and a smart sensor (electromagnetic linear encoder with local controller 2). The local controllers represent wireless nodes based on ARM Cortex-M3 that run at 96 MHz [12] augmented with IEEE 802.15.4-compliant wireless transceiver Microchip MRF24J40MA [13]. This dataset [14] was obtained by acquiring communicated data between the local controller 1 and local controller 2. The signal recorded during the piston's movement along a

trajectory of 3 positions was selected for further analysis; the sampling rate was 33.3 Hz. Since the dataset includes only signals recorded during normal behavior (without attacks), a total of 6 different attacks were created to test the performance of IDS in [10]. These attacks will be used to compare the performance of the IDSs based on the teacher and student models.

4.1 Generation of the student model

The generation of the student models is carried out in the same way as in the previously explained procedure, except that in equation (1) where the prediction given by the teacher model \hat{y}_i is used as the output instead of the y_i ; in this way, knowledge is transferred from teacher to the student. The selection of a suitable student model is based on the second criterion (Section 3). This means that the first model that satisfies this criterion is selected as appropriate and used in the online phase for attacks detection.

The preprocessing procedure (normalization, FIR filtering, ordered pairs generation, and shuffling) is applied to input signals. A buffer size of $v=16$ samples was used to predict the current value. The datasets are divided into training, validation, and data for model selection, with a share of 70/10/20%, respectively. The model was trained for 10 epochs using the Adam optimizer with a learning rate 0.001, and the cost function was the mean squared error (MSE).

To make the model development process less time-consuming and reduce the number of unique models, we employed a general architecture that has proven effective [10]. This architecture is comprised of two sequentially placed blocks containing two 1D-CNN layers and a max pooling layer. A flattening layer follows the second max pooling layer, and the network ends with two fully connected layers (Fig. 2). The CNN hyperparameters that will be varied during the development of unique ML models are the number of filters f_i ($i \in \{1, \dots, 4\}$) and filter size fs in 1D-CNN layers, as well as the number of neurons in the first fully connected layer d_1 . The downsampling rate in the max

pooling layers is set to $p=2$, whereas the number of neurons in the output (fully connected) layer is determined by the number of output parameters ($d_2=1$).

The sets of hyperparameter values are defined so that even the most complex student model has fewer parameters than the simplest teacher model (table 1). The filter size was the only hyperparameter whose sets were the same for both models.

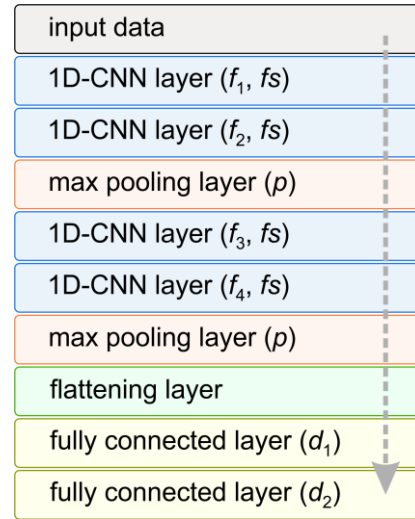


Figure 2. General 1D-CNN architecture

Table 1. Varied 1D-CNN parameters

hyperpar.	teacher	student
f_1	4, 8, 16	2, 4, 8
f_2	8, 16, 32	2, 4, 8
f_3	8, 16, 32	2, 4, 8
f_4	16, 32, 64	2, 4, 8
fs	2, 3, 4	2, 3, 4
d_1	30, 40, 50	5, 10, 20

Table 2 represents the architectures of obtained teacher and student models for considered sensory signals. The complete procedure for generation of teacher models is presented in [10], whereas the student models are created using the procedure from Section 2. The architectures of the created models differ in the number of filters $f_1 \dots f_4$ and the number of neurons in the first fully connected layer d_1 . The filter size for each signal and model is set to $fs=2$ and it is not presented in table 2.

4.2 Comparison of teacher and student models

As can be observed from table 2, the number of parameters in the selected student models ranges from 87 to 603. Comparing student models to the teacher models used for knowledge distillation confirms that the numbers of parameters have been successfully reduced for all sensory signals. A notable instance is observed in the AIT401 sensor signal, where the teacher model originally had 10,209 parameters but was distilled down to 211. The student models have 282.6, whereas the teacher models have 5585.8 parameters in average, which shows that the number of parameters has been reduced over 19 times in average.

Table 2. Teacher and student models architectures

sensor	model	$f_1 \dots f_4$	d_1	param.
FIT101	teacher	4-8-8-64	30	9,049
	student	4-4-4-4	5	211
LIT301	teacher	4-8-8-16	30	2,473
	student	4-4-4-4	10	301
AIT401	teacher	4-8-16-64	30	10,209
	student	4-4-4-4	5	211
PIT501	teacher	4-8-8-16	30	2,473
	student	2-2-2-2	5	87
DisEPP	teacher	8-8-32-16	30	3,725
	student	8-8-8-8	5	603

During the online phase, an attack is detected if the discrepancy between the real and values estimated using generated model exceeds the threshold T for $z=15$ consecutive signal samples. The threshold is defined as a sum of the mean value (μ) and three times the standard deviation (σ) of the discrepancies between real and estimated values of the subset of the data used for model selection:

$$T = \mu_{ms} + 3\sigma_{ms} \quad (2)$$

Using IDs based on student models, all 18 attacks on considered sensors and adjacent devices were successfully detected without false positive results (table 3). Table 3 shows the same results were achieved using IDs based on the teacher models. The obtained results confirm that using the knowledge distillation technique based on existing models we can generate models with significantly fewer parameters that will provide the same detection performance as the original models.

Table 3. Performances of the selected models

model	number of detected attacks on:				
	FIT101	LIT301	AIT401	PIT501	DisEPP
teacher	/	7	/	5	6
student	/	7	/	5	6

Fig. 3 presents the examples of 3 out of 7 detected attacks on LIT301 sensor. Blue and red lines represent received data and obtained prediction, whereas the start and moment of

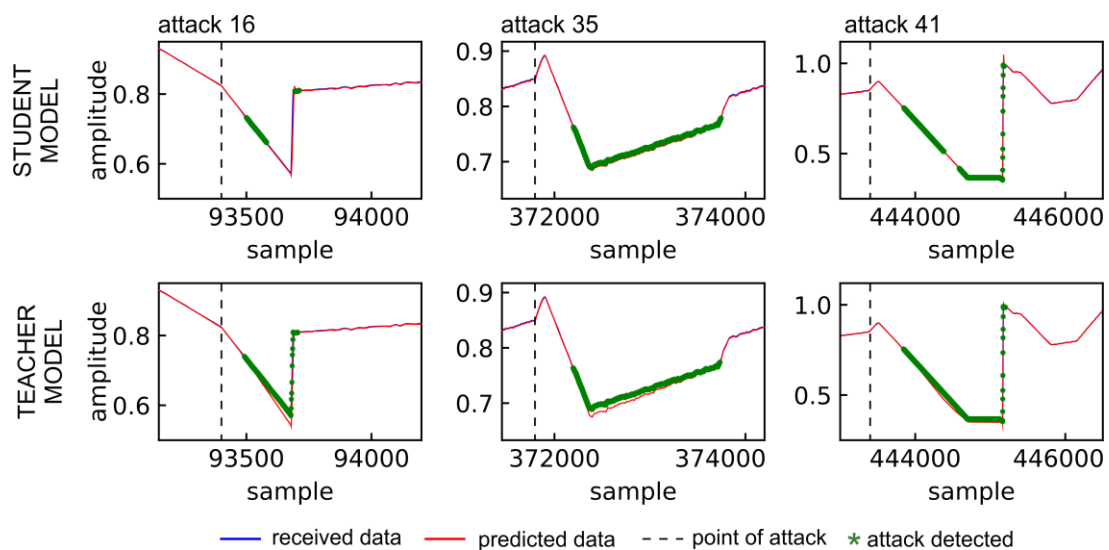


Figure 3. Example of the three detected cyber-attacks on LIT301

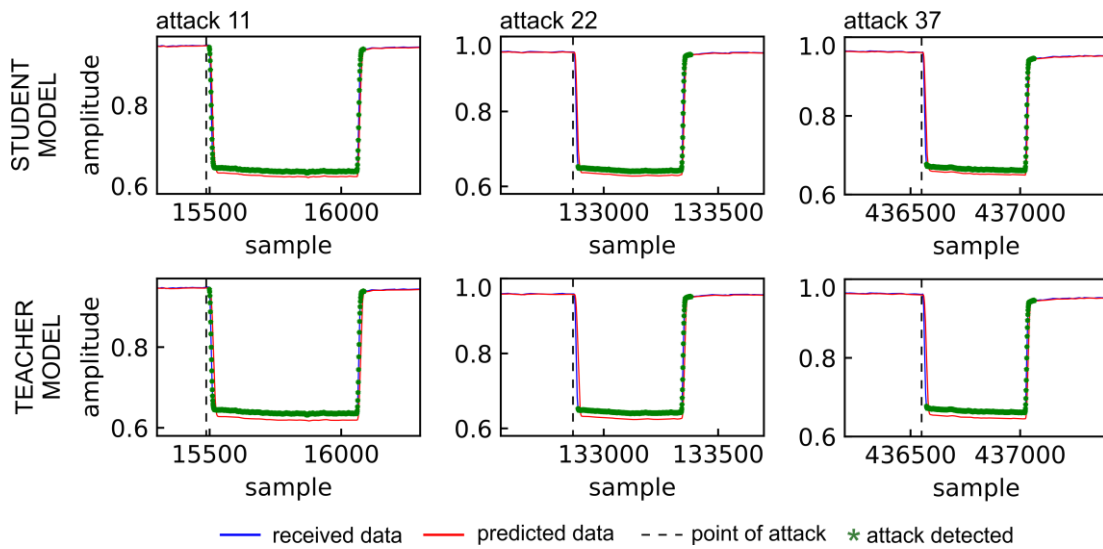


Figure 4. Example of the three detected cyber-attacks on PIT501

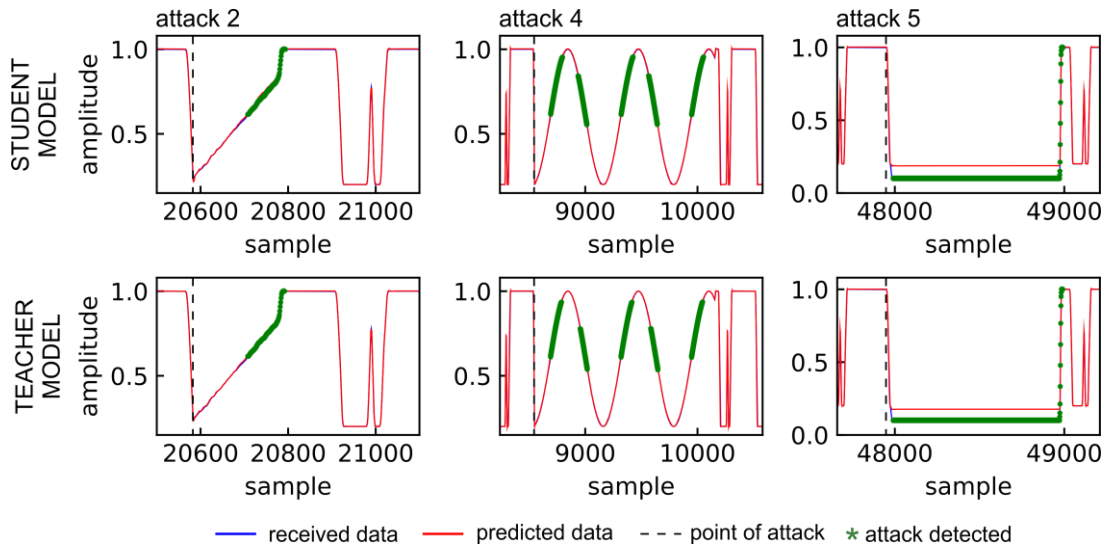


Figure 5. Example of the three detected cyber-attacks on DisEPP

the detection of the attack are marked with a black dashed line and a green marker, respectively. A linear increase/decrease in the signal value characterizes the shown attacks on LIT301.

Examples of detected attacks (3 out of 5) on PIT501 are shown in Fig. 4. The received data, prediction, start of the attack, and the moment of its detection are represented in the same way as in Fig. 3. Attacks (11, 22, and 37) on PIT501 have similar dynamics characterized by oscillating around the set signal value. For the signal from DisEPP, 3 out of 6 detected attacks are shown in Fig. 5. In addition, the same format of lines and markers was used to represent received data, prediction, and the moments of start and detection of attacks. The shown attacks on DisEPP have different

dynamics defined by a linear increase (attack 2), changing the signal value as a harmonic function (attack 4) or setting the signal value to a constant for a certain period (attack 5).

In addition to the capability of IDSs based on the student models to detect all attacks, it can be noted that the moments of detection are almost the same as in the case of IDSs based on teacher models.

5. CONCLUSION

This paper explored the utilization of knowledge distillation to generate lightweight models for cyber-attack detection in ICS. The development of lightweight models was based on the proven 1D-CNN models obtained in previous research. Appropriate models were

chosen based on specific criteria, resulting in a significant reduction in the number of parameters (e.g., from 10,209 to 211 parameters for the AIT401 signal), which can be a crucial factor for the timely detection of cyber-attacks in real-time tasks. The performance of cyber-attacks detection algorithms based on the generated models was tested on five signals from two publicly available datasets. Using algorithms based on the student models, all 18 attacks were detected with no false positives, which was also the case with teacher models (models before distillation). In this way, it is shown that models with a very small number of parameters (e.g., 87 parameters in the case of PIT501 signal) can be used as successfully as models with a few thousand parameters.

In future work, we will implement the IDS based on the distilled model on the local controller within DisEPP to test its performance in real-world conditions. Further research will also include the application of the knowledge distillation technique to models for cyber-attacks detection algorithms on sequences of two-dimensional signals.

ACKNOWLEDGEMENT

This research was supported by the Ministry of Science, Technological Development and Innovations of the Serbian Government under the contract No. 451-03-47/2023-01/200105.

REFERENCES

[1] H. Kagermann, J. Helbig, A. Hellinger, W. Wahlster: Recommendations for Implementing the Strategic Initiative INDUSTRIE 4.0, Forschungsunion, 2013.

[2] H. S. Sánchez, D. Rotondo, T. Escobet, V. Puig, J. Quevedo: Bibliographical review on cyber attacks from a control oriented perspective, *Annual Reviews in Control*, Vol. 48, pp. 103-128, 2019.

[3] M. Macas, C. Wu, W. Fuertes: A survey on deep learning for cybersecurity: Progress, challenges, and opportunities, *Computer Networks*, Vol. 212, art. 109032, 2022.

[4] M. M. H. Shuvo, S. K. Islam, J. Cheng, B. I. Morshed: Efficient acceleration of deep

learning inference on resource-constrained edge devices: A review, *Proceedings of the IEEE*, 2022.

[5] M. Zhu, T. Zhang, Z. Gu, Y. Xie: Sparse tensor core: Algorithm and hardware co-design for vector-wise sparse neural networks on modern gpus, in: *Proceedings of the 52nd Annual IEEE/ACM International Symposium on Microarchitecture*, 12-16.10.2019, Columbus, USA, pp. 359-371.

[6] K. Ullrich, E. Meeds, M. Welling: Soft weight-sharing for neural network compression. arXiv preprint arXiv:1702.04008, 2017.

[7] Y. Cheng, D. Wang, P. Zhou, T. Zhang: Model compression and acceleration for deep neural networks: The principles, progress, and challenges, *IEEE Signal Processing Magazine*, Vol. 35, No. 1, pp. 126-136, 2018.

[8] G. Hinton, O. Vinyals, J. Dean: Distilling the knowledge in a neural network, arXiv preprint arXiv:1503.02531, 2015.

[9] J. Gou, B. Yu, S. J. Maybank, D. Tao: Knowledge distillation: A survey, *International Journal of Computer Vision*, Vol. 129, pp. 1789-1819, 2021.

[10] D. Nedeljkovic, Z. Jakovljevic: CNN based method for the development of cyber-attacks detection algorithms in industrial control systems, *Computers & Security*, Vol. 114, art. 102585, 2022.

[11] J. Goh, S. Adepu, K. N. Junejo, A. Mathur: A dataset to support research in the design of secure water treatment systems, in: *Critical Information Infrastructures Security: 11th International Conference*, 10-12.10.2016, Paris, France, pp. 88-99.

[12] NXP Semiconductors N.V., LPC1769/68/66/65/64/63 32-bit ARM Cortex-M3 microcontroller, available at: https://www.nxp.com/docs/en/data-sheet/LPC1769_68_67_66_65_64_63.pdf, accessed: 02.10.2023.

[13] Microchip Technology Inc., MRF24J40MA 2.4 GHz IEEE Std. 802.15.4TM RF Transceiver Module, available at: <http://ww1.microchip.com/downloads/en/DviceDoc/70329b.pdf>, accessed: 02.10.2023.

[14] D. Nedeljkovic, Z. Jakovljevic: New datasets obtained from experimental installations with centralized control – v2.0, 2021, available at: <https://zenodo.org/record/5514351>, accessed: 02.10.2023.



Society of Production
Engineering

SPMS 2023

39. Savetovanje proizvodnog mašinstva Srbije

ICPES 2023

39th International Conference on Production Engineering of
Serbia



Faculty of Technical
Sciences
University of Novi Sad

Novi Sad, Serbia, 26. – 27. October 2023

IMPLEMENTATION OF INDUSTRY 4.0 IN THE METAL INDUSTRY TO ACHIEVE SMART PRODUCTION PROCESSES

Isak KARABEGOVIĆ^{1,*}, Mehmed MAHMIĆ², Edina KARABEGOVIĆ², Ermin HUSAK²

¹Academy of Sciences and Arts of Bosnia and Herzegovina, Sarajevo,

²University of Bihać, Technical faculty Bihać, Bihać

*Corresponding author: isak1910@hotmail.com

Abstract: *The automation of production processes begins with the implementation of the first industrial robot patent (patent approved on June 13, 1961) in the General Motors company, which continues to this day. Research and development in the world is going very fast so that today we are in the fourth industrial revolution, where companies are widely implementing Industry 4.0. Methods of production in the world is changing, so the production processes are focused on the implementation of the basic technologies of Industry 4.0 such as: Robotics, Automation, Internet of Things (IoT), Big Data, computing in the "cloud" (Cloud Computing), 3D Printing, Smart Sensors, Radio Frequency Identification (RFID), Virtual and Augmented Reality (AR), Artificial Intelligence (AI), Advanced Security Systems, etc. The metal industry, together with the electrical industry, are the first industries to experience the transformation and implementation of Industry 4.0, and the reason is that they are the base industry in the production of vehicles in the world. Increasing automation is occurring through the introduction of industrial and service robots in all industrial branches, and the metal industry is aiming for complete automation by introducing both first and second generation industrial robots, as well as service robots for logistics in the production process itself. The paper presents the trend of the implementation of industrial and service robots in the metal industry, as well as the prediction of implementation in the future. The paper provides an economic analysis of why there are completely smart production processes in the metal industry.*

Keywords: *Industry 4.0, Automation, Smart Processes, Metal Industry, Robotics, Advanced Technologies.*

1. INTRODUCTION

We are witnessing major changes taking place on the world industrial and digital scene. The WEF – World Economic Forum (held in Davos in 2016) called them the fourth industrial revolution, whereas the Germans named these changes "Industry 4.0" for the first time at the Hanover fair in 2011 [1,2,3]. All companies in the world face global competition, and in order to keep up with the competition and meet the increasing demands on the market, it is

necessary to use new technologies in production processes, i.e., implement Industry 4.0. The concept of Industry 4.0 is defined by many technologies (over 40 technologies), some of which are: robotics, automation, Internet of Things (IoT), Big Data, Cloud Computing, 3D printing, smart sensors, radio frequency identification (RFID), virtual and augmented reality (AR), Artificial Intelligence (AI), advanced security systems, Cyber-Physical Systems (CPS), etc., as shown in Figure 1 [1-3].

Cyber-Physical Systems (CPS), Internet of Things (IoT), Artificial Intelligence (AI), Additive Manufacturing, Cloud Computing, and other aforementioned technologies combine to construct dynamic, real-time optimized and self-organizing networks values between production processes and companies. All listed components are necessary for the implementation of Industry 4.0. Through its implementation, we can make a connected company that enables production processes to discover new ways of increasing productivity and improving overall business performance. Industry 4.0 helps to increase productivity as well as improve the overall business performance of the company. In order to ensure this, it is necessary to have a secure connection between different production systems and processes throughout the company. The new way of managing production processes aims to improve performance and better use of data that already exists, by using a combination of tools that can be applied to improve the system or production process [4, 5, 7]. Vehicle manufacturing companies are the first to implement Industry 4.0 in order to be competitive on the world global market. The reason lies in the fact that the role of workers in the production process, who in today's conditions of production processes are an important factor in the process, is changing in all industrial branches, including and the metal industry. The tasks performed by workers in difficult, physically and psychologically tiring and dangerous routine operations, which damaged health and safety on a daily basis, are transferred into other forms of easier intellectual work, which requires individuals to be educated in trends that are now focused on designing, monitoring and controlling manufacturing processes. The development of robotic technology and other new technologies has led to the second-generation industrial robots. Compared to first-generation robots, collaborative robots have a number of advantages. Robotic technology is one of the most important technologies in "Industry 4.0", so the application of robots in the automation

of production processes, with the support of information technology, is leading towards "smart automation", i.e., "smart production processes". Among the first processes are the ones in the metal industry. The reason for the rapid transformation is the global market. The implementation of robotic technology in the metal industry brings a number of advantages, some of which are:

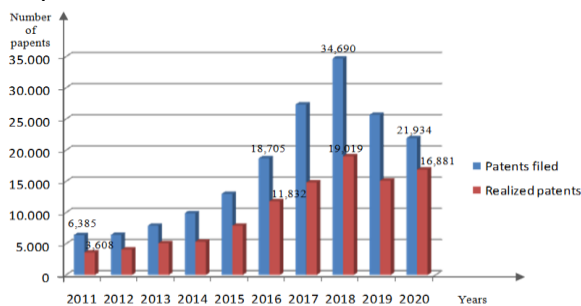
- increased productivity of the production process,
- increased flexibility of the production process,
- increased accuracy in the production process, thus providing better product quality,
- increased work safety in inadequate working conditions,
- reduced production and maintenance costs,
- reduced participation of workers in the production process,
- reduced workforce in the conditions of performing difficult and repetitive tasks,

This represents only a small part of the advantages, which are very significant in conditions of production of larger capacities, as evident in the metalworking industry.

2. TREND OF INNOVATION AND PATENTS IN ROBOTIC TECHNOLOGY AS A BASE TECHNOLOGY OF INDUSTRY 4.0

It is well-known that the automation of any production process requires the implementation of robots, whose automation dates back to the early 1960s. We can say that robot technology is one of the most represented basic technology of Industry 4.0. Since the implementation of the first industrial robot, scientists have been working on their development, improvement and research, as well as their implementation in any human environment. From the very beginning, automation has been expanding and increasing in all production processes in the world, because the increase in automation can be realized by investing in research and

development which brings benefits to both companies and society as a whole. All countries in the world invest in research and development in robotic technology. Most advanced countries invest in the development of the automotive and electro-electronic industries, because automation is most represented in these industrial branches and have the highest number of implemented robots. Investment in research and development in robotic technology is reflected in the trend of registered and realized patents in robotic technology in the world for the period 2011-2020, as shown in Figure 1 [6-8]. Based on Figure 1, we can conclude that the trend of registered patents in robotic technology for the period 2011-2018 has a positive growth that takes place almost according to an exponential function., which is the period of implementation of Industry 4.0 in all developed countries, including the robotics as the first base Industry 4.0 technology. The number of realized patents in robotic technology is somewhat lower, as shown in Figure 1. We can see that in 2018, 34.690 patents were applied for, while the realization is slightly lower and amounted to 19.019 patents. This is the year with the maximum number of registered and realized patents for this period.

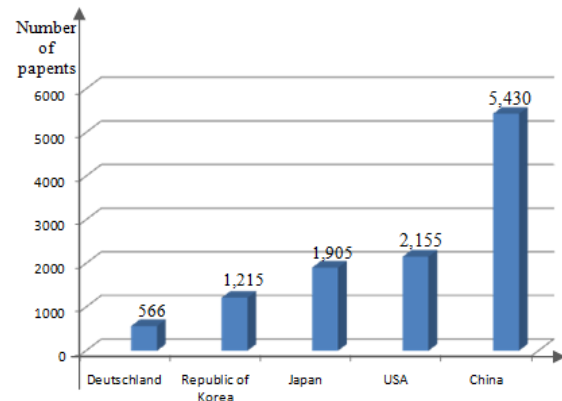


Source: GlobalData Patent Analytics

Figure 1. Trend of registered and realized patents from robotics as the base technology of Industry 4.0 for the period 2011-2020

Due to the outbreak of the Covid-19 pandemic in the world in the period 2019-2020, the number of registered and realized patents is lower compared to 2018, so that in 2020 there were 21.934 registered patents and 16.881 realized patents in robotics. Given that the Covid-19 virus pandemic has ended, we expect

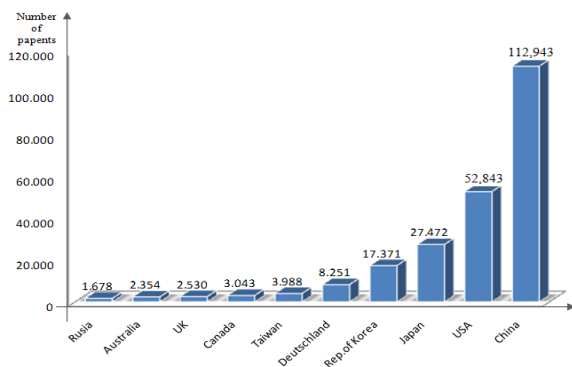
that the trend of growth in the number of applications and realized patents will grow on annual basis. An analysis of approved patents in robotics as the base technology of Industry 4.0 in 2019 in five technologically developed countries: Germany, Japan, the Republic of Korea, China and the USA was prepared and shown in Figure 2 [7-9].



Source: 1790 Analytics robotics patent dataset.

Figure 2. Trend of approved robotics patents for 2019 in the countries: Germany, Republic of Korea, Japan, USA and China

The most developed companies in the analyzed countries belong to the automotive and electrical/electronic industry, in which the implementation of robotic technology is the most represented [14, 15]. Companies invest in research and development of this technology, which can be seen in the number of patents. The analysis of the diagram of international patent families (IPFs) from robotics technology as the base technology of Industry 4.0 in five developed countries depicted in Figure 2, shows that China holds the first place with 5.430 approved patents, while the USA is in second place with 2.155 approved patents in robotics. Comparing the USA and China, we can see that China has more than twice as many robotics patents compared to the USA in 2019. In order to get a true picture of the development and research of robotics technology, an analysis of the registered patents from robotics as the base technology of Industry 4.0 for the period 2011-2020 was created and shown in Figure 3 [6, 7, 9].



Source: GlobalData Patent Analytics

Figure 3. Trend of registered patents in the top ten countries in the world in robotics as the base technology of Industry 4.0 for the period 2011-2020

The analysis of Figures 2 and 3 provided us with the conclusion that in the period 2011-2020, China and the USA were the leading countries in terms of the number of registered and implemented patents from robotic technology as the base technology of Industry 4.0. China holds the first place, followed by the USA with twice less registered and approved patents in robotics technology. In our opinion, there are three most important reasons why China holds the first place in terms of the number of registered and approved patents in robotics technology, although there are more [16-18]:

- The first reason is that the Chinese government adopted the “Made in China 2025” strategy, which aims to position China as the technologically most advanced country in the world by 2025. They have already divided the strategy into three periods: the second period is until 2039 and the third period until the 2049.
- The second reason is that China is in first place in the production of vehicles in the world, i.e., about 30% of the world’s production, and is among the first in the production of electronic devices. These two industries are known for implementing the highest number of robots.
- The third reason is that in China, the price of workers’ labor has been increasing in recent years, from 5 euros/hour to 15 euros/hour, and the

price of robot labor per hour is decreasing, so that it amounts to about 10 euros/hour. In the European Union, the price of a worker is around 30 euros/hour.

These are technologically developed countries that invest in development and research into the basic technologies of Industry 4.0, the main one being the robotic technology. Both China and the USA have their own Strategy for the implementation of Industry 4.0 in order for their companies to be competitive on the global market. In order to have a complete picture of the implementation of the basic robotic technology of Industry 4.0, we will analyze the implementation of industrial and service robots in the world in the last ten years. The discovery of a large number of innovations from digital technologies and their implementation in production processes through the use of computer hardware, software and networks are becoming increasingly sophisticated and intelligent, which results in its transformation in all segments of society, which echoes the global economy in the world [8, 21-23].

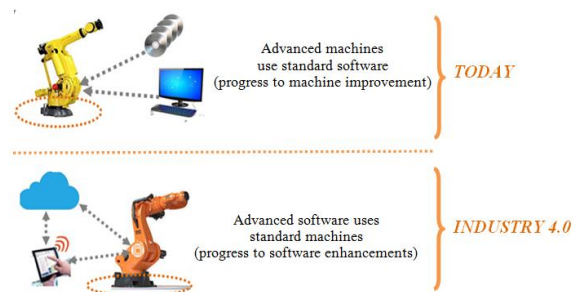


Figure 4. The advantages of Industry 4.0 in the automation of production processes in the metalworking industry

Industry 4.0, like every industrial revolution, creates an increase in knowledge in the world through the implementation of innovations from all of the aforementioned new technologies and the use of advanced software, as shown in Figure 4.

All production processes nowadays, including the metalworking industry, use advanced machines with standard software, while the fourth industrial revolution uses advanced software for typical machines, as shown in

Figure 4. In the fourth industrial revolution, the fundamental technologies of Industry 4.0 are based on innovations that are much faster and more widely implemented in the production processes of the automotive industry. The reason for such trend is the influence of the global market. In order for the companies to survive on the market, they must constantly modernize and innovate their production processes, i.e., implement Industry 4.0, which especially refers to the metal industry as the basis of the automotive industry [10-13]. Similar to the automotive industry, the metal industry is moving from a linear production process to a network production process, as shown in Figure 5, where the machine communicates with the machine - M2M. The machines are serviced by collaborative robots, and the transport itself is resolved with service robots for logistics, because completely smart local transport solutions have already been implemented with mobile robots for logistics.

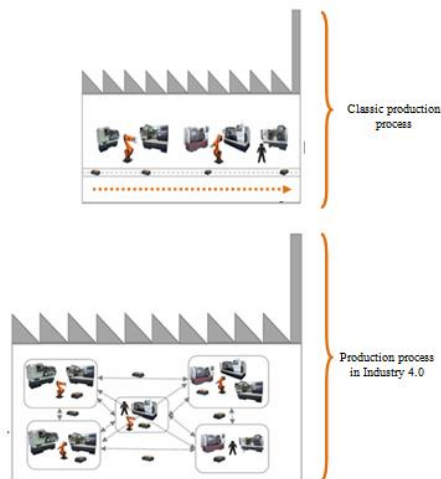


Figure 5. Line production process is transformed into network production process of Industry 4.0

Industrial robots of the second generation and service robots for logistics are implemented in the production processes of the metal industry within the fourth industrial revolution, i.e., Industry 4.0. The line production process is transferred to a network production process, because the machines communicate with each other, and communication is provided by the basic technology of Industry 4.0. The production processes in the metal industry have many advantages, such as [21-23]:

- when complete automation is complex, we are able to partially automate the execution of tasks, i.e., we have the possibility of different levels of automation,
- we turn rigid automation into flexible automation,
- it is characterized by simple and easy-to-handle tasks,
- when dividing the execution of operations between workers and robots, we have improved performance,
- the role of industrial and service robots in Industry 4.0 is of great importance, because it connects the factory of real life with virtual reality, which opens greater perspectives of application in global production,
- we can significantly improve non-ergonomic workstations using collaborative robots, where we must remember that worker safety is an absolute prerequisite,
- reducing the product life cycle and increasing the variety of products, require flexible automation, which will result in an increase in the use of collaborative robots, etc.

The above analysis provides us with the conclusion that the concept of production processes in all industrial branches, including the metal industry, aims the following: to implement second-generation industrial robots, i.e., collaborative robots, as well as service robots for logistics; to move line production process to the network production process; to ensure machine-to-machine communication; to implement a large number of smart sensors; to monitor the production process and make decisions online; to enable permanent maintenance; to quickly change serial production, etc. The production process in the metalworking industry is moving in the direction of a smart production process with the implementation of Industry 4.0 [24-26]. The first-generation industrial robots play the role of automation tools for learning the existing

knowledge. Implementation of innovations in robotic technology and basic technologies of Industry 4.0, such as sensors, microcontrollers, microprocessors and other equipment on which artificial intelligence technology is upgraded such as machine learning, computer vision in cloud computing, industrial robots, is being transformed in the direction of intelligent tools, and even innovative tools [14,26,27]. In the recent years, industrial robots are gradually showing the characteristics of intelligent tools, such as second-generation industrial robots, i.e., collaborative robots. The impact of collaborative robots is reflected in increased productivity and replaced programmed work, but also filling the labor shortage gap and creating new jobs.

3. IMPLEMENTATION OF ROBOTS IN PRODUCTION PROCESSES WITH SPECIAL OVERVIEW OF METAL INDUSTRY

In order to obtain a real representation of the implementation of industrial robots, it is necessary to make an analysis of the implementation of industrial robots in the world in the last ten years and the expected predictions of the implementation in the coming period. The analysis was made on the basis of statistical data on the implementation of industrial and service robots obtained from the International Federation of Robotics (IFR), the UN Economic Commission for Europe (UNECE) and the Organization for Economic Cooperation and Development (OECD). The trend of the implementation of industrial robots on an annual basis in the world is shown in Figure 6 [28-30].

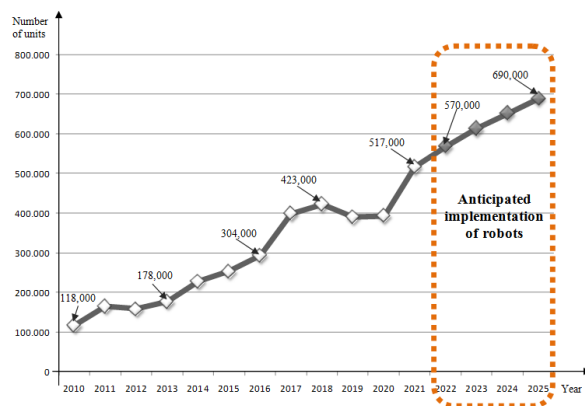


Figure 6. The trend of the implementation of industrial robots in the world on an annual basis in the period 2010-2021 and the estimation of implementation until 2025

Based on the trend of the use of industrial robots in the period 2010-2021, shown in Figure 8, we can conclude that the use of industrial robots is increasing every year, going from 118.000 units used in 2010 and increasing until 2018. In 2019 and 2020, there was a decline in the use of industrial robots due to the Covid-19 virus pandemic. Therefore, slightly fewer industrial robots were used compared to the previous year: 391.000 robot units were applied in 2019, and 394.000 units of robots were applied in 2020. After the end of the pandemic, there was an increase in the trend of the implementation of industrial robots, and in 2021, 517.000 robot units were applied. Based on the diagram shown in Figure 6, we see that in the period 2022-2025, an increase in the implementation of industrial robots is predicted every year. It is estimated that in 2025, about 690.000 industrial robot units will be implemented. The implementation of industrial and service robots in the production processes of the metal industry aims to increase productivity, reduce costs and achieve better product quality. With their implementation, we will achieve exactly what Industry 4.0 advocates: a greater degree of automation with satisfactory flexibility and greater production with economic justification, whether it is about existing production processes or the introduction of new production processes. The metalworking industry covers all production and service processes, from the production of parts to

assembly into semi-finished or finished products. Industrial and service robots in the metalworking industry are used in many tasks in the production process, from the transportation of materials before and after processing, process operations, assembly processes of subsets/sets/finished products, control processes (interoperation control and control of final products), etc. The application of the basic technology of Industry 4.0, especially second-generation industrial robots, as well as service robots for logistics, in the production processes of the metal industry leads to greater flexibility and efficiency in production processes. The analysis of the implementation of industrial robots in the metalworking industry was carried out on the basis of statistical data on the implementation of industrial and service robots obtained from the International Federation of Robotics (IFR), the UN Economic Commission for Europe (UNECE) and the Organization for Economic Cooperation and Development (OECD), as shown in Figure 7 [28-30].

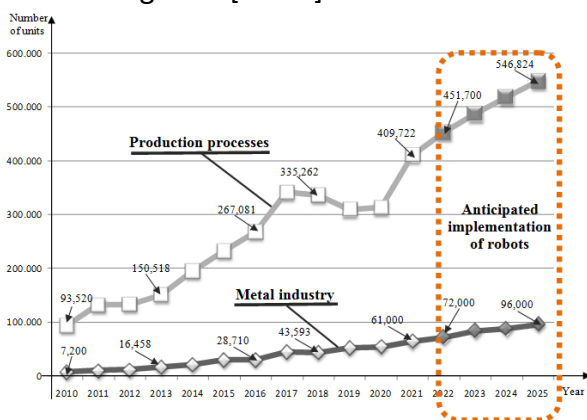


Figure 7. Trend of the annual implementation of industrial robots in the production processes of all industrial branches and the metal industry in the world in the period 2010-2021 and estimates of implementation until 2025.

The trend of implementation of industrial robots in the production processes of all industrial branches in the world has a growing trend on an annual basis, so that in 2010, 93.520 robot units were implemented, in 2016 the implementation increased to 267.081 robot units, and in 2021 the implementation amounted to 409.722,300 robot units. The trend of implementation of industrial robots in

production processes in the world is predicted to grow in the coming years, so that in 2025, around 546.000 robot units will be implemented. This trend in the implementation of industrial robots is expected due to the fact that companies are introducing Industry 4.0 into their production processes, which is not possible without the introduction of industrial robots. The largest number of robots is implemented in the production processes of the automotive industry, and the largest part is used in the welding of bodies, production engines and various elements necessary in the automotive industry. In order to get a real picture of the implementation of industrial robots in the production processes of the metal industry, an analysis was made and shown in Figure 7. The trend of implementation of industrial robots in production processes in the metal industry has a growing trend, with 7.200 robot units implemented in 2010. In just three years, the implementation increased to 16.458 robot units, which is an increase of about 2.2 times. In the next three years, in 2016, the increase amounted to 28.710 robot units, which is an increase of 1.75 times. The total increase in the implementation of industrial robots in metal industry processes for the period 2010-2021 was 8.8 times, which shows a steady growing trend. An increase in the implementation of industrial robots is expected in the coming years, so that in 2022, the implementation of around 72.000 robot units is expected, whereas in 2025, the implementation of around 96.000 units of robots is expected. In addition to industrial robots, service robots for logistics are also implemented in the production processes of the metal industry, which are used for the transport of materials and semi-finished products from machine to machine, the transport of finished products and the transport of finished products in the warehouse during commissioning. Figure 8 depicts the trend of their implementation [28-30].

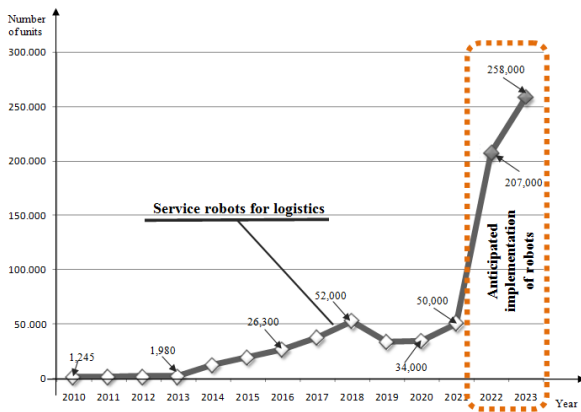


Figure 8. Trend of the annual implementation of service robots for logistics in production processes in the world for the period 2010-2021 and estimates of application until 2023

The development of the basic technologies of Industry 4.0 had a significant impact on the development of service robots, especially service robots for logistics. Many companies have developed different constructions of service robots for logistics that are implemented in all production processes in the world. The largest part of these robots is implemented in production of metal industry processes. Based on Figure 7, we see that the trend of implementation of service robots for logistics takes place according to an exponential function, so that from the 1.245 robot units implemented in 2010, there was an increase to about 52.000 service robot units in 2018, which represents an increase of 40 times. In the period of the Covid-19 virus pandemic, there was a slight decline in the implementation of service robots for logistics. However, in 2021, about 50.000 robot units were implemented. It is predicted that the increase in the implementation of service robots for logistics will continue, and in 2023, the implementation of about 258.000 units of service robots for logistics is expected. This indicates that Industry 4.0 is widely implemented in production processes, including the production processes of the metal industry. The objective is for production processes to become smart-intelligent without employees who currently perform monotonous and tiring tasks, i.e., the employees will be replaced by second-generation industrial robots and service robots.

4. CONCLUSION

Every company strives to survive on the global market, and in order to achieve this, it is necessary to reduce costs, and increase productivity, efficiency and quality of the final product, which can only be achieved by implementing the basic technologies of Industry 4.0. Among the first basic technologies of Industry 4.0 is the robot technology, i.e., the implementation of second-generation industrial robots - collaborative robots and service robots in production processes, especially in the metal industry. When designing any metal processing procedure in the metal industry, care must be taken to organize the process with as little human participation in operational tasks as possible. Companies in the metal industry around the world are implementing Industry 4.0, because any deviation or slowdown in development reduces competitiveness on the market and inevitably leads to stagnation. The trend of implementation of industrial robots and professional service robots in the production processes of all industries is growing and it will continue to increase in the coming years, as presented in this paper, especially in the metal industry. The decision to introduce robots into the mentioned segments of production processes in the metal industry would represent one of the conditions for achieving greater efficiency in the work of production processes in the metal industry. The use of robots is no longer limited to industrial robots with specific requirements for a safe working environment, because the achieved robot-human interaction has created the conditions for their joint work using collaborative robots, which will result in an increase in their implementation. The development and improvement of new technologies, including robotic technology where artificial intelligence is being introduced, are expected in the coming years. The implementation of robotic technology with other advanced technologies of Industry 4.0 in the production processes of all industrial branches, especially in the metal

industry, aims to make production processes smart-intelligent. The ultimate goal is to reach smart-intelligent factories.

Acknowledgements. The authors acknowledge the financial support from the Ministry of Science, Higher Education and Youth, Canton Sarajevo, Bosnia and Herzegovina, grant for cofinancing of scientific research/artistic research and research projects of special interest to Sarajevo Canton for 2022. (Number 27-02-35-37081-14/23, Sarajevo: 14.09.2023).

REFERENCES

- [1] I. Karabegović, A. Kovačević, L. Banjanović-Mehmedović, P. Dašić, *Handbook of Research on Integration Industry 4.0 in Business and Manufacturing*, IGI Global, Hershey, Pennsylvania, USA, 2020.
- [2] B. Pelster, J. Schwartz, (Ed.) *Rewriting the rules for the digital age*, Deloitte Global Human Capital Trends, Deloitte University Press. 2017.
- [3] K. Schwab, *The Fourth Industrial Revolution*, World Economic Forum, Geneva, Switzerland, 2016.
- [4] d'A. Mathieu: Data analytics beyond data processing and how it affects Industry 4.0, *Insight Centre for Data Analytic, Dublin, Irska*, 2017.
- [5] V. Doleček, I. Karabegović, *Roboti u industriji*, Technical faculty Bihać, B&H, 2008.
- [6] Trademarks and patents in China: The impact of non-market factors on filing trends and IP systems." January 2021.
<https://www.uspto.gov/sites/default/files/documents/USPTOTrademarkPatentsInChina.Pdf>
- [7] I. Karabegović, M. Bičo Ćar, M. Šestić, S. Stupar, i dr., (2022), *Industry 4.0 of Bosnia and Herzegovina Within Industry 4.0*, International Scientific Conference, Application of Industry 4.0 an Opportunity for a New Step Forward in all Industrial Branches, 14 April Sarajevo, 2022, Bosnia and Herzegovina, pp. 49-68. https://www.anubih.ba/images/news/PDF/20220526_Aplikacija_industrije_4.pdf; DOI: 10.5644/PI2022.202.20
- [8] E. Karabegović, *The Application of Robotics in the Metal Industry*, Karabegović, I., Banjanović-Mehmedović, L. *Industrial Robots, Design, Application and Technology*, NOVA Science Publishers, New York, USA, p. 293-324., 2020.
- [9] https://www2.deloitte.com/content/dam/insights/us/articles/4340_DSN-Logistics-and-distribution/figures/4340_fig1.png [Accessed: Dec..20.2022]
- [10] K.-L. Kusmin, *Industry 4.0 Analytical Article*, IFI8101 - Information Society Approaches and ICT Processes, School of Digital Technologies, Tallinn University, Estonia, 2016.
- [11] R. Davies, *Industry 4.0: Digitalisation for productivity and growth*, Briefing for the European Parliament (PE 568.337), European Parliamentary, 2015.
- [12] B. Bunse, H. Kagermann, W. Wahlster, *Smart Manufacturing for the Future*, Germany Trade & Invest, Berlin, Germany, 2017.
- [13] E. Freund, O. Stern, *Robotertechnologie I*, Institut für Roboterforschung, Dortmund, Germany, 1999.
- [14] Li. Shiyun, Xu. Chenghong. Research on the Impact of Industrial Robots on China's Regional Industrial Structure, *Journal of Autonomous Intelligence*, Volume 5 Issue 1. pp:1-12., 2022. doi: 10.32629/jai.v5i1.498
- [15] I. Karabegović, R. Turmanidze, P. Dašić, *World Trend of Implementation of Industrial Robots With a Focus on the Industry 4.0*, Grabchenko International Conference on Advanced Manufacturing, Odessa, Ukraine, pp. 128-136. 2019.
- [16] E. Karabegović, I. Karabegović, E. Hadžalić *Industrial Robot Application Trend in World s metal Industry, Inzinerine ekonomika-Engineering Economics*, vol. 4, no. 23, p. 368-378, 2012. DOI:10.5755/j01.ee.23.4.25.67.
- [17] I. Karabegović, E. Husak, M. Đukanović, *Applications intelligent systems-robot the manufacturing process*, 19th Conference Information Tehnology – IT 2014, Faculty of Electrical, Engineering University Montenegro, Žabljak, Montenegro, Conference Proceedings, p. 177-180. 2014.
- [18] I. Karabegović, *The Role of Industrial and Service Robots in Fourth Industrial Revolution with Focus on China*, *Journal of Engineering and Architecture*, vol. 5, No. 2, pp. 110-117. 2018.
- [19] I. Karabegović, E. Karabegović, M. Mahmić, M. E. Husak, *Contribution of Fourth Industrial Revolution to Production Processes in China*, 1st International Conference "Engineering and Entrepreneurship", ICEE-2017, Tirana, Albania Conference Proceedings, p. 295-301. 2017.
- [20] I. Karabegović, E. Karabegović, M. Mahmić, E. Husak, *Dissemination of Patent of the Base Technologies of the Fourth industrial*

- revolution-Industry 4.0, New Technologies, Development and Application III, Sarajevo, B&H, Conference Proceedings, p.3-15.2020.
- [21] E. Ulrich, H. Maximilian, *Industrial IoT Risk Assessment of Smart Factories*, PLUS-2016, Munchen, Germany, 2016.
- [22] B. Buchmeister, D. Friscic, I. Palcic, Impact of demand changes and supply chain's level constraints on bullwhip effect, *Advances in Production Engineering & Management*, vol. 8, no. 4, p.199-208.2013. DOI:10.14743/apem2013.1.128.
- [23] G. Papa, D. Torkar, Visual Control of an Industrial Robot manipulator: Accuracy Estimation, *Strojniški vestnik-Journal of Mechanical*, vol.55, no.12, p781-787, UDC 007.52, 2009.
- [24] M. Dev Anand, T. Selvaraj, S. Kumanan, T. Ajith Bosco Raj, Robotics in online inspection and quality control using moment algorithm, *Advances in Production Engineering & Management*, vol. 7, no. 1, p.27-38., 2012. DOI:10.14743/apem2012.1.128..
- [25] E. Karabegović, Implementation of Industry 4.0 and Robots in Production Processes of the Metal Industry, *International Journal of Advanced Engineering Research and Science*, Vol-7, Issue-12, pp:169-176, 2020. <https://dx.doi.org/10.22161/ijaers.712.26>, www.ijaers.com
- [26] M. Dev Anand, T. Selvaraj, S. Kumanan, Fault detection and fault tolerance methods for industrial robot manipulators based on hybrid intelligent approach, *Advances in Production Engineering & Management*, vol. 7, no. 4, p.225-236, 2012. DOI:10.14743/apem2013.4.144.
- [27] I. Karabegović, E. Karabegović, M. Mahmić E. Husak, The application of service robots for logistics in manufacturing processes, *Advances in Production Engineering & Management*, vol. 10, no. 4, p. 185-194, 2015. DOI:10.14743/apem2015.4.201.
- [28] IFR, "World Robotics Report: 'All-Time High' with Half a Million Robots Installed in one Year," *IFR International Federation of Robotics*. <https://ifr.org/ifr-press-releases/news/wr-report-all-time-high-with-half-a-million-robots-installed> [Accessed; Dec. 16, 2022].
- [29] M. Bill, C. Müller, W. Kraus, W., and S. Bieller, World Robotics Report 2022, 2022. [Online]. Available: https://ifr.org/downloads/press2018/2022_W_R_extended_version.pdf
- [30] International Federation of Robotics, "Executive Summary World Robotics 2022 Industrial Robots." 2022. [Online]. Available: https://ifr.org/img/worldrobotics/Executive_Summary_WR_Industrial_Robots_2022.pdf



Society of Production
Engineering

SPMS 2023

39. Savetovanje proizvodnog mašinstva Srbije

ICPES 2023

39th International Conference on Production Engineering of
Serbia



Faculty of Technical
Sciences
University of Novi Sad

Novi Sad, Serbia, 26. – 27. October 2023

COMPARISON OF SIGNAL FEATURES FROM TIME AND FREQUENCY DOMAIN FOR CHATTER DETECTION

Nikola VORKAPIC¹, Branko KOKOTOVIC¹, Sasa ZIVANOVIC¹

¹Faculty of Mechanical Engineering, Belgrade, Serbia

*Corresponding author: nvorkapic@mas.bg.ac.rs

Abstract: *This paper presents the results of the research into the applicability of the features derived by statistical analysis of signals from the machining process in the recognition of occurrence and evolving of chatter vibration. Selected set of statistical features were discussed, 3 of them in the time domain, an one in the frequency domain. Effects of these signal features were discussed through analysis of the results of two experiments with machining. It was shown that standard deviation and the skewness of the force or acceleration signal have some desirable properties in recognition of the moment when chatter vibrations occur.*

Keywords: *chatter vibrations, signal processing, feature extraction*

1. INTRODUCTION

In early days of theory of machining processes significance of chatter vibrations was recognized, with all types of degradation of process outputs, referred to this phenomenon. From pioneer works by Tlusty, Tobias and Meritt, until present time, during more than seven decades, chatter is permanently in focus of different research projects.

The main directions of these researches are aimed at predicting of chatter vibrations, online identification of chatter occurrence and techniques for its suppression. In the prediction of chattering, models based on the interaction of the cutting process model and experimentally identified dynamic parameters of the machine structure, tool, and workpiece are used [1]. More reliable results in form of stability lobes were achieved through extension

of such model with process damping [2]. Finally, the most accurate stability lobes can be created using more complex experimental identification procedure [3].

For applications for machining process monitoring there were presented a number of procedures, based on various types of sensors, and especially numerous algorithms for signal parameter classification in order to recognition of occurrence of chatter vibrations [4]. Most of them are based on fast Fourier transform, wavelet transform and Huang-Hilbert transform. One systematic overview of research achievements aimed for developing techniques for chatter suppression, as a specific kind of adaptive control of machining processes is given in [5].

This paper is related to the domain of on-line identification of chatter occurrence during machining process. The aim was to examine

potential use of statistic features of signals, acquired in process, in recognition of the moment in which the chatter vibrations start to evolve. These features derived from time series, of course, cannot be substitute for algorithms based on frequency content of the signal.

A potential benefit is reflected in the possibility that the monitoring system can be of a dual nature. The processing of signal segments in the time domain, as less demanding in terms of processing time, would serve to act as a trigger for signal processing procedures in the frequency domain based on such classified parameters.

This paper primarily is considering the applicability of selected set of statistical features derived from signal in time domain. It is also considered one of the statistical features of the signal in frequency domain. Definitions of these features is given in Section 2. Nature of these features are illustrated on 2 examples with machining, in Section 3. Results obtained from experiments, and potential use of these signal features is discussed in Section 4.

2. STATISTICAL FEATURES OF THE SIGNAL

In Literature source [6], specific sets of statistical features from both the time and frequency domains of a signal as a candidate for parameter classification with specific values that strongly correlate with certain changes in process. In the following, the correlation of some of these features with the stability of the machining process will be discussed using concrete examples. A selected set of these features is shown in Table 1. The first of them refers to the signal transformed into the frequency domain, and the remaining to the signal in the time domain.

Real-time applications imply that processing is performed not for the entire record, but in successive time windows of finite width and certain overlap. The power spectrum of a signal indicates the relative magnitudes of the frequency components composing the signal, identifies the frequencies that carry the highest signal energy. The Mean Square Frequency (MSF) represents the energy of the vibration

signal in the frequency domain, where f_j ($j=1, 2, L, \dots, m$) is the j -th frequency of the power spectrum [7].

Table 1. Statistical features from frequency and time domain

Formulation	Statistical features	Domain
$MSF = \frac{\sum_{j=1}^m f_j^2 S(f_j)}{\sum_{j=1}^m S(f_j)}$	Mean square frequency	Frequency domain
$x_m = \frac{1}{n} \sum_{i=1}^n x_i$	Mean value	Time domain
$x_{std} = \sqrt{\frac{1}{n-1} \sum_{i=1}^n (x_i - x_m)^2}$	Standard deviation	
$x_p = \max(x_i)$	Pick	
$x_{ske} = \frac{\sum_{i=1}^n (x_i - x_m)^3}{(n-1) \cdot x_{std}^3}$	Skewness	
$x_{kur} = \frac{\sum_{i=1}^n (x_i - x_m)^4}{(n-1) \cdot x_{std}^4}$	Kurtosis	

The 'Peak' feature represents the maximum value of the signal, while 'Mean' signifies the mean value of the signal, with x_i representing the current value of the signal. These values serve as a basis for calculating other features listed in Table 1. Skewness is a statistical measure assessing the asymmetry of a probability distribution, quantifying the extent to which the data is skewed or shifted to one side. Positive skewness indicates a longer tail on the right side of the distribution, while negative skewness indicates a longer tail on the left side. Kurtosis is a statistical parameter used to characterize a signal, offering a measure of the "peakedness" of a random signal. This feature is widely used in systems for monitoring of assemblies with rolling bearings. Signals with higher kurtosis values have more peaks greater than three standard deviations. The standard deviation measures the extent of signal distortion from the mean value.

3. EXPERIMENTAL EXAMPLES

The specific processing of the signals from the machining process is illustrated by two examples. The first refers to the internal turning with a linearly variable depth of cut. In the experiment, a time record of the acceleration is formed from the accelerometer placed on the tool shank. In the second experiment an internal planar contour was machined with flat end mill with variable axial and radial depth of cut. Recorded signal was referred to the one force component in the XY plane, using a dynamometer on which the workpiece is placed. The dynamometer, in this case, represents a substructure of maximum compliance.

3.1 EXP1: Internal turning

The first case refers to internal turning with a linearly variable cutting depth, as in Fig. 1. In such setting of the experiment, cutting tool was the element with dominant compliance in the whole mechanical structure. Internal turning is particularly interesting from the point of view of chatter vibrations, because the usual logic contained in stability lobes does not apply in this case.

That is the reason for development of special tool holders for such operations [7]. An unstable process is expected in the zone of small depths and especially in cases with small feeds.

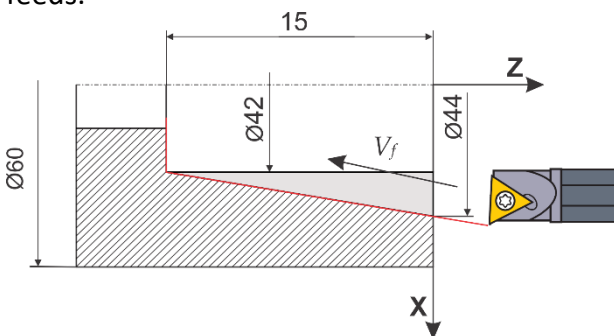


Figure 1. Cutting area in machining test

For this tool setup, an experimental modal analysis was performed, along with a dynamic analysis in Ansys software. Dominant modes have following frequencies: 372.5Hz for X direction, and 409.27Hz for Y direction. (Fig. 2).

During machining tests, the workpiece material was 42CrMo4 steel. Machine: Echo-Eng TCN410 - 2 axis CNC lathe. Tool: R S36.8 - 25-16 with TPMR 160312 4C40 P40 TiN coated carbide insert. Cutting speed 90m/min.

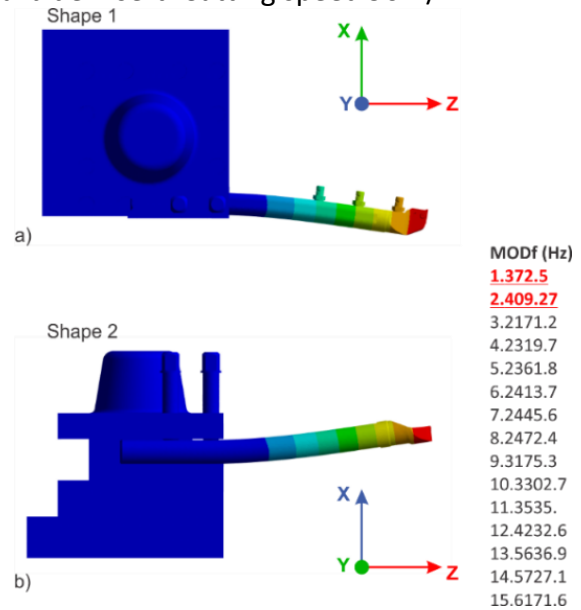


Figure 2. Results of dynamic analysis for tool shank and tool holder (ANSYS)

Set of 3 experiments was performed with different value of feed: 0.15, 0.16, and 0.18 mm/rev. An accelerometer, the PCB Piezotronics 352C03, was affixed to the tool shank. The cDAQ NI 9174, with S/V Input Module NI9234, driven by NI-LabView, were used for data acquisition. Sampling frequency was set on 1024 S/s. Acquired acceleration signal for example with 0.16 mm/rev is shown in Fig. 3.

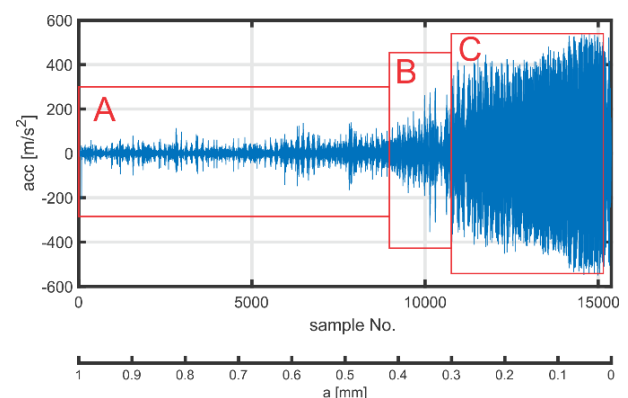


Figure 3. EXP1: Acceleration along X axis of the tool shank

Three zones can be observed in Fig. 3. Area A represents a stable process. The transition region is marked with B, while the chatter

region is marked by C. Acceleration signal processing is performed in a sliding window (here called buffers). The width of the window is 450 samples, and the overlapping factor is 0.5 (225 samples).

Figure 3 shows the spectrogram (amplitude spectrum in successive buffers), calculated using FFT. The dominant frequency in all buffers is 372.5 Hz, which is also the frequency of the first mode, determined by the modal analysis of the tool holder. A sudden increase in amplitude at this frequency over time is not noticeable. This can be interpreted as a consequence of the slightly changing process damping.

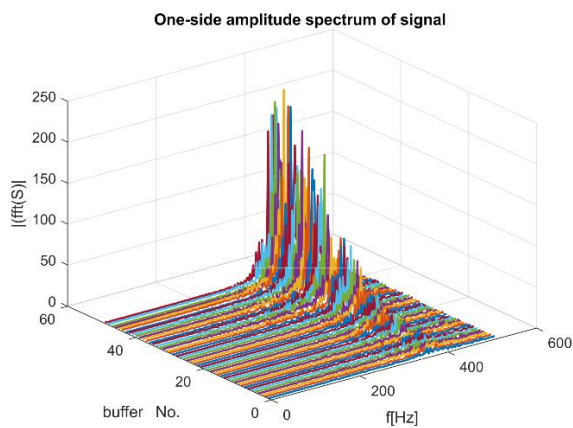


Figure 4. EXP1: Amplitude spectrum in successive buffers

Mean square frequency, defined as in table 1, for this case is shown by the diagram in Fig. 5.

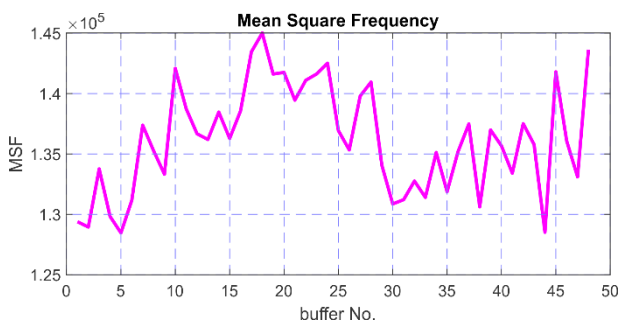


Figure 5. EXP1: Mean square frequency in successive buffers

Figure 6 presents three selected statistics features derived from acceleration signal in time domain.

Here, some conclusions can be made, observing original signal and its different

presentation, shown in figures 4-6. In the amplitude spectrum, the dominant frequency is the natural frequency of the structure during whole time.

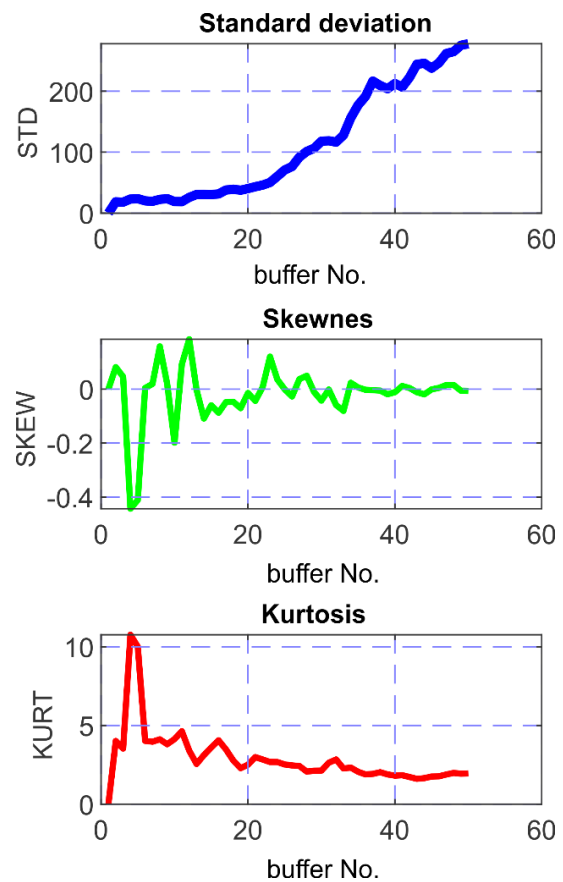


Figure 6. EXP1: Statistical features (time domain) of acceleration signal

In the first part, the amplitudes are smaller, which is explained by higher process damping. It is not possible to clearly identify the moment of chattering. Mean square frequency (MSF, figure 5) has a profile that cannot be clearly correlated with moment of chatter occurrence. The same can be conclude for the profile of kurtosis (KURT). It should be noticed that, in the graph of skewness (SKEW), evolving of chatter vibrations is related with SKEW value near to the zero.

3.2 EXP2: End milling

In This example is referred to milling operation. Measurements was a part from an earlier research project [8]. Figure 7 shows a signal recorded during the milling process (closed internal contour in XY plane), where

variations were made through variable axial (0-8mm) and radial (0-16mm) depth of cut along the tool path. Feed rates along tool path was variable, according to results of the algorithm for federate scheduling. In this experiment one pre-machined part made of ENAW 7019 alloy was milled on horizontal machining center (LOLA HMC500). Tool was an HSSE end mill $\phi 16$, with 4 flutes. Dynamometer was 4-component, with strain gauges. Workpiece was fixed to the plate of the dynamometer. Force signal (y direction of the dynamometer) was recorded with sampling rate of 2000 S/s.

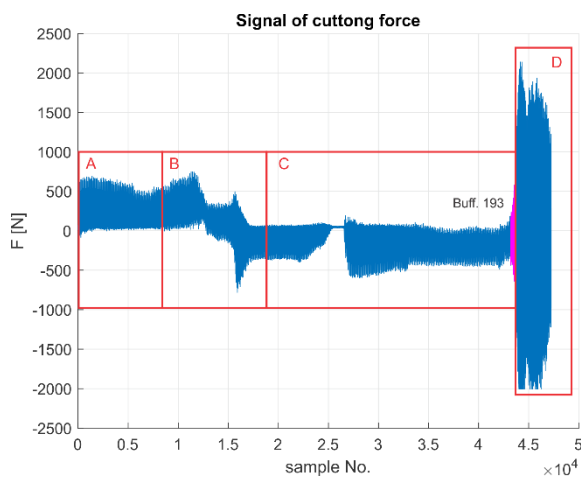


Figure 7. EXP2: Force signal during test with end milling

Time series of measured force contains several zones, regarding chatter vibrations. With A and C there are marked zones of stable cutting process. Specific zone is marked with B, and it was referred to early stage of chatter evolving. Further amplitude rise was suppressed with change in subsequent cutting parameters. Finally, zone B represents true chatter vibrations. Such flow of considered milling operation has clear explanation in spectrogram, shown in Fig. 8.

In the stages of the stable process, the frequency of the mill teeth entering (39Hz) is dominant. Unstable phases of the process have spectrum with dominant frequency equal to the one of the natural frequencies of the dynamometer (280Hz).

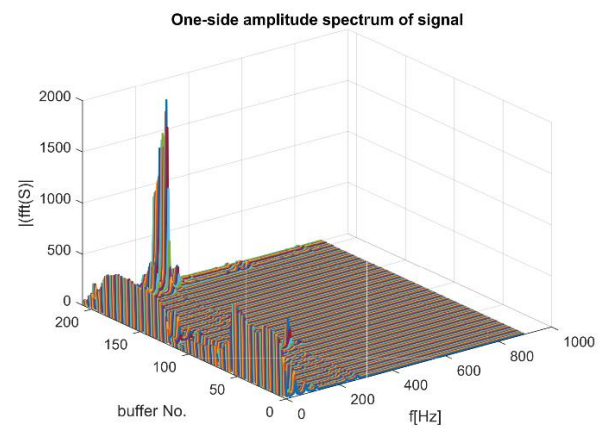


Figure 8 EXP2: Amplitude spectrum in successive buffers

Figure 9 presents the mean square frequency of the signal from this example.

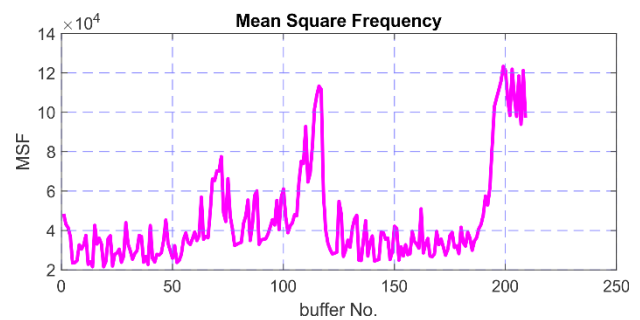


Figure 9. EXP2: Mean square frequency

Figure 10 presents three selected statistics features derived from force signal in time domain.

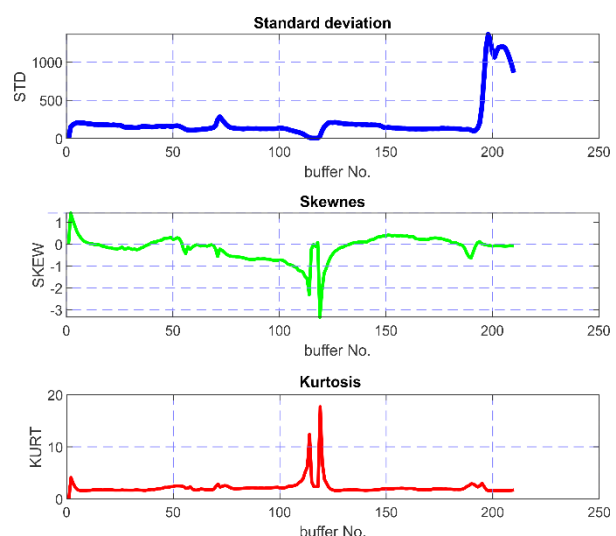


Figure 10. EXP2: Statistical features (time domain) of force signal

Some conclusions can be made, observing original signal and its different presentation,

shown in Figs. 7-10. In the amplitude spectrum, evolving of chatter vibrations can be recognized in two zones of original force signal. These situations are followed by changing in frequency of dominant component in amplitude spectrum of considered buffer, shifting this frequency to the natural frequency of the structure (transition from forced to self-exciting vibrations). Evolving of the first occurrence of chatter was broken by change of cutting parameters along tool path. In the second case this evolving is not damped and the sudden rise and high amplitudes of measured force was notable.

These phenomena cannot be recognized by MSF profile (Fig.9) or by kurtosis (KURT, Fig.10). The standard deviation STD, of the force signal (Fig.10) has sudden rise in the zone where chatter occurs. These moments in force signal also correlated with zero values of the skewness (SKEW, Fig.10).

4. CONCLUSION

The paper illustrates the potential of standard deviation and skewness of the signals from machining process in the detection of the occurrence of chatter vibrations. They cannot replace identification algorithms based on fast Fourier transform and wavelet transform, but they can be an additional criterion in the procedures for monitoring the stability of the machining process. This limitation stems from the fact that chattering is accompanied by a marked increase in amplitude (force, acceleration), but that the recognition of high amplitudes in the signal does not mean the occurrence of chattering. In the further work, it is planned to formulate additional derived quantities, for which it is possible to clearly define the threshold, and with the aim of more precisely identifying the moment when chattering occurs.

ACKNOWLEDGEMENT

The presented research was supported by the Ministry of Education, Science and Technological Development of the Republic of Serbia through the project "Integrated research in macro, micro, and nano mechanical engineering" (contract no. 451-03-47/2023-01/200105 dated 3 February 2023).

REFERENCES

- [1] Y. Altintas: Manufacturing automation: Metal cutting mechanics, Machine tool vibrations, and CNC design, Second Edition, University of British Columbia, 2012.
- [2] O. Andreas, et al.: Extension of Tlustý's law for the identification of chatter stability lobes in multi-dimensional cutting processes. *International Journal of Machine Tools and Manufacture*, Vol. 82, pp. 50-58, 2014.
- [3] C. Mladenović, A. Košarac, M. Zeljković, M. Knežev: Experimental Definition of Machining Systems Stability Lobe Diagram, in *Proceedings of the XIII International Scientific Conference MMA 2018 – Flexible Technologies*, 28-29.9.2018, Nov Sad, Serbia, pp. 95-98.
- [4] C.H. Lauro, L.C. Brandão, D. Baldo, R.A. Reis, J.P. Davim: Monitoring and processing signal applied in machining processes – A review, *Measurement*, Vol. 58, pp.73-86, 2014.
- [5] J. Munoa, X. Beudaert, Z. Dombovari, Y. Altintas, E. Budak, C. Brecher, G. Stepan: Chatter suppression techniques in metal cutting, *CIRP Annals*, Vol.65, No.2, 2016, pp. 785-808, 2016.
- [6] Z. Qingzhen, G. Chen, A. Jiao, Chatter detection in milling process based on the combination of wavelet packet transform and PSO-SVM, *The International Journal of Advanced Manufacturing Technology*, Vol. 120, No. 1-2, pp.1237-1251, 2022.
- [7] B. A. G. Yuvaraju, B. K. Nanda, J. Srinivas, Investigation of stability in internal turning using a boring bar with a passive constrained layer damping. *FME Transactions*, Vol. 49, No. 2, pp. 384-394, 2021.
- [8] B. Kokotović, N. Vorkapić: Feedrate optimization for 2.5D milling operations, *FME Transactions*, Vol. 47, No. 3, pp. 613 – 623, 2019.



Society of Production
Engineering

SPMS 2023

39. Savetovanje proizvodnog mašinstva Srbije

ICPES 2023

39th International Conference on Production Engineering of
Serbia



Faculty of Technical
Sciences
University of Novi Sad

Novi Sad, Serbia, 26. – 27. October 2023

DATA INTEROPERABILITY IN COMMUNICATION BETWEEN REAL AND DIGITAL MEASURING TWIN

Vidoje KASALICA^{1*}, Slavenko STOJADINOVIĆ¹

¹ University of Belgrade, Faculty of Mechanical Engineering, Belgrade, Serbia

*Corresponding author: vidoje.kasalica@gmail.com

Abstract: *The development of computer technologies and software packages, along with their increasingly advanced capabilities, has brought forth new requirements in the field of coordinate metrology. As an essential response to the challenges of modern production and measurement approaches, the concept of the digital twin has emerged and is actively evolving. This concept is becoming increasingly significant in the industry, enabling the monitoring, control, and simulation of measurement as well as inspection of objects or processes within a digital environment. Integration within the industrial context opens doors to novel methods of analysis, optimization, and management of production systems. The contribution offered by this study lies in addressing the issue of interoperability between output data obtained from physical coordinate measuring machines (.dms) and output data derived from inspection process simulations (.ncl) on virtual machines. This constitutes a pivotal part of the communication process between the virtual and real twins. The approach is grounded in the identification of key parameters and analysis of the structure of generated DMIS file codes originating from PTC Creo software and PC-DMIS software for real machines. The findings of this research contribute to the development of efficient tools for analysis, processing, and translation of codes for communication between the virtual and real components of digital twins. This provides a foundation for semantic understanding of their structure, precise communication, and broader application across industries. The development of this interoperable model serves to advance towards the goal of enabling the direct implementation of obtained simulation code on coordinate measuring machines (CMM). Such implementation in an on-line and, crucially, real-time mode would facilitate the interconnection of diverse digital twins, realizing the potential for integration within complex technological systems.*

Keywords: *Digital twin, Data Interoperability, Simulation, CMM, Inspection planning*

1. INTRODUCTION

Today, as we find ourselves deeply immersed in a new chapter of the industrial revolution, called Industry 4.0, we are facing inevitable and accelerated technological advancements and transformation of the physical into the digital environment. The global presence of digital technology and computing is profoundly altering the traditional

approach to industry and manufacturing. The concept of Industry 4.0 could be described as the integrated application of artificial intelligence (AI), robotics, additive manufacturing (3D printing), and the Internet of Things (IoT) as well as digital twin. Within this comprehensive integration, the concept of digital twins has emerged as a key model promising a revolutionary transformation in various industries including manufacturing, and

thereby, measurement inspection and product quality management. Digital twins represent digital replicas of real-world objects, systems, or processes. They enable the physical world to become digitally visible and functional, facilitating the monitoring of its characteristics, performance, and real-time changes. This technology has the potential to optimize processes, alert to possible collisions, and thus reduce costs and increase profits.

One of the key challenges in realizing the full potential of a digital twin is data interoperability. To ensure that a digital twin accurately represents a real system, efficient data exchange between digital and physical entities is essential. This lays the foundation for a deep and precise analysis, simulation, and control of real systems through their digital counterpart.

This paper specifically addresses the crucial issue of data interoperability in the context of communication between the digital and physical measurement twin based on Coordinate Measuring Machine (CMM). The main idea is to compare the data obtained from measurement inspections on a virtual CMM and real CMM with the data obtained after simulating measurements. The focus is on identifying similarities in the syntax of these codes, as well as differences that actually hinder the smooth flow of information between these parallel systems.

The next chapter will provide a detailed description of the digital twin concept, both individual systems, and the modeling and simulation of the digital twin based on CMM.

Afterwards, the concept of data interoperability in the measurement inspection of machine parts will be introduced within the framework of the digital twin model. The contribution of this paper is a detailed analysis and comparison of the structure, syntax and content of DMIS codes obtained from virtual and real measurement inspections. Their ability and compatibility to offer seamless digital twin interaction is highlighted.

2. DIGITAL TWIN

The concept of Industry 4.0 has gained great importance in recent years. The increase in usage of computerized systems, Industry 4.0 deals with creating more digitized systems and network integration via smart systems [1].

In the field of mechanical engineering, specifically in manufacturing, one model has drawn particular attention within Industry 4.0, and that is the model of digital twins (DT). The DT represents a virtual replica of a real system or machine. There are two approaches, or bidirectional information flows. In the first working principle, it is based on continuous data collection from the real system through various types of sensors and their application to the virtual one. While in the second approach, data from the digital simulation of the process is implemented into the physical system.

The concept itself was first introduced in Michael Grieves' work in 2003 [2], during a presentation in a product lifecycle management course. The first use of the DT was a year later (2004), by NASA, in technology roadmaps [3]. They used it to replicate conditions in space and conduct tests to prepare for their spacecraft's flights. Since then, the DT has advanced technologically and expanded its scope of use. There has been a noticeable exponential increase in the use of this model in the last ten years. Manufacturing relies on high-cost equipment that generates a high volume of data which facilitates creating DTs. There is also an expected significant increase in the potential of the DT in every branch of industry, especially in manufacturing [4].

2.1. Real twin

The real twin in this work represents the realization and verification of measurements for a specific workpiece, the CMM DEA Epsilon 2304, as shown in Figure 1. During real measurement inspection, the RENISHAW PH10M PLUS measuring head was used, connected to a post-processor from the same manufacturer. The measuring machine's

measuring range along the X/Y/Z axes is 3000 x 1950 x 500 mm. Positioning errors: 3.5 μm +5 L/1000. Measurement uncertainty: 7 μm +7 L/1000. The PC-DMIS software was used to configure the measurement inspection plan, which is implemented in the control unit of the measuring machine.

CMM are used, first, in assessing product quality and conformance with regard to original design intent, second, in providing feedback upstream. Usually, the measurement system is composed of four major phases (definition of dimensional and geometric specifications, unfolding of a measurement plan, measurement execution, and results analysis) [5].



Figure 1. Real measuring machine DEA Epsilon 2304. - Physical twin

Prior to commencing the actual measurement and following the positioning and setup of the measuring object on the machine's worktable, it is necessary to perform the probe calibration. This step is crucial due to the digital twin model itself, as well as data interoperability. Information about the performed calibration process of the measuring probe is only found in the output code of the PC-DMIS software (AUTOCALIBRATE/PROBE, PARAMETER_SET=, QUALTOOL_MOVED=Y/Y/N, SHOW_SUMMARY=Y/N, OVERWRITE_RESULTS FILE=Y/N), that is, during inspection on a real CMM. This should be highlighted as one of the factors that can influence the complexity of creating an interoperable model.

After the measurement is completed, the software generates a graphical measurement

report (achieved tolerances), Figure 2. In addition to the visual representation, information about the measurement is obtained in an analytical form, representing the coordinates of the measuring probe's movement, using an output (.dmis) file, which will be discussed in detail in the next chapter.

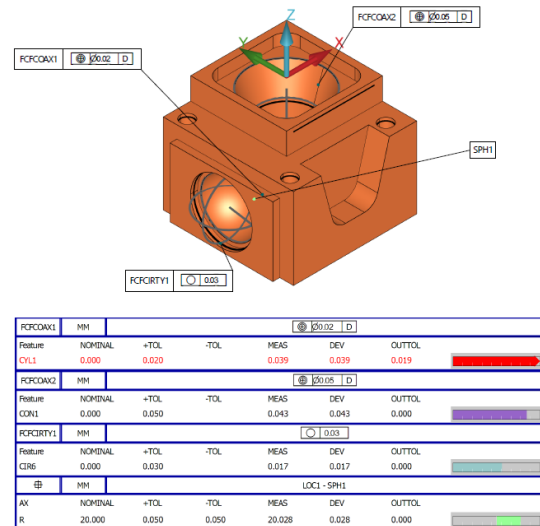


Figure 2. Graphic report of measurement inspection

The parameters verified after obtaining the measurement inspection report, related to the decision-making about the correctness of the measuring part, are as follows:

- **NOMINAL:** Represents the nominal (theoretical) value.
- **+TOL/-TOL:** Represents tolerance values.
- **MEAS:** Represents the actual measured value on the measuring machine.
- **DEV:** Represents arguably the most important parameter of the measurement displacement, which is the difference between the nominal (desired) and measured (achieved) values [6].

2.2. Virtual twin – modeling, simulation and measurement verification

In the previous subsection, the real part of the digital twin was extensively described. Here, the focus will be on the virtual part, which involves modeling and simulating the measurement inspection. As part of the

modeling process, it is necessary to create an identical representation of the real measurement inspection, from the dimensions on the technical drawing of the workpiece to every individual component used during physical measurements. Accordingly, for the purposes of this work, in the CAD/CAM environment, PTC Creo Parametric software, was used to model the workpiece, auxiliary clamping equipment, measuring sensor, and measuring machine, Figure 3,4.

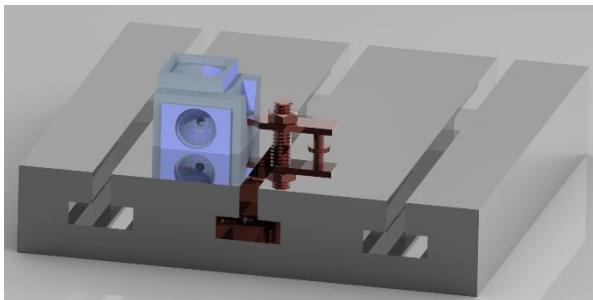


Figure 3. Modeled components of the virtual twin

Simulating the measurement inspection process using software offers many advantages before the work piece is placed on the table of the numerically controlled measuring machine. Some of the advantages include the elimination of the need to design and manufacture expensive prototypes, timesaving, real-time visualization and monitoring of the measurement inspection process, detection and avoidance of collisions on the real system. By combining all of these factors, it can be concluded that significant cost savings are achieved.

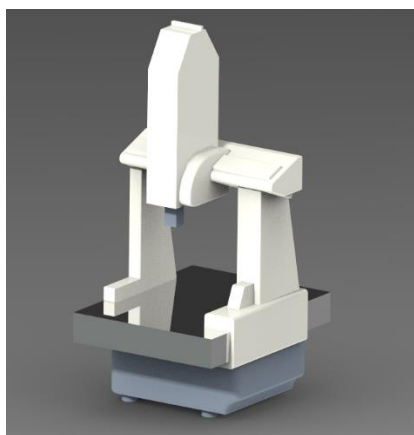


Figure 4. Modeled measuring machines - Virtual twin

After modeling the mentioned components, defining the workspace of the virtual measuring machine, and establishing the coordinate origin of the measuring part (which must be identical in real and virtual inspections), it is necessary to configure the measuring probe. The basic parameters for configuration include: the length of the measuring probe (error due to deflection increases with increasing length), the size of the sphere of the contact part of the measuring probe, the rotation angle, and the orientation angle. After defining these parameters, virtual measurement inspection can be conducted using the CMM module within the PTC Creo Parametric software, as shown in Figure 5. As an output of virtual metrology, in addition to the visual representation, you also receive an .ncl (dmis) file with all relevant measurement data in digital format. In terms of the measurement principle, the two codes are the same, but upon closer examination of its syntax and scrutiny of each line of code, certain differences are identified, which will be described in detail in the following chapter.

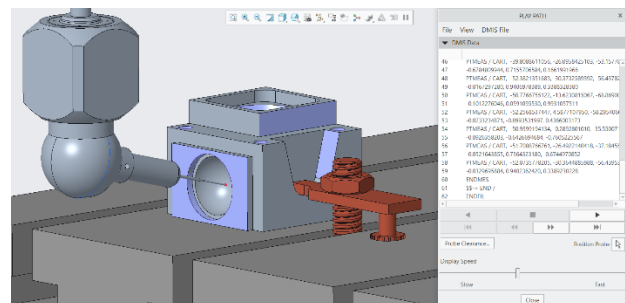


Figure 5. Verification process through the output DMIS code

3. DATA INTEROPERABILITY

Data interoperability in the context of mechanical engineering refers to the ability of various software systems, machines, devices, and components to efficiently exchange, interpret, and utilize data among themselves. This concept is intended to overcome factors such as different protocols, formats, or platforms on which these elements operate. Data interoperability plays a crucial role in Industry 4.0 (and consequently in the digital twin model) and the digitization of

manufacturing processes, enabling more informed decision-making, production optimization, and more efficient resource utilization.

Therefore, one goal should be to analyze the collected product data and utilize it in (sophisticated) models to improve the currently applied production processes [7].

Currently data is typically either (i) not stored at all, (ii) only retained locally, i.e., stored in isolated data buffer, or (iii) not transferable between systems by different manufacturers due to vendor-specific solutions (as identified by [8]).

In this study, the analysis will be focused on examining two DMIS codes, comparing their structures, syntax, and content. As mentioned in the previous chapters, the two codes obtained by measurement inspection (virtual and real) are used for data communication, in order to confirm the concept of a digital twin during the inspection of the tolerance range of the measurement part. The first code (.dms) is generated by simulating the measurement inspection process within the PTC Creo Parametric software package, while the code (.ncl) from the real twin is obtained through measurements on the CMM DEA Epsilon 2304. In order for their further analysis to be comprehensive, it was chosen to perform code interoperability for four primitives: plane, cylinder, cone, and sphere. The selected segments of the code for sphere inspection are shown in Figure 6. The first part of the figure contains the code obtained from PTC Creo Parametric, while the second part is the code obtained from measurements on a real CMM.

A detailed analysis has revealed that these two DMIS codes share a very similar overall structure, consisting of various sections for defining modes, characteristics, and commands for measurement inspection. However, there are certain differences in these codes that can pose challenges when creating a universal model (at least for this specific software and measuring machine manufacturer) for data interoperability.

The main difference between the PC-DMIS program and the inspection in the PTC Creo is

the measurement protocol record, more precisely the Edit window. In the same window, you can write the original measurement protocol from the program PC-DMIS, as well as the import of already created and generated .ncl code from the program PTC Creo [9].

The drawbacks are reflected in the following factors, primarily in the aforementioned calibration of the measuring probe. It has been stated what the calibration of the probe contributes to and how important this procedure is in real inspection. Therefore, the adjustment of calibration parameters holds a special place in the pre-inspection setup of the PC-DMIS software, as well as in the output code it generates. This part of the procedure and structure does not exist and cannot be implemented in the digital twin.

```

MODE / PROG, MAN
SNSLCT / S(4)
FEDRAT / MESVEL, MPM, 0.2500000000
FEDRAT / POSVEL, MPM, 5.0000000000
ACLRAT / MESACL, MPMM, 3.0000000000
ACLRAT / POSACL, MPMM, 3.0000000000
PRCOMP / OFF
SNSSET / APPRCH, 3.0000000000
SNSSET / RETRCT, 3.0000000000
SNSSET / CLRSRF, 0.0000000000
F(M_SP01)= FEAT / SPHERE, INNER, CART, $
-52.7000000000, -12.5000000000, -50.0000000000, 40.0000000000
MEAS / SPHERE, F(M_SP01), 12
RAPID / 1.000000
GOTO / -40.1490317409, -9.3330530436, -51.2015168473
PTMEAS / CART, -34.3562771598, -7.8713852175, -51.7560630846, $
-0.9654590969, -0.2436113043, 0.0924243729
PTMEAS / CART, -39.9329356516, -26.2244756002, -53.1049697944, $
-0.6719507552, 0.7223408211, 0.1634194629
PTMEAS / CART, -39.4125773235, -14.2934665203, -63.4620903450, $
-0.6993380356, 0.0943929748, 0.7085310708
PTMEAS / CART, -40.3137678464, 1.7320341166, -52.2428682397, $
-0.6519069555, -0.7490544272, 0.1180456968

$$$$definition: ID
$$
$$ F(SPH1)=FEAT/SPHERE,INNER,CART,-55,-12.5,-50,40,-0.9995559,-0.0297951,$$$
$$ -0.00044395$
$$ CALL/M(PCD_AUTO_SPHERE_605),(SPH1),-55,-12.5,-50,-0.9995559,-0.0297951,$$$
$$ -0.0004439,'THICKNESS_NONE',0,'BOTH',10,12,3,0,0,0,-103,256.9,$
$$ -77.23,$$$
$$ -1.707,-0.0004441,0,0.9999999,'-35.504,-0.697,-45.978,-0.9714223,$$$
$$ -0.1406073,-0.1912283,-41.987,-19.911,-63.13,-0.6472633,0.3700645,$$$
$$ 0.0664102,-42.618,1.194,-57.586,-0.6156853,-0.6851711,0.3801942,$
$$ -12.463,$$$
$$ -4.339,-36.469,-0.6234628,-0.408247,-0.6666346,-41.831,-25.449,$
$$ -41.995,$$$
$$ -0.6550475,0.6469524,-0.39034,-41.986,-19.934,-63.117,-0.6472976,$
$$ 0.371227,$$$
$$ 0.6657299,-54.028,-22.596,-67.049,-0.045217,0.504302,0.8623427,$
$$ -53.757,$$$
$$ -32.011,-45.525,-0.0587725,0.9750908,-0.2138777,-54.287,-14.465,$
$$ 29.908,$$$
$$ -0.0322739,0.0977587,-0.9946867,-54.886,5.807,-41.771,-0.0023238,$$$
$$ -0.9158337,-0.4015511,-54.726,0.003,-64.727,-0.0102921,-0.6656091,$$$
$$ 0.7462290,-54.029,-22.505,-67.067,-0.0451725,0.5027967,0.8632235'$
$$ $$

```

Figure 6. Output codes from PTC Creo Parametric and PC_DMIS software

The next factor that is important in ensuring accurate and repeatable measurement results, and which is again related only to CMM (real twin), is temperature compensation. Figure 7 displays a segment of code obtained from the PC-DMIS software (Command Mode), related

to temperature compensation, which is entered into the measurement routine.

```
TEMPCOMP/METHOD = AUTOMATIC, MATERIAL = Aluminium, CTE=23
,SET WARNING LIMIT = TRUE, MINIMUM = 18, MAXIMUM = 22
,PART SENSOR NUM=DEFAULT,X SCALE= 19.85,Y SCALE= 20.625,Z SCALE= 20.95,PART TEMP=21.27
```

Figure 7. Code segment for temperature compensation in PC-DMIS software

Temperature compensation on CMM refers to adjusting measurement data based on the effects of temperature variations on the machine and the workpiece being measured. Temperature changes can cause expansion or contraction of machine components, measuring probes, work tables, and the overall machine structure, which directly contributes to increased errors in measurement inspection. In Figure 8, you can see a graphical representation of the impact of temperature change on measurement results [10].

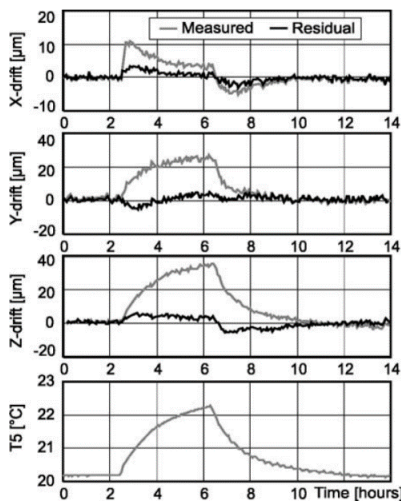


Figure 8. Drift model results under targeted temperatures [9]

The coordinates of measuring (planned) points, coordinate systems, and defined measurement parameters, there are also a difference in their interpretation. An analysis of the output from PTC Creo Parametric software reveals that each measurement characteristic requires a separate call for the coordinate system and all relevant parameters such as approach speed, measuring speed, distances, and accelerations. The problem with this approach to writing output files is the large

volume of code, with information repeated for each specified function. On the other hand, in the PC-DMIS environment, the coordinate system and relevant alignments are defined at the very beginning and are applied to all subsequent measurement characteristics unless there is a need to redefine them.

Another important factor worth mentioning is the alignments with CMM axes, which are crucial in real inspection to guarantee measurement accuracy. On the other hand, the DMIS code obtained from virtual simulation in PTC Creo Parametric software generates boundary planes. It could be said that this is a way to compensate for the lack of alignments. This is another element that increases the volume of code obtained through virtual measurement inspection.

4. CONCLUSION

In terms of production metrology, the DT's role is to monitor the measurement process, improve processing quality, dimension accuracy, and surface roughness, and thus reduce production costs in an efficient, dynamic, and intelligent manner.

In this paper, one approach to data interoperability has been successfully demonstrated. Also, the paper provided a detailed overview of the advantages and disadvantages of application this concept (DT). It is also important to emphasize that each software and each manufacturer of measuring machines has its own way of creating and interpreting output code. As is the case in this model, the operating principle is relatively similar for all. This raises the question of whether it is possible to create a universal model for data interoperability, specifically for data obtained from the measurement inspection process.

The contribution of this paper is a detailed analysis and comparison of the structure, syntax and content of DMIS codes obtained from virtual and real measurement inspections. Their ability and compatibility to offer seamless digital twin interaction is highlighted.

The feature research in this field would be to create a computer model for data interoperability. It is sufficient for the model to have a unidirectional data flow, meaning that data from the simulated measurement inspection (virtual twin) is converted into the control unit of the measuring machine. To achieve this goal, it is necessary to find suitable solutions for all the mentioned problems when networking data between the virtual and real world.

ACKNOWLEDGMENT

We would like to take this opportunity to express our gratitude to the Military Technical Institute for providing formatted data from the CMM for the purpose of completing Master's thesis.

REFERENCES

- [1] Erboz, G. 2017. How to Define Industry 4.0: The Main Pillars of Industry 4.0. Managerial Trends in the Development of Enterprises in Globalization Era, Nitra, 761-767.
- [2] Grieves, M., 2015. Digital Twin: Manufacturing Excellence through Virtual Factory Replication This paper introduces the concept of a A Whitepaper by Dr . Michael Grieves. https://www.researchgate.net/publication/275211047_Digital_Twin_Manufacturing_Excellence_through_Virtual_Factory_Replication
- [3] Shafto, M., Rich, M.C., Glaessgen, D.E., Kemp, C., Lemoigne, J., Wang, L., 2010. DRAFT MoDeling, SiMulATion, inFoRMATion Technology & PRocESSing RoADMAP Technology Area 11. Technical ReportJ.K. Lancaster: Severe metallic wear, in: *Proceedings of the Conference on Lubrication and Wear*, 01-03.10.1957, London, UK, pp. 1-7 or Paper 7
- [4] Vidoje Kasalica, Slavenko Stojadinović, Srđan Živković, 2022. Jedan pristup razvoju digitalnog mernog blizanca na bazi numerički upravljane merne mašine; DOI: 10.5937/tehnika2206707K
- [5] Raoudha Gaha, Alexandre Durupt, Benoit Eynard. Towards the implementation of the Digital Twin in CMM inspection process: opportunities, challenges and proposals. Volume 54, 2021, Pages 216-221, <https://doi.org/10.1016/j.promfg.2021.07.033>
- [6] S. Stojadinovic, V. Majstorovic, N. Durakbasa, "An approach to development of the digital inspection twin based on CMM" Measurement, Sensors 18 (2021), 100300. <https://doi.org/10.1016/j.measen.2021.100300>.
- [7] Gleim, L., Pennekamp, J., Liebenberg, M., Buchsbaum, M., Niemietz, P., Knappe, S., ... & Wehrle, K. (2020). FactDAG: formalizing data interoperability in an internet of production. IEEE Internet of Things Journal, 7(4), 3243-3253.
- [8] E. Sisinni, A. Saifullah, S. Han, U. Jennehag, and M. Gidlund, "Industrial Internet of Things: Challenges, Opportunities, and Directions," IEEE Trans. Industr. Inform., vol. 14, no. 11, 2018.
- [9] Slavenko M. Stojadinovic, Vidosav D.Majstorovic, Numan M. Durakbasa, Dusan Stanic, 2022. Contribution to the development of a digital twin based on CMM to support the inspection process. <https://doi.org/10.1016/j.measen.2022.100372>
- [10] J.-P. Kruth, P. Vanherck, C. Van den Bergh, 2001. Compensation of Static and Transient Thermal Errors on CMMs. [https://doi.org/10.1016/S00078506\(07\)62144-1](https://doi.org/10.1016/S00078506(07)62144-1)



Society of Production
Engineering

SPMS 2023

39. Savetovanje proizvodnog mašinstva Srbije

ICPES 2023

39th International Conference on Production Engineering of
Serbia



Faculty of Technical
Sciences
University of Novi Sad

Novi Sad, Serbia, 26. – 27. October 2023

PRODUCTION MODELS OF DIGITAL GOODS

Ernad KAHROVIĆ^{1,*}

¹ State University of Novi Pazar, Novi Pazar, Serbia

*Corresponding author: ekahrovic@np.ac.rs

Abstract: *The digital economy, as an economy that functions primarily through digital technology, has caused the emergence of a wide range of digital products and services that can be distributed through digital business platforms. The paper points out the characteristics of goods and services in the digital environment, as well as certain differences compared to physical goods. Also, the existence of zero marginal cost for digital goods, which enables them to access a wide market area, is especially highlighted. The paper elaborates on different ways of producing digital goods and special emphasis is placed on in-house production, commons-based peer production (CBPP), and crowdsourcing.*

Keywords: *digital economy, digital technology, digital goods, digital services, production models.*

1. INTRODUCTION

The fourth industrial revolution is often identified with the concepts of the digital revolution and/or the digital economy. Namely, the first industrial revolution was related to the second half of the 18th and the first half of the 19th century when manual production began to be replaced by steam engines, thus beginning the development that changed earlier political, economic and social systems in much of the world. The second half of the 19th century and the beginning of the 20th century were marked by the second industrial revolution with the introduction of alternating electricity and the emergence of mass production of consumer goods. The Third Industrial Revolution is characteristic of the period from 1960 to 1995 when production automation took place using the advantages of

electronics and information technology. The main determinant of the fourth industrial revolution or digital economy becomes capable employees who develop new technological ideas and digitally innovate the business of enterprises.

Don Tapscott, one of the world's foremost authorities on the impact of technology on business and society, in his first published book on the digital economy in the world, *The Digital Economy: Promise and Peril in the Age of Networked Intelligence*, in which he points out that the digital economy represents an economy based on intellectual property and knowledge workers. He explains that in the digital economy, companies retain a competitive advantage only if their workers are constantly educated and acquire useful knowledge faster than competing companies. Useful knowledge, which should be in the

function of the new economy, refers, among others, to the intensive application of digital, i. e. information and communication technology in business, which creates radical changes in the understanding of business resources – from physical, tangible, to digital, electronic, or intangible. The intensive application of the digital way of doing business applies not only to technological features, but also to all economic activities, processes, structures, models, which ultimately means that the way economic value is created is radically changed [11]. On the occasion of the 20th anniversary of the first edition of this book, the aforementioned author published a second edition analyzing where he was right and what can be stated about the digital economy today. Interestingly, he very well predicted the development trends of the digital economy, but also confirmed the existence of negative sides of the digital economy, such as its impact on the labor market, privacy, social inequality, family ties, government, democracy and education [12]. The most relevant infrastructural factors of the digital economy are digital technologies, relating to the use of digital resources (technologies, algorithms and apps), through which digital goods in a computing environment are found, analysed, created, shared and used efficiently. Digital technologies may be classified into two groups, or more specifically as: [2] *primary* and *secondary*. The primary digital technologies that have transformed the world economy into a digital economy in the last few years are: [8] *mobile technologies, social networks, cloud computing, Internet of Things, IoT and big data analytics*. The mentioned primary digital technologies represent the convergent forces of digital disruption that significantly affect the changes taking place in the market. These forces are innovative and revolutionary on their own, but combined, they are radically transforming society and business, eliminating old business models and creating new digital leaders [9]. Apart from the primary ones, other – secondary digital technologies are often used, which include: *3D printers, robotics, drones, wearable technology and artificial intelligence*.

The main purpose of this article is to point out that the digital economy, as an economy that functions primarily through the aforementioned digital technologies, has caused the emergence of a wide range of digital products and services that can be distributed through digital business platforms. The paper points out the characteristics of goods and services in the digital environment, as well as certain differences compared to physical goods. Also, the existence of zero marginal cost for digital goods, which enables them to access a wide market area, is especially highlighted. Digital technologies have not only permitted the creation of many new goods or services, but has also dramatically changed the way an entire category of goods in the economy are created, produced, distributed, exchanged and consumed [7]. The paper elaborates on different ways of producing digital goods and special emphasis is placed on *in-house production, commons-based peer production (CBPP), and crowdsourcing*.

2. DIGITAL GOODS AND SERVICES

Speaking about the possibility of using digital technologies in developing modern and modifying existing products, authors often use the term "smart, connected products" [6]. According to their opinion, these products, apart from physical components, which include mechanical and electronic parts, also have the so-called "smart" components (sensors, software, operating system, user interface) and "connectivity" components. Thanks to these devices, networking and collecting a huge amount of data, these products can provide monitoring, control, optimization and autonomous functioning [3]. A *digital good*, also known as a digital product or digital asset, is a type of product or item that exists in a digital or electronic form, and it can be accessed, transmitted, or consumed primarily through digital devices and computer networks. Digital goods have several defining characteristics: 1. *no physical presence*: digital goods do not have a physical form. They are purely digital files or data that can be stored,

transmitted, and processed electronically; 2. *instant delivery*: they can be delivered or accessed almost instantly over the internet. For example, when you purchase and download a digital song or e-book, you can typically access it immediately; 3. *easy reproduction*: digital goods can be replicated or copied without any loss of quality. This makes it possible for the same digital good to be distributed to multiple users without the need for physical production or shipping; 4. *low marginal cost*: once created, the cost of producing additional copies of digital goods is typically very low or negligible. This is often referred to as "zero marginal cost", which will be discussed below.

Digital goods can be bought online, consumed immediately, and used without worry for their degradation or loss. All of a person's digital books, documents, music, photographs, and videos can be stored in one pocket-sized device, providing the individual access to a library of content anywhere at any time. Examples of digital goods include: digital music files (MP3s), e-books and digital publications, video games and downloadable content (DLC), software applications and programs, digital art and graphic design files, stock photos and images, online courses and educational materials. The digital goods market has grown significantly with the advent of the internet and digital technologies, allowing for the easy distribution and consumption of these digital products. Consumers can purchase, download, and use digital goods from various online platforms and stores.

Digital goods have proliferated widely. Digital photographs, for instance, were first commercialized in 1990 and now are taken more often than print photographs. Similar advances in technology have given rise to the widespread digitization of many other consumer goods, including books, magazines, newspapers, music, movies, and even academic journals [1]. Examples of digital goods that satisfy aforementioned definition include Microsoft Word documents, music tracks on Spotify, webpages on the Internet, apps on iPhone, Wikipedia articles, e-mails, data stored on electronic bank accounts, private data

stored on Dropbox accounts, and the list of apartments on an Airbnb web page. These goods are all virtual objects; they have value for someone; they can be replicated without any cost; and they can be delivered to consumers over the Internet. Examples of non-digital goods are computers, mobile phones, and mobile base stations. These goods have value for someone, but none of them are virtual objects; they have non-zero marginal cost and cannot be sent over the Internet.

On the other side, a *digital service* also known as an online service or web-based service, is a service that is provided over the internet or through digital platforms and does not require a physical presence. Digital services are intangible and are typically delivered electronically. They can encompass a wide range of offerings and functions, and they have become an integral part of the digital economy. Here are some key characteristics and examples of digital services: 1. *online delivery*: Digital services are delivered through the internet or other digital networks. Users can access these services from their devices, such as computers, smartphones, or tablets. 2. *no physical product*: Unlike traditional goods, digital services do not involve the production, distribution, or physical delivery of a tangible product. 3. *instant access*: Users can often access digital services immediately upon purchase or registration, making them convenient and accessible. 4. *subscription-based*: Many digital services operate on a subscription model, where users pay recurring fees for ongoing access to the service. Examples include streaming platforms like Netflix and software-as-a-service (SaaS) applications. 5. *global reach*: Digital services can be accessed from anywhere in the world, as long as there is an internet connection, making them accessible to a global audience. Examples of digital services include:

1. *Streaming Services*: Platforms like Netflix, Amazon Prime Video, Spotify, and YouTube offer digital streaming services for movies, TV shows, music, and other media content.

2. Social Media Platforms: Social networking sites like Facebook, Twitter, Instagram, and LinkedIn provide digital services for connecting with others, sharing content, and networking.

3. Cloud Computing Services: Providers like Amazon Web Services (AWS), Microsoft Azure, and Google Cloud offer digital services for cloud storage, computing, and infrastructure.

4. Online Banking and Financial Services: Banking, payment processing, and investment services are increasingly offered online.

5. E-learning and Online Education: Platforms like Coursera, edX, and Khan Academy offer digital educational services and courses.

6. Software as a Service (SaaS): SaaS companies provide digital services through web-based software applications, such as Google Workspace (formerly G Suite), Microsoft Office 365, and Salesforce.

7. Digital Marketing Services: Services related to online advertising, search engine optimization (SEO), and social media marketing fall into this category.

8. Telemedicine and Telehealth: Remote healthcare services, including virtual doctor's appointments and medical consultations, are delivered digitally.

Digital goods and services are different from physical products (or tangible goods). Physical products are tangible products that have a physical presence. They can be touched, seen, and physically handled. They are typically manufactured, packaged, and physically shipped to consumers or retailers. Physical goods require physical storage space, whether in warehouses, stores, or homes. Businesses often need to manage inventory levels to meet demand and avoid overstocking or stockouts. Shipping and distribution logistics are necessary to deliver physical goods to customers. Customers can physically return or exchange defective or unwanted physical goods. On the other side, digital goods are intangible and exist in digital form as data or files. They have no physical presence. They can be delivered or accessed electronically over the

internet and are available almost instantly. There is no need for manufacturing, packaging, or physical shipping, which reduces costs. Digital goods do not require physical storage space. Since they are not physical, there is no need for inventory management. Once downloaded or accessed, digital goods are not typically returnable or exchangeable due to their replicable nature.

3. Classification of digital goods

The usual classification of goods can be done on the basis of two basic characteristics: [4] 1. Is exclusivity characteristic of a certain good? Can people be prevented from using it? and 2. Is rivalry inherent in a certain good? Does one person's use of a good reduce another person's ability to use it? Excludability and rivalry help economists and policymakers understand how goods are consumed and shared within society. *Excludability* refers to the degree to which consumption of a good or service is limited to paying customers. *Rivalry* in consumption refers to the degree to which one person consuming a particular unit of a good or service precludes others from consuming that same unit of a good or service. A excludable good is such that it is possible to prevent consumers from accessing or using the good. A non-excludable good is such that consumers cannot be prevented from accessing or using the good. A good is classified as rival if it is reduced in quantity after consumption or if the usage of the good prevents others from using it. A non-rival good is the opposite of a rival good; it is neither reduced by consumption nor does the usage of the good prevent others from using it [5]. From these characteristics, four different types of goods based on excludability and rivalry, can be classified either as private goods, public goods, club goods, or common-pool resource [10].

On one side, private goods are excludable, meaning it is possible to prevent individuals who have not paid for the good from consuming it. Private goods are rivalrous, meaning consumption by one individual reduces the quantity available for others. Public goods are non-excludable, meaning it is difficult or impossible to exclude individuals from

enjoying the benefits of the good, even if they haven't paid for it. Public goods are non-rivalrous, meaning consumption by one individual does not reduce the quantity available for others. On the other side, club goods are excludable, meaning access to the good can be restricted, and individuals can be charged for its use. Club goods are non-rivalrous or have low rivalry, meaning consumption by one individual has little or no impact on the availability for others. Common-pool resources are non-excludable, meaning it's challenging to exclude individuals from using them. Common-pool resources are rivalrous, meaning consumption by one individual diminishes the quantity available for others.

Understanding the excludability and rivalry characteristics of digital goods and services is important for various reasons, including pricing models, copyright and intellectual property considerations, and the design of digital platforms and services. These characteristics can also impact the business models and strategies of companies in the digital economy. Figure 1 provides examples of digital goods and services classified according to the aforementioned classification.

Digital goods and services can also be classified based on the concepts of excludability and rivalry, similar to physical goods. Here's how digital goods fit into these categories: [5]

1. **excludable and rivalrous digital goods:**

Some digital goods are excludable, meaning access to these goods can be restricted, and individuals can be charged for their use. These digital goods are rivalrous, meaning consumption by one individual reduces the availability or quality of the good for others. Online multiplayer video games and certain premium software applications are excludable and rivalrous. To access these goods, users typically need to purchase a license or subscription, and when one user is actively playing or using the software, it may not be available to others simultaneously.

2. **excludable and non-rivalrous digital goods:**

These digital goods are excludable,

meaning access can be restricted, and users can be charged for their use. Consumption by one individual does not reduce the availability or quality of the good for others. E-books, digital music, and software downloads often fall into this category. Once purchased or licensed, users can access these goods without diminishing their availability to others.

3. **non-excludable and rivalrous digital goods:** These digital goods are non-excludable, meaning it's challenging to prevent individuals from accessing them, even if they haven't paid for them. Consumption by one individual reduces the availability or quality of the good for others. Peer-to-peer file-sharing networks and certain online forums or communities may host content that is non-excludable and rivalrous. Users can access and share such content freely, and heavy usage can lead to slower access or degradation of the content's quality.

4. **non-excludable and non-rivalrous digital goods:** These digital goods are non-excludable, meaning it is challenging or impossible to exclude individuals from enjoying the benefits of the good. Consumption by one individual does not reduce the availability or quality of the good for others. Publicly available information on the internet, open-source software, and some forms of online content (like freely accessible educational resources) are non-excludable and non-rivalrous digital goods. They are accessible to anyone without restrictions.

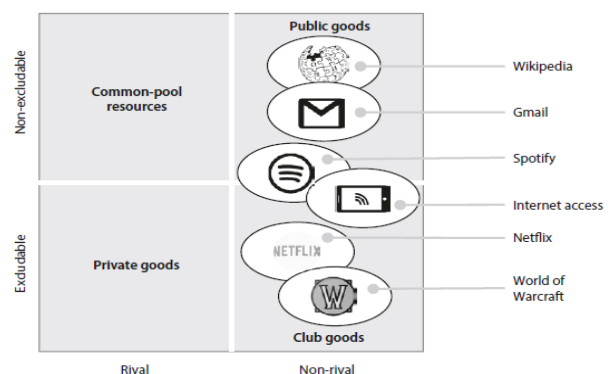


Figure 1. Classification of digital goods

Digital goods that are both non-rivalrous and non-excludable fall into the category of public goods. A good is non-rival in consumption if the consumption activity of each consumer does

not decrease the quantity of good available in the economy.

A good is non-excludable if no one can be prevented from consuming it [7]. Public goods hold a special place in economic theory because they often encounter market failures, necessitating governmental regulation or other interventions to ensure proper market functioning. One key reason for this market failure is the "free rider" problem. Public goods can be accessed by anyone without requiring payment, which creates a situation where private actors lack incentives to provide these goods, and users have no motivation to pay for access or usage to sustain the public good. An exemplar of a public good in the digital realm is Wikipedia, which offers a free online encyclopedia. Private actors typically find few financial incentives to support or invest in Wikipedia. Instead, Wikipedia primarily relies on two income sources to sustain its operations: financial donations from benefactors and voluntary contributions from authors who write and update articles. In contrast to public goods, common-pool resources are susceptible to the "tragedy of the commons," a scenario in which shared resources are overused and depleted. Despite individuals acting in their self-interest, the collective behavior of all individuals can lead to the overuse or depletion of these resources. Examples of this tragedy in real life include overfishing in the oceans and air pollution. The concept of the tragedy of the commons also extends to the digital economy, even though digital goods and services are inherently non-rivalrous. Given the near-zero marginal cost and close-to-unlimited supply of digital goods and services, the tragedy of the commons manifests differently in the digital realm. This can result in issues such as the dissemination of unwanted and illegal information and content, spam, denial-of-service attacks, and service abuse, as outlined by Øverby and Audestad in 2018.

3. ZERO MARGINAL COST

One of the fundamental characteristics of digital goods is their zero or near-zero marginal

cost. This means that the cost of producing additional copies or units of a digital good is extremely low once the initial creation or development has occurred. Here's why this characteristic is significant: *no physical production costs*: Unlike physical goods that require materials, manufacturing, and transportation, digital goods are created and stored as digital files or data. There are no costs associated with physical production or distribution; *easy replication*: Digital goods can be duplicated or copied at almost no cost. Whether you're downloading a software application, streaming a video, or sharing a digital file, making additional copies doesn't require additional resources or expenses; *scalability*: Digital goods can be distributed to a large number of users without significantly increasing production or distribution costs. This scalability is a key advantage for digital businesses; *global distribution*: Since digital goods are transmitted electronically, they can be distributed globally with minimal additional cost. This allows for worldwide access and reach; *flexible pricing models*: The low marginal cost of digital goods has led to various pricing models, such as subscription services, freemium models, and one-time purchases, where the pricing is often based on perceived value rather than production cost.

Indeed, there is a stark contrast between the marginal cost associated with physical goods and that of digital goods. For physical goods, the production cost encompasses expenses like raw materials (such as steel or plastic), labor, and logistics. This means that the cost of creating each additional physical unit increases with each unit produced. Even in e-commerce businesses like Amazon, which primarily operate online, there is a notable marginal cost attributed to the shipping and handling of physical goods. In contrast, digital trade transactions have a marginal cost of essentially zero. This is a significant advantage of digital goods. While digital goods may have substantial fixed costs, which can include expensive development, building, and operational expenses (such as software development costing millions of US dollars,

requiring large development teams, and taking several years from concept to finished product), these fixed costs do not necessarily translate into direct charges to consumers. The business model of the company plays a crucial role in this regard. For example, companies like Facebook and Google have high ongoing operational costs, but they do not pass these costs directly to users. Instead, they generate revenue indirectly by collecting extensive user data and selling it to advertisers for targeted advertising or to other data processing firms for various purposes. This approach raises significant privacy concerns. The discrepancy between fixed and marginal costs is a defining characteristic of digital goods. Take the example of an app: the primary cost is in its development, which can span from a few days to several years. As mentioned, the marginal cost of each additional copy of a digital good, such as the app, is effectively zero. Therefore, distributing copies of the app, even for free, does not result in financial loss for the developer. Once total sales cover the development costs, subsequent sales contribute directly to profits, making digital goods highly profitable in the long run.

Under these conditions, the average cost of a copy of the digital good equals:

$$AC = \frac{F}{n} + MC = \frac{F}{n},$$

where AC is the average cost, F is the fixed costs, n is the number of copies of the good produced during its lifetime, and MC is the marginal cost. Figure 1.1 shows the average cost as a function of n . Observe that the average cost approaches zero as n gets large.

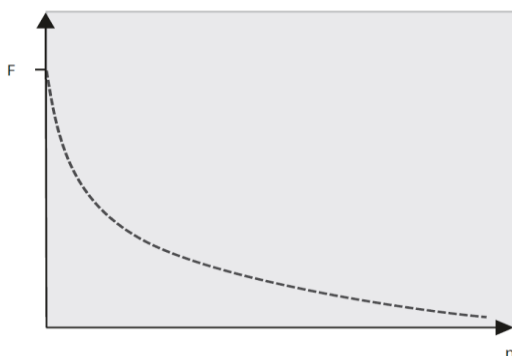


Figure 2. The average cost as a function of the number of units produced

Economies of scale are the cost advantages that companies obtain as the number of units produced increases. This is so because the fixed cost per unit decreases as the production volume increases as shown in . Fig. 2 and may tend to zero if the number of units produced is large. Companies producing physical goods benefit from cost advantages as the number of units produced increases only up to a certain point. The marginal cost per unit produced is independent of production volume and sets a lower limit for the cost of the product. Moreover, expanding the production beyond a certain threshold may also necessitate that more production infrastructure must be built, thereby increasing the cost of administration and support- functions so that the benefits from economies of scale are marginalized. This is different in the digital economy. This is so because the marginal cost is zero and that there is no limit to the number of units that can be produced without increasing the fixed costs. Hence, the cost per unit produced will be zero independently of the production volume. This is one of the reasons why companies producing digital goods and service get so big [5].

4. PRODUCTION MODELS

The general characteristics of digital goods generate new ways of production. The key distinction from physical products is that digital products can be created through online collaboration, leading to entirely new production methods. In this context, production encompasses both product development and the subsequent processes of production and distribution to customers. There exist multiple avenues for the development and production of digital goods, with three fundamental methods being *in-house production*, *commons-based peer production (CBPP)*, and *crowdsourcing*. Production relying on CBPP and crowdsourcing occurs predominantly on the Internet.

The three fundamental production models are not mutually exclusive, as a company may employ a combination of them when creating and delivering a digital service. In this context,

it's important to recognize that some digital services can be relatively straightforward to develop, requiring minimal resources. This category includes even large-scale services such as the World Wide Web, Facebook, Airbnb, and TCP/IP. However, certain digital services demand extensive collaboration from hundreds of individuals over extended periods. Examples of such services encompass the development of operating systems like UNIX and Linux, public mobile networks (GSM, 3G, 4G, and 5G), and local access networks (Wi-Fi, WiMAX, Ethernet, and Bluetooth) [5].

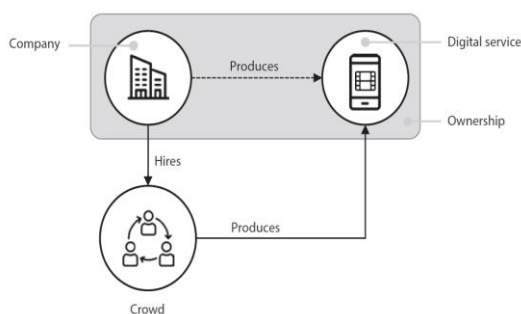
In-house production of digital goods refers to the practice of creating digital goods or content within an organization or company, using its own resources and personnel rather than outsourcing or purchasing these digital assets from external sources. This approach is common in various industries and has several advantages. When an organization produces digital goods in-house, it has direct control over the quality and standards of the content or product. This ensures that it meets the company's specific requirements and brand standards. In-house production allows for customization and tailoring of digital goods to align with the organization's unique needs, objectives, and target audience. Depending on the scale and frequency of content creation, in-house production can be cost-effective over the long term, as there may be reduced reliance on external vendors or content providers. The organization retains full ownership of the intellectual property rights associated with the digital goods created in-house, providing more control over licensing, distribution, and monetization. In-house teams can respond quickly to changing market conditions, trends, and audience demands, resulting in faster content production and release. Sensitive or proprietary information can be better protected when production is kept in-house, reducing the risk of data breaches or leaks.

Commons-based peer production (CBPP), sometimes referred to as social production, is an approach to creating digital goods in a collaborative and decentralized manner. In the context of digital goods, CBPP involves

individuals and communities coming together to produce and share digital content, software, or other digital assets. CBPP in the realm of digital goods involves a networked community of contributors who collaborate to create digital products, such as open-source software, online content (like Wikipedia), or digital art. These contributors often work together voluntarily and share their expertise and efforts. Digital goods produced through CBPP are typically made available with open access principles. This means that the resulting digital products are often released under open licenses, allowing anyone to use, modify, and distribute them freely. CBPP relies on peer-to-peer interaction, where participants interact directly with one another to contribute, review, and improve the digital goods. This collaborative process is facilitated by online platforms and tools. CBPP projects often involve community governance models, where participants collectively make decisions about the direction of the project. Decisions may be made through discussions, consensus-building, or other democratic processes. CBPP is widely seen in the digital world. Examples include open-source software development communities like Linux, collaborative content platforms like Wikipedia, and online communities where digital artists or musicians share their creations openly. Participants in CBPP projects are often motivated by intrinsic factors, such as a passion for the subject matter, a desire to contribute to a shared cause, or the satisfaction of seeing their work benefit others. Monetary rewards are not always the primary motivation. CBPP has led to the creation of high-quality digital goods that are freely accessible to a wide audience. It has played a significant role in the development of open-source software, the growth of free knowledge resources, and the promotion of digital creativity. While CBPP has many advantages, it can also face challenges, including sustaining participation over time, addressing governance issues, and ensuring the long-term sustainability of digital goods and communities. The most famous example of the CBPP model is the operating system Linux in which hundreds

of computer scientists contributed to the evolution of the Linux software over many years. Wikipedia is also the result of the CBPP model—no one is coordinating the content or the evolution of the encyclopedia. Arbitrary readers are checking the validity of the articles, correcting errors, adding novel material, and writing new articles (Øverby & Audestad, 2018).

Crowdsourcing is a production model of digital goods that leverages the collective intelligence, skills, and contributions of a large and often decentralized group of individuals or a "crowd" to create digital products, services, or content. In the context of digital goods, crowdsourcing involves soliciting input, ideas, labor, or resources from a broad online community. In the crowdsourcing production model, both organizations and individuals collaborate to create digital services by motivating the general public to contribute to the project. This might initially appear similar to outsourcing, but there's a crucial distinction between the two. Outsourcing typically involves contracting work to another company under formal commercial and legal agreements. In contrast, crowdsourcing entails enlisting the efforts of diverse groups of individuals without the formalization seen in outsourcing arrangements. Crowdsourcing can yield results that are more diverse and less predictable, but it also has the potential to generate superior, cost-effective, and highly adaptable solutions. Because numerous participants can engage in the project, it's more likely that design flaws will be identified at an early stage, leading to the discovery of improved and more cost-effective designs. The crowdsourcing production model is depicted in Figure 3.



Source: (Øverby & Audestad, 2018)

Figure 3. The crowdsourcing production model

Crowdsourcing is a form of peer production. The difference is that CBPP may follow arbitrary development paths sometimes resulting in a viable product, whereas a crowdsourcing project aims at developing a predefined product. Crowdsourcing may be used in any stage of product development from the initial idea to development, production, testing, and marketing. The prerequisite is that the collaboration can take place over the Internet. A company may use crowdsourcing at all stages of production or only parts of production, leading to a final digital service.

5. CONCLUSION

The traditional production method is in-house production in which the entire production of the good takes place within the company. This method is used for almost all physical products. This is also the dominating production method in the digital economy. Microsoft, Facebook, Google, Netflix, and all the other big companies in the digital economy base their production method on in-house production. In-house production of digital goods offers advantages in terms of quality control, customization, and cost efficiency. However, it also comes with resource and expertise requirements, and organizations need to carefully assess their specific needs and capabilities to determine the most suitable production approach. CBPP is a collaborative and open approach to producing digital goods, fostering communities of individuals who work together to create valuable assets that can benefit society while adhering to principles of open access and shared ownership. The Internet has created more flexible production methods based on collaboration over the network. Commons-based peer production (CBPP) is founded on voluntary participation and takes place without (or with only little) central coordination. This has led to large projects such as Linux, digitization of books and documents, development of free and open-source software (FOSS), and production of technical standards and recipes. CBPP has created vast amounts of freely available

resources such as statistics, encyclopedia, software, and digital books and documents. Crowdsourcing implies that a firm invites individuals to participate in the development or production of a good. The project is managed by the firm, but the work is done by a group of arbitrary individuals. Crowdsourcing does not depend on the Internet but is facilitated by it. Crowdsourcing offers an innovative and cost-effective way to tap into the collective wisdom and creativity of diverse online communities to produce a wide range of digital goods. It has played a significant role in democratizing digital content creation and problem-solving.

REFERENCES

- [1] Atasoy, O., & Morewedge, C. K. (2017). Digital Goods Are Valued Less Than Physical Goods. *Journal of Consumer Research*, 44(6), 1343-1357.
- [2] Kahrović, E., & Avdović, A. (2023). Impact of Digital Technologies on Business Performance in Serbia. *Management: Journal of Sustainable Business and Management Solutions in Emerging Economies*, 28(2), 37-53. doi:10.7595/management.fon.2021.0039
- [3] Kahrović, E. (2023). Business Strategy in the Digital Economy. *International May Conference on Strategic Management – IMCSM23* (pp. 1-9). Bor: University of Belgrade, Technical Faculty in Bor, Engineering.
- [4] Mankju, G. N. (2013). *Principi ekonomije*. Beograd: Centar za izdavačku delatnost Ekonomskog fakulteta u Beogradu.
- [5] Øverby, H., & Audestad, A. J. (2018). *Introduction to Digital Economics*. Springer.
- [6] Porter, M., & Heppelmann, E. (2014). How Smart, Connected Products Are Transforming Competition. *Harvard Business Review*, 92(11), 64-88.
- [7] Rayna, T. (2008). Understanding the Challenges of the Digital Economy: The Nature of Digital Goods. *Communications & Strategies*(71), 13-16.
- [8] Rogers, D. (2016). *The Digital Transformation Playbook: Rethink Your Business for the Digital Age*. Columbia Business School Publishing.
- [9] Schwertner, K. (2017). Digital transformation of business. *Trakia Journal of Science*, 15(1), 388-393.
- [10] Stiglitz, J. (2015). *Economics of the public sector*. W. W. Norton & Company.
- [11] Tapscott, D. (1995). *The Digital Economy: Promise and Peril in the Age of Networked Intelligence*. New York: McGraw-Hill.
- [12] Tapscott, D. (2015). *The Digital Economy ANNIVERSARY EDITION: Rethinking Promise and Peril in the Age of Networked Intelligence*. New York: McGraw-Hill Education.

SPMS/ICPES 2023

**39TH INTERNATIONAL CONFERENCE ON
PRODUCTION ENGINEERING OF SERBIA**

**SESSION 2:
MATERIALS, METAL FORMING, CASTING AND WELDING**

Novi Sad, 26 – 27 October 2023



Society of Production
Engineering

SPMS 2023

39. Savetovanje proizvodnog mašinstva Srbije

ICPES 2023

39th International Conference on Production Engineering of
Serbia



Faculty of Technical
Sciences
University of Novi Sad

Novi Sad, Serbia, 26. – 27. October 2023

MECHANICAL PROPERTIES VARIATION DUE TO BUILDING ORIENTATION OF ABS RESIN MATERIAL

Božica BOJOVIĆ^{1*}, Zorana GOLUBOVIĆ¹, Ivana JEFTIĆ², Žarko MIŠKOVIĆ¹, Aleksandar SEDMAK¹

¹University of Belgrade, Faculty of Mechanical Engineering, Belgrade, Serbia

²Innovation Centre of Faculty of Mechanical Engineering, Belgrade, Serbia

*Corresponding author: bbojovic@mas.bg.ac.rs

Abstract: Considering that additive manufacturing technology, has evolved significantly over the past few decades, understanding of materials mechanical properties became important part of researches with the goal of further improvement of production. Among the seven different AM technologies, in this research is used digital light processing (DLP) 3D printing process with LCD projector. The thermoplastic polymer material acrylonitrile butadiene styrene (ABS) is a widely used material for 3D plastics printing, and in this study, it is chosen in the resin form. So far, this type of material has not been sufficiently studied, and the aim of this study was to determine the mechanical properties for two different specimens' building orientations (45° and 90°). Specimen's geometry is chosen according to the respective standards for mechanical testing's. Because of the difficulties and warping which occur when printing the flat, thin and long specimens, orientation 'on edge', i.e., 90° is chosen, as well as the 45° orientation, for comparison. Tensile, three point bending and compression mechanical tests were performed and Matlab is used to create stress-strain curves. Additionally, microscopy is performed for more comprehensive insight of the behaviour of the ABS resin printed via DLP-LCD technology. Comparison of mechanical properties for two orientations leads to the overview of printing parameters which result in better mechanical properties regard to specific application. Better behaviour and compression mechanical properties are noticed in 90° orientation printed ABS resin specimens, compared to 45° ones, while flexure behaviour of ABS is the same regardless to building orientation.

Keywords: additive manufacturing, DLP-LCD, ABS resin, mechanical properties, microscopy.

1. INTRODUCTION

Additive manufacturing (AM), also known as 3D printing, has been developing since the 1980s and has quickly become an important technology with various applications in different industries e.g. in the automotive, aerospace, equipment, or medical industry [1,2,3]. Polymer based AM technology enables cost-effective manufacture in small batches of

user-specific products regarding their shape, size and aesthetics [4].

According to the ISO/ASTM 52900:2021 standard, there are seven types of AM technologies. Among them vat polymerisation technology was chosen, particularly Digital Light Processing (DLP) technology due to versatility and low energy demand [4,5].

The latest developed 3D printing vat technology is DLP-LCD. Photosensitive liquid

polymer is exposed to projections of UV light emitted by a digital projector that uses LCD device in which each pixel acts as a small window that blocks or let's light through. Projected image of the entire layer solidifies through photo-polymerization at once. For highly-detailed parts made by DLP-LCD the various photopolymers are available: ABS-like, rigid PC-like, semi-flexible PE-like, durable PP-like [4,6].

Overall, the preferred AM material is Acrylonitrile Butadiene Styrene – ABS and variations of it [4]. Therefore, for research is chosen ABS-like photopolymer suitable for DLP-LCD. ABS-like resin consists of three parts, acrylonitrile-styrene copolymer, SAN in the matrix and grafted polybutadiene rubber in a dispersed phase.

For the ABS specimens were reported that raster orientation largely affects the mechanical properties [5]. Various raster angle orientations (0° , 90° , 45° , -45°) were investigated and the majority of results are by utilizing the FDM technology. Rankouhi et al. suggested that 0° raster angle ensures the highest tensile strength [7]. Ziemian et al. suggested 0° raster orientation for the largest flexural yield strength, and for the highest compression strength suggests axial build orientation [8]. Exploitation of viscous materials for 3D printing suggests that 90° raster angle gives better mechanical properties [9]. Naik and Kiran were testing the various building on-edge orientations (0° , 15° , 30° , 45° , 60° , 75° , 90°) of specimens printed by photo-polymerisation technology, and confirmed better tensile properties in case of on-edge than in case of flat building orientation [11]. Brighenti et al. examined fracture toughness were it was concluded that maximum mode I fracture toughness was for 0° specimen orientation. Decrease of the fracture toughness happens for the orientation of 90° , which is logic because of the arrangement of the printed layers parallel to the crack plane [12].

The objective of this research was to examine the mechanical properties obtained by tensile, three point bending and compression testing of ABS similar resin samples build using

DLP-LCD printing technology. Additionally, specimens were 3D printed in two different building orientations in order to compare mechanical properties for two cases. Microscopy was performed to get a better overview of the material properties.

2. METHODOLOGY

Specimens were modelled in SOLIDWORKS software in compliance with the specified standards ISO 527-2, ISO 178:2019 and ISO 604:2002 for tensile, flexure and compression respectively (see Fig1). ABS like resin material (Crealty, Shenzhen, China) was used for common desktop DLP-LCD 3D printer (Crealty LD-002R, Shenzhen, China). Five specimens were printed with 100% infill density, per two print orientations (90° and 45°) that are presented as ChituBox screenshots in Figure 1.

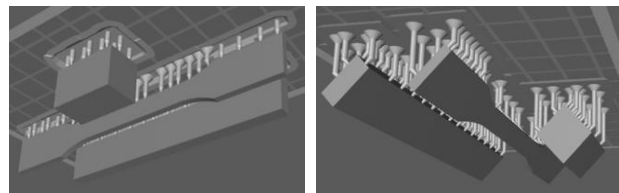


Figure 1. Specimens' STL models according to ISO 527-2, ISO 178:2019 and ISO 604:2002 standards in two building orientations: left -90° , right -45° .

Since the flattened dog-bone shape parts' orientation is problematic because it's the flat, thin and long part, the building orientation of 90° is chosen as the quickest one, considering building time. Building orientation of 45° is chosen as the comparing orientation. The main printing parameters were the same: exposure time – 8s, bottom exposure time – 80s, layer height – 0.05mm, lift distance – 5mm, lift and retract speed – 100mm/min. After printing, all the specimens were stored and tested at room temperature of 23°C and humidity of 55% RH.

Universal testing machine Shimadzu AGS-X (Shimadzu Corp., Kyoto, Japan) with load cell of 100 kN and the testing speed of 1 mm/min was used for the three type of mechanical testing.

After tensile, flexure and compression testing, the microscopy was performed using a digital optical microscope (Mustool, Shenzhen, China). Obtained images of the fractured

surfaces provide qualitative assessment of the material's structure.

3. RESULTS AND DISCUSSION

Visual inspection before and after mechanical testing were performed. DLP-LCD built specimens of ABS resin material are more rubbery and have a silicon-like touch effect. This effect is quite unexpected, since ABS material in filament form is more like firm plastic. A representative specimen of each mechanical test showed the brittle fracture: (a) in a normal direction to the tensile stress localized in adequate position at narrowing part of geometry (Figure 2a); (b) in a middle of specimens with either clear and straight fracture line for on-edge printing specimen, or step-like fracture line for slanted printed specimen (Figure 2b); (3) after the initial barrelling, splinters separate from conical core (Figure 2c).

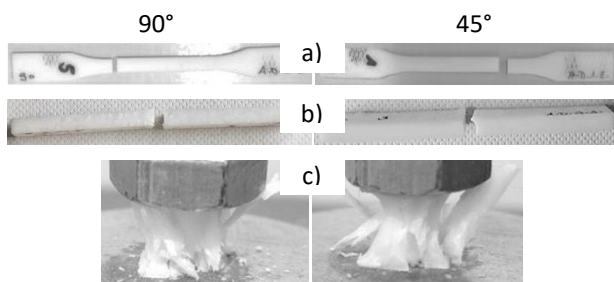


Figure 2. Fractured specimens printed by DLP-LCD after: a) tensile, b) flexure and c) compression testing.

2.1 Microscopy

Digital optical microscopy is used in order to additionally observe topography and morphology of examined specimens at magnification 50x. Similarity in fractured surfaces' appearance for the both orientations is expected and obvious, as it can be seen in Figure 3. DLP-LCD prints isotropic material regardless to building orientation.

Fractured surface of the tensile specimen built on-edge exhibits irregularities in shape of bubbles, which are in a middle of image in Figure 3a-left. The bubbles have been found quite often in ABS resin parts and caused fracture in that specific region. Tensile tested

specimen built in 45° orientation has slanted striation at fractured surface that evolves along layers (Figure 3a-right side).

Two zones can be differentiated on the fractured surfaces of 3 point bended specimens: (1) ductile zone with striation and (2) the brittle zone as dark, flat and shiny (Figure 3b). Distinction between orientations is mainly in stair-like fractured surface in case of slanted building orientation (Figure 2b-right and Figure 3b-right).

The sharp splinters in Figure 3c) confirm brittle mode that compressed specimens undertake. Splinters could be monolith spear-like (Figure 3c-left) altogether with layers or tiny spikes separated from core, which has stress lines along shiny zone (see Figure 3c-right).

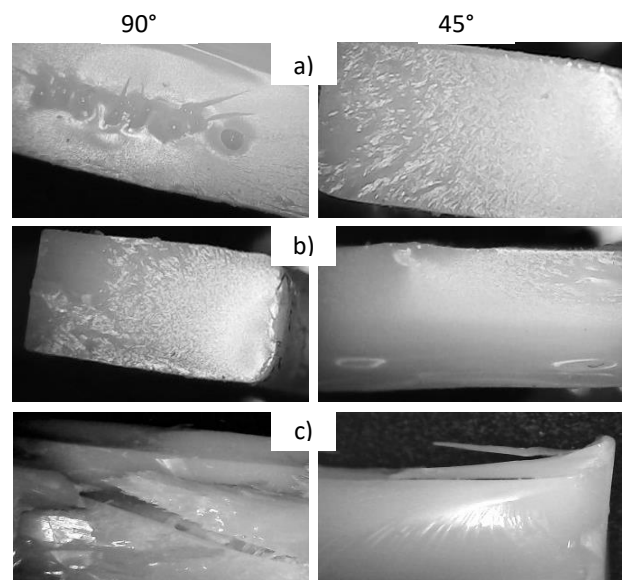


Figure 3. Fractured surfaces of DLP-LCD printed specimens after: a) tensile, b) flexure and c) compression testing.

2.2 Mechanical testing

The charts, which are presented in Figure 4, show average values along with standard error of main mechanical properties for each type of testing. Mechanical properties for flexural testing have similar values regardless to building orientation. Flexure modulus is the highest compared to the tensile and compressive. Tensile modulus for on-edge specimen is higher compared to slanted printed specimen. Oppose to it, compressive modulus is lower for on-edge specimen compared to

slanted printed one. Ultimate stress and max strain values are the highest in case of compression compared to other tests regardless to building orientation. Tensile and compressive ultimate stress for building orientation of 90° are higher than for 45° orientation. Strain value for building orientation of 90° is lower for tensile and higher for compressive test.

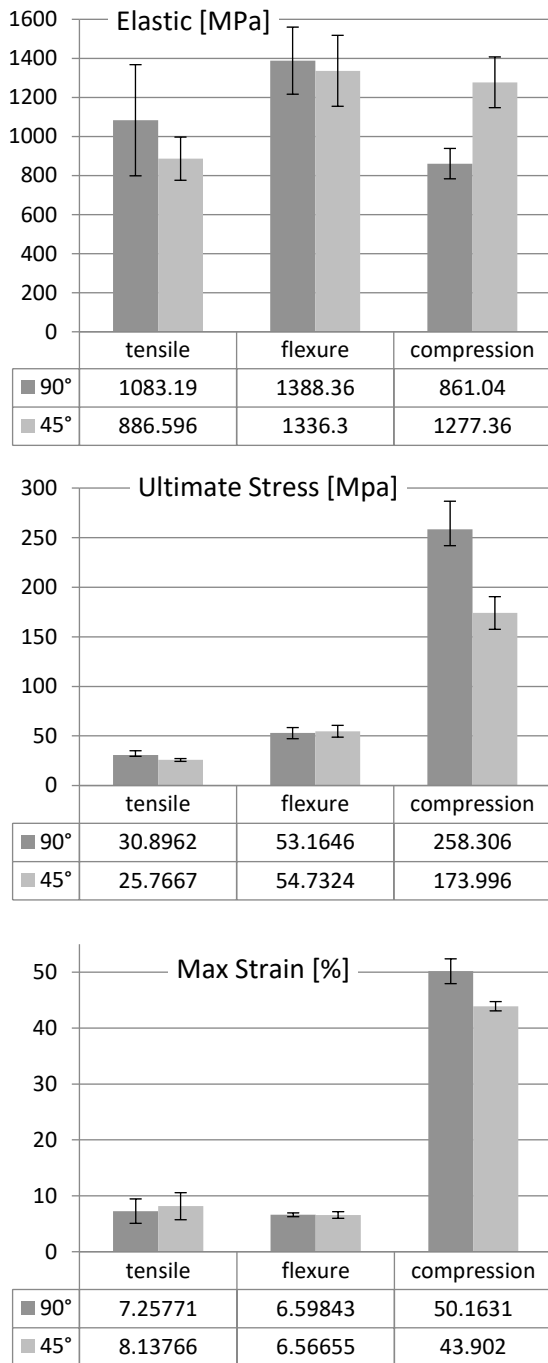


Figure 4. The main mechanical properties of ABS specimens DLP-LCD printed in two building orientations.

Matlab software was used to compute the average stress–strain curves for five ABS specimens that undertake each of three mechanical tests. The curves dedicated to DLP-LCD built specimens in particular orientation have same line type at diagrams (Figure 5).

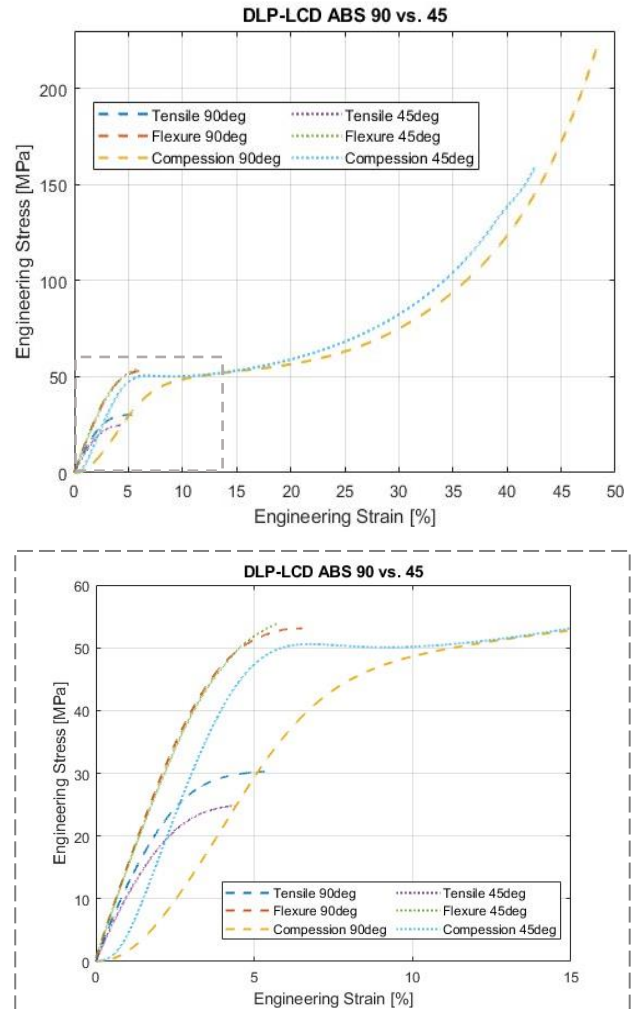


Figure 5. Stress-strain curves of DLP-LCD printed specimens made of ABS resin in two building orientations.

Specimens reveal slightly different stress-strain curves under tension, where on-edge building orientation shows better behaviour. Comparison of curves' slope in zoomed Figure 5, shows concurrence in flexure, divergence in tensile, and initial disparity in compression case. Regardless to printing orientation, specimens demonstrate same behaviour for flexure and very similar values of mechanical parameters. Generally, mechanical testing perceives dominant behaviour under compression, especially for 90° building orientation since the max strain value is 50% and ultimate stress is

higher 5 to 8 times compare to flexure and tensile respectively.

4. CONCLUSION

It should be noted that

The mechanical properties compared in charts reveal:

- similar values regardless to building orientation for flexural case,
 - dominant behaviour under compression, especially for 90° building orientation,
 - flexure modulus is the highest in comparison with tensile and compressive,
- Generally, DLP-LCD printed ABS parts are more appropriate for compression applications. In case of flexure applications printed parts are suitable, regardless to building orientation. Whenever possible, 3D printed part should align the load/stresses in a part with the strongest orientation. This research provide additional notion regarding building orientation.

ACKNOWLEDGEMENT

This research was financially supported by the Ministry of Education, Science and Technological Development of the Republic of Serbia by Contract No. 451-03-47/2023-01/200105 from 03.02.2023.

REFERENCES

- [1] S. Thiede, M. Wiese, C. Herrmann, L. Marşavina: Upscaling strategies for polymer additive manufacturing: an assessment from economic and environmental perspective for SLS, MJF and DLP, *Procedia CIRP*, Vol.104, pp.653–658, 2021.
- [2] A. Al Rashid, W. Ahmed, M. Y. Khalid, M. Koça: Vat photopolymerization of polymers and polymer composites: Processes and applications, *Additive Manufacturing*, Vol. 47 102279, 2021.
- [3] M. Wiese, A. Kwaukaa, S. Thiedeb, C. Herrmann: Economic assessment for additive manufacturing of automotive end-use parts through digital light processing (DLP), *CIRP Journal of Manufacturing Science and Technology*, Vol. 35, pp. 268–280, 2021.
- [4] T. Kermavnar, A. Shannon, L. W. O’Sullivan: The application of additive manufacturing/3D printing in ergonomic aspects of product design: systematic review, *Applied Ergonomics*, Vol. 97, 103528, 2021.
- [5] J. C. Dizona, A. H. Espera, Q. Chena, R. C. Advincula: Mechanical characterization of 3D-printed polymers, *Additive Manufacturing*, Vol. 20, pp. 44–67, 2018.
- [6] D.M. Shah, J. Morris, T.A. Plaisted, A.V. Amirkhizi, C.J. Hansen: Highly Filled Resins for DLP-based Printing of Low Density, High Modulus Materials, *Additive Manufacturing* Vol. 37, 101736, 2020.
- [7] B. Rankouhi, S. Javadpour, F. Delfanian: Failure Analysis and Mechanical Characterization of 3D Printed ABS With Respect to Layer Thickness and Orientation, *J Fail. Anal. and Preven.* Vol. 16, pp. 467–481, 2016.
- [8] C. Ziemian, M. Sharma, S. Ziemian: Anisotropic mechanical properties of ABS parts fabricated by fused deposition modelling, *Mechanical engineering*, Vol. 23, pp. 159-180, 2012.
- [9] F. D. Siacor, Q. Chen, J. Y. Zhao, L. Han, A. D. Valino, E. Taboada, E. B. Caldon, R. C. Advincula: On the additive manufacturing (3D printing) of viscoelastic materials and flow behavior: From composites to food manufacturing, *Additive Manufacturing*, Vol. 45, 102043, 2021.
- [10] D.L. Naik, R. Kiran: On anisotropy, strain rate and size effects in vat photopolymerization based samples, *Additive Manuf.* Vol. 23, pp.181–196, 2018.
- [11] Y. Wang, X. Li, Y. Chen, C. Zhang: Strain rate dependent mechanical properties of 3D printed polymer materials using the DLP technique, *Additive Manufacturing*, Vol. 47, 102368, 2021.
- [12] R. Brighenti., L. Marsavina, M. Marghitas, M. Montanari, A. Spagnoli, F. Tatar: The effect of process parameters on mechanical characteristics of specimens obtained via DLP additive manufacturing technology, *Materials Today: Proceedings* 78, 331–336, 2023.



Society of Production
Engineering

SPMS 2023

39. Savetovanje proizvodnog mašinstva Srbije

ICPES 2023

39th International Conference on Production Engineering of
Serbia



Faculty of Technical
Sciences
University of Novi Sad

Novi Sad, Serbia, 26. – 27. October 2023

THE EFFECT OF CRITICAL WATER CONCENTRATION ON THE EMBRITTLMENT OF AUSTEMPERED DUCTILE IRONS

Petar JANJATOVIC¹, Dragan RAJNOVIC¹, Sebastian BALOS¹, Miroslav DRAMICANIN¹,
Olivera ERIC CEKIC², Milan PEĆANAC¹, Danka LABUS ZLATANOVIC¹, Lepasava SIDJANIN¹

¹Department of Production Engineering, Faculty of Technical Science, University of Novi Sad,
Trg Dositeja Obradovica 6, 21000 Novi Sad, Serbia

²Department of General Engineering Education, Faculty of Mechanical and Civil Engineering in
Kraljevo, University of Kragujevac, Dositejeva 19, 36000 Kraljevo, Serbia

*Corresponding author: janjatovic@uns.ac.rs

Abstract: In this work, the influence of different water concentrations on the mechanical tensile properties of ADI material with a fully ausferrite microstructure was studied. The concentration of water in ethyl alcohol was 0.2; 4; 10 vol.%. Also, the samples were tested both in 100 vol.% water and in a dry condition. The values obtained by testing in the dry state are used as reference. The ADI material with an ausferrite microstructure was produced by heat treatment consisted of austenitizing at a temperature of 900 °C for 2 hours, followed by isothermal transformation at 400 °C for 1 hour. The results indicated that even a small water concentration of 0.2 vol.% caused the creation of an embrittled zone on the fracture surface, however it does not significantly influence the value of the tensile properties. It was established that the critical influence on ultimate tensile strength and elongation has a water concentration of 4%, while 10% causes the degradation of proof strength.

Keywords: austempered ductile iron, ausferrite, water embrittlement, mechanical tensile properties, fracture behavior.

1. INTRODUCTION

Austempered ductile irons (ADI materials) represent the latest advancements in the ductile iron family of materials. The process of austempering produce a unique microstructure – ausferrite which is a mixture of ausferritic ferrite and carbon enriched retained austenite [1]. Ausferrite provides ADI materials with properties that can be similar to those found in forged steels. The ADI materials have an extraordinary combination of high strength, ductility, and toughness, together with good

machinability, vibration damping, high wear, and fatigue resistance [1–3]. The combination of these properties makes ADI a unique engineering material that may substitute cast, forged, and/or heat-treated steel or aluminum in applications where a combination of strength and weight ratio is important [4]. The ADI can be produced with a wide array of ultimate tensile strengths, ranging from 850 MPa to 1600 MPa and elongations between 10 and close to 0%, respectively [5].

The ADI has been used in many different sectors including automotive, trucks,

construction, earthmoving, agricultural, railway and military industries [6]. While in use, the ADI materials may come into contact with different fluids. It is established that the mechanical properties of ADI materials degrade when in contact with water. The most significant decrease is observed in elongation.

Shibutani et al. [7], in their innovative study, were the first to research the impact of water on the characteristics of Austempered Ductile Iron. Their research unveiled an interesting result: under dry testing conditions, ADI specimens demonstrated impressive tensile strengths of approximately 1000 MPa and an elongation of 8%, however, when the same specimens encountered a testing environment with moisture, their tensile strengths plummeted to around 700 MPa, while elongation diminished significantly to approximately 1.5%. These findings indicate that the presence of water can have a pronounced adverse effect on both the strength and ductility of the ADI.

This phenomenon of embrittlement induced by water exposure was further proved by Martínez et al. [8]. Their study repeated the conclusions drawn by Shibutani et al., solidifying the notion that ADI's mechanical properties can be substantially compromised in the presence of water.

On the other hand, research investigations [9-11], have shown that after a period of drying, the specimens returned to their original tensile properties. Also, the effect of water and the underlying cause of this phenomenon remain not fully understood.

For that reason, in this paper a comprehensive investigation of ADI behavior in different water concentration was investigated and presented.

2. MATERIALS AND METHODS

The chemical composition of ductile iron was: 3.5C; 2.5Si; 0.35Mn; 0.05Ni; 0.06Cr; 0.031Mg; 0.018P; 0.015S wt%. The graphite spheroidization was more than 90%. The average graphite volume fraction was cca 12% and nodule count distribution was from 125 to

175 mm² with nodule size was from 15 to 30 μm. The microstructure after etching by 2% nital (2% nitric acid—HNO₃ in alcohol) uncovered a predominantly ferritic metal matrix with 10% of pearlite, as depicted in Figure 1a.

The described nodular cast iron was heat-treated to produce ADI material. The heat treatment process consisted of two main steps: austenitization and isothermal transformation. Austenitization was carried out at 900°C for 2 hours in a protective argon atmosphere. This was followed by austempering at 400°C for 1 hour in a salt bath. At the end, after isothermal transformation, the specimens were allowed to cool in ambient air to room temperature. The resulting samples have been designated as ADI-904.

The microstructure of obtained samples ADI 904 is fully ausferritic and consisting of a mixture of ausferritic ferrite and carbon enriched retained austenite, Figure 1b. The morphology of ausferritic is plate-like with a 29.6 ± 2.1% volume fraction of the retained austenite.

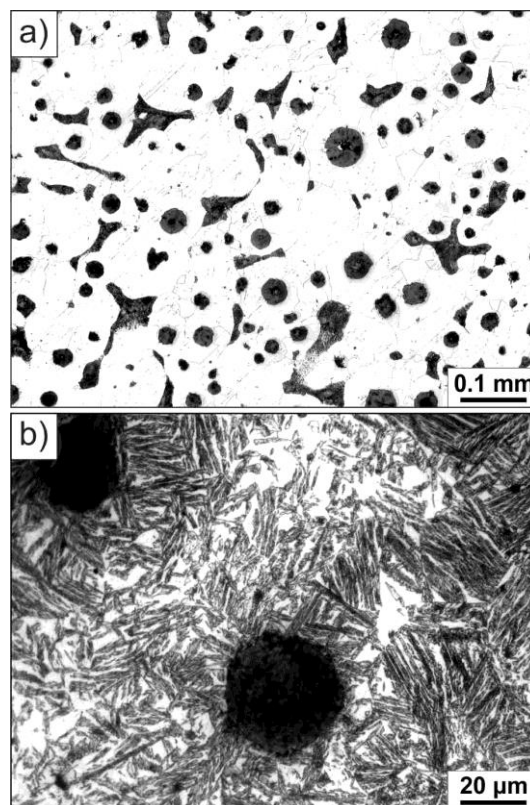


Figure 1. Microstructures of: a) ductile iron, b) ADI material

The mechanical properties of the starting materials, including $R_{p0.2}$ (0.2% proof strength), R_m (ultimate tensile strength), and A (elongation), are provided in Table 1.

Table 1. The mechanical properties of ductile cast iron and ADI 904 material

Material	$R_{p0.2}$ (MPa)	R_m (MPa)	A (%)
Ductile iron	318	456	19.1
ADI 904	722	959	11.5

The specimens were tested in dry condition, distilled water, and various water-ethanol mixtures. These mixtures contained 0.2%, 4%, and 10% distilled water by volume, with ethanol (C_2H_5OH).

3. RESULTS AND DISCUSSION

Table 2 presents the tensile properties of ADI 904 in both dry conditions and various water environments, along with the P parameter, in addition to the mean values.

Table 2. The mechanical properties of ADI 904 material tested in different environment.

Material	Environment	$R_{p0.2}$ (MPa)	R_m (MPa)	A (%)
ADI 904	Dry	722	959	11.5
	0.2% Water	707	952	8.7
	4% Water	711	901*	5.2*
	10% Water	678*	864*	4.2*
	Water	675*	814*	2.1*

* $p < 0.05$ denotes a statistically significant difference in relation to dry environment.

The results for proof strength indicate a slight decrease in the samples tested in dry conditions. Statistically significant differences in ADI 904 testing under dry conditions were observed between specimens tested in environments containing 10% and 100% water.

Greater sensitivity to the influence of water was noted for ultimate tensile strength and elongation. As in the previous case, the results for ultimate tensile strength indicate a clear tendency to decrease with increasing water content compared to the samples tested in dry conditions. Additionally, the presence of 0.2%

water content in the environment did not lead to a statistically significant decrease. The reduction in ultimate tensile strength for ADI 904 in a water environment was 17.8%.

The most significant decrease in mechanical properties was recorded during the elongation test. It can be clearly observed from Table 2 that a noticeable tendency for a decrease in elongation is noted as the water content in the tensile testing environment is increased, when compared to the samples tested in a dry condition. The reduction in elongation for specimens tested in a water environment was 82%.

3.1 Fracture Behavior

Depending on the testing environment, the fracture surfaces can be different. In the dry condition, the entirety of the fracture surface exhibits uniformly distributed dimples and graphite nodules. Conversely, when samples were subjected to testing at various water concentrations, two separate fracture zones became apparent: one featuring a flat, bright appearance near the specimen surface, and a larger zone exhibiting dimples across the remaining portion of the fracture surface, Figure 2. The fracture zones near the surface of the sample, respectively the water embrittled zone area is increasing as the water concentration in the environment rises.

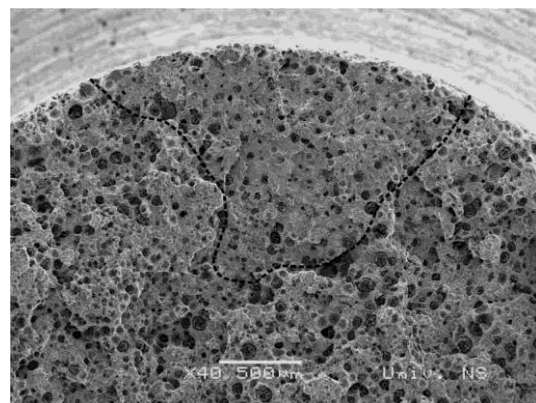


Figure 2. Embrittlement zone (100% water)

The characteristic fracture surfaces of the dry sample and the sample tested in water are shown in Figure 3. Figures 3b and c both the outside and inside of the embrittlement zone same specimen when tested in water.

It is evident that there is no significant difference between the fracture mode of samples tested in dry condition, and the fracture mode outside the embrittlement zone, Figure 3a and 3b. In all specimens, the fracture mode has an appearance of a mix mode fracture: ductile dimpled fracture and dispersed cleavage facets associated with brittle fracture, that is a quasi-cleavage fracture.

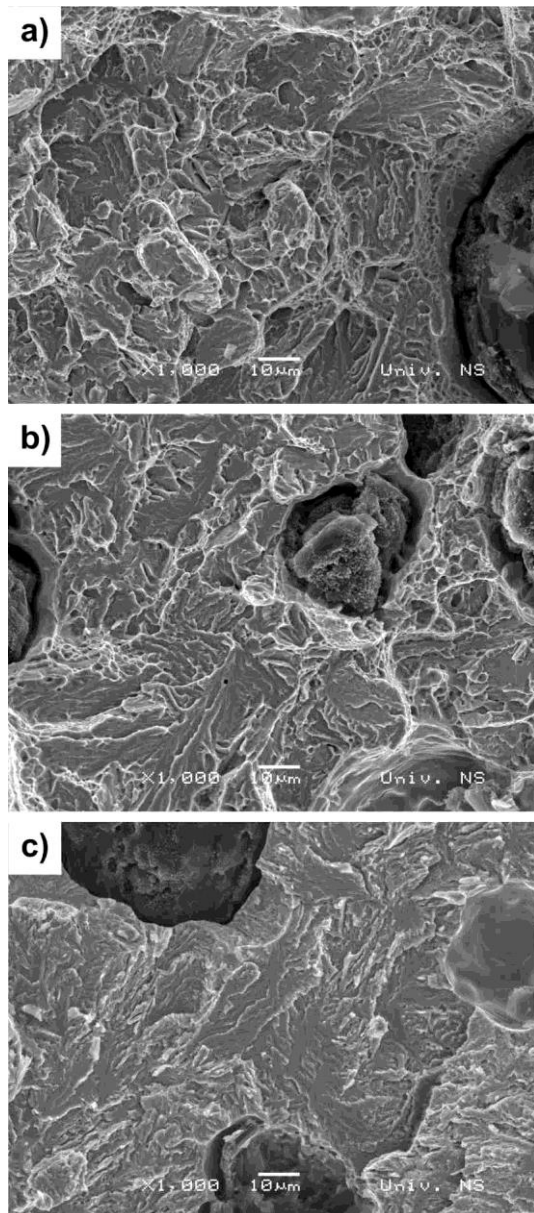


Figure 3. Fracture mode: a) in dry condition, b) in water, outside of the embrittlement zone; and c) in water, inside of the embrittlement zone.

The water embrittlement zone was observed for all water concentrations, from the lowest amounts of 0.2 vol.% to 100% water.

The fracture morphology of the embrittlement zone consists of the narrow serrated facets, forming shallow steps and tear ridges. The serrated facets are stretching from the free sample surface or from graphite spheres. The repeating appearance of the brittle zone morphology may be attributed to the cyclic propagation of crack. This is due to the cyclic nature of atomic hydrogen chemisorption into the narrow region under the specimen surface under strained conditions, thus inducing local micro-embrittlement, followed by brittle micro-fracture and formation of the new free surface where chemisorption start again [10, 12]. The cyclic embrittlement nature is further supported by the large size of the embrittlement zone, since hydrogen diffusion over few millimeters of embrittlement zone in few minutes (the time of test) would indicate an anomalous hydrogen diffusion coefficient which is not possible under given conditions.

4. CONCLUSION

Based on the test results and their analysis, the following conclusions can be summarized:

The presence of water in the environment significantly decreases the tensile properties of ADI materials.

Elongation is the most affected, followed by ultimate tensile strength, while proof strength is affected to a lesser extent.

The primary factor leading to the formation of the embrittlement zone, which acts as a critical point for crack initiation and subsequent fracture, is the phenomenon of chemisorption of hydrogen atoms from water onto the material surface.

ACKNOWLEDGEMENT

The authors gratefully acknowledge research support by the project entitled “Advanced materials, joining and allied technologies” in the Department of Production Engineering, Faculty of Technical Sciences Novi Sad, Serbia.

REFERENCES

- [1] L. Sidjanin, R.E. Smallman, J.M. Young: Electron microstructure and mechanical properties of silicon and aluminium ductile irons. *Acta Metallurgica Materialia*, Vol. 42, No. 9, pp. 3149-3156, 1994.
- [2] L. Sidjanin, D. Rajnovic, O. Eric, R.E. Smallman: Austempering study of unalloyed and alloyed ductile irons. *Mater. Sci. Technol.*, Vol. 26 No. 5 pp. 567-571, 2010.
- [3] O. Eric, D. Rajnovic, S. Zec, L. Sidjanin, J. Jovanovic: Microstructure and fracture of alloyed austempered ductile iron. *Mater. Charact.*, Vol. 57, pp. 211, 2006.
- [4] D. Rajnovic, O. Eric, L. Sidjanin: Transition temperature and fracture mode of as-cast and austempered ductile iron. *J. Microsc.*, Vol. 232, No. 3, pp. 605-610, 2008.
- [5] R.A. Martinez, S.N. Simison, R.E. Boeri: Environmentally Assisted Embrittlement of ADI—Current Understanding, *2002 World Conference on ADI*, 26–27 September 2002, Louisville, KY, USA.
- [6] R.A. Harding: The production, properties and automotive applications of austempered ductile iron. *Kov. Mater.* Vol. 45, pp. 1–16, 2007.
- [7] S. Shibutani, S. Komatsu, Y. Tanaka: Embrittlement of Austempered Spheroidal Graphite Cast Iron by Contact with Water and Resulting Preventing Method, *Int. J. Cast Met. Res.*, Vol 11, pp. 579–585, 1999.
- [8] R.A. Martínez, R.E. Boeri, J.A. Sikora: Embrittlement of ADI caused by contact with water and other liquids. *Int. J. Cast Met. Res.*, Vol. 13, pp. 9–15, 2000.
- [9] R.A. Martinez, S.N. Simison, R.E. Boeri: Environmentally Assisted Embrittlement of ADI—Current Understanding, in: *2002 World Conference on ADI*, 26-27 September 2002, Louisville, KY, USA.
- [10] S. Komatsu, Y. Osafune, Y. Tanaka, K. Tanigawa, S. Shibutani, H. Kyogoku: Influence of water embrittlement effect on mechanical properties of ADI, *Int. J. Cast Met. Res.* Vol. 16, pp. 209–214, 2003.
- [11] L. Masud, R. Martínez, S. Simison, R. Boeri: Embrittlement of austempered ductile iron on contact with water—Testing under applied potential, *J. Mater. Sci.*, Vol. 38, pp. 2971–2977, 2003.
- [12] D. Rajnovic, S. Balos, L. Sidjanin, O. Eric Cekic, J. Grbovic Novakovic: Tensile properties of ADI material in water and gaseous environments, *Mater. Charact.*, Vol. 101, pp. 26–33, 2015.



Society of Production
Engineering

SPMS 2023

39. Savetovanje proizvodnog mašinstva Srbije

ICPES 2023

39th International Conference on Production Engineering of
Serbia



Faculty of Technical
Sciences
University of Novi Sad

Novi Sad, Serbia, 26. – 27. October 2023

AN EXPERIMENTAL METHOD FOR STRAIN STATE DETERMINATION IN BULK METAL FORMING

Plavka SKAKUN^{1, *}, Dragan RAJNOVIĆ¹, Petar JANJATOVIĆ¹, Miroslav DRAMIĆANIN¹

¹ University of Novi Sad, Faculty of Technical Sciences, Novi Sad, Serbia

*Corresponding author: plavkas@uns.ac.rs

Abstract: Determination of process parameters in metal forming, such as forming load and work, is based on stress and strain analysis which are different for every forming method. In this paper an experimental method for strain state determination in bulk metal forming is presented. This method is based on the dependence between recrystallized grain size and prior deformation. Method is used for strain state determination of cold extruded gear-like element made of Al99.5. Experimental method procedure is presented and described in details. The obtained results accurately shows the strain distribution inside the element, as well as the way material flows during forming process.

Keywords: bulk metal forming, strain state, experimental method

1. INTRODUCTION

Stress and strain state in a metal forming process is of great importance when it comes to a process design. Nowadays numerical simulation usually gives good insight where the critical values of stress and strain could occur during a forming process, however an experimental approach, even if it is usually more demanding than numerical simulation, gives more realistic and accurate values of analyzed parameters.

One method which is widely used for strain state determination is the Digital Image Correlation (DIC) [1,2,3]. Its application is more suitable for plane strain state in sheet metal forming.

Another experimental approach uses the relation between material hardness and related values of strain [4,5,6]. An advantage of this method is that hardness measurement tests are widely used and equipment is accessible, but this method requires that relationships between hardness and strain should be determined earlier.

In this paper an experimental metallographic method intended for strain state determination in bulk metal forming is presented [7,8]. The method is based on the relation between recrystallized grain size and prior deformation of material. It was applied for strain values determination in cold extruded aluminium gear-like element. To apply this method, it is necessary to determine calibration curve, which gives relation between grain size and achieved deformation.

2. SPECIMEN PREPARATION

For this study specimens were made of Al 99.5 with following chemical composition: 0.02% Cu, 0.003% Mn, 0.016% Mg, 0.13% Si, 0.28% Fe, 0.05% Zn, 0.018% Ti, 0.006% Pb, 0.005% Sn and balance Al.

In order to apply this method for strain state determination in a cold bulk forming process, all specimens for calibration curve and for the extrusion experiment must undergo same procedure.

Procedure for specimen preparation consisted of:

- initial heat treatment at 600°C for 16 h,
- upsetting for effective strain of $\varphi=0.25$
- second heat treatment at 500°C for 1 h.

The result of the initial heat treatment was chemical homogenization and grain growth. The following upsetting process (compressive deformation) was used to enable some energy storage, which would be released in the second heat treatment, recrystallisation.

In this way uniform initial microstructure was achieved, Figure 1.

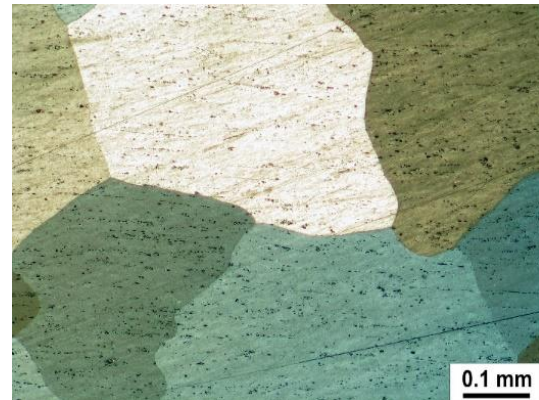


Figure 1. Initial microstructure

3. CALIBRATION CURVE

A part of the initially prepared samples was used for calibration curve determination. The calibration curve shows dependence between mean grain diameter of recrystallized grain and effective strain, Figure 2.

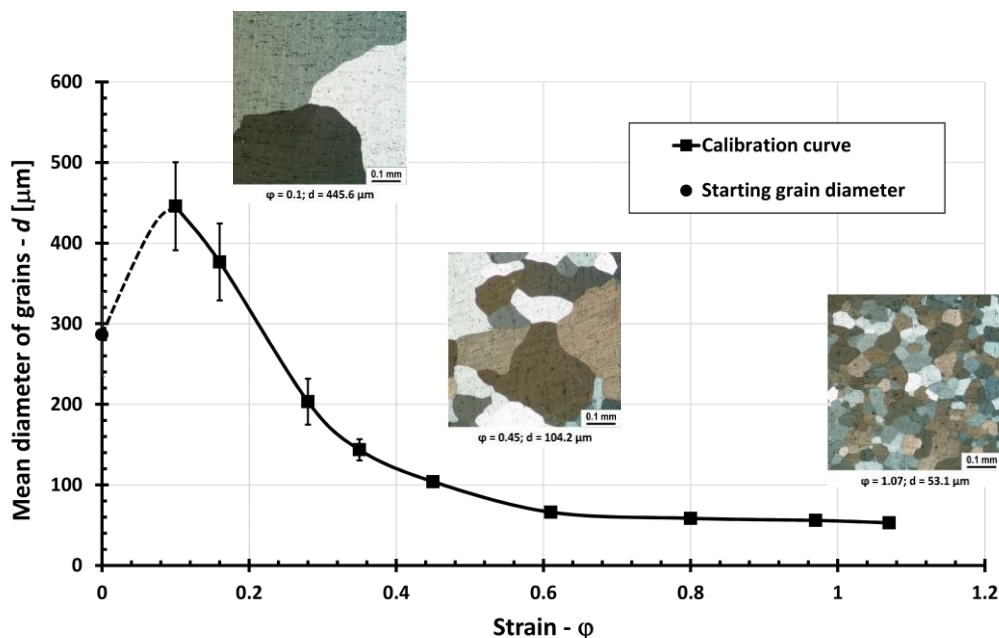


Figure 2. Calibration curve

In order to achieve uniform grain size in specimens used for calibration curve, they were deformed in such a way that even distribution of strain values was enabled. For this purpose, uniaxial compression was used (upsetting by

Rastegaev method) [9]. In the conventional upsetting, friction on contact surfaces between billet and die, affects the way material flows, and at the end of the forming process of cylindrical billet barreling occurs. To eliminate

friction, in Rastegaev method, on the contact surfaces of the billet shallow indentations (lubrication pockets) are made, where solid lubricant (stearic acid) can be placed. Another way of friction elimination in this process is application of PTFE (Teflon) foil. However, for larger strain values, it could happen that process has to be conducted incrementally, because foil can break. The cylindrical shape of the billet after upsetting indicates that friction was eliminated or maximally reduced to negligible level. Billets were deformed for the values of logarithmic strain ϕ between 0.1 and 1.07 and for each billet grain size was determined (procedure is explained later). The curve was approximated by the power function (Equation 1):

$$\phi = 44.357 \cdot d^{-0.973} \quad (1)$$

4. EXTRUSION EXPERIMENT AND RESULTS

The extrusion experiment was performed on the hydraulic press (model 630t, Sacks und Kiesselbach, Germany) by special tooling for radial extrusion. Gear-like element obtained in this experiment is presented in figure 3.

From extruded element one twelfth section (0-30°) was made for microstructure analysis. The metallographic examinations for all specimens were done after the standard

metallographic preparation: (i) grinding with SiC papers (from 220 up to 2500 grid); (ii) polishing with diamond suspension (6, 3, 1 and 1/4 μm grain size); and finally (iii) polishing with colloidal silica polishing suspension. To develop the Al grains the anodic oxidation etching in Barkers reagent HBF_4 (5 mL HBF_4 + 200 ml distilled H_2O) was applied. All specimens were examined with an Orthoplan (Leitz, Germany) light microscope under polarized light (polarized LM).

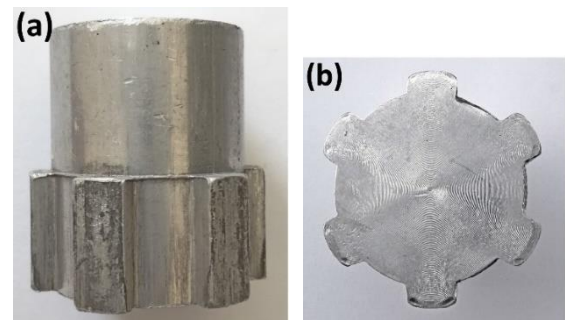


Figure 3. Extruded gear-like element

In Figure 4a, the macrostructure of the representative section of one twelfth of the extruded element, is presented. It can be seen that grain size and their distribution are ununified as a result of different strain values obtained during the extrusion process.

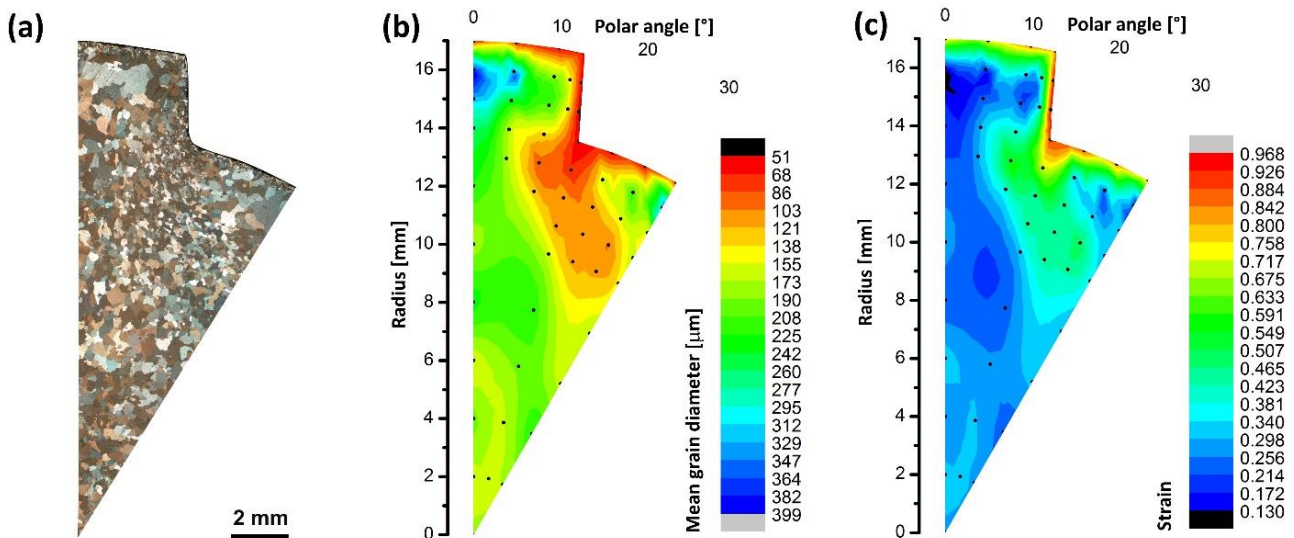


Figure 4. Grain size in the 30° segment: a) Grain size zones; b) The grain diameter; c) Strain

The results of microstructure grain size for section are presented graphically in Figure 4b, (black dots represent the position of measurement in polar coordinates). The grain diameter varies from 51 to 399 μm . The highest grain size is in the middle of the tooth and in the zone between the teeth, close to the surface. The smallest grains were obtained at the root of the tooth and at the surface of the element. Between each tooth root, there is the zone with grains from very fine to fine in the middle between tooth roots. This "circlet" is surrounded by large grains between teeth close to the surface and medium size grains in the intermediate zone between surface and center. In the center of the cylindrical part of the element, grain size values are slightly lower than in the intermediate zone.

Based on the calibration curve (Equation 1) and measured grain size (Figure 4b), the strain state was determined, and graphically presented in Figure 4c.

5. CONCLUSION

In this paper an experimental metallographic method for strain state determination in bulk metal forming processes is presented. The method was applied for strain state determination within cold extruded gear like element made of Al 99.5.

In order to apply this method, it is necessary to prepare specimens and to determine calibration curve, which makes this procedure, in a certain way, demanding. On the other hand, results obtained by this method show true state of strain distribution and material flow. Furthermore, through flow curve, effective stress values also can be determined.

In this study, the method was applied on a single-phase material. This represents the base for future strain state research in the case of multi-phase materials.

ACKNOWLEDGEMENT

The authors gratefully acknowledge research support by the project entitled "Advanced materials, joining and allied technologies" in the Department of Production Engineering, Faculty of Technical Sciences Novi Sad, Serbia.

REFERENCES

- [1] B. Pan: Digital image correlation for surface deformation measurement: historical developments, recent advances and future goals, *Measurement Science and Technology*, Vol. 29, No. 8, pp. , 2018.
- [2] J. Agirre, L. Galdos, E.S. Argandona, J. Mendiguren, Hardening prediction of diverse materials using the Digital Image Correlation technique, *Mechanics of materials*, Vol.124, pp. 71-79, 2018.
- [3] I.I. Ailinei, S. V. Galatanu, L. Marsavina: Influence of anisotropy on the cold bending of S600MC sheet metal, *Engineering failure analysis*, Vol. 137, 2022.
- [4] D. Tabor: *The Hardness of Metals*, Oxford University Press, London, 1951.
- [5] G. Sundararajan, Y. Tirupataiah: The hardness - flow stress correlation in metallic materials, *Bulletin of Materials Science*, Vol. 17, No. 6, pp. 747-770, 1994.
- [6] M. L. Alves, J. M. C. Rodrigues, P. A. F. Martins: Cold forging of gears: experimental and theoretical investigation, *Finite Elements in Analysis and Design*, Vol. 37, Issues 6-7, pp. 549-558, 2001.
- [7] B. O. Oyekanmi, T. A. Hughes, A. N. Bramley: A microstructural evaluation technique for deformation studies in metal forming processes, *Journal of Materials Processing Technology*, Vol. 21, Issue 1, pp. 75-89, 1990.
- [8] P. Skakun, D. Rajnovic, P. Janjatovic, S. Balos, A. Shiskin, P. Novak, L. Sidjanin, Metallographic determination of strain distribution in cold extruded aluminium gear like element, *Metals*, Vol.10, April 2020,
- [9] International Cold Forging Group. 40 Years History Document; Document No18/07; ICFG: Los Angeles, CA, USA, 2007.



Society of Production
Engineering

SPMS 2023

39. Savetovanje proizvodnog mašinstva Srbije

ICPES 2023

39th International Conference on Production Engineering of
Serbia



Faculty of Technical
Sciences
University of Novi Sad

Novi Sad, Serbia, 26. – 27. October 2023

HIGH TEMPERATURE TRIBOLOGICAL EVALUATION OF NANOLAYER TiAlN/TiSiN COATING DEPOSITED ON TOOL STEEL

Vladimir TEREK^{1, *}, Lazar KOVAČEVIĆ¹, Zoran BOBIĆ¹, Branko ŠKORIĆ¹, Aljaž DRNOVŠEK², Miha ČEKADA², Peter PANJAN², Pal TEREK¹

¹University of Novi Sad, Faculty of Technical Sciences, Novi Sad, Serbia

²Jožef Stefan Institute, Ljubljana, Slovenia

*Corresponding author: vladimirterek@uns.ac.rs

Abstract: In this investigation, nanolayer TiAlSiN coating was deposited by alternating TiAlN and TiSiN layers. The coating was deposited on hot-work tool steel (EN X38CrMoV5) and plasma nitrided (PN) hot-work tool steel samples using industrial magnetron sputtering unit. Tribological behavior of the coating was evaluated using high temperature pin-on-disk tribometer. Tribo-tests were performed in air atmosphere against Al₂O₃ counterball at room temperature (RT), 300, 400, 500, 600, and 700 °C. After the tribo-tests, wear tracks were examined using confocal microscopy, stylus profilometry, scanning electron microscopy, focused ion beam and energy dispersive spectroscopy. To determine mechanical properties and adhesion of the coating, nanoindentation and HRC tests were performed before and after the tribological tests. It was found that after exposure to the testing temperatures the coating retained its hardness and adhesion. Visual analysis of the wear tracks suggests the presence of abrasive wear mechanism at room temperature, while at high temperatures both abrasive and oxidative wear mechanisms are present. Steady state coefficient of friction (COF) at room temperature was approximately 0.85 for coating on both substrate materials. At 300, 400, and 500 °C the COF values increased due to the formation of oxide tribo-layer inside the wear tracks. The coating on non-nitrided substrate exhibited an additional increase in COF values at these temperatures due to the micro-cracks and steps that form inside the wear tracks. Further increase of the testing temperature to 600 and 700 °C leads to decrease of COF because of the coating failure and formation of Fe-O inside of the wear track. The highest wear rate was observed at RT, while at high temperature the wear rate was ~10 times lower due to the formation of the protective oxide tribo-layer. At 700 °C the coating on non-nitrided substrate was completely destroyed due to oxidation of substrate material, while coating on PN substrate was only partially destroyed. It is concluded that PN layer slightly extended coating's application to the higher temperatures.

Keywords: TiAlN/TiSiN, high temperature, tribology, PDV coating, thin films, tribological coatings

1. INTRODUCTION

Hot-work tool steel is widely used for tools in hot-extrusion, high pressure die casting and forging processes [1]. However, due to harsh

conditions and relatively low hardness of the material, these tools need to be additionally protected to endure aggressive wear conditions [2]. One way of protecting tool surfaces and increasing its hardness and

tribological behaviour is a well-known plasma nitriding process. Still, this way of protecting tools is often not sufficient during high demanding production regimes. In those cases, plasma nitriding treatment is combined with a subsequent deposition of PVD hard coatings.

Ti-based nitrided coatings are widely used for this purpose. First the TiN was used for several decades and was later replaced by TiAlN due to the higher hardness, oxidation resistance and thermal stability [3]–[5]. Ever increasing demands for productivity encouraged further development of these coatings and a quaternary Ti-Al-Si-N coatings were developed. These coatings display high hardness (~40 GPa), high thermal stability (~1200 °C) and high oxidation resistance (~1100 °C) [6]–[8]. However, the high temperature tribological behaviour of these coatings was investigated only to a limited extent. Therefore, in this study nanolayer, TiAlN/TiSiN was evaluated using high temperature pin-on-disk tribometer. The coating was deposited in industrial magnetron sputtering unit, on hot-work tool steel and plasma nitrided hot-work tool steel.

2. MATERIALS AND METHODS

In this study hot-work tool steel (EN X38CrMoV5), in a form of disk-shaped samples, was used as a substrate material for the coating deposition. The samples were quenched and double tempered. After the heat treatment a group of samples was plasma nitrided. Before the deposition, the substrates were mirror polished and cleaned in ultrasonic bath. Nanolayer TiAlSiN coating (3.6 µm thick) was deposited using an industrial magnetron sputtering device (CC800/9, CemeCon). The deposition unit contains four unbalanced magnetrons, positioned in the corners of the deposition chamber. The coating was deposited using two TiAl and two TiSi targets. Additionally, the substrates were placed on a two-fold rotary table, which resulted in a nanolayered design with an alternating TiAlN and TiSiN layers.

Mechanical properties of the coating were measured at room temperature by nanoindentation (H100C, Fischerscope), before

and after the tribological tests. To minimize the indentation depth and influence of the substrate material, the load of 50 mN was used. Adhesion of the coating and hardness of the substrate materials, before and after the tribological tests, were determined by the standard HRC test.

Tribological testing was performed using high temperature pin-on-disk tribometer (THT, Anton Paar). Tribo-tests were performed in ambient air atmosphere at room temperature (RT), 300 °C, 400 °C, 500 °C, 600 °C, and 700 °C. The tests were conducted against alumina (Al₂O₃) counterballs, with a diameter of 6 mm. The load of 5N and linear velocity of 5 cm/s were used, and the tests lasted for 2000 cycles.

After the tribological tests, wear tracks were first analysed using confocal microscopy (CFM) (Axio CSM700, Zeiss) and measured using 2D profilometry (Talysurf, Taylor Hobson). Profilometry scans were used to determine the cross-section of the wear tracks, which was used to calculate the coating's worn volume. The wear rate was calculated as follows: $K = V / (w \cdot s)$ [9], where V is the worn volume (mm³), w is the normal load (N), and s is the sliding distance (m).

More detailed characterization of the wear tracks was performed using scanning electron microscope (SEM) (Quanta 650 ESEM, FEI) and focused ion beam (FIB) (Helios Nanolab 650i, FEI), while chemical analysis was performed using energy dispersive spectroscopy (EDS).

3. RESULTS AND DISCUSSION

3.1 Mechanical properties

Figure 1 presents hardness of the substrate materials, measured at room temperature before and after the tribological tests. Both substrates retained their hardness up to 600 °C, while at 700 °C the hardness of both substrates decreased by approximately half.

Adhesion of the coating is presented in Fig. 2. Coating on non-nitrided (NN) substrate contains circular cracks around the HRC indents while for the coating on nitrided (PN) substrate only thin radial cracks are present around the indents. The coating on both substrates

displayed good adhesion, delamination is not observed, and according to HF classification it can be characterized as HF3 for coating on NN substrate and HF1 on PN.

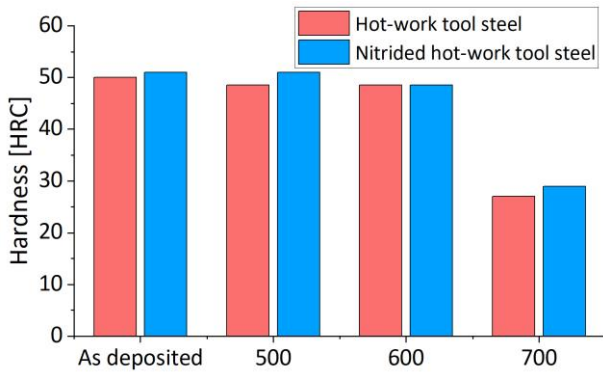


Figure 1. Hardness of the substrate material before and after the tribo-tests

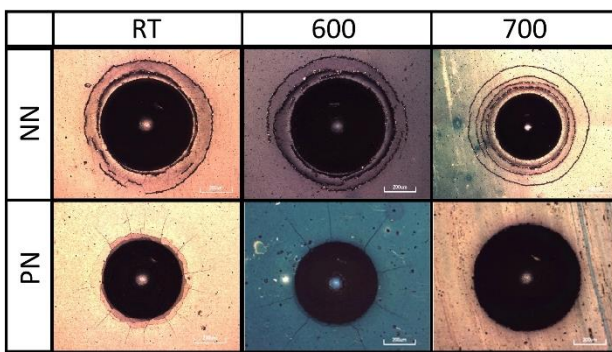


Figure 2. HRC indents before and after the tribo-tests.

Hardness and modulus of elasticity of the coating on both substrate materials is presented in Fig. 3. The coating exhibited only a minor change in mechanical properties after annealing at the testing temperatures. Rahman et al [10] observed similar behaviour.

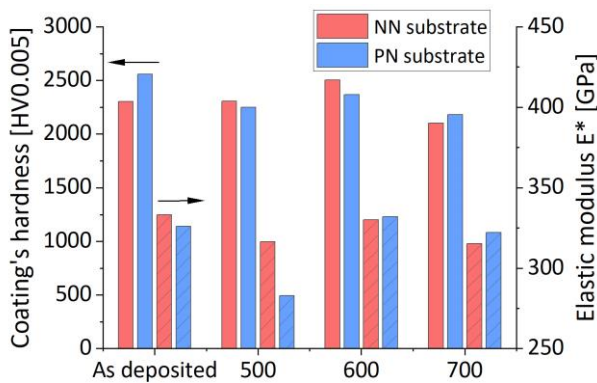


Figure 3. Hardness and elastic modulus of the coating, at room temperature before and after tribo-tests.

2.1 CFM analysis

Figure 4 presents CFM images of the wear tracks at RT, 300 °C, 400 °C, 500 °C, 600 °C and 700 °C for coating on both substrates. At RT both wear tracks are approximately of the same width and are characterized with smooth areas which suggest the presence of an abrasive wear mechanism. At 300, 400 and 500 °C the wear tracks are similar and significantly narrower than at RT, which indicates a lower wear rate. Apart from smooth areas inside the wear track, grooves and adhered material can also be observed. This suggests that the wear mechanism has changed, possibly to a combination of abrasive and oxidative wear. Additionally, cracks perpendicular to the counterball movement are found inside the wear tracks. The cracks inside the wear track at 500 °C are more pronounced in the coating on NN substrate.

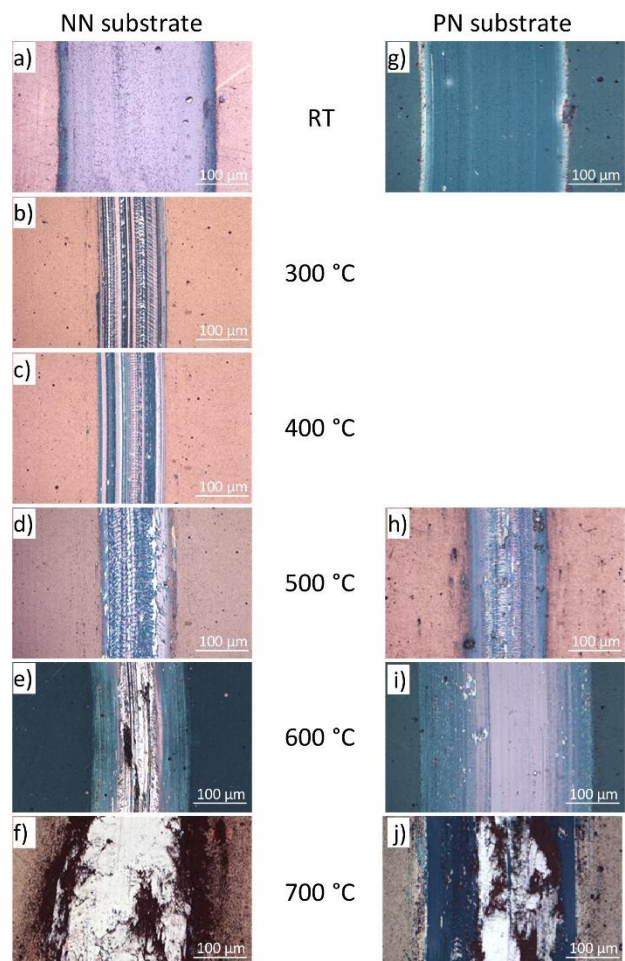


Figure 4. CFM images of the wear tracks.

At 600 °C the width of the wear tracks increases. Wear tracks are smoother, and the cracks are now present only in the coating on NN substrate. However, in the middle of the wear track of this sample the coating layer exhibited damage due to the substrate material oxidation. This is not observed for the coating on PN substrate. Finally, at 700 °C the coating inside of the wear track on NN substrate is completely destroyed, while on PN substrate the coating is only partially destroyed.

2.2 FIB, SEM and EDS analysis

After the tribological tests, detailed FIB, SEM, and EDS analysis was performed inside of the wear tracks at 500 °C, 600 °C and 700 °C. Figure 5a presents the SEM top view images of the wear tracks at 500 °C on NN substrate. EDS analysis was performed at marked location inside the wear track, and it was found that the oxide tribo-layer formed on the surface of the coating (Table 1). The exact chemical composition of the oxide layer cannot be determined by means of used technique. However, in the literature it is reported that Al_2O_3 , TiO_2 and SiO_2 usually form on top of the TiAlN/TiSiN (TiAlSiN) coatings [6], [11]. Inside the wear track, the marks on the coating are also visible. In order to analyse these marks in more detail, FIB cross-section was prepared at their location (Fig. 5b). It was found that these marks are cracks that span through the whole coating to the substrate. It is suggested that the cracks formed due to decrease of substrates mechanical properties at high temperatures and consequently its load-bearing capacity. This resulted in formation of small steps on the interface between substrate and the coating which then transferred to the coating's surface.

SEM images of the coating on NN substrate tested at 600 °C are presented in Figure 6. EDS analysis on marked location (Fig. 6a) revealed the presence of Fe inside the wear track (Table 1), apart from constituents of the coating. Fe originated from the substrate material and is suggested to be present on the surface of the coating as Fe-O. This suggests that the substrate material oxidized, and Fe-O started

filling the wear track through the damaged coating layer. The steps can be also observed inside the wear track. Detailed SEM (Fig. 6b) and FIB (Fig. 6c) analysis revealed that the oxides are filling the cracks inside the coating and accumulating on the steps. This effect can also be observed at 500 °C, but notably milder.

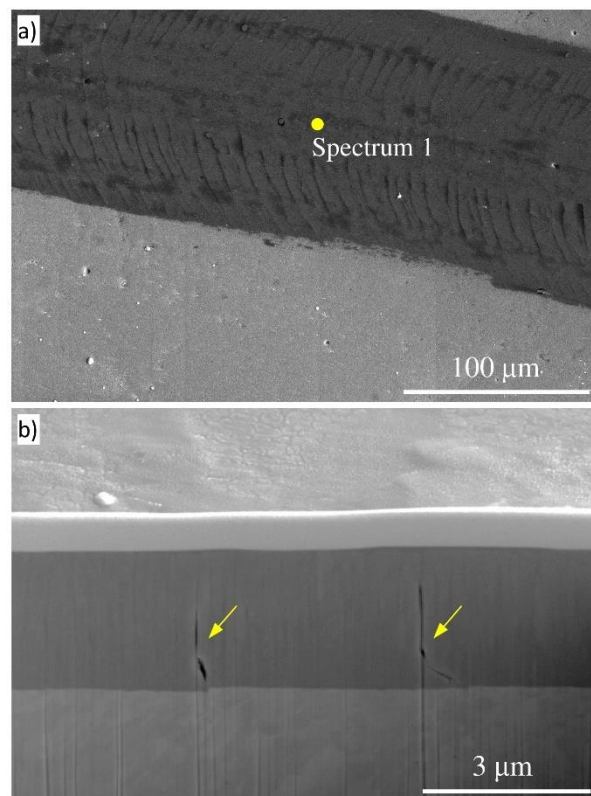


Figure 5. SEM images of coating on NN substrate tested at 500 °C: a) top view of the wear track, b) FIB cross-section of the wear track, yellow arrows indicate the cracks.

EDS analysis of the wear track of the coating on PN substrate tested at 600 °C (not shown here) showed the presence of oxides on the surface, however Fe was not detected. This confirms that plasma nitriding treatment postponed the oxidation of substrate material. The reason for this behaviour is suggested to be the absence of crack because they can facilitate movement of Fe to the coating's surface.

Table 1. Chemical analysis performed by EDS

Chemical composition [At %]						
Spectrum	Ti	Al	Si	N	O	Fe
1	29.9	10.2	3.2	21.9	34.5	0.4
2	16.1	6.5	2.4	-	58.8	16.2
3	3.5	1.2	1.2	-	54.4	39.8*

*Fe+Cr+Mo

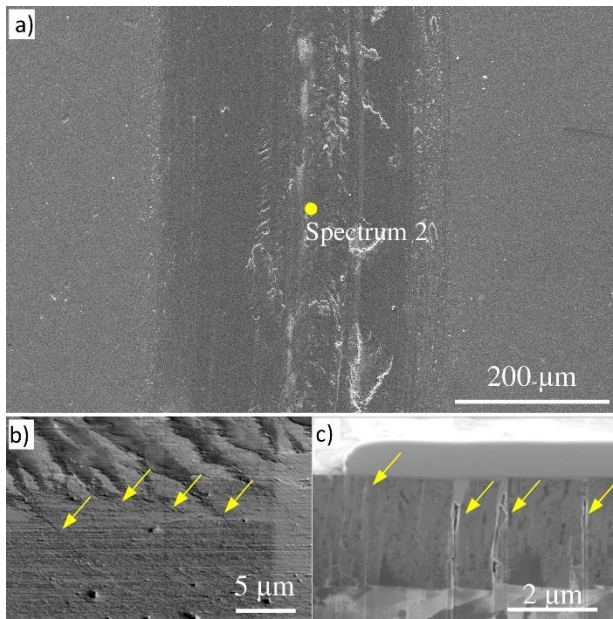


Figure 6. SEM images of coating on NN substrate tested at 600 °C: a,b) top view of the wear track, c) FIB cross-section of the wear track. Yellow arrows indicate the cracks.

At 700 °C on NN substrate the wear track is completely filled with Fe-O (Fig. 7a, Table 1), while on PN substrate the Fe-O is detected only in the middle of the wear track (Fig. 7b). Therefore, it can be concluded that the plasma nitriding treatment provided better thermal and oxidation resistance of hot-work tool steel and slightly extended its application to a higher temperature [2].

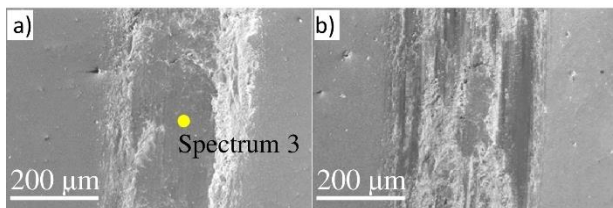


Figure 7. SEM top view of the coating tested at 700 °C, deposited on: a) NN, and b) PN substrate.

2.3 Coefficient of friction and wear rate

Figure 8 shows the typical coefficient of friction (COF) curves obtained from tribological tests at different temperatures. At room temperature the coating on both substrates displayed similar COF curves and value of steady state COF was approximately 0.85 in both cases. However, as the testing temperature increased, different behaviour was observed between these two cases.

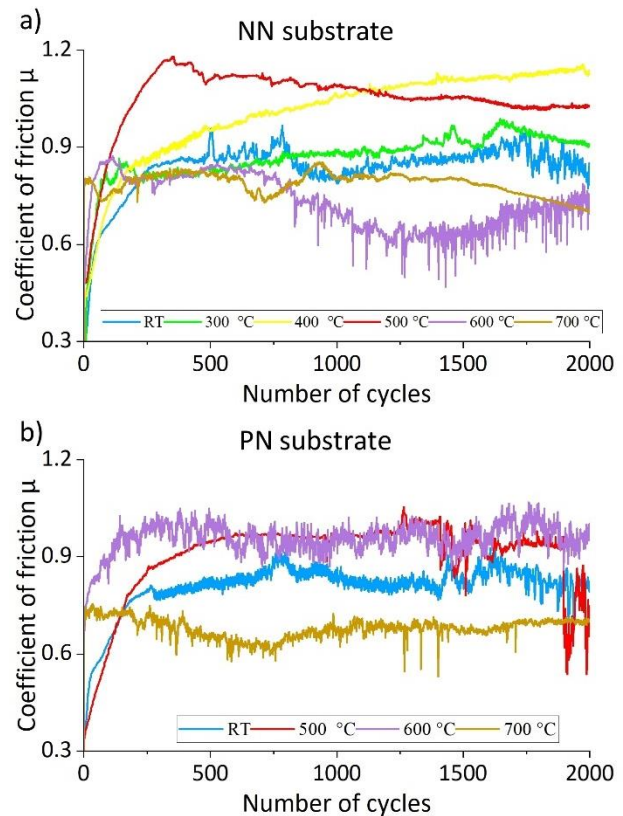


Figure 8. COF curves as a function of number of cycles for tribo-test on coating deposited on: a) NN, and b) PN substrate.

As temperature increased up to 500 °C, the coating on NN substrate displayed significant increase in values of COF (up to 1.2). This increase is suggested to be due to two main reasons. First is self-mated Al_2O_3 contact between counterball and oxide that forms inside the wear track [12], [13]. The second are the steps that formed inside the wear track as a result of substrate losing its load-bearing capacity. These steps act as small obstacles that hinder the movement of the counterball which consequently increases the values of COF. However, the value of COF in tribo-test at 500 °C decreases over time. This is suggested to be due to oxide accumulation on the steps which created a smoother surface. At 600 and 700 °C the values of COF significantly decreased and were lower than at RT test. In these cases, the decrease of values of COF is attributed to even more pronounced oxide accumulation on the steps and Fe-O formation inside the wear tracks [14].

The coating on PN substrate exhibited slightly different behaviour. The values of COF increased at 500 and 600 °C when compared to RT.

However, this increase was lower than in case of the coating on NN substrate. This is mainly due to less pronounced steps (500 °C) and absence of steps (600 °C), that increased the values of COF in previous case, so the increase is only a result of self-mated Al₂O₃. Additionally, the Fe-O was not detected at 600 °C, therefore the values of COF did not decrease. At 700 °C the Fe-O formed inside the wear track and the value of COF consequently decreased.

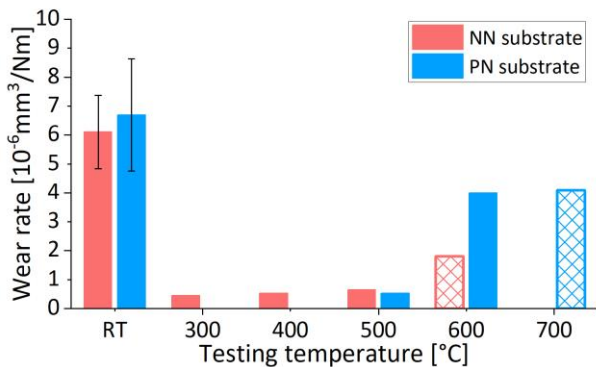


Figure 9. The wear rate of TiAlN/TiSiN coating at different testing temperatures

Figure 9 shows the wear rate of the coatings tested at different temperatures. At room temperature similar wear rates were observed for the coating on both substrates. This were also the highest wear rates observed in this study. At high temperatures the wear rate was significantly lower than at RT. The decrease in wear rate is attributed to formation of Al-O and Si-O in the wear track, which are known to have protective properties [6]. However, as the temperature increased from 300 °C to 700 °C, the wear rate also increased. This increase in the wear rate is attributed to the decrease in hardness of both substrate and the coating at high temperatures (hot hardness). Even though both coating and substrate retained their hardness, the hardness was measured at room temperature after tribological tests at specific temperatures, and not directly at high temperatures. Arsić et al. [15] showed that the mechanical properties of X38CrMoV5 hot-work tool steel, measured directly at high temperatures, are significantly lower than after annealing at those temperatures and measuring after samples cool down. Additionally, Drnovšek et al. [16] showed that the hardness of the coating is lower while at

high temperatures and it returns to original values after cooling down to room temperature.

The wear rates of the coating on NN substrate tested at 600 and on PN substrate tested at 700 are on Fig. 9 presented with hatched pattern. This is because in these test the Fe-O started filling the wear tracks, which omitted the calculation of the wear rate and caused an invalid results.

4. CONCLUSION

In this investigation the nanolayer TiAlN/TiSiN was deposited on two substrate materials, hot-work tool steel (EN X38CrMoV5) and plasma nitrided hot-work tool steel, using industrial magnetron sputtering unit. The coating was tribologically tested at room temperature, 300 °C, 400 °C, 500 °C, 600 °C, and 700 °C. The presented results led to following conclusions:

- Both nitrided and non-nitrided hot-work tool steel substrate material retained its hardness up to 600 °C, while the coating retained its hardness up to maximal testing temperature.
- The morphology of the surface inside the wear tracks and wear mechanisms are similar for coatings on both substrates. At room temperature the abrasive wear mechanism is present while at high temperatures abrasive and oxidative wear mechanism are combined.
- Steps inside of the wear tracks at high temperatures formed as a result of cracks in the coating that originated due to loss of load-bearing capacity of the substrate. The steps are more pronounced on the coating deposited on non-nitrided substrate and played a significant role in increasing the values of coefficient of friction. However, to better understand the origin of the cracks and formation of steps, additional analyses are required.
- The highest wear rate was observed at room temperature for coating on both substrates. At high temperatures the wear rate decreased due to formation of protective Al-O and Si-O on the surface of the coating.
- Intense oxidation of substrate material inside the wear track at 700 °C completely destroyed

the coating deposited on non-nitrided substrate which resulted in failure of the coating, while plasma treatment slightly postponed this effect and increased working temperature of the investigated system.

ACKNOWLEDGEMENT

This research has been supported by the Ministry of Science, Technological Development, and Innovation through project no. 451-03-47/2023-01/200156 "Innovative scientific and artistic research from the FTS (activity) domain".

This work was also funded by the Slovenian Research Agency (program P2-0082) and European Regional Development Funds (CENN Nanocenter, OP13.1.1.2.02.006).

REFERENCES

- [1] Y. Y. Chang and S. Amrutwar: Effect of plasma nitriding pretreatment on the mechanical properties of AlCrSiN-coated tool steels, *Materials*, vol. 12, no. 5, 2019.
- [2] B. Navinšek, P. Panjan, and F. Gorenjak: Improvement of hot forging manufacturing with PVD and DUPLEX coatings, *Surf. Coatings Technol.*, vol. 137, no. 2–3, pp. 255–264, 2001.
- [3] P. Panjan, A. Drnovšek, P. Terek, A. Miletić, M. Čekada, and M. Panjan: Comparative Study of Tribological Behavior of TiN Hard Coatings Deposited by Various PVD Deposition Techniques, *Coatings*, vol. 12, no. 3, p. 294, 2022.
- [4] A. Vennemann, H. R. Stock, J. Kohlscheen, S. Rambadt, and G. Erkens: Oxidation resistance of titanium-aluminium-silicon nitride coatings, *Surf. Coatings Technol.*, vol. 174–175, pp. 408–415, 2003.
- [5] S. Veprek, M. G. J. Veprek-Heijman, P. Karvankova, and J. Prochazka: Different approaches to superhard coatings and nanocomposites, *Thin Solid Films*, vol. 476, no. 1, pp. 1–29, Apr. 2005.
- [6] N. He, H. Li, L. Ji, X. Liu, H. Zhou, and J. Chen: High temperature tribological properties of TiAlSiN coatings produced by hybrid PVD technology, *Tribol. Int.*, vol. 98, pp. 133–143, 2016.
- [7] Y. Y. Chang and S. M. Yang: High temperature oxidation behavior of multicomponent TiAlSiN coatings, *Thin Solid Films*, vol. 518, no. 21 SUPPL., pp. S34–S37, 2010.
- [8] Z. W. Xie, L. P. Wang, X. F. Wang, L. Huang, Y. Lu, and J. C. Yan: Influence of oxidation on the structural and mechanical properties of TiAlSiN coatings synthesized by multi-plasma immersion ion implantation and deposition, *Nucl. Instruments Methods Phys. Res. Sect. B Beam Interact. with Mater. Atoms*, vol. 271, pp. 1–5, 2012.
- [9] K. H. Matthews: *Coating Tribology*, Elsevier, Amsterdam, 1994.
- [10] M. M. Rahman et al: Effects of annealing temperatures on the morphological, mechanical, surface chemical bonding, and solar selectivity properties of sputtered TiAlSiN thin films, *J. Alloys Compd.*, vol. 671, pp. 254–266, 2016.
- [11] L. Rebouta, F. Vaz, M. Andritschky, and M. F. da Silva: Oxidation resistance of (Ti,Al,Zr,Si)N coatings in air, *Surf. Coatings Technol.*, vol. 76–77, pp. 70–74, 1995.
- [12] X. Dong, S. Jahanmir, and S. M. Hsu: Tribological Characteristics of α -Alumina at Elevated Temperatures, *J. Am. Ceram. Soc.*, vol. 74, no. 5, pp. 1036–1044, 1991.
- [13] R. Rodríguez-Baracaldo, J. A. Benito, E. S. Puchi-Cabrera, and M. H. Staia: High temperature wear resistance of (TiAl)N PVD coating on untreated and gas nitrided AISI H13 steel with different heat treatments, *Wear*, vol. 262, no. 3–4, pp. 380–389, 2007.
- [14] C. Courbon, M. Fallqvist, J. Hardell, R. M'Saoubi, and B. Prakash: Adhesion tendency of PVD TiAlN coatings at elevated temperatures during reciprocating sliding against carbon steel, *Wear*, vol. 330–331, pp. 209–222, 2015.
- [15] D. Arsic, V. Lazic, A. Sedmak, S. Aleksandrovic, J. Zivkovic, M. Djordjevic, G. Mladenovic: Effect of elevated temperatures on mechanical properties of ultra high strength hot work tool steel H11, *Trans. Famena*, vol. 44, no. 2, pp. 71–82, 2020.
- [16] A. Drnovšek, M. Rebelo de Figueiredo, H. Vo, A. Xia, S. J. Vachhani, S. Kolozsvari, P. Hosemann, R. Franz: Correlating high temperature mechanical and tribological properties of CrAlN and CrAlSiN hard coatings, *Surf. Coatings Technol.*, vol. 372, no. February, pp. 361–368, 2019.



Society of Production
Engineering

SPMS 2023

39. Savetovanje proizvodnog mašinstva Srbije

ICPES 2023

39th International Conference on Production Engineering of
Serbia



Faculty of Technical
Sciences
University of Novi Sad

Novi Sad, Serbia, 26. – 27. October 2023

INFLUENCE OF SHOULDER PINCHING GAP ON MECHANICAL PROPERTIES OF THE BOBBIN TOOL FSW WELDED JOINTS

Milan PECANAC^{1*}, Danka LABUS ZLATANOVIC^{1,2}, Nenad KULUNDZIC¹, Miroslav DRAMICANIN¹,
Petar JANJATOVIC¹, Mirjana TRIVKOVIC¹, Dragan RAJNOVIC¹, Sebastian BALOS¹,
Leposava SIDJANIN¹

¹Faculty of Technical Sciences, Department for Production Engineering, Novi Sad, Serbia,
pecanac.milan@uns.ac.rs, danlabus@uns.ac.rs, kulundzic@uns.ac.rs, dramicanin@uns.ac.rs,
janjatovic@uns.ac.rs, mirjana.trivkovic@uns.ac.rs, draganr@uns.ac.rs, sebab@uns.ac.rs,
lepas@uns.ac.rs

²Technical University in Ilmenau, Ilmenau, Germany, danka.labus-zlatanovic@tu-ilmenau.de

*Corresponding author: pecanac.milan@uns.ac.rs

Abstract: In modern industry, there is a great tendency for effective and eco-friendly technologies. Friction Stir Welding (FSW) is such a technology. FSW welding is predominantly used for welding aluminium and its alloys. A great advantage of FSW technologies is the fact that they do not require filler material for the welding process. Bobbin Tool Friction Stir Welding (BTFSW) is one of many iterations of FSW technology. This procedure is distinctive because it uses the tool with a dual shoulder. This feature enables the dual heat and stirring effect of the base material, thus producing more effective joints. Welding parameters dictate the properties of welded joints. However, the shoulder-pinching gap plays a significant role in welded joints as presented in this paper. Dimension of the shoulder pinching gap can dictate the shape of the welded joint, as well as welded joint properties. Interferences of the shoulder pinching gap used in the experiments were 4%, 6%, and 8%. Welded joints produced are in compliance with ISO 25239-5 standard. Tension, bend, and Charpy impact test results are reported.

Keywords: Welding, Friction Stir Welding, Bobbin tool, Welding parameters, Shoulder Pinching gap, Welded joint properties

1. INTRODUCTION

Friction welding has gained popularity in recent years because it enables the welding of materials that are considered un-weldable by conventional welding by localized melting. In the UK, at the end of 1991. Friction Stir Welding (FSW) was developed and patented at the Welding Institute [1–4]. This welding procedure

is quite unique because it is a solid-state welding procedure. The absence of localized melting of the base material enables lower heat input in the base material which results in lower stress input in the base material. The heat necessary for the welding process is generated by a combination of friction and pressure of the toll on the base material[5,6]. The friction-generated heat softens the base material and

the axial rotation of the tool mixes two plates, thus welding the parts together [4,7]. Another distinguishable thing about FSW is a spindle-like tool with specialized geometry. Tool geometry directly influences the quality of the welded joint [8]. Nowadays, more commonly known as conventional tool geometry consists of a tool shoulder and pin (figure 1a).

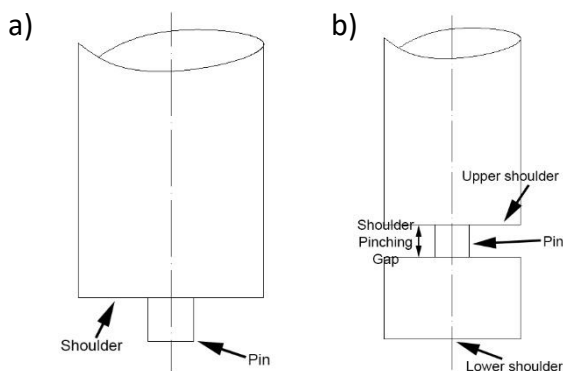


Figure 1. Friction Stir Welding tools; a) Conventional FSW tool, b) Bobbin FSW tool.

Since its arrival on the scene, FSW has been intensely developed and many variations of the tools have been created. Such as are Stationary shoulder tool, double-driven tool, bobbin tool, and many others. The bobbin tool is a very interesting concept of the FSW process, and a schematic depiction of the tool is presented in figure 1b.

Bobbin FSW tool has an upper and lower shoulder interconnected with the pin which is also known as the Shoulder Pinching Gap (SPG). Bobbin tool has certain advantages in comparison to the conventional FSW process. One of the biggest advantages of bobbin tool is dual-sided heat and stirring effect, as well as the elimination of vertical force which is essential for the conventional FSW process [9]. Also, the lower shoulder acts as a support for the base material and serves as secondary heat input and additional mixing of the softened base material. FSW equipment is relatively expensive, but it is common practice to adjust existing machines to do welding procedures. Most commonly engineers adjust vertical milling machines to perform simpler weld

designs[7,10]. FSW technology is also used for welding of the steels [11]. FSW is commonly used for welding of dissimilar materials that are considered not weldable with conventional welding fusion processes [12–14]. Main advantages of the FSW technology is low heat input (solid state procedure) that enables the welding of thin sheet metal [14], welding of dissimilar materials, refined grain structure of the weld [6], etc. Application of the FSW welding process is wide range of application that includes automotive, aerospace, nautical, railway, and many other industries. Disadvantages of the FSW process are expensive and robust equipment necessary for the welding process, defects that can occur if parameters are not adequate.

2. EXPERIMENTAL

To perform the FSW experiment, it was necessary to modify the vertical milling machine for the experiment. The milling machine used for the experiments was performed on FSSGVK-3 (Prvomajska, Zagreb, Croatia) vertical milling machine. The experimental setup is presented in Figure 2.

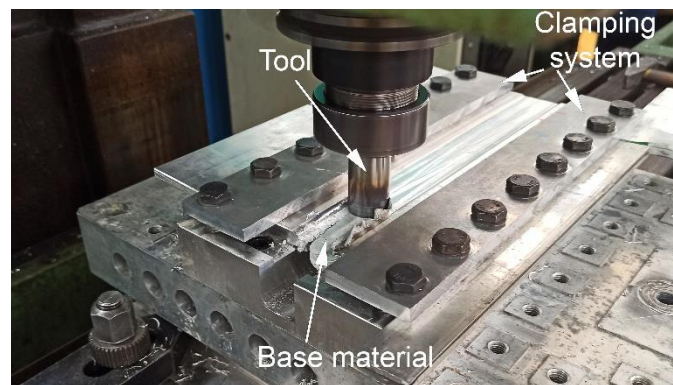


Figure 3. Experimental setup

The base material used was 5 mm thick aluminium-magnesium alloy (AA5005 H32). The chemical composition of the base material was obtained by an Optical emission spectrometer (ARL 3580) and the results are presented in Table 1. Mechanical properties of the base material were obtained via universal tension testing machine ZDM5/91 (VEB, Leipzig,

Germany). Tension test results are presented in table 2.

Table 1. Chemical composition of the base material.

Cu	Mn	Mg	Si	Fe	Zn	Ti	Al
0.04	0.14	0.6	0.22	0.29	0.06	0.02	Bal.

Table 2. Characteristics of the base material.

Rp [MPa]	Rm [MPa]	A [%]	Z [%]
120	135	15	60

The bobbin tool was made of H13 (X40CrMoV5-1) hot work tool steel in accordance with the drawing presented in Figure 3.

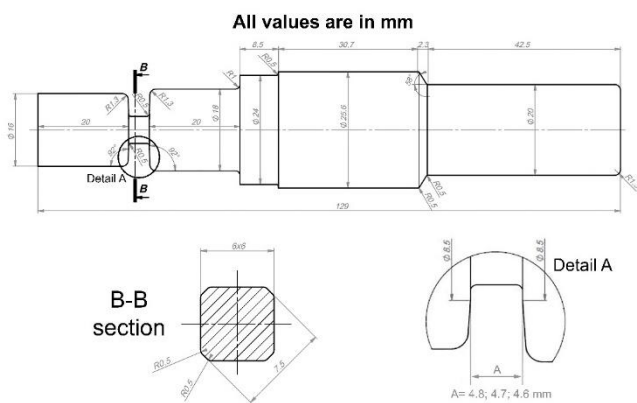


Figure 3. Drawing segment of the Bobbin FSW Tool

Three tools have been manufactured with different Shoulder pinching gaps (4.6; 4.7 and 4.8 mm). Weld designation system and parameters are shown in table 3.

Table 3. Sample designation system and welding parameters

Weld designation	SPG [mm]	Interference [mm]	Interference [%]	Tool rotation speed [rpm]	Weld. Speed [mm/min]
1	4.8	0.2	4	1400	20
2	4.7	0.3	6		
3	4.6	0.4	8		

After the welding, samples were cut for specimen manufacture. Metallographic specimens were prepared with the standard metallographic procedure: Grinding with SiC grinding paper starting with roughest (P300) and going to finest (P2500). Afterwards the grinding samples were polished with diamond suspension to achieve a mirror-like reflection. In the end, polished samples were electrolytically etched with Barker's reagents (1.8% Fluoboric acid in distilled water; 20÷47 V,

up to 2 minutes) to develop a coloured structure of the welded samples. Samples were observed with optical microscope Leitz Orthoplan. Samples for tension testing were tested on universal tensile testing machine VEB ZDM5-91 in accordance with EN ISO 4136:2012 [15]. Three-point bending was conducted also on universal tension testing machine VEB ZDM5-91 in accordance with EN ISO 5173:2010 [16]. Charpy impact test was performed on JWT-450 instrumented Charpy impact testing machine in accordance with EN ISO 148-1:2010 [17] the V-notch was placed in the middle of the welded joint.

3. RESULTS AND DISCUSSION

Samples that are etched with Barker's reagent and observed through a Leitz Orthoplan light microscope are presented in Figure 5.

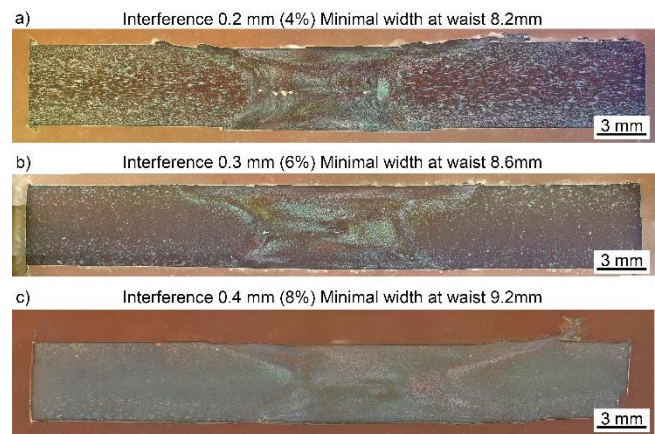


Figure 5. Etched samples; a) Sample 1; b) Sample 2; c) Sample 3

From Figure 5, it can be seen that samples have distinctive hourglass shape, while samples 1 and 2 have defects (tunnels) at the left side of the welded joint, represented by white marks. Sample 3 is the only one without defects. In accordance with EN ISO 25239-5 [18], only sample 3 can pass the B Acceptance level, which is most rigorous. All samples can pass C Acceptance level which tolerate defects with equation:

$$d \leq 0.2s \text{ or } 4\text{mm} \quad (1)$$

Where d stands for dimension of the defect (tunnel or a wormhole), and s is thickness of the

welded plate. Microstructural images were also taken on light microscope. Microstructural images are presented on figures 6 and 7.

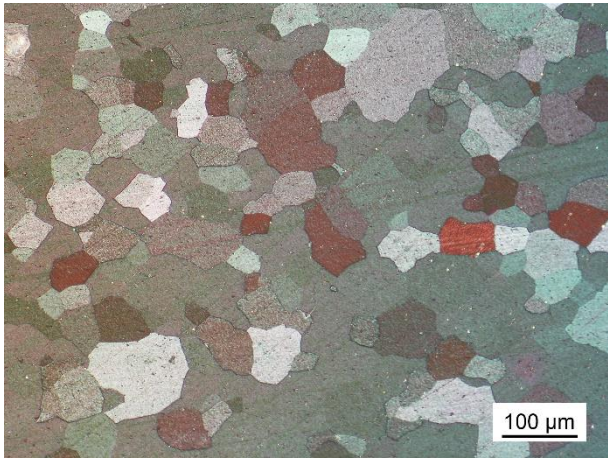


Figure 6. Base material microstructure.

From figure 6 it can be seen typical aluminium structure with grain average size 2.5 in accordance with ASTM E112-13 [19], which corresponds to 151 µm of average grain diameter. Nugget microstructure is presented on figure 7.

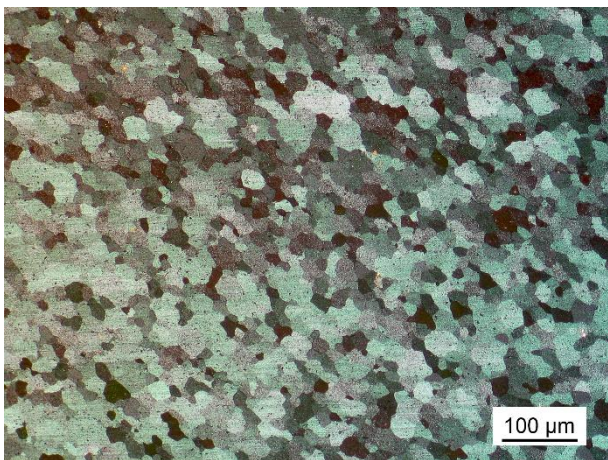


Figure 7. Nugget microstructure.

From figure 7 it can be seen that grain structure is refined with average grain size of 8.5 in accordance with ANST E112-13 [19], which corresponds with average grain diameter of 18.9 µm. This phenomenon is the result of dynamic recrystallization that occurs during the mixing of the softened base material by the tool [4,7].

Tension testing results are graphically presented in figure 8. Figure 8 shows that sample 3 has the highest value of ultimate strength and

reduction of the section. Lower tension characteristics of samples 1 and 2 can be attributed to the defects in the welded joint. Defects (tunnels) can be seen on figure 5.

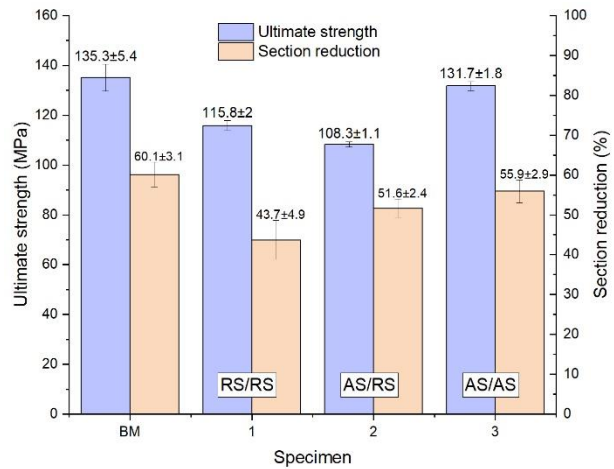


Figure 8. Tension test results.

Bend test samples are presented in Figure 9. All samples are bent to an angle of 180° without crack appearance or fracture of the sample. This can be explained from the tool's perspective because welded joint is heated and deformed from both sides. In conventional FSW, the tool has one shoulder, while the weld root is formed by the tool pin and backing plate.



Figure 9. Bend test samples.

Charpy impact test results are graphically presented in Figure 10. It can be seen that all samples have increased impact energy in comparison to base material. In sample, the highest value. This phenomenon can be attributed to the position of the notch in the sample and refined grain structure in the stir zone (nugget). Finer grain structure implicates the grain boundary hardening mechanism. Also,

it can be seen that crack initiation energy represented by orange bars is lower compared to green bars that correspond to the crack propagation energy. This trend is retained in all welded specimens as in base material.

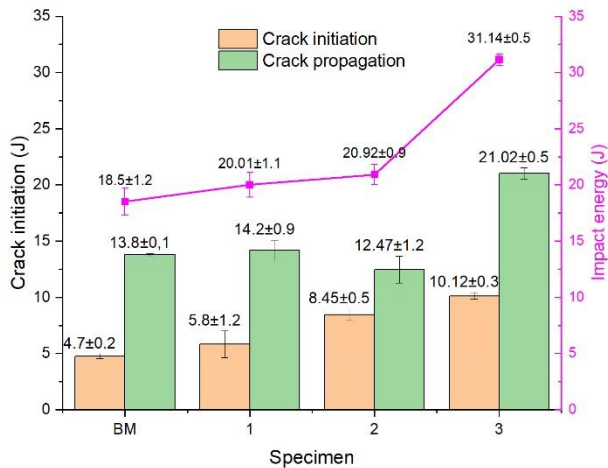


Figure 10. Charpy impact test results

4. CONCLUSIONS

From the results presented in this paper it can be concluded that:

- Welded samples have distinguishable hourglass shape.
- Samples have good tension characteristics, especially sample 3 with SPG 0.4mm
- All samples can be bent to 180° without crack appearance or fracture.
- Refined grain structure of the welded joint resulted in good impact energy of the tested samples.

5. ACKNOWLEDGEMENT

The authors gratefully acknowledge research support by the project entitled “Advanced materials, joining and allied technologies” in the Department of Production Engineering, Faculty of Technical Sciences Novi Sad, Serbia.

6. REFERENCES

[1] K. Fuse, V. Badheka, Bobbin tool friction stir welding: a review, *Sci. Technol. Weld. Join.* 24 (2019) 277–304.

<https://doi.org/10.1080/13621718.2018.1553655>.

[2] R.S. Mishra, M.W. Mahney, *Friction Stir Welding and Processing*, ASM International, 2007. <https://doi.org/10.1361/fswp2007p001>.

[3] S.S. Chaudhary, K.H. Bhavsar, A Review of Bobbin Tool Friction Stir Welding (FSW) Process, *Int. J. Sci. Technol. Eng.* 2 (2016) 630–633.

[4] M. Pecanac, D. Labus Zlatanovic, N. Kulundzic, M. Dramicanin, Z. Lanc, M. Hadzistevic, S. Radisic, S. Balos, Influence of Tool and Welding Parameters on the Risk of Wormhole Defect in Aluminum Magnesium Alloy Welded by Bobbin Tool FSW, *MDPI Met.* 12 (2022) 14. <https://doi.org/https://doi.org/10.3390/met12060969>.

[5] M.B. Đurđanović, M.M. Mijajlović, D.S. Milčić, D.S. Stamenković, Heat generation during friction stir welding process, *Tribol. Ind.* 31 (2009) 8–14.

[6] S. Kumar, A. Mahajan, S. Kumar, H. Singh, Friction stir welding: Types, merits & demerits, applications, process variables & effect of tool pin profile, *Mater. Today Proc.* 56 (2022) 3051–3057. <https://doi.org/10.1016/j.matpr.2021.12.097>.

[7] M. Pecanac, *Uticaj geometrije ramena alata na osobine zavarenih spojeva dobijenih zavarivanjem trenjem sa mešanjem*, Univerzitet u Novom Sadu, 2017.

[8] D. Labus Zlatanovic, *Friction stir spot welding of ultrathin sheets made of aluminium – magnesium alloy PhD Thesis*, University of Novi Sad, 2020.

[9] M. Habba, M. Ahmed, M. Seleman, A. EL-Nikhaily, An Analytical Model of Heat Generation for Friction Stir Welding Using Bobbin Tool Design, *J. Pet. Min. Eng.* 20 (2018) 1–5. <https://doi.org/10.21608/jpme.2019.37963>.

[10] S. Balos, D.L. Zlatanovic, N. Kulundzic, P. Janjatovic, M. Dramicanin, Z. Lanc, M. Hadzistevic, S. Radisic, D. Rajnovic, M. Pecanac, Influence of Tool – Base Metal Interference on the Performance of an Aluminium – Magnesium Alloy Joined via Bobbin Tool Friction Stir Welding, *MDPI Met.* (2023). <https://doi.org/https://doi.org/10.3390/me>

t13071215.

- [11] D.G. Mohan, C.S. Wu, A Review on Friction Stir Welding of Steels, Chinese J. Mech. Eng. (English Ed. 34 (2021).
<https://doi.org/10.1186/s10033-021-00655-3>.
- [12] Z. Boumerzoug, Joining of dissimilar materials by friction stir welding, MATEC Web Conf. 224 (2018).
<https://doi.org/10.1051/matecconf/201822401118>.
- [13] N. Kumar, W. Yuan, R.S. Mishra, Friction Stir Welding of Dissimilar Alloys and Materials, Waltham, USA, 2015.
<https://doi.org/10.1016/b978-0-12-802418-8.00001-1>.
- [14] M. Haghshenas, A.P. Gerlich, Joining of automotive sheet materials by friction-based welding methods: A review, Eng. Sci. Technol. an Int. J. 21 (2018) 130–148.
<https://doi.org/10.1016/j.jestch.2018.02.008>.
- [15] ISO, BS EN ISO 4136: Destructive tests on welds in metallic materials - Transverse tensile test (ISO 4136:2012), (2013) 1–20.
- [16] ISO, EN ISO 5173:2009 Destructive tests on welds in metallic materials.pdf, (209AD) 26.
- [17] ISO, EN ISO 148-1 - 2010 Charpy Part 1 Test method.pdf, (2010).
- [18] ISO, ISO 25239-5 Quality and inspection requirements, (2020).
- [19] ASTM, ASTM E112 - 13 Standard Test Methods for Determining Average Grain Size, (2013) 28.



Society of Production
Engineering

SPMS 2023

39. Savetovanje proizvodnog mašinstva Srbije

ICPES 2023

39th International Conference on Production Engineering of
Serbia



Faculty of Technical
Sciences
University of Novi Sad

Novi Sad, Serbia, 26. – 27. October 2023

ISPITIVANJE BALISTIČKE OTPORNOSTI ŠLJEMA OJAČANOG ARAMIDNIM VLAKNIMA

Stanko SPASOJEVIĆ^{1*}, Katarina ILIĆ¹, Ana BRDAR¹, Miroslav DRAMIĆANIN¹, Milan PEĆANAC¹,
Petar JANJATOVIĆ¹, Mirjana TRIVKOVIĆ¹, Dragan RAJNOVIĆ¹, Sebastian BALOŠ¹, Lepasava
ŠIĐANIN¹

¹Departman za proizvodno mašinstvo, Fakultet tehničkih nauka, Univerzitet u Novom Sadu, Srbija,
*spasojevic@uns.ac.rs; anab@uns.ac.rs, katailic@uns.ac.rs., dramicanin@uns.ac.rs,
pecanac.milan@uns.ac.rs, janjatovic@uns.ac.rs., mirjana.trivkovic@uns.ac.rs, draganr@uns.ac.rs,
sebab@uns.ac.rs, lepas@uns.ac.rs

Apstrakt: U radu je izvršeno balističko ispitivanje kompozitnog šljema izrađenog od epoksidne smole ojačane aramidnim vlaknima. Ispitivanja su izvršena streljačkim oružjem u različitim kalibrima kako bi se dobila balistička otpornost kompozitnog šljema. Pored toga, izvršena su mjerenja deformacije šljema, kao i koliko je slojeva šljema probijeno tokom udara. Rezultati koji su dobijeni korišteni su za utvrđivanje balističkih osobina samog šljema, kao i poređenje preformansi kompozitnog sa čeličnim šljedom. Upoređivanjem osobina utvrđeno je da kompozitni šljemovi imaju veću balističku otpornost od svojih prethodnika od čelika, pre svega zahvaljujući visokim mehaničkim osobinama aramidnih vlakana, kao i većoj debljini zbog manje gustine kevlaru u odnosu na čelik.

Ključne reči: kompozitni šljem, balističko ispitivanje, deformacija, proboj.

1. UVOD

Šljemovi imaju dugu istoriju koja datira još od Arsije tačnije iz 800. godine p.n.e. Od tada pa sve do danas prošli su dug razvojni put, gdje su pored oblika, ključnu ulogu imali i materijali od koga su se izrađivali. Prvi šljemovi koji su se izrađivali imali su manju izdržljivost, odnosno bili su podložni deformacijama, jer su se izrađivali od bronz. U periodu od starog rata do kraja 70tih šljemovi su se pretežno izrađivali od čelika, a od kraja 70tih godina prošlog vijeka počeli su se izrađivati od kompozitnih materijala. Šljemovi su ključna i najupotrebljivija kopnena zaštita vojnika, koja treba da štiti glavu vojnika od parčadi

artiljerijskih sredstava i streljačkog naoružanja, jer prema ispitivanju glava predstavlja 9% tijela izloženog u borbi, a ujedno i 20% svih smrtnih slučajeva je rezultat pogotka u glavu [1].

2. SAVREMENI ŠLJEMOVI

Nedostaci prethodnih šljemova u vidu male balističke izdržljivosti i lake deformacije su bili neprihvatljivi, a zbog straha od novog rata tragalo se za novim i boljim materijalom za izradu šljemova. Tako da potpuno nova era započinje otkrićem kevlaru. Šljemovi izrađeni od ovog materijala dobijaju naziv PASGT (Personnel Armor System for Ground Troops u slobodnom prevodu – lični oklopni sistem za

kopnene trupe), slika 1 [2]. Ovi šljemovi imaju odličan bilans između svih neophodnih zahtjeva koje treba da ispuni savremeni šljem [3].



Slika 1. Izgled PASGT šljema [4].

Kevlar kao materijal posjeduje visoku čvrstoću kao i visok odnos čvrstoće i mase, otpornost na udare velike brzine što čini ovaj materijal u pojedinim oblastima povoljniji od metala, odnosno legura. On je vrsta vlakna koje se zove aramid, skraćeno od „aromatični aramidi“ [5].

3. EKSPERIMENTALNI DIO

Predmeti eksperimenta su tri šljema od različitih materijala: dva šljema od kompozitnih materijala i jedan od čelika. Jedan kompozitni šljem je ojačan staklenim vlaknima, a drugi aramidnim vlaknima. Cilj rada je da se utvrde probojni mehanizmi različitim vrstama municije i balistička otpornost šljemova.

Tokom eksperimenta šljemovi su postavljeni na tri drvene letve, koje su zabijene u zemlju kako ne bi došlo do pomjeranja. Dok su oko njih postavljene gume radi dodatne sigurnosti.

Šljemovi koji su korišteni u eksperimentu prikazani su na slici 2:

1. M-59/85 iz perioda SFRJ je izrađen od manganskog čelika. Debljina šljema je 1,3 mm.
2. M-89 je takođe iz perioda SFRJ, izrađen je od staklenih vlakana vezanih polifitalatnim estrima.
3. ACH (Advanced Combat Helmet- napredni borbeni šljem), takođe izrađen od kompozitnog materijala, ali za razliku

od M-89 koji je izrađen od staklenih vlakana ovaj šljem je izrađen od aramidnih vlakana vezanih epoksidnom smolom. Masa „školjke“ ovog šljema bez vezivih kaiševa i boje je 1 kg.



Slika 2. Šljemovi i pistolji sa revolverima koji su korišteni za balističko ispitivanje.

Prilikom eksperimenta u šljem je pucano iz sledećih kalibara:

- I. CZ-75 poluautomatski pištolj češke proizvodnje, u kalibru 9x19 mm Parabellum, sa municijom:
 - Full metal Jacket (FMJ) - sa punom košuljicom, masom zrna 124 gr (8g), power factor-om 128 (PF 128) i početnom brzinom 315 m/s.
 - Full metal Jacket (FMJ) - sa punom košuljicom, masom zrna 145 gr (8g), power factor-om 145 (PF 145) i početnom brzinom 356 m/s.
- II. Zastava M-57 poluautomatski pištolj u kalibru 7,26x25 mm Tokarev, sa municijom:
 - Full metal Jacket (FMJ) - sa punom košuljicom, masom zrna 85 gr (5,5g) i početnom brzinom 356 m/s.
- III. Revolver Ruger GP100 proizveden u SAD-u, u kalibru .357 Magnum sa municijom:
 - Flat Point Jacket (FMJ) – sa tupim vrhom, mase 158 gr (10,2 g) i početnom brzinom 430 m/s.

- Flat Point Jacket (FMJ) – sa oštirim vrhom, mase 158 gr (10,2 g) i početnom brzinom 410 m/s.
- IV. Just Right Carbine (JRC) – Karabin u kalibru 9x19 mm, sa power faktorom 145 (PF 145) i početnom brzinom 430 m/s.

4. REZULTATI I DISKUSIJA

Za mjerenje deformacije šljema nastalih prilikom proboja metaka korišćeno je mjerilo za zavarene spojeve.

Tabela 1. Rezultati ispitivanja na probojnost.

Oružja/kalibri	Šljemovi*		
	M-59/85	M-89	ACH
CZ-75 (9x19 mm PF128)	NE (17 mm)	NE (2 mm)	NE (18 mm)
CZ-75 (9x19 mm PF145)	NE (10mm)	NE (7 mm)	NE (15 mm)
M-57 (7,62x25 mm)	DA	DA	NE (11 mm)
Ruger GP100 (.357 tupo zrno)	NE (26 mm)	DA	NE (24 mm)
Ruger GP-100 (357 oštro zrno)	NE (17 mm)	DA	NE (14 mm)
JRC (9x19 mm PF145)	NE (15 mm)	DA	NE (14 mm)

* NE-nije došlo do proboja, DA-došlo je do proboja, a u zagradama se nalazi veličina deformacije.

U tabeli 1 se mogu vidjeti rezultati uticaja metaka na probojnost šljemova i njihovu deformaciju. Primjetno je da kod šljema M-59/85 dolazi do proboja samo kod kalibra 7,62x25 mm, a kod ostalih kalibara nemamo proboj, ali je prisutna deformacija od 10 mm do 26 mm. Kod deformacija većih od 25,4 mm sa prednje i zadnje strane, a 16 mm sa bočne i gornje strane smatra se da nemaju zaštitu jer prouzrokuju teške povrede vojnika. Takva deformacija se javlja kod kalibra .357 Magnum sa tupim zrnom, tako da se ne može smatrati da ovaj šlem pruža zaštitu od te municije.

Prilikom ispitivanja šljema M-89 do proboja dolazi kod kalibara 7,62x25 mm, .357 tupo zrno, 357 oštro zrno, 9x19 mm PF145. Dok se

deformacija u maloj mjeri javila kod kalibra 9x19 mm PF128, 9x19 mm PF145.

Kao poslednji šljem na kome je vršeno ispitivanje je ACH kod koga nije došlo do proboja ni kod jednog gađanja, a deformacija se kretala u granicama od 11 mm pa do 24 mm sa boka kod kalibra .357 (tupo zrno) gdje možemo reći da je to izuzetna velika deformacija koja može ostaviti teške povrede vojnika. Tako da hitac ostvaren sa municijom .357 Magnum sa tupim zrnom smatra se opasnim po nosioca šljema ACH i da ne štiti vojnika od te municije.

Nakon gađanja sva zrna koja su ostala unutar kompozitnih šljemova su izvađena i analizirana. Kod svih kalibara osim kod metka .357 (oštro zrno) postignut je pogodak pod približno pravim uglom i pri tome zrno dobija oblik pečurke koji je karakterističan za pogotke pod pravim uglom, slika 3.



Slika 3. Izgled metka 9x19 (128) nakon što je izvađen iz šljema.

Za .357 Magnum sa oštirim zrnom smatra se da nije ušlo pod pravim uglom u odnosu na površinu šljema. Metak .357 (oštro zrno) je pronađen na nekih 50 mm od samog ulaza metka u šljem. Zbog toga se smatra da metak nije ušao pod pravim uglom i da je zbog oštrog vrha koji može indukovati nestabilnost pri proboju, kao i zbog slojeva kevlar koji pružaju otpor prilikom proboja primoran da ide linijom manjeg otpora, gdje je zaustavljen posle kratke razdaljine. Izgled metka .357 (oštro zrno) je prikazan na slici 4, gdje je primjetno da nema karakterističan oblik pečurke nego neravnomjerno izdeformisan vrh.



Slika 4. Izgled metka .357 (oštro zrno) nakon što je izvađen iz šljema.

Nakon što je zrno izvađeno iz šljema pristupljeno je još jednom eksperimentu, a to je određivanje broja slojeva šljema i broja slojeva koji su pomenuti kalibri probili. Zbog preklapanja slojeva ustanovljeno je da broj slojeva nije jednak u svim dijelovima šljema i da je prosjek slojeva 11.

Tabela 2. Prikaz probijenih slojeva

	Broj slojeva	Postotak proboja
CZ-75 (9x19 mm PF128)	3	27%
CZ-75 (9x19 mm PF145)	3	27%
M-57 (7,62x25 mm)	5*	45%
Ruger GP-100 (357 oštro zrno)	4	36%
JRC (9x19 mm PF145)	4*	36%

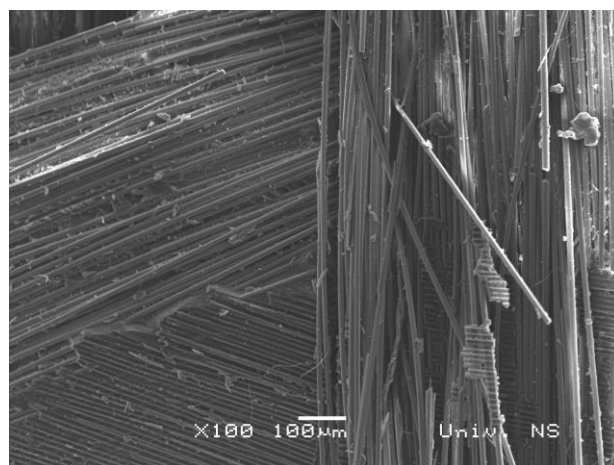
*ostešen naredni sloj

Kalibri koji su ispaljeni iz pištolja CZ-75 su pokazali najmanju stetu po broju probijenih slojeva, ali su oni i najslabiji kalibri u ovom slučaju. Takođe, kalibar koji je ispaljen iz pištolja M-57 ima najveću probojnu moć sa pet probijenih slojeva i oštećenim šestim slojem, što je približno pola debljine šljema.

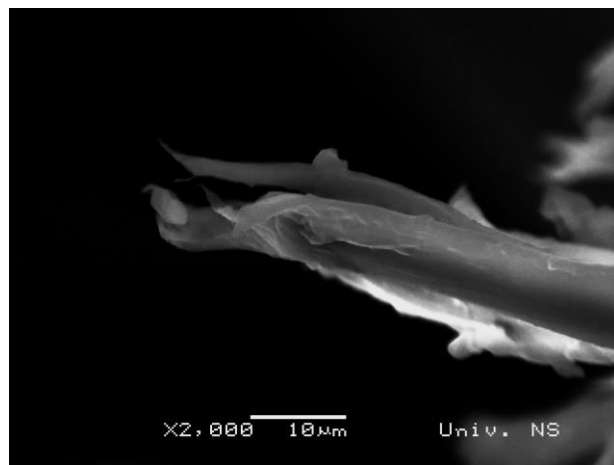
Za posmatranje uzoraka pod SEM mikroskopom korišćen je uređaj „JEOL JSM 6460 Scanning Electron Microscope“ sa zadatim standardnim parametrima 20 kV na 10 mm u visokom vakumu.

Zona loma staklenih i aramidnih vlakana koja je posmatrana na SEM-u prikazana na slici 5 i 6. Gdje je uočljiv sloj vlakana koji je utisnut u

vezivo prilikom udara projektila. Kod aramidnih vlakana vidljiva je plastična deformacija vlakana, odnosno kako dolazi do suženja vlakana na više mjesta, što se najvjerovatnije odnosi na mikrofibrile unutar jednog aramidnog vlakna. Staklena vlakna nemaju izraženu plastičnu deformaciju nego se kod njih javlja krta lom. Iako ova dva materijala imaju sličnu zateznu čvrstoću (3445 MPa staklo [6], odnosno 3620 MPa aramid [7]) ova pojava predstavlja glavnu razliku između njih.



Slika 5. Kompozitni materijal sa staklenim vlaknima snimljen na SEM-u.



Slika 6. Kompozitni materijal sa aramidnim vlaknima snimljen na SEM-u.

5. ZAKLJUČCI

- Zahvaljujući visokim mehaničkim karakteristikama aramidnih vlakana, ACH šljem ima bolju balističku otpornost u poređenju sa šljemovima M-59/89 i M-89, koji imaju slične osobine.

- Prilikom upotrebe kalibra .357 Magnum sa tupim zrnom dolazi do deformacije unutrašnje strane ACH šljema koja je veća od preporučene vrijednosti, što ukazuje da ovaj šljem ne pruža dovoljnu zaštitu pri upotrebi ovog kalibra i municije ovog tipa.
- Dobra karakteristika kevlar je što zadržava masu koja je na nivou čeličnih šljemova, koji nisu uspjeli odoliti većini kalibara.
- Prednosti šljema ACH mogu da se pripišu dobrim karakteristikama aramidnih vlakana da se plastično deformišu i na taj način obezbijede veću balističku otpornost.
- Pri udaru projektila pod uglom manjim od 90° u odnosu na površinu šljema, kod čeličnog šljema dolazi do rikošeta i deformacije šljema, a kod kompozitnih šljemova javlja se proboj površinskih slojeva i kretanje zrna između slojeva što dovodi do relativno male deformacije.

6. ZAHVALNOST

Ovaj rad je rezultat rada autora u okviru projekta pod naslovom „Savremeni materijali, tehnologije spajanja i srodni postupci“ Laboratorije za ispitivanje materijala i Laboratorije za zavarivanje, Departmana za proizvodno mašinstvo, Fakulteta tehničkih nauka.

7. LITERATURA

- [1] Shadrake D. "Putting a lid on it (First World War equipment design)": Engineering & Technology (2014), vol 9, pp: 44- 47.
- [2] Michael E. Carey, M.D., Matthew Herz, Ph.D., Brian Corner, Ph.D., Joseph McEntire, M.E., Malabarba, M.A., Steven Paquette, M.A., James B. Sampson, Ph.D., Ballistic Helmets and Aspects of Their Design Department of Neurosurgery (MEC), Louisiana State University Health Sciences Center, New Orleans , Natick Soldier Center (MH, BC, DM, SP, JBS), Natick, Massachusetts; and U.S. Army Aeromedical Research Laboratory (JM), Fort Rucker, USA, 2000
- [3] Carey M.E., Joseph A.S., Morris W.J., McDonnell D.E., Rengachary S.S. Brain wounds and their treatment in VII Corps during Operation Desert Storm, February 20 to April 15, 1991., Mil Med (1998), vol. 163, pp: 581-586.
- [4] <https://unitedshield.uk/images/products/helmets/pasgt-feature.jpg> (pristupljeno u oktobru 2023.)
- [5] Tanner D., Fitzgerald J. A., Phillips B. R. The Kevlar Storyan Advanced Materials Case Study: Advanced Materials (1989) vol. 28, pp: 649-654.
- [6] Sathishkumar T.P., Satheeshkumar S., Naveen J., Glass fiber-reinforced polymer composites - a review, Journal of Reinforced Plastics and Composites, Vol. 33: 1258, 2012.
- [7] Pourdeyhimi B., Wagner H. D., Schwartz P., A comparison of mechanical properties of discontinuous Kevlar 29 fibre reinforced bone and dental cements: Journal of Material Science, Vol. 21, 4468-4474, 2012

TESTING OF THE BALLISTIC RESISTANCE OF A HELMET REINFORCED WITH ARAMID FIBERS

Abstract: *In the paper, a ballistic test of a composite helmet made of epoxy resin reinforced with aramid fibers was performed. Tests were performed with firearms in different calibers in order to obtain the ballistic resistance of the composite helmet. In addition, measurements were made of the deformation of the helmet, as well as how many layers of the helmet were broken during the impact. The obtained results were used to determine the ballistic properties of the helmet itself, as well as to compare the performance of the composite and steel helmet. By comparing the properties, it was determined that composite helmets have a higher ballistic resistance than their steel predecessors, primarily due to the high mechanical properties of aramid fibers, as well as greater thickness due to the lower density of Kevlar compared to steel.*

Keywords: *composite helmet, ballistic testing, deformation, penetration*



Society of Production
Engineering

SPMS 2023

39. Savetovanje proizvodnog mašinstva Srbije

ICPES 2023

39th International Conference on Production Engineering of
Serbia



Faculty of Technical
Sciences
University of Novi Sad

Novi Sad, Serbia, 26. – 27. October 2023

INFLUENCE OF WAAM TECHNOLOGY PARAMETERS ON PROPERTIES OF STRUCTURAL STEEL WALLS

Katarina ILIC¹, Albert HAUCK¹, Ana BRDAR¹, Stanko SPASOJEVIC¹, Miroslav DRAMICANIN¹, Milan PECANAC¹, Petar JANJATOVIC^{1*}, Mirjana TRIVKOVIC¹, Dragan RAJNOVIC¹, Sebastian BALOS^{1*}, Leposava SIDJANIN¹

¹Department of Production Engineering, Faculty of Technical Science, University of Novi Sad, Trg Dositeja Obradovica 6, 21000 Novi Sad, Serbia

*Corresponding author: sebab@uns.ac.rs

Abstract: Wire Arc Additive Manufacturing (WAAM) is an innovative welding technology that combines Gas Metal Arc Welding (GMAW) and welding robot. The production process of WAAM is carried out by welding robots that are depositing layers of metal on top of each other. The presented research focuses on the influence of different welding parameters and deposition strategies of WAAM on the mechanical properties and microstructures. On the obtained samples in form of walls, the following tests were carried out: visual and macro cross-section examination, tensile testing, impact energy testing, and bend testing. It was found that welding parameters, especially welding current and voltage have a significant effect on the porosity and mechanical properties and geometry of the material.

Keywords: Wire Arc Additive Manufacturing (WAAM), Gas Metal Arc Welding (GMAW), mechanical properties, robot welding, welding parameters

1. INTRODUCTION

Wire arc additive manufacturing (WAAM) is a process which uses the electric arc to melt and deposit the consumable in form of wire, guided by an automatic device, typically a robot. This process was invented in 1925, within the framework of the patent entitled "The Use of an Electric Arc as a Heat Source to Generate 3D Objects Depositing Molten Metal in Superimposed Layers" [1,2]. In parallel to this,

Escholz proposed the application of an electric arc to deposit metal to create various ornamentation using a layering method [3]. These patents created a foundation for a further development, that ultimately resulted in WAAM as we know it today. Muller Albert proposed the application of wire feed for so called Shape welding" [4]. Ujiie, from Mitsubishi fabricated the whole pressure vessel by submerged arc welding (SAW) and TIG welding processes, applying different wires to

create functionally graded walls, in 1971. Kussmaul [5] used shape welding to fabricate large parts for nuclear power plants weighing 79 t. Research of Acheson and Dickens [6,7] shed light in the field of automation and process parameters such as voltage, wire feed rate, nozzle distance, etc. Finally, in 2002, GMAW was vastly improved by the application of CAD/CAM (Computer Aided Design/Manufacturing) system [8]. Subsequently, cold metal transfer (CMT) was successfully applied in the fabrication of massive Ti-alloy parts, with full control of the weld bead geometry through welding parameters [9,10]. Today, WAAM technology combines the benefit of welding processes (GMAW/TIG) and robotic guidance.

Compared to Selective Laser Melting (SLM), the equipment for WAAM is cheaper, more effective (over 80 % and closing to 100 %, compared to 40-60 %), higher deposition rate, higher safety, very wide wire types equivalent to welding consumables, but, the surface quality is lower, requiring machining finishing [11].

The aim of this paper is to find the influence of different GMAW welding parameters and deposition strategies of WAAM on the mechanical properties and microstructures using SG2 wire.

2. EXPERIMENTAL PART

WAAM process was done on Fanuc ARC Mate 100iC/8L robot coupled to EWM Phoenix puld 500 A GMAW welding machine, Figure 1.



Figure 1. WAAM setup

Base material used for WAAM hardfacing and deposition is S355 structural steel, 10 mm thick, and the dimensions of 500x150 mm. Consumable used was Thyssen Energomag 2; SG2 1.2 mm wire, having the nominal chemical composition and mechanical properties of the deposited layer given in Tables 1 and 2. Shielding gas used in all experiments was C18 (82 % Ar, 18 % CO₂), with 15 l/min flow.

Table 1. Nominal chemical composition of the SG2 wire; EN ISO 14341-A-G 42 4 C1/M21 3Si1 (mass.%; Fe balance)

%C	%Si	%Mn	%P	%S	%Cu	%Cr	%Ni	%Ti
0.07	0.85	1.45	0.02	0.02	0.25	<0.15	<0.15	< 0.05

Table 2. Mechanical properties of the deposited layer; EN ISO 14341-A-G 42 4 C1/M21 3Si1

Yield strength R _e [MPa]	Tensile strength R _m [MPa]	Elongation A [%]
450	550	>24

Two basic welding strategies were used, Figure 2, to fabricate three specimens:

a) Specimen 1 was welded with strategy 1 (Figure 2a), welding was done in 52 passes, with current declining from 160 to 107 A and wire feed from 6 to 3,5 m/min.

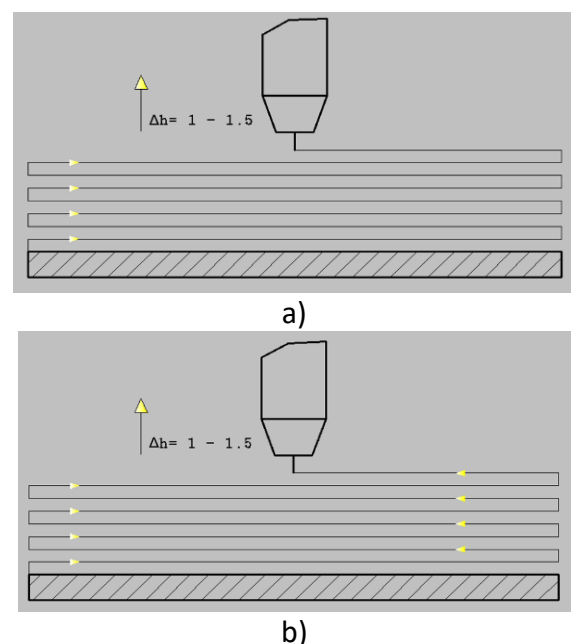


Figure 2. Welding strategies: a) welding in one direction indicated by arrow (specimen 1); b) welding in both directions (specimens 2, 3)

b) Specimen 2 was welded with strategy 2 (Figure 2b), in 56 passes, with 160 A and 6 m/min feed.

c) Specimen 3 also with strategy 2 (Figure 2b), in 61 passes, 184 A and 7 m/min feed.

Metallographic study, tensile, bend and impact tests were performed in order to characterize the obtained specimens. Tensile and bend testing were done on VEB ZDM 5/91 tensile testing machine, impact strength on JWT-450 Charpy pendulum tester. Metallographic testing was performed after a standard preparation which consisted of cutting, grinding with abrasive papers, from the coarsest to the finest (P120 to P2500), polishing with diamond suspensions (6, 3, 1 and $\frac{1}{4}$ μm) and etching by 3 % Nital (HNO_3 in ethyl-alcohol).

3. RESULTS AND DISCUSSION

WAAM specimens are shown in Figure 3. Specimen 1 is notably smoother than Specimens 2 and 3, however, it can be seen that the finishing side collapsed, a common macro defect in WAAM. The main cause is the excessive heat accumulation at the end of each pass, which is similar to the results obtained by Duarte et al. [12].



a)



b)



c)

Figure 3. Welded specimens: a) Specimen 1; b) Specimen 2; c) Specimen 3

WAAM macro sections taken 20 mm from the end of the specimens (Specimen 1 20 mm from the point of collapse) are shown in Figure 4. The thicknesses vary from 6,4 mm on average in Specimen 1, to 7 mm in Specimen 2 and 6.9 mm in Specimen 3. It can be seen that the edges in Specimen 1 are the smoothest, which is in accordance to Figure 3. Also, the porosity is the highest in Specimen 3, which is the most pronounced in the middle of the specimen, towards the surface. These pores are the result of a relatively high welding speed, so that the gases are still entrapped within the crystallized material.



a)



b)



c)

Figure 4. Cross sections: a) Specimen 1; b) Specimen 2; c) Specimen 3

Tensile properties are shown in Table 3. The highest yield and tensile strength values were obtained in Specimen 2. This is the result of the lack of porosity, which can be observed in Figure 4. These values are well within the nominal properties of S355 structural steel. The lowest standard deviations are also in Specimen 2, while the highest are in Specimen 3, which are the least uniform in terms of porosity. In all specimens, ductile fracture is present, with a more intensive deformation in Specimens 1 and 2, also due to a high porosity in Specimen 3, which is reflected by a lower elongation in Table 3.

Table 3 Average tensile properties

	R_p [MPa]	R_m [MPa]	A [%]
Specimen 1	430±21	500±18	31±2
Specimen 2	471±11	540±5	29±2
Specimen 3	365±88	384±79	17±10
Nom. values for S355 steel	355-550	490-630	>22



Figure 5. Representative tensile specimens: a) Specimen 1; b) Specimen 2; c) Specimen 3

Impact properties are shown in Table 4. All specimens comply with nominal values for S355 steel.

Table 4 Average impact strengths

	KV [J]
Specimen 1	67±2
Specimen 2	56±4
Specimen 3	30±8
Nominal values for S355 steel	>27

The highest average value was obtained in Specimen 1, which complies well with the

highest elongation presented in Table 3. As in tensile testing, fractures are ductile, with intensive plastic deformation, Figure 6. Specimens 1 and 2 suffered an incomplete fracture.

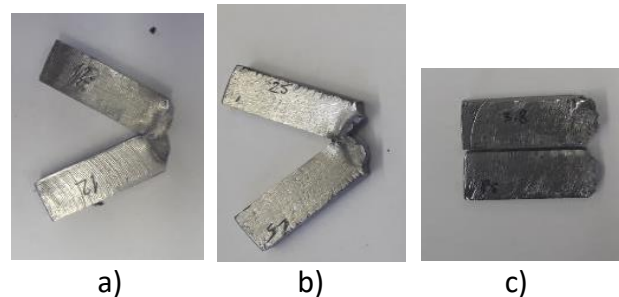


Figure 6. Representative impact testing specimens: a) Specimen 1; b) Specimen 2; c) Specimen 3

Bend testing results are shown in Figure 7. It can be seen that some defects are present in convex, tensile area of the specimens 1 and 2, however, these are minor, less than 2 mm in size. In Specimen 3, large irregularities can be observed, which are also the result of porosity in this specimen.

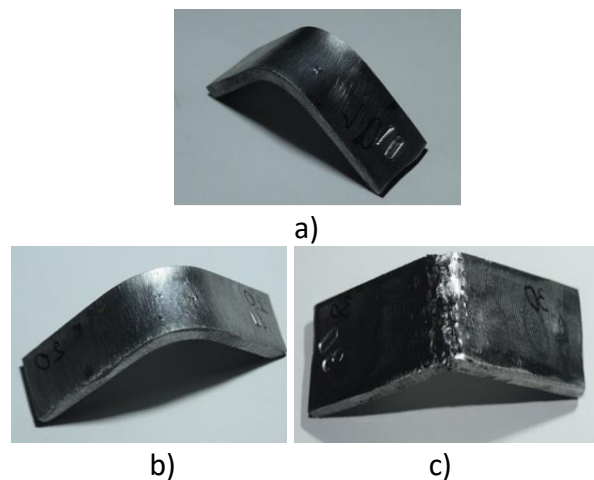


Figure 7. Representative bend testing specimens: a) Specimen 1; b) Specimen 2; c) Specimen 3

4. CONCLUSION

Based on the results obtained and within the limitations of this work, the following conclusions can be drawn:

- The specimen 1 welded in one direction suffered a collapse at the end of each pass, which largely restricts the useful macro-defect-free area of the specimen.
- Macro images reveal a significant porosity in specimen 3, welded with the highest welding speed and welding in both directions.
- The highest porosity is the result of the highest welding speed, preventing the entrapped gasses to escape from the weld.
- Tensile properties are the highest in specimen 2, fully complying to S355 steel tensile properties. Impact properties are the highest in specimen 1. In both tests, ductile fracture is present.
- Bend testing resulted in acceptable defects in the convex area.

ACKNOWLEDGEMENT

The authors gratefully acknowledge research support by the project entitled “Advanced materials, joining and allied technologies” in the Department of Production Engineering, Faculty of Technical Sciences Novi Sad, Serbia.

REFERENCES

- [1] US423647A, Method of Making Decorative Articles. Baker Ralph; Perth, Australia, 1925.
- [2] Baker: The Use of an Electric Arc as a Heat Source to Generate 3D Objects Depositing Molten Metal in Superimposed Layers, Baker, Chicago, IL, USA: 1926.
- [3] US1533239A, Ornamental Arc Welding. CBS Corp.; New York, NY, USA, 1925.
- [4] US2504868A, Electric Arc Welding. Airco Inc.; Punta Gorda, FL, USA, 1950.
- [5] K. Kussmaul, F.W. Schoch, H. Luckow: High-quality large components shape welded by a SAW process, *Weld. J.* Vol. 62, pp. 17-24, 1983.
- [6] US4952769A, Automatic Welding Apparatus for Weld Build-Up and Method of Achieving Weld Build-Up. Bow Mills Bank and Trust; South Street Bow, NH, USA, 1990.
- [7] P.M. Dickens, M.S. Pridham, R.C. Cobb, I. Gibson, G. Dixon: Rapid Prototyping Using 3-D Welding in: *1992 International Solid Freeform Fabrication Symposium*, 3-5 Aug. 1992, The University of Texas at Austin; Austin, TX, USA, pp. 1-11.
- [8] H.F. Wang, Y.L. Zhang: CAD/CAM integrated system in collaborative development environment, *Robot. Comput. Integr. Manuf.* Vol 18, pp. 135–145, 2002.
- [9] A. P. Williams. Innovative process model of Ti–6Al–4V additive layer manufacturing using cold metal transfer (CMT) in: *21st Annual International Solid Freeform Fabrication Symposium—An Additive Manufacturing Conference, SFF*. January 2010, University of Texas at Austin; Austin, Texas, pp 1-12.
- [10] J.S. Gaddes: Parametric Development of Wire 3D Printing, Auburn University; Auburn, AL, USA, 2015.
- [11] S.W. Williams, F. Martina, A.C. Addison, J. Ding, G. Pardal, P. Colegrove: Wire + arc additive manufacturing, *Materials Science and Technology*, Vol. 32, pp. 641–647, 2016.
- [12] R. D. Valdemar, A. R. Tiago, N. Schell, R.M. Miranda, J.P. Oliveira, T. G. Santos: Hot forging wire and arc additive manufacturing (HF-WAAM), *Additive Manufacturing*, Vol. 35, pp. 1-10, 2020, 101193



Society of Production
Engineering

SPMS 2023

39. Savetovanje proizvodnog mašinstva Srbije

ICPES 2023

39th International Conference on Production Engineering of
Serbia



Faculty of Technical
Sciences
University of Novi Sad

Novi Sad, Serbia, 26. – 27. October 2023

INFLUENCE OF STRAIN RATE ON METALLURGICAL AND MECHANICAL PROPERTIES OF FRICTION STIR SPOT WELDED ALUMINIUM JOINTS

**Danka LABUS ZLATANOVIC^{1,2*}, Jean Pierre BERGMANN¹, Sebastian BALOS², Petar JANJATOVIC²,
Dragan RAJNOVIC¹, Lepasava SIDJANIN²**

¹Department of Production Technology, Technische Universität Ilmenau, 98693 Ilmenau, Germany

²Department of Production Engineering, Faculty of Technical Science, University of Novi Sad,
21000 Novi Sad, Serbia

*Corresponding author: danlabus@uns.ac.rs

Abstract: Nowadays, the substitution of copper with aluminium is widely pursued in order to save weight and material costs, for battery components and wire connectors. Additionally, cost reductions can be further enhanced with effective reduction of energy consumption through efficient manufacturing. Therefore, friction stir spot welding as a solid-state welding technique is a potential choice with low energy demands and high joining performances. However, the joining of aluminium and its alloys with solid-state welding techniques is still a challenging task due to a persistent and chemically stable aluminium oxide layer formed at the sheets prior to the welding, due to the reaction between aluminium and atmospheric oxygen. In this paper, the influence of strain rate induced during friction stir spot welding process on the metallurgical, mechanical and electrical properties of friction stir spot welding of AA 5754-H111 was studied. The strain rate was calculated according to the rotational speed of the tool and the effective (average) radius and depth of the stir zone. It was observed that the specimens welded with a lower strain rate endured a 15 % higher average strain failure load compared to the specimens welded at a higher share rate. The microhardness profiles of the specimens obtained at low strain rates imply strain hardening mechanisms in the weld zone, while the microhardness of specimens welded at high strain rates expressed thermal softening. It was also found that the friction welded sheets, regardless of the strain rate, show increased electrical resistance compared to the base material, however, it decreases with an increase in strain rate. Microstructural analysis reveals a stress-induced metallurgical transformation in the narrow zone around the weld-faying interface.

Keywords: friction stir spot welding, strain rate, residual oxide defects, al-mg alloy, strain hardening, thermal softening, dynamic precipitation.

1. INTRODUCTION

Automotive and aerospace industry requirements for low-weight components have caused aluminium and its alloys to become key choices in today's manufacturing. Economic

motives, competitive market demands and weight reduction, provided the substitution of copper (8.96 g/cm³) for aluminium (2.7 g/cm³) to gain full attention for battery components, strand-terminal connectors, etc. [1]. Consequently, the challenge of establishing the

improved joining technologies for aluminium and its alloys with suitable weld characteristics and lowest energy consumption has emerged [2,3]. However, the joining of aluminium and its alloys, with solid-state welding techniques is demanding due to the chemically stable oxide layer on the top and at the surface of the sheet before joining, as a consequence of the reaction between aluminium and atmospheric oxygen [4].

Friction stir spot welding (FSSW) offers a number of advantages compared to the other welding techniques such as high mechanical properties, small or no distortion of welds, low energy consumption, and no consumable or shielding gas needed [5]. Compared to conventional friction stir spot welding (CFSSW), where a keyhole is left behind, causing a reduction of mechanical properties, probe-less tool friction stir spot welding (PLT-FSSW) was used. During PLT-FSSW, the deformation brought by the tool results in stretch-induced strain in the workpieces causing fragmentation of the brittle oxide layer between the sheets at the weld-faying interface (WFI). As these fragments remain entrapped within WFI, they reduce the homogeneity in the diffusion bonding resulting in non-uniform weld joint quality and becoming nucleation hotspots for joint fracture [10].

Sato et al. [6] first analysed the influence of the oxide layer on the mechanical properties of friction stir welded joints (AA 1050). It was shown that entrapped residual oxides cause kissing bond defects, which are responsible for delamination during bending tests. Due to a different joint geometry during lap joining (FSSW vs. FSW) the residual oxide defects cause the formation of bonding ligaments, which are responsible for the reduction of joining strength [7]. Tier et al. [8] studied the influence of rotational speed on the length of bonding ligaments during refill friction stir spot welding. They found that the reduction of rotational speed from 1900 to 900 RPM increases the length of BL. Li et al. [9] studied the effects of rotational speed on the weld quality during RFSSW of 2A12- T4 aluminium alloy. The tensile-shear properties of welds depend on hook geometry and the distribution of bonding ligament. With increasing rotational speed from 900 to 1300 RPM, the bonding ligaments of the weld periphery were more dispersed, and the hardness of the stir zone decreased. Recently

Labus Zlatanovic et al. [10,11] analysed the origins of delamination in multiple sheets of AA 5754 aluminium alloy joined by FSSW. Detailed microscopic characterisation revealed the complex interfacial layer formed because of stress-assisted metallurgical transformation at the intersection of WFI.

In this study, the influence of strain rate caused by different rotational speeds during probe-less friction stir spot welding of AA 5754-H111 on mechanical and electrical properties was studied. Micro- and macroscopic analysis with light and transmission electron microscopy was carried out, together with tensile shear and hardness tests.

2. EXPERIMENTAL PART

Specimens used for FSSW were cut from rolled aluminium alloy sheets (5754-H111) to 45 × 110 × 0.3 mm dimensions. The chemical composition and mechanical properties are shown in Table 1. and Table 2, respectively. The four sheets were placed one above another and welded together.

Table 1. Chemical composition of commercial AA 5754 - H111 aluminium alloy

Element	Si	Fe	Cu	Mn	Mg	Cr	Zn	Ti	Al
wt. (%)	0.19	0.24	0.03	0.30	3.10	0.03	0.005	0.014	bal.

Table 2. Mechanical properties of AA 5754 – H111 aluminium alloy quoted by the material supplier

Base material	Min. Yield Strength (MPa)	Tensile Strength (MPa)	Elongation – A50 (%)
AA 5754 – H111	80	190-240	10

Experimental tests were carried out on a force-controlled EJOWELD C50R FSSW machine with a maximal rotational speed of 9000 RPM, maximum force of 8 kN and maximum welding time of 5 s. Joining of the sheets was done with a convex pin-less tool, used in previous studies [11], made from H13 (X40CrMoV51) hot-work tool steel. Process parameters are shown in Table 3.

Table 3. Process parameters

Rotational speed (RPM)	Penetration depth (mm)	Axial load (kN)	Welding time (s)
1000			1.43±0.07
2500	0.25	4	1.07±0.08
4000			0.98±0.04

After the joining, the standard metallographic preparation (grinding and polishing) followed by electrolytic etching with Barker's reagent was performed. The cross-section morphology of the joints was analysed by light microscope Zeiss AxioScope.A, for etched specimens and Zeiss Axio Vert.A1 MAT, for polished specimens with crossed polarised light and sensitive tint.

The weld faying interface was analysed with a 200 kV transmission electron microscope (TEM, Tecnai Osiris, FEI) additionally equipped with a scanning unit (STEM) including a high-angle annular dark-field (HAADF, Fischione Co.) detector and energy dispersive X-ray spectrometer (EDX, Super-X system with 4 Bruker silicon drift detectors, Thermo Fisher Co.). Electrical properties were determined according to the explanation in previous work [11].

Microhardness test was done by using standard Vickers microhardness test with Struers DuraScan 70 machine with 0.1 kg loading and distance between indentations of 0.33 mm. A Hegewald & Peschke Inspect Retrofit universal tensile testing machine with a maximal load of 20 kN was used to test tensile shear specimens. The testing speed was set to be 10 mm/min, and the test set-up was explained in previous work [11]. Testing was performed on all three weld-faying interfaces.

3. RESULTS AND DISCUSSION

3.1 Coefficient of friction and strain rate calculations

The variation in the coefficient of friction (CoF) was calculated by using Equation (1) [12]. In this paper, the CoF was calculated by using

axial force and torque data generated from the FSSW equipment. Although the axial force was constant at the beginning of the process, monitored axial force, which slightly differs from fixed, was used in the calculation to obtain a date with higher accuracy contact. Also, the radius of the tool calculated according to equation (2) used for the estimation of the CoF changed during the process from 0 to 3.34 mm. Therefore, in CoF equation time-dependent torque, axial load and contact radius were used, and results are also presented as time-dependent diagrams.

$$\mu(t) = \frac{\tau}{\sigma_n} = \frac{2 \cdot T(t)}{F_N(t) \cdot r(t)} \quad (1)$$

τ - shear stress (MPa)

σ_n - normal stress (MPa)

$T(t)$ - torque (N·mm)

$F_N(t)$ - axial load (N)

$r(t)$ - tool contact radius [mm] calculated from the equation:

$$r(t) = \frac{\sqrt{4 \cdot R^2 - (2 \cdot R - 2 \cdot h)^2}}{2} \quad (2)$$

where R is the fixed tool radius (mm), $h(t)$ is the axial displacement of the tool (penetration depth) (mm) [13].

The CoF vary from 0.6 to 2 as shown in Figure 1. In a specimen welded with 1000 RPM where the CoF increases with welding time, the strain hardening overcomes thermal softening. The frictional properties are governed by the properties of the strain-hardened workpiece. In specimens where CoF increases shortly at the beginning and then decreases with the increase of welding time, thermal softening overcame strain hardening after reaching the highest value of the CoF. Between them is a specimen welded at 2500 RPM where CoF swings without significant increase or decrease, making the strain hardening and thermal softening almost equally influential in the evolution of CoF.

Kumar et al.[14] and Farhat et al. [15] reported, that during the initial interaction between the tool and workpiece, friction is driven by the grains from base material. As the interaction increases, the material in the sub-surface deforms and due to strain hardening of the material competing against

thermal softening the hardness increases. Thus, the two opposite driving forces are working against each other to impose the conditions and microstructure of the workpiece at the end of the process.

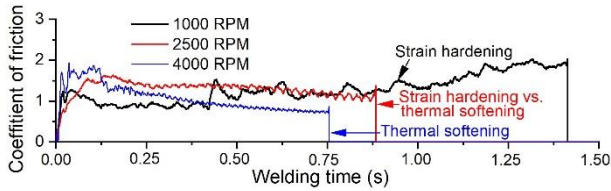


Figure 1. Variation in the coefficient of friction over dwell time

Materials like aluminium-magnesium alloys tend to express Portevin-Le Chatelier (PLC) effect during inhomogeneous plastic deformation. Under conditions of local increase of the strain rate above a certain limit, softening of the material locally occurs. Next, the formula proposed by Chang et al. [16] was used to perform calculations for estimating the applied strain rate as a function of rotational speed.

$$\dot{\epsilon} = \frac{R_m \cdot 2 \cdot \pi \cdot r_e}{L_e} \quad (3)$$

where r_e and L_c are the effective (average) radius and depth of the stir zone measured with the ImageJ software from cross-sections of etched specimens. Chang *et al.* [16] estimated the average material flow R_m to be half of the tool rotation speed. The results of strain rate calculations are presented in Table 4. Together with process temperatures.

Table 4. Maximal temperature and strain rate obtained from equation (3)

Rotational speed (RPM)	Max. temperature (°C)	Strain rate (s ⁻¹)
1000	101±5	175
2500	135±4	441
4000	156±10	612

Values in table show that during FSSW, the strain rate increases with rotational speed and maximal temperature. According to stress-cycle time plots, CoF vs. time plots and

hardness measurements, it can be concluded that strain hardening is more pronounced at strain rates lower than 441 s⁻¹ and low process temperature and thermal softening is more pronounced at strain rates >441 s⁻¹ followed by higher process temperature.

3.2 Macro and microstructural evaluation

Cross-sections of polished and etched specimens obtained at rotational speeds 1000, 2500 and 4000 RPM are shown in Figure 2. The polished specimens do not reveal delamination or any other defects in the welded specimen. A uniform weld zone without a visible weld interface can be observed. However, after etching of the specimen, bonding ligaments at all three WFI become visible.

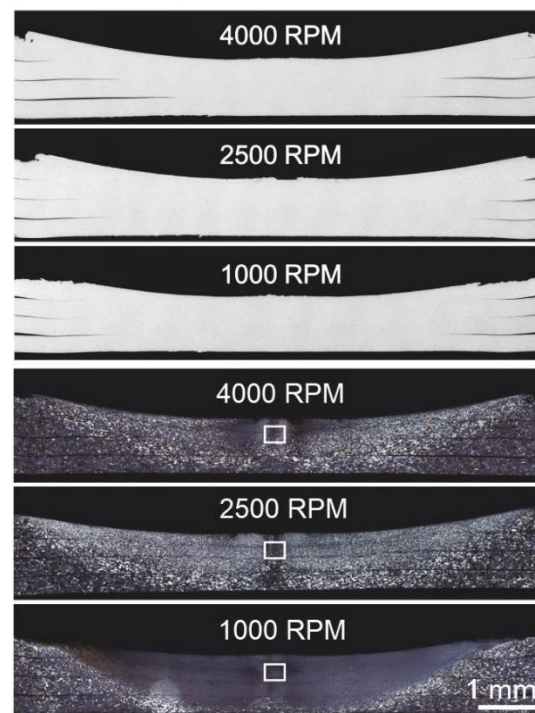


Figure 2. Polished and etched cross-section views of the welded joints (4000, 2500 and 1000 RPM)

The variations in the grain size are presented in Figure 3, respectively. It was observed that the low RPM (low strain rate < 441 s⁻¹) leads to small grain sizes while high RPM (strain rate > 441 s⁻¹) causes grains to be coarse. Jata et al. [17] proposed that the main grain refinement mechanism during FSSW is continuous dynamic recrystallisation (CDRX). This process is driven by temperature and strain rate. Furthermore,

the interaction between precipitates and solute atoms with dislocations has a high influence.

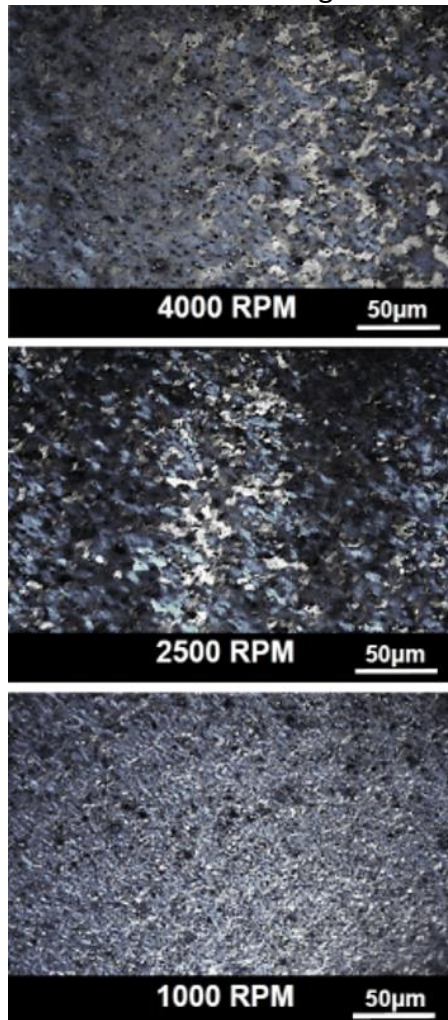


Figure 3. Micrographs of specimens welded at 4000, 2500 and 1000 RPM (taken in the area of the white square in Figure 2.)

The STEM bright-field image of the weld faying interface between the last two sheets, including the recrystallised stir zone, is presented in Figure 4. The image shows the presence of ultrafine globular precipitates in grain boundaries of WFI, originating from dynamic precipitation [10]. A high number of precipitates can be seen at the boundary between the recrystallised stir zone and the weld faying interface. Polygonal grains in recrystallised stir zone and fibrous grains in weld faying interface, both contain randomly dispersed globular $Al_6(FeMn)$ precipitates which are typical in an AA 5754 alloy [10]. At the centre of the weld faying interface, which is the junction of the two sheets, the disturbed oxide layer combined with nano and micro pits can be

found. The aluminium oxide layer acted as a barrier to prevent metal atoms from diffusing from one sheet to form stable bonds with another sheet,

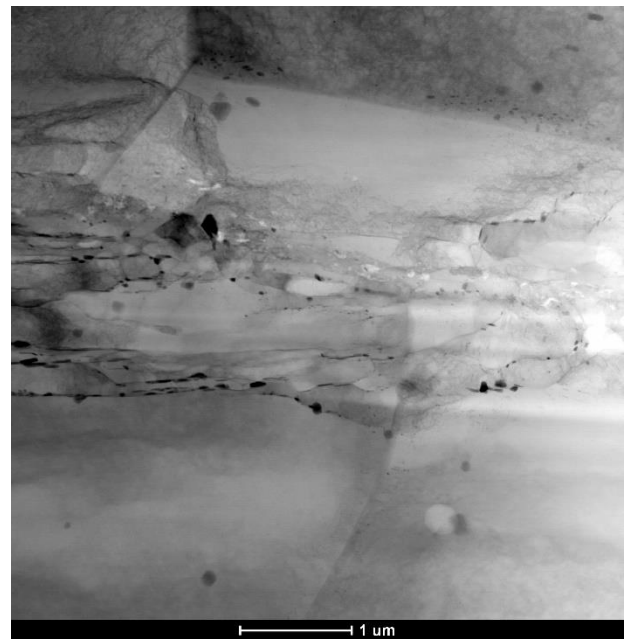


Figure 4. Scanning transmission electron micrographs of third weld faying interface of specimen welded at 1000 RPM

EDX analysis was used to determine chemical composition of the oxide and shown in Figure 5. At the weld faying interface, the disturbed oxide layer combined with nano and micro pits is present. The disturbed oxide layer prevents metal atoms from diffusing from one sheet to another. During solid-state bonding, usually the oxide layer is about 5–10 nm thick Al_2O_3 , however, when alloy contains active elements such as magnesium, amorphous Al_2O_3 can react with Mg to form crystalline MgO [18].

Shen et al. [19] found that the welding interface of AA 6061-T4 obtained by the conventional FSSW contained an array of discontinuous oxide particles causing poor welding. Furthermore, Reilly et al. [20] also proposed that the penetration of the tool into the weld zone stretches the weld interface as well as brittle oxide. Thus, diffusion occurs between oxide fragments

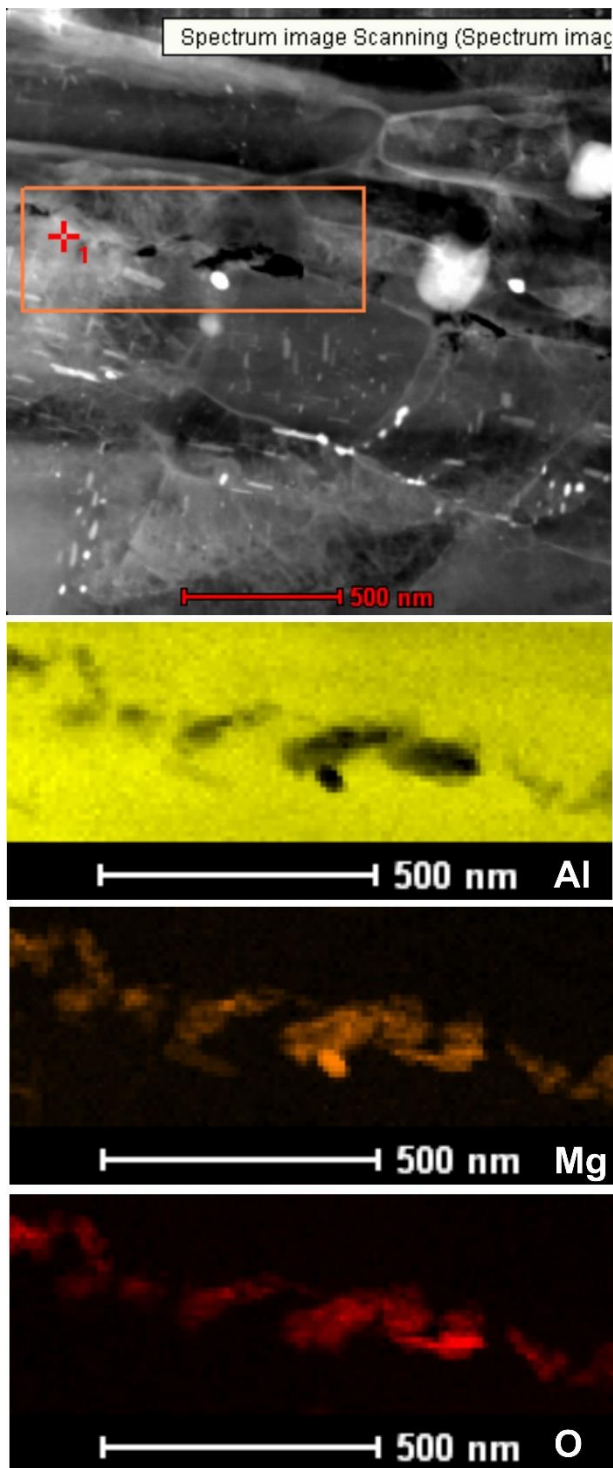


Figure 5. High-angle annular dark-field scanning transmission electron microscope image of the boundary between weld faying interface and recrystallised stir zone with corresponding energy dispersive X-ray spectroscopy (STEM/EDX) elemental mappings of the area marked in overview

3.3 Mechanical properties

To understand the effect of size and composition of weld faying interface on the mechanical properties of the weld,

microhardness and shear-tensile tests were done. The effect of strain hardening at low RPMs was verified by Vickers hardness maps presented in Figure 6., revealing that the microhardness on the surface was highest in the welded zone for specimens welded at low rotational speeds. Therefore, in specimens welded at 1000 RPM, the strain hardening mechanism dominates over thermal softening, and conversely, in specimens welded at 2500 and 4000 RPM, thermal softening was more pronounced.

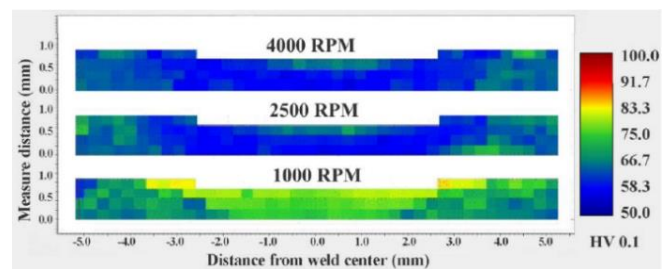


Figure 6 Vickers microhardness maps at the cross-section of specimens processed at rotational speeds 1000, 2500 and 4000 RPM.

Thermal softening of the stir zone in the specimens welded at 4500 RPM causes shear failure load to reduce as shown in Figure 7. On the other hand, the strain hardening of the stir zone in the specimens welded at 1000 RPM significantly improves the mechanical properties of the weld which is supported by microhardness maps.

The rotational speed also influences the size of the welded surface which can be seen on polished specimens in Figure 2. The difference in the size of the welded surface is most pronounced in the I and III weld faying interface, while the II weld faying interface in all specimens are approximately the same. However, even though the size of the welded surface in the I weld faying interface for the specimen welded at 4000 RPM is significantly higher compared to that of 1000 RPM, the shear failure load was almost the same (Figure 7.). This was caused by the higher mechanical properties of the strain-hardened stir zone of the weld obtained at 1000 RPM compared to the thermal softened stir zone of the specimen welded at 4000 RPM.

Furthermore, the welded surface of the I weld faying interface is larger than that of the II weld faying interface, but the shear failure load is higher in II. For that was responsible significant thinning of the first sheet due to the penetration of the tool. The size of the III weld faying interface was the smallest of all three, which caused the shear load to be the lowest as well.

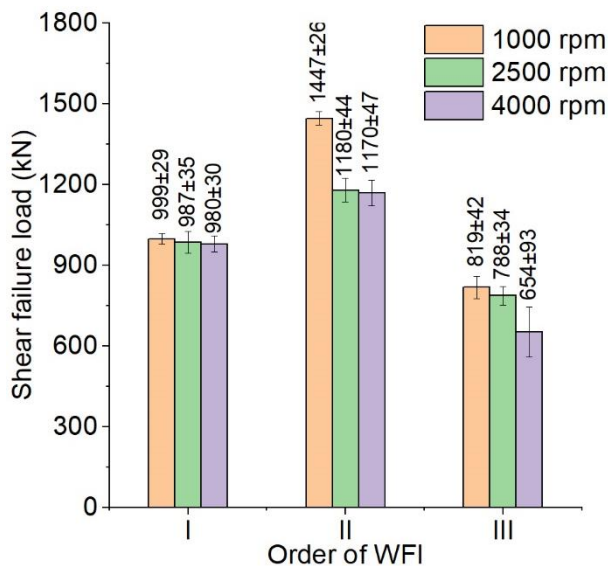


Figure 7. Influence of rotational speed and order of WFI on the shear failure load

The variation in specific electrical resistance of the base material and specimens welded at 1000 and 4000 RPM is presented in Table 5. The specimens welded at 1000 RPM showed higher specific electrical resistance, followed by the specimen welded at 4000 RPM. The lowest specific resistance was for the base material. In the specimens welded at 1000 RPM, strain hardening is leading, and this causes the dislocations accumulation.

The increase in dislocation density causes an increase in the specific resistance. In the specimen welded at 1000 RPM, there were three faying interface regions with a large number of intermetallics. Furthermore, there is also an oxide layer in the middle of every WFI with a very high electrical resistance combined with nano pits. All those facts combined to cause the electrical resistance of the weld to vary, and this influence in weld quality.

Table 5. Specific electrical resistance

Specimen	Specific electrical resistance (mΩ·mm)
Base material	42.9±0.8
1000 RPM	77.0±2.3
4500 RPM	52.0±1.8

4. CONCLUSIONS

Friction stir spot welding (FSSW) is becoming promising technology for welding battery components, connectors, standard-thermal and terminals. However, one of the biggest issues driven by this technique is to provide quality weld joints with low electrical resistance, which is an important requirement of the electrical industry. The conclusions drawn from this research can be summarised as follows:

- (i) The coefficient of friction (CoF) was found to vary with the rotational speed. At low rotational speeds, as a strain hardening effect prevails, the CoF increased up to the end of the process. However, in specimens welded at higher rotational speeds thermal softening caused a decrease of CoF upon the welding time.
- (ii) The origins of the delamination between weld sheets were observed to be due to the metallurgical transformations in the narrow region at the weld interface. This narrow zone was composed of precipitates of $Al_6(FeMn)$ and a weld faying interface, which had significantly smaller fibrous grains with a high volume of precipitates of Al_3Mg_2 . Additionally, within the weld faying interface, sites of nano- and micropits combined with a rich presence of MgO were found to be present as well.
- (iii) Shear strength and microhardness were highest in specimens obtained at 1000 RPM. The II weld faying interface expressed the highest shear strength in all specimens, while the III weld faying interface showed the lowest. In specimens welded at 1000 RPM, microhardness increased compared to the base material due to strain hardening, whereas in specimens welded at 4000 RPM,

the microhardness of the stir zone decreased below the base material due to a predominant thermal softening mechanism.

- (iv) It was noted that the electrical resistance of the weld joints depends on the rotational speed. Although the electrical resistance of the welds was found to be higher in all cases compared to the base material, concerning the base material, it increases for low rotation speed more than for higher rotation speed.

ACKNOWLEDGEMENT

The authors gratefully acknowledge research support by the project entitled "Advanced materials, joining and allied technologies" at the Department of Production Engineering, Faculty of Technical Sciences Novi Sad, Serbia.

REFERENCES

- [1] Pryor L, Schlobohm R, Brownell B. A Comparison of Aluminum Vs. Copper As Used in Electrical Equipment. *Corrosion*, 2008, p. 1–7.
- [2] Regensburg A, Petzoldt F, Benss T, Bergmann JP. Liquid interlayer formation during friction stir spot welding of aluminium / copper. *Weld World* 2018;63:117–25.
- [3] Labus Zlatanovic D. Friction stir spot welding of ultrathin sheets made of aluminium – magnesium alloy, PhD thesis. University of Novi Sad, 2020.
- [4] Labus Zlatanovic D, Bergmann JP, Balos S, Hildebrand J, Bojanic-Sejat M, Goel S. Effect of surface oxide layers in solid-state welding of aluminium alloys – review. *Sci Technol Weld Join* ISSN 2023:1–21. <https://doi.org/10.1080/13621718.2023.2165603>.
- [5] Sun Y, Morisada Y, Fujii H, Tsuji N. Ultrafine grained structure and improved mechanical properties of low-temperature friction stir spot welded 6061-T6 Al alloys. *Mater Charact* 2018;135:124–33. <https://doi.org/10.1016/j.matchar.2017.11.033>.
- [6] Sato YS, Takauchi H, Park SHC, Kokawa H. Characteristics of the kissing-bond in friction stir welded Al alloy 1050. *Mater Sci Eng A* 2005;405:333–8. <https://doi.org/10.1016/j.msea.2005.06.008>.
- [7] Sarkar R, Pal TK, Shome M. Material flow and intermixing during friction stir spot welding of steel. *J Mater Process Technol* 2016;227:96–109. <https://doi.org/10.1016/j.jmatprotec.2015.08.006>.
- [8] Tier MD, Rosendo TS, Dos Santos JF, Huber N, Mazzaferro JA, Mazzaferro CP, et al. The influence of refill FSSW parameters on the microstructure and shear strength of 5042 aluminium welds. *J Mater Process Technol* 2013;213:997–1005. <https://doi.org/10.1016/j.jmatprotec.2012.12.009>.
- [9] Li G, Zhou L, Luo L, Wu X, Guo N. Microstructural evolution and mechanical properties of refill friction stir spot welded alclad 2A12-T4 aluminum alloy. *J Mater Res Technol* 2019;8:4115–29. <https://doi.org/10.1016/j.jmrt.2019.07.021>.
- [10] Labus Zlatanovic D, Balos S, Bergmann JP, Rasche S, Zavašnik J, Panchal V, et al. In-depth microscopic characterisation of the weld faying interface revealing stress-induced metallurgical transformations during friction stir spot welding. *Int J Mach Tools Manuf* 2021;164:103716. <https://doi.org/10.1016/j.ijmactools.2021.103716>.
- [11] Labus Zlatanovic D, Bergmann JP, Balos S, Gräzel M, Pejic D, Sovilj P, et al. Influence of rotational speed on the electrical and mechanical properties of the friction stir spot welded aluminium alloy sheets. *Weld World* 2022. <https://doi.org/10.1007/s40194-022-01267-8>.
- [12] Kalpakijan S. *Manufacturing Processes for Engineering Materials*. Addison Wesley Publishing Company; 1991.
- [13] Labus Zlatanovic D, Baloš S, Bergmann JP, Rasche S, Pecanac M, Goel S. Influence of Tool Geometry and Process Parameters on the Properties of Friction Stir Spot Welded Multiple (AA 5754 H111) Aluminium Sheets. *Materials (Basel)* 2021;14. <https://doi.org/10.3390/ma14051157>.
- [14] Kumar K, Kalyan C, Kailas S V, Srivatsan TS. An Investigation of Friction During Friction

- Stir Welding of Metallic Materials. *Mater Manuf Process* 2009;24:438–45.
<https://doi.org/10.1080/10426910802714340>.
- [15] Farhat ZN, Ding Y, Northwood DO, Alpas AT. Effect of grain size on friction and wear of nanocrystalline aluminum. *Mater Sci Eng A* 1996;206:302–13.
- [16] Chang CI, Lee CJ, Huang JC. Relationship between grain size and Zener-Holloman parameter during friction stir processing in AZ31 Mg alloys. *Scr Mater* 2004;51:509–14.
<https://doi.org/10.1016/j.scriptamat.2004.05.043>.
- [17] Jata K, Semiatin S. Continuous dynamic recrystallization during friction stir welding of high strength aluminum alloys. *Scr Mater* 2000;43:743–9.
[https://doi.org/10.1016/S1359-6462\(00\)00480-2](https://doi.org/10.1016/S1359-6462(00)00480-2).
- [18] Shirzadi AA, Assadi H, Wallach ER. Interface evolution and bond strength when diffusion bonding materials with stable oxide films. *Surf Interface Anal* 2001;31:609–18.
<https://doi.org/10.1002/sia.1088>.
- [19] Shen Z, Yang X, Zhang Z, Cui L, Yin Y. Mechanical properties and failure mechanisms of friction stir spot welds of AA 6061-T4 sheets. *Mater Des* 2013;49:181–91.
<https://doi.org/10.1016/j.matdes.2013.01.066>.
- [20] Reilly A, Shercliff H, Chen Y, Prangnell P. Modelling and visualisation of material flow in friction stir spot welding. *J Mater Process Technol* 2015;225:473–84.
<https://doi.org/10.1016/j.jmatprotec.2015.06.021>.



Society of Production
Engineering

SPMS 2023

39. Savetovanje proizvodnog mašinstva Srbije

ICPES 2023

39th International Conference on Production Engineering of
Serbia



Faculty of Technical
Sciences
University of Novi Sad

Novi Sad, Serbia, 26. – 27. October 2023

ULTRASONIC WELDING OF COPPER CONDUCTORS

Ana BRDAR.¹, Katarina ILIC¹, Stanko SPASOJEVIC¹, Danka LABUS-ZLATANOVIC.^{1,2}, Petar JANJATOVIC.¹, Ivan ZABUNOV.³, Miroslav DRAMICANIN.¹, Milan PECANAC.^{1*}, Mirjana TRIVKOVIC.¹, Dragan RAJNOVIC¹, Sebastijan BALOS.¹, Leposava. SIDANIN¹

¹ Department of Production Engineering, Faculty of Technical Sciences, University of Novi Sad, Serbia, anab@uns.ac.rs; katailic@uns.ac.rs, spasojevic@uns.ac.rs, danlabus@uns.ac.rs, janjatovic@uns.ac.rs, dramicanin@uns.ac.rs, pecanac.milan@uns.ac.rs, mirjana.trivkovic@uns.ac.rs, draganr@uns.ac.rs, sebab@uns.ac.rs, lepas@uns.ac.rs

² Technical University Ilmenau, Germany, e-mail: danka.labus-zlatanovic@tu-ilmenau.de

³ Proficut doo, Backi Petrovac, Serbia, zabunov@proficut.rs

*Corresponding author: pecanac.milan@uns.ac.rs

Abstract: This study delves into the fundamentals of ultrasonic welding (USW), categorizing the process by metal type and investigating critical parameters and their impact on welding outcomes. The theoretical section outlines the pros and cons of ultrasonic welding and showcases its diverse industrial applications, underscoring its significance. Two copper conductors were ultrasonically welded with various pressures, a parameter recognized as the most influential in the welding process. Following welding, specimens underwent metallography post-cutting. Subsequently, the assessment of mechanical properties included tensile testing and microhardness testing. All specimens achieved successful welds, with the best results obtained at pressures between 4.5 and 6 bars. These findings enhance our understanding of ultrasonic welding and its potential across industries, providing a foundation for further research and development.

Keywords: Ultrasonic welding (USW), Ultrasonic welding parameters, Pressure variation, Mechanical properties

1. INTRODUCTION

Ultrasonic welding (USW) is a solid-state welding process whereby high-frequency ultrasonic acoustic vibrations are applied to base material held together by a specially designed clamping system [1]. Basically, USW uses the basic principle of friction joining processes, where the adherent is subjected to high frequency (15-75 kHz) and low amplitude (10-300 μm) mechanical vibrations with

constant welding force applied. USW is characterized by relatively low heat input, a short welding time, cost-effectiveness, and suitability to weld thin workpieces [2]. Materials that are typically welded with the USW process are aluminium, titanium, magnesium, copper and their alloys, steels, fibre-reinforced composites, and thermoplastics, in various industrial areas, such as packing, electronics, aerospace, automotive, and transportation [3]. The base materials

listed and their advantages make USW ideal for industrial applications involving the welding of conductors and dissimilar joints [4]. Some welded joints are shown in Figure 1.

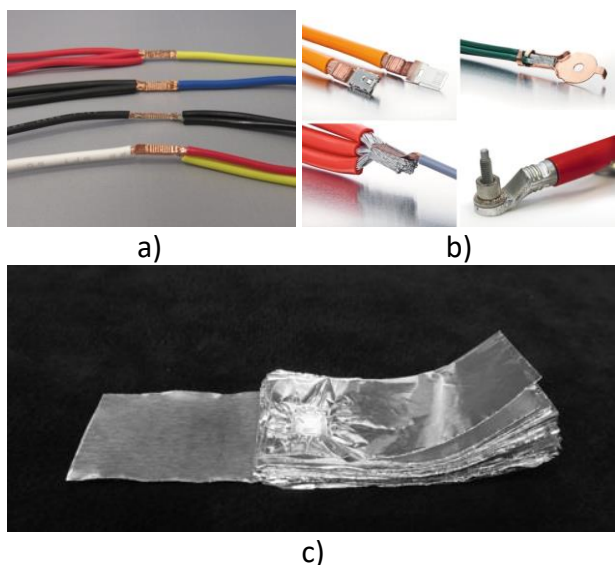


Figure 1. USW applications: a) multi-conductor cables; b) high-voltage conductors; c) 60 aluminium foils, 25 µm thick [5]

In this paper, the influence of USW pressure and welding time on multiwire conductor joint rupture force and hardness was studied.

EXPERIMENTAL PART

The base material used in this study was a multiwire conductor with 10 mm² cross-section, Figure 1. The nominal chemical composition of this 99.95 % Cu is given in Table 1 and physical properties are given in Table 2.

Table 1 Nominal chemical composition, maximal values, Cu balance

As	Sb	Bi	Pb	S	Fe
0.002	0.002	0.001	0.003	0.005	0.003

Table 2 Physical properties

Melting temperature	1083 °C
Electric conductivity at 20 °C	60·106 S/m

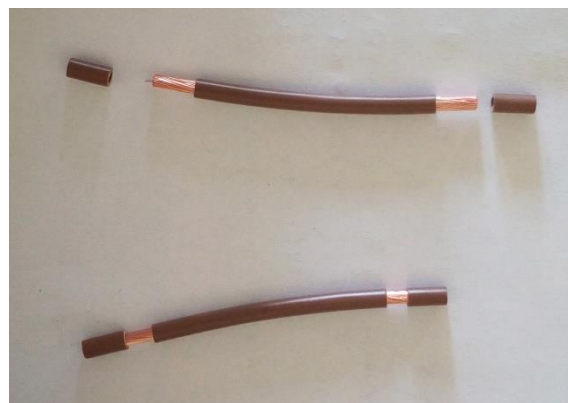


Figure 2. Multiwire conductors with insulation removed.

Ultrasonic welding was done by Schunk Sonosystems Minic-III, used for welding various conductors and foils, Figure 3.



Figure 3. Ultrasonic welding machine: 1- ultrasonic generator, 2- welding device, 3- display

Pressure was varied in a wide margin: 2.4, 2.7, 3, 3.3, 3.6, 3.9, 4.2, 4.5, 4.8, 5.1, 5.4, 5.7, 6 bar, which, together with energy involved, caused the synergic system of the welding device to adjust the time and sonotrode travel.

Tensile testing of welds was done on the mechanical testing machine Toyoseiki AT-L-118B. Three specimens of each pressure were tensile tested. Furthermore, welds were subsequently prepared in accordance with common metallographic preparation procedure: cutting, mounting, grinding (SiC abrasive papers, P220 to P2000), and polishing (diamond suspensions of 6, 3, 1, and ¼ µm). Preparation was conducted on Struers equipment. Afterward, Microhardness was measured by the Wilson Tukon 1102 device, with a 1 kg load, in accordance with the schematic representation in Figure 4.

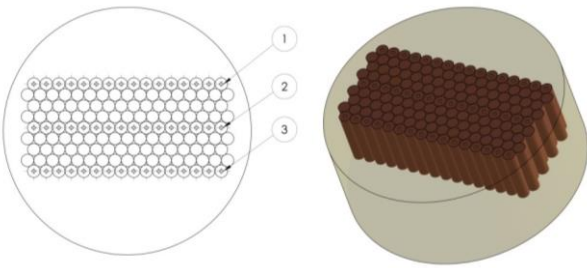


Figure 4. Microhardness measurement scheme

RESULTS AND DISCUSSION

In Figures 5 and 6. As the pressure increases, the welding time is shorter, Figure 4. An opposite trend was obtained in Sonotrode travel, which is larger as the pressure increases, Figure 6

Macro images of weld cross-sections obtained with three selected pressures of 2.4, 4.5 and 6 bar are shown in Figure 7. It can be seen that a higher USW pressure results in a higher density (fill factor). However, this increase in density is not proportional since the increase in pressure from 4.5 to 6 bar results in just a marginal increase in density. Obviously, a certain threshold was reached, which prevents a significant further increase in density from being reached in case a higher pressure would have been applied.

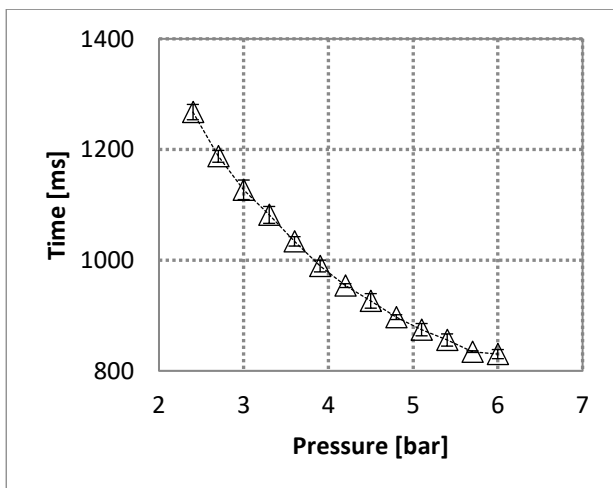


Figure 5. Time vs. pressure chart

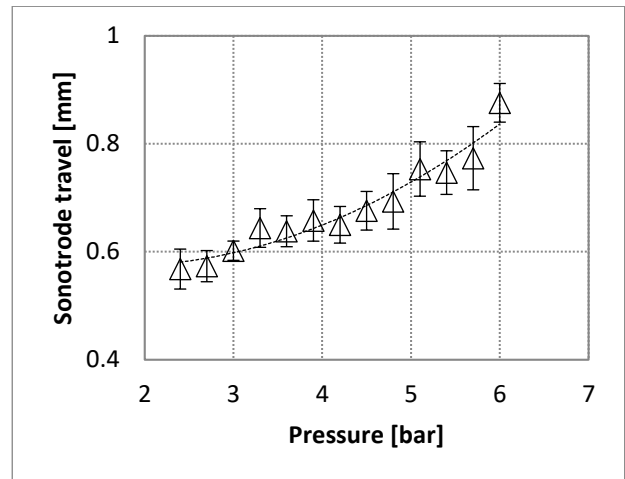
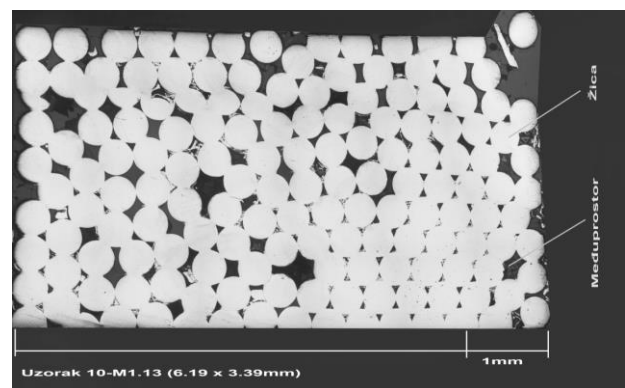
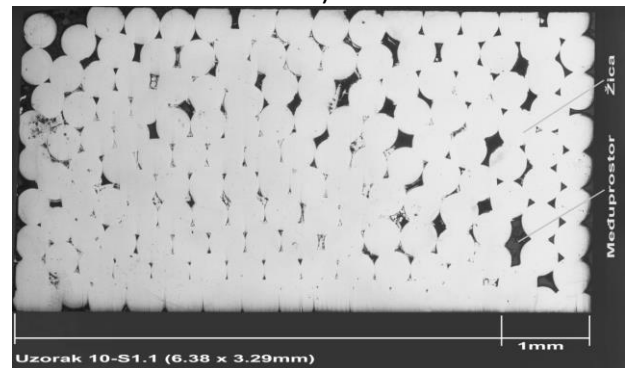


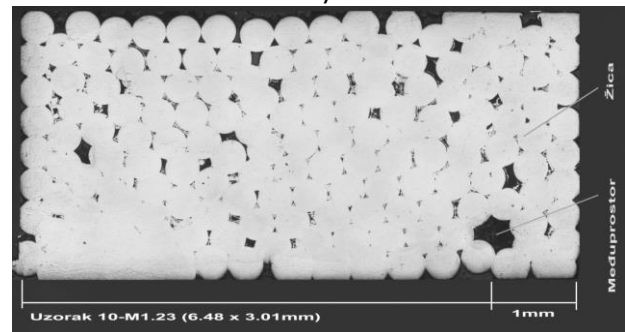
Figure 6. Sonotrode travel vs. pressure chart



a)



b)



c)

Figure 7. Specimen macros: a) 2.4 bar (84 % fill factor); b) 4.5 bar (92.8 % fill factor); c) 6 bar (93 % fill factor)

Rupture force vs. welding pressure is shown in Figure 6. Rupture forces increase as the welding pressure increases until 4.5 bar pressure is reached. Afterwards, a further increase in pressure results in a drop in rupture forces.

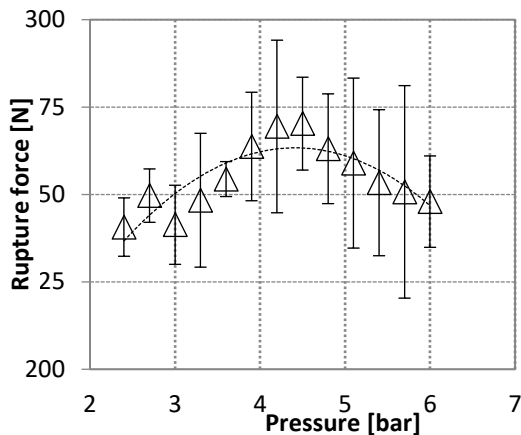


Figure 8. Rupture force related to welding pressures.

Microhardnesses in specimens welded with 2.4, 4.5 and 6 bar pressure are shown in Figure 9. The highest values were obtained in specimen welded with 6 bar, closely followed by the specimen welded with 4.5 bar pressure. It can be observed that the highest microhardness was obtained in the row at the anvil side, followed by values in the centre. Finally, differences in microhardnesses are represented by dashed bars in Figure 9. They show that an increase in welding pressure makes the differences between minimum and maximum values smaller.

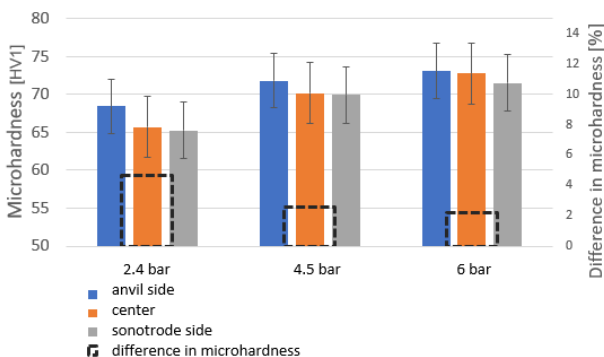


Figure 9. Microhardness at anvil side, centre and sonotrode side, as well as the difference in microhardness

CONCLUSIONS

Based on the obtained results, and within the limitations of this study, the following conclusions can be drawn:

- Increased pressure during USW, from 4.5 to 6 bar does not result in increased rupture force.
- By increasing the pressure from 4.5 to 6 bar, a marginal increase in microhardness and fill factor was obtained. The only tangible benefit is related to a shortened welding time.
- An increased microhardness is the result of strain hardening effect during welding.
- The drop in rupture force can be the result of excessive straining in wires.

Optimal USW welding pressure is 4.5 bar, with only merit of increasing it to 6 bar can be the reduction of welding time, at the cost of weld rupture force.

ACKNOWLEDGEMENT

The authors gratefully acknowledge research support by the project entitled “Advanced materials, joining and allied technologies” in the Department of Production Engineering, Faculty of Technical Sciences Novi Sad, Serbia.

REFERENCES

- [1] S. Mostafavi, D.F. Hesser, B. Markert, Effect of process parameters on the interface temperature in ultrasonic aluminum wire bonding, *J. Manuf. Process.* 36 (2018) 104–114. <https://doi.org/10.1016/j.jmapro.2018.09.020>.
- [2] T.G. Unnikrishnan, P. Kavan, A review study in ultrasonic-welding of similar and dissimilar thermoplastic polymers and its composites, *Mater. Today Proc.* 56 (2022) 3294–3300. <https://doi.org/10.1016/j.matpr.2021.09.540>.

- [3] S. Tilahun, M.D. Vijayakumar, C. Ramesh Kannan, S. Manivannan, J. Vairamuthu, K.P. Manoj Kumar, A Review on Ultrasonic Welding of Various Materials and Their Mechanical Properties, IOP Conf. Ser. Mater. Sci. Eng. 988 (2020). <https://doi.org/10.1088/1757-899X/988/1/012113>.
- [4] H.T. Fujii, Y. Goto, Y.S. Sato, H. Kokawa, Microstructure and lap shear strength of the weld interface in ultrasonic welding of Al alloy to stainless steel, Scr. Mater. 116 (2016) 135–138. <https://doi.org/10.1016/j.scriptamat.2016.02.004>.
- [5] M.P. Matheny, K.F. Graff, Ultrasonic welding of metals, Elsevier Ltd., 2015. <https://doi.org/10.1016/B978-1-78242-028-6.00011-9>.



Society of Production
Engineering

SPMS 2023

39. Savetovanje proizvodnog mašinstva Srbije

ICPES 2023

39th International Conference on Production Engineering of
Serbia



Faculty of Technical
Sciences
University of Novi Sad

Novi Sad, Serbia, 26. – 27. October 2023

FEM ANALYSIS FORWARD EXTRUSION PROCES OF HOLLOW ELEMENTS

Saša RANĐELOVIĆ^{1*}, Nikola VITKOVIĆ¹, Marina TRAJKOVIĆ MILENKOVIĆ², Andrija ZORIĆ²

¹University of Nis, Faculty of Mechanical Engineering, 18000 Niš, Serbia

² University of Nis, Faculty of Civil Engineering and Architecture, 18000 Niš, Serbia

*Corresponding author: sassa@masfak.ni.ac.rs

Abstract: *The industrial process of forward extrusion of hollow elements represent complex metal forming plastic deformation in volumetric area. In order for such processes to be competitive today, it is necessary to apply modern numerical methods of finite elements to simulate the behavior of metals inside the tool. They monitor the mechanical parameters within the deformable continuum (stress, strain, temperatures, strain rates, etc.) in order to find the optimal tool solution for the given product even in the design phase. Very complex processes of plastic flow take place in the mold cavity itself because it is a continuous deformation. The metal continuum is first split (separated), then plastically deformed and finally joined into a continuous product that comes out of the tool with an opening of a given cross-section.*

Keywords: *Extrusion, FEM, Stress, Strain, Deformation velocity, tool, profile.*

1. INTRODUCTION

FEM modeling of the process of forward extrusion of hollow elements represent a complex task that is usually solved by software nowadays. Part of the research is directed towards the materials that are extruded, part towards the construction of the tool, but the whole process gains significance when a software simulation is generated that come together all these elements.

To model the extrusion process with the FEM, three formulations can be used. The transient updated Lagrangian formulation, where the FEM mesh is attached to the deforming billet, is able to capture the material flow in a very intuitive way [1]. Runtimes can be long, but this method can produce some results

that are difficult or impossible to obtain from other simulation methods. Some available results include: material splitting over the bridge and merging in the welding chamber for a hollow extrudate, front end formation, curling or twisting of the entire extrudate, and complete load vs. stroke behavior. Parallel computing can speed up updated Lagrangian simulations. The steady state Eulerian approach, in which the mesh is fixed in space, is fast but can not provide any transient information and the thermal-mechanical stationarity may not be well established in reality [2].

The ALE (Arbitrary Lagrangian Eulerian) approach falls somewhere between the other two methods. It is efficient for this class of problems, [3] since the frequent remeshing

inevitable in updated Lagrangian can be eliminated. Also, some of the shortcomings of the steady state approach can also be circumvented since the procedure is incremental in nature.

The ALE method is an attempt to combine the advantages of both the Eulerian and Lagrangian formulations. It was first introduced by Hirt, et al.,[4] and Donea, et al.,[3,4] in modeling the solid-fluid interaction. It was subsequently applied to problems of solid mechanics with large deformation.

2. FEM ANALYSIS FORWARD EXTRUSION PROCESS HOLOW ELEMENTS

The general ALE method uses two mesh systems: the computational reference mesh system, on which the finite element calculations are performed, and the material reference mesh system, which follows the material as it deforms. The relationship between the computational reference mesh system and material reference mesh system in each of the Lagrangian, Eulerian, and ALE descriptions consists in the position of the nodes at the end of one time iteration. At the beginning of a new ALE step, the material reference mesh system is made to be the same as the computational reference mesh system. In a time increment, the nodes move together with the material for the Lagrangian formulation. For the Eulerian formulation, the nodes are fixed in space [4,5]. For the ALE method, the new position of the computational reference mesh nodes can be designed based on the need of the simulation (Fig. 1).

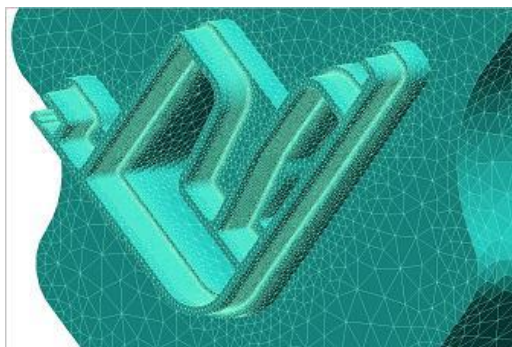


Figure 1. FEM model of finished part at the end of process (www.qform.com)

In the ALE formulation, both material reference mesh system and computational reference mesh system consist of hexahedral, tetrahedral (volumetric problems) or triangle elements (plane problems) that are moving in the extrusion direction. The movement of the computational reference mesh system differs in the three or two directions. The nodes are fixed in the extrusion direction, while they are updated in a Lagrangian fashion in the plane perpendicular to the extruding direction. To implement this, the computational reference mesh system is superimposed with the material reference mesh system at the beginning of the simulation. The increment proceeds exactly as that for the pure Lagrangian description using the computational reference mesh system through the end of the solution phase. As the computational mesh deforms and changes its geometry, new coordinates and deformation state variables are obtained during the simulation and then are transferred to the material reference mesh system at the end of each increment to update it. The computational reference mesh system remains unchanged at this stage. Since the initial nodes and elements of the computational mesh belong to the material mesh, no interpolation of the state variables is needed. Instead, nodal and elemental values are simply registered to the material mesh [3,4,5].

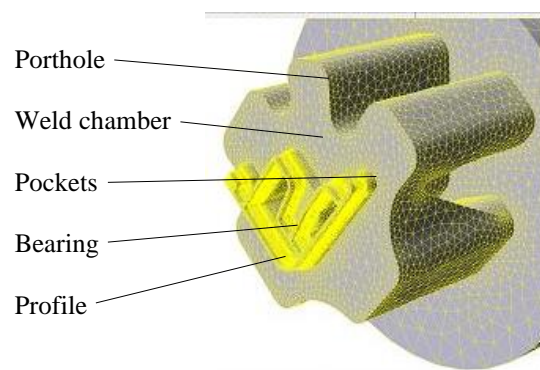


Figure 2. Deformable metal volume inside of tool (www.qform.com)

The subject of the analysis are hollow and semi-hollow aluminum elements, and therefore, this tool model implies the existence of a mandrel, which ensures obtaining a profile

with the given internal shape and dimensions (Fig. 2).

On the example of extruding a pipe (5) with a circular cross-section (Fig. 3) on a partial section, the parts of the tool in direct contact with the deformable aluminum material (2) can be recognized. Due to the axial movement of the tool ram (1) and the high pressure in contact with the deformable material, it first encounters four bridges (6) that separate the deformable material into eight parts filling the chambers (7) that direct the material around the mandrel (3) to the die matrix (4) which forms the exit section with the bearing length (9). Its length defines, on the one hand, the quality and accuracy of the finished part, but also the quality of the tool itself and its working life.

The arrangement of the bridges and the configuration of the tools are dictated by the geometry of the finished part.

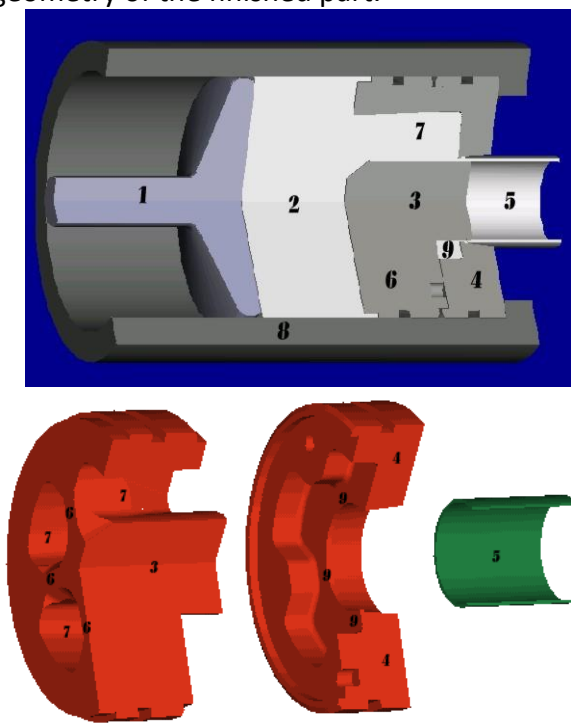


Figure 3. Partial section of deformable aluminum volume inside of tool

In most cases, these are cylindrical billet (2) which at elevated temperatures (for aluminum $t \approx 450^\circ\text{C}$) flow around the bridges (6) and one or more mandrels (3) of the tool into complex cylindrical or prismatic profiles (5) with smaller or larger deviations from regular geometric shapes [5,6]. For the mechanical model itself, it

is assumed that in the exit zone of the tool, in different axial sections, it is a plane deformation state. Such a model is imposed as a solution, because in the majority of cases, the output profile has a very small wall thickness, around 1mm, and a significantly larger width on the circumference.

For this analysis, a finite element with the name Element 11 (MSC.Marc), an arbitrary square element, with four nodes, which is recommended for the plane deformation state, was used. Nodes are marked counter-clockwise.

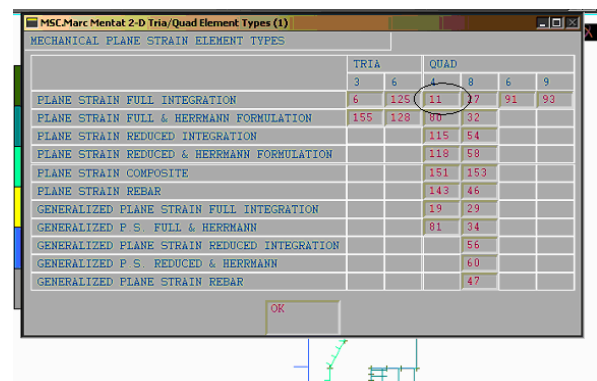


Figure 4. Choice of the FEM element

Its complete geometry is defined by twelve nodes. If any of the nodes on the page of the element is not defined, it retains its initial straight line shape, without nodes. A quadratic element is created by mapping the unit square with a third-order polynomial. For these reasons, it can be used to approximate curved boundary surfaces. As this element uses a bilinear interpolation function, the deformations on its surface tend to be equal. For these reasons, this element is not favorable for the discretization of continua loaded in shear and bending. This behavior can be corrected to some extent by using alternative interpolation functions [7].

The stiffness of this element is formed via four Gaussian points inside the element. It can be used for all types of constitutive relations.

The ability to adapt the behavior of the network, in this solution, implies an increase in the number of elements, of the same type, by dividing the original element by its interior at a certain level (four new ones are obtained from one existing one) [5,7,8].

Each adaptive process takes place according to a precisely determined and chosen iterative criterion until its fulfillment in each step. Also, the restoration of the deformed network is performed according to one, two, three or all four criteria set in advance. These are the criteria of element distortion, contact penetration, incremental and angular deviation.

For adaptive models, there are three sources of nonlinearity in the plastic deformation processes of metals, the nonlinear behavior of the continuum itself, the nonlinear geometry, and the nonlinear boundary conditions. Non-linearity of the material comes as a result of non-linear connections between stress and strain in the area of plasticity, as well as the strengthening effect present during the deformation process [5,7].

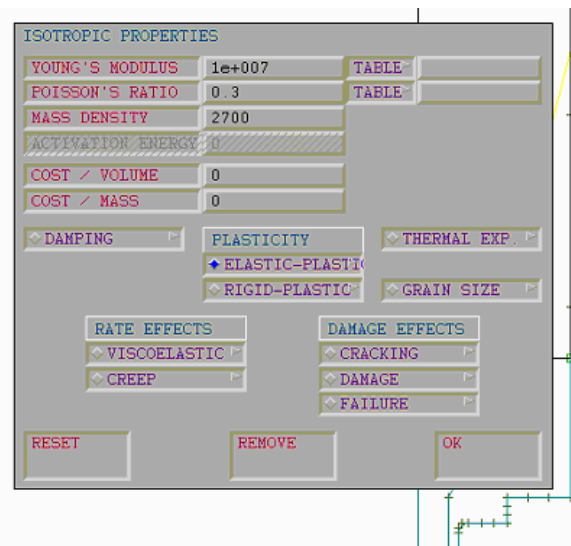


Figure 5. Mechanical characteristic aluminium alloy

The model of the billet itself has the characteristics of aluminum with recognizable physical parameters (Fig. 6) and the law of strengthening which is given through the diagram (Fig. 7).

Geometric nonlinearity refers to the relationship between deformation and displacement, that is, to the relationship between stress and deformation force [5,6,7].

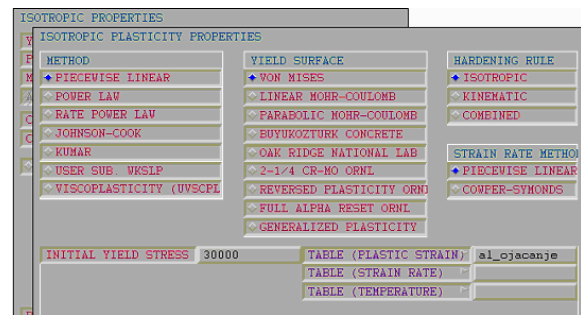


Figure 6. Input plastic parameters

The nonlinearity of the boundary conditions refers to contact stresses and changes in the friction force during the deformation process.

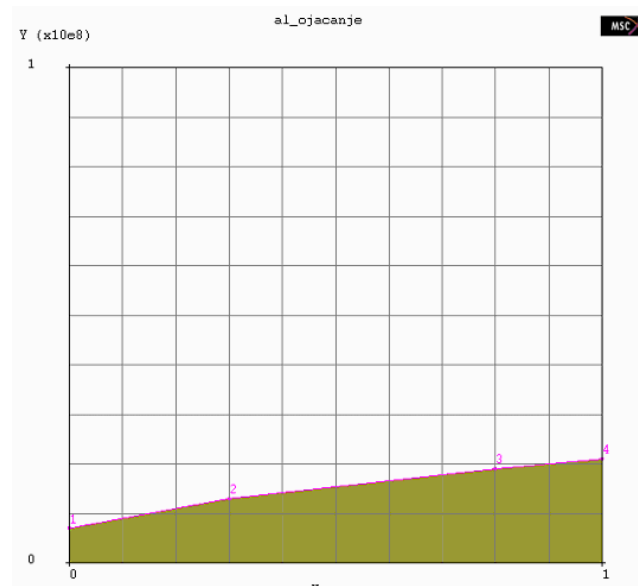


Figure 7. Curve of aluminium hardening

On the generated plane model of the longitudinal section, a two-dimensional model of the billet whose plasticity parameters are monitored during the process of filling the mold cavity and forward extruding it into the calibration zone of the tool can be recognized, the model of the rigid matrix, which here plays the role primarily of limiting the space in which the simulation is monitored and the mandrel model that conditions the obtaining of hollow aluminum elements (Fig. 8).

For the billet volume, a relative movement along the y-axis with a negative sign and a sufficient number of finite elements (336) was assigned to fill the entire mold cavity and extrude into the calibration zone. The size of

the square element was varied at two levels of 0.04 and 0.05, thus creating a balance between two opposite requirements, the fineness of the simulation and its duration. The criterion for restoring the network is defined by the frequency of increase 5 (Fig. 8).

Numerous test and analysis of existing solutions indicate that when defining the load, it is best to separate two intervals, an initial and much smaller one, when the process of plastic flow is established and begins, and another that includes the entire analysis until the end of the simulation. For these reasons, the first and second load periods were formed during the process of plastic deformation. Only setting the number of steps, that is, the total duration of the load, has a decisive role on the number of iterations reached in the simulation of the entire process of plastic deformation (Fig. 9). For these reasons, a lot of attention and a large number of trials have been devoted to this problem in order to obtain the most accurate and realistic solution [5,7,8].

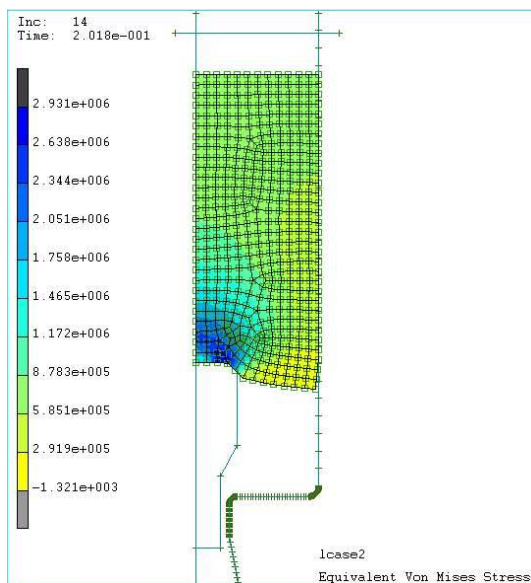


Figure 8. FEM adaptive model of stress distribution in y direction, increment 14

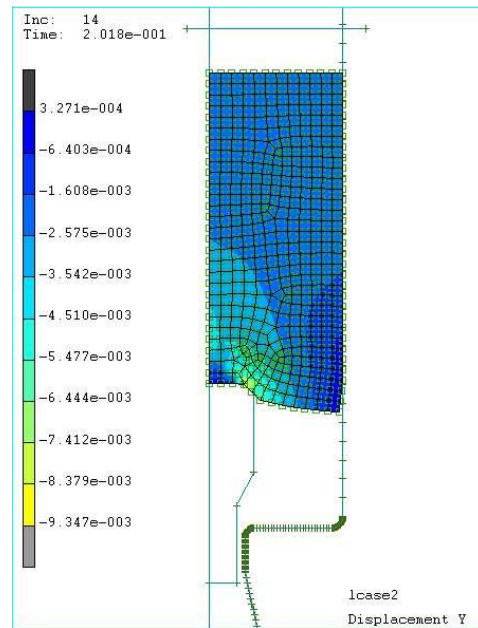


Figure 9. FEM adaptive model of displacement distribution in y direction, increment 14

After defining the number and duration of different loads, the conditions and criteria for the case of the plane deformation state are defined. An updated Lagrange procedure was chosen with a maximum number of segments, that is, nodes in contact of 2000. There is also the option of selecting output results that can be monitored at the end of the simulation (Fig. 10).

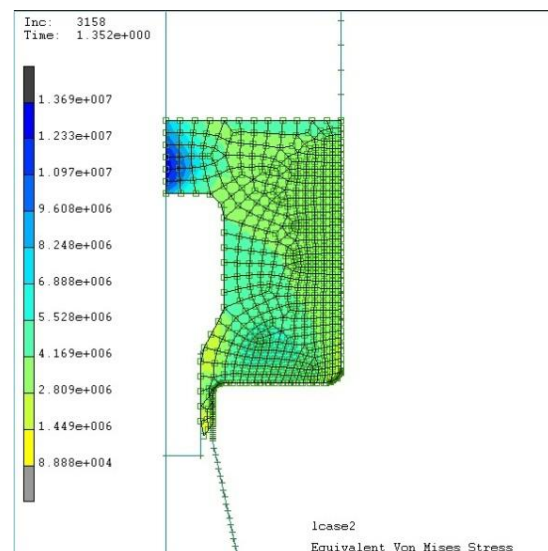


Figure 10. The Equivalent stress at the moment of exit die orifice, increment 3158

The simulation of the plastic deformation process itself provides outstanding

opportunities for detailed monitoring and analysis of results in the focus of deformation under different geometric conditions. Here, the case of unidirectional extrusion of hollow elements is analyzed when the mandrel face is flat in order to reduce the load on the tool bridge and improve the uniformity of extrusion of aluminum in the tool cavities before entering the calibration zone (Fig. 10). In order to reduce the dead zones, different structural transitions are performed on real tools, which, with their shape and number, improve the entry of aluminum into the calibration zone. Their number and size are the subject of many researches, while this paper presents only one example and the simulation of plastic deformation in their vicinity.

3. CONCLUSION

Numerical analysis of the forward extrusion process aims to generate a simulation model that, even in the design phase, can indicate problems that are visible only on the finished part. By correcting the dimensions and angles of the tool on the geometric model, in several iterations, a constructive solution of the tool is obtained, which at the output gives a finished part with the correct dimensions and the specified surface quality. With all these tools, the working length and its small correction by volume remains the parameter that solves the greatest number of problems.

REFERENCES

- [1] F. Belytschko, W. K. Liu, B. Moran: *Nonlinear Finite Elements for Continuous and Structures*, John Wiley & Sons, New York, 2000.
- [2] A. Rodriguez-Feran, , F. M. Casadei, and A. Huerta: ALE stress update for transient and quasistatic, *International Journal for Numerical Methods in Engineering*, l.41:241-262, 1998.
- [3] F. K. Chen, W. C. Chuang, S. Torng: Finite element analysis of multi-hole extrusion of aluminum-alloy tubes, *J. Mater. Process. Technol.* 201, pp. 150–155. 2008.
- [4] L. Donati, B. Reggiani, R. Pelaccia, M. Negrozio, S. Di Donato: Advancements in extrusion and drawing: a review of the contributes by the ESAFORM community, *J. of Mater. Form.* pp. 40-68, 2022.
- [5] S. Randelović, Modeliranje procesa istosmernog istiskivanja šupljih elemenata koji obezbeđuje visoku sposobnost procesa, *Doktorska disertacija*, pp.149, Niš, Oktobar 2006.
- [6] C. Zhang, Y. Dong, G. Zhao, L. Chen: Experimental and numerical investigation on transverse weld of hollow aluminum profile during porthole extrusion process. *Procedia Eng.* 207, 1653–1658, 2017.
- [7] F. Krumphals, I. Flitta, S. Mitsche, T. Wlanis, A. Jahn, C. Sommitsch, Comparison of experimental and Finite Element Modelling of the extrusion of AA6082 on both tools and extrudate as a function of process parameters. *Int J Mater Form* 1: pp. 427–430. 2008, <https://doi.org/10.1007/s12289-008-0086-0>
- [8] H. Valberg, W. Misiolek: Plastic deformation in hot extrusion of an aluminum alloy characterised by FEM-analysis with experiment. In: *The 9th International Conference on Material Forming ESAFORM 1*: pp. 587–590. 2006, ISBN 83–89541–66–1



Society of Production
Engineering

SPMS 2023

39. Savetovanje proizvodnog mašinstva Srbije

ICPES 2023

39th International Conference on Production Engineering of
Serbia



Faculty of Technical
Sciences
University of Novi Sad

Novi Sad, Serbia, 26. – 27. October 2023

IZRADA KALUPA ZA LIVENJE U SOLIDWORKSU

Andelija MITROVIĆ^{1,*}, Jelena BARALIĆ¹, Aleksandar JOVIČIĆ¹

¹Fakultet tehničkih nauka u Čačku, Srbija, andjelija.mitrovic@ftn.kg.ac.rs ;
jelena.baralic@ftn.kg.ac.rs; aleksandar.jovicic@ftn.kg.ac.rs ;

Apstrakt: U radu je prikazan postupak izrade složenog kalupa pomoću programskog paketa SolidWorks. Kalup je konstruisan u modulima Sketch, Features i Mold Tools pomoću kojih je napravljen 3D model viljuške a zatim su konstruisani gornji i donji kalup. Najveći problem prilikom konstruisanja kalupa je definisanje linije razdvajanja alata, koja seče alat na dva dela. Nakon 3D modeliranja kalupa, izrađena je simulacija 3D obrade glodanja u programskom modulu SolidCAM, gde je nakon definisanja obrade generisan G-kod za glodalicu HAAS VF-3 na kojem je kalup i izrađen.

Ključne reči: modeliraje, kalup, SolidWorks, Mold Tools, 3D glodanje

UVOD

SolidWorks je programski paket za mašinsko projektovanje i automatizaciju procesa pomoću parametarskog modelovanja punih tela. Omogućava da se osnovna 2D skica pretvori u model punog tela pomoću jednostavnih, ali visoko efikasnih alata za modeliranje. Uz to, SolidWorks generiše i tehničke crteže međusobno povezanih elemenata, delova i sklopova. Omogućava izradu virtuelnog prototipa od lima i razvijenog omotača, radi lakše realizacije plana projektovanja i izrade odgovarajućeg proizvoda. Pomoću ovog programskog paketa moguće je izdvojiti jezgro i šupljinu modela koji treba da se izlije u kalupu a pruža i mogućnost kreiranja složene parametarske površine [1].

U ovom programskom paketu radni prostor povećan je tako što su grupisane alatke sa sličnim funkcijama i namenama. Alatke s palete

Standard dostupne su i na paleti menija (Menu Bar). Navedena paleta se nalazi iznad prostora za crtanje u okoviru kojih se nalaze panoi za skice, za tipske oblike, za kotiranje limova, pano sa alatima za kalupe i drugi [2].

Upotrebom programskih paketa moguće je napraviti geometrijski veoma složene modele. CAM/CAD tehnologije predstavljaju deo ukupne podrške procesima konstruisanja i proizvodnje. Srž njihove primene čini model proizvoda, odnosno računarska predstava stvarnog proizvoda. Svaki od skupova programskih paketa vezan je za podršku pojedinim fazama razvoja proizvoda [3]. Korišćenjem CAD/CAM tehnologije moguće je konstruisati geometrijski komplikovani predmet u prirodnoj veličini i zatim napraviti simulaciju obrade tog predmeta. Korekcijom parametara tokom simulacije smanjuje se mogućnost greške pri obradi, čime se štedi vreme zbog nepotrebnih obrade sirovine dok se

ne dobije tačno željeni model. U radu je kao primer složenog modela, odnosno kalupa za njega, izabrana viljuška.

OBLIKOVANJE MODELA KALUPA

U SolidWorksu u modulima Sketch i Features napravljen je model viljuške (slika 1). Nakon toga konstruisan je alat za livenje plastične viljuške u aluminijumu. Sam alat se sastoji od dva dela, gornjeg i donjeg.

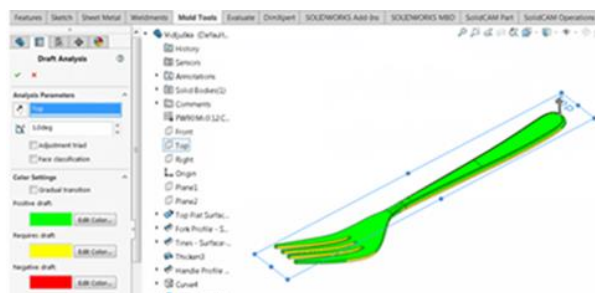


Slika 1. Model viljuške u SolidWorksu

Da bi se napravio alat, potrebno je izraditi kalup na modelu kako bi viljuška mogla da se lije. Za taj postupak neophodan je modul Mold Tools u Solidworks-u. Ova opcija daje mogućnost kreiranja šupljina u kalupu za deo za koji se želi napraviti alat.

Alatke sa ovog modula, koriste se pri izradi kalupa i izdvajanju jezgra i šupljine izlivenog modela. Da bi se kreirao željeni alat, potrebno je definisati odlivak pomoću panoa skice i panoa za tipske oblike. Model viljuške je odlivak za koji će biti izrađen kalup [3].

Pre samog postupka izrade kalupa, neophodno je utvrditi, kroz opciju Draft Analysis da li su stranice odlivka u blagom zakošenju (minimum 1%) u odnosu na ravan sečenja kalupa (slika 2). Ukoliko stranice odlivka nisu u blagom zakošenju, to može predstavljati problem pri vađenju odlivka iz kalupa. U ovom slučaju odlivak je blago zakošen u odnosu na ravan sečenja.



Slika 2: Prikaz dela kroz opciju Draft Analysis

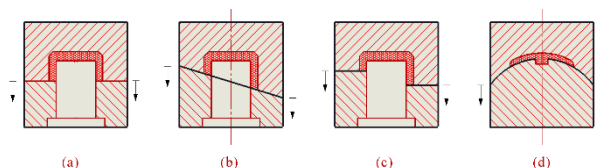
U datom prikazu program korisniku daje obaveštenja putem boja da su sve površine blago zakošene što omogućava izvlačenje odlivka iz kalupa. Žuta boja predstavlja delove koji su upravni na ravan sečenja kalupa i ti delovi bi mogli ostati u samom kalupu [4].

U konkretnom slučaju, u ovom radu, žutom bojom su obeleženi samo vrhovi viljuške i oni ne predstavljaju problem za izvlačenje, zbog svoje male površine. Crvena boja na delu predstavlja površine koje se ne bi mogle izvaditi iz kalupa, ali tih površina u ovom slučaju nema, tako da se može preći na sledeći korak izrade kalupa.

Pomoću opcije Parting lines definiše se linija razdvajanja kalupa, koja seče kalup na gornji i donji deo. Zbog složenog oblika proizvodnog dela, neophodno je koristiti ovu opciju koja prati samu konturu viljuške. U slučaju da se odabere druga vrsta preseka kalupa, ravan ili stepenast, sam alat ne bi bio funkcionalan i ne bi zadovoljio postavljene kriterijume.

Opcija Parting surface daje mogućnost kreiranja nove površine, koja je neophodna za konstruisanje gornjeg i donjeg dela kalupa. Razdvojne površine kalupa su one površine ploče, koje su susedne otiscima i međusobno se spajaju da bi stvorile zaptivku i sprečile gubitak plastičnog materijala od otiska.

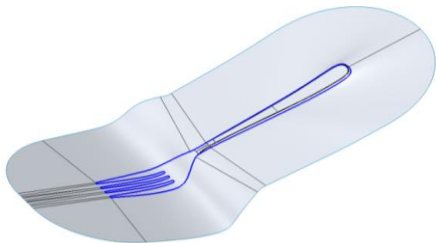
Postoji više vrsta razdvajanja kalupa: ravno razdvajanje kalupa; razdvajanje kalupa pod uglom; stepenasto razdvajanje kalupa i lučno razdvajanje kalupa (slika 3).



Slika 3. Vrste preseka kalupa

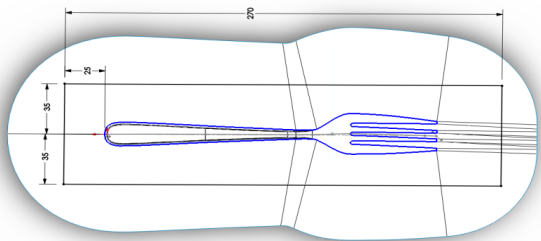
U zavisnosti od samog oblika kalupa i njegovih fizičkih karakteristika, bira se neka od

ponuđenih vrsta razdvajanja kalupa. Linija razdvajanja mora da prati sam oblik kalupa. U ovom slučaju koristiće se lučno razdvajanje kalupa. Pomoću opcije Parting surface kreira se nova površina (slika 4) a sa opcijom Tolling split kreira se gornji i donji deo kalupa.



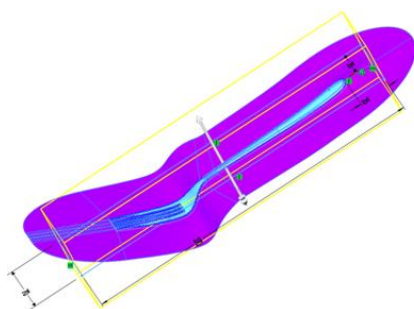
Slika 4. Prikaz nove površine pomoću opcije Parting surface

Sledeći korak je izrada skice, koja je neophodna zbog pozicioniranja i definisanja dimenzija (slika 5).



Slika 5. Izrada skice i definisanje dimenzija alata

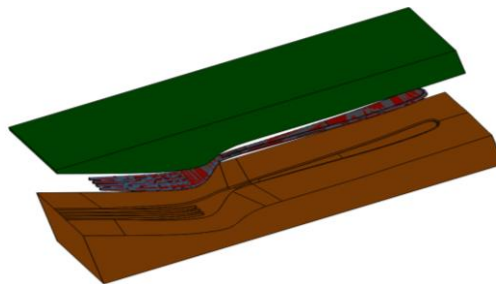
Kada je završeno modeliranje potrebno je definisati debljinu tako što se dodaje sloj materijala u željenom smeru (slika 6).



Slika 6. Definisane debljine alata

U sledećem koraku je neophodno odrediti debljinu gornjeg i donjeg dela kalupa. Iz menija pomoćnih alata, na polju Insert iz padajućeg menija bira se opcija Surface i u okviru nje, opcije Move and Copy, kako bi se izvršilo razdvajanje gornjeg i donjeg dela kalupa. Radi boljeg pregleda detalja, preporučljivo je odrediti druge boje novim telima.

Kalup za ubrizgavanje ima dve glavne komponente: pokretnu polovinu i fiksnu polovinu (slika 7). Tokom procesa ubrizgavanja liva u kalup, ove dve polovine se čvrsto pritisnu i čine zapečaćenu šuplinu kako bi se izbeglo curenje toka rastopine i održao određeni pritisak zadržavanja. Pritisnuta površina se naziva razdelna površina. Obično su razdelne površine najveći obris projekcije dela [5].

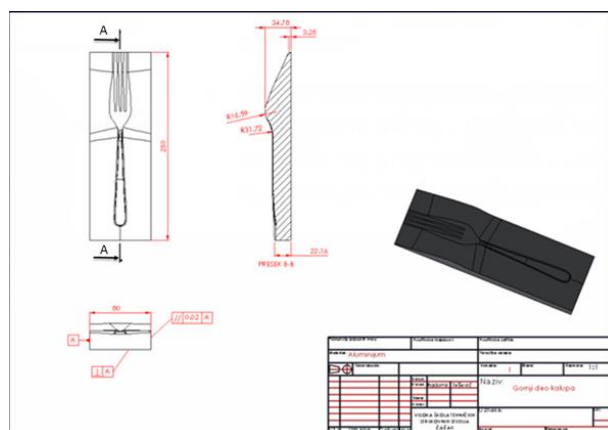


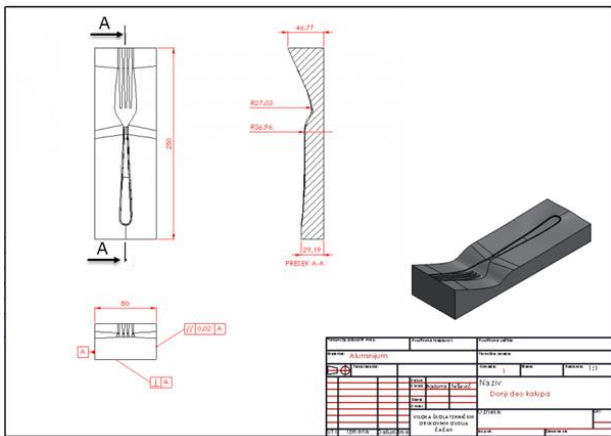
Slika 7. Prikaz gornjeg i donjeg dela kalupa

DEFINISANJE OPERACIJA GLODANJA U SOLIDCAMU

Pre nego što se započne postupak obrade u SolidCAM-u, neophodno je uraditi par koraka: sačuvati model u poseban fajl u koji će biti sačuvan i CAM fajl, uraditi radionički crtež i odrediti način stezanja izradka.

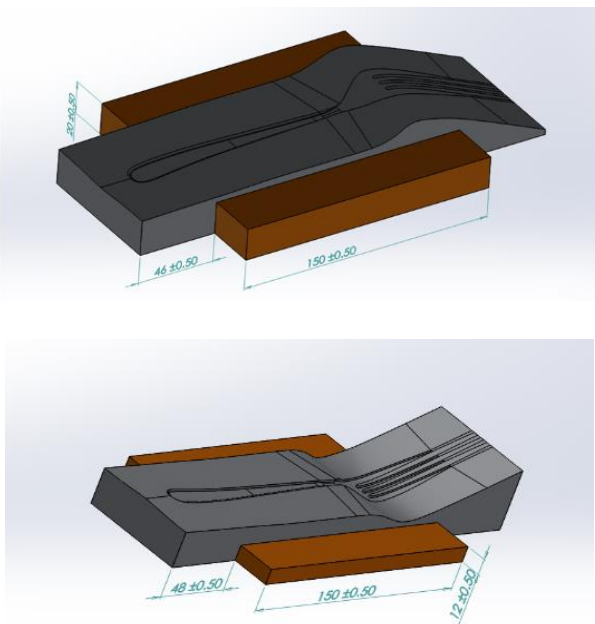
Pomoću opcije Make Drawing from Part kreira se radionički crtež (slika 8). Svi neophodni detalji koji su vezani za proces izrade, prikazani su na samom crtežu.





Slika 8. Radionički crtež gornjeg i donjeg kalupa

Pored svih detalja koji se nalaze u radioničkom crtežu, neophodno je i definisati način stezanja komada kako alat kojim se vrši obrada, ne bi zakačio fiksni i pokretni deo stega (slika 9).



Slika 9: Plan stezanja gornjeg i donjeg kalupa

Nakon generisanja geometrije, izbora postprocesora, definisanja koordinatnog sistema, definisanja pripremnika i gotovog dela, potrebno je u tehnološkom stablu definisati preostale parametre.

Pomoću kartice Tool Sheet dobija se tabela alata koji se koristi u samom postupku obrade, sa svim parametrima koji su vezani za alate. Klikom na ikonicu Operation, otvara se padajući meni sa paletom različitih programa koji se biraju pri izradi samog dela. Većina opcija koje

nam nudi program opisane su u samom naslovu, kao npr. Face, ali zbog složenih površina na samom kalupu, koristiće se opcije HSM i HSR za izradu složenih površina.

Tabela 1. Alati koji se koriste u postupku obrade

Wednesday, November 25, 2020		Tool Table For GORNJI KALUP		SolidCAM	
1-Spindle-1	FACE MILL	D: 25 mm R: 1 mm TD: 25 mm A: 0 AD: 32	TL: 60 mm OHL: 40 mm CL: 20 mm SL: 30 mm H: 100 mm	H 1	D 1 Flutes: 4
2-Spindle-1	END MILL	D: 6 mm AD: 6	TL: 80 mm OHL: 60 mm CL: 24 mm SL: 30 mm H: 100 mm	H 2	D 2 Flutes: 2
3-Spindle-1	BALL NOSE MILL	D: 6 mm R: 3 mm AD: 6	TL: 80 mm OHL: 60 mm CL: 24 mm SL: 30 mm H: 100 mm	H 3	D 3 Flutes: 2
5-Spindle-1	BALL NOSE MILL	D: 4 mm R: 2 mm AD: 6	TL: 80 mm OHL: 60 mm CL: 24 mm SL: 30 mm H: 100 mm	H 5	D 5 Flutes: 2

Wednesday, November 25, 2020		Tool Table For DONJI KALUP		SolidCAM	
1-Spindle-1	FACE MILL	D: 25 mm R: 0 mm TD: 25 mm A: 0 AD: 32	TL: 60 mm OHL: 40 mm CL: 20 mm SL: 30 mm H: 100 mm	H 1	D 1 Flutes: 4
2-Spindle-1	END MILL	D: 6 mm AD: 6	TL: 80 mm OHL: 60 mm CL: 24 mm SL: 30 mm H: 100 mm	H 2	D 2 Flutes: 2
3-Spindle-1	BALL NOSE MILL	D: 6 mm R: 3 mm AD: 6	TL: 80 mm OHL: 60 mm CL: 24 mm SL: 30 mm H: 100 mm	H 3	D 3 Flutes: 2
4-Spindle-1	BALL NOSE MILL	D: 4 mm R: 2 mm AD: 6	TL: 80 mm OHL: 60 mm CL: 24 mm SL: 30 mm H: 100 mm	H 4	D 4 Flutes: 2
5-Spindle-1	END MILL	D: 4 mm AD: 6	TL: 80 mm OHL: 60 mm CL: 24 mm SL: 30 mm H: 100 mm	H 5	D 5 Flutes: 2

Na kraju programiranja uz pomoć opcije GCode program je generisao celokupan G kod u formi Notepad fajla, koji će biti prebačen na mašinu.



Slika 10. Prikaz gotovog gornjeg i donjeg kalupa

ZAKLJUČAK

U radu je prikazan postupak izrade složenog kalupa u SolidWorksu. Za primer je uzet 3D model viljuške a nakon toga je konstruisan alat za livenje plastične viljuške u aluminijumu.

Može se zaključiti da je sam postupak izrade šupljina u kalupima u današnje vreme gotovo nezamisliv bez programskog paketa kao što je SolidWorks. Programski paket SolidWorks, daje mnoštvo mogućnosti pri kreiranju samog alata i omogućava sagledavanje samog postupaka izrade, od početka do kraja, uz mogućnost korekcije grešaka pre postupka izrade. Na taj način, mnoge geške se otklanjaju u fazi kreiranja, što postupak izrade čini lakšim i jeftinijim.

LITERATURA

- G. Čučković: *SolidWorks i SolidCAM osnove*, CET, Beograd, 2017.
- Š. Tiku: *SOLIDWORKS 2020 za mašinske inženjere*, Mikro knjiga, Beograd, 2020.
- G. Devedžić, S. Ćuković, S. Petrović, J. Maksić: *3D modeliranje proizvoda*, Mašinski fakultet u Kragujevcu, CIRPIS centar, Kragujevac, 2016.
- J. Bethune: *Solidworks 2014 inženjerski dizajn i grafika*, Kompjuter biblioteka, Beograd, 2014.
- R. Lueptow, M. Minbiole: *Naučite Solidworks*, CET, Beograd, 2013.

PROCEDURE OF MAKING CASTING MOLD IN SOLIDWORKS

Abstract: *The paper shows the procedure for making a complex mold using the SolidWorks software package. The mold was constructed in the Sketch, Features and Mold Tools modules, with which a 3D model of the fork was created and then the upper and lower molds were constructed. The biggest problem when constructing a mold is defining the tool parting line, which cuts the tool in two. After 3D modeling of the mold, a simulation of 3D milling processing was created in the SolidCAM program module, where after defining the processing, G-code was generated for the HAAS VF-3 milling machine on which the mold was made.*

Keywords: *modelling, mold, SolidWorks, Mold Tools, 3D milling*



Society of Production
Engineering

SPMS 2023

39. Savetovanje proizvodnog mašinstva Srbije

ICPES 2023

39th International Conference on Production Engineering of
Serbia



Faculty of Technical
Sciences
University of Novi Sad

Novi Sad, Serbia, 26. – 27. October 2023

INFLUENCE OF SURFACE ROUGHNESS ON MATERIAL TRANSFER OCCURRING IN ALUMINIUM DRY SLIDING APPLICATION

Dragan DzUNIC^{1, *}, Vladimir KOCOVIĆ¹, Suzana PETROVIĆ SAVIĆ¹, Aleksandar DjORDJEVIĆ¹,
Aleksandra KOKIĆ ARSIĆ², Slobodan MITROVIĆ¹

¹Faculty of Engineering, University of Kragujevac, Kragujevac, Serbia

²Kosovo and Metohija Academy of Applied Studies, Leposavic, Serbia

*Corresponding author: dzuna@kg.ac.rs

Abstract: Aluminium and its alloys are highly represented in industrial application. Despite of good mechanical and conductive properties, both thermal and electric, in tribological manner material transfer that may occur during the dry sliding conditions has great influence on friction and wear of the contact elements. This study represents an attempt one in a row to define the parameters that leads to the material transfer occurring, and in this paper influence of surface roughness was investigated. Tribological test were performed in dry sliding conditions using CSM nanotribometer with ball-on-plate contact configuration and linear reciprocating motion with 0,5mm amplitude and sliding speeds of 1, 5 and 10 mm/s under constant load of 200mN. Obtained results indicated presents of material transfer for all three investigated surfaces prepared using sand paper with different grit sizes 240 and 1000 and polished sample. Appearance of transferred layer, on the steel counter body, and penetration depth value plots refers to cyclic nature of material transfer. Material transfer during the dry sliding contact result in increase of coefficient of friction and wear of tested aluminium samples.

Keywords: Aluminium, Friction Coefficient, Wear, Material Transfer, Nanotribometer.

1. INTRODUCTION

Aluminium and his alloys as a material has a wide industrial application since it is recognized as lightweight metal in comparison to other market available metals and due to its good, mechanical and structural properties and electric and thermal conductivity. Also numerous improvement are possible using aluminium as a matrix material for wide range of composites, reinforced with various types of materials, shapes and sizes [1-3]. In tribological

manner, it is possible to improve physical appearance of the contact surface, by lowering the surface roughness and in the same way improving the mechanical properties, using nonconventional techniques such as ball and roller burnishing [4-5].

Despite mentioned improving the problem of material transfer still, exist in dry sliding conditions, which can occur as a result of construction of tribo-mechanical system itself or inadequate lubrication, lubrication medium or due to breakage of lubrication or protection

film. Tribological investigations of different aluminium alloy indicated to presence of material transfer to the counter body surface [6-8]. Material transfer were noticed in all dry sliding tests of automotive cylinder aluminium alloy [8], and in some cases of zinc aluminium alloy (ZA-27, 27% of aluminium) nano composite [6]. In both cases it is very hard to predict and to conclude the moment and the reason for material transfer. It can occur at the early begging of the sliding contact, but also in the same contact condition it can be prolonged much later.

In our previous investigations, we have tried to avoid material transfer by varying material of the counter body (Inox 440c, Ruby, Sapphire, Alumina Al_2O_3 and Silicon Nitride Si_3N_4) [9] or at least define contact parameters without material transfer. In this paper, we investigated influence of surface roughness on mentioned phenomenon of material transfer under dry sliding.

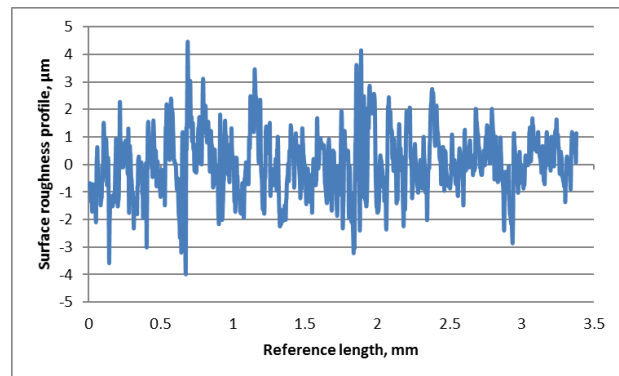
2. EXPERIMENT

Tribological testing were performed using CSM Nanotribometer with ball-on-plate contact geometry and linear reciprocating motion. 100Cr6 steel was used as a counter body (ball, 1.5 mm in diameter) material. Test samples were prepared from aluminium alloy 6082 (AlMgSi1) T651 grinded with sand paper with different grit size, 240p, 1000p, while the third one is polished. Pilishing was performed using polishing emulsion with 6, then 1 and finish with $0,42\mu m$ abrasive particles. Surface roughness were measured using INSIZE C002 profilometer. Friction and wear tests were performed under constant load (200mN), with 0.5 mm amplitude, sliding distance of 1m or 500 cycles and three different sliding speeds (1, 5 and 10 mm/s). Each test were repeated three times. Obtained wear tracks were measured and analysed using optical microscope.

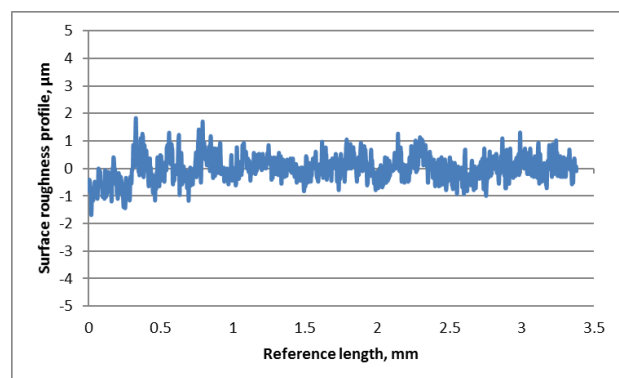
3. RESULTS AND DISCUSSION

Surface roughness measurement result were presented on figure 1. As it is mentioned

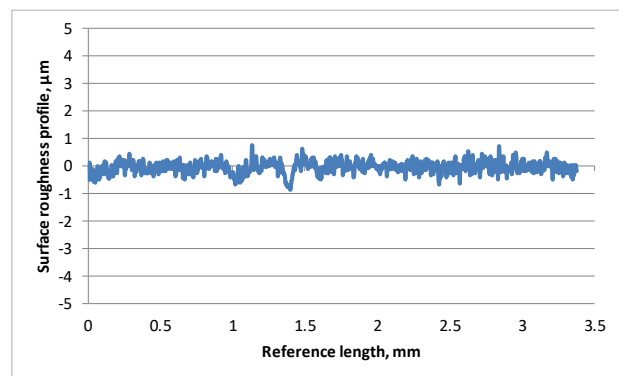
before three aluminium samples, with different surface finish (240p, 1000p and polished), were on test.



a)



b)



c)

Figure 1. Surface roughness of prepared Aluminium samples with sandpapers with different grit sizes: a) 240p, b) 1000p and polished

Coefficient of friction and penetration depth values are presented on the following plots (Figure 2-4) in comparison to the sliding time, sliding distance and number of cycles. Penetration depth parameter proved to be very useful for analysing the material transfer process. Presented plots represents one tribological test from three that were performed under the same contact conditions.

Figure 2 represents COF and PD values for the samples with 240p grit finish under three sliding speeds value. From these plots, it can be concluded that material transfer starts at early beginning of the contact, which followed with the sharp change of both observed parameters.

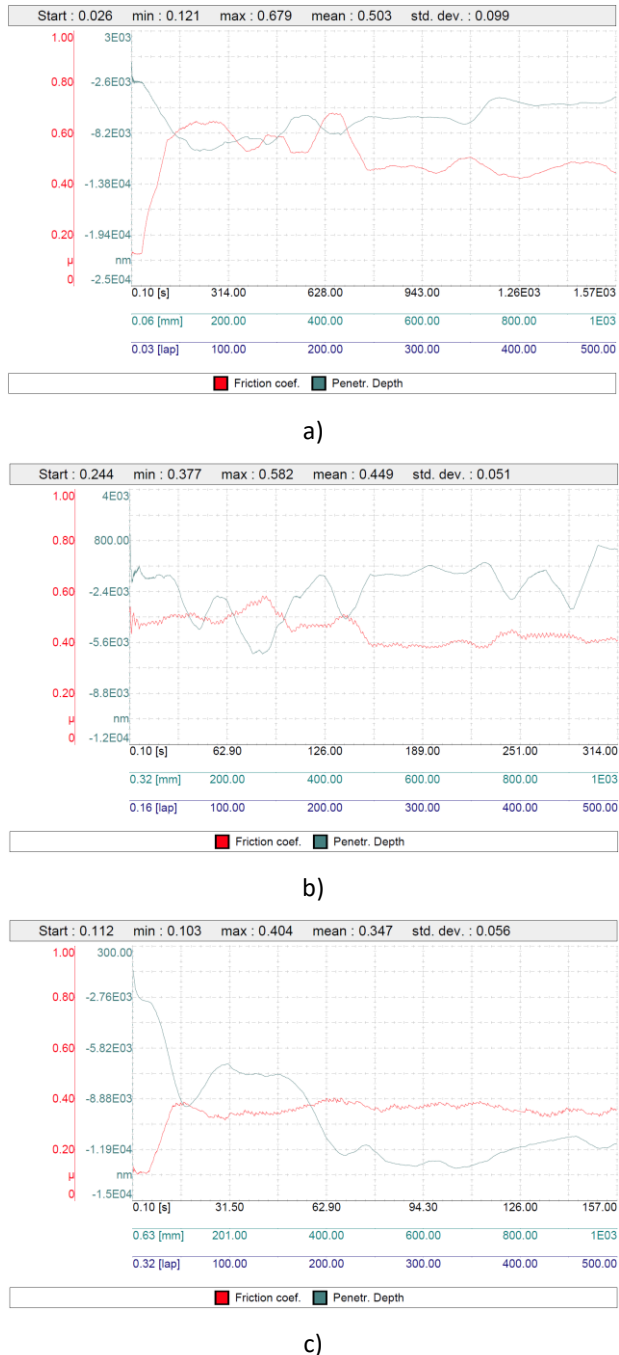


Figure 2. Coefficient of friction and Penetration depth plots for 240p grit size Aluminium sample under three sliding speeds: a) 1mm/s, b) 5mm/s and c) 10mm/s.

In case of 5mm/s sliding speed material transfer starts almost instantly while for others sliding speeds material transfer occurs in period of 10-20s. Figure 3 represents obtained results for sample prepared with 1000 grit size. Sample

prepared with sandpaper with 1000p grit size manifests almost the same trends for COF and PD as previous prepared with 240p grit size.

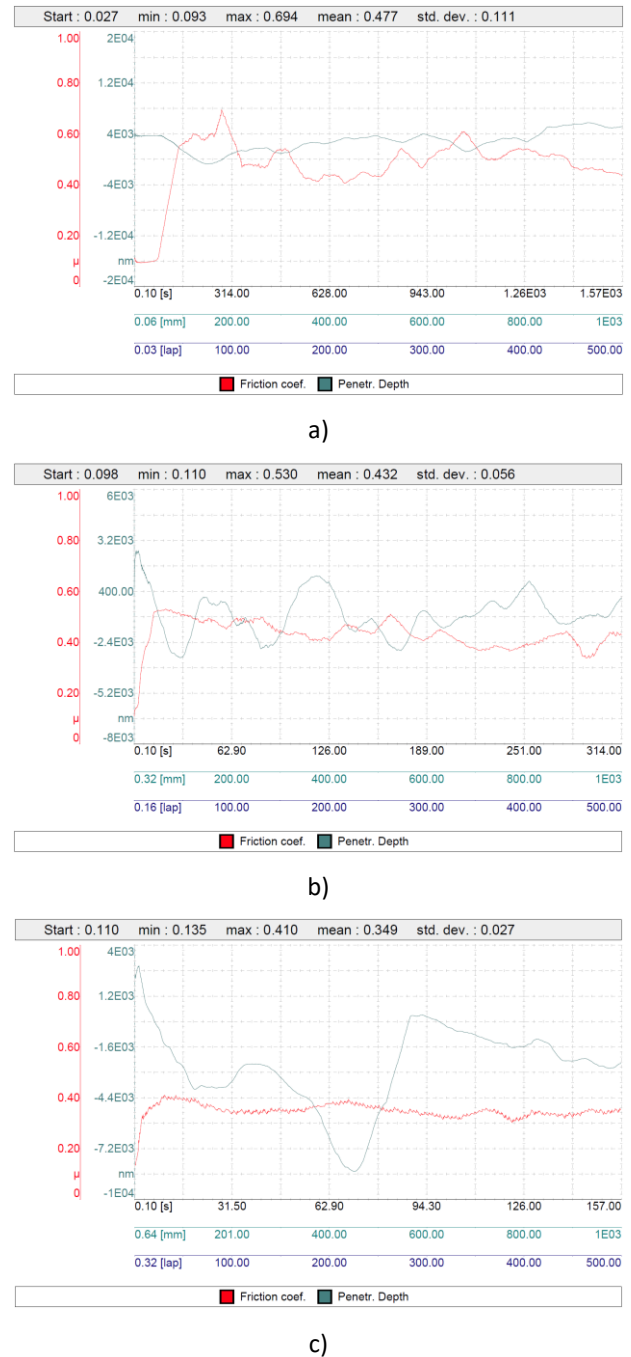
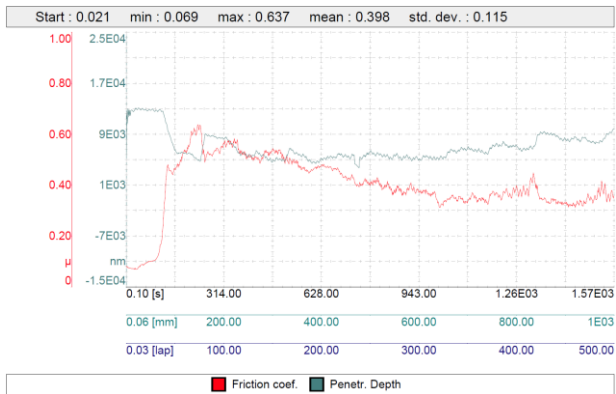


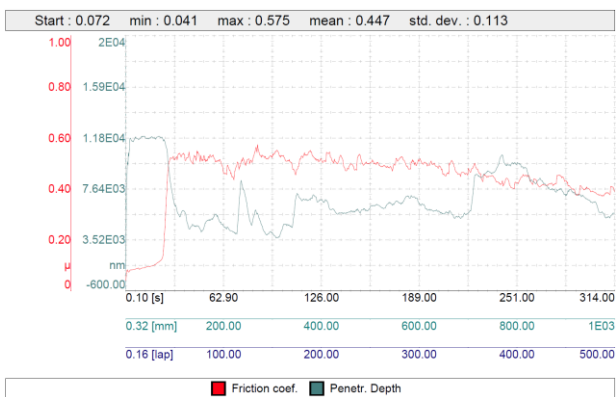
Figure 3. Coefficient of friction and Penetration depth plots for 1000p grit size Aluminium sample under three sliding speeds: a) 1mm/s, b) 5mm/s and c) 10mm/s.

On the figure 4 COF and PD plots are related to the polished sample. As it can be seen from presented plots, material transfer is postponed 10-20s, but in all tests there were no immediate material transfer. Some authors indicated that material transfer is related to the contact temperature, and that with temperature rise material transfer is more frequent and starts

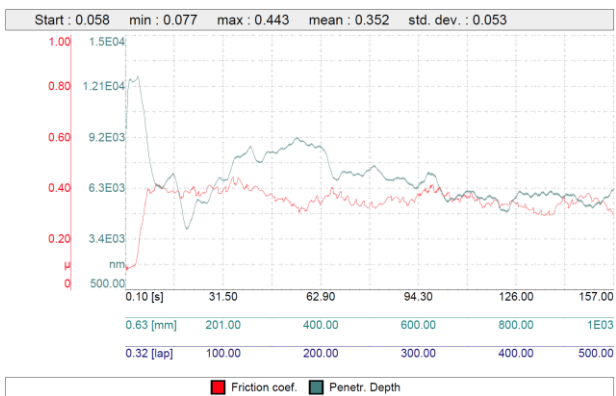
much earlier [7], but in the present investigation that's not a case since all tests were performed at the room temperature.



a)



b)



c)

Figure 4. Coefficient of friction and Penetration depth plots for polished Aluminium sample under three sliding speeds: a) 1mm/s, b) 5mm/s and c) 10mm/s.

From all presented plots it is obvious that penetration depth has numerous sharp changes during the sliding period that indicated on unstable and variable thickness of transferred layer on the counter body surface. Transferred layer thickness increases until the critical value that is not able to withstand the tangential force. In that moment part of the

transferred layer is detached and become wear debris. That process repeats numerous times during the sliding contact and the change in PD value is more pronounced for rougher surfaces.

Wear tracks were measured and analysed using optical microscope. Measurement were done by measuring the appeared area of the wear track and then analytically wear volume was calculated. Wear volume and standard deviation of measured wear tracks is presented on figure 5. Polished samples exhibits better wear resistance in comparison to the rougher surfaces accept in case of 10mm/s sliding speed.

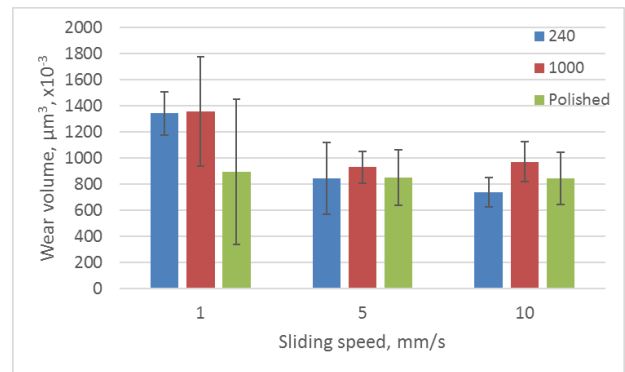
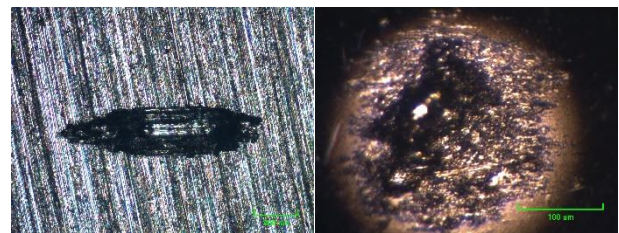
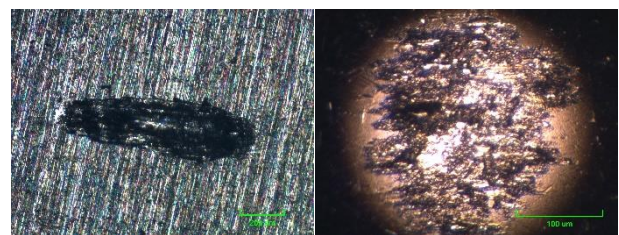


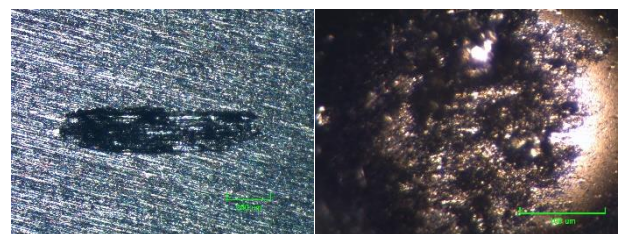
Figure 5. Wear volume of all tested samples



a)



b)



c)

Figure 6. Wear tracks and transferred layer appearance obtained under 5mm/s sliding speed: a) 240p, b) 1000p and c) polished sample.

As a representative example of wear track and transferred layer appearance, those obtained under 5mm/s sliding speed was chosen. Uneven distribution of transferred material on the counter body surface indicates uneven height, which is in corresponding to the presented PD plots. This kind of distribution of transferred material and its unpredictable behaviour are the reason for high deviations in measured wear tracks volume values.

4. CONCLUSION

Influence of surface roughness on material transfer occurring, from aluminium samples to the steel counter body, during the dry sliding contact was presented. It can be concluded that surface roughness has no greater influence material transfer occurring but polished samples has lower wear volume and also PD change is less pronounced in comparison to the samples with rougher surfaces.

Material transfer process is not progressive by its nature, but more cyclic, which correspondents to the presented PD plots.

Material transfer occurring is followed by sharp change in COF and PD value. COF is increased more than four times in comparison to the starting values.

ACKNOWLEDGEMENT

This research was funded by the Ministry of Science, Technological Development and Innovation of Republic of Serbia.

REFERENCES

- [1] T. Ma, H. Yamaura, D. Koss, R. Voigt: Dry sliding wear behavior of cast SiC-reinforced Al MMCs, *Materials Science and Engineering: A*, vol. 360, no. 1-2, pp. 116-125, 2003.
- [2] M, R.P., Saravanan, R. and Nagaral, M.: Fabrication and wear behavior of particulate reinforced Metal Matrix Composites-an overview, *IOSR Journal of Mechanical and Civil Engineering*, 14(01), pp. 10–20. Available at: <https://doi.org/10.9790/1684-1401041020>.
- [3] Y. Sahin: Wear behaviour of aluminium alloy and its composites reinforced by SiC particles using statistical analysis', *Materials & Design*, vol. 24, no. 2, pp. 95-103, 2003.
- [4] Đ. Vukelić, B. Tadic, D. Džunić, Vladimir Kočović, Lj. Brzaković, M. Zivković, G. Simunović: Analysis of ball-burnishing impact on barrier properties of wood workpieces, *International Journal of Advanced Manufacturing Technology*, Vol.92, No.1-4, pp. 129–138, ISSN 0268-3768, Doi 10.1007/s00170-017-0134-3, 2017.
- [5] M.H. El-Axir, O.M. Othman, A.M. Abodiena: Study on the inner surface finishing of aluminum alloy 2014 by ball burnishing process, *Journal of Materials Processing Technology*, Volume 202, Issues 1–3, Pages 435-442, 2008.
- [6] M. Babic, B. Stojanovic, D. Dzunic, M. Pantic: Micro/nanoscale structural, mechanical and tribological characterization of ZA-27/SiC nanocomposites, *Journal of Composite Materials*, Vol. 54, Iss. 16, pp. 2113-2129, 2019.
- [7] Tarasov SYu, Filippov AV, Kolubaev EA, et al. Adhesion transfer in sliding a steel ball against an aluminium alloy, *Tribol Int*, Vol. 115, pp. 191–198, 2017.
- [8] S. Milojević, D. Džunić, D. Marić, T. Skrúcaný, S. Mitrović, R. Pešić, *Tribological Assessment of Aluminum Cylinder Material for Piston Compressors in Trucks and Buses Brake Systems*, *Tehnički vjesnik/Technical Gazette*, Vol.28, No.4, pp. 1268-1276, 2020
- [9] D. Džunić, S. Petrović Savić, V. Kočović, S. Kostić, A. Đorđević, A. Kokić Arsić, S. Mitrović: Influence Of Counter Body Material On Material Transfer During Ball On Plate Dry Sliding, *18th International Conference On Tribology*, Kragujevac, Serbia, 17 – 19 May, pp. 242-247, 2023.



Society of Production
Engineering

SPMS 2023

39. Savetovanje proizvodnog mašinstva Srbije

ICPES 2023

39th International Conference on Production Engineering of
Serbia



Faculty of Technical
Sciences
University of Novi Sad

Novi Sad, Serbia, 26. – 27. October 2023

NUMERICAL AND EXPERIMENTAL RESEARCH OF SHRINKAGE AND SINK MARKS ON INJECTION MOLDED PLASTIC PARTS

Ivan MATIN^{1*}, Branko ŠTRBAC¹, Miloš RANISAVLJEV¹, Miodrag HADŽISTEVIĆ¹, Zorana LANC¹

¹University of Novi Sad, Faculty of Technical Sciences, Novi Sad, Serbia

*Corresponding author: matini@uns.ac.rs

Abstract: Injection molding (IM) is the most efficient and cost-effective method for mass-production of plastic parts. This method aids in reducing the time and cost required to create appropriate shape. To achieve accurate dimensional precision of the part, these defects should be carefully minimized to improve operational characteristics and product life. The influence of packing pressure, packing time, and melt temperature on dimensional shrinkage, and sink marks of plastic material was studied numerically and experimentally. Experimental and numerical study indicated minimum shrinkage of 1.51% and 1.68%, respectively, with the identical injection molding process parameters. The minimal depth of sink marks was found 0.05 mm and 0.58 mm, respectively, in experimental and numerical study.

Keywords: measurement, injection molding, sink marks, numerical simulation.

1. INTRODUCTION

Injection molding (IM) is one of the most important manufacturing processes to produce plastic products. The process converts the plastic pellets to the finished components without grinding and polishing. However, injection molded plastic parts undergo shrinkage during cooling and after the ejection stage, which remains a point of concern owing to its effect on performance. Manufacturer suffers higher losses if the component's size is over the part's permitted tolerance limit. Therefore, the minimization of shrinkage is important. In IM, part geometry, mold design, part material and injection molding process parameters are the critical factors that decides the characteristics of the manufactured

components such as shrinkage and sink marks. Hence, these factors must be carefully determined. The part should have uniform wall thickness to ensure uniform cooling [1]. In recent years, injection molded products have been widely used in various devices, ranging from automobiles to home electric appliances, electronic devices and mechanical components. When embossed decorative products are used as substrate for optical disks, automobiles, home appliances, mechanical components, etc. Surface property plays an important role to evaluate the quality of final product. The sink marks affect the surface quality that is requires the research. One of the key requirements of the good quality injection molding of plastic materials is a thin and consistent wall thickness. In the case of the injection molding of thick-

walled products, either aesthetic problems occur sink marks or production can only be executed by applying an unacceptably long cycle time [2]. Shrinkage occurs at a molecular level when plastics melt and cool. Volumetric shrinkage is caused by thermal contraction, which affects all plastics (semi-crystalline and amorphous), and influences how the material changes in volume as it transitions from a liquid to a solid state [3]. The mold design consists of design of gates, runner, sprue and waterline channel. The gate design includes finding the number of gates, locations, shape and dimensions. Many authors have carried out numerical study to determine best gate location and gate numbers using numerical simulation [4-7].

The injection molding parameters namely packing pressure, packing (holding) time, melt temperature, mold temperature, injection pressure, injection time and cooling time should be carefully selected to minimise the defects [8-10].

Many authors determined IM parameters and gate numbers to minimize shrinkage, weld line, warpage, and air traps on selected plastic material. The authors observed that the volumetric shrinkage has increased with melt temperature, but it has decreased as the packing pressure and mold temperature increases [11]. They had studied experimental and numerical approach to characterize shrinkage and optimized dimensional deviation of injection-molded plastic part. The authors advocated that cooling rate has highest contribution on shrinkage while melt temperature has highest contribution on dimensional deviation. The authors developed procedure to analyse internal mechanism of deviation between numerical simulation and experiment, and investigated influence of molding conditions on the shrinkage and roundness of injection molded parts. They concluded that melt temperature and packing pressure has dominating effect on part shrinkage. The sink marks are undesired depressions on the surface of injection-molded components, and appear frequently on

sections with the highest plastic concentration [7, 9, 12, 13, 14].

The quality of injected part which is affected by many parameters and the number of variables is high, that is why the studying task which is required to perform by computer aided engineering (CAE) can be remarkable. Hence, design of experiment (DOE) is an acceptable method to reduce the number of numerical experiments and obtain enough information which is used in real experiments, [6, 12, 14].

Therefore, it can be reported that packing pressure, packing time, melt and mold temperature were the most influential process parameters. It was observed from the literature that the impressive study of IM processing parameters on part shrinkage have been carried out over the years and advocated the significance of packing pressure, packing time and melt temperature. However, a little work has been reported on sink marks. Furthermore, complex plastic part need more research in this domain.

This research aims to design and develop mold and conduct experimental and numerical study to discover the impact of IM processing factors on shrinkage, and sink marks of the plastic part. The outcomes of this study are hoped to be useful to academics and manufacturers.

2. NUMERICAL AND EXPERIMENTAL METHODOLOGY

2.1 CAD model and material

The CAD model of the part is tailor-made from the point of manufacturing (radius, chamfer, draft, shrinkage etc.) and ensures uniform plastic material flow. The wall-thickness of the part has constant value of 2 mm. The CAD model is meshed using simple tetrahedron structure using PTC CREO Parametric software. The CAD drawing of the part is presented in Figure 1.

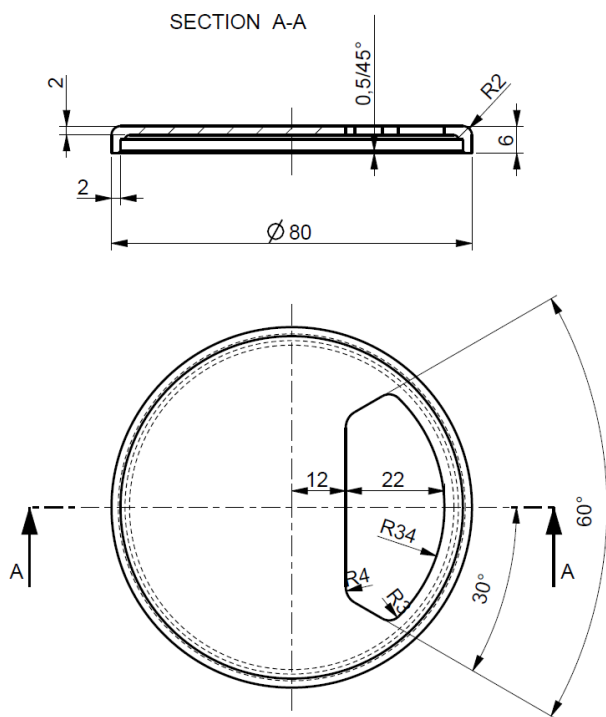


Figure 1. Technical draft of the part

Polypropylene (PP) is a widely used semi-crystalline polymer, which imparts high tensile strength to weight ratio, excellent chemical inertness, resistance to moisture, good fatigue life and low density. Therefore, PP K110 was selected as a plastic material in case study. This is general purpose homopolymer having easy processability and high strength. The PP granules have spherical shape with diameter of 3.8 to 4.8 mm, as shown in Figure 2.

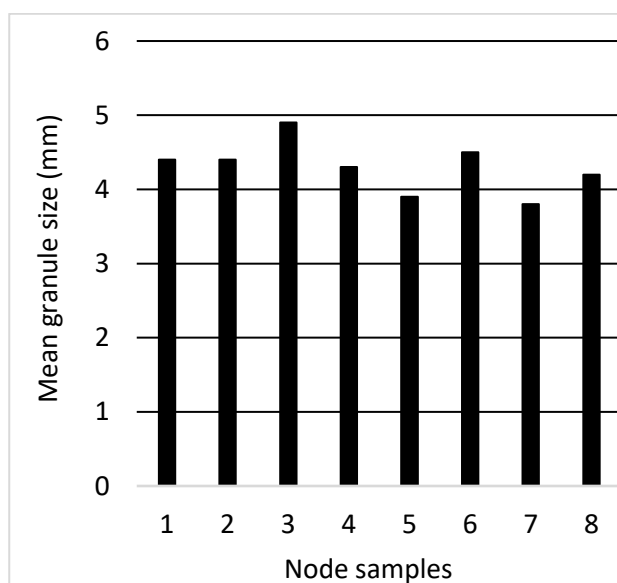


Figure 2. Granule diameter of PP

Variation of the diameter is not considered significant for IM process. Recommended injection molding conditions are selected from MoldFlow Database. The properties of the PP is presented in Table 1.

Table 1. Properties and molding conditions of PP

The parameters	Unit	Values
Solid density	g/cm ³	0,89
Liquid density	g/cm ³	0,74
Tensile strength at yield	MPa	40
Tensile elongation at yield	%	6
Glass transition temperature	°C	110
Mold temperature	°C	30-50
Elastic modulus	MPa	1340
Shear modulus	MPa	480
Maximal shear stress	MPa	0,25
Melt temperature range	°C	210-290
Maximal shear rate	1/s	100000
Ejection temperature	°C	102
Transition temperature	°C	111

2.2 Numerical simulation

The numerical simulation process begins with the import of geometry, mesh generation, plastic material, analysis sequence selection, injection molding condition implementation, and IM process parameter selection. This was carried out to predict the shrinkage and sink marks at a set of IM parameters and compare the same with experimental results. The first step of numerical simulation is determination number and gate location. The best gate location analysis for experimental part was carried out to find the most suitable area to locate the gates for easy cavity filling. The “gate region locator” algorithm was used to find the “best gate location”. The results are obtained in terms of the best region to locate the specific number of gates at a location having minimum flow resistance. Figure 3 shows „best gate location regions“ of the simulation model.

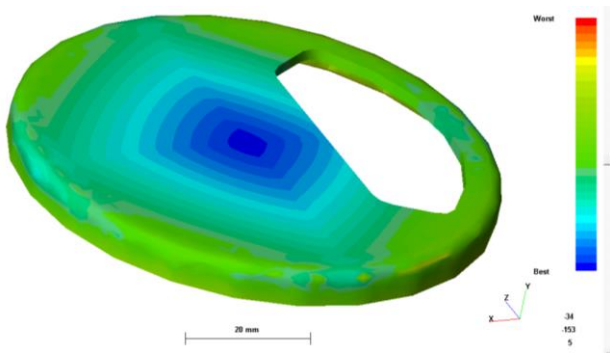


Figure 3. Best gate location

The highlighted regions (dark zones) represent the region where gate can be located as these regions offer minimum flow resistance. Many of the highlighted regions were found on the surface. Sink marks is estimate by numerical simulation is presented in Figure 4.

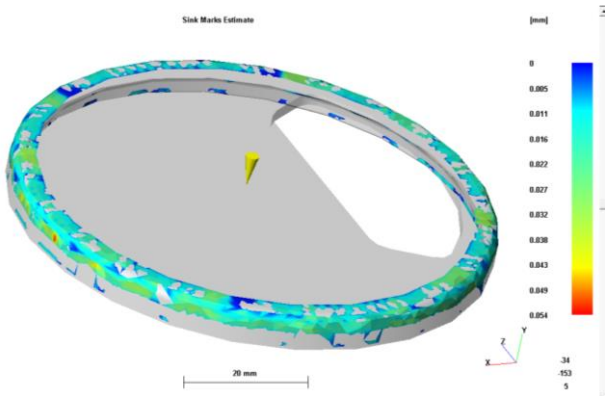


Figure 4. Sink mark using numerical simulation

The minimal depth of sink marks was found to be 0.005 mm, and maximal 0.054 mm, respectively, in numerical simulation.

Prediction of the quality of part using current IM process parameters is presented in Figure 5.

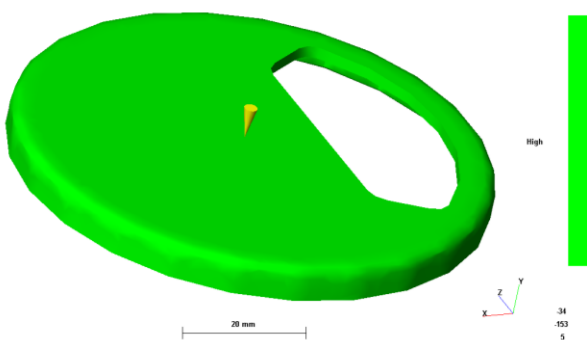


Figure 5. Confidence of fill the cavity of the mold

The Confidence of fill result displays the probability of plastic filling a region within the

cavity under conventional injection molding conditions. This result is derived from the pressure and temperature results. The part is easily filled and part quality should be acceptable because all regions on the CAD model of the part are green. Green color is presented High filling quality.

2.3 Experimental setup

The authors are selected „All Rounder 270s Compact” injection molding machine by ARBURG company using SAPA software. The specification of the injection molding machine according to EUROMAP is shown in Table 2.

Table 2. Specifications of IM machine

The parameters	Values
Distance between tie bars [mm]	270x270
Injection unit	100
Mold mount platens [mm]	380x380
Maximal clamping force [kN]	35
Unit of screw diameter [mm]	20
Maximal opening force [kN]	90
Minimal mold height fixed [mm]	200
Maximum injection pressure [MPa]	250
Maximal holding pressure [MPa]	250
Maximal screw stroke [mm]	100
Maximal injection flow [cm ³ /s]	146
Maximal ejector force [kN]	20
Maximal theoretical shot weight [g]	23
Maximal opening force [kN/mm]	350

In this study, injection molding machine had been operated in automatic mode, monitored using SELOGICA software.

2.4 Measurement of shrinkage and sink marks

The shrinkage is a ratio of the difference in addendum dimension of cavity and part. The shrinkage percentage presented here with is statical average of all measured shrinkage. The sink marks are areas in an injection molded part where the surface is deformed into a deformation. The sink marks was measured by micrometer. It is clear that the high injection and packing pressure results in the high clamping force and small volume shrinkage. For

crystalline, especially semi-crystalline materials the problem is very complex. The selected PP displays anisotropy in shrinkage such that shrinkage along the flow direction is greater than that measured transverse to flow. However, under some conditions, this anisotropy is reversed. The shrinkage percentage and percentage improvement in shrinkage and sink marks were calculated using following equations (1-3):

$$\text{Shrinkage } [\%] = \left(\frac{D_m - D_p}{D_m} \right) \cdot 100 \quad (1)$$

$$\Delta_1 [\%] = \left(\frac{S_{max} - S_{min}}{S_{max}} \right) \cdot 100 \quad (2)$$

$$\Delta_2 [\%] = \left(\frac{SM_{max} - SM_{min}}{SM_{max}} \right) \cdot 100 \quad (3)$$

Where are:

- D_m – dimension of mold cavity in mm,
- D_p – dimension of manufactured part in mm,
- Δ_1 – Improvement in shrinkage in percentage,
- S_{max} – Maximum value of shrinkage in percentage,
- S_{min} – Minimum value of shrinkage in percentage,
- Δ_2 – Improvement in sink marks in percentage,
- SM_{max} – Maximum depth of sink marks in mm,
- and,
- SM_{min} – Minimum depth of sink marks in mm.

3. RESULTS AND DISCUSSION

The effect of IM process parameters on shrinkage and sink marks has been discussed for many decades. As a matter of fact, shrinkage is inherent property of plastic material and it should be precisely handled to improve the product quality. Especially in the thick part improper setting of packing pressure, packing time and melt temperature may stimulate localize shrinkage that generates the sink marks. Hence, these IM parameters were carefully monitored and their impact was recorded in terms of diametric shrinkage, mass and depth of sink marks. The obtained results would have to make a balance between the selected outputs. Effect of melt temperature on shrinkage using experimental and numerical simulation method is presented in Figure 4.

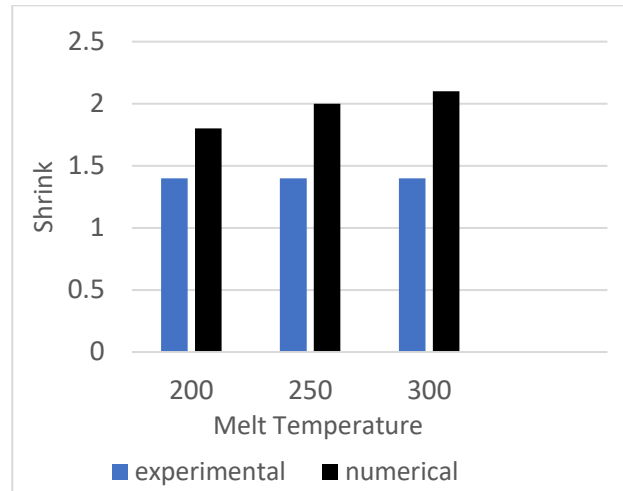


Figure 4. Effect of melt temperature on shrinkage

4. CONCLUSION

The sink marks was measured by micrometer, the results are provided satisfactory. Further work will be to verify presented shrinkage and sink marks measuring by GOM and/or CMM.

Pro/Plastic Advisor software was used for numerical simulation to determine the best gate location. The experimental and numerical analysis was carried out to observe the effects of packing pressure, packing time, and melt temperature on the shrinkage, and sink marks on the part. The following conclusions may be drawn from the case study. Experimental and numerical study indicated minimum shrinkage of 1.51% and 1.68%, respectively, with the determined injection molding parameters. The minimal depth of sink marks was found 0.05 mm and 0.58 mm, respectively, in experimental and numerical study. The PP granules have spherical shape with diameter of 3.8 to 4.8 mm, that is not considered into IM process. The experimental and numerical results showed similar trends of shrinkage, and depth of sink marks, and thereby validating simulation model of the plastic part. Validation of the model would help in redesigning the CAD free of the limitations of the existing mold and cavity design. These studies also presented the relationship between IM process parameters and defects on manufactured part. The enough high packing pressure had significantly

improved the shrinkage, and depth of sink marks. Melt temperature should be low to avoid shrinkage and sink marks.

ACKNOWLEDGEMENT

The results presented in this paper are part of the research within the project "Application of advanced production and information technologies in education, research and cooperation with the economy", at the Department of Production Engineering, Faculty of Technical Sciences, University of Novi Sad, Republic of Serbia.

REFERENCES

- [1] J. Z. Liang, J. N. Ness: The calculation of cooling time in injection moulding, *Journal of Material Process Technology*, Vol. 57, pp. 62-64, 1996.
- [2] G. Dogossy, T. Morauszki, F. Ronkay: Experimental Investigation and Applicability of Multi-Stage Simulations in the Case of a Thick-Walled Injection-Moulded Composite, *Applied Sciences*, Vol. 12, No. 17, pp. 415-426, 2022.
- [3] G. Guo: Investigation on surface roughness of injection molded polypropylene parts with 3D optical metrology, *International Journal on Interactive Design and Manufacturing*, Vol. 16, pp. 17-23, 2022.
- [4] B. S. Solanki, T. Sheorey, H. Singh: Experimental and numerical investigation of shrinkage and sink marks on injection molded polymer gears: A case study, *International Journal on Interactive Design and Manufacturing*, Vol. 16, pp. 1653-1667, 2022.
- [5] I. Matin, B. Štrbac, M. Hadžistević, M. Ranisavljev: The plastic product development using CAD/CAE advanced tools, in: *Proceedings of the 43th JUPITER conference*, University of Belgrade, Faculty of Mechanical Engineering, Belgrade, 2022.
- [6] I. Matin, B. Štrbac, M. Hadžistević, M. Ranisavljev: The advanced design and manufacture of the plastic part, in: *Proceedings of the 38th International Conference on Production Engineering of Serbia*, University of Kragujevac, Faculty of Technical Sciences Čačak, Čačak, 2021.
- [7] X. He, W. Wu: A practical numerical approach to characterizing non-linear shrinkage and optimizing dimensional deviation of injection-molded small module plastic gears, *Polymers*, Vol. 13, No. 13, 2021.
- [8] M. Mohan, M. N. M. Ansari, R. A. Shanks: Review on the effects of process parameters on strength, shrinkage, and warpage of injection molding plastic component, *Polymer Plastics Technology and Engineering*, Vol. 56, No. 1, pp. 1-12, 2017.
- [9] M. Kurt, Y. Kaynak, O. S. Kamber, B. Mutlu, B. Bakir, U. Koklu: Influence of molding conditions on the shrinkage and roundness of injection molded parts, *The International Journal of Advanced Manufacturing Technology*, Vol. 46, pp. 571-578, 2010.
- [10] S. M. Nasir, Z. Shayfull, S. Sharif, A. E. Abdellah, M. Fathullah, N. Z. Noriman: Evaluation of shrinkage and weld line strength of thick flat part in injection moulding process, *Journal of the Brazilian Society of Mechanical Sciences and Engineering*, Vol. 43, No. 452, 2021.
- [11] A. Torres-Alba, J. M. Mercado-Colmenero, J. Caballero-Garcia, C. Martin-Donate: Application of new conformal cooling layouts to the green injection molding of complex slender polymeric parts with high dimensional specifications, *Polymers*, Vol. 15, No. 558, 2023.
- [12] M. Moayyedian, K. Abhary, R. Marian: Gate design and filling process analysis of the cavity in injection molding process, *Advances in Manufacturing*, Vol. 4, pp. 123-133, 2016.
- [13] Cao-Tsai. Huang, Yi-H. Hsu, Bo-Syuan. Chen: Investigation on the internal mechanism of the deviation between numerical simulation and experiments in injection molding product development, *Polymer Testing*, Vol. 75, pp. 327-336, 2019.
- [14] T. B. Nguyen, Th. A. Yokoyama, S. Hamanaka, K. Kodama, K. Yamashita, C. Nonomura: Numerical and experimental evaluation of surface properties of embossed decorative injection-molded parts, *Polymer Testing*, Vol. 53, pp. 188-196, 2016.



Society of Production
Engineering

SPMS 2023

39. Savetovanje proizvodnog mašinstva Srbije

ICPES 2023

39th International Conference on Production Engineering of
Serbia



Faculty of Technical
Sciences
University of Novi Sad

Novi Sad, Serbia, 26. – 27. October 2023

UTICAJ PVD GREŠAKA RASTA NA KOROZIONU OTPORNOST EN X2CrNiMo18-14-3 HIRURŠKOG ČELIKA SA TiN PREVLAKOM

Zoran BOBIĆ¹, Lazar KOVAČEVIĆ¹, Atila CSIK², Peter RODIČ³, Branko ŠKORIĆ¹, Vladimir TEREK¹,
Pal TEREK¹

¹Univerzitet u Novom Sadu, Fakultet Tehničkih Nauka, Novi Sad, Srbija, zoranbobic@uns.ac.rs

²Institut za Nuklearna Istraživanja, Debrecen, Mađarska

³Institut Jožef Stefan, Ljubljana, Slovenija

Apstrakt: Ortopedski implanti zahtevaju materijale sa adekvatnom oseointegracijom i otpornošću na koroziju. Metalni materijali za ortopedске implantе imaju određena ograničenja u ovim aspektima. Nanošenjem prevlaka primenom tehnologije fizičke depozicije iz parne faze (PVD) istovremeno se može poboljšati otpornost na koroziju i oseointegraciju. Prevlake koje se nanose primenom PVD postupaka nanošenja imaju nesavršenosti u vidu greške rasta u sloju. Ove greške koje intenziviraju efekte korozije na podlozi usled pojave efekta korozije u zazoru i pukotinama. U ovom istraživanju, ispitivan je uticaj grešaka rasta PVD TiN slojeva na koroziju hirurškog čelika EN X2CrNiMo18-14-3. Karakterizacija broja i veličinu grešaka rasta PVD slojeva, sprovedena je primenom taktilne profilometrije na lokacijama gde su izvođeni testovi korozije. Smanjenje gustine grešaka rasta u kombinaciji sa povećanjem prosečne visine grešaka rasta, koje su identifikovane pomoću parametara hrapavosti Sds i Spk, rezultuje smanjenjem impedance. Vrednosti parametra Smr₁ su slične za sve ispitivane lokacije i kretale su se između 12 i 25%. Značajna odstupanja u vrednostima parametra Sz su prouzrokovala različite pragove detekcije određenog vrha u parametru Sds. Shodno tome, svaka lokacija je imala svoj prag za detekciju određenog vrha kao vrha u parametru Sds. Gustina grešaka rasta nije relevantna za predviđanje otpornosti na koroziju, budući da su različite veličine grešaka rasta prouzrokovalе varijacije u intenzitetu promene impedance.

Ključne reči: Korozija, TiN, PVD, EN X2CrNiMo18-14-3, greške rasta

UVOD

Materijali koji se primenjuju za ortopedске implantate moraju imati adekvatne osobine u pogledu poput čvrstoće, tvrdoće, žilavosti, otpornosti na habanje i koroziju. Osim predhodno navedenog, materijal oseoinduktivnih ortopedskih implantata mora omogućiti adekvatnu oseointegraciju. Metalni materijali koji se primenjuju za ortopedске implantate imaju ograničenja u pogledu korozione otpornosti i oseointegracije [1–3].

Ljudsko telo je agresivna korozivna sredina u kojoj se mogu naći različiti anjoni, katjoni, proteini i rastvoreni kiseonik, koji mogu izazvati korozione procese na metalnim materijalima koji se primenjuju za ortopedске implantate [2,4,5].

Primenom različitih prevlaka moguće je postići istovremeno poboljšanje korozivnih osobina i oseointegracije [6]. Jedna od grupe metoda koja se koristi za nanošenje prevlaka na materijale ortopedskih implantata su tehnologije fizičke depozicije iz parne faze.

Slojevi neneti ovim tehnikama nude brojne prednosti u pogledu poboljšanja bioaktivnosti i korozivnih osobina ortopedskih implantata.

Tehnologije fizičke depozicije iz parne faze uzrokuju nastanak rešaka rasta u slojevima prevlaka koji mogu imati negativne efekte na korozionu otpornost materijala implantata. Greške rasta su mesta u prevlaci kod kojih tečni medijum može doći do međupovršine prevlaka-podloga [7]. Usled velike razlike u površini katode i anode u kontaktu sa tečnošću dolazi do intenzivnih korozivnih efekata galvanske korozije i korozije u procepu, nagreškama rasta, na podlozi [8–10]. U literaturi je dokumentovano da povećanje gustine grešaka rasta dovodi do smanjenja korozivne otpornosti [11–13].

U zavisnosti od uzroka nastanka greške i debljine prevlake zavisi vrsta i veličina greške rasta PVD sloja [7,13,14]. U istraživanjima [7,13,14] je pokazano da se na osnovu debljine prevlake geometrijski može proračunati prečnik greške rasta PVD slojeva čiji se uzrok nastanka nalazi na međupovršini prevlaka-podloga.

Iako su razvijeni modeli koji ukazuju da se na osnovu veličine greške rasta može utvrditi da li određena greška rasta ima procep koji omogućava prolaz tečnosti do međupovršine [7,13,14], u brojnim istraživanjima efekat grešaka rasta na korozionu otpornost se posmatra preko gustine svih grešaka rasta [11–13]. Stoga, ovo istraživanje ima za cilj da ispita uticaj veličine i gustine grešaka na promenu korozivnih osobina materijala koji namenjeni za primene na oseinduktivnim ortopedskim implantatima.

EKSPERIMENTALNA ISPITIVANJA

Na polirane uzorke od hirurškog čelika EN X2CrNiMo18-14-3 naneta je TiN prevlaka PVD postupkom naparavanja sa elektronskim snopom.

Korozivni testovi sprovedeni su na površinama 3 uzorka i to na po 2 lokacije. Pre korozivnih testova izvršena su topografska merenja izabranih lokacija primenom taktilnog profilometra Bruker Dektak XT. Profilometrijska

merjenja izvršena su na oblastima veličine $0,5 \times 0,5$ mm sa rezolucijama u brzom i sporom pravcu $0,3 \mu\text{m}$ i $2 \mu\text{m}$.

Karakterizacija korozivnog ponašanja izvršena je primenom metode spektroskopija elektrohemijske impedanse (EIS) u sistemu sa tri elektrode. Grafitna i Ag/AgCl elektrode su korišćene kao referentna i merna (*counting*) elektroda, dok je radna elektroda uzorak. EIS merenja koja su sprovedena na uređaju Autolab, izvršena su u opsegu frekvencije $0,01$ Hz do 1×10^6 Hz. Površina izložena korozivnom medijumu, odnosno, površina radne elektrode je $7,065 \text{ mm}^2$. Merenja su izvršena sat vremena nakon početka izlaganja korozivnom medijumu. Kao korozivni medijum korišćen je Hankov rastvor sa hemiskim sastavom datom u tabeli 1.

Za obradu i analizu topografskih snimaka korišćen je SPIP 6.2.0 softver uz pomoć kojeg su određeni i parametri hrapavosti. Površinski parametri hrapavosti koji su korišćeni u analizama u ovom istraživanju su: visina deset tačaka (S_z), redukovana visina vrhova (S_{pk}), odnos razvijene površina (S_{dr}), gustina vrhova (S_{ds}) i udeo materijala vrhova (S_{mr1}).

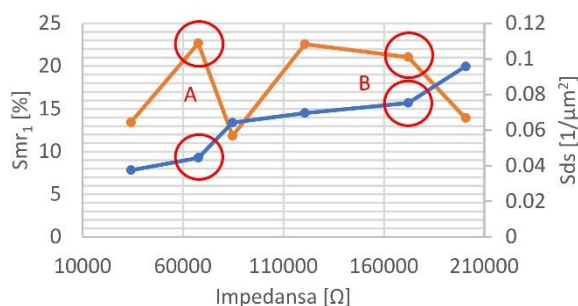
Tabela 1. Sastav Hankovog rastvora

Komponenta	Koncentracija
NaCl	0.14 M
KCl	0.005 M
CaCl ₂	0.001 M
MgSO ₄ ·H ₂ O	0.0004 M
MgCl ₂ ·6H ₂ O	0.0005 M
Na ₂ HPO ₄ ·2H ₂ O	0.0003 M
KH ₂ PO ₄	0.0004 M
D-glukoza	0.006 M
NaHCO ₃	0.004 M

REZULTATI

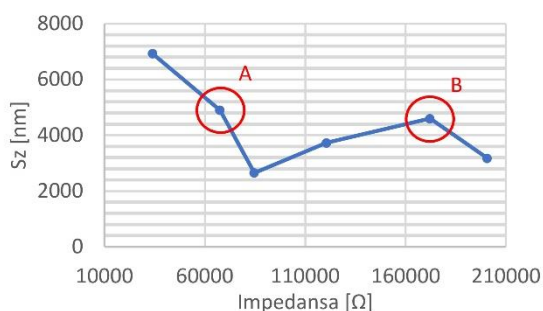
Na dijagramu na slici 1 prikazane su zavisnost promene impedanse (na $0,01$ Hz) i parametara hrapavosti S_{ds} i S_{mr1} . Može se videti da porastom parametra S_{ds} , odnosno porastom gustine nodularnih grešaka dolazi do povećanja otpornosti na koroziju. Vrednost R^2 je $0,91$, odnosno promena S_{dr} parametra dobro opisuje promenu impedanse. Vrednosti

parametara sa Abot-ove krive nosivosti Smr_1 , grupisale su se na oko vrednosti 12 i 25. Ova vrednost predstavlja udeo materijala koji se nalazi u vrhovima neravnina, odnosno nodularnim greškama.

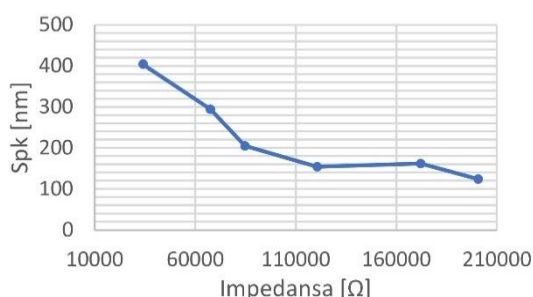


Slika 1. Zavisnost impedanse i parametara Smr_1 i Sds

Na dijagramu na slici 2 prikazana je zavisnost promene impedanse sa prametrom Spk . Sa dijagrama se vidi da postoji izvestan trend. Odnosno smanjenje Spk parametra praćeno je povećanjem impedanse. Vrednost R^2 je oko 0,77.



Slika 2. Zavisnost impedanse i Sz



Slika 3. Zavisnost impedanse i Spk

Na dijagramu na slici 3 prikazana je zavisnost promene impedanse sa prametrom Sz . Sa dijagrama se vidi da impedansa ne zavisi od promene Sz parametara.

DISKUSIJA

Rezultati u ovom istraživanju ukazuju da povećanje gustine grešaka rasta, definisana preko Sds parametra, dovodi do povećanje impedanse. Ovaj rezultat je u suprotnosti sa rezultatima dobijenim u istraživanjima [11–13] gde je ukazano da povećanje gustine grešaka rasta dovodi do smanjenja impedanse.

Smanjenje parametra Spk , za koje se može pripisati da je uzrokovano smanjenju prosečne visine nodularnih grešaka rasta, uzrokovalo je povećanje impedanse.

Ovaj rezultat je u skladu sa predhodnim istraživanjima [7,13,14] gde je pokazana zavisnost prečnika i visine nodularnih grešaka rasta sa time gde je uzrok nastanka ove greške. Odnosno u istraživanjima [7,13,14] je ukazano na vezu između prečnika nodularne greške rasta sa debljinom prevlake. Dok je visina nodularne greške rasta, u slučaju da potiče od međupovršine, jednaka debljini sloja prevlake (u idealizovanom slučaju).

Sds parametar, koji određuje gustinu vrhova, zavisi od parametra Sz . Konkretno, smatra se da određeni region sadrži lokalne vrhove ukoliko visina lokalnih vrhova prelazi 5% vrednosti parametra Sz . Sa slike 3 može se videti da ispitivane lokacije imaju značajne razlike u vrednostima parametra Sz , što posledično uzrokuje drugačiji prag detekcije. To uzrokuje da određeni lokalni vrh na površini bude uvršten u vrhove u okviru parametra Sds .

Na slikama 1 i 3 označena su merenja koje imaju slične vrednosti parametra Sz . Ovi regioni takođe imaju sličnu vrednost parametra Smr_1 , što ukazuje na količinu materijala prisutog u vrhovima. Ovo implicira da su u oba slučaja slični prag detekcije i količina materijala u vrhovima.

Uzimajući predhodno u obzir, možemo zaključiti da u slučaju B, gde je ustanovljen znatno veći broj grešaka rasta, da su greške značajno manje veličine nego u slučaju A. Odnosno slučaj A koji ima manji broj grešaka rasta, koje su većih dimenzija, izazvao je veće smanjenje impedanse nego slučaj B kad su greške rasta manjih dimenzija a veće količine.

Promena impedanse, odnosno promena korozijske otpornosti ne može biti objašnjena samo promenom gustine grešaka rasta PVD sloja. Takođe, da bi odredili greške koje zaista utiču na korozijsku otpornost moraju se razmatrati i veličina grešaka rasta PVD slojeva.

Parametar hrapavosti Sds omogućava dobijanje informacija o gustini vrhova. Međutim, prag detekcije za parametra Sds zavisi od Sz parametra čije vrednosti mogu značajno varirati u zavisnosti od lokacije. Posledično, na različitim lokacijama detektovati će se lokalni vrhovi, odnosno greške rasta, sa drugačijim minimalnim visinama. Shodno tome, posmatranje uticaja gustine grešaka rasta na promenu impedanse nije moguće adekvatno izvršiti primenom Sds zbog različitih kriterijuma za detektovanje grešaka rasta.

ZAKLJUČAK

Rezultati dobijeni u ovom istraživanju dovode nas do sledećih zaključaka:

- Gustina grešaka rasta, karakterisana parametrom Sds, nije adekvatna za precizno predviđanje korozijske otpornosti.
- Nemaju sve greške rasta isti uticaj na vrednosti impedanse u karakterizaciji korozijske EIS merenjima. Odnosno, sama gustina grešaka rasta nije relevantna sa stanovišta predviđanja impedanse.
- Da bi greške rasta uticale na korozijsku otpornost one moraju preći neku visinu i dimenziju u prečniku.

ZAHVALNOST

Istraživanje prikazano u ovom radu je finansirano iz bilateralnog projekta Srbija-Mađarska (2021-2023) ugovor br. 1. Zahvaljujemo se kompanijama Narcissus d.o.o., Ada i Termometal d.o.o., Ada na njihovoj podršci u vidu pripreme uzoraka za ovo istraživanje.

LITERATURA

- [1] Ali, S.; Abdul Rani, A.M.; Baig, Z.; Ahmed, S.W.; Hussain, G.; Subramaniam, K.; Hastuty, S.; Rao, T.V.V.L.N. Biocompatibility and Corrosion Resistance of Metallic Biomaterials. *Corros. Rev.* **2020**, *38*, 381–402, doi:10.1515/corrrev-2020-0001.
- [2] Manivasagam, G.; Dhinasekaran, D.; Rajamanickam, A. Biomedical Implants: Corrosion and Its Prevention - A Review. *Recent Patents Corros. Sci.* **2010**, *2*, 40–54, doi:10.2174/1877610801002010040.
- [3] Thanka Rajan, S.; Subramanian, B.; Arockiarajan, A. A Comprehensive Review on Biocompatible Thin Films for Biomedical Application. *Ceram. Int.* **2022**, *48*, 4377–4400, doi:10.1016/j.ceramint.2021.10.243.
- [4] Li, Y.; Shi, C.; Guan, L.; You, Y.; Tang, W. Correlation between Protein Adsorption and Electrochemical Corrosion Behavior of Niobium for Bio-Implant Application. *J. Solid State Electrochem.* **2020**, *24*, 1325–1336, doi:10.1007/s10008-020-04634-x.
- [5] Talha, M.; Ma, Y.; Kumar, P.; Lin, Y.; Singh, A. Role of Protein Adsorption in the Bio Corrosion of Metallic Implants – A Review. *Colloids Surfaces B Biointerfaces* **2019**, *176*, 494–506, doi:10.1016/j.colsurfb.2019.01.038.
- [6] Sheng, X.; Wang, A.; Wang, Z.; Liu, H.; Wang, J.; Li, C. Advanced Surface Modification for 3D-Printed Titanium Alloy Implant Interface Functionalization. *Front. Bioeng. Biotechnol.* **2022**, *10*, doi:10.3389/fbioe.2022.850110.
- [7] Merl, D.K.; Panjan, P.; Panjan, M.; Čekada, M. The Role of Surface Defects Density on Corrosion Resistance of PVD Hard Coatings. *Plasma Process. Polym.* **2007**, *4*, 613–617, doi:10.1002/ppap.200731416.
- [8] Pierre R. Roberge, Ph.D., P.E. *Corrosion Engineering Principles and Practice*; 2008; Vol. 1; ISBN 0071640878.
- [9] Schweitzer, P.A.; Systems, C.P.; Schweitzer, P.A. *Corrosion Mechanisms*

- in Theory and Practice*; 1996; Vol. 34; ISBN 9781420094626.
- [10] Makhlof, A.S.H.; Botello, M.A. *Failure of the Metallic Structures Due to Microbiologically Induced Corrosion and the Techniques for Protection*; Elsevier Ltd, 2018; ISBN 9780081019283.
- [11] Panjan, P.; Drnovšek, A.; Gselman, P.; Čekada, M.; Panjan, M.; Bončina, T.; Merl, D.K. Influence of Growth Defects on the Corrosion Resistance of Sputter-Deposited TiAlN Hard Coatings. *Coatings* **2019**, *9*, 1–16, doi:10.3390/coatings9080511.
- [12] Panjan, P.; Čekada, M.; Panjan, M.; Kek-Merl, D.; Zupanič, F.; Čurković, L.; Paskvale, S. Surface Density of Growth Defects in Different PVD Hard Coatings Prepared by Sputtering. *Vacuum* **2012**, *86*, 794–798, doi:10.1016/j.vacuum.2011.07.013.
- [13] Balzer, M. Identification of the Growth Defects Responsible for Pitting Corrosion on Sputter-Coated Steel Samples by Large Area High Resolution Mapping. *Thin Solid Films* **2015**, *581*, 99–106, doi:10.1016/j.tsf.2014.12.014.
- [14] Penttinen, I.M.; Korhonen, A.S.; Harju, E.; Turkia, M.A.; Forsén, O.; Ristolainen, E.O. Comparison of the Corrosion Resistance of TiN and (Ti,Al)N Coatings. *Surf. Coatings Technol.* **1992**, *50*, 161–168, doi:10.1016/0257-8972(92)90057-H.

INFLUENCE OF PVD COATING DEFECTS ON CORROSION RESISTANCE OF TiN COATED EN X2CrNiMo18-14-3 SURGICAL STEEL

Abstract: *Orthopedic implants require materials with adequate osseointegration and corrosion resistance. The metallic material for orthopedic implants exhibits limitations in these aspects. Deposition of coatings using physical vapor deposition (PVD) can simultaneously enhance corrosion resistance and osseointegration. Coatings applied by PVD processes exhibit imperfections, the growth defects, which can intensify corrosion effects on the substrate, due to crevice and gap corrosion phenomena. In this study, the influence of growth defects in PVD TiN layers on the corrosion protection of EN X2CrNiMo18-14-3 was investigated. To characterize the number and size of growth defects in PVD layers, tactile profilometry is conducted in areas where corrosion tests were performed. A decrease in the density of growth defects coupled with an increase in the average defect height, characterised by roughness parameters S_d and S_{pk} , results in a decrease in impedance. The S_{mr1} parameter values are similar for all locations, ranging between 12 and 25%. A significant deviation in the S_z parameter caused a different detection threshold for a particular peak in the S_d parameter. Consequently, each area has its own detection threshold for a specific peak. Since different defect sizes caused varying intensity changes in impedance the density of growth defects is not relevant for predicting corrosion resistance.*

Keywords: *Corrosion, TiN, PVD, EN X2CrNiMo18-14-3, growth defects*



Society of Production
Engineering

SPMS 2023

39. Savetovanje proizvodnog mašinstva Srbije

ICPES 2023

39th International Conference on Production Engineering of
Serbia



Faculty of Technical
Sciences
University of Novi Sad

Novi Sad, Serbia, 26. – 27. October 2023

THE INFLUENCE OF STRAIN ON FREE SURFACE ROUGHNESS AT UNIAXIAL UPSETTING

Vladimir GAŠIĆ¹, Nemanja DAČEVIĆ^{1, *}, Pal TEREK¹, Zoran BOBIĆ¹, Marko VILOTIĆ¹

¹Faculty of Technical Sciences, Novi Sad, Serbia

*Corresponding author: dacevic@uns.ac.rs

Abstract: While the upsetting process is also used for near-net shape manufacturing, it primarily serves as a preparatory or intermediate step within other forming technologies. In both scenarios, understanding how processing parameters impact the quality and precision of the resulting part is of utmost importance. This paper aims to investigate the effect of strain magnitude on the surface roughness of cylindrical specimens during uniaxial compression. To ensure a uniaxial stress state, Rastegaev's samples were used. The paper presents and discusses four roughness parameters: R_a , R_{z10} , R_{ku} , and R_{sk} . An analysis of these parameters leads to the conclusion that an increase in deformation leads to an increase in the roughness of the specimen's free surface.

Keywords: Surface roughness, Uniaxial upsetting, Rastegaev's specimen, C15E

1. INTRODUCTION

The advancement of manufacturing processes has always been closely associated with the pursuit of enhanced material properties and product quality. In this context, metal forming techniques have played a pivotal role in shaping the evolution of engineering materials and components. One such method that stands at the crossroads of traditional manufacturing and modern materials science is upsetting. In the realm of metal forming, the versatility and adaptability of upsetting processes make them a compelling choice as a preparatory step for various downstream technologies such as forging or extrusion. Upsetting, with its inherent ability to create significant plastic deformation, serves as a

foundational stage for shaping raw materials into forms that are more amenable to subsequent processes. By employing upsetting as an initial step, manufacturers can efficiently reduce the cross-sectional area of workpieces and alter their geometrical and material characteristics. This not only simplifies the material flow in subsequent forming operations but also allows for better control over the resulting mechanical properties. The uniformity and consistency achieved through upsetting lay a robust foundation for downstream processes like forging, which require precise control over the starting material's dimensions and microstructure. Similarly, when used as a preparatory stage for extrusion, upsetting can help control material flow and reduce the risk of defects, ensuring the seamless transition

from one forming technology to another. The ability to tailor material properties and geometries through upsetting provides manufacturers with a valuable tool to enhance the efficiency and quality of their metal forming processes, making it an indispensable component of modern manufacturing strategies. Its significance further extends to the realm of cost-efficiency. By substituting machining for the manufacturing of specimens with specific dimensions, upsetting offers a more resource-efficient approach, minimizing waste and optimizing material utilization [1,2].

Given that the upsetting process is mostly used as a preparatory or intermediate stage in metal forming, the characteristics of the part after upsetting directly affect the subsequent stages of forming and, consequently, the quality and accuracy of the finished part. A profound understanding of how variations in forming parameters manifest in the final product quality is essential for optimizing manufacturing processes, reducing defects, and enhancing the mechanical properties of components. Forming parameters, which encompass a spectrum of variables such as strain, temperature, and strain rate, exert a substantial influence on the surface characteristics of the workpiece. These parameters govern the intricate interplay between material flow and deformation during the upsetting process, making them pivotal determinants of free surface roughness. Aim of this paper is to determine the effect of imposed strain on the free surface roughness during uniaxial upsetting of cylindrical specimens.

2. EXPERIMENTAL WORK

The stress state in the sample during upsetting with flat dies depends to the greatest extent on the friction that occurs on the contact surfaces. The magnitude of the friction is mostly influenced by the roughness of the surface and the chosen lubricant [3,4]. In order to reduce friction to a minimum and ensure a uniaxial stress state, Rastegaev's specimen was chosen for this research [5]. Rastegaev's specimen is primarily used to determine the

flow curve in the range of large deformations ($\phi > 1$). These specimens are cylindrical in shape and are characterized by the existence of a groove for placing the lubricant on the base surface of the specimen (Figure 1). For lubrication stearic acid was used. The specimens are made of low carbon steel C15E widely used for construction and mechanical engineering parts with low core strength, such as levers, joints, bushings, bolts, pins, pivots, gears, etc. The final processing of the cylindrical sample is fine machining.

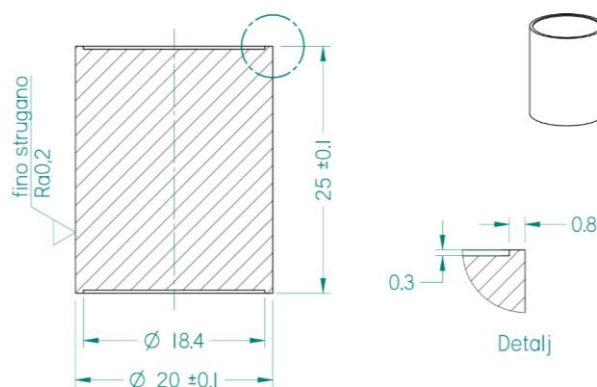


Figure 1. Rastegaev's specimen

Four Rastegaev's specimens, marked S1, S2, S3 and S4, were provided for research purposes. In the first phase of the experimental research, the roughness of the cylindrical surface of each of the samples was measured in three positions. Before the actual measurement, they were cleaned in an ultrasonic bath "ASonic", while a 95-96% ethanol solution from the manufacturer "Zorka" was used as a cleaning agent. To measure the surface roughness a 2D tactile profilometer "HOMMEL TESTER 2000" was used, which is located at the Faculty of Technical Sciences - Center for Surface Engineering and Nanotechnology. The measurement length was 4.8 mm, the measurement resolution was 10nm, while the measurement speed was 0.5mm/s. A measuring probe TK100 with a radius of 5 μ m was used for the measurement.

In order to examine the influence of the degree of deformation, each of the specimens was compressed for a different value of the tool stroke. The tool stroke was determined based on the targeted effective strain values.

Specifically, specimens S1, S2, S3, and S4 were subjected to the upsetting process until effective strain values of 0.25, 0.5, 0.85, and 1 were achieved, respectively (Figure 2.). The upsetting process was carried out on a "Sack & Kieselbach" hydraulic press for cold forming with a nominal force of 6.3 MN. Flat dies used for upsetting were polished before the experiment. The experiment was conducted in the Metal Forming Laboratory at the Faculty of Technical Sciences.

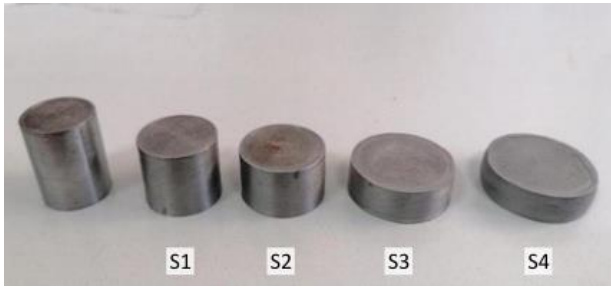


Figure 2. Specimens before and after forming

After upsetting the specimens were cleaned and roughness was measured according to the previously described procedure.

3. RESULTS AND DISCUSSION

The following roughness parameters were obtained using the previously described experimental procedure:

1. R_a – Average roughness:

$$R_a = \frac{1}{L} \int_0^L |z(x)| dx \quad (1)$$

where L is measurement length.

Table 1. Rougness parameters:

Roughness parameters		S1		S2		S3		S4	
		$\phi_{ef} = 0$	$\phi_{ef} = 0.25$	$\phi_{ef} = 0$	$\phi_{ef} = 0.5$	$\phi_{ef} = 0$	$\phi_{ef} = 0.85$	$\phi_{ef} = 0$	$\phi_{ef} = 1$
R_a [nm]	1.	947.4	2762.7	1082.8	3515.4	963.3	4963.9	831.4	4707.5
	2.	807.6	2458.2	1139.1	3473.5	1280.9	4837.7	527.0	5232.6
	3.	1462.0	2514.1	1188.2	3836.8	951.6	4402.2	615.7	4465.6
R_{sk}	1.	-0.53958	-0.73829	-0.8799	-0.47993	-1.1478	-0.26548	-2.1634	-0.67038
	2.	-1.4522	-0.85033	-0.95902	-0.27710	-2.2319	-0.21599	-2.0631	-0.51517
	3.	-0.93991	-0.55809	-1.2323	-0.12765	-1.7486	0.22015	-1.598	-0.40924
R_z [nm]	1.	6261.3	17710	8042.8	24909	6304.3	33668	7543.1	36835
	2.	7334.0	20143	6794.1	30310	12356.0	43966	5803.9	40868
	3.	10646.0	19480	9391.8	29410	8873.3	32831	5622.9	34814
R_{ku}	1.	2.9465	3.1145	4.0537	3.1007	3.967	2.7961	9.0358	3.9045
	2.	6.4653	4.1425	3.5902	3.3861	9.0654	3.6027	9.601	3.4870
	3.	4.5116	3.5159	5.1515	2.7180	7.0427	2.8476	6.4762	3.5095

2. R_z - the mean value of the difference of the five highest and five lowest points of the profile:

$$R_{z10} = \frac{P_1 + P_2 + \dots + P_5 - V_1 - V_2 - \dots - V_5}{5} \quad (2)$$

where P_1, P_2, P_3, P_4, P_5 are five highest points and V_1, V_2, V_3, V_4, V_5 are the five lowest points on the surface.

3. R_{sk} – Surface skewness:

$$R_{sk} = \frac{1}{R_q^3} \sum_{n=1}^N \frac{1}{N} |Z_n - \bar{z}|^3 \quad (3)$$

4. R_{ku} – Kurtosis:

$$R_{ku} = \frac{1}{R_q^4} \sum_{n=1}^N \frac{1}{N} |Z_n - \bar{z}|^4 \quad (4)$$

where R_q is mean squared deviation, N is number of measured points, Z_n is the height of the n th point and \bar{z} is mean height of measured points.

In table 1. values of specified roughness parameters for each specimen, before and after the upsetting process, are presented.

The comparison of the average values of the measured roughness parameters before and after the upsetting process is shown graphically in figures 3-6. Comparison is done for all four specimens.

By comparing the values of the roughness parameter R_a before and after the forming process (Figure 3.), a notable increase in roughness becomes evident as the degree of

deformation increases. The surface quality after forming can be described as medium to rough and is akin to the surface quality achieved after cold forging.

The results of measuring the parameter R_z (Figure 4.) confirms the previous observation and indicate an increase in the difference between the peaks and valleys on the surface as the degree of deformation increases.

The negative value of the R_{sk} parameter before and after the upsetting process (Figure 5.) indicates a negative polarity of the surface, which means that valleys prevail over peaks. Compared to the state of the surface before forming, after the upsetting this difference is significantly reduced.

In the case of the parameter R_{ku} (Figure 6.), its value is observed to converge toward the value of 3 during forming process, signifying that the surface is becoming more uniform and the normal distribution of heights narrower.

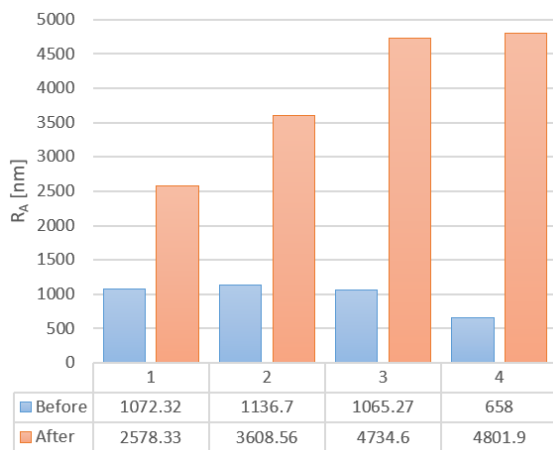


Figure 3. Comparison of average value of R_A before and after upsetting

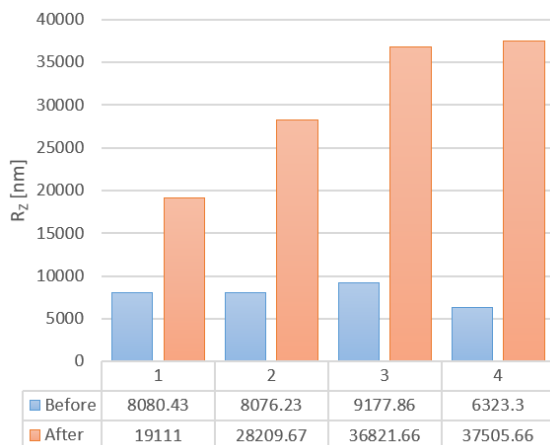


Figure 4. Comparison of average value of R_z before and after upsetting

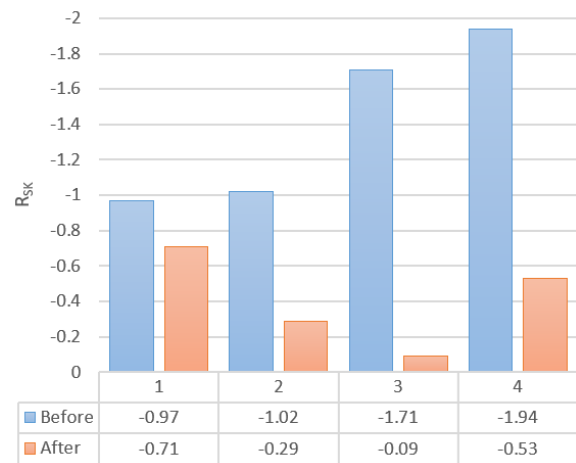


Figure 5. Comparison of average value of R_{sk} before and after upsetting

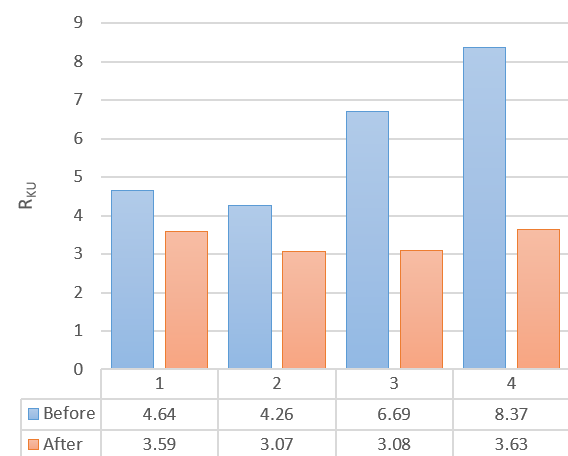


Figure 6. Comparison of average value of R_{ku} before and after upsetting

4. CONCLUSION

Following conclusions can be drawn:

1. Based on the shape of the specimens we can conclude that uniaxial stress state was present;
2. Roughness parameters R_A and R_z confirm that with the increase in deformation, the roughness of the free surface also increases, which is in accordance with the research of other authors [6,7,8].
3. Although the surface retained negative polarity after upsetting, the forming process influenced the closing of deep valleys.
4. After forming, value of parameter R_{ku} is close to 3 indicating more uniform surface compared to the initial state.

REFERENCES

- [1] SCHULER GmbH: Metal forming handbook, Springer Verlag, Berlin, 1998.
- [2] E. Doege: Handbuch Umformtechnik, Springer-Verlag, Berlin, 2010.
- [3] M. Plančak: Технологија пластичног деформисања, ФТН, Нови Сад, 2012.
- [4] B. Devedžić: Plastičnost I obrada metala deformisanjem, Naučna Knjiga, Beograd, 1992.
- [5] W. Reiss, K. Pöhlandt: The Rastegaev Upset Test-A Method To Compress Large Material Volumes Homogeneously, Experimental Techniques, 10, 20-24, 1986.
- [6] T. Furushima, H. Tsunozaki, K.I. Manabe, and S. Alexandrov: Ductile fracture and free surface roughening behaviors of pure copper foils for micro/meso-scale forming. International Journal of Machine Tools and Manufacture, 2014.
- [7] T. Furushima, Z. Jiang, D. Wei, K. Manabe, X. Zhao, D. Wu, L. Liang: Effects of surface roughness on micro deep drawing of circular cups with consideration of size effects, Finite Elements in Analysis and Design, 2016.
- [8] K. Osakada, and M. Oyane: On the roughening of free surface in deformation processes', Bulletin of JSME, 14(68), 171–177, 1971.

SPMS/ICPES 2023

**39TH INTERNATIONAL CONFERENCE ON
PRODUCTION ENGINEERING OF SERBIA**

**SESSION 3:
MATERIAL REMOVAL TECHNOLOGIES**

Novi Sad, 26 – 27 October 2023



Society of Production
Engineering

SPMS 2023

39. Savetovanje proizvodnog mašinstva Srbije

ICPES 2023

39th International Conference on Production Engineering of
Serbia



Faculty of Technical
Sciences
University of Novi Sad

Novi Sad, Serbia, 26. – 27. October 2023

MATERIAL REMOVAL RATE DURING ELECTRICAL DISCHARGE MACHINING OF ZIRCONIUM OXIDE

Dragan RODIĆ^{1, *}, Marin GOSTIMIROVIĆ¹, Milenko SEKULIĆ¹, Borislav SAVKOVIĆ¹,
Andjelko ALEKSIĆ¹

¹University of Novi Sad, Faculty of Technical Sciences, Department for Production Engineering, Trg
D. Obradovica 6, 21000 Novi Sad, Serbia

*Corresponding author: rodicdr@uns.ac.rs

Abstract: *The use of non-conductive ceramic materials is increasingly used in industrial and engineering applications due to their remarkable properties. Machining components made of these materials poses a great challenge, mainly due to their pronounced brittleness. Therefore, conventional machining methods often prove unsuitable for these materials. To solve this problem, the electrical discharge machining with assisting electrode is effectively used. In order for the processing of non-conductive material to be possible, the vital factor for the uninterrupted functioning of EDM is the presence of a pyrolytic carbon layer. This layer plays a crucial role in the process. The establishment and durability of the pyrolytic carbon layer depend on several factors, primarily the discharge current and pulse duration. Experiments were conducted to investigate how variations in these factors affect the material removal rate and to clear up the underlying material removal mechanisms.*

Keywords: EDM, discharge current, pulse duration, duty factor, assisting electrode.

1. INTRODUCTION

Electrical discharge machining (EDM) is an unconventional but widely used material removal process. It can effectively machine all electrically conductive materials regardless of their physical and metallurgical properties. EDM is widely used for machining challenging materials and shaping complex geometric components that are often impossible to produce using conventional methods. A basic requirement for the successful implementation of the EDM process is that the workpiece has a minimum level of electrical conductivity [1].

Despite their remarkable properties compared to metallic materials, ceramic

materials are becoming increasingly popular in the metalworking industry [2]. One of the obstacles standing in the way of widespread acceptance is the limitations imposed by the sintering process, which makes it difficult to produce complicated geometries and limits the options for machining the final product [3]. Machining of ceramic materials has gained importance in various industrial applications due to their exceptional strength, heat, corrosion and wear resistance. Various machining techniques such as diamond grinding, ultrasonic machining, laser cutting, abrasive waterjet cutting, ion beam machining and others can be used for machining ceramic materials [4]. However, these methods have

certain limitations in terms of productivity, quality, and cost efficiency, and may not fully meet the requirements of modern manufacturing. Therefore, it is imperative to explore alternative approaches for machining ceramic materials [5].

By placing an electrically conductive layer (Assisting Electrode - AE) on the top surface of the workpiece, it is possible to process electrically non-conductive ceramic materials called Assisting Electrode Electrical Discharge Machining – AEEDM [6]. The fundamentals of Electric Discharge Machining with an assisting electrode were established in the early 1990s. The first appearance of Assisting Electrode Electrical Discharge Machining (AEEDM) technology in academic circles was recorded in 1995 by Japanese scientists Fukuzawa, Tani, Iwane, and Mohri [7]. This paper describes a new method that enables the electroerosion machining of electrically conductive ceramic materials using an adhesive metal plate (assisting electrode) attached to the workpiece and a tool made of soft metal material. They concluded that AEEDM machining is achieved due to the modification of the ceramic surface, specifically the continuous formation of an electrically conductive layer.

The assisting electrode plays a critical role by facilitating the initial electrical discharge between the tool and the workpiece. Once the auxiliary electrode layer is eliminated due to the high temperatures in the discharge zone, the process of dielectric dissolution takes place. During this phase, carbon particles are deposited on the surface, creating an electrically conductive layer often referred to as a carbon layer. Throughout the AEEDM this electrically conductive carbon layer continuously forms on the workpiece and plays a critical role in maintaining process stability. The process of formation of this electrically conductive layer is also explained by Tany et al [8], who highlight the necessity of using a carbon-based dielectric oil for stable erosion of non-conductive ceramics. Similar phenomena have been observed and documented by Mohri et al [9] and Hanaoka et al [10] who emphasize the importance of a carbon-based dielectric oil

for stable machining of nonconductive ceramic materials.

The impact of the material referred to as AE on the technological characteristics of AEEDM was thoroughly examined by Hanaoka et al. [11]. Their research involved a comparative analysis of various supported electrode designs. Initially, they utilized a metal plate as the electrode and subsequently experimented with a multi-layered metal grid. The results revealed that the use of a copper grid significantly reduced surface roughness. In another study conducted by the same authors [8], they processed zirconium oxide using both copper and graphite tools. Interestingly, it was observed that when copper tools were employed, the formation of the carbon layer was incomplete, resulting in a rougher surface finish. Moving forward, in the subsequent work [12] researchers investigated the influence of the thermal conductivity of alumina with a purity level of 99.99% on machining productivity. Their findings indicated that higher thermal conductivity values in the material led to increased machining efficiency. In a separate study [13], die-sinking EDM was performed on alumina with high discharge energy. This involved using elevated discharge voltage and very high capacitance per unit area, resulting in an exceptionally high discharge energy and explosive force. The researchers concluded that the polarity of the tool was the most significant factor affecting crater volume, depth, and relative tool wear. Furthermore, reference [14] identified that the formation and stability of the carbon layer, aside from being influenced by the workpiece and tool materials, the dielectric type, and the tool polarity, were also dependent on the discharge energy. Discharge energy, in this context, is defined as the product of voltage, discharge current, and pulse duration.

However, it is important to acknowledge that the current application of AEEDM has limitations, mainly related to the relatively low material removal rate. This drawback has hindered its wide application in various industries and manufacturing processes. In view of this, this research focuses on the study

of electrically non-conductive ceramics, with particular emphasis on zirconia, also known as ZrO_2 . In this research is used a hybrid assisting electrode consisting of a self-adhesive copper metal foil and a graphite layer. The main objective of this study is to analyze the material removal rate in the context of AEEDM, especially to investigate its dependence on pulse duration. The inclusion of zirconia as a ceramic material in conjunction with the innovative hybrid auxiliary electrode highlights the contribution of this research. By investigating the material removal rate at different pulse durations, this study should provide valuable insights for optimizing and improving future research of AEEDM processes.

2. MATERIAL AND METHODS

A series of experiments was carried out on a die-sinking EDM machine Agie Charmilles of the SP1-U type. The isotropic graphite with a cross-section of $10 \times 10 \text{ mm}^2$ was used as an electrode for machining insulating zirconium oxide ZrO_2 . The reason for using graphite tools is that the formation of the electrically conductive layer is more stable than other types of tools, such as copper.

In this study, the workpiece material was a nonconductive ceramic. Therefore, for the application of EDM to process insulating ceramic material, a basic technique was developed in which a graphite layer (Graphite 33 lacquer) and an adhesive layer of copper foil (3M grade 1181) were applied to the workpiece surface. Adhesive aluminum and copper metal foils and graphite coatings are most commonly used. The combination of metal foil and graphite coating is called hybrid auxiliary electrode. Table 1 shows the processing conditions for zirconium oxide. In these experimental setups, the discharge current was kept constant at 1.5 A along with other relevant parameters, while the pulse duration was deliberately adjusted to observe its effects on the machining process. This systematic variation of the pulse duration allows a detailed study of its influence on the machining results and helps to establish a clear correlation

between pulse duration and material removal rates in the context of zirconia.

The machining performance characteristics selected for this study is material removal rate (MRR). The workpiece's erosion depth is measured directly from the machine's display, with a precision of $1 \text{ } [\mu\text{m}]$, and then manually confirmed using a comparator.

Table 1. Machining conditions

Parameters	Experiments		
	Test 1	Test 2	Test 3
Discharge current [A]	1.5	1.5	1.5
Pulse on time [μs]	42	75	100
Open circuit voltage [V]	300	300	300
High tension current[A]	0.5	0.5	0.5
Polarity	(-)	(-)	(-)
Duty factor [%]	50	50	50

The material removal rate is quantified in cubic millimeters per minute (mm^3/min) and serves as an indicator of the EDM process efficiency, as defined in equation 1. Where, CSE - cross section electrode", DOC - depth of cut and TM – time of machining.

$$MRR = \frac{CSE(mm^2) \times DOC(mm)}{TM(min)} \left[\frac{mm^3}{min} \right] \quad [1]$$

3. RESULTS AND DISCUSSION

During electrical discharge machining (EDM) of ZrO_2 ceramic workpieces, a pyrolytic carbon layer is formed on the machined surface. This layer is formed by using carbon oil as a dielectric fluid and by using adhesive copper foil together with coated graphite as the first auxiliary electrode. The primary material removal mechanism in EDM of non-conductive ceramic materials such as ZrO_2 is spalling. Nevertheless, a small portion of the ceramic material can also be removed by melting and evaporation. This phenomenon is due to the high melting point of zirconium and its remarkable electrical resistivity.

In the field of assisted electrode electrical discharge machining (AEEDM) for ZrO_2 , it proved difficult to initiate electrical discharges within the machining gap between the tool

electrode and the ceramic workpiece when operating at an open voltage of 100 V. This problem resulted from the insufficient discharge energy available during the process, which hindered the formation of an efficient carbon layer. However, by introducing an auxiliary current of 0.5 A and increasing the voltage to 300 V, it was possible to process insulating ceramics with the SPU-1 machine.

Based on the research [15], the main input parameters are discharge current and pulse duration where they are also commonly considered the most important parameter in EDM of insulating ceramics. According to the previous studies in the field of AEEDM, discharge currents up to 6 A have been used for tool cross sections up to 1 cm². To determine the pulse duration at which the EDM process is stable under the set machining conditions, a test experiment was conducted at a constant discharge current of 1.5 A. The pulse on time was 42 μs and 100 μs, and the duty cycle τ was constant 50%.

For pulse durations below 42 μs, there was no formation of a carbon layer on the ceramic surface, making the AEEDM process for ZrO₂ entirely unfeasible. It was observed that at pulse durations exceeding 100 μs, the surface roughness significantly deteriorates, and the process becomes unstable (leading to unwanted interruptions in the process).

Figure 1 illustrates that increasing the pulse duration at constant discharge current leads to improved productivity. This is mainly due to the significant influence that these parameters exert on the energy input.

The input energy generated during this process results in increased temperatures, which subsequently cause local melting of the material, vaporisation, and decomposition of the workpiece material, often referred to as 'spalling'.

It is known that the discharge current and the pulse duration are equally involved in the discharge energy. In this case, since the discharge current is a constant value, the change in pulse duration is observed. In other words, as the pulse duration increases, the discharge energy also increases. A minimum

input power is essential for the formation of a pyrolytic carbon layer on the ceramic surface. Initial experiments have shown that when lower input powers were used (e.g., a pulse duration of 40 μs), the EDM process on ZrO₂ could not be sustained.

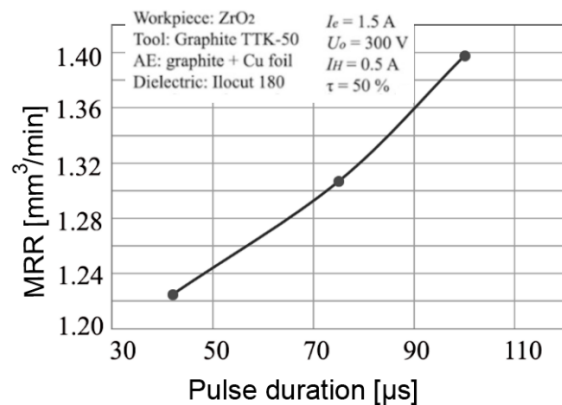


Figure 1. Influence pulse duration on material removal rate

Only at a minimum input power could the machining process begin, resulting in the formation of a thin layer of pyrolytic carbon characterized by a remarkably low material removal rate (MRR). Stable machining conditions were achieved in the range of 40 to 100 μs pulse duration, resulting in greater material removal. It is evident that MRR increases with increasing pulse duration. Nevertheless, it is imperative to perform further experiments to confirm this observed trend.

4. CONCLUSION

This article investigates the effect of pulse duration on material removal rate (MRR) during electrical discharge machining of nonconductive ceramics. A hybrid assisting electrode made by applying a graphite coating and attaching a copper strip to the workpiece enables successful machining of zirconia. Pulse duration significantly affects MRR, with performance decreasing with increasing duration. In summary, this research enhances our understanding of AEEDM, a relatively new

machining process with potential for continued improvement and refinement.

ACKNOWLEDGEMENT

This paper has been supported by the Provincial Secretariat for Higher Education and Scientific Research through the project no. 142-451-3175/2023-01/01: "Research of the innovative electrical discharge machining process of non-conductive materials"

REFERENCES

- [1] J. H. Zhang, T. C. Lee, W. C. Lau: Study on the electro-discharge machining of a hot pressed aluminum oxide based ceramic, *Journal of Materials Processing Technology*, Vol. 63, No., pp. 908-912, 1997.
- [2] C. S. Treuman, J. Huddleston: Material removal by spalling during EDM of ceramics, *Journal of the European ceramic society*, Vol. 20, No. 10, pp. 1629-1635, 2000.
- [3] B. Lauwers, J. Vleugels, O. Malek, K. Brans, K. Liu: Electrical discharge machining of composites, *Machining technology for composite materials*, No., pp. 202-241, 2012.
- [4] M. Sekulic, *Inovacione tehnologije obrade*, Skripta. 2013, Novi Sad: Fakultet tehničkih nauka.
- [5] K. H. Ho, S. T. Newman: State of the art electrical discharge machining (EDM), *International Journal of Machine Tools and Manufacture*, Vol. 43, No. 13, pp. 1287-1300, 2003.
- [6] A. M. Gadalla, B. Bozkurt, N. M. Faulk: Modeling of Thermal Spalling During Electrical Discharge Machining of Titanium Diboride, *Journal of the American Ceramic Society*, Vol. 74, No. 4, pp. 801-806, 1991.
- [7] Y. Fukuzawa, T. Tani, E. Iwane, N. Mohri: A New Machining Method for Insulating Ceramics with an Electrical Discharge Phenomenon, *Journal of the Ceramic Society of Japan*, Vol. 103, No. 10, pp. 1000-1008, 1995.
- [8] T. Tani, Y. Fukuzawa, T. Kawase, K. Futurani, N. Mohri, N. Saito: Machining Characteristics of ZrO₂ Ceramics by Electrical Discharge Machining, *Journal of The Japan Society of Electrical Machining Engineers*, Vol. 32, No. 71, pp. 18-26, 1998.
- [9] N. ohri, Y. Fukuzawa, T. Tani, N. Saito, K. Furutani: Assisting Electrode Method for Machining Insulating Ceramics, *CIRP Annals - Manufacturing Technology*, Vol. 45, No. 1, pp. 201-204, 1996.
- [10] D. Hanaoka, Y. Fukuzawa, K. Kaneko, T. Harada: Discharge Machining of Insulating Si₃N₄ Ceramics with added Al₂O₃, *The 16th International Symposium on Electromachining*, No., 2014.
- [11] T. Tani, Y. Fukuzawa, N. Mohri, N. Saito: Effects of Assisting Electrode Material on the EDM Characteristics for Insulating Sialon Ceramics, *Journal of the JAPAN society of electrical machining engineers*, Vol. 30, No. 65, pp. 17-23, 1996.
- [12] Y. Fukuzawa, N. Mohri, T. Tani, A. Muttamara: Electrical discharge machining properties of noble crystals, *Journal of Materials Processing Technology*, Vol. 149, No. 1-3, pp. 393-397, 2004.
- [13] J. Renije, L. Yonghong, Z. Yanzehn, F. Wang, C. Baoping, F. Xingsheng: Single discharge machining insulating Al₂O₃ ceramic with high instantaneous pulse energy in kerosene, *Materials and Manufacturing Processes*, Vol. 27, No. 12, pp. 676-682, 2012.
- [14] A. Sabur, M. Y. Ali, A. Malaque, A. A. Khan: Investigation of material removal characteristics in EDM of nonconductive ZrO₂ ceramic, *Procedia Engineering*, Vol. 56, No., pp. 696-701, 2013.
- [15] Y. Fukuzawa, N. Mohri, H. Gotoh, T. Tani: Three-dimensional machining of insulating ceramics materials with electrical discharge machining, *Transactions of Nonferrous Metals Society of China* Vol. 19, No., pp. 150-156, 2009.



Society of Production
Engineering

SPMS 2023

39. Savetovanje proizvodnog mašinstva Srbije

ICPES 2023

39th International Conference on Production Engineering of
Serbia



Faculty of Technical
Sciences
University of Novi Sad

Novi Sad, Serbia, 26. – 27. October 2023

MODELLING AND ANALYSIS OF CHIP COMPRESSION RATIO IN TURNING OF POM-C

Milan TRIFUNOVIĆ^{1, *}, Miloš MADIĆ¹, Predrag JANKOVIĆ¹

¹University of Niš, Faculty of Mechanical Engineering in Niš, Niš, Serbia

*Corresponding author: milan.trifunovic@masfak.ni.ac.rs

Abstract: Turning process is affected by synergistic effects of a number of parameters which ultimately define machining mechanisms and resulting process performances. Chip morphology is essential for machining evaluation and can be quantified using chip compression ratio. This parameter can be used as a quantitative measure of the total plastic deformation, tends to indicate the amount of energy consumed during the cutting process and indicates the frictional behaviour at the interaction points of chip and cutting tool. This study focuses on modelling and analysis of chip compression ratio in dry longitudinal turning of polyoxymethylene copolymer (POM-C) using a polycrystalline diamond (PCD) tool. To this aim turning experiment was realized using a face-centred central composite design in which three main parameters (depth of cut, feed rate and cutting speed) were arranged. Upon realization of the experiment and measurement data collection, a second-order mathematical model for relating turning parameters and chip compression ratio was developed. The results of statistical analysis indicate pronounced main effects of the depth of cut and feed rate, quadratic effect of the depth of cut and interaction effect of the feed rate and cutting speed on the change in chip compression ratio values.

Keywords: turning, chip compression ratio, POM-C, PCD, modelling

1. INTRODUCTION

Turning is the most prevalent machining technology capable of producing rotary parts of various shapes [1]. From the aspects of physical realization of the process and involved cutting mechanics and physics, turning is a complex process in which synergistic effects of a number of parameters ultimately define resulting process performances. For a given workpiece material and used machining system (cutting tool, machine tool, cooling/lubricating conditions), machinability, referring to the ease or difficulty of machining certain workpiece

material into desired shape, is predominantly affected by the selected cutting parameters. There are a number of criteria upon which material machinability is evaluated, and they are classified as basic (tool life, wear rate, surface roughness), and auxiliary (cutting forces, cutting temperature, chip morphology, etc.) [2]. Analysis of chip morphology gives information about the stability of machining processes. Usually, chip morphology is quantified using different parameters, like chip compression ratio (CCR), chip segmentation ratio, chip thickness, chip curling, radius of curvature of chips, etc. [3, 4]. Given that chip

morphology can be quantitatively analysed using chip compression ratio (CCR) [5], a number of studies were focused on the analysis of CCR in machining of different engineering materials, since this parameter can be used as a quantitative measure of the total plastic deformation [6]. As discussed by Santos Jr et al. [7], this post-process parameter is very important machining output parameter that can be related to the amount of plastic deformation that the material experiences during the chip formation process and tends to indicate the amount of energy consumed during the cutting process. Moreover, it directly indicates the frictional behaviour at the chip-tool interaction points (rake surface) [8].

Some recent studies related to chip morphology analysis are as follows. Hameed et al. [9] investigated the machinability indices such as chip compression ratio, shear plane angle and specific cutting energy in conventional and electropulsing-assisted turning of steel S235 and aluminium 6060. Chandra Behera et al. [3] presented experimental research aimed to understand the chip formation mechanisms in Inconel 718 turning process through metallographic technique. Analysis of the effect of feed rate and cutting speed on plastic deformation and CCR in turning of C45 medium carbon steel and 62SiMnCr4 tool steel was conducted by Kuruc et al. [10]. Younas et al. [11] analysed tool wear and specific energy consumption in turning Ti-6Al-4V alloys under varying cutting conditions and concluded that tool wear and energy consumption are strongly influenced by the chip compression ratio, shear angle and the tool-chip contact length. There are also studies focused on the optimization of cutting regime with respect to chip-tool interaction parameters. Application of Taguchi optimization approach to optimize cutting conditions in turning of titanium alloy with respect to the CCR was reported by Kumar et al. [12]. Mia et al. [4] presented a grey relational based Taguchi approach for multi-objective optimization of AISI 1060 steel turning process with respect to several representative indices of chip-tool interaction, such as chip

compression ratio, effective shear angle, friction coefficient and the chip-tool interface temperature. Measurement of chip morphology and multi-objective optimization, based on RSM-desirability approach, of cutting conditions in turning of AISI 4340 steel with respect to the CCR, surface roughness and chip tooth height was presented by Singh et al. [13]. With the use of genetic algorithm (GA), Santos Jr et al. [7] determined the cutting conditions (cutting speed, depth of cut and feed rate) that simultaneously minimize the machining force and CCR in turning of aluminum alloys.

Given in mind the significance of the CCR, the present study deals with the analysis of the effects of turning parameters on the CCR in turning of polyoxymethylene copolymer (POM-C). Empirical mathematical model, developed upon realization of a face-centered central composite design in which three main parameters (depth of cut, feed rate and cutting speed) were arranged, was used for the analysis of the CCR.

2. EXPERIMENTAL DETAILS

Longitudinal turning experiment was conducted on a universal lathe machine (POTISJE PA-C 30) in dry machining environment. Experimental units were in the form of bar with a diameter of 100 mm, made of a polyoxymethylene (acetal) copolymer POM-C produced by Zell-Metall, Austria. Cutting experiments were performed using a Walter VCGT160408FS-1 PCD insert mounted on a toolholder Sandvik Coromant SVJBR 3225P 16. The experimental trials were conducted in accordance with the face-centered central composite design and cutting parameter levels given in Table 1. Cutting parameter levels were selected considering industrial plastics machining recommendations, machine tool characteristics and recommended cutting conditions for the insert.

Table 1. Cutting parameter levels used in the experiment

Parameter	Level 1	Level 2	Level 3
Depth of cut, a_p [mm]	1	2.5	4
Feed rate, f [mm/rev]	0.049	0.214	0.392
Cutting speed, v [m/min]	188.5	345.6	510.5

The realization of the experiment, among other important performances, made it possible to estimate CCR (R_c) as the ratio of actual chip thickness (t_2) to the un-deformed (uncut) chip thickness (t_1) [6, 14]:

$$R_c = \frac{t_2}{t_1} = \frac{t_2}{f \cdot \sin \kappa} \quad (1)$$

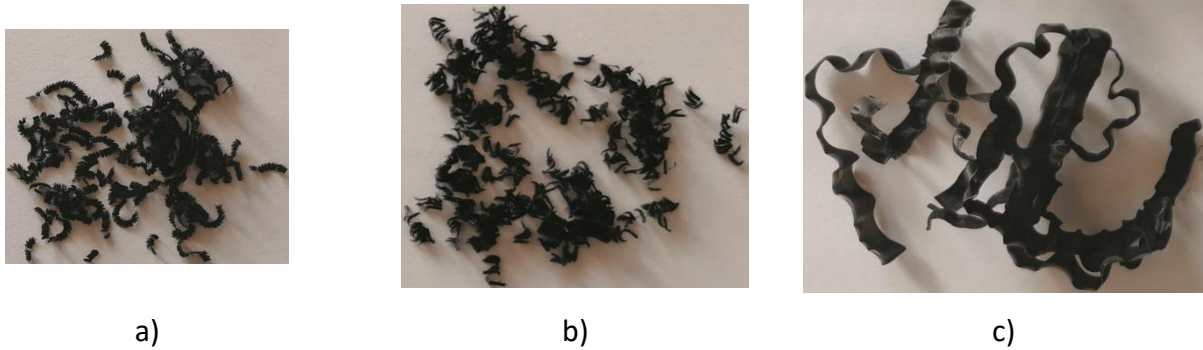


Figure 1. Chips obtained with different cutting regimes: a) $a_p = 1$ mm, $f = 0.214$ mm/rev, $v = 345.6$ m/min; b) $a_p = 2.5$ mm, $f = 0.392$ mm/rev, $v = 345.6$ m/min; c) $a_p = 4$ mm, $f = 0.049$ mm/rev, $v = 510.5$ m/min

As given in Equation 1, the resulting CCR in turning is higher than 1 because the actual chip thickness is greater than the corresponding un-deformed chip thickness, due to the frictional conditions existing at the chip-tool interface and the plastic deformation of the chip [14].

Higher values of CCR necessitate more work to perform the process [10] and, therefore, indicate higher plastic energy requirement for the chip formation [3]. That is, the chip, in the process of slipping over the rake face of the tool,

$$R_c = 1.303 + 0.125 \cdot a_p - 0.18 \cdot f - 0.026 \cdot v + 0.105 \cdot a_p^2 - 0.012 \cdot f^2 + 0.05 \cdot v^2 + 0.0125 \cdot a_p \cdot f + 0.026 \cdot a_p \cdot v - 0.073 \cdot f \cdot v \quad (2)$$

It should be noted that in addition to considerably high values of coefficients of determination ($R^2 = 0.94, R_{pred}^2 = 0.66, R_{adj}^2 = 0.89$) and p value much less than 0.05, residuals were scattered randomly without any significant pattern around zero, which indicates that the developed empirical

where f is the feed rate and κ is the cutting edge angle.

In Equation 1, the un-deformed chip thickness is affected only by the feed rate given that the tool cutting edge angle was held constant during experimentation ($\kappa = 93^\circ$). The actual chip thickness was measured using a Mitutoyo digital micrometer with measurement range of 0 - 25 mm and a resolution of 0.001 mm. After each experimental trial, the chips were collected and randomly selected for measurement of chip thickness. Three measurements were taken in order to obtain average chip thickness for all cutting conditions. Some of measured chip samples are shown in Figure 1.

has encountered enormous restrictions that impair chip movement and has thus become thicker and vice versa [7].

3. EMPIRICAL MODEL

Upon realization of the experiment and measurement data collection a second-order mathematical model for relating turning parameters (a_p, f and v) and CCR was developed in the following form:

model is suitable for prediction and analysis of the change in CCR values with respect to independent variables (a_p, f and v).

4. RESULTS AND DISCUSSION

Graphical visualization of the developed model for the prediction of CCR is presented in

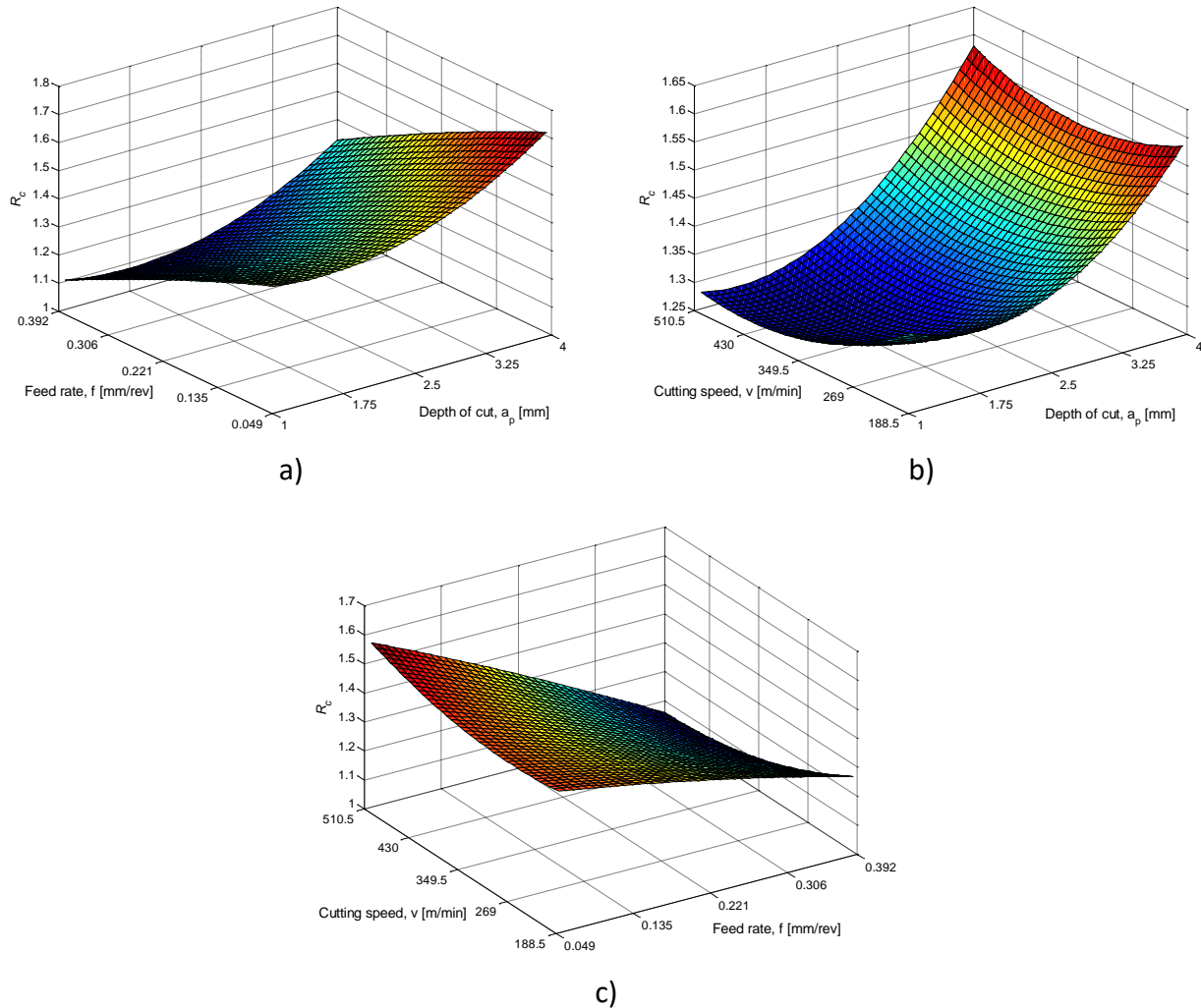


Figure 2. Surface plots of CCR: a) interaction of depth of cut and feed rate, b) interaction of depth of cut and cutting speed, c) interaction of feed rate and cutting speed

As could be observed from Figure 2 a) and b) an increase in the depth of cut consistently nonlinearly increases the CCR regardless of the values of the cutting speed and feed rate. In a related study, Singh et al. [13] also observed that at constant cutting speed and feed rate values, due to the more material removal from the workpiece, CRC gradually increases with the rise in depth of cut. Actually, any increase of depth of cut or feed rate increases the cross-sectional area of the undeformed chip, and thus CCR tends to decrease.

The approximately linear decrease in CCR with an increase of the feed rate, as a consequence of the increased undeformed chip thickness, may be observed in Figure 2 a) and c).

Figure 2 in order to analyse the main and interaction effects of the depth of cut, feed rate and cutting speed on the resulting CCR.

On the other hand, the lower the feed rate, there is a higher plastic deformation of the chip. This phenomenon can be explained by a greater strain-hardening effect occurring at a lower feed (thinner unreformed chip removed) and the associated size effect [2] as well as higher specific cutting pressure [15]. One could also observe that at higher cutting speeds, the decrease in CCR is more pronounced due to the effect of feed rate increase. Astakhov and Shvets [6] also note that the effect of feed rate may have a different influence at different cutting speeds, however in machining of steels the general trend of decrease of CCR with an increase in feed rate, for different cutting speed values, can be observed. Similar conclusions

were made by Chandra Behera et al. [3] in turning of Inconel 718. The authors quoted that possible reason is that with increasing cutting speed, chip velocity increases, which in turn reduces the friction on the contact between the chip and the tool [16].

Figure 2 b) and c) shows that the effect of the cutting speed on the resulting CCR is least pronounced and that it has a variable character. Namely, as shown in Figure 2 b), an increase in the cutting speed up to approximately 350 m/min results in CCR decrease, but afterwards, an increase in the cutting speed again increases CCR, and that increase is higher for greater values of the depth of cut. One may notice that for a constant feed rate there is a combination of cutting speed and depth of cut which produces minimal CCR. Research by Astakhov and Shvets [6] showed that in machining copper, steel, and aluminum, for a constant feed rate and depth of cut ($f = 0.07$ mm/rev, $a_p = 1$ mm), there exists a particular cutting speed which results in minimal CCR. The conducted machining test also confirmed the existence of variable influence of cutting speed on the CCR. It has been pointed out that the cutting speed influences the energy spent on the deformation of the chip through the temperature, dimensions of the deformation zone adjacent to the cutting edge and velocity of deformation.

Further, from Figure 2 c) one may notice that there exists a certain level of interaction between the cutting speed and feed rate. Namely, for low feed rates, and increase in the cutting speed leads to a slight increase in CCR, however, for high feed rates, and increase in the cutting speed results in a decrease in CCR. The experimental investigation by Yilmaz et al. [17], showed that increased cutting speed influences the chip formation by producing less thick chips, and this may justify the observed decrease of CCR for higher cutting speed.

Figure 2 shows that there are significant effects of both feed rate and depth of cut on CCR. The combination of high feed rate and low depth of cut decreases CCR, while CCR attains higher values when using higher depth of cut values and minimum feed rate values. These observations are in line with the results of Singh

et al. [13]. The authors explained this phenomenon mainly due to dominating effect of material removal rate, which is directly linked with depth of cut.

5. CONCLUSION

The study presented experimental results regarding CCR in turning of unreinforced polyoxymethylene copolymer POM-C material using a PCD cutting tool. Based on developed empirical model for the prediction of CCR, and analysis of the obtained results, the following conclusions could be drawn:

- The developed empirical model proved to be statistically valid and the predicted CCR values are found to be in good agreement with experimental data.
- In the performed experiment CCR values were in the range of 1.1 - 1.6, which is not a wide range, given that covered experimental hyperspace encompassed cutting conditions for finishing and medium machining. In fact, this could have been foreseen given that specific cutting force for POM-C is several times lower compared to steels, aluminum alloys and cast irons.
- From the obtained results it can be clearly concluded that the depth of cut is most significant factor affecting CCR, followed by feed rate, cutting speed and interaction effect of cutting speed and feed rate.
- From the conducted analysis one can observe that depth of cut is directly proportional to the CCR, while the cutting speed and feed rate are inversely proportional with certain degree of interaction between the feed rate and cutting speed.
- Given that CCR indicate the energy spent in the cutting process, the empirical models for the prediction of CCR can be used as objective function, of minimization type, in the formulation of single and multi-objective turning optimization problems for comprehensive process enhancement.

- It has been revealed that CCR and material removal rate are not conflicting objectives. However, minimization of CCR and maximization of MRR should be considered in relation to other important machining performances, such as surface roughness and formation of favourable chip forms.

ACKNOWLEDGEMENT

This research was financially supported by the Ministry of Science, Technological Development and Innovation of the Republic of Serbia (Contract No. 451-03-47/2023-01/200109).

REFERENCES

- [1] M. Trifunović, M. Madić, P. Janković, D. Rodić, M. Gostimirović: Investigation of cutting and specific cutting energy in turning of POMC using a PCD tool: Analysis and some optimization aspects, *Journal of Cleaner Production*, Vol. 303, Article ID: 127043, 19 pages, 2021.
- [2] W. Grzesik: *Advanced Machining Processes of Metallic Materials: Theory, Modelling, and Applications*, Second Edition, Elsevier, Amsterdam, 2017.
- [3] B. Chandra Behera, C. Sudarsan Ghosh, V.R. Paruchuri: Study of saw-tooth chip in machining of Inconel 718 by metallographic technique, *Machining Science and Technology*, Vol. 23, No. 3, pp. 431-454, 2019.
- [4] M. Mia, A. Rifat, M.F. Tanvir, M.K. Gupta, M.J. Hossain, A. Goswami: Multi-objective optimization of chip-tool interaction parameters using Grey-Taguchi method in MQL-assisted turning, *Measurement*, Vol. 129, pp. 156-166, 2018.
- [5] I. Shyha, S. Gariani, M.A. El-Sayed, D. Huo: Analysis of Microstructure and Chip Formation When Machining Ti-6Al-4V, *Metals*, Vol. 8, No. 3, Article ID: 185, 20 pages, 2018.
- [6] V.P. Astakhov, S. Shvets: The assessment of plastic deformation in metal cutting, *Journal of Materials Processing Technology*, Vol. 146, No. 2, pp. 193-202, 2004.
- [7] M.C. Santos Jr, A.R. Machado, M.A.S. Barrozo, M.J. Jackson, E.O. Ezugwu: Multi-objective optimization of cutting conditions when turning aluminum alloys (1350-O and 7075-T6 grades) using genetic algorithm, *The International Journal of Advanced Manufacturing Technology*, Vol. 76, No. 5-8, pp. 1123-1138, 2015.
- [8] M.A. Shalaby, M.A. El Hakim, M.M. Abdelhameed, J.E. Krzanowski, S.C. Veldhuis, G.K. Dosbaeva: Wear mechanisms of several cutting tool materials in hard turning of high carbon-chromium tool steel, *Tribology International*, Vol. 70, pp. 148-154, 2014.
- [9] S. Hameed, H.A. Gonzalez Rojas, J.I. Perat Benavides, A. Napoles Alberro, A.J. Sanchez Egea: Influence of the Regime of Electropulsing-Assisted Machining on the Plastic Deformation of the Layer Being Cut, *Materials*, Vol. 11, No. 6, Article ID: 886, 10 pages, 2018.
- [10] M. Kuruc, T. Vopat, J. Peterka, M. Necpal, V. Šimna, J. Milde, F. Jurina: The Influence of Cutting Parameters on Plastic Deformation and Chip Compression during the Turning of C45 Medium Carbon Steel and 62SiMnCr4 Tool Steel, *Materials*, Vol. 15, No. 2, Article ID: 585, 18 pages, 2022.
- [11] M. Younas, S.H.I. Jaffery, A. Khan, M. Khan: Development and analysis of tool wear and energy consumption maps for turning of titanium alloy (Ti6Al4V), *Journal of Manufacturing Processes*, Vol. 62, pp. 613-622, 2021.
- [12] A.R. Kumar, K.K. Joshi, R.K. Das: Analysis of Chip Reduction Coefficient in Turning of Ti-6Al-4V ELI, *IOP Conference Series: Materials Science and Engineering*, Vol. 390, Article ID: 012113, 7 pages, 2018.
- [13] B.K. Singh, H. Roy, B. Mondal, S.S. Roy, N. Mandal: Measurement of chip morphology and multi criteria optimization of turning parameters for machining of AISI 4340 steel using Y-ZTA cutting insert, *Measurement*, Vol. 142, pp. 181-194, 2019.
- [14] J.P. Davim, F. Mata: A comparative evaluation of the turning of reinforced and unreinforced polyamide, *The International Journal of Advanced Manufacturing Technology*, Vol. 33, No. 9-10, pp. 911-914, 2007.
- [15] P. Nieslony, W. Grzesik, K. Żak, P. Laskowski: 3D FEM simulations and experimental studies of the turning process of Inconel 718 superalloy, *Journal of Machine Engineering*, Vol. 14, No. 2, pp. 16-26, 2014.
- [16] N.R. Dhar, M.W. Islam, S. Islam, M.A.H. Mithu: The influence of minimum quantity of

lubrication (MQL) on cutting temperature, chip and dimensional accuracy in turning AISI-1040 steel, *Journal of Materials Processing Technology*, Vol. 171, No. 1, pp. 93-99, 2006.

[17] B. Yilmaz, S. Karabulut, A. Gullu: Performance analysis of new external chip breaker for

efficient machining of Inconel 718 and optimization of the cutting parameters, *Journal of Manufacturing Processes*, Vol. 32, pp. 553-563, 2018.



Society of Production
Engineering

SPMS 2023

39. Savetovanje proizvodnog mašinstva Srbije

ICPES 2023

39th International Conference on Production Engineering of
Serbia



Faculty of Technical
Sciences
University of Novi Sad

Novi Sad, Serbia, 26. – 27. October 2023

THE TOOL LIFE MODEL BY THE USE OF GENETIC ALGORITHM

Pavel KOVAČ^{1*}, Vladimir PUCOVSKI¹, Borislav SAVKOVIĆ^{1*}, Dušan JEŠIĆ², Branislav DUDIĆ^{3,4}

¹University of Novi Sad, Faculty of Technical Sciences, 21000 Novi Sad, Serbia

²International Technology Management Academy, 21000 Novi Sad

³Comenius University Bratislava, Faculty of Management, Slovakia

⁴University Business Academy, Faculty of Economics and Engineering Management, Serbia

*Corresponding author: pkovac@uns.ac.rs

Abstract: *It is widely known that genetic algorithms could be used in search space and modeling problems. In this paper their ability to model a function while varying tool life input data is tested. Function which is used for this research is a tool life function. This concept is chosen because by being able to predict tool life, workshops can optimize their production rate – expenses ratio. Also, they would gain profit by minimizing number of experiments necessary for acquiring enough input data in process of modeling tool life function. Tool life by its nature is a multiple factor dependent problem. By using four factors, to acquire adequate tool life function, vivid complexity is simulated while acceptable duration of computational time is maintained. As a result, almost clear threshold, of data quantity inputted in optimization model to gain acceptable results in means of output function accuracy, is noticed.*

Keywords: *modeling; genetic algorithms; tool life; milling; heuristic crossover.*

1. INTRODUCTION

From early days when artificial intelligence was introduced, there is a prevailing trend of discovering capabilities which lies inside this branch of science. As all machine related domain, with this one being no exception, there are limits. These limits and boundaries of usage are often expanded and new purposes are constantly discovered. To be able to achieve this goal one must be a very good student of a best teacher that is known to mankind; mother nature. With an experience of more than five billion years our nature is a number one scientist and we are all proud that we have an opportunity to learn whatever she

has to offer. Mastery of creation such a variety of living beings is no easy task and maintaining this delicate balance between species is something that requires time, experience and understanding. No scientist is able to create something graceful, like variety of life on Earth, by share coincidence. There has to be a consistency in process of creating and maintaining this complexity of living beings. Law which lies behind this consistency had prevailed more than we can remember and is a simple postulate which tells us that only those who are most adaptable to their environment will survive. By surviving more than others, less adaptable individuals, every living organism is increasing chance to mate,

with equally adaptable member of same species and creating offspring which possess the same, or higher level of adaptability to their environment. This law of selection is something that enabled creation of this world that we live in. Seeing its effectiveness yet understanding simplicity of this concept, we decided to model it [1,2]. One way of succeeding in this is through genetic algorithms (GA). Since they have been introduced, in early 1970's, GA present a very powerful tool in space search and optimization fields. Introduce them to a certain area and, with a proper guidance, they will create a population of their own and eventually yield individuals [3,4].

2. EXPERIMENT

Tests were performed on a 14-kW vertical milling machine without cooling lubrication fluid. A single-tooth face, milling cutter of 125 mm diameter, with a carbide P 25 insert SPAN 12 03 ER was used. The working material was a block of 100x120x600 mm of **steel AISI 1060** and was fixed on milling machine table (Kovac et al., 2012). Experimenting mode included varying following parameters: cutting speed v [m/s], respectively number of revolutions on machine n [°/min], feed per tooth f_t [mm/t], respectively corresponding feed rate f [mm/min], depth of cut a [mm] and width of flank wear VB [mm]. Each variation of mentioned parameters provided value for tool life T [min] which was carefully measured during whole experiment. Results of experiment are shown in Table 1.

Table 1. Results of experiments

No (i)	v [m/s]	f_t [mm/t]	a [mm]	VB [mm]	T [min]	T_{mod} [min]
1	2.32	0.178	1	0.12	8	8.48
2	3.67	0.178	1	0.12	6	3
3	2.32	0.28	1	0.12	9	5.85
4	3.67	0.28	1	0.12	2	2.07
5	2.32	0.178	2.25	0.12	8	9.1
6	3.67	0.178	2.25	0.12	5.2	3.22
7	2.32	0.28	2.25	0.12	7	6.27
8	3.67	0.28	2.25	0.12	4	2.22

9	2.32	0.178	1	0.28	42	40.72
10	3.67	0.178	1	0.28	16.6	14.4
11	2.32	0.28	1	0.28	30	28.07
12	3.67	0.28	1	0.28	9.2	9.93
13	2.32	0.178	2.25	0.28	43.5	43.68
14	3.67	0.178	2.25	0.28	18.5	15.45
15	2.32	0.28	2.25	0.28	32	30.11
16	3.67	0.28	2.25	0.28	6.5	10.65
17	2.95	0.223	1.5	0.18	13.3	8.97
18	1.83	0.223	1.5	0.18	20	26.48
19	4.65	0.223	1.5	0.18	3.2	3.2
20	2.95	0.142	1.5	0.18	13	13
21	2.95	0.351	1.5	0.18	7	6.18
22	2.95	0.223	0.67	0.18	14	8.37
23	2.95	0.223	3.37	0.18	13	9.62
24	2.95	0.223	1.5	0.08	2	2
25	2.95	0.223	1.5	0.4	28	39.35

3. MODELING FUNCTION

To model the function of tool life T , predefined second-order model is used:

$$T = C_1 \cdot v^{x_1} \cdot f_t^{x_2} \cdot a^{x_3} \cdot VB^{x_4} \quad (1)$$

The objective of GA optimization is to get such solutions for values of the coefficients C_1 , x_1 , x_2 , x_3 , and x_4 that the difference between experimental values and values predicted by model are as smaller as possible [5]. This in other words is something to be considered as a fitness function or a measure of success for every individual. Number of individuals that participate in every generation is n . Every individual (chromosome) has five distinctive features (genes) which are before mentioned coefficients C_1 , x_1 , x_2 , x_3 and x_4 .

General form of fitness function is defined as:

$$\Delta(j) = \sum_{i=1}^{25} \left| 1 - \frac{M(i, j)}{P(i)} \right| \times 100\% \quad (2)$$

4. IMPLEMENTATION OF GENETIC ALGORITHMS

GA consists of several steps whose execution leads to the solution (Figure 1).

For practical realization of the model, software MatLab is used. At the very beginning an initial population of 50 individuals is created. Theirs genes (coefficients) are randomly generated from interval 0÷1 using

uniform distribution. This indicates that real number coding was used. As a fitness scaling function rank method was used. Most fit individual, respectively individual with best raw score is assigned as first on the scaling list, next to fittest is ranked number two and so on. This method is ranking every individual in generation comparing to best individual in that same generation, no matter how good or bad fitness value is. It was selected because it allowed fastest convergence toward the best solution. Selection of individuals for presence in mating pool was executed by roulette wheel method. Size of area on wheel, occupied by a single individual is defined by rank score - better the score, bigger the area. Wheel is then spun and individual with largest area has the most chances to be assigned a slot in mating pool. This action is repeated until all slots in mating pool are assigned. In each generation two of the best individuals are automatically transferred to next generation. This act is called elitism and it guarantees that the best genetic material is passed onto next generation. By setting this parameter high the genetic diversity is quickly reduced which leads to prolonged convergence time. On the other hand setting it low, elite genetic material of every generation may be lost and algorithm stuck in local minimum. Number of individuals created by heuristic crossover is, in this case, 43. Heuristic crossover is carried out by creating children that randomly lie on the line containing the two parents, a small distance away from the parent with the better fitness value, in the direction away from the parent with the worse fitness value. After transferring two elite individuals from previous generation and creating 43 by crossover, to complete a full population with 50 members, last 5 individuals are created by mutating 5 of their predecessors. With the process of mutation a completely new genetic material is introduced into the population which helps in expanding genetic diversity and search space. It also prevents jamming an algorithm in a local minimum of the function. Uniform mutation is selected with the rate of 0.2. This type of mutation is basically a two-step process. Firstly,

the algorithm selects a gene of an individual for mutation, where each gene has the same probability as the mutation rate of being mutated. In the second step, the algorithm replaces each selected entry by a random number selected uniformly from the range for that entry. This whole process of selection, recombination and mutation lasted 500 generations.

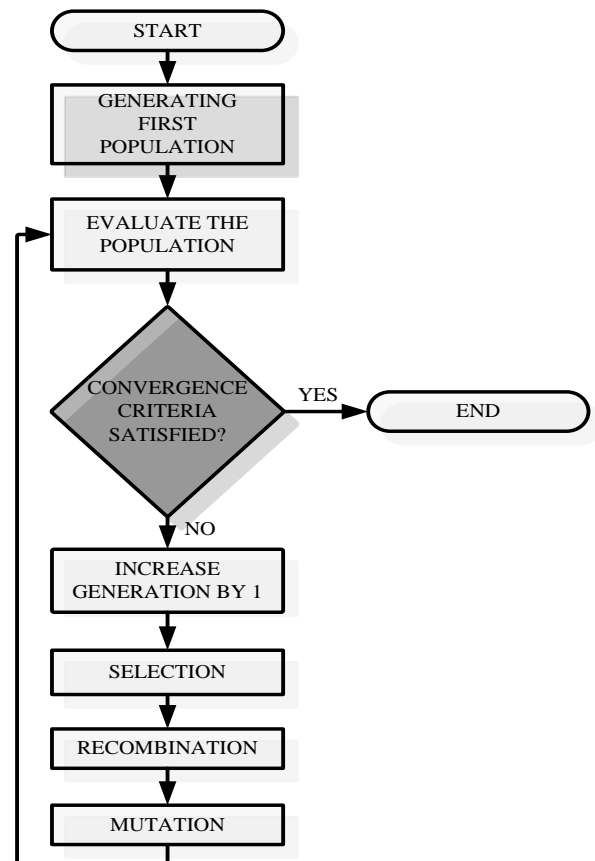


Figure 1. Structure of genetic algorithm

5. ANALYSIS OF RESULTS

Best results obtained by GA, gave average absolute deviation E of just above 20%. Function with implemented obtained coefficients now looks like:

$$T = 701.407 \cdot v^{-2.2661} \cdot f_t^{-0.8211} \cdot a^{0.0865} \cdot VB^{1.8512} \quad (3)$$

Using this equation to calculate the tool life, obtained results are shown in last column of Table 1. Figure 2 presents graphical interpretation of comparison experimental and modeled values.

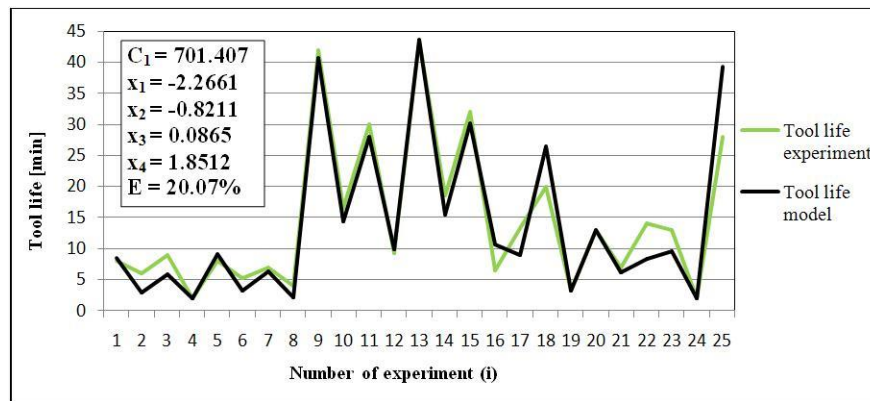


Figure 2. Correlation of tool life values with 20 experiments on input

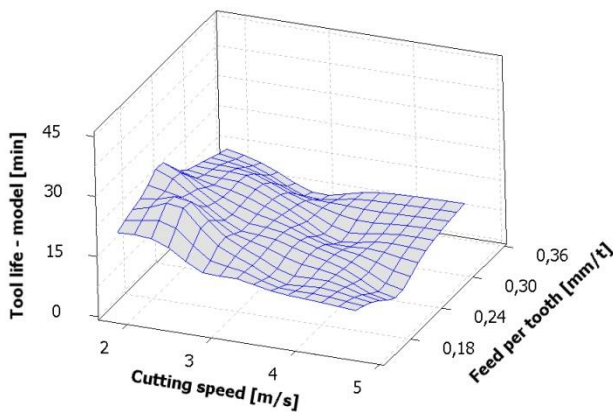


Figure 3. 3D representation of modeled dependencies of v , f , T

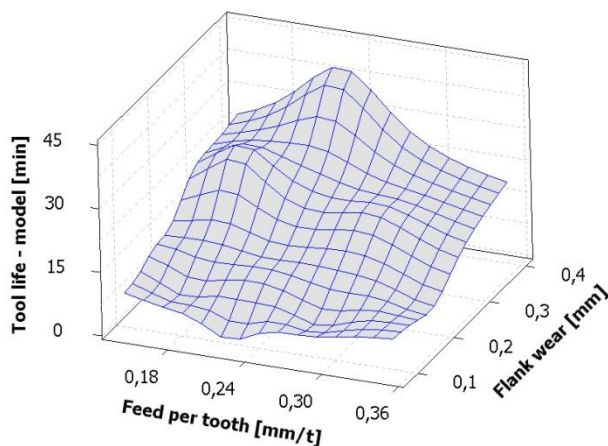


Figure 4. 3D representation of modeled dependencies of f , VB , T

6. CONCLUSION

As expected, lowering the number of experiments used for modeling tool life function did have an influence on final accuracy of modeled function. Step of 5 experiments was selected because it was considered an optimal change, not too big –

which would lead to rapid changes, nor too small – to unnecessary increase the computing time. It can be noticed that lowering experimental data to only 10 didn't dramatically change an accuracy of modeled function. Eventually with enough data collected a rule of thumb could be extracted which would spare engineers and researchers of unnecessary experiments.

REFERENCES

- [1] Čuš, F. and Balič, J. (2003). Optimization of Cutting Process by GA Approach. *Robotics and Computer Integrated manufacturing*, 19(1-2):113–121.
- [2] Ezzaine, Z. (2002). Solving the 0/1 Knapsack Problem Using an Adaptive Genetic Algorithm. *Artificial Intelligence for Engineering Design, Analysis and Manufacturing*, 16(1): 23–30.
- [3] Ficko, M., Brezočnik, M. and Balič, J. (2005). A Model for Forming a Flexible Manufacturing System Using Genetic Algorithms. *Strojniški vestnik - Journal of Mechanical Engineering*, 51(1): 28–40.
- [4] Kovac, P., Rodic, D., Pucovsky, V., Savkovic, B. and Gostimirovic, M. (2012). Application of Fuzzy Logic and Regression Analysis for Modeling Surface Roughness in Face Milling. *Journal of Intelligent Manufacturing*, doi: 10.1007/s10845-012-0623-z.
- [5] Sovilj, B., Brezočnik, M., Sovilj-Nikić, I. and Kovač, P. (2009). Tool Life Function Modeling by the Use of Genetic Algorithm and Response Surface Methodology During Profile Production. *Conference on Production Engineering of Serbia. 2009, Beograd, Serbia, June 16-17.*



Society of Production
Engineering

SPMS 2023

39. Savetovanje proizvodnog mašinstva Srbije

ICPES 2023

39th International Conference on Production Engineering of
Serbia



Faculty of Technical
Sciences
University of Novi Sad

Novi Sad, Serbia, 26. – 27. October 2023

INTEGRATED OPTIMIZATION OF TOOL PATH AND CUTTING PARAMETERS IN CONTOUR MILLING USING GENETIC ALGORITHM

Predrag MITIĆ^{1*}, Aleksandar ĐORĐEVIĆ², Suzana PETROVIĆ SAVIĆ², Dragan DŽUNIĆ²,
Vladimir KOČOVIĆ²

¹Metalika SMTR, Sopot, Serbia

²Faculty of Engineering, University of Kragujevac, Serbia

*predrag2904@gmail.com

Abstract: *The optimization of the cutting parameters and the tool path has attracted the attention of a large number of researchers in the past two decades. Cutting parameters and the tool path have a great influence on the production time and the quality of the machined surface, and therefore on the production costs. Optimization of cutting parameters and tool path are still the main directions of research in the field of machining process optimization. However, in the majority of research, the optimization of cutting parameters and tool path is done independently and their mutual influence is ignored. This paper discusses the possibility of integrated optimization of tool path and cutting parameters on the example of rough contour milling using genetic algorithm.*

Keywords: *Integrated optimization, tool path, cutting parameters, genetic algorithm*

1. INTRODUCTION

The problem of tool path generation and optimization in chip removal machining processes has attracted the attention of a large number of researchers for several past decades. In addition to the optimal tool path it is necessary to determine the optimal cutting parameters while respecting the multiple technological constraints imposed by the machine, the tool and the part geometry in order to achieve optimal part quality in minimal machining time. Machining in general and milling in particular is one of the main production processes used to manufacture durable goods. The cost optimization of

production processes remains one of the major focus points of machine builders world-wide [1].

The conventional ways of selecting the tool path and the cutting parameters or programming the NC code used data from machining handbooks and the knowledge of programmer for optimal processing. However, the conventional NC programming has many disadvantages for instance increasing time and cost production and, decreasing accuracy and quality of the work piece. Modern CNC machine programming relies on commercial CAM software that speed up and facilitate CNC programming but the price of these software is high and to work with them, a highly skilled workforce is needed. These software's,

however, do not offer optimization of the tool path and cutting parameters, but rely on empirical data and built-in, ready-made algorithms. In the literature there is a growing trend of development and application of models for automatic generation and tool path optimization and also for cutting parameters optimization. The developments of such models will not only shorten the reaction time of manufacturing system, but also improve the machine productivity through optimal selection of cutting parameters [3]. The most common approach is the application of artificial intelligence and metaheuristic algorithms, but there are very few works that simultaneously optimize tool path and cutting parameters. Although the tool path generation and optimization and the cutting parameters selection and optimization can be performed independently, the mutual influence of the tool path and cutting parameters on the production costs should not be ignored. There are three major issues in the process of integrated optimization of tool path and cutting parameters:

- recognition of geometric information of the work piece
- selection and optimization of cutting parameters
- tool path generation and optimization

Assuming that the geometry of the work piece is already recognized in a suitable manner, it is necessary to integrate activities that in modern CAM systems are implemented through interaction with the knowledge of programmers and as mentioned above, built-in, ready-made algorithms. Also, the programmer or operator on the machine enters the cutting depth, the number of revolutions of the main spindle, the speed of the auxiliary movement, the place where the tool starts moving as well as the place where the tool exits the machining zone, the clamping method, the position of clamping accessories and similar.

The aim of this paper is to present the theoretical framework of the integrated optimization of the tool path and cutting parameters mode as a basis for the automatic generation of NC code, that is, technological

procedures in the narrower sense.

2. DEVELOPMENT OF MODULE FOR THE INTEGRATED OPTIMIZATION OF CUTTING PARAMETERS AND TOOL PATH

The basis for making parts by machine processing is the technical documentation (technical drawing, 3D model of the part being processed, etc.) and also the initial shape of the raw material from which the part is made. Figure 1 shows a typical industrially inspired part in 3D model representation.

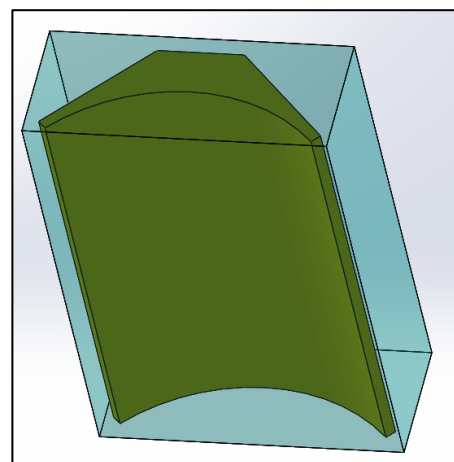


Figure 1. 3D model of work piece

Figure 2 shows a plane view of the same part, where the hatched surface represents the material that must be removed in order to obtain the shape marked in red, i.e. the final contour of the part. The shape and dimensions of the initial work piece (marked blue in Figure 1) is predetermined and as such, represents one of the input data in the model.

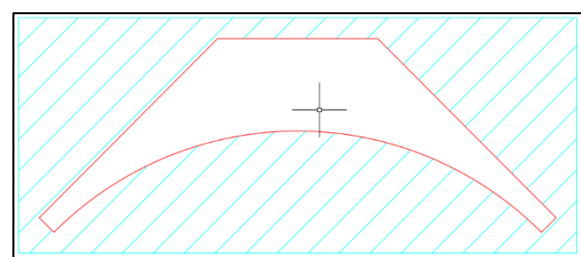


Figure 2. 3D model of work piece

In order for the part to be machined it is necessary to determine the tool, the cutting parameters (speed, feeds, radial and axial cutting depth) and the tool path. The cutting parameters and tool path must be determined in such a way that there is an economic profitability of the machining process, that is, their optimization must be performed in

accordance with the optimization objectives and constraints imposed by various limitations of the tool, the CNC machine, the clamping tools, work piece material, the required accuracy and the required quality of the processed surface. Formally, the problem can be described as stated in [4]: For a work piece with given machine, cutting tool and clamp, there are a large number of feasible combinations $P = \{p_1, \dots, p_i, \dots, p_m\}$ of cutting parameters including spindle speed n , feed per tooth fz , cutting depth a_p and cutting width a_e . Each combination p_i corresponds to numbers of feasible tool paths $L_i = \{L_{i1}, \dots, L_{ij}, \dots, L_{in}\}$, where each tool path L_{ij} consists of void tool path L_a and cutting path L_c . In addition, cutting parameters and tool path affect each other and constitute processing space F . Then, the problem is defined as: for a given processing space F of a work piece, this paper aims to optimize the combination of P_i and L_{ij} to achieve coordinative optimization of objectives set O which can be expressed as:

$$F_{\text{optimal}} = \operatorname{argmin}\{O(P_i, L_{ij})\} \quad (1)$$

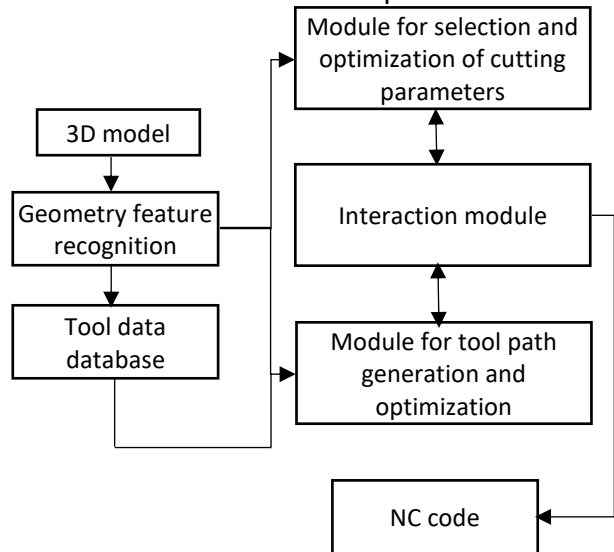
Optimization objectives will be discussed later in the paper. The initial assumptions of the model are:

- the integrated optimization is done after the machine, cutting tool and clamping fixtures are chosen
- there are no tool change in the machining process of contour milling

It is clear that the process of integrated optimization of cutting parameters and tool path must take place in three stages. The first stage should be optimization of cutting parameters, the second stage is generation and optimization of the tool path and the final stage is interaction between optimized cutting parameters and the tool path. Figure 3 shows block diagram of proposed concept.

In [2] the authors stated that determining the optimal machine tool path has been proven to lead to high productivity and minimal production costs. Furthermore, they provide statistical data related to the methods used by various authors in researches, with the conclusion that Genetic Algorithms (GA) and

Particle Swarm Optimization (PSO) method are largely used to optimize machining efficiency and when compared with other methods, the GA has been successfully applied for many optimization problems with various parameters related to tool path and effective in improving the robustness of feature selection over a range of problems. A similar analysis of methods used to optimize cutting mode parameters is given in [4], so GA was chosen as the most suitable method for the research presented in this



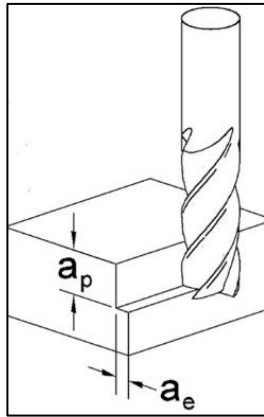
paper as well.

Figure 3. Block diagram of integrated optimization

2.1 Module for selection and optimization of cutting parameters

The task of optimizing the contour milling machining is defined at the following way: select the milling parameters speed and feed that meet the quality limits surfaces and optimization criteria [5]. The traditional methods for milling parameters calculation are widely known and are well described in the literature. Although the mentioned methods are applicable in everyday practice, nowadays, especially in the conditions of individual and small-batch production, data from the tool manufacturer's catalogue are most often used to determine the tool and milling parameters for the selected cutter. These catalogues are available in electronic form, so determining the tool and parameters using this data is very easy and fast. Based on the geometry of the surface and the required quality of processing, a tool of

the appropriate diameter is chosen in such a way that all segments of the contour can be processed with that tool. The manufacturer of the tool according to the type of engagement (Figure 4) and according to the recommended values of the axial (a_p) and radial (a_e) depth of cut gives the recommended values of the



milling parameters.

Figure 4. Tool engagement

The recommended values of cutting parameters are always given in the interval from the minimum to the maximum as shown in Table 1 as an example. In addition to data shown in Table 1 there are also recommended values for the axial (a_p) and radial (a_e) depth of cut in function of tool diameter D . Radial depth of cut a_e or *stepover* can be also defined as the percentage of the tool diameter engaged in material (Figure 5).

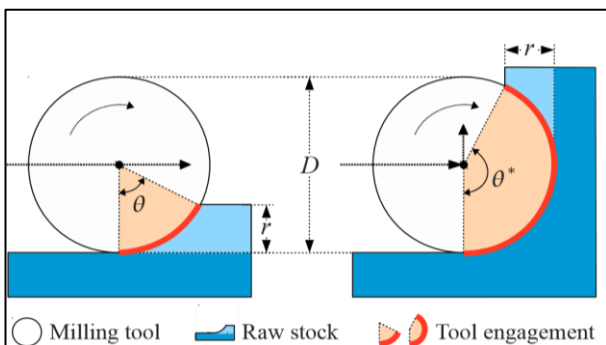


Figure 5. Radial depth of cut and TEA

The stepover determines the material removal rate (MRR) and reflects the cutting forces, but only for straight line motions. A parameter which better reflects the cutting force, regardless of the toolpath shape, is the *tool engagement angle-TEA* [6] as the amount of sweep subtended by each cutting edge as it engages and leaves the stock. TEA plays an

important role in the formation of the tool path and is dependent on the axial depth of cut [5]. The engagement angle reaches its maximum (360°) when plunging the tool vertically into the material. The next maximum value, 180° , is encountered during a slotting operation; this condition may lead to high thermal stress on the tool, since the chips cannot be evacuated properly. Tool engagement is also known to increase at internal corners in toolpath. The engagement angle also has direct influence on the chip shape, therefore keeping TEA constant ensures consistent chip size and shape throughout the milling process [6]. A large value of the TEA would result in a large amount of material removed, which certainly increases productivity, but then the cutting resistance is high and the wear of the tool is intense. In the model presented in this paper TEA will be considered in the process of forming feasible tool paths as one of the constraints. The maximum value of TEA marked as Θ_{max} can be easily calculated from the data shown in Table 1 and Table 2 and is often found in tool manufacturers' catalogs as a value given in degrees.

Input values for GA that generates sets of cutting parameters, chosen from a tool manufacturers' catalog are:

- tool diameter D (mm)
- number of teeth z
- cutting speed V_c (m/min) within the limits $V_{cmin} < V_c < V_{cmax}$
- feed per tooth f_z (mm/tooth) within the limits $f_{zmin} < f_z < f_{zmax}$
- radial depth of cut a_e (mm) within the limits $a_{emin} < a_e < a_{emax}$
- axial depth of cut a_p (mm) within the limits $a_{pmin} < a_p < a_{pmax}$

Also, maximum TEA defined as Θ_{max} is considered as maximum possible value for above cutting parameters values within the given limits. The above given limits of cutting parameters are constraints of the presented model and must be included in GA through chromosome feasibility check. In addition to the above mentioned constraints, it is necessary to take into account the constraints related to tool shaft breakage (cutter bending

strength), tool deflection and the speed of main spindle.

Table 1. The recommended value of cutting parameters

	Strength [N/mm ²]	Work piece material DIN	Vc [m/min]	fz [mm/tooth] at Diameter				
				2-4	4-8	8-12	12-16	16-20
1. Work piece material								
1.1 Free cutting steel	< 900	9 S 20	220-230	0.03-0.04	0.04-0.09	0.09-0.13	0.13-0.18	0.18-0.22
1.2 Structural steel	<500	ST 37-2	220-230	0.03-0.04	0.04-0.09	0.09-0.13	0.13-0.18	0.18-0.22
1.3 Structural steel	> 500	ST 60-2	190-200	0.025-0.035	0.035-0.08	0.08-0.12	0.12-0.16	0.16-0.02
1.4 Tempered steel	<1000	42 CrMo 4	150-160	0.025-0.035	0.035-0.08	0.08-0.12	0.12-0.16	0.16-0.02
1.5 Cast steel	<1000	GS-45	120-130	0.02-0.03	0.03-0.07	0.07-0.1	0.1-0.14	0.14-0.17
1.6 Case-hardened steel	<1200	16 MnCr 5	190-220	0.02-0.03	0.03-0.07	0.07-0.1	0.1-0.14	0.14-0.17
1.7 Stainless steel ferritic/martensitic	<1100	X 10 Cr 13	110-120	0.01-0.02	0.02-0.04	0.04-0.06	0.06-0.08	0.08-0.1

The calculation of maximum cutter bending stress and tool deflection, in detail, can be found in [3] and must be incorporated in GA mechanism as constraints during feasibility check. Using wide known formula for spindle speed

$$n (o/min) = \frac{V_c \cdot 1000}{\pi \cdot D} \quad (2)$$

it is easy to determine n_{max} and n_{min} using V_{cmin} and V_{cmax} obtained from Table 1. Now, all constraints of the presented model are defined.

In GA acceptable representation of chromosome is the most critical factor influencing all other phases of the GA [7]. In the present model a single chromosome binary bit string is chosen to represent four cutting parameters as shown in Table 2. The number of bits in a chromosome which represents coded chromosome size is set to 24. Cutting parameters are mapped from the 24-bit chromosome by segmenting it into four equal parts.

Table 2. Chromosome representation

1	0	1	1	1	1	0	1	0	1	1	1	0	0	1	1	1	1	0	0	0	1	0	1
<i>ap (mm)</i>						<i>ae (mm)</i>						<i>n(o/min)</i>						<i>fz (mm/tooth)</i>					

Each part of the chromosome string represents a percentage value of the predefined range of the cutting parameter and is obtained using equation (3) [3]. The maximum value for each part is 63, which is value obtained from binary to decimal conversion of maximum value, and the value of zero correspond to the upper and lower bounds of the cutting parameter, as shown in Table 1.

$$X = \frac{X_{max} - X_{min}}{63} \cdot Y + X_{min} \quad (3)$$

where X is mapped value of the cutting parameter, X_{max} and X_{min} correspond to the cutting parameter's upper and lower bound, while Y is the decoded value of respective chromosome part.

Furthermore, an algorithm for forming a set of parameters, based on a GA, will be given. For every chromosome, Material Removal Rate (MRR) is calculate given by an equation (4)

$$\max(MRR) = \max(f_z \cdot z \cdot n \cdot a_p \cdot a_e) \quad (4)$$

A set of cutting mode parameters is formed, which is passed to the interaction module, which will be discussed later. The algorithm is repeated m times, and m is the value that represents the input data to the algorithm for integrated optimization. As the mechanism of action of GA is widely known [7], in this part only specific details related to the algorithm for forming a set of parameters will be given.

Step 1: Entry of input parameters-population size, no. of generations, no. of parents, mutation probability, crossover probability

Step 2: Randomly generation of a bit binary string-chromosome

Step 3: Checking feasibility of chromosome. If chromosome is feasible then go to step 4. If not go to step 2.

Step 4: Calculate MRR of chromosome

Step 5: Store chromosome p_i in the set P

Step 6: Checking if population size is equal to the cardinality of set P. If it equal go to step 7. If not go to step 2

Step 7: Transmit the set P to the interaction module via data in data interface

Now, the set of feasible chromosome is formed which representation the set of cutting parameters with MRR calculated for each of them.

2.2 Module for tool path generation and optimization

In contour milling, the tool path represents an ordered set of points where the tool is positioned, moving in the direction of the auxiliary motion velocity vector. If n is the number of points in that set, then theoretically there are $n!$ potential toolpaths. If restrictions are taken into account, then that number decreases but is still very large. Discretization can be modelled as pixelization-mapping of the surface being processed with a large number of squares [8], basically cover the surface being processed very well, but then their number, that is, the resolution of the grid of squares goes up to 0.01 mm is the usual resolution of today's CNC machines. Such a data set is very

large for processing by metaheuristic methods, especially GA, which can lead to the fact that it is not possible to find a solution that converges to the optimal one in an acceptable time [9]. Other approach is surface discretization by placing up an equidistant grid of points on the surface to be processed, but this method gives good results only in cases of rough contour milling [10]. For the purpose of integrated optimization of tool path and cutting parameters discretization of the surface is done by placing points at a distance equal to the radial cutting depth a_e which is part of the set of parameters of the cutting mode. Example of discretization is shown in Figure 6.

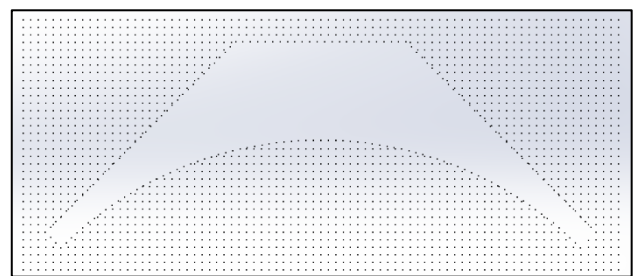


Figure 6. Surface discretization

Distance between points in point grid is equal to a_e with the exception of the points located on the offset contour of the work piece. It is clear that contour of work piece is offset for half of tool diameter D . The algorithm for tool path generation and optimization can be found in [11] and here a brief description of the most important features will be given. It is based on, in the literature, widely known problem of the Traveling Salesman Problem (TSP) [7].

A 3 axes CNC machine moves in both x and y directions simultaneously and Euclidean distance function is to be used to calculate the distance between points. In this way a distance matrix $D=[d_{ij}]$ between points (Figure 6) is created. Let M is a set of points obtained by surface discretization

Let i and j be two arbitrary points from set M .
Input variables of the proposed model

- the set of points described by the point map $M=[m_{ij}]$,
- the distance matrix $D=[d_{ij}]$ between the points of the set M
- maximum TEA θ_{max} in degrees

- tool diameter d in mm
- speed of main spindle n (rev/min)
- feed rate $F = f_z \cdot z \cdot n$ (mm/min)
- rapid feed rate F_{bh} (mm/min)

Control variables of the proposed model

$$X_{ij} = \begin{cases} 1 & \text{if point } i \text{ is immediately by } j \\ 0 & \text{otherwise} \end{cases} \quad (5)$$

$$Y_{ijk} = \begin{cases} 1 & \text{if tool travels from } i \text{ to } k \text{ in same dir.} \\ 0 & \text{otherwise} \end{cases} \quad (6)$$

$$Z_{ij} = \begin{cases} 1 & \text{if } j \text{ is machined} \\ 0 & \text{otherwise} \end{cases} \quad (7)$$

$$\Theta_{ij} \text{ TEA when moving from } i \text{ to } j \quad (8)$$

Constraints of the proposed model

- 1) Constraint that ensure that every point from set M is visited by the tool at least once

$$\forall j \in \{0 \dots N\} \sum X_{ij} > 0 \quad (9)$$

- 2) Constraint that ensure that tool leaves each point after visiting for another

$$\forall j \in \{0 \dots n\} \sum_{i=0}^n X_{ij} \sum_{k=0}^n X_{jk} \quad (10)$$

- 3) Constraint that ensure that every point is followed by a different point and path moves on

$$\forall j \in \{0 \dots n\} X_{ii} = 0 \quad (11)$$

- 4) From each subset of points the tool must be positioned at least once in another point that is not part of the of that subset of points

$$\forall Q \subset \{0 \dots n\}: Q \neq \emptyset$$

$$\sum_{\{i,j \in N\}: i \in Q, j \in N \setminus Q} X_{ij} + \sum_{\{i,j \in N\}: i \in Q, j \in N \setminus Q} X_{ji} \geq 2 \quad (12)$$

- 5) Constraint to ensure that the tool engagement angle Θ_{ij} must be smaller or equal than the maximum allowed engagement angle Θ_{max}

$$\forall j \in \{0 \dots n\} \sum_{i=0}^n X_{ij} \cdot \theta_{ij} \leq \theta_{max} \quad (13)$$

- 6) Constraint that ensure that during the chip removal process, the movement of the tool is allowed only towards neighbor points.

$$\forall j \in \{0 \dots n\} \sum_{i=0}^n Z_{ij} \cdot X_{ij} = 0 \quad (14)$$

The objective function

The objective function of the proposed model represents the criteria of optimization. In the observed model the goal is to achieve high productivity, thus minimization of processing time, with minimization of the jerk effect with as uniform tool angle of engagement as possible and also

Minimization of the processing time, can be written as:

$$F_{c1} = \min \sum_{i=1}^n \sum_{j=1}^n \left(\frac{d_{ij}}{F} + \frac{r_{ij}}{F_{bh}} \right) \cdot X_{ij} \quad (15)$$

where d_{ij} are the distance between the points of the path in which the tool moves in a feed rate and r_{ij} the distance between the points of the path in which the tool moves in a rapid rate.

The minimization of the number of changes in the direction of movement of tool, taking into account the control variable defined by expression (6) can be written as:

$$F_{c2} = \min \sum_{i=1}^{n-2} \sum_{j=2}^{n-1} \sum_{k=3}^n \frac{1}{Y_{ijk}} \quad (16)$$

The third goal of optimization is the smallest possible deviation of the TEA from the target value and can be defined as:

$$F_{c3} = \min \sum_{i=1}^n \sum_{j=1}^n |\theta_{ij} - \theta_c| \cdot X_{ij} \quad (17)$$

that is, as a minimization of the deviation of the TEA value at each point of the path in relation to the target value.

The problem of milling path optimization is clearly multi objective optimization problem. For the purpose of this research the method of weight coefficients will be applied. Determining the weight coefficients can be a problem [7] because the vector of weight coefficients controls the optimal solution. Mathematically,

the optimal solution obtained with equal weighting coefficients should lead to the smallest conflict between the optimization goals, but in practice it is often not a satisfactory solution, so when determining the weighting coefficients, it is always necessary to have information in the order of priority of the goals. For the purposes of this paper, the greatest weight will be given to achieving maximum productivity so objective function is defined by following expression

$$F_c = 0,5 \cdot F_{c1} + 0,25 \cdot F_{c2} + 0,25 \cdot F_{c3} \quad (18)$$

Chromosome representation

Now it is necessary to define an appropriate genetic representation or an appropriate coding method. In the model being observed so that the chromosome coding solution with a vector of real components will be given.

As mentioned earlier in this paper the geometry of working piece is already recognized. The coordinates of every point is known so the distance matrix $D=[d_{ij}]$ can be easily determined. In the observed model, the tool can pass through any point of the map of points several times, with the fact that it only passes once to remove chips, and it can pass through the same point again only for the purpose of approaching the cutting zone. Thus, the gene in the chromosome is marked with a natural number and represents the ordinal number of the point of the point map through which the tool passes. The tool can move from one point to another either at feed rate or rapid rate depending on whether the chip is removing or tool positioning is performed. Therefore, it is necessary to know the speed with which the tool moves from the point i and arrives at the point j . The next segment that describes the trajectory of the cutter is the engagement angle θ_{ij} which can be $\theta_{ij} = 0$ if the tool is moving at rapid rate or $\theta_{ij} > 0$ if the tool is moving at feed rate. In addition to knowing the x and y coordinates of each path point, it is also necessary to know the z coordinate, i.e. the plane in which the center of the tool moves and the condition of the point i.e. if is previously machined or no. An example

of fully decoded chromosome is given in Table 3.

Initial population

Using the distance matrix $D=[d_{ij}]$, it is necessary to form another set of points which is very important for generating the initial population. That set K is the set of the closest points of each point of the point map, which contains all the k closest points to the point where the center of the tool is located. In the observed model, there can be up to 24 closest points to each point of the point map, and the x and y coordinates of the members of that set tell to which point the tool can move from any current point of the path. By forming the set K, a part of unacceptable or illegal paths is eliminated, i.e. the constraint defined by expression (13) is implemented. When all points of set K is visited by the tool then next random point of tool path is chosen. At the initial moment. only the points located in the first and last row and the first and last column of the map of points have the condition *machined=true* and that point are peripheral points status of peripheral points, all other points have the status *machined=false*, i.e. the status of unprocessed points. It is clear that the first point of any milling path must be one of the points with status *machined=true*. Furthermore, the algorithm for forming the initial population is given below:

Step 1: Randomly select the initial point from the set of points M with *machined=true*

Step 2: For a randomly selected point from step 1, load the previously determined set of nearest points K to the randomly selected point.

Step 3: Randomly choose one point from the set K in the label j that has the status of an unprocessed point i.e. *machined=false*

Step 4: Calculate the milling angle θ_{ij} when moving from i to j.

Step 5: If $\theta_{ij} \leq \theta_{max}$, point j becomes a tool path point. If $\theta_{ij} \geq \theta_{max}$ max then go to step 10.

Step 6: Assign status *machined=true* at point j.

Step 7: Calculate the vector product of vectors and $\vec{ix}\vec{j}$ if the vector product is different from zero, increase the control variable $t=t+1$, if it is equal to zero, the control variable t keeps its previous value.

Step 8: Calculate $|\theta_{ij} - \theta_c|$. Control variable $d = d + |\theta_{ij} - \theta_c|$.

Step 9: Check the statuses of the neighboring points of point j . If the statuses are machined=true, then point j becomes a peripheral point, i.e. the status of point j machined=true

Step 10: Repeat steps 3-9 for each point from the set K .

Step 11: Repeat steps 1-10 for each point in the set M until all points from the set M have status machined=true

Step 12: Repeat steps 1-11 for each individual from the initial population

Table 1. Decoded chromosome

	1	3	8	5	4	2	10	7	9	8	3	5	6
F (mm/min)	F_{bh}	F	F	F	F	F	F	F	F	F_{bh}	F_{bh}	F	F
θ_{ij} (°)	0	40	42	25	30	35	39	41	42	0	0	0	30
x (mm)	20	22	24	26	28	30	32	32	34	24	22	26	26
y (mm)	6	6	6	6	6	6	6	6	6	6	6	6	10
z (mm)	50	0	0	0	0	0	0	0	0	50	50	0	0
Machined	true	false	false	false	false	false	false	false	false	true	true	false	false

By forming the initial population whose size is the input parameter of the genetic algorithm, the initial set of possible tool paths is formed. By choosing the parents, that is, two tool paths, and applying the genetic operators of crossover and mutation, and calculating fitness for each individual, that is, for each tool path, a path that converges to the optimal path is reached. Furthermore a pseudo code of proposed GA for tool path generation and optimization will be given. The detail description of fitness calculation, parents selection, crossover and mutation operator as mentioned can be found in [11].

Input parameters for GA are: Set of point M , TEA target value, diameter of the tool, the population size, the number of parents, mutation rate and the number of generations.

Start

Enter the input parameters
 Create Points map, Distant matrix and Matrix of neighbors K of each point
 Create Initial population
 Calculate the fitness of individuals of the first generation

 Generation = 1
 Repeat
 Selection of parents
 Children = 0
 Repeat

 Pick of two parents for a crossover (Parent1, Parent2)
 Crossover OX (Parent1, Parent2)
 Mutation
 Children = Children + 1
 Until Children = population size-total number of parents
 Generation = Generation + 1
 Calculate the fitness of individuals for the current generation
 Until generation = total number of generations
End.

In the next section algorithm for interaction between cutting parameter optimization and tool path generation and optimization will be shown.

2.3 Interaction module

In this chapter, a two-stage algorithm based on analysis presented in [4], will be given that combines a GA for cutting parameter optimization and a GA for toolpath generation and optimization.

Step 1: Setting the parameters of both algorithms which includes population size, maximum number of iterations m , crossover probability, mutation probability, number of parents and number of generations.

Step 2: Execution of cutting parameters optimization algorithm which generates set of cutting parameters.

Step 3: Transmission of a set of generated cutting parameters to tool path optimization module via data interface.

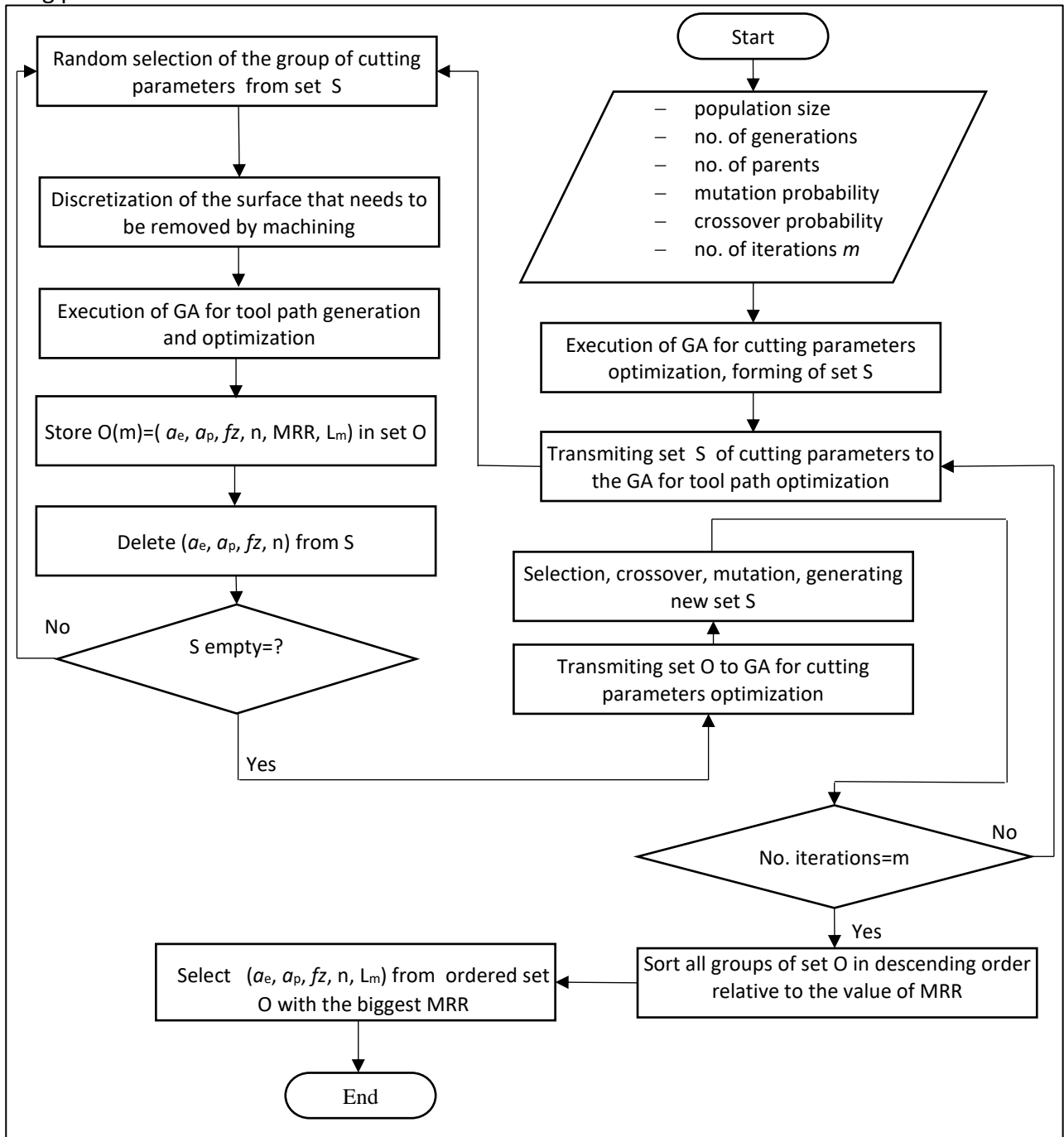


Figure 7. Flowchart of proposed algorithm for integrated optimization

Step 4: One group (a_e, a_p, fz, n) of cutting parameters is randomly selected from the set P.

Step 5: Discretization of the surface that needs to be removed by machining, by imposing a grid of points, based on the selected radial depth of cut a_e

Step 6: Execution of tool path generation and optimization algorithm, which give the

optimum tool path for used set of cutting parameters.

Step 7: The group of cutting parameters with MRR and optimum tool path is stored in set O

Step 8: The extracted group of cutting parameters is deleted from set P

Step 9: Is set P empty=?

Step 10: If yes, optimum objective set O is transmitted to the cutting parameters module via data interface, if not go to step 4.

Step 11: In the cutting parameters module a series of operations is conducted, including selection, crossover and mutation to obtain new population of cutting parameters.

Step 12: Is reached maximum number of iterations for cutting parameters optimization algorithm=?

Step 13: If yes, then the process of generation the optimum objective set O (group of cutting parameters and the tool path) is finished, if not go to step 3.

Step 14: Sort all groups of set O in descending order relative to the value of MRR

Step 15: The first group of ordered set O is selected as the optimal set of cutting mode parameters with the corresponding tool path.

Step 16: Information about optimal set of cutting parameters and corresponding tool path is transmitted to the module for generating NC code via data interface

For better understanding of proposed algorithm for integrated optimization a flowchart is given in a Figure 7. The basic idea is that the set of groups of the cutting parameters is formed several times, that is, that more populations of individuals are formed, which would significantly increase the diversity of population. Each of those individuals is sent to the tool path generation and optimization module, which increases the diversity of the individuals represented by the tool paths, and the information about the best tool path for the corresponding group of cutting parameters is sent to the cutting parameter optimization module, where by applying elitism can be selected the best individuals or groups of cutting mode parameters in the next iteration. In this way, the diversity of individuals in the GA is preserved, but this prevents its premature convergence towards the optimal solution, and at the same time bad individuals are eliminated from the population.

3. CONCLUSION

The classic method of creating NC programs relies on CAM software and the experience of the programmer. Even then, the time of creating the program can be long and there is no guarantee that the machining time will be as short as possible which is necessary condition for minimizing the production costs. In the recent decades, there has been a growing trend in the literature in developing models for tool path generation and optimization as well as cutting parameters optimization in order to automate the process of NC code generation. These problems are being observed separately, regardless of the fact that the cutting parameters affect the generation of the tool path. This research deals with the possibility of integrated optimization of cutting parameters and tool path generation and optimization. For this purpose, the theoretical framework of integrated optimization as well as the algorithm that integrates the optimization of cutting parameters and tool path are given, as a prerequisite for the automatic generation of the NC code, that is, the technological procedure in the narrower sense.

REFERENCES

- [1] D. Khatiwada, D. Nepali, N. Raj, A. Bhattarai: Tool path optimization for drilling holes using genetic algorithm, *International Journal of Machine Tools and Maintenance Engineering*, 1(1):36-42, 2020
- [2] S. Bharath, K.R. Natraj: Application of Artificial Intelligence Methods of Tool Path Optimization in CNC Machines, *International journal of engineering research and technology*, Volume 06, Issue 14, 2018
- [3] J. Rai. D. Brand, M. Slama. P. Xirouchakis: Optimal selection of cutting parameters in multi-tool milling operations using a genetic algorithm. *International Journal of Production Research*, Volume 49, No. 10, 3045-3068. 2011
- [4] S. Jia, S. Wang, N. Zhang et al.: Multi-objective parameter optimization of CNC plane milling for sustainable manufacturing, *Environmental Science and Pollution Research*,

<https://doi.org/10.1007/s11356-022-24908-3>,
2022

- [5] Lj. Tanović, Y. Petrakov: Teorija i simulacija procesa obrade, *Mašinski fakultet*, Beograd, 2007
- [6] A. Dumitrache, T. Borangiu, A. Dogar: Automatic Generation of Milling Toolpaths with Tool Engagement Control for Complex Part Geometry, in: *IFAC Proceedings*, Volumes, 43, 252-257, 2010
- [7] S. R. Singiresu: Engineering optimisation-theory and practice, Fourth edition, *John Wiley & Sons, Inc.*, Hoboken, New Jersey, 2009
- [8] M. Kumar, P. Khatak: Implementation of Genetic Algorithm in Multiobjective Optimization of Milling Toolpath, *International Journal of Emerging Technologies and Innovative Research*, ISSN:2349-5162, Vol.5, Issue 5, page no.1147-1155
- [9] J. Barclay, V. Dhokia, A. Nassehi: Generating milling tool paths for prismatic parts using genetic programming. *Procedia CIRP*, 33, 490-495. 2015
- [10] W. Essink, A. Nassehi, S. T. Newman: Toolpath Generation for CNC Milled Parts Using Genetic Algorithms, Enabling Manufacturing Competitiveness and Economic Sustainability (pp.189-193), doi:10.1007/978-3-319-02054-9_32, 2015
- [11] P. Mitić, M. Zahar Đorđević, V. Petronijević, N. Abadić. A. Đorđević: Automatic tool path generation in contour milling using genetic algorithm, *14th International Quality Conference, Quality Festival 2023*, Kragujevac, 2023, 24-27 May, pp. 663-680, ISBN 978-86-6335-104-2



Society of Production
Engineering

SPMS 2023

39. Savetovanje proizvodnog mašinstva Srbije

ICPES 2023

39th International Conference on Production Engineering of
Serbia



Faculty of Technical
Sciences
University of Novi Sad

Novi Sad, Serbia, 26. – 27. October 2023

REVIEW OF THE FIRST GENERATION OF THE ADVANCED HIGH-STRENGTH STEELS (AHSS) AND THEIR MANUFACTURING PROCEDURES

Djordje IVKOVIĆ^{1*}, Dragan ADAMOVIĆ¹, Dušan ARSIĆ¹, Nada RATKOVIĆ¹, Ružica NIKOLIĆ²

¹Faculty of Engineering, University in Kragujevac, Serbia

²Research Centre, University of Žilina, Slovakia

*Corresponding author: djordje.ivkovic@fink.rs

Abstract: *The objective of this paper was to present the first generation of Advanced High-Strength Steels (AHSS) and their manufacturing processes, as well as to emphasize their complexity. The AHSSs were created as a solution to reduce the weight of parts and structures in transportation industries (automotive, airplane and truck industry). Regarding the development of the AHSSs, it was divided in three generation. The first generation, to which this paper relates, includes the DP (Dual-Phase), CP (Complex-Phase), TRIP (TRansformation Induced Plasticity) and martensitic steels. Besides implementation of materials with higher strength, lower mass of structures could be achieved by application of materials of a lower density (e.g., aluminum and titanium). Application of the lightweight materials directly results in lowering the structures' mass, and it positively affects energy efficiency, preservation of the environment and lowering the pollution levels. However, there are still numerous problems and disadvantages, related to application of lightweight materials, primarily with processing (low machineability, deformability, as well as weldability). Besides the processing problems, mentioned materials have higher prices than steel; therefore, development of new steel grades, as well as development of new methods for realizing the higher strength was initiated. It is already well known from the literature that by implementing the selected heat treatment procedures (varying the heating and cooling regimes), the steel properties could be altered. It was thus concluded that combination of the heat treatment and plastic deformation in steel production can result in increasing the steel strength, while simultaneously keeping the good deformability and even weldability.*

Key words: AHSS, heat treatment, strength, quenching, annealing, tempering.

1. INTRODUCTION

As the trends in modern industry are increasingly oriented towards the preservation of natural resources, increasing energy efficiency, reducing the harmful gases emission, as well as the carbon footprint, it is necessary to make adequate changes to fulfill the mentioned requirements. In the transportation industry, the change that effectively provides for these requirements to be met is actually

related to reducing the mass of the steel structures. By using the composite or light-weight materials (Al, Ti and their alloys) that have the lower density and/or higher strength than steels, the mass of the structure can be significantly reduced. At the expense of the smaller mass, obtained by use of these materials, the production process is made more difficult due to their poor machinability by cutting and deforming, as well as poor weldability of the composite and light-weight

materials, which all result in the price increase of the final product. To keep the processing method as simple as possible and the products' price as low as possible, development of the special high-strength steels started in the last decades of the 20th century. Compared to the classic steels, the new materials have significantly higher strength, with their machinability by cutting and deforming, as well as weldability, being at the required level. The high strength of these steels is a result of application of the complex thermal (heat), thermomechanical and mechanical processing procedures. Thus, the high strength allows the dimensions of the cross-sections of parts to be smaller; subsequently the amount of material used and the weight of structures became smaller.

2. REVIEW OF THE GENERAL CHARACTERISTICS OF THE AHSSs OF THE FIRST GENERATION

Sheets of tensile strength higher than 500 MPa belong to a group of the so-called high-strength steels (HSS). They possess a complex microstructure, which is usually composed of ferrite, bainite, martensite and residual austenite. The first generation AHSSs includes the Dual Phase steels (DP), Complex Phase steels (CP), TRansformation Induced Plasticity steels (TRIP) and the martensitic steels. These steels were created as a result of the need for materials of a greater strength as compared to the classic steels. As with other steel materials, the rule applies here that as the strength

increases, the plasticity decreases. From figure 2.1 one can conclude that the TRIP steels have the lowest strength but the highest plasticity, while for the martensitic steels the situation is quite opposite. They have the highest strength, but the lowest plasticity, [1].

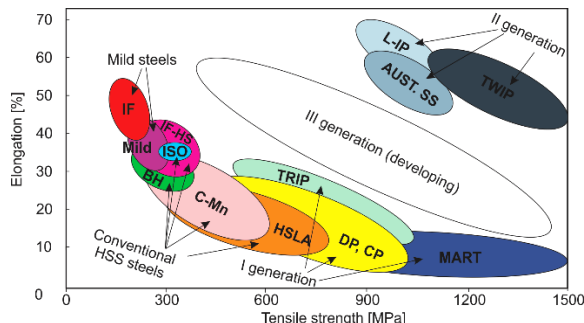


Figure 2.1 Mechanical characteristics of the advanced high strength steels

2.1 The DP (Dual-phase) steels

Due to the favorable relationship between the strength and plasticity, the DP steels have the greatest application in the automotive industry. The tensile strength value ranges from 420 to 1030 MPa, and the elongation from 5 to 28 %. The chemical composition of some of the DP steels is shown in table 2.1, while their mechanical properties are shown in table 2.2. The microstructure of the DP steel is made of a ferritic matrix containing martensite. The maximum share of martensite is 40 % and the steels' mechanical characteristics depend on it [1, 2]. An example of microstructure of the DP steel is shown in Figure 2.2.

Table 2.1 Chemical composition of certain DP steels' classes, [2]

Notation according to EN 10336:2006	max %C	max %Si	max %Mn	max %P	max %S	%Al	max %Cu	max %B	max %Ti+Nb	max %Cr + %Mo
HCT490X	0.14	0.5	1.8	0.05	0.01	0.01-1.5	0.2	0.005	0.15	1.0
HCT780X	0.18	0.8	2.5	0.05	0.01	0.015-1.0	0.2	0.005	0.15	1.4
HCT1180G2	0.23	1.0	2.9	0.05	0.01	0.015-1.0	0.2	0.005	0.15	1.0

Table 2.2 Mechanical characteristics of certain DP steels' classes, [2]

Notation according to EN 10336:2006	$R_{p0.2}$, MPa	R_m , MPa	A_{80} , %
HCT490X	290-380	490-600	24
HCT780X	440-550	780-900	14
HCT1180G2	900-1100	1180-1350	5

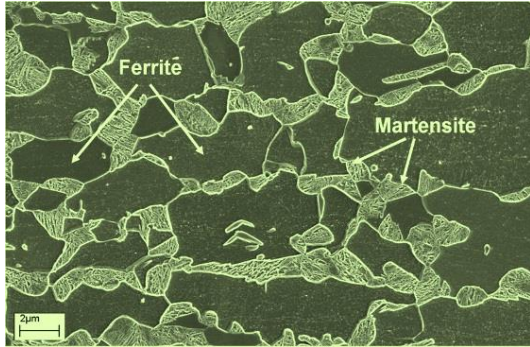


Figure 2.2 Ferritic-martensitic microstructure of the DP steels, [3]

different structural phases. The chemical composition of these steels is similar to composition of the DP steels. They are characterized by the high strength, while their plasticity is very low. They are the most widely used for production of columns and beams, as well as other simpler parts in the automotive industry [4].

As an example, the CP 800 steel microstructure is shown in Figure 2.3. It contains 42 % ferrite, 40 % bainite, 13 % martensite and 5 % residual austenite, [1, 4].

2.2 The CP (Complex Phase) steels

These steels were so named due to their microstructure, which contains several

Table 2.3 Chemical composition of certain CP steels' classes, [4]

Notation according to EN 10346:2009	max %C	max %Si	max %Mn	max %P	max %S	%Al	max %Cu	max %B	max %Ti + %Nb	max %Cr+%Mo
HCT600C	0.1	0.4	1,6	-	-	-	-	-	-	-
HCT780C	0.18	1.0	2.5	0.05	0.01	0.15-1.0	0.2	0.005	0.15	1.0
HCT980C	0.23	1.0	2.7	0.05	0.01	0.015-1.0	0.2	0.005	0.15	1.0

Table 2.4 Mechanical characteristics of certain CP steels' classes, [4]

Notation according to EN 10336:2006	$R_{p0.2}$, MPa	R_m , MPa	A_{80} , %
HCT600C	360-440	600-700	19
HCT780C	570-720	780-920	10
HCT980C	780-950	980-1140	6

2.3 The transformation induced plasticity (TRIP) steels

Steels of this class contain carbon in the range of 0.1 to 0.4 % and alloying elements, such as Si, Al, Ti, Ni and V. Depending on the chemical composition of these steels, their strength ranges from 500 to 1050 MPa, and elongation from 12 to 32 %. Due to the good ratio of strength and plasticity, they are intended for the manufacturing the complex parts of automobile structures. The chemical composition and mechanical characteristics of some of the TRIP steels are presented in tables 2.4 and 2.5, respectively, [1,4].

The microstructure of the TRIP steels is complex. It basically consists of a ferrite-bainite matrix containing 5 to 20 % residual austenite. Thanks to this microstructure, these steels have good deformability properties. The share of ferrite in the ferrite-bainite matrix has the greatest impact on mechanical properties of these steels, [1, 5].

Table 2.4 Chemical composition of the TRIP steels, [5]

Notation according to EN 10346:2009	max %C	max %Si	max %Mn	max %P	max %S	%Al	max %Cu	max %B	max %Ti + %Nb	max %Cr+ %Mo
HCT690T	0.24	2.0	2.2	0.05	0.01	0.015-2.0	0.2	0.005	0.2	0.6
HCT780T	0.25	2.2	2.5	0.05	0.01	0.015-2.0	0.2	0.005	0.2	0.6

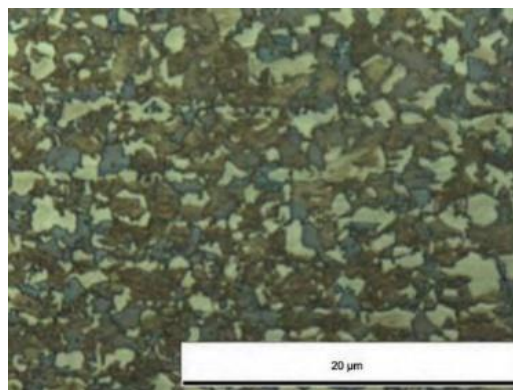


Figure 2.3 Microstructure of the CP800 steel, [1]

Figure 2.4 shows an example of the TRIP steel's microstructure.

A special feature of the TRIP steels is the increase in strength during deformation, since the residual austenite is transformed into martensite [6]. That is why these steels are primarily used for production of the car body parts that are the most often exposed to deformation during a collision. The increase in strength of the parts during their deformation directly affects the increase in the safety of passengers in the car [1, 5].

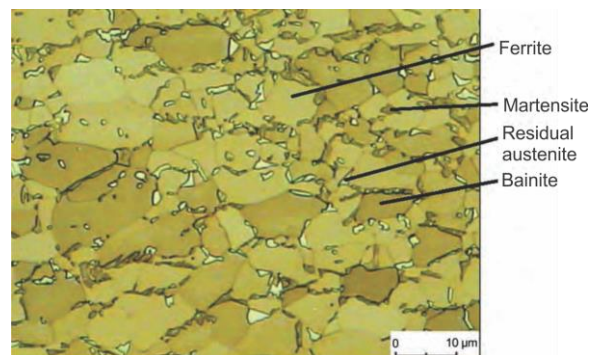


Figure 2.4. Microstructure of TRIP steels [1]

Table 2.5 Mechanical characteristics of the TRIP steels, [5]

Notation according to EN 10346:2009	$R_{p0.2}$, MPa	R_m , MPa	A_{80} , %
HCT690T	40-520	690-800	24
HCT780T	450-570	780-910	21

2.4 Martensitic steels

These steels were developed due to the need for steels with extremely high values of tensile strength. Their microstructure contains predominantly martensite, due to which the tensile strength of these steels is within range 720 to 1680 MPa, and the elongation is within range 3 to 15 %. The chemical composition and mechanical characteristics of some martensitic steels

are shown in tables 2.6 and 2.7, respectively. Due to those exceptionally high mechanical properties, these steels are often subjected to tempering prior to forming, or the forming is done with preheating, and the forming itself is done in a tool that is cooled by the flowing water. In this way, the molded part obtains the martensitic structure, which comes as a result of the contact between the material in the initial state and the working surfaces of the tool [1, 7].

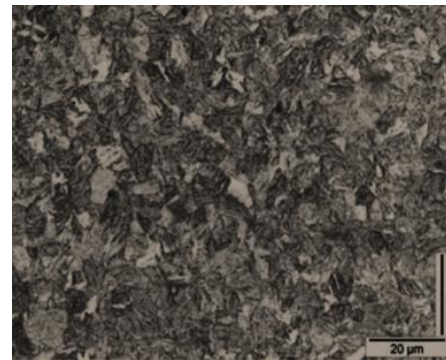
Table 2.6 Chemical composition of certain martensitic steels' classes, [7]

Notation according to VDA 239-100	Max %C	Max %Si	Max %Mn	Max %P	Max %S	%Al	Max %Cu	Max %B	Max %Ti + %Nb	Max %Cr+ %Mo
CR1030Y130T-MS	0.28	1.0	2.0	0.02	0.025	≥ 0.010	0.2	0.01	0.15	1
CR1220Y1500T-MS	0.28	1	2	0.02	0.025	≥ 0.010	0.2	0.01	0.15	1
CR1350Y1700T-MS	0.35	1	3	0.02	0.025	≥ 0.010	0.2	0.01	0.15	1

Table 2.7 Mechanical characteristics of certain martensitic steels' classes, [7]

Notation according to VDA 239-100	$R_{p0.2}$, MPa	R_m , MPa	A_{80} , %
CR1030Y130T-MS	1030-1330	1300-1550	3
CR1220Y1500T-MS	1220-1520	1500-1750	3

As emphasized at the beginning, these steels' microstructure is composed of a martensitic matrix containing small shares of ferrite and bainite. The martensitic steel CR1220Y1500T-MS microstructure is presented in figure 2.5.

**Figure 2.5** Microstructure of the martensitic steels, [1]

3. REVIEW OF PROCEDURES FOR OBTAINING THE THIN SHEETS OF INCREASED STRENGTH STEELS OF THE FIRST GENERATION

3.1 Thermal and thermomechanical processes for obtaining the DP steels

The name of these steels indicates that there are two phases in their microstructure. That structure consists of a ferrite matrix in which martensite particles are wedged. The maximum share of martensite in the microstructure of these steels is 40 %, and with that share increase in the microstructure, the strength and hardness increase, as well, [1].

The production of the cold-rolled DP steels is primarily based on the heating and heating-through of the previously obtained cold-rolled steel strips of the appropriate chemical composition, to a temperature in the interval between A_{c1} and A_{c3} . In this temperature interval, the microstructure of the steel consists of ferrite and austenite. With an increase in the heating temperature (approaching the critical temperature A_{c3}), the proportion of austenite increases, as well as the amount of carbon that can be dissolved in the austenite. To limit the share of martensite to 40 %, the maximum heating and heating-through temperature of these steels should be 800 °C, [1].

The heating-through is followed by cooling, where the cooling rate is higher than the critical one. In that way, the austenite with dissolved carbon forms martensite particles, which are distributed in the ferrite matrix. Figure 3.1 shows the thermal cycle for obtaining the cold-rolled DP steel, [1].

Obtaining the hot-rolled DP steel first assumes that the appropriate semi-finished product from the ironworks is heated to a temperature between 1180 and 1250 °C, when it is rolled. After obtaining a strip of appropriate thickness, it is slowly cooled to a temperature between A_{c1} and A_{c3} , to obtain a mixture of ferrite and austenite in the microstructure. This is followed by the rapid cooling from that range, which results in the two-phase microstructure.

The schematics of this procedure is presented in Figure 3.2, [1].

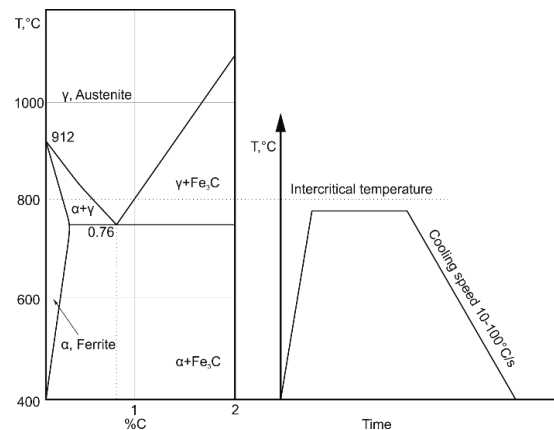


Figure 3.1 Thermal cycle for obtaining the cold-rolled DP steels

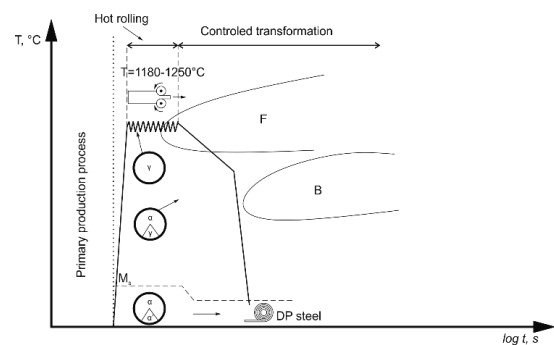


Figure 3.2 Schematics of producing the hot-rolled DP steels

3.2 Thermal and thermomechanical processes for obtaining the CP steels

The CP steels have an interphase microstructure. It consists of a ferrite-bainite matrix in which there are small shares of martensite, residual austenite and pearlite. Obtaining these steels implies that the starting semi-finished product is first heated to the high-austenitic temperature region, where the carbon content is 0.2 %. After the heating, the steel is cooled down to a temperature between 800 and 900 °C, when it is rolled. After the rolling, the part is heated-through for 60 s, during which the ferrite-austenitic structure is obtained, and the carbon content increases to 0.4 %. The heating-through is then followed by the slow cooling to a temperature of 450 °C, where the steel is isothermally held for 90 s, which results in formation of a small share of bainite, and the carbon share increases to 1.2 %. After the

isothermal holding, the thin strips are wound and then cooled to a room temperature. The thermal process of obtaining these steels is shown in Figure 3.3, [1].

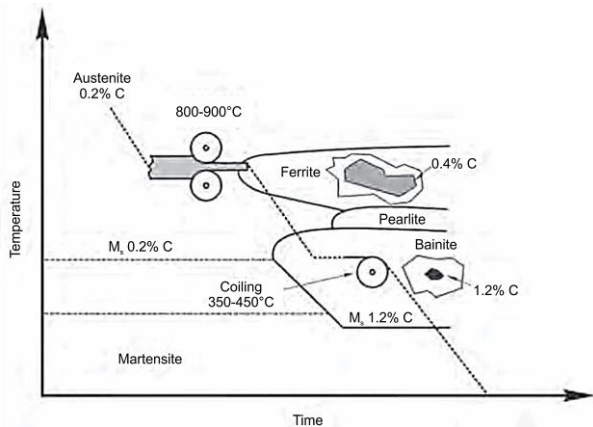


Figure 3.3 Thermomechanical process of obtaining the CP steels

3.3 Thermal and thermomechanical processes for obtaining the TRIP steels

The microstructure of these steels is also the interphase one. It is formed from a ferrite matrix in which the residual austenite and bainite are wedged. The process starts with rolling in the austenitic region, followed by cooling to 800 °C. At this temperature, the steel is heated-through for 60 s, which is followed by rapid cooling to 450 °C, where the steel is held isothermally for 90 s. This isothermal holding results in formation of a certain amount of bainite in the ferrite matrix. After the holding at 450 °C, the steel is wound to a coil and cooled to ambient temperature. The comparison of procedures for obtaining the DP and TRIP steel is schematically shown in Figure 3.4, [1].

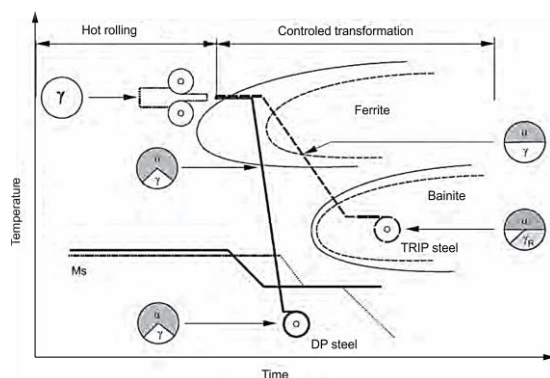


Figure 3.4 Comparison of production procedures of the DP and TRIP steels

3.4 Thermal and thermomechanical processes for obtaining the martensitic steels

Steels of this kind predominantly contain martensite in microstructure. It is obtained in two ways, while both ways imply the rapid cooling of the steel from the austenite region.

The first way of obtaining refers to the hot-rolled steels, which are cooled down quickly, immediately after the rolling at elevated temperatures is finished, [1].

The second method implies that the previously obtained sheet metal strips are heated above the critical temperatures; they are then heated-through at those temperatures and then cooled quickly, [1].

In both cases, due to heating to temperatures within the range 900 - 950 °C and rapid cooling, the final microstructure of the steel is martensite, [1].

Figure 3.5 shows the thermomechanical and thermal processes for obtaining these steels.

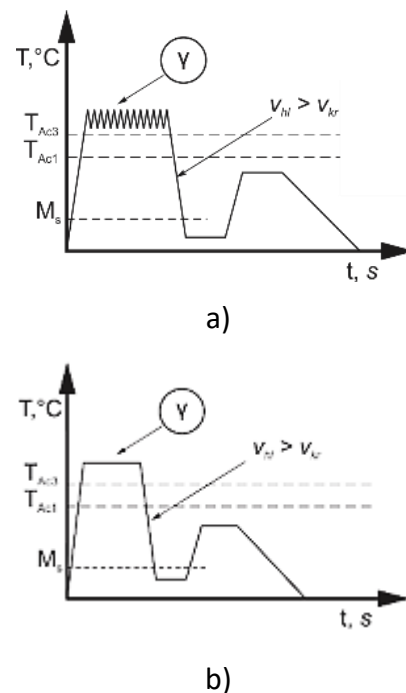


Figure 3.5 Thermomechanical (a) and thermal (b) ways of obtaining the martensitic steels

4. CONCLUSIONS

Due to the increase in people's awareness of the necessity to reduce the environmental pollution, to use natural resources more rationally, development of the new steel

materials, which compared to Al and Ti alloys, have a significantly higher specific mass and strength, but a lower price, better workability and weldability (special requirements related only to cleaning and preheating of parts prior to welding), has been initiated. As an answer to this tendency, the new grades of advanced high strength steels (AHSS) have been developed. Depending on the level of development, three groups of advanced high-strength steels are distinguished. A review of the first generation of the AHSSs and some procedures for their production was conducted. From the presented data, one can conclude that these steels have high strength; however, simultaneously they are characterized by low deformability, which has caused numerous difficulties. This is why the development of the second generation AHSSs has begun. The advanced high-strength steels of the second generation are characterized by slightly lower strength than the first-generation steels; however, they possess the significantly better deformability.

ACKNOWLEDGEMENT

This research was partially financially supported through the projects TR35024 and TR33015 financed by the Ministry of Science of the Republic of Serbia. Research was also partially financed by statutory research of the Czestochowa University of Technology.

REFERENCES

- [1] M. Demeri, *Advanced High-Strength Steels*, Science, Technology and Application, ASM International, USA, 2013
- [2] https://automotive.arcelormittal.com/products/flat/first_gen_AHSS/DP, Excerpts from the manufacturer's catalogue *ArcelorMittal*, electronic form; accessed on 24.12.2021.
- [3] <https://www.ispatguru.com/dual-phase-steels/>, accessed on, 24.12.2021.
- [4] https://automotive.arcelormittal.com/products/flat/first_gen_AHSS/CP, Excerpts from the manufacturer's catalogue

ArcelorMittal, electronic form; accessed on 24.12.2021.

- [5] https://automotive.arcelormittal.com/products/flat/first_gen_AHSS/TRIP, Excerpts from the manufacturer's catalogue *ArcelorMittal*, electronic form; accessed on 24.12.2021.
- [6] D. Radović, *Modern steels: Transformation induced plasticity, Welding and welded structures*, 4/2011 pp. 167-170.
- [7] https://automotive.arcelormittal.com/products/flat/martensitic_steels/martinsite, Excerpts from the manufacturer's catalogue *ArcelorMittal*, electronic form; accessed on 24.12.2021.



Society of Production
Engineering

SPMS 2023

39. Savetovanje proizvodnog mašinstva Srbije

ICPES 2023

39th International Conference on Production Engineering of
Serbia



Faculty of Technical
Sciences
University of Novi Sad

Novi Sad, Serbia, 26. – 27. October 2023

EFFECTS OF APPLYING A HYBRID MILLING PROCESS ASSISTED BY ULTRASONIC VIBRATIONS

Borislav SAVKOVIĆ^{1*}, Milenko SEKULIĆ¹, Aleksandar KOŠARAC², Dragan RODIĆ¹, Anđelko ALEKSIĆ¹, Slaviša MOLJEVIĆ², Jelica ANIĆ²

¹University of Novi Sad, Faculty of Technical Sciences, 21000 Novi Sad, Serbia

²University of East Sarajevo, Faculty of Mechanical Engineering, 71126 Lukavica, East Sarajevo, Republic of Srpska, Bosnia and Herzegovina

*Corresponding author: savkovic@uns.ac.rs

Abstract: *The combination of conventional milling and ultrasonic processing, or rather ultrasonic vibrations, resulted in a hybrid processing called milling supported by ultrasound. This paper includes a series of experiments comparing the output characteristics obtained by conventional milling and milling supported by ultrasound. Emphasis is placed mainly on the roughness of the processed surface, cutting forces, durability of the tool, etc. The article also deals with the process of longitudinal-torsional ultrasonic milling as well as the effects that are manifested during the processing of the difficult-to-machine alloy Ti-6Al-4V with an emphasis on the application of simulation based on the finite element method. It then shows the principles of ultrasonic milling of carbon fiber reinforced plastics. At the very end, final considerations are given and a conclusion based on the effects of introducing this hybrid procedure into production processes is presented.*

Keywords: *milling, hybrid process, ultrasound, characteristics, effectiveness.*

1. INTRODUCTION

In the modern machine industry, which is developing rapidly, the demand for better quality products with shorter production times is increasing day by day. This includes, in addition to the accuracy of production, the quality of the processed surface and other output characteristics, the choice of materials itself. Modern machine materials that have superior mechanical properties, such as Inconel 718, AISI 420 stainless steel, glass-ceramics, titanium alloys, nickel-based

superalloys, etc. are widely used in aviation, rocket (space), automotive and other industries, mainly in extreme working conditions, such as elevated temperature, corrosive environment, for responsible parts, parts under constant load, etc. Of course, such long-lasting and high-quality materials are very difficult to process, and thus represent a huge problem with conventional processing methods. This problem caused the intensification of hybrid processing, i.e. the combination of conventional processing procedures with non-conventional procedures.

One of the many hybrid processing procedures, which was the subject of this paper, is ultrasound-supported milling. The essence of this processing is to apply ultrasonic vibration of low amplitude, on the order of μm or nm , and high frequency, on the order of kHz , to the tool or workpiece. Many experimental studies, some of which are presented, have indicated the convenience and improvement of the output characteristics of this processing compared to conventional milling.

1.1 Practical application of ultrasound to the cutting process using plastic deformation and fracture of materials

Figure 1 shows the turning process in which workpiece 1 is machined with cutting tool 2. Cutting forces are mainly caused by plastic deformation of the layer being machined and by overcoming the external frictional forces present on the working surfaces of the tool. When ultrasonic vibration is applied to a cutting tool, both major components of the cutting force are reduced. The result is most pronounced if the direction of vibration coincides with the direction of cutting.

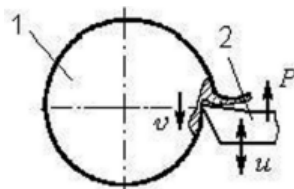


Figure 1. Applying ultrasound to the cutting process

The dependence of the cutting force P on the cutting speed v was obtained in experiments and is shown in Figure 2.

Curve 1 refers to traditional turning, while curve 2 is encountered when ultrasonic vibration is applied to the cutting tool during machining. An important observation of the experiment is the "disappearance" of the cutting force for values of velocity close to zero. The constant component of the cutting force is considered here. This is measured either by the torque generated by the workpiece, or the stress generated by the cutting tool during turning. As the cutting speed increases to a value of $v = a\omega$, the

cutting force increases monotonically to the value it would take in the absence of vibrations. Such a relationship between constant force and relative displacement speed is typical for systems with dry friction, under the influence of vibration within the friction zone.

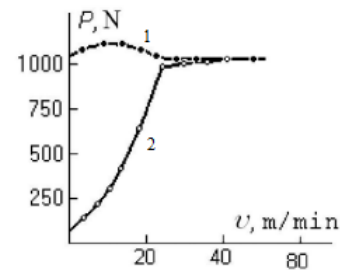


Figure 2. Dependence of cutting force on cutting speed [1]

2. ULTRASOUND SUPPORTED MILLING (USM)

USM is an advanced machining process that combines ultrasonic vibrations as an auxiliary mechanism in the milling process. Various studies have shown that ultrasound-supported cutting contributes to a reduction in temperature and cutting force, due to less contact friction between the tool and the workpiece. This results in greater stability, which can be up to 40% higher, while the roughness of the treated surface can be reduced up to two times. Today, the vibrating mechanism can be installed directly on the cutting tool or on the workbench. When a low-amplitude vibration is applied to a cutting tool or workpiece, it positively affects the machining process compared to conventional processing. A piezoelectric actuator is one of the devices that can produce a precise vibration amplitude (on the order of μm or nm) of high frequency (on the order of kHz) [3].

Many modern materials containing high strength, high temperature resistance such as stainless steels, titanium alloys, ceramics and other non-metallic materials are very difficult to machine with traditional machining methods. Using traditional cutting methods when processing such materials leads to breakage or destruction of the surface layer of the part, which results in poor quality of the

processed surface. It is also known that when machining some soft materials such as copper or aluminum, the cutting process is followed by a process in which the workpiece material sticks to the edge of the cutting tool. This also affects the deterioration of the surface quality of the workpiece.

The processing quality is improved by transforming the cutting process, by applying high-frequency (ultrasonic) vibrations to the very cutting edge of the tool. This is precisely why this process is called ultrasonic cutting. With this process, a number of effects were experimentally found during its realization. One of these effects is the reduction of the cutting force in the presence of vibrations, and it is most noticeable when the vibrations occur in the cutting direction. In addition to reducing the cutting force, ultrasound-supported cutting also leads to a decrease in temperature due to reduced friction between the tool and the workpiece, which contributes to an increase in the durability of the tool.

3. APPLICATION OF HYBRID MILLING PROCEDURE AND ITS EFFECTS

3.1. The effect of rotary ultrasonic elliptical milling (RUEM) on the surface integrity of Ti-6Al-4V

Titanium alloy Ti-6Al-4V is an extremely attractive material used in the aerospace industry due to its strength-to-weight ratio, resistance to corrosion and fatigue. However, due to poor machinability, Ti-6Al-4V is susceptible to surface damage and has low fatigue strength during machining. Surface integrity has an important impact on the performance, reliability and durability of manufactured components. In paper [2], the experiment was performed on a four-axis CNC milling machine (BV100) equipped with a tool holder with ultrasonic ellipsoidal vibrations. The influence of cutting speed and feed on the roughness of the machined surface is shown in Figure 3. The figure shows that a better roughness of the machined surface is obtained during conventional milling (CM).

In addition to this negative effect regarding the roughness of the treated surface, the authors also showed a positive contribution of RUEM. The values of residual compressive stresses in RUEM can be changed in a narrow range by varying the vibration frequency and are lower than in CM.

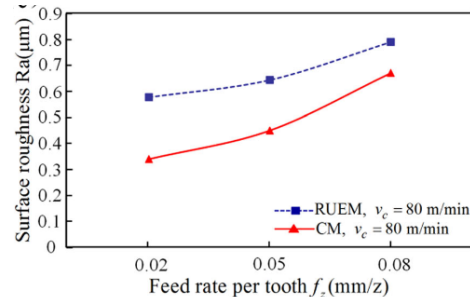
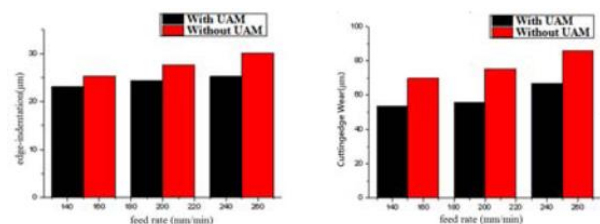


Figure 3. Influence of feed rate on surface roughness (Ra) [2]

3.2. The influence of USM in the processing of glass-ceramics

In glass-ceramic cutting processes, high temperature quickly accumulates around the cutting edge of the tool due to the very contact between the workpiece and the tool, as well as due to the very poor thermal conductivity of the workpiece. Figure 4 shows a comparison of edge wear and tool wear versus feed with and without USM, using cutting fluid [3].



(a) edge-indentation vs F (b) cutting-tool wear vs F

Figure 4. Comparison of edge-indentation and cutting-tool wear versus feedrate for the use of water soluble with or without USM, respectively [3]

3.3. Feasibility of USM for machining components in the aerospace industry

Superalloys have found their ideal for the production of parts intended for work in extreme conditions [4]. Cutting force is a key variable applied as an indicator of tool wear among indirect online wear monitoring methods. The results of the experiment are shown in Figure 5.

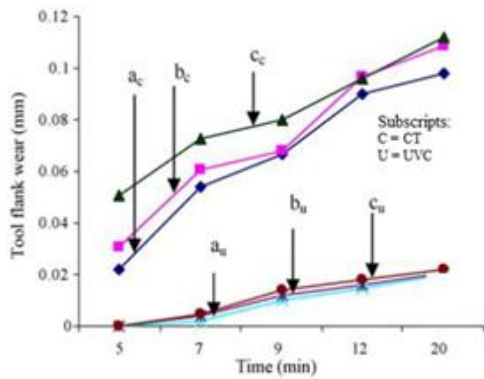


Figure 5. Tool wears condition at three cutting speeds for both CT and UVC processes: feed rate at 0.1 mm/rev [4]

3.4. Influence of ultrasonic vibrations on side milling of AISI 420 stainless steel

AISI 420 martensitic stainless steel is widely used in places where a combination of corrosion resistance and high strength is necessary, such as turbine blades, shafts, propellers and surgical instruments [5]. In this experimental model of the cutting force of a unidirectional USM is presented and ultrasound-supported milling is applied to test the cutting force and the quality of the machined surface in different cutting conditions. It can be seen from Figure 6 that the cutting forces in USM are smaller than in CM, and that is for the displacement $a_{fz} = 0.05$ mm/t amounts 19 %.

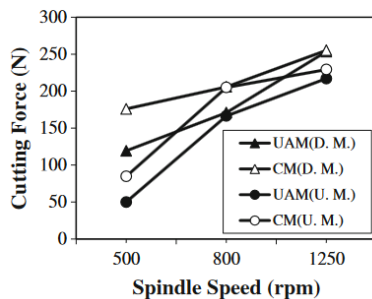


Figure 6. Effect of spindle speed and the type of milling process on cutting force in feed per tooth of $a_{fz} 0.05$ mm/tooth [5]

3.5. Performance analysis of longitudinally torsional USM

In previous years longitudinal ultrasonic vibration milling (SLUVM) was applied to process Ti-6Al-4V (TC4). Compared to conventional milling (CM), this process belongs to non-conventional machining methods that

apply longitudinal vibrations to the milling process. Mauroto [6] applied an ultrasonic vibration load to the cutting tool during machining and the cutting force significantly decreased compared to CM after which improvements in the quality of the machined surface were observed.

In addition to SLUVM, longitudinal-torsional ultrasonic vibration milling has also been introduced to process materials that are more difficult to machine. This method uses a discontinuous cutting mode that can reduce the cutting force and cutting heat, but also improve the surface quality and tool life. Wong studied the feasibility of longitudinal-torsional ultrasonic vibrations for processing brittle materials. He observed that this method showed better performance compared to SLUVM. Amini [7] investigated the effect of using longitudinal-torsional ultrasonic vibration on drilling Al 7075. He found that longitudinal-torsional ultrasonic vibration improved the hole quality by reducing the cutting force and changing the helix angle of the tool. Inspired by the superiority of longitudinal-torsional ultrasonic vibration in drilling difficult-to-machine materials, this experiment is devoted to improving the face milling performance of TC4 using longitudinal-torsional ultrasonic vibration. To achieve longitudinal torsional ultrasonic vibration milling (LTUVM), an ultrasonic sonotrode with helical slots was fabricated and used in the cutting experiments.

3.5.1. Working principle of LTUVM

Compared to conventional milling, the LTUVM path was applied with ultrasonic vibration in both the circumferential and axial directions. Figure 7 shows that there are longitudinal and torsional harmonic vibrations in the Z and X-Y directions. The tool tip path equation CO in LTUVM is (1) [9]:

$$\begin{cases} x = r \sin\left(\frac{2\pi nt}{60} + \frac{A_T}{r} \cos(2\pi ft) + \varphi_0\right) \\ y = r \cos\left(\frac{2\pi nt}{60} + \frac{A_T}{r} \cos(2\pi ft) + \varphi_0\right) + v_y t \\ z = A_L \sin(2\pi ft) \end{cases} \quad (1)$$

where r is the radius of the tool, [mm]; v_f is the feed rate, [mm/min]; n is the number of revolutions of the spindle, [rpm]; f is the ultrasonic frequency, [Hz]; A_T is the torsional amplitude and A_L is the longitudinal amplitude, [μ m]; and ϕ_0 is the starting angle, [rad].

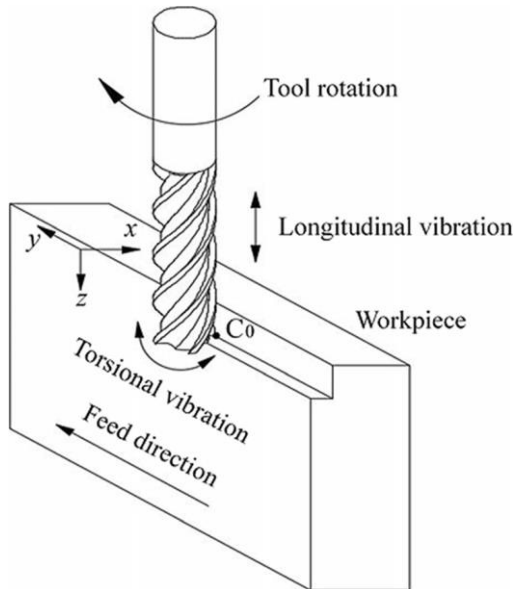


Figure 7. The principles of the LTUVM [8]

The stress distribution shown in Figure 8 shows that longitudinal torsional ultrasonic milling (LTUVM) can effectively reduce the stress concentration and value. Although the SLUVM process did not reduce the stress concentration, the maximum stress value was reduced compared to CM.

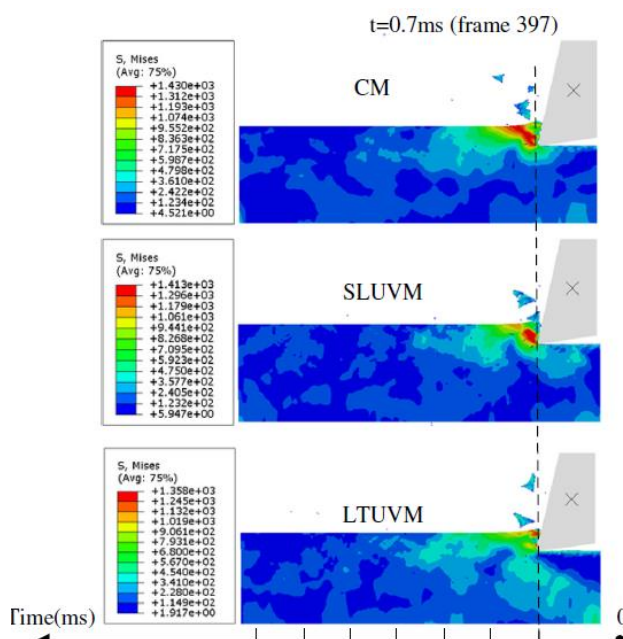


Figure 8. Stress distribution of the three cutting methods [8]

3.6. Ultrasonic milling of plastic reinforced with carbon fibers (CFRP)

In addition to fiber reinforced plastic (CFRP) drilling, CFRP milling is important during aircraft panel production to remove excess material and to achieve final part dimensional accuracy with surface integrity that is not detrimental to mechanical properties. However, several problems have been reported in conventional milling of CFRP. The main problems are; delamination, fiber pull-out, rapid tool wear and poor surface finish [10]. Since CFRP machining always occurs at the end of the production cycle, it is very important that the machining process is able to consistently produce high quality results.

The obtained cutting force data were consistent with the observations related to the adhesive material on the cutting tools. Cutting forces recorded during USM CFRP were reduced by 15 to 20%, Fig. 9, with the higher average force in CM being associated with increased adhesion. CFRP covering the diamond tool reduced the active cutting edges of the tool. Consequently, the cutting tool in CM used more energy and generated higher shear forces during material removal during machining compared to USM. Furthermore, the higher cutting force generated by CM eventually produced micro cracks, resulting in diamond grain breakage, fracture and loss of coating again reducing the cutting efficiency. This was not observed with USM.

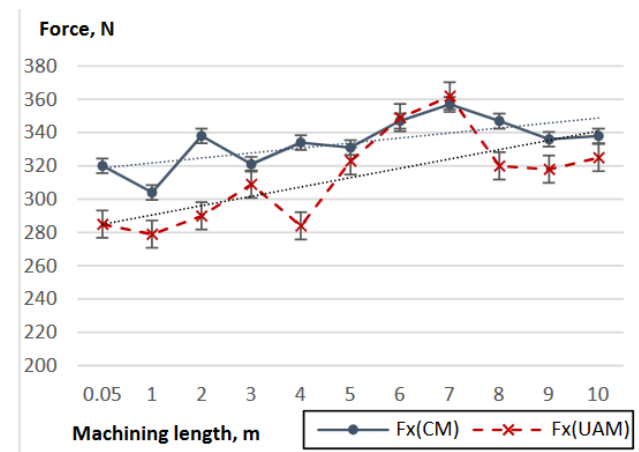


Figure 9. Average machining force for conventional machining and USM [11]

4. CONCLUSION

The processing of modern materials by conventional milling is possible, but at the cost of longer production time, intensive tool wear, reduced accuracy and quality of the processed surface, increased cutting forces and many other factors. In order to reduce these factors, two conventional and non-conventional machining procedures, milling and ultrasonic processing, have been combined into one functional unit called ultrasound-assisted milling.

Some of the modern materials that were processed by ultrasound supported milling are Inconel 718, AISI 420 stainless steel, titanium alloys, nickel-based superalloys, glass-ceramics, etc. have given clear results that a constant supply of vibration can have a positive effect on their workability and the output characteristics themselves. The reason for this is that the vibration affects the separation of the contact surface between the tool and the workpiece more often, which results in a better flow of the cooling and lubricating agent and the removal of the accumulated working heat.

It can be concluded that USM is a good processing technology and that the best results are achieved in experiments where the object of processing was glass. From this it can be concluded that USM is most suitable for processing hard and brittle materials.

ACKNOWLEDGEMENT

This research (paper) has been supported by the Provincial Secretariat for Higher Education and Scientific Research AP of Vojvodina through project No. 142-451-334/2023-01/2: "Advanced processing technologies of modern engineering materials".

REFERENCES

- [1] A. Isaev, V. Anokhin: Application of ultrasonically vibrating tool to metal cutting, *Vestnik machinostroenia*, 1961.
- [2] J. Liu, X. Jiang, X. Han, Z. Gao, D. Zhang: Effects of rotary ultrasonic elliptical machining for side milling on the surface integrity of Ti-6Al-4V, *The International Journal of Advanced Manufacturing Technology*, Vol. 101, pp. 1451-1465, 2019.
- [3] S. Lin, C. Kuan, C. She, W. Wang: Application of Ultrasonic Assisted Machining Technique for Glass-Ceramic Milling, *International Journal of Mechanical and Mechatronics Engineering*, Vol.9, No.5, pp. 802-807, 2015.
- [4] M. Hafiz, M. Kawaz, W. Mohamad, M. Kasim, R. Izamshah, J. Saedon, S. Mohamed: A review on feasibility study of ultrasonic assisted machining on aircraft component manufacturing, *IOP Conference Series: Materials Science and Engineering*, Vol. 270, No. 1, p. 012034, 2017.
- [5] M. M. Abootorabi Zarchi, M. R. Razfar, A. Abdullah: Influence of ultrasonic vibrations on side milling of AISI 420 stainless steel. *The International Journal of Advanced Manufacturing Technology*, Vol.66, pp. 83-89, 2013.
- [6] A. Maurotto, R. Muhammad, A. Roy, VV. Silberschmidt, Enhanced ultrasonically assisted turning of a β -titanium alloy, *Ultrasonics*, Vol. 53, No. 7, pp. 1242-1250, 2013.
- [7] S. Amini, M. Soleimani, H. Paktinat, M. Lotfi: Effect of longitudinal-torsional vibration in ultrasonic assisted drilling, *Mater Manuf Process*, Vol. 32, pp. 616-622, 2016.
- [8] Y. Pang, P. Feng, J. Wang, H. Zha, J. Xu: Performance analysis of the longitudinal-torsional ultrasonic milling of Ti-6Al-4V, *The International Journal of Advanced Manufacturing Technology*, Vol. 113, pp. 1255-1266, 2021.
- [9] G. Gao, Z. Xia, Z. Yuan, D. Xiang, B. Zhao: Influence of longitudinal-torsional ultrasonic-assisted vibration on micro-hole drilling Ti-6Al-4V, *Chinese Journal of Aeronautics*, Vol. 34, No. 9, pp. 247-260, 2021.
- [10] J. Y. Sheikh-Ahmad, *Machining of polymer composites*, Vol. 387355391, New York: Springer, 2009.
- [11] H. Ascroft, S. Barnes, A.N. Dahnel, A. Gupta, N. F. H. B. Abd Halim, D. Ray: Ultrasonic assisted machining. *The 17th International Conference on Machine Design and Production, Conference proceedings*, Vol. 1, pp. 15-30, 2016.



Society of Production
Engineering

SPMS 2023

39. Savetovanje proizvodnog mašinstva Srbije

ICPES 2023

39th International Conference on Production Engineering of
Serbia



Faculty of Technical
Sciences
University of Novi Sad

Novi Sad, Serbia, 26. – 27. October 2023

TRANSFORMING MANUFACTURING AND INDUSTRY 5.0

Bogdan NEDIĆ^{1*}, Gordana GLOBOČKI LAKIĆ²

¹Faculty of Engineering, Kragujevac, Serbia

²Faculty of Mechanical Engineering, University of Banja Luka, RS, BiH,

*Corresponding author: nedic@kg.ac.rs

Abstract: Industry 4.0 is based on the introduction of innovative information and communication technologies in production, while Industry 5.0 changes it. Many subjects of Industry 4.0 are not new, but the way and their application are new. In Industry 4.0, the physical world merges with the virtual, where information technology, telecommunications and production are intertwined and connected.

Industry 5.0 is not a simple development continuation of Industry 4.0, but a completely new approach to solving problems in production and society as a whole. It is intended for the production of personalized products that require the creativity and skills of people and conditions where a high degree of automation is not profitable, to further increase productivity and efficiency, whereby the customer and the creativity of workers are placed at the center of the production process, and robots and highly automated production are the means of production.

The paper presents the basic concepts of Industry 4.0 and Industry 5.0 and points to the directions of the development of new tools for industrial production.

Keywords: Industry 4.0, Industry 5.0, artificial intelligence, robots

1. INTRODUCTION

Industry 4.0 was created by the application of innovations in technologies, whereby traditional industrial practices and business procedures were transformed into new techniques and technologies. Industry 4.0 is a consequence of the digital revolution, that is, the description and conversion of technologies into a digital format. By integrating a real production environment with advanced technologies such as artificial intelligence, robots, 3D printing, IoT, cloud computing, etc., great flexibility and quick decision-making is enabled in companies that have adopted the

Industry 4.0 concept. Industry 5.0 is an upcoming concept in which man and machine are connected by combining their unique specificities, human cognitive abilities, precision and reliability of robot work.

The first three industrial revolutions were driven by mechanization, electrification and automation that gradually transformed the agrarian economy into an economy based on industrial production. This contributed to improving the life and work of workers in factories and improving the overall quality of life [1]. Adapting to change has led to massive increases in commodity production, competitive advantage, and international

business. We are witnessing the fourth industrial revolution (known as Industry 4.0), whereby the world begins a new big step, the fifth industrial revolution or Industry 5.0.

Industry 5.0 is currently a vision whose goal is to further increase productivity and efficiency by placing the customer and worker at the center of the production process. The emphasis is on research and sustainable innovation. It is "the next step, involving cooperation between increasingly powerful and precise machines and the unique creative potential of the human being" [2].

2. INDUSTRY 1.0 TO 4.0

The first industrial revolution [3] is characterized by the appearance and use of the steam engine in the 18th century [4], mechanization and the transformation of the agricultural into the industrial world. It started with the introduction of water- and steam-powered machines into production [5, 6]. Its foundations are the production of steam engines and the textile industry [6]. Also, there was progress in transporting products and people over long distances with the advent of steamships and locomotives.

The second industrial revolution is related [3] to mass production and intensive use of electricity, it started at the end of the 19th century [7]. It is characterized by the introduction of electricity and oil into production, intensive division of labor and the development of the railway and steel industry [7]. There was mass production using assembly lines [8].

The third industrial revolution [3] is characterized by automation and digitalization, i.e. computerization. Industry 3.0 began in the middle of the twentieth century with the significant use of electronics, information and communication technologies (ICT) in industry. Those technologies made it possible to replace and significantly ease the work of workers, after which its transformation into a new era of industrialization, the fourth industrial revolution, continues [7].

The fourth industrial revolution, industry 4.0 [3] or the digital revolution, is characterized by the connection of real objects and people with virtual objects using computer networks. A key element of Industry 4.0 is a significant change in the interconnection of production systems thanks to the integration of ICT, the Internet of Things (IoT) and machines into the so-called Cyber-Physical Systems (CPS) [4, 8]. The beginning is related to the year 2011, when the concept of industry 4.0 first appeared at the HannoverMesse fair [9]. Industry 4.0 concepts then spread to other countries.

An important aspect of Industry 4.0 is the increased power of lower-cost computers, the spread of wireless communication and networks, the availability of increasingly "intelligent" robots and machines, and the ubiquitous use of sensors. The fourth industrial revolution leads to an increase in industrial efficiency and productivity [10, 11], while care must be taken to reduce the risk of losing millions of jobs [12].

The key concept of Industry 4.0 is the "Smart Factory" in which people, machines and resources communicate with each other as in a social network [8]. The factory should be flexible and safe and capable of producing both large series and individual products.

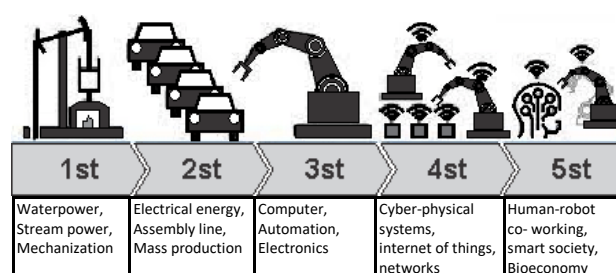


Figure 1. Industry 1.0 to 5.0

Industry 4.0 today is transitioning to Industry 5.0, when it will be possible to adapt products to the needs of individual customers. With Industry 4.0, products are already designed for individual customers, and the selected manufacturer has the appropriate technology, which produces and delivers directly to the customer. This can be seen in the example of cars where one can choose the

type of car in thousands of different variables, not only colors, headlights and interior, but also with many other applications. Industry 5.0 takes the concept of personalization to a higher level.

The concept of Industry 4.0 is essentially related to increased automation and digital information transfer in production [1]. OK, with Industry 4.0 the focus is on mass and smart production, with Industry 5.0 the focus is on a smart and sustainable society with production in which humans and robots collaborate.

Industry 4.0 is characterized by:

- **Cyber physical systems** connect the concepts of Internet of Things that enables real-time data sharing between all parts of industrial systems, information and communication technology, Internet services, connectivity, wireless networks, cloud computing and services, machine-to-machine communication. The Internet of Things has led to sensors of all kinds (biosensors, smart sensors, photonic sensors) being used almost everywhere today [14].
- **Advanced monitoring**, diagnostics and maintenance are related to the use of sensors, wireless sensor networks, real-time data collection and analysis, signal processing, remote access and control, and remote maintenance.
- **Advanced energy saving technologies** include ecological or green technologies, alternative energy conversion (solar, wind and hydrogen energy production), energy recovery.
- **Advanced manufacturing** solutions include flexible production lines, supervisory control and data acquisition (SCADA), computer-aided design and manufacturing (CAD, CAM) and additive manufacturing [14].
- **Advanced engineering technologies and materials** include laser, plasma, ultrasound, radiation and optical technologies, microtechnologies for microelectromechanical systems (MEMS), nanotechnologies, new polymers,

composite and ceramic materials and coatings, new efficient and intelligent materials,

- **Machine learning** refers to the ability of software to analyze large amounts of data and learn how to solve problems automatically.
- **Adaptive control** (the system's ability to identify a problem and decide how to modify its operation to achieve the best possible way of operation).
- **Human-machine** interaction includes augmented and virtual reality, wearable technologies, human-machine interface (HMI) or men-machine interface (MMI) (speech recognition interfaces, touch screens, 3D scanner).
- **Robotics** includes autonomous robots, interconnected robots, co-robots (or collaborative robots, robots that work together with humans) that allow human work to be directed towards activities with greater added value.

3. INDUSTRY 5.0

Industry 5.0 includes everything mentioned for Industry 4.0, whereby Industry 5.0 focuses on the human aspect of production. Industry 5.0 emphasizes the connection between human work in production and automation and robots as production tools. Humans, machines and robots work together, with manufacturing machines and robots enhanced and equipped with AI technologies, which require less complex programming through machine learning. The production environment is integrated into complex systems of networks and interconnection of devices, sensors, wireless communications, transport (autonomous systems), logistics (fuzzy logic, AI), etc. [15].

Industry 5.0 is not a technological revolution but a systemic transformation where Industry 4.0 technologies are implemented, used and adapted to the goals of sustainable development, increasing people's living standards and improving

production and working conditions without increasing the unemployment rate [16].

The new generation of production systems in Industry 5.0 includes [17]:

- **Green machines:** These are machines with a significantly reduced impact on the environment during their entire life cycle. These include a significant reduction in energy consumption, the use of recycled materials for the manufacture of machine parts, zero-waste production, minimal application of MQL which reduces liquid waste from the processing process and recycling of the machine at the end of its life,
- **Autonomous machines:** Machines with a high degree of controllability and autonomy are used, the machine is subordinate to the operator and supports him. They have improved ergonomics, reduced maintenance requirements, built-in many applications and increased operational capabilities. The machines have high productivity, adaptability because they use databases and have integrated intelligent modules for recognizing and predicting the output parameters of the production system.
- **Machines of increased productivity** will be achieved by increasing the accuracy of the elements of all subsystems of the machine, using a system of self-calibration, self-maintenance, measurement and control, high speeds and acceleration of the main and auxiliary movements.
- **Machines with a high degree of utilization:** The high flexibility, autonomy and productivity of the machine will enable its use both for the production of products and for providing services to other companies. The machine works 24 hours a day.

The development of new production systems is based on a new approach to the development and design of machines capable of rapid adaptation to the demands of personalized customers, with systems for self-

control, self-maintenance, etc. The development is based on:

- **Miniaturization** (micro milling, micro laser, micro EDM wire processing and micro ECM),
- **The development of machines with low mass** (in conventional machines, most of the mass of the machine is used to ensure the necessary rigidity for precise work). Application of mechatronic systems ensures controlled flexibility, i.e. mechatronic rigidity. In addition to weight reduction, the machines have an ecological design, optical servo devices, mechatronic systems with numerous controllers and smart materials with actuators and sensors. All machine systems are subordinated to hardware/software solutions.
- **Development of new materials** with active vibration elimination methods using sensors and actuators to dampen externally induced vibrations. New materials (eg, polymer concrete shows low density and high vibration damping properties) and knowledge of their properties enable simulation of the designed model using numerical methods (FEM) and dynamic behavior.
- **Visualization**, which implies visual control in automated production and assembly lines. The process involves smart cameras and machine learning that mimics the human eye and measurement and control activities to make good/not good decisions.

4. CONCLUSION

Industry 5.0 is not a simple development continuation of Industry 4.0, but a completely new approach to solving problems in production and society as a whole. It is intended for conditions where a high degree of automation is not profitable, for the production of personalized products that require the creativity and skills of people, further increasing productivity and efficiency, where the customer and the creativity of the workers are placed at the center of the production process.

Industry 4.0 was abandoned as a goal by the bureaucracy from the EU only ten years after its establishment, and it became an outdated concept of development. The new development paradigm is a consequence of the search for a better model of the progress of the entire society, which is faced with the biggest challenges so far: climate change and the collapse of biological diversity. Until now, the models of development and capitalism that exist today in a large part of the world are the generators of the problems humanity is in. Industry 4.0 is characterized as an inadequate model of development because it is focused on exclusively technological development based on cybernetic-physical objects and systems that produce technological monopolies and large social inequalities. Comprehensive digitization of value creation chains, isolated from other content, does not have sufficient capacity to solve the climate and ecological "state of emergency" on the planet, nor to solve the accumulated tensions resulting from various forms of social inequalities [18]. EU bureaucrats are now offering through Industry 5.0 a departure from the existing practices of neoliberal capitalism and its exclusive focus on production for profit, and consider it necessary to steer towards a more balanced view of values over much longer time frames (as opposed to immediately and everything).

By analyzing many literary sources and events in many manufacturing companies in Serbia, it can be concluded that the importance of implementing many advanced technologies of the Industry 4.0 concept is recognized in some companies, which creates the prerequisites for Industry 5.0. These companies recognize the importance of hiring highly qualified human resources. The main obstacle to a greater and faster implementation of the concept of Industry 4.0 and thus to the aspiration towards Industry 5.0 is, first of all, the lack of high-quality human resources and a significant investment in their training. These are engineers of all profiles (in the first place: engineers of electronics, informatics, mechatronics, robotics,

manufacturing and industrial engineering and others). In addition to engineers, highly skilled staff are needed in the fields of economics, human rights, social and environmental aspects of society, as well as many others.

The current global economy and technological environment for domestic companies create a climate and impose the need for faster mastering of advanced technologies. The growing problems in many EU countries, which will surely become even more complicated in the long term, create an opportunity for domestic companies to better position themselves on the world market.

Much greater investment in trained professional staff is needed (education by the state, incentives to stay in the country and incentives for experts from around the world to come and work in Serbia). Domestic companies must be more significantly involved in the training of professional staff.

REFERENCES

- [1] Nedić B., Globočki Lakić G., Tribology and Industry 4.0, Serbiatrib- 18th International Conference on Tribology – Serbiatrib '2023, Kragujevac, Serbia, pp. 102-111. ISBN: 978-86-6335-103-5
- [2] Ciulli E. (2019a)., Tribology and Industry: From the Origins to 4.0. *Frontiers in Mechanical Engineering*, Vol. 5, No 55, 2019, pp.1-12,
- [3] Xu, L. D., Xu, E. L., and Li, L. (2018). Industry 4.0: state of the art and future trends. *Int. J. Prod. Res.* 56, 2941–2962.
- [4] Dalenogare, L. S., Brittes Benitez, G., Ayala, N. F., and Frank, A. G. (2018). The expected contribution of Industry 4.0 technologies for industrial performance. *Int. J. Prod. Econ.* 204, 383–394.
- [5] Dowson, D. (1998). *History of Tribology*. 2nd Edn. London and Bury St Edmunds: Professional Engineering Publishing Limited.
- [6] Khonsari, M. M., and Booser, E. R. (2008). *Applied Tribology Bearing Design and Lubrication*. Chichester: Wiley.
- [7] Lele, A. (2019). "Industry 4.0. chapter 13," in *Disruptive Technologies for the Militaries and Security*. Smart Innovation, Systems and Technologies, Vol. 132 (Singapore: Springer).

- [8] Kagermann, H., Wahlster, W., and Helbig, J. (2013). Securing the Future of German Manufacturing Industry. Recommendations for Implementing the Strategic Initiative INDUSTRIE 4.0. Final Report of the Industrie 4.0 Working Group. Munich: Acatech, National Academy of Science and Engineering.
- [9] Kagermann, H., Lukas, W.-D., and Wahlster, W. (2011). Industrie 4.0: Mit dem Internet der Dinge auf dem Weg zur 4. Industriellen Revolution (Industry 4.0: with the Internet of Things towards the 4th Industrial Revolution). Available online at: <http://www.vdi-nachrichten.com/Technik-Gesellschaft/Industrie-40-Mit-Internet-Dinge-Weg-4-industriellen-Revolution> (4.04.2023.)
- [10] Holdren, J. P. (2008). Science and technology for sustainable well-being. *Science* 319, 424–434.
- [11] Van Camp, V. (2018). Industry's Fourth Big Wave. Available online at: <http://evolution.skf.com/industrys-fourth-big-wave/> (4.04.2023.)
- [12] Devezas, T., Leitão, J., and Sarygulov, A. (2017). *Industry 4.0-Entrepreneurship and Structural Change in the New Digital Landscape*. Oxford: Springer International Publishing AG.
- [13] Winters, J. (2018). By the numbers: sensing excitement. *Mech. Eng.* 140, 28–29.
- [14] Brown, A. S. (2018a). Chain reaction. Why additive manufacturing is about to transform the supply chain. *Mech. Eng.* 140, 30–35.
- [15] Čočkalo D., Bakator M., Đorđević D., Vorkapić M., Stanisavljev S., *Industry 5.0: A New Paradigm in Manufacturing*, PaKSoM 2021 3rd Virtual International Conference Path to a Knowledge Society-Managing Risks and Innovation, Serbia, Niš, 15-16.11.2021, pp. 245-250, ISBN 978-86-80593-72-3
- [16] Volotka, V., Shloma, O., & Stambulzhi, N. (2021). The future belongs to Industry 5.0. *InterConf.*, Available online at <https://ojs.ukrlogos.in.ua/index.php/interconf/article/view/9923> (10.09.2023.)
- [17] *Transforming the tools of production, Strategy for a sustainable European machine tools industry*, European Communities, 2009, ISBN 978-92-79-11213-3
- [18] Petrović P. *Industrija 5.0 - Nova holistička platforma za održivu budućnost Evrope*, *Journal Industrija* (in Serbian), Available online at <https://www.industrija.rs/vesti/clanak/industrija-5.0-nova-holisticka-platforma-za-odrzivu-buducnost-evrope>

TRANSFORMACIJA PROIZVODNJE I INDUSTRIJA 5.0

Abstract: *Industrija 4.0 je zasnovana na uvođenju inovativnih informacionih i komunikacionih tehnologija u proizvodnju, dok je industrija 5.0 menja. Mnogi subjekti industrije 4.0 nisu novi, ali su način i njihova primena novi. U industriji 4.0 fizički svet se spaja s virtualnim, pri čemu su informacione tehnologije, telekomunikacije i proizvodnja međusobno isprepletani i povezani.*

Industrija 5.0 nije prost razvojni nastavak industrije 4.0, već je sasvim nov pristup rešavanja problema u proizvodnji i društvu u celini. Namenjena je za proizvodnju personalizovanih proizvoda koji zahtevaju kreativnost i veštine ljudi i uslove gde nije isplativ visok stepen automatizacije, za dalje povećanje produktivnosti i efikasnosti pri čemu se kupac i kreativnost radnika stavljaju u centar proizvodnog procesa a roboti i visoko automatizovana proizvodnja su sredstva za proizvodnju.

U radu se predstavljene osnovni koncepti industriji 4.0 i industrije 5.0 i ukazano na pravce razvoja novih alata za industrijsku proizvodnju.

Keywords: *Industrija 4.0, Industrija 5.0, veštačka inteligencija, roboti,*



Society of Production
Engineering

SPMS 2023

39. Savetovanje proizvodnog mašinstva Srbije

ICPES 2023

39th International Conference on Production Engineering of
Serbia



Faculty of Technical
Sciences
University of Novi Sad

Novi Sad, Serbia, 26. – 27. October 2023

BASICS OF DEVELOPMENT OF AN EXPERT SYSTEM FOR THE SELECTION OF GRINDING TOOLS

Vladimir TODIĆ^{1*}, Milan DELIĆ¹

¹University of Novi Sad, Faculty of Technical Sciences, Republic of Serbia,

delic@uns.ac.rs

*Corresponding author: vladimir.todic@uns.ac.rs;

Abstract: Digitization of the preparation of production, in the part related to programming the grinding processing on CNC grinders, multifunctional machining systems for scraping and grinding, and machining centers for grinding or grinding modules within flexible technological systems, is most often based on the application of modern CAD/CAM systems and specific artificial intelligence tools. Within the programming of the process on the above processing and technological systems for grinding, the automated selection of tools and processing modes for grinding can be carried out by applying an appropriate expert system as one of the tools of artificial intelligence. The paper presents an expert system model for the automated selection of grinding tools as well as the basics of its development.

Keywords: expert system, model, grinding tool

INTRODUCTION

The basic characteristics of the modern market, which relate to products of the metal processing industry, include requirements for the production of a wide and changing range of products of superior quality and design, low, often limited prices, short delivery times and fierce competition.

These market requirements determine the directions of development, the production and application of appropriate technological and production systems, the main characteristics of which are related to digitization, automation and robotization.

The development, production and application of modern processing and technological systems, such as hybrid,

multifunctional and flexible technological systems, along with digitization and automation of all functions of the production system, enable its successful operation in modern conditions.

These modern machining and technological systems, including machining centers for grinding, as well as grinding modules within flexible technological systems, require digitization of the production management function, within which a significant place belongs to the preparation of the production, especially in the part related to programming the grinding process, as well as the choice of quality tools and processing modes for grinding.

The paper presents the model of an expert system (ES) for the automated selection of

grinding tools, as well as the basis of development of this system.

EXPERT SYSTEM MODEL

The basic elements of the adopted ES consist of the knowledge base, user interface and automatic conclusion [1], [2], Figure 1.

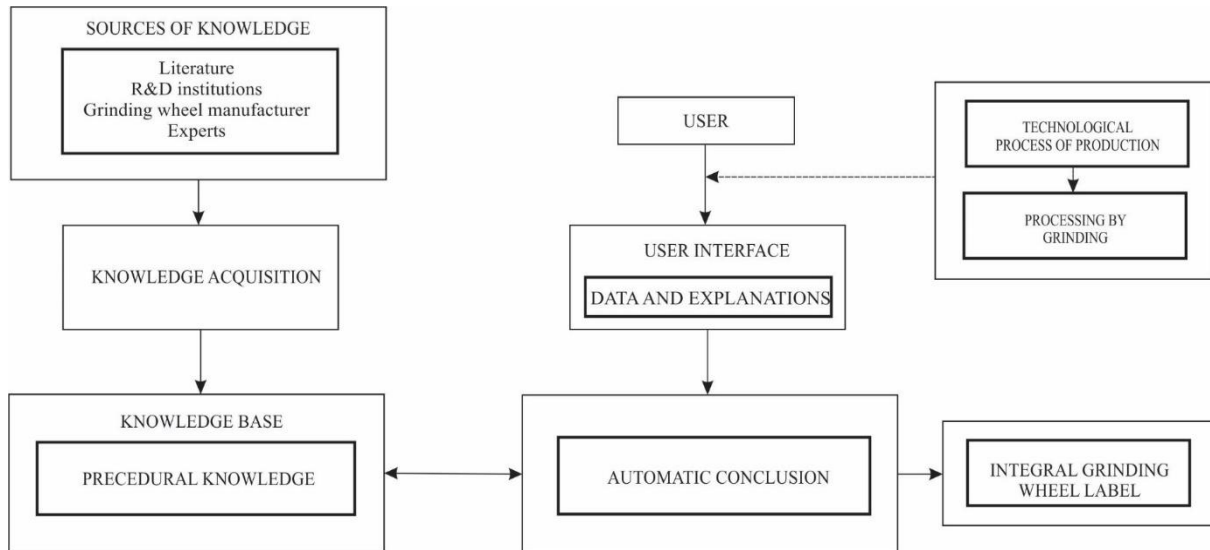


Figure 1. Expert system model

The collected and arranged data within the framework of knowledge acquisition enable the formation of a knowledge base based on a procedural principle, most often in the form of production rules, which can be presented in a familiar form:

IF(conditions) **THEN**(actions)

Procedural knowledge is a set of specific rules and procedures, used when solving certain tasks. In essence, it is the knowledge collected from the specified knowledge sources, which has been translated into corresponding rules and procedures, known as the rule base.

The user interface enables to select the code of the appropriate type of grinding and the code of the workpiece material, which has been defined in the corresponding technological process of producing the product.

Automatic conclusion enables to obtain the integral label of the corresponding grinder, on the basis of the developed knowledge base, i.e.

For the acquisition of knowledge, which makes the basis for the development of the knowledge base, data sources from literature, research and development institutions, data from grinder manufacturers and expert knowledge are used.

the corresponding production rules, by assigning the code of the given grinding operation and the code of the workpiece material.

SYSTEMATIZATION AND CODING OF GRINDING TYPES

Grinding is one of the best-known methods of finishing products, i.e., pieces in the metalworking industry, which enables achieving high accuracy of dimensions, as well as accuracy of geometric shapes and quality of surfaces [3], [4], [5].

In contrast to traditional grinding, which is performed after previous treatments, defined by the technological process of producing the given workpiece, deep or highly productive grinding is used when making certain products from solid materials [6].

The basic types of grinding can be classified in two groups, such as circular and flat grinding.

Circular grinding includes external circular, radial, internal and profile grinding. Table 1 shows the adopted ways of coding these processing processes.

Flat grinding is used for the finishing of flat surfaces on grinders with rectangular and rotary tables.

Table 1. Basic types of grinding

TYPES OF GRINDING		PROCESSING CODE
CIRCULAR GRINDING	<ul style="list-style-type: none"> External circular Radial Profile 	SB
	<ul style="list-style-type: none"> Internal 	UB
FLAT GRINDING	<ul style="list-style-type: none"> Grinders with rectangular table Grinders with rotary table 	RB

Basic types of grinding tools

Grinding tools, or grinders, can be classified into three basic groups: standard round and profile wheels, spindle-shaped grinders of various shapes, and pot- or plate-shaped grinders (Figure 2).

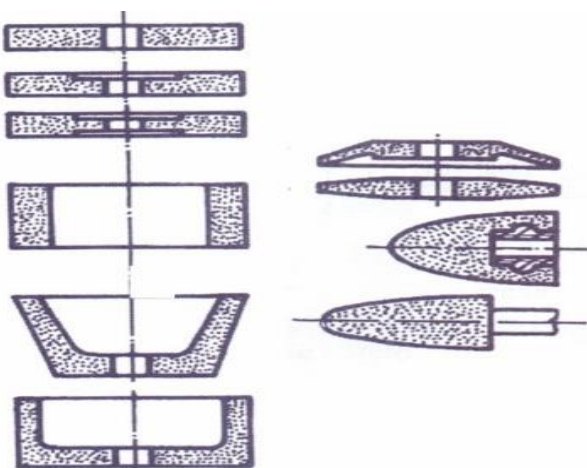


Figure 2. Examples of wheel, pot, plate and spindle grinding tools

Wheel grinders are used for circular external and flat grinding, spindle-shaped grinders for internal grinding, while pot-shaped and plate-

shaped grinders are used for flat grinding. Profile wheel grinders are used for grinding various profile surfaces.

Characteristics of grinding tools

Grinding tools, as tools with undefined cutting geometry, due to their specificity, require the necessary knowledge of their basic characteristics, which depend on [3]:

- Type of the abrasive grain material
- Thickness of the abrasive grains
- Hardness
- Structure of the grinding wheel
- Binding agent.

Abrasive grain materials can be natural, which are rarely used in the metalworking industry, in contrast to artificial materials that are regularly used in this industry (Table 2).

Table 2. Artificial abrasive grains and their standard labels

ABRASIVE GRAIN MATERIAL	LABEL
Aluminum oxide Al_2O_3	A
	B
Silicon carbide SiC	C
Boron carbide B_4C	BC
Cubic boron nitride CBN	BN
Synthetic semi crystal diamond	D

Thickness of the abrasive grains is expressed by the number of sieve openings on the length of one 1" through which the grinding grains passed during separation. Grain thickness is taken according to the following recommendations:

- For rough grinding 40-60,
- For fine grinding 60-100,
- For the finest grinding 100-320.

The hardness of the grinding wheel is measured by the resistance of the binding agent against losing the grains, which according to the standard is marked with capital letters:

- Extremely soft A, B, C, D,
- Very soft E, F, G,
- Soft H, I, J, K
- Medium soft L, M, N, O

- Hard P,Q,R,S
- Very hard T,U,V,W
- Extremely hard X,Y,Z.

The structure or the porosity of the wheel is grouped into fourteen classes, from which six characteristic groups are taken, such as:

- Strongly closed 1,2,
- Closed 3,4,
- Medium 5,6,7,8,
- Open 9,10,11,
- Very open 12,13,14.

Binding agents can be organic and inorganic, with appropriate markings according to the standard (Table 3).

Table 3. Binding agents and their labels

ORGANIC BINDERS	LABEL	INORGANIC BINDERS	LABEL
Bakelite	B	Ceramic binder	V
Fiber-strengthened bakelite	BF	Silicate binder	S
Rubber	R	Magnesium binder	Mg
Fiber-strengthened rubber	RF	Metal binder	M

Figure 3 briefly presents the characteristics of grinding wheels, which affect their cutting ability, processing quality and durability, which are included in the integral label of the grinder.

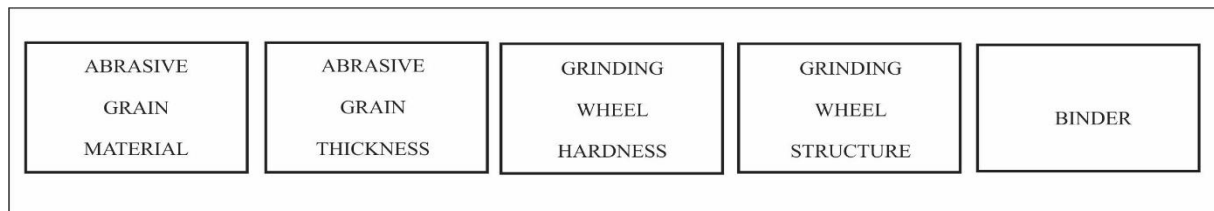


Figure 3: Integral label of the grinding wheel

GROUPING AND CODING OF PROCESSING MATERIALS

For the development and application of the user interface of the adopted ES model in addition to the coding of specific types of grinding (Table 1), it is necessary to group and code the materials of the workpieces, based on which the appropriate types of grinding tools are recommended. The paper adopts a method of coding specific groups of materials (Table 4).

The literature specifies several ways of grouping workpiece materials that influence the choice of grinding tool characteristics. Thus, for example, in [3], [7], five groups of materials are presented, such as tempered steels, untempered steels, cast iron, copper, brass and bronze and light metals, while in [8], 17 groups of materials were formed for choosing wheels for external circular grinding, for internal grinding and wheels for flat grinding.

Table 4. Coding workpiece materials

WORKPIECE MATERIAL	CODE
Aluminum and aluminum cast	M01
Copper and soft bronze	M02
Bronze, hard and tough	M03
Grey iron	M04
Cast hard metal	M05
Crucible steel	M06
Messing	M07
Hard metal	M08
Carbon steel, untempered	M09
Carbon steel, tempered	M10
Cr-Ni steel, uncemented, untempered	M11
Cr-Ni steel, cemented, tempered	M12
Non corroding steel	M13
Nitride steel	M14
Manganese steel	M15
High speed steel, untempered	M16
High speed steel, tempered	M17

DISPLAYING PART OF THE KNOWLEDGE BASE OF THE EXPERT SYSTEM

The knowledge base in the ES model is developed as production rules of the following form:

IF (grinding type code and workpiece material code) **THEN** (grinding wheel label)

Based on recommendations for the selection of grinding wheels for circular external, internal and flat grinding [8], several production rules were formed for the selection of suitable grinding wheels:

IF (SB and M05) **THEN** (C 80 J 8 V)

IF (SB and M12) **THEN** (C,B,A 36-80 L-K 5 V)

IF (UB and M05) **THEN** (C 54-80 K-I 5 V)

IF (UB and M12) **THEN** (B 36-80 K-N 5,6 V)

IF (RB and M05) **THEN** (C 30-60 K-H 8 V)

IF (RB and M12) **THEN** (B 30-46 J-H 5 V)

CONCLUSIONS

The ES model enables the development and its application for the automated selection of tools for grinding, the corresponding characteristics for a specific type of grinding and the given workpiece material.

The adopted method of coding of grinding the types and workpiece materials enables the development of the ES knowledge base on a procedural principle in the form of production rules and the development of the user interface.

The reliability of data for the selected tool for grinding using ES, mostly depends on the acquisition of knowledge, as well as the regular update of data in the knowledge base.

ACKNOWLEDGEMENT

The results presented in this paper are part of the research within the project "Implementation of the results of scientific research work in the field of Industrial Engineering and Management in DIIM teaching processes with the aim of their continuous improvement", at the Department of Industrial Engineering and Management, Faculty of

Technical Sciences, University of Novi Sad, Republic of Serbia.

REFERENCES

- M. Jocković Z. Ognjanović S. Stankovski: *Veštačka inteligencija*, Krug, Beograd, 1997.
- M. Manić :*Ekspertni sistemi za projektovanje tehnoloških procesa pri rezanju u obradi rotacionih delova*, PhD thesis, Mašinski fakultet, Niš, 1995.
- D. Milikić: *Tehnologija obrade rezanjem, Opšta i primenjena teorija*, Fakultet tehničkih nauka, Novi Sad, 1999.
- P. Stanković: *Mašinska obrada rezanjem- obrada metala rezanjem*, Građevinska knjiga, Beograd, 1979.
- M. Jovičić B. Kršljak R. Vukasojević V. Drobnjak: *Obrada brušenjem, Identifikacija karakteristika stanja i optimizacija procesa*, Mašinski fakultet, Beograd, 1986.
- R. Cebalo: *Duboko brušenje*, Školska knjiga, Zagreb, 1990.
- W. König: *Fertigungsverfahren, Band 2- Schleifen, Honen, Looen*, VDI-Verlag GmbH, Dusseldorf, 1980.
- A. Romček: *Tehnologija brušenja, Izbor tocila i elemenata režima obrade*, LŽTK, Kikinda, 1990.



Society of Production
Engineering

SPMS 2023

39. Savetovanje proizvodnog mašinstva Srbije

ICPES 2023

39th International Conference on Production Engineering of
Serbia



Faculty of Technical
Sciences
University of Novi Sad

Novi Sad, Serbia, 26. – 27. October 2023

KINEMATIKA PROCESA OBRADE SEČENJA ŽICOM

Goran VASILIĆ^{1*}, Saša ŽIVANOVIĆ², Milan MILUTINOVIĆ¹, Zoran DIMIĆ³

¹Akademija tehničkih strukovnih studija Beograd, Srbija

²Mašinski fakultet, Univerzitet u Beogradu, Srbija

³Lola institut, Beograd, Srbija

*gvasilic@atssb.edu.rs

Apstrakt: Proces obrade sečenja materijala je jedan od značajnijih metoda obrade u savremenoj industriji. Sa ciljem da se proces obrade u određenoj meri unapredi, u okviru ovoga rada je analizirano kretanje alata tokom procesa obrade kao i uticaj kretanja alata na kretanja mehanizma mašine alatke. Pažnja je posvećena kompleksnoj višeosnoj mašini alatki koja je konfigurisana pomoću dva ravanska rekonfigurabilna mehanizma sa paralelnom kinematikom. Mašine alatke zasnovane na paralelnim mehanizmima, a namenjene za proces obrade sečenja žicom su nedovoljno izučavane te rezultati ovoga rada daju značajan doprinos u njihovom budućem razvoju.

Ključne reči: Sečenje žicom, Kompleksne mašine alatke, Paralelni mehanizmi, Rekonfigurabilni mehanizmi, Kinematički problemi.

UVOD

Proces obrade sečenja žicom spada u nekonvencionalne metode obrade. Sam proces obrade sečenja materijala žicom je veoma zastupljen ta je veliki broj istraživača svoja istraživanja usmerio ka analizi i unapređenju procesa. Grubo govoreći, istraživanja vezana za proces obrade sečenja žicom se mogu podeliti u sledeće grupe: i) analize režima obrade pri sečenju metala nekonvencionalnom W-EDM (Wire Electrical discharge machining) metodom [1,2]; ii) sečenje penastih materijala usijanom žicom [3,4]; iii) mašine alatke i roboti namenjeni za proces obrade sečenja žicom [5,6]; iv) programiranje i upravljanje mašinama alatkama namenjenih za proces obrade sečenja žicom [7,8]. Oslanjajući se na prethodno dobijene rezultate, ali i na rezultate istraživanja drugih autora, u okviru ovoga rada je

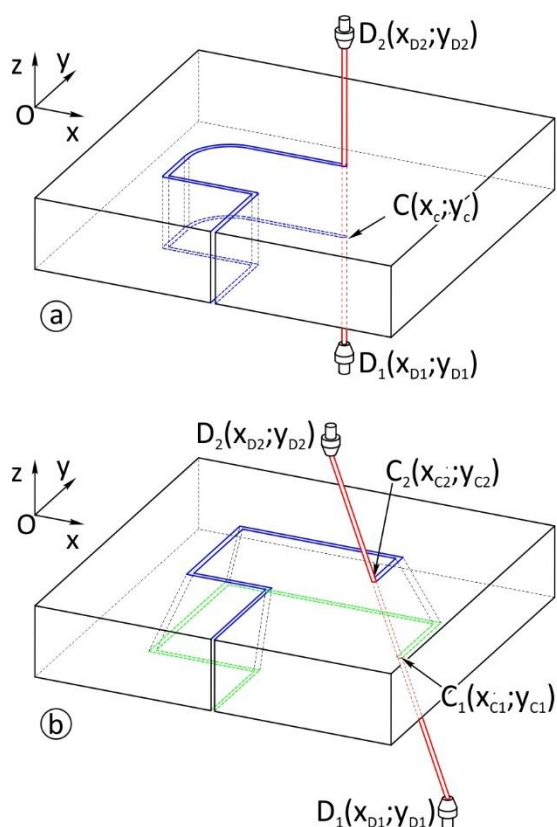
analizirana kinematika višeosne obrade sečenja materijala žicom koja važi za sve mašine alatke namenjene za ovaj proces obrade, bez obzira na konfiguraciju same mašine.

U okviru ovoga rada, najpre je razmatrana kinematika procesa obrade sečenja žicom tj. kretanje žice (alata) po programiranoj putanji a potom, uticaj kinematike procesa obrade na kinematiku mehanizma mašine alatke.

PROCES OBRADE SEČENJA ŽICOM

Proces obrade sečenja žicom je proces obrade koji se karakteriše kao konturna obrada. Tokom procesa obrade, alat (žica) se kreće po programiranoj konturi. U zavisnosti od složenosti konture, proces obrade se može realizovati kretanjem alata po konturi bez promene orijentacije, pri čemu je žica upravna na Oxy ravan u kojoj leži kontura (slika 1.a) i

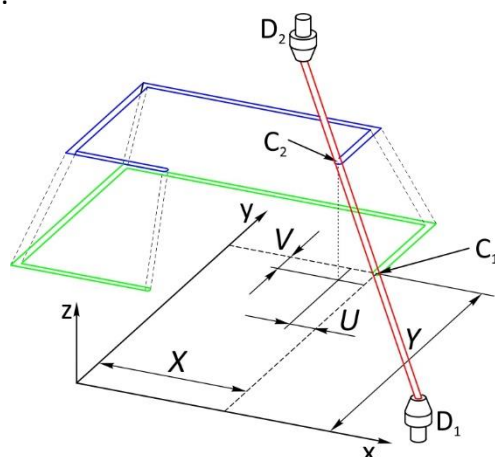
kretanjem alata po konturi sa promenom orijentacije (slika 1.b).



Slika 1. Proces obrade sečenja žicom: a) sa konstantnom orijentacijom žice; b) sa promenljivom orijentacijom žice

U prvom slučaju (slika 1.a), prema standardu ISO 6983 [9], karakteristične tačke konture se zadaju koordinatama X i Y . Kontura po kojoj se kreće žica (na slici prikazana plavom bojom), definisana je koordinatama karakterističnih tačaka C . Prema slici 1.a, koordinate tačke C i koordinate dizni D_1 i D_2 koje vode žicu po programiranoj konturi su u svakom trenutku procesa obrade iste tj. $x_C = x_{D1} = x_{D2}$ i $y_C = y_{D1} = y_{D2}$. U drugom slučaju (slika 1.b), tokom procesa obrade, žica se kreće po dve različite konture. Na ovaj način obezbeđuje se promena orijentacija žice. Karakteristične tačke prve konture (na slici 1.b prikazana zelenom bojom), definisane su koordinatama x_{C1} i y_{C1} , dok su karakteristične tačke druge konture (na slici 1.b prikazana plavom bojom) definisane koordinatama x_{C2} i y_{C2} . Kao što se može primetiti, u drugom slučaju koordinate karakterističnih tačaka C_1 i C_2 i koordinate dizni koje vode žicu po zadatim konturama D_1 i D_2 međusobno se razlikuju, tj. $x_{C1} \neq x_{C2} \neq x_{D1} \neq x_{D2}$ i

$y_{C1} \neq y_{C2} \neq y_{D1} \neq y_{D2}$. Prema standardu ISO 6983 [9], koordinate karakterističnih tačaka prve konture su definisane koordinatama X i Y dok su koordinate karakterističnih tačaka druge konture definisane koordinatama U i V . Koordinate tačke X i Y su apsolutne koordinate tačke C_1 u koordinatnom sistemu obratka a koordinate U i V su relativne koordinate tačke C_2 u odnosu na tačku C_1 kako je i prikazano na slici 2.



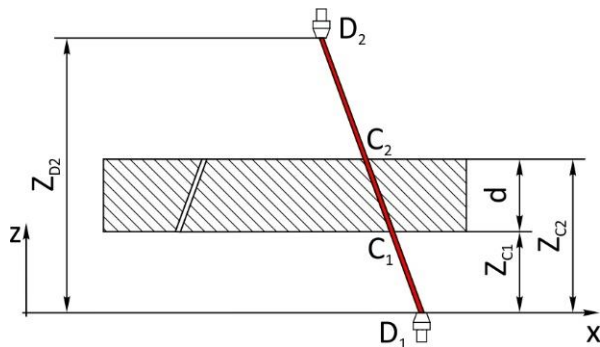
Slika 2. Koordinate karakterističnih tačaka kontura tokom procesa obrade sečenja žicom sa promenom orijentacije

Problematika koja se razmatra u ovom radu, odnosi se na kretanje dizni koje obezbeđuju kretanje žice po programiranoj putanji. U okviru rada, razmatra se proces obrade sečenja žicom sa promenom orijentacije. Pažnja se posvećuje određivanju koordinata dizni koje obezbeđuju programirano kretanje žice. Takođe, razmatra se i uticaj programirane brzine alata (žice) po programiranim konturama na brzine dizni tokom procesa obrade kojima se ostvaruju programirana brzina alata.

KINEMATIKI MODEL PROCESA OBRAD SEČENJA ŽICOM

Kao što je već rečeno, koordinate dizni D_1 i D_2 koje svojim kretanjima obezbeđuju kretanje žice po programiranim konturama zavise od koordinata karakterističnih tačaka kontura C_1 i C_2 . Kako su koordinate tačaka C_1 i C_2 poznate, neophodno je odrediti zavisnost koordinata dizni od koordinata karakterističnih tačaka. Posmatrajući sliku 3, kojom su definisane koordinate karakterističnih tačaka C_1 i C_2 kao i Z

koordinate dizni D_1 i D_2 i uzimajući u obzir sliku 2, može se napisati grupa jednačina (1).



Slika 3. Z koordinate karakterističnih tačaka C_1 i C_2 i Z koordinate dizni D_1 i D_2

$$\begin{aligned} x_{D1} &= K_1 \cdot (x_{C2} - x_{C1}) + x_{C1} \\ y_{D1} &= K_1 \cdot (y_{C2} - y_{C1}) + y_{C1} \\ x_{D2} &= K_2 \cdot (x_{C2} - x_{C1}) + x_{C1} \\ y_{D2} &= K_2 \cdot (y_{C2} - y_{C1}) + y_{C1} \end{aligned} \quad (1)$$

Jednačinama (1) daje zavisnost koordinata dizni D_1 i D_2 od programiranih koordinata koordinata karakterističnih tačaka C_1 i C_2 . U jednačinama (1), koordinate tačke C_2 su date u apsolutnim koordinatama. Uzimajući u obzir navedenu činjenicu da su koordinate tačke C_2 zadate koordinatama U i V koje predstavljaju relativnu poziciju tačke C_2 u odnosu na poziciju tačke C_1 (definisane koordinatama $X=x_{C1}$ i $Y=y_{C1}$), vrednosti apsolutnih koordinata tačke C_2 su date jednačinama (2).

$$\begin{aligned} x_{C2} &= U + X \\ y_{C2} &= V + Y \end{aligned} \quad (2)$$

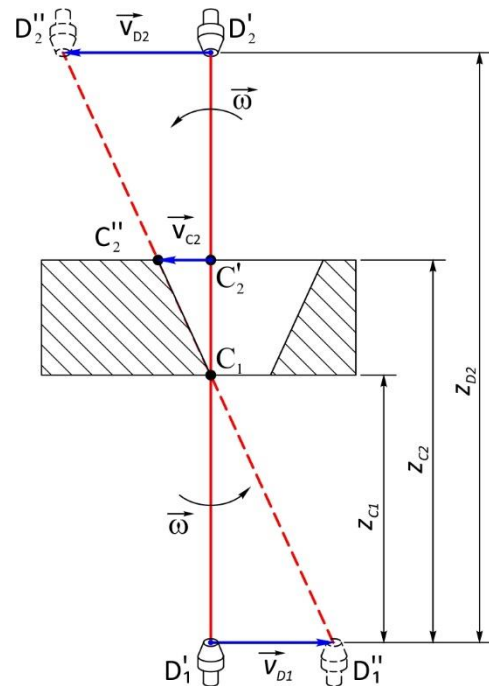
U jednačinama (1) figurišu koeficijenti K_1 i K_2 koji uzimaju u obzir Z koordinate tačaka C_1 i C_2 kao i Z koordinate dizni D_1 i D_2 . Koeficijenti K_1 i K_2 su određeni jednačinama (3).

$$\begin{aligned} K_1 &= \frac{Z_{D1} - Z_{C1}}{Z_{C2} - Z_{C1}} \\ K_2 &= \frac{Z_{D2} - Z_{C1}}{Z_{C2} - Z_{C1}} \end{aligned} \quad (3)$$

Jednačinama (1)-(3) određuju se koordinate dizni D_1 i D_2 na osnovu programiranih

koordinata tačaka C_1 i C_2 , i deo su postprocesorskog računa koji obavlja upravljački deo mašine.

Ako se uzme slučaj kada žica tokom procesa obrade menja orijentaciju, brzine dizni D_1 i D_2 koje svojim kretanjima obezbeđuju kretanje žice programiranim brzinama određuju se prema slici 4.



Slika 4. Brzine dizni D_1 i D_2 tokom procesa obrade sečenja žicom

U slučaju prikazanom na slici 4. kada žica ne menja poziciju ali menja orijentaciju, brzine žice u tački C_1 iznosi $\vec{v}_{C1} = 0$ dok brzina u tački C_2 ima vrednost \vec{v}_{C2} . Razlike u vrednostima brzina \vec{v}_{C1} i \vec{v}_{C2} uzrokuju promenu orijentacije žice. Uzimajući u obzir teoriju kinematike krutog tela, brzina jedne tačke krutog tela (\vec{v}_{C2}) u odnosu na drugu tačku (\vec{v}_{C1}), određuje se vektorskom jednačinom (4)

$$\vec{v}_{C2} = \vec{\omega} \times \overline{C_1 C_2} \quad (4)$$

pri čemu je $\vec{\omega}$ ugaona brzina žice pri promeni orijentacije. U slučaju da žica tokom procesa obrade vrši i translaciju i rotaciju, brzina \vec{v}_{C2} se određuje prema vektorskoj jednačini (5).

$$\vec{v}_{C2} = \vec{v}_{C1} + \vec{\omega} \times \overline{C_1 C_2} \quad (5)$$

Obzirom da se programom za mašinu osim putanje alata (žice) programira i brzina kretanja alata, brzine \vec{v}_{C1} i \vec{v}_{C2} su poznate te se na osnovu njih može odrediti ugaona brzina $\vec{\omega}$. Uz poznatu ugaonu brzinu $\vec{\omega}$ i poznata rastojanja dizni D_1 i D_2 od obratka (slika 3), jednačinom (6) se određuju brzine dizni \vec{v}_{D1} i \vec{v}_{D2} .

$$\vec{v}_{Di} = \vec{v}_{C1} + \vec{\omega} \times \overline{C_1D_i} \quad (i=1,2) \quad (6)$$

Do istih rezultata se dolazi i primenom Jakobijan matrice dobijene na osnovu jednačine (1), a čiji je oblik dat jednačinom (7). Jakobijan matrica se odnosi na obradni proces te nosi oznaku J_{OP} .

$$J_{OP} = \begin{bmatrix} \frac{\partial x_{D1}}{\partial x_{C1}} & \frac{\partial x_{D1}}{\partial y_{C1}} & \frac{\partial x_{D1}}{\partial x_{C2}} & \frac{\partial x_{D1}}{\partial y_{C2}} \\ \frac{\partial y_{D1}}{\partial x_{C1}} & \frac{\partial y_{D1}}{\partial y_{C1}} & \frac{\partial y_{D1}}{\partial x_{C2}} & \frac{\partial y_{D1}}{\partial y_{C2}} \\ \frac{\partial x_{D2}}{\partial x_{C1}} & \frac{\partial x_{D2}}{\partial y_{C1}} & \frac{\partial x_{D2}}{\partial x_{C2}} & \frac{\partial x_{D2}}{\partial y_{C2}} \\ \frac{\partial y_{D2}}{\partial x_{C1}} & \frac{\partial y_{D2}}{\partial y_{C1}} & \frac{\partial y_{D2}}{\partial x_{C2}} & \frac{\partial y_{D2}}{\partial y_{C2}} \end{bmatrix} \quad (7)$$

Diferenciranjem jednačina (1), i uzimajući u obzir uvedene smene date jednačinama (2) i (3), konačan oblik Jakobijan matrice je dat jednačinom (8) na osnovu koje se određuju brzine dizni \vec{v}_{D1} i \vec{v}_{D2} na osnovu poznatih brzina \vec{v}_{C1} i \vec{v}_{C2} . Brzine dizni se određuju pomoću matrice jednačine (9).

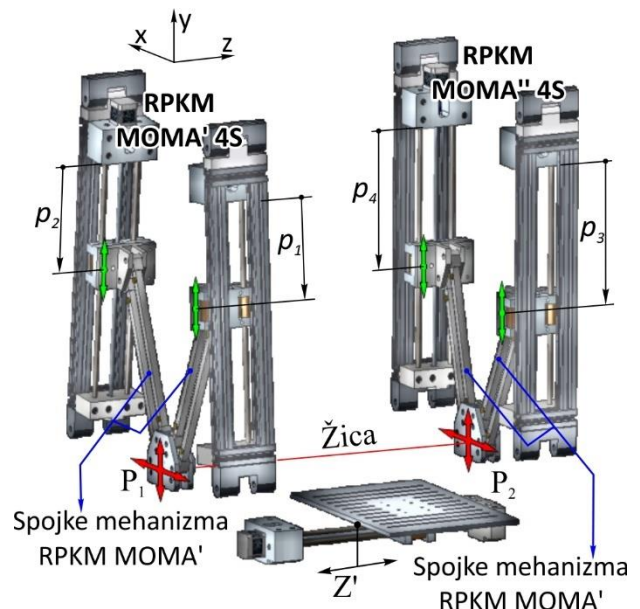
$$J_{OP} = \begin{bmatrix} 1 - K_1 & 0 & K_1 & 0 \\ 0 & 1 - K_1 & 0 & K_1 \\ 1 - K_2 & 0 & K_2 & 0 \\ 0 & 1 - K_2 & 0 & K_2 \end{bmatrix} \quad (8)$$

$$\begin{bmatrix} \dot{x}_{D1} \\ \dot{y}_{D1} \\ \dot{x}_{D2} \\ \dot{y}_{D2} \end{bmatrix} = J_{OP} \cdot \begin{bmatrix} \dot{x}_{C1} \\ \dot{y}_{C1} \\ \dot{x}_{C2} \\ \dot{y}_{C2} \end{bmatrix} = \begin{bmatrix} 1 - K_1 & 0 & K_1 & 0 \\ 0 & 1 - K_1 & 0 & K_1 \\ 1 - K_2 & 0 & K_2 & 0 \\ 0 & 1 - K_2 & 0 & K_2 \end{bmatrix} \cdot \begin{bmatrix} \dot{x}_{C1} \\ \dot{y}_{C1} \\ \dot{x}_{C2} \\ \dot{y}_{C2} \end{bmatrix} \quad (9)$$

Matrična jednačina (9) kojom se određuju brzine \vec{v}_{D1} i \vec{v}_{D2} , složenija je od jednačina (4) do (6), ali je pogodnija za dalje analize kinematike procesa obrade sečenja žicom.

KOMPLEKSNA VIŠEOSNA MAŠINA ALATKA MOMA-W

U slučaju da se kretanja dizni u dva pravca realizuju tradicionalnim dvoosnim serijskim mehanizmima, izvedene brzine \dot{x}_{Di} i \dot{y}_{Di} su brzine koje realizuje svaka od pogonskih osa. Međutim, ako kretanja dizni D_1 i D_2 obezbeđuju paralelni mehanizmi, kinematika celog procesa obrade se usložnjava. Mašina alatka namenjena za proces obrade sečenja žicom je već bila predmet istraživanja autora [10-11] i prikazana je na slici 5.



Slika 5. Kompleksna mašina alatka MOMA-W namenjena za proces obrade sečenja žicom

Mašinu alatku namenjenu za proces obrade sečenja žicom prikazane na slici 5, nazvana je MOMA-W (W-wire) i čine je dva mehanizma sa paralelnom kinematikom MOMA (RPKM) čija se konfiguracija može menjati [12-14]. Konfiguracije paralelnih mehanizama se mogu lako i brzo menjati promenom orijentacije pogonskih osa ili promenom dužine spojki mehanizama. Paralelni mehanizmi su međusobno nezavisni dok su platforme mehanizama međusobno povezane žicom. Platforme mehanizama se mogu kretati u

pravcima osa X i Y , a pozicije platformi su određene unutrašnjim koordinatama kompleksne mašine alatke p_1, p_2, p_3 i p_4 . Spoljašnje koordinate mašine alatke su koordinate programiranih tačaka, odnosno X, Y, U i V za koje važi jednačina (2). Na platformama mehanizma se nalaze dizne D_1 i D_2 koje obezbeđuju programirane pozicije i orijentacije žice tokom procesa obrade, te se jednačine (1) do (4) u ovom slučaju odnose na koordinate platformi mehanizama. Usled promene orijentacije žice, njena dužina se menja tokom procesa obrade pa se opisana veza dva paralelna mehanizma ne može okarakterisati kao serijska veza. Iz tog razloga, mašina alatka sa slike 5 je okarakterisana kao kompleksna mašina alatka. Koordinate dizni x_{D1}, x_{D2}, y_{D1} i y_{D2} date jednačinom (1) su ujedno i koordinate platformi mehanizama i polazne su jednačine za rešavanje kinematičkih problema višeosne mašine alatke sa slike 5. Postupak rešavanja kinematičkih problema se zasniva na rešavanju kinematičkih problema dvoosnih paralelnih mehanizama [12-14], a rešenja su data u radovima [10-11].

Uzimajući u obzir već određene brzine dizni D_1 i D_2 , za kompleksnu mašinu alatku MOMA-W neophodno je odrediti brzine kojima se kreću klizači duž vođica pogonskih osa kako bi se realizovale željene brzine platformi sa samim time i programirane brzine alata (žice). Jakobijan matrica kompleksne mašine alatke MOMA-W data je jednačinom (10). Kako se Jakobijan matrica odnosi na kompleksnu mašinu alatku MOMA-W, u označena je sa J_W .

$$J_W = \begin{bmatrix} \frac{\partial p_1}{\partial x_{D1}} & \frac{\partial p_1}{\partial y_{D1}} & \frac{\partial p_1}{\partial x_{D2}} & \frac{\partial p_1}{\partial y_{D2}} \\ \frac{\partial p_2}{\partial x_{D1}} & \frac{\partial p_2}{\partial y_{D1}} & \frac{\partial p_2}{\partial x_{D2}} & \frac{\partial p_2}{\partial y_{D2}} \\ \frac{\partial p_3}{\partial x_{D1}} & \frac{\partial p_3}{\partial y_{D1}} & \frac{\partial p_3}{\partial x_{D2}} & \frac{\partial p_3}{\partial y_{D2}} \\ \frac{\partial p_4}{\partial x_{D1}} & \frac{\partial p_4}{\partial y_{D1}} & \frac{\partial p_4}{\partial x_{D2}} & \frac{\partial p_4}{\partial y_{D2}} \end{bmatrix} \quad (10)$$

Pomoću Jakobijan matrice J_W određuju se brzine klizača na pogonskim osama \dot{p}_i ($i=1,2,3,4$)

okjima se realizuju brzine platformi mehanizama i to putem jednačine (11).

$$\begin{bmatrix} \dot{p}_1 \\ p_2 \\ \dot{p}_3 \\ \dot{p}_4 \end{bmatrix} = J_W \cdot \begin{bmatrix} \dot{x}_{D1} \\ \dot{y}_{D1} \\ \dot{x}_{D2} \\ \dot{y}_{D2} \end{bmatrix} \quad (11)$$

Konačno, brzine klizača duž pogonskih osa kompleksne mašine alatke MOMA-W koje obezbeđuju programirane brzine alata (žice) tokom procesa obrade, prema do sada izvedenim jednačinama, određuju se matricnom jednačinom (12).

$$\begin{bmatrix} \dot{p}_1 \\ p_2 \\ \dot{p}_3 \\ \dot{p}_4 \end{bmatrix} = J_W \cdot \begin{bmatrix} \dot{x}_{D1} \\ \dot{y}_{D1} \\ \dot{x}_{D2} \\ \dot{y}_{D2} \end{bmatrix} = J_W \cdot J_{OP} \cdot \begin{bmatrix} \dot{x}_{C1} \\ \dot{y}_{C1} \\ \dot{x}_{C2} \\ \dot{y}_{C2} \end{bmatrix} \quad (11)$$

ZAKLJUČAK

U okviru rada je prikazana kinematička analiza procesa obrade sečenja žicom pri čemu se pažnja posvetila jednoj kompleksnoj mašini alatki koja je sačinjena od dva paralelna mehanizma. Značaj prikazane analize se ogleda u tome što se zbog nelinearne zavisnosti unutrašnjih od spoljašnjih koordinata kompleksne mašine alatke ne mogu predvideti brzine klizača duž pogonskih osa. Drugačije rečeno, male programirane brzina alata, zbog opšte poznatih karakteristika paralelnih mehanizama, mogu zahtevati izuzetno velike brzine klizača duž pogonskih osa koje se ne mogu realizovati. Prikazanom analizom, prema programiranoj brzini alata mogu se odrediti brzine klizača u svakom delu programirane putanje. U slučaju da se brzine klizača ne mogu realizovati, kompleksna mašina alatka se može rekonfigurisati kako bi se dobila konfiguracija koja može realizovati željene brzine alata.

Izneta pretpostavka da se konfiguracija mašine alatke može prilagoditi programiranoj putanji i programiranoj brzini alata je jedan od pravaca budućih istraživanja koja za osnovu imaju višeosne mašine alatke namenjene za proces obrade sečenja žicom.

ZAHVALNOST

Predstavljeno istraživanje je podržalo Ministarstvo prosvete, nauke i tehnološkog razvoja Republike Srbije ugovorom br. 451-03-47/2023-01/200105 od 03.02.2023. godine i ugovorom 451-03-47/2023-01/200066 od 2023. godine.

LITERATURA

- [1] R. Chalisgaonkar, J. Kumar: Multi-response optimization and modeling of trim cut WEDM operation of commercially pure titanium (CPTi) considering multiple user's preferences, *Engineering Science and Technology, an International Journal*, Vol. 18, pp. 125-134, 2015.
- [2] R. Ramakrishnan, L. Karunamoorthy; Multi response optimization of wire EDM operations using robust design of experiments, *The International Journal of Advanced Manufacturing Technology*, Vol. 29, pp. 105-112, 2006.
- [3] S. H. Lee, D. G. Ahn, D. Y. Yang: Calculation and verification of rotation angle of a four-axis hotwire cutter for transfer-type variable lamination manufacturing using expandable polystyrene foam, *The International Journal of advanced Manufacturing Technology*, Vol.22, pp. 175-183, 2003.
- [4] R.F. Hamade, F. Zeineddine, B. Akle, A. Smaili: Modelangelo: a subtractive 5-axis robotic arm for rapid prototyping, *Robotics and Computer-Integrated Manufacturing*, Vol.121, No.2, pp.133-144, 2005.
- [5] M. Jovanović, M. Raković, B. Tepavčević, B. Borovac, M. Nikolić: Robotic fabrication of freeform foam structures with quadrilateral and puzzle shaped panels, *Automation in Construction*, Vol. 74, pp. 28-38, 2017.
- [6] X. Cheng, Z. G. Wang, S. Kobayashi, K. Nakamoto, K. Yamazaki: Development of a six-axis wire electrical discharge machine for the fabrication of micro end mills, *Journal of Engineering Manufacture*, Vol.23, No.2, pp.121-131. 2009.
- [7] S. Živanović, R. Puzović: Simulacija elektro erozijske obrade žicom na temelju STEP-NC programa, *Tehnički vjesnik*, Vol. 23 No. 6, 2016.
- [8] S. Zivanovic, R. Puzovic: Off-line Programming and Simulation for 2-axis Wire EDM, *Faculty of Mechanical Engineering, Belgrade, FME Transactions*, Vol. 43, No. 2, pp. 138-143, 2015.
- [9] ISO 6983-1, *Automation systems and integration — Numerical control of machine — Program format and definitions of address words — Part 1: Data format for positioning, line motion and contouring control systems*, 2009.
- [10] G. Vasilić, S. Živanović: Configuring and analysis of complex multi-axis reconfigurable machine for wire cutting process, *Mechanism and Machine Theory*, Vol.149, pp.203833, 2020.
- [11] G. Vasilić: *Koncepcijsko projektovanje jedne klase kompleksnih mašina alatki*, doktorska disertacija, Mašinski fakultet Univerziteta u Beogradu, 2023.
- [12] G. Vasilić, S. Živanović, B. Kokotović, Z. Dimić: Configuring and analysis of a class of generalized reconfigurable 2-axis parallel kinematic machine, *Journal of Mechanical Science and Technology*, Vol. 33, pp. 3407-3421, 2019.
- [13] G. Vasilić, S. Živanović: Analiza radnog prostora rekonfigurabilnog dvoosnog paralelnog mehanizma MOMA, *40. JUPITER konferencija, NU-Roboti-FTS*, Univerzitet u Beogradu, Mašinski fakultet, 2016.
- [14] G. Vasilić, S. Živanović: Modelling and Analysis of 2-Axis Reconfigurable Parallel mechanism MOMA with translatory Actuated Joints. *TECHNICS-magazine of the union of engineers and technicians od Serbia*, Special edition, pp. 59-66, 2016.

KINEMATICS OF THE WIRE CUTTING PROCESS

Abstract: *The wire-cutting process is one of the most important processing methods in modern industry. To improve the machining process to a certain extent, the movement of the tool during the machining process as well as the influence of the movement of the tool on the movement of the mechanism of the machine tool were analyzed in this paper. Attention is devoted to a complex multi-axis machine tool, which is made up of two planar reconfigurable mechanisms with parallel kinematics. Machine tools based on parallel mechanisms, intended for the wire-cutting process, are insufficiently studied, and this work's results significantly contribute to their future development.*

Keywords: *Wire cutting process, Complex machine tools, Parallel mechanisms, Reconfigurable mechanisms, Kinematics problems*



Society of Production
Engineering

SPMS 2023

39. Savetovanje proizvodnog mašinstva Srbije

ICPES 2023

39th International Conference on Production Engineering of
Serbia



Faculty of Technical
Sciences
University of Novi Sad

Novi Sad, Serbia, 26. – 27. October 2023

THERMOCOUPLE AND INFRARED SENSOR-BASED MEASUREMENT OF TEMPERATURE IN METAL CUTTING

Milan IVKOVIĆ¹, Bogdan NEDIĆ^{1*}, Suzana PETROVIĆ SAVIĆ¹

¹Faculty of engineering University of Kragujevcu, Serbia,

*Corresponding author: nedic@kg.ac.rs

Abstract: *The high temperature that occurs during metal cutting processing has a negative impact on the durability of the cutting tool and can also have a negative effect on the object of processing. Therefore, it is very important to have information about the temperature in the cutting zone and the workpiece. Accurate real-time temperature measurement is still a challenge. Efforts to accurately measure the cutting temperature today are directed in two directions. One direction refers to placing artificial thermocouples as close as possible to the cutting zone, and the other direction is the application of infrared thermography and thermovision. The paper presents the results of temperature measurement using an artificial thermocouple placed directly under the top of the cutting tool insert of the turning knife and using an IR non-contact thermometer to measure the temperature on the surface of the workpiece at different cutting speeds of two different materials.*

Key words: *temperature metal cutting, turning, thermocouple, IC thermometer*

INTRODUCTION

The processing of metals by cutting is highly non-linear in nature, where complex processes take place in an extremely small cutting zone with high cutting temperatures and high specific pressures [1, 2].

During the cutting process, most of the mechanical work (approximately 90%) is converted into thermal energy in a very narrow cutting zone directly at the tip of the cutting tool. High temperature significantly affects tribological processes on the cutting tool, wear of the tool and reduction of its service life. In addition, high cutting temperatures and tool wear affects the quality of the machined surface (inaccuracy of measurements and surface roughness

increases). Also, high temperature can lead to structural changes in the surface layer of the processing object [1, 3, 4]. Cutting speed has the greatest influence on heat generation in the cutting zone, followed by depth and pitch. In addition to processing parameters, the cutting temperature is influenced by the type of material being processed. An increase in hardness and tensile strength leads to an increased cutting temperature. Also, when processing more difficult to process alloy steels, higher cutting heat is generated.

In order to efficiently select and use adequate cutting parameters, it is necessary to measure the cutting temperature in real time. On-line measurement of the cutting temperature can prevent high cutting temperatures at the very beginning of

processing, and also stop the cutting process in case of unwanted changes (eg tool wear, unplanned changes in cutting depth, etc.) [5, 6].

In addition to the impact on tool durability, the heat generated in the cutting process also affects the productivity of the machining process, the quality of the machined surface, machining accuracy and other output factors of the machining process. Hence, examination, measurement and knowledge of the size and distribution of the cutting temperature in the tool and the workpiece is of first-rate practical importance. On the basis of this knowledge, optimal processing conditions and regimes, quality, productivity and economic efficiency of the process, durability of tools, etc. can be determined.

So far, a number of different cutting temperature measurement methods have been developed, but precise measurement in real time is still a challenge. The reason for this is the movement of tools and workpieces, frequent changes in cutting depth, the creation of chips whose course cannot be controlled, very small cutting zones, complex geometry of the cutting tool, etc. [7, 8].

The cutting temperature measuring methods can be divided into two groups, based on:

- thermal conductivity and
- thermal radiation.

In the case of thermal conductivity, thermal energy leads to the creation of a thermal voltage that can be measured by suitable measuring systems. Thermocouples are most often used, because they have a low price, can work in a wide temperature range, and can be easily installed. They are used to measure the mean temperature in the immediate environment of the thermocouple [9].

Artificial thermocouple. Pre-formed thermocouples made of special materials are implanted in places close to the cutting zone. This is achieved by drilling holes in the workpiece [10, 11] or the tool [12, 13, 14, 15] at one or more points at the same time, or by placing the tip of the thermocouple on the outer surface of the tool. The accuracy of

measurement using this method primarily depends on the proximity of the set measuring point to the cutting zone [16, 17, 18].

Methods based on thermal radiation (infrared pyrometer to measure the temperature at a point, and thermography, thermovision to measure the temperature of the surface). These methods are non-contact methods that have a number of advantages over the previously described contact methods. The main disadvantage is that the method depends on the optical properties of the measured object, i.e. shavings or cooling and lubricating agents can cover the surface whose temperature is measured or damage to the measuring equipment can occur [19, 20]. Also, the problem is the necessity of knowing the exact value of the thermal emission coefficient of the surface whose temperature is measured [21, 22, 23, 24].

TEMPERATURE MEASUREMENT DURING TURNING PROCESSING

In order to test the possibility of measuring the temperature on the cutting tool and the object of processing and the influence of the cutting speed and the type of material of the object of processing, appropriate measurement systems were formed, Figure 1.

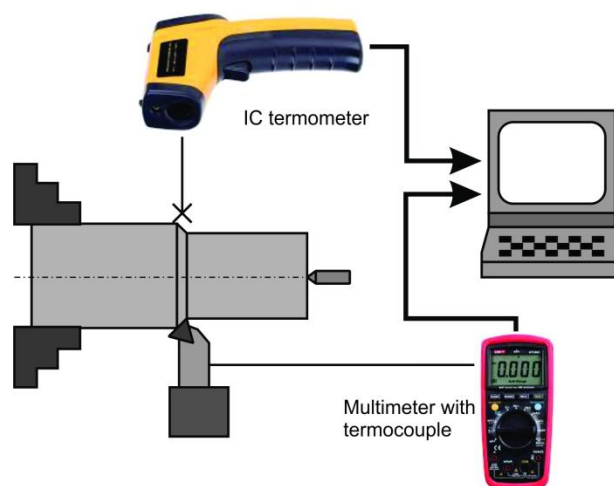


Figure 1. Measuring systems for measurement of the cutting temperature

During turning processing, a special artificial thermocouple is formed, placed between the cutting plate and the base plate immediately below the top of the cutting plate. The tool is a turning knife CSDNR 2020K12 with an

interchangeable insert SPMX 12T3AP-75. A cutting insert without coatings was used for the tests. Figure 2 shows the position of the measuring point and the method of placing the thermocouple. A groove was formed on the base plate by drilling, in which the thermocouple was placed.

The special thermocouple was formed using a type 2 AB AC 15 thermocouple from the "Termocoax" series of the "PHILIPS" company. Thermocouple elements are NiCr(+) and Ni(-) wires. The thermocouple is pre-calibrated.

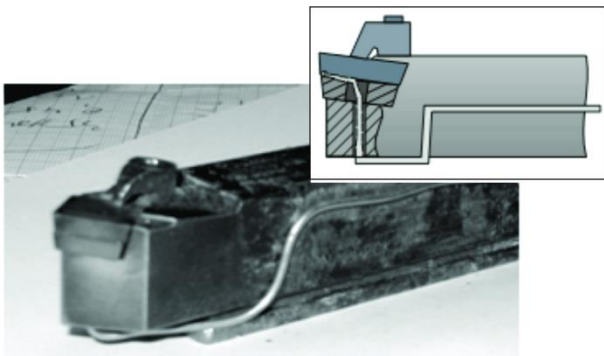


Figure 2. Position and measuring spot for artificial thermocouple at turning tools

A TENMA 72-7750 digital multimeter was used to measure the temperature

The 72-7750 multimeter has the standard measurement modes (voltage, current capacitance, resistance, conductivity), also measures frequency, temperature, and TENMA has an opto-coupled RS-232 cable with connector and datalogging software, figures 3 and 4.

The temperature measurement range is -40°C to +1000°C with resolution 1°C. Measurement speed - updates 2 times/second.



Figure 3. Digital multimeter TENMA 72-7750

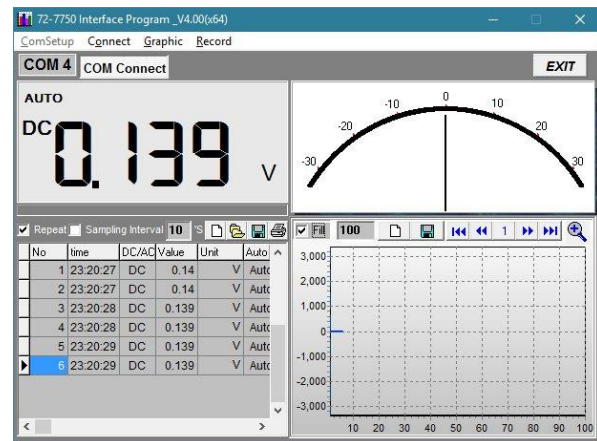


Figure 4. 72-7750 Interface Program

IR thermometer DT-8855 was used to measure the temperature of the surface of the workpiece on the newly processed surface on the opposite side from the place of the cutting, Figure 5. Infrared temperature range -50 to 1050°C with resolution 0.1°C. The Model DT-8855 is supplied with a Wireless USB (RF 433 MHz) datalogging system for use with a PC and software, interface to figure 6.

Experimental tests in turning processing were carried out under the following conditions:

- cutting speeds $v = \sim 60, \sim 80 \text{ i } \sim 100 \text{ m/min}$,
- step $s = 0,2 \text{ mm/o}$
- cutting depth $a = 0,3 \text{ mm}$,
- the material of the processing object
 - 25CrMo4 (Č4730), diameter 45 mm, processing length - 300 mm,
 - C45 (Č1530), diameter 30 mm. processing length - 320 mm,



Figure 5. IC termometer DT-8855

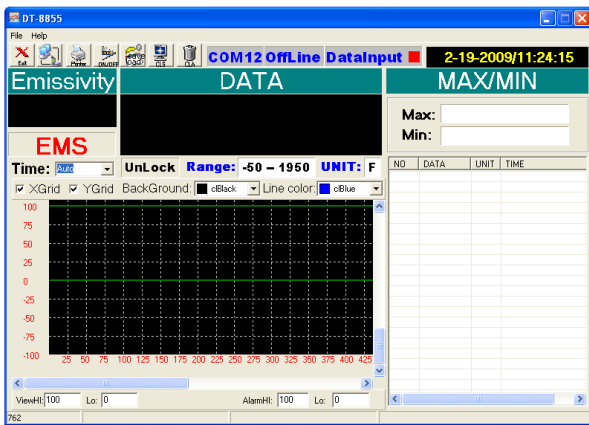


Figure 6. Interface IC thermometer

MEASUREMENT RESULTS

Longitudinal machining by turning was performed on a universal lathe Prvomajska TNP-480, power 10 KW. Figure 7 shows the position of the processing object, tool with thermocouple and IR thermometer.



Figure 7. Position of the turning knife and IR thermometer during longitudinal turning

Figure 8 shows a monitor with active software for temperature measurement using the methods described.

Temperature measurements were always performed with the initial ambient temperature: 23.6 °C.

Figure 9 shows the change in the measured temperature in the tool and on the workpiece from C45. It can be seen that the temperature in the tool rises and that after processing the 320 mm object, it is 107°C. Measuring the temperature on the surface of the object to be

processed with an IR thermometer showed that there was very little heating, i.e. from the initial 23.6°C the surface reached 28.2°C. However, it can be seen that there are significant deviations in the value of the measured signal, which occurs due to the accumulation of continuous chips on the tool and the object in the immediate vicinity of the processing zone. Its breakage in a short period of time enables measurement with an IR thermometer.

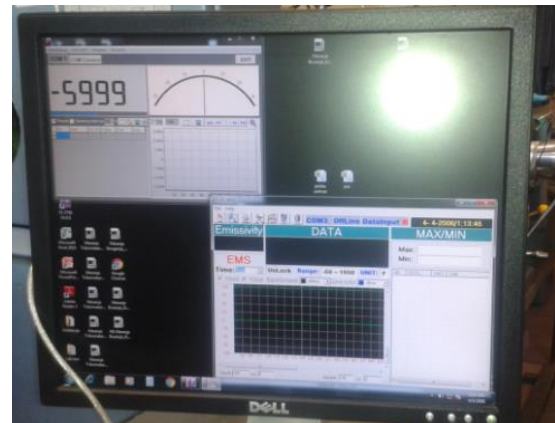


Figure 8. Temperature measurement applications

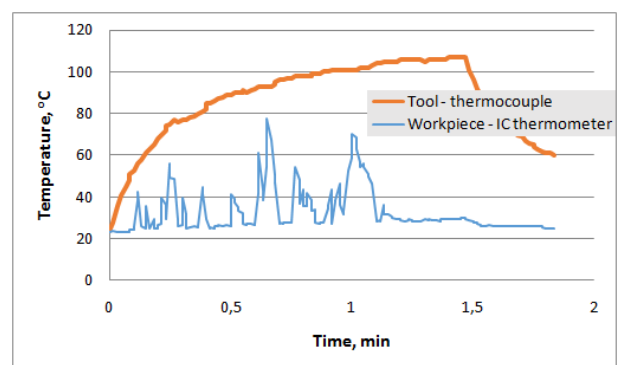


Figure 9. Cutting temperature when processing steel C45 and cutting speed 80 m/min

Figure 10 shows the temperature change during processing of 25CrMo4 material at the same cutting speed. It can be seen that after processing a length of 300 mm, a higher temperature was reached: 120°C. In this case too, the established maximum temperature was not reached. The temperature signal on the workpiece shows that the chip removal flow is more favorable and that it does not accumulate on the tools and the workpiece. The temperature of the surface of the processing object increased from 23.6°C to 28.5°C.

Figures 11 and 12 show the changes in cutting temperatures for two different steels and three cutting speeds.

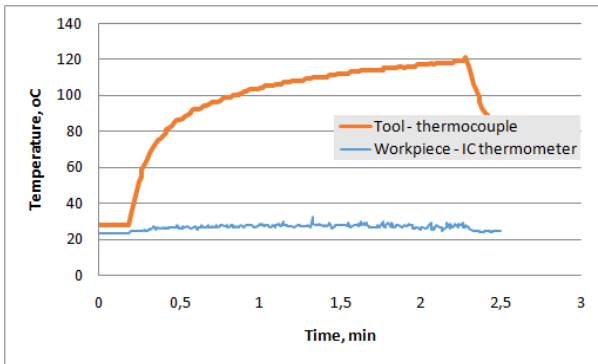


Figure 10. Cutting temperature when processing steel 25CrMo4 and cutting speed 80 m/min

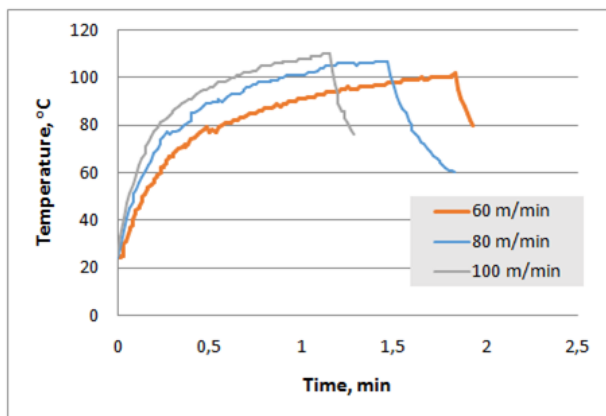


Figure 11. Temperature in the cutting tool when processing C45 with different cutting speeds.

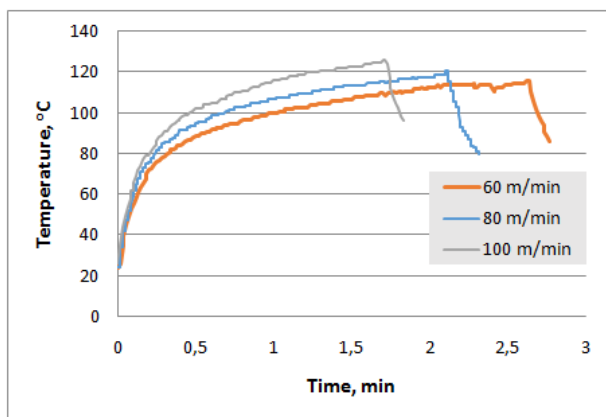


Figure 12. Temperature in the cutting tool when machining 42CrMo4 with different cutting speeds.

CONCLUSION

The tests carried out in this work are a continuation of long-started tests aimed at the development of methods for monitoring the cutting process, in which the resistance and temperature of cutting and tool wear are

measured, and the formation of a database on material machinability and tool wear.

Based on the obtained measurement results, the following conclusions can be drawn:

- the presented methods for measuring the cutting temperature during turning processing using a thermocouple placed on the surface of the substrate immediately below the cutting edge of the insert and measuring the temperature of the object being processed using an IR thermometer are: simple, reliable, economical and sufficiently sensitive methods,

- these methods enable direct examination of the influence of technological processing parameters (processing mode, tool material and processing object, cutting geometry, etc.) on the cutting temperature,

- with the developed method of temperature measurement, it is possible to compare the machinability of the material of the processing object,

- the obtained results show that in order to draw general conclusions, it is necessary to continue the tests, where it is necessary to expand the area of the processing mode and prevent the penetration of chips between the processing object and the IR thermometer.

LITERATURE

1. Abukhshim, N.A.; Mativenga, P.T.; Sheikh, M.A. Heat generation and temperature prediction in metal cutting: A review and implications for high speed machining. *Int. J. Mach. Tools Manuf.* 2006, 46, 782–800
2. Bruno G., José R., Cristina M. F., Daniel F., Hernâni L., Olga C. P., Filipe S. S., Georgina M., Real-Time Cutting Temperature Measurement in Turning of AISI 1045 Steel through an Embedded Thermocouple—A Comparative Study with Infrared Thermography, *Journal of Manufacturing and Materials Processing*, vol. 7, No. 50, 2023, 1-12
3. Bhirud, N.L.; Gawande, R.R. Measurement and prediction of cutting temperatures during dry milling: Review and discussions. *J. Braz. Soc. Mech. Sci. Eng.* 2017, 39, 5135–5158.
4. Grzesik, W. Heat in Metal Cutting. In *Advanced Machining Processes of Metallic*, 2nd ed.; Grzesik, W., Ed.; Elsevier: Amsterdam, The Netherlands, 2017; pp. 163–182.
5. Guimarães, B.M.P.; Fernandes, C.M.D.S.; de Figueiredo, D.A.; da Silva, F.S.C.P.; Miranda,

- M.G.M. Cutting temperature measurement and prediction in machining processes: Comprehensive review and future perspectives. *Int. J. Adv. Manuf. Technol.* 2022, 120, 2849–2878.
6. Kovac, P.; Gostimirovic, M.; Rodic, D.; Savkovic, B. Using the temperature method for the prediction of tool life in sustainable production. *Measurement* 2018, 133, 320–327.
 7. Rosas, J.; Lopes, H.; Guimarães, B.; Piloto, P.A.; Miranda, G.; Silva, F.S.; Paiva, O.C. Influence of Micro-Textures on Cutting Insert Heat Dissipation. *Appl. Sci.* 2022, 12, 65–83.
 8. Brito, R.F.; Carvalho, S.R.; Silva, S.L.E. Experimental investigation of thermal aspects in a cutting tool using comsol and inverse problem. *Appl. Therm. Eng.* 2015, 86, 60–68.
 9. Abdil K., Yahya I., M. C.C., Salih C., Kadir Ö., Thermocouple and Infrared Sensor-Based Measurement of Temperature Distribution in Metal Cutting, *Sensors* 2015, 15 1274–1291.
 10. Fang F. Z., Lee L.C., Liu X.D., Mean Flank Temperature Measurement in High Speed Dry Cutting of Magnesium Alloy, *Journal of Materials Processing Technology*, Volume 167, Issue 1, 25 August 2005, Pages 119–123.
 11. Brandao L.C., Coelho R.T., Malavolta A.T., Experimental and Theoretical Study on Workpiece Temperature when Tapping Hardened AISI H13 Using Different Cooling Systems, *Journal of Brazilian Society Mechanical Science & Engineering*, Vol. XXXII, No. 2, April-June 2010, pp. 154–159.
 12. Jie Liu, Y. Kevin Chou, On temperatures and tool wear in machining hypereutectic Al–Si alloys with vortex-tube cooling, *International Journal of Machine Tools & Manufacture* 47 (2007) 635–645
 13. Theo Ian van Nieker, Monitoring and diagnosis for control of an intelligent machining process, Ph.D Thesis, Faculty of Electrical and Mechanical Engineering, Port Elizabeth Technikon, George, South Africa, 2001.
 14. Nedić B., Erić M., Cutting Temperature Measurement and Material Machinability, *Thermal Science*, 2014, Vol. 18, No. 1, s259–s268.
 15. Carvalho S.R., Lima e Silva S.M.M., Machado A.R., Guimaraes G., Temperature determination at the chip–tool interface using an inverse thermal model considering the tool and tool holder, *Journal of Materials Processing Technology* 179 (2006) 97–104
 16. Zhao J., Liu Z., Shen Q., Wang, B., Wang, Q., Investigation of Cutting Temperature during Turning Inconel 718 with (Ti,Al)N PVD Coated Cemented Carbide Tools. *Materials* **2018**, 11, 1281.
 17. Xie J., Luo M., Wu K., Yang L., Li D., Experimental study on cutting temperature and cutting force in dry turning of titanium alloy using a non-coated micro-grooved tool. *Int. J. Mach. Tools Manuf.* **2013**, 73, 25–36.
 18. Campidelli A.F.V., Lima H.V., Abrão A.M., Maia A.A.T., Development of a wireless system for milling temperature monitoring. *Int. J. Adv. Manuf. Technol.* **2019**, 104, 1551–1560.
 19. Goyal A., Dhiman S., Kumar S., Sharma R., A study of experimental temperature measuring techniques used in metal cutting. *Jordan J. Mech. Ind. Eng.* **2014**, 8, 82–93.
 20. Saez-De-Buruaga, M.; Soler, D.; Aristimuño, P.; Esnaola, J.; Arrazola, P. Determining tool/chip temperatures from thermography measurements in metal cutting. *Appl. Therm. Eng.* **2018**, 145, 305–314
 21. Tanikić D., Manić M., Radenković G., Mančić D., Metal cutting process parameters modeling: an artificial intelligence approach, *Journal of Scientific & Industrial Research*, Vol. 68, June 2009. pp. 530–539
 22. Tanikić D., Manić M., Devedžić G., Modeliranje temperature strugotine korišćenjem metoda veštačke inteligencije, *Tehnička dijagnostika*, 2008, vol. 7, br. 4, str. 3–11
 23. Dogu Y., Aslan E., Camuscu N., A numerical model to determine temperature distribution in orthogonal metal cutting, *Journal of Materials Processing Technology* 171 (2006), 1–9
 24. János K., Viktor M., Investigation of cutting temperatures' relation to the tool wear, *Annals of Faculty Engineering Hunedoara - International Journal of Engineering*, Tome IX (Year 2011), Fascicule 2. pp. 169–172

PRIMENA VEŠTAČKOG TERMOPARA I IC TERMOMETRA ZA MERENJE TEMPERATURE PRI OBRADI METALA STRUGANJEM

Apstrakt: *Visoka temperatura koja nastaje prilikom obrade metala rezanjem ima negativan uticaj na postojanost reznog alata a može imati i negativan uticaj na predmet obrade. Zbog toga je od velike važnosti imati informacije o temperaturi u zoni rezanja i predmetu obrade. Precizno merenje temperature u realnom vremenu je i dalje izazov. Napori za precizno merenje temperature rezanja danas su usmereni u dva pravca. Jedan pravac se odnosi na postavljanje veštačkih termoparova što bliže zoni rezanja, a drugi pravac je primena infracrvene termografije i termovizije. U radu su prikazani rezultati merenja temperature primenom veštačkog termopara postavljenog neposredno ispod vrha rezne pločice strugarskog noža i primenom IC beskontaktnog termometra za merenje temperature na površini predmeta obrade pri različitim brzinama rezanja dva različita materijala.*

Ključne reči: *temperatura rezanja, struganje, veštački termopar, IC termometar, monitoring rezanja*



Society of Production
Engineering

SPMS 2023

39. Savetovanje proizvodnog mašinstva Srbije

ICPES 2023

39th International Conference on Production Engineering of
Serbia



Faculty of Technical
Sciences
University of Novi Sad

Novi Sad, Serbia, 26. – 27. October 2023

OPTIMIZATION OF SURFACE ROUGHNESS IN TURNING OF ALUMINUM ALLOY 2024-T3 USING TAGUCHI METHOD

Andjelko ALEKSIĆ^{1,*}, Marin GOSTIMIROVIĆ¹, Milenko SEKULIĆ¹, Borislav SAVKOVIĆ¹,
Dragan RODIĆ¹

¹Faculty of Technical Sciences, Novi Sad, Serbia

*Corresponding author: andjelkoa94@uns.ac.rs

Abstract: Determining optimal machining parameters is crucial for cost reduction and achieving the desired surface quality in production. This study investigates the influence of cutting parameters on surface roughness during the turning of aluminum alloy 2024-T3. The experiments were performed on a lathe machine using a cemented carbide tool. The turning experiments were designed following the Taguchi L9 orthogonal array method, with spindle speed, feed rate, and depth of cut selected as the cutting variables at three different levels. The obtained experimental data were analyzed using signal-to-noise ratios and analysis of variance. Furthermore, optimal cutting conditions were determined. Ultimately, the optimization of cutting parameters using the Taguchi method was validated through confirmation experiments.

Keywords: Aluminium alloys, machining parameters, surface roughness, dry turning, Taguchi method, ANOVA, S/N ratio.

1. INTRODUCTION

Aluminum, the third most abundant metal in the Earth's crust, posed a significant challenge to early scientists due to its stable oxygen compounds. The breakthrough in converting aluminum into a pure metal came in 1824 when it was first achieved in the laboratory of H.C. Ørsted in Denmark. It took nearly half a century for scientists to develop a method for mass production.

The pivotal moment in the history of aluminum production occurred in 1886 when P.L.T. Héroult invented the electrolytic reduction process. At the inception of the industry, aluminum production amounted to a

modest 45,000 tons annually. However, the landscape dramatically evolved, with production reaching 25 million tons in 1999 [1].

Today, the global demand for aluminum has soared to a staggering 67 million tons annually, and projections indicate a continual increase, reaching an estimated 78.4 million tons per year by 2029. The primary areas of application are in transportation (32%), containers and packaging (21%), and construction (13%). Remarkably, the aluminum content in an average automobile has escalated from 36 kg in 1973 to 161 kg in 2010 [2], [3]."

In their study, Xu et al. conducted an analytical investigation into the machining performance of 2024-T351 aluminum alloy

using TiAlN-coated carbide cutting tools in both low and high-speed machining scenarios. The findings indicated that high-speed milling of the 2024-T351 alloy resulted in reduced surface roughness and superior surface quality compared to low-speed machining [4].

Rubio et al. in their research examined chip formation during dry machining of aluminum alloys 2024 (Al-Cu) and 7050 (Al-Zn). The study considered parameters such as feed rate, cutting speed, and depth of cut, employing TiN-coated WC-Co turning inserts. Surface roughness was measured using a MAHR profilometer/roughness meter (Perthometer MI). Chips produced under various cutting conditions were classified based on their shapes using ISO 3685, a standard for steels and cast iron. The study aimed to relate chip formation to workpiece surface finish by comparing form and Ra parameters across different cutting scenarios. The results showed no significant correlation between chip classification in AA2024 and AA7050 alloys and the ISO standard for steels and cast iron [5].

Ramreddy and Varvatte conducted an experiment on the aluminum alloy Al 7075 using hard metal cutting tools on a lathe. The experiment was based on the Taguchi L9 experimental design, with data analysis carried out using ANOVA. The input parameters included cutting depth, feed rate, and cutting speed, while the output characteristics were surface roughness and material removal rate. Optimal processing parameters for minimizing surface roughness were found to be $a = 0.8$ mm, $s = 0.1$ mm/rev, and $v = 1500$ m/min, while for maximizing material removal rate, the optimal parameters were $a = 0.4$ mm, $s = 0.20$ mm/rev, and $v = 1500$ m/min [6].

2. TAGUCHI METHOD

Robust Design method, also called the Taguchi method, pioneered by Dr. Genichi Taguchi, greatly improves engineering productivity. The Taguchi method is a well-known technique that provides a systematic and efficient methodology for process optimization and this is a powerful tool for the design of high quality systems. Taguchi

parameter design is based on the concept of fractional factorial design. The main objective of parameter design is to minimize the process or product variation and to design robust and flexible processes or products that are adaptable to environmental conditions [7].

Taguchi's approach to design of experiments is easy to adopt and apply for users with limited knowledge of statistics; hence it has gained a wide popularity in the engineering and scientific community. This is an engineering methodology for obtaining product and process condition, which are minimally sensitive to the various causes of variation, and which produce high-quality products with low development and manufacturing costs. Many companies around the world have saved hundreds of millions of dollars by using the method in diverse industries: automobiles, xerography, telecommunications, electronics, software, etc.

Taguchi proposed a standard procedure for applying his method for optimizing any process. The steps suggested by Taguchi are [8]:

1. Determine the quality characteristic to be optimized
2. Identify the noise factors and test conditions
3. Identify the noise factors and test conditions
4. Design the matrix experiment and define the data analysis procedure
5. Conduct the matrix experiment
6. Analyze the data and determine the optimum levels for control factors
7. Predict the performance at these levels

The Signal-to-Noise Ratio (S/N ratio) and orthogonal arrays are two fundamental tools utilized in robust design. Orthogonal arrays enable designers to concurrently investigate numerous design parameters and provide a means to estimate the effects of each factor independently. The S/N ratio serves as a quality measurement with a specific focus on variation, while orthogonal arrays facilitate the handling of multiple design factors simultaneously [6].

The S/N ratio characteristics can be divided into three categories when the characteristic is continuous:

nominal is the best,

$$S/N = 10 \log \frac{\bar{y}}{s_y^2} \quad (1)$$

smaller the better

$$S/N = -10 \log \left(\frac{1}{n} \sum_{i=1}^n y_i^2 \right) \quad (2)$$

and

larger is better characteristics

$$S/N = -10 \log \left(\frac{1}{n} \sum_{i=1}^n \frac{1}{y_i^2} \right) \quad (3)$$

where \bar{y} is the average of observed data, s_y^2 the variance of y , n is the number of replication and y_i is the measured value of output variable. In the context of characteristic types, the higher the S/N ratio transformation, the more favorable the outcome.

For each characteristic type, following the above S/N ratio transformation, a smaller S/N ratio indicates a better result. The experiment's objective is to optimize the turning parameters to achieve improved surface roughness, utilizing the "smaller is better" criteria as defined in equation (2). The impact of each control factor can be more effectively visualized through response graphs. Additionally, optimal cutting conditions for the control factors can be readily determined from S/N response graphs.

3. EXPERIMENTAL SETUP

The experimental work was carried out at the Faculty of Technical Sciences in the Conventional Machining Laboratory. The conditions for the experimental tests are given in this chapter.

The conditions apply to:

- The workpiece material,
- the machine tool,
- the cutting tool and
- the machining conditions,
- the measuring technique.

The workpiece material: The experimental tests were carried out with the aluminum alloy 2024-T3. This material is used in almost all

fields, especially in aerospace, marine and automotive industries. The chemical structure is shown in Table 1. The workpiece had a length of 550 mm (cut length) and a diameter of 62 mm.

Table 1. Chemical structure of AL 2024-T3

Si	Cu	Fe	Zn	Mg	Mn
0,22	4,48	0,23	0,14	1,42	0,5
Ni	Pb	Sn	Ti	Cr	Ti+Zr
0,03	<0,04	<0,04	0,02	0,03	0,01

Machine tool: Machining was performed on universal lathe machine in dry condition.

Cutting tool: A turning cutter SDJCR2020K11, with cemented carbide inserts ("SECO" type DCGT11T308F- AL KX). Table 2 illustrates the geometrical characteristics of the cutting tool on the tool holder [9].

Table 2. Geometrical specifications of DCGT11T308F-AL KX insert

Geometrical Characteristics of DCGT11T308F-AL KX insert	Value
Clearance angle major	7°
Insert included angle	55°
Theoretical cutting edge length	11,60 mm
Corner radius	0,80 mm
Insert thickness	3,97 mm

Machining conditions: Depth of cut, feed rate, and cutting speed were used as cutting conditions. In Table 3 lists the cutting parameters and their values depending on the workpiece material of the workpiece and the tool manufacturer's recommendations.

Table 3. Machining parameters and their levels

Symbol	Parameters	Levels		
		1	2	3
A	Cutting speed v , [m/min]	200	250	315
B	Feed rate s , [m/rev]	0,1	0,155	0,2
C	Depth of cut a , [mm]	0,5	0,75	1

Measuring technique: A Mitutoyo SurfTest SJ-210 was used for the surface roughness measurements. Measurements were taken

three times for each experiment, and the mean value was selected for data processing.

4. RESULTS AND DISCUSSION

The experimental tests following the Taguchi orthogonal array $L_9 (3^4)$ were analyzed using the MINITAB software. In Table 4 shows the experimental setup and the measured results of average surface roughness R_a .

Table 4. The setup of experiments and results of average surface roughness R_a

Exp no.	A	B	C	v	s	a	R_a [μm]
1	1	1	1	200	0,1	0,5	1,508
2	1	2	2	200	0,155	0,75	1,942
3	1	3	3	200	0,2	1	3,504
4	2	1	2	250	0,1	0,75	1,921
5	2	2	3	250	0,155	1	2,449
6	2	3	1	250	0,2	0,5	3,116
7	3	1	3	315	0,1	1	2,415
8	3	2	1	315	0,155	0,5	1,936
9	3	3	2	315	0,2	0,75	3,057

In this study, all the analysis based on the Taguchi method was conducted using Minitab

software to determine the main effects of the cutting parameters, perform Analysis of Variance (ANOVA), and establish the optimum conditions [10], [11]. Table 5 displays the transformation of experimental results into signal-to-noise ratios.

Table 5. Results of signal-to-noise ratio.

Exp no.	A	B	C	R_a [μm]	Calculated S/N ratio
1	1	1	1	1,508	-3,568
2	1	2	2	1,942	-5,765
3	1	3	3	3,504	-10,891
4	2	1	2	1,921	-5,670
5	2	2	3	2,449	-7,779
6	2	3	1	3,116	-9,872
7	3	1	3	2,415	-7,658
8	3	2	1	1,936	-5,738
9	3	3	2	3,057	-9,706

Table 6 shows the S/N ratios with each factor and the corresponding level for the average surface roughness. The factors with the largest difference in mean values (max–min) have the greatest influence on the output size. From the table, it can be seen that the feed rate has the greatest influence on the average surface roughness, followed by the cutting speed, and depth of cut.

Table 6. Response table of S/N ratio for average surface roughness R_a

No.	Factors		Levels			Min-Max	Rang
			1	2	3		
1	A	Cutting speed v, [m/min]	-6,741*	-7,774	-7,701	1,033	3
2	B	Feed rate s, [mm/rpm]	-5,634*	-6,428	-10,157	4,523	1
3	C	Depth of cut a, [mm]	-6,393*	-7,048	-8,777	2,384	2

The influence of individual input parameters on the output performance of the machining process can be represented using a response graph, which demonstrates the change in the S/N ratio when the control parameter level changes from 1 to 3. Consequently, the impact of individual parameters on the output characteristic of the machining process is graphically expressed through the slope of the

line connecting different parameter levels (Fig. 1).

The highest value of the S/N ratio on the corresponding graph provides the answer to the question of which level of the control parameter is optimal. Optimizing the cutting parameters within the specified factor levels, based on the 'the smaller, the better' criterion, yields the optimal combination of control factors: A=1, B=1, and C=1.

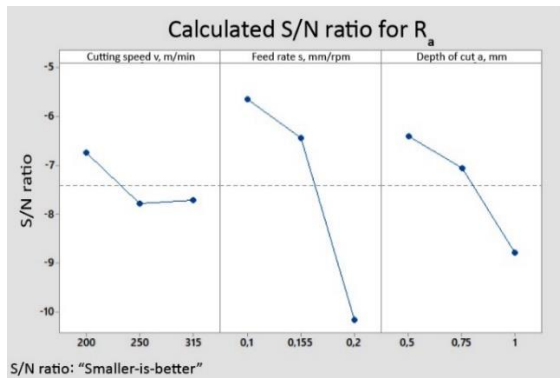


Figure 1. Response ANOVA graph for average surface roughness R_a

Table 7. Optimal setting of input parameters with confirmation experiment.

Factors	Level	Value	Obtained R_a using the Taguchi Method	Confirmation Experiment
v [m/min]	1	200	S/N=-3,956 $R_{a,opt}=1,577$ [μm]	$R_a=1,508$ [μm]
s [mm/rpm]	1	0,1		
a [mm]	1	0,5		

According to the research of [12], a prediction is considered good if the average error is up to 10%. Therefore, the single-objective optimization of the input parameters of the turning aluminum alloy 2024-T3 can be considered successful.

5. CONCLUSION

This paper presents the application of Taguchi method for optimizing surface roughness in turning of Al 2024-T3 under dry condition. Using signal to noise (S/N) ratio and ANOVA results the significance of cutting parameters was determined to get better surface roughness. The experimental results revealed that:

- Taguchi method is a powerful technique for designing and analyzing the experimental results in machining researches.
- The feed rate has the most significant influence on the average surface roughness, followed by the cutting depth, while the cutting speed has the least impact.
- By optimizing the input parameters for the minimum output size ($R_a=1,577$ μm),

The confirmation test (Table 7) is the final step to verify the improvement in the average surface roughness at the optimal level of process parameters. The average error between the values of average surface roughness obtained by the prediction based on the Taguchi analysis and the values obtained after the verification experiments (with the optimal input parameter values) was only 4,37%.

the minimum levels for all three input factors were obtained.

- The error of 4.37% between the measured size based on optimal input factors and the calculated size confirms the success of the experiment.

Further research in the field of machining aluminum alloys with carbide inserts could focus on expanding the factors that influence surface roughness during turning. This might include investigating the impact of coolant and lubricant usage as well as the nose radius.

ACKNOWLEDGEMENT

This research (paper) has been supported by the Provincial Secretariat for Higher Education and Scientific Research AP of Vojvodina through project No. 142-451-334/2023-01/2: "Advanced processing technologies of modern engineering materials".

REFERENCES

- [1] T. Cock, "Aluminium - A Light Metal," *TALAT - Training in Aluminium Application Technologies*, pp. 1–10, 1999.
- [2] Statista, "Global aluminum consumption projections from 2021 to 2029," Statista Research Department. Accessed: Jan. 19,

2023. [Online]. Available: <https://www.statista.com/statistics/863681/global-aluminum-consumption/>
- [3] B. Stempel, "The Road Ahead Looks Brighter and Lighter," in *American Metal Market's North American Aluminum Conference*, Chicago, Jun. 2007.
- [4] D. Xu, P. Feng, W. Li, Y. Ma, and B. Liu, "Research on chip formation parameters of aluminum alloy 6061-T6 based on high-speed orthogonal cutting model," *The International Journal of Advanced Manufacturing Technology*, vol. 72, no. 5–8, pp. 955–962, May 2014, doi: 10.1007/s00170-014-5700-3.
- [5] E. M. Rubio, A. M. Camacho, J. M. Sánchez-Sola, and M. Marcos, "Chip arrangement in the dry cutting of aluminium alloys Manufacturing and processing," *Journal of Achievements in Materials and Manufacturing Engineering*, vol. 16, no. 1–2, pp. 164–170, 2006, [Online]. Available: www.journalamme.org
- [6] B. Ramreddy and G. Varvatte, "Optimization of Process Parameters in Cnc Turning of Aluminium Alloy 7075 By Taguchi Method Using Regression Analysis," *Indian J Sci Res*, vol. 12, no. 1, pp. 203–208, 2015, [Online]. Available: <https://go.gale.com/ps/i.do?p=AONE&u=googlescholar&id=GALE%7CA454619925&v=2.1&it=r&sid=AONE&asid=9d22dcb9>
- [7] Ranjit K. Roy, *Design of Experiments Using The Taguchi Approach: 16 Steps to Product and Process Improvement*. John Wiley & Sons, 2001.
- [8] S. Kumar Bathini, G. Ramya, B. S. Kumar, and N. Gopikrishna, "Optimization of Milling Process Parameters using Taguchi Parameter Design Approach," 2017. [Online]. Available: <http://www.ripublication.com>
- [9] "Secotools.com," "Elektronski katalog reznih alata za obradu struganjem." Accessed: Feb. 21, 2023. [Online]. Available: https://www.secotools.com/article/p_00040400
- [10] A. Aleksic, M. Sekulic, B. Savkovic, M. Gostimirovic, I. Kamenko, and P. Kovac, "Optimization of cutting parameters by nature-inspired algorithms," *Acta Technica Corviniensis - Bulletin of Engineering*, vol. 13, no. 4. pp. 41–44, 2020.
- [11] A. Aleksić, M. Sekulić, M. Gostimirović, D. Rodić, B. Savković, and A. Antić, "EFFECT OF CUTTING PARAMETERS ON CUTTING FORCES IN TURNING OF CPM 10V STEEL," *Journal of Production Engineering*, vol. 24, no. 2, pp. 5–8, Dec. 2021, doi: 10.24867/JPE-2021-02-005.
- [12] P.J. Ross, *Taguchi Techniques for Quality Engineering*. OH: McGraw-Hill International Book Company, 1996.

SPMS/ICPES 2023

**39TH INTERNATIONAL CONFERENCE ON
PRODUCTION ENGINEERING OF SERBIA**

**SESSION 4:
MACHINE TOOLS AND AUTOMATIC FLEXIBLE TECHNOLOGICAL
SYSTEMS, CAx AND CIM PROCEDURES AND SYSTEMS**

Novi Sad, 26 – 27 October 2023



Society of Production
Engineering

SPMS 2023

39. Savetovanje proizvodnog mašinstva Srbije

ICPES 2023

39th International Conference on Production Engineering of
Serbia



Faculty of Technical
Sciences
University of Novi Sad

Novi Sad, Serbia, 26. – 27. October 2023

AN APPROACH FOR AUTOMATIC FREE FORM SURFACE MILLING MACHINING TECHNOLOGY DESIGN

Goran MLADENOVIC^{1,*}, Radovan PUZOVIC¹, Jagos STOJANOVIC¹, Ivana JEVTIC², Mihajlo
POPOVIC¹, Milos PJEVIC¹

¹University of Belgrade – Faculty of Mechanical Engineering, Kraljice Marije 16, Serbia

²Innovation Centre of the Faculty of Mechanical Engineering, Kraljice Marije 16, Belgrade
Serbia

*Corresponding author: gmladenovic@mas.bg.ac.rs

Abstract: Parts with free form surfaces are commonly used in wide area of engineering, not only in mechanical engineering. When it comes to the area of mechanical engineering, the main problem is how to produce such parts. One of the commonly used methods is milling with ball end mill cutter on 3, 4 or 5 axis mill machines. A usual approach for production of such parts is to generate NC code in some of commercial CAM software and afterwards load it on CNC machine. In this paper is presented the software for automatic technology design which is developed at the department of production engineering of the Faculty of Mechanical engineering in Belgrade, Serbia. Based on loaded CAD models of the final product and workpiece which will be used for production software automatically gives the NC code for machining according to implemented machining strategies. The core of software is a module for machining simulation process which allow multicriteria optimization method for machining. Verification of the generated NC code was done on horizontal machining center and after that measurement of machined part where was verified quality of machined part in predefined tolerances.

Keywords: CAD/CAM, free form surface, milling, force prediction, ball end mill cutter.

1. INTRODUCTION

It is widely known that use of parts with free form surfaces is widely used in almost every field of engineering, not only in mechanical engineering. When it comes to the area of mechanical engineering, especially in area of production engineering the main challenge is how to produce such parts. The most used method for this is by machining with ball end mill cutter on 3, 4 or 5 axis CNC milling machines. For this purpose, free form surface is

approximated with triangles i.e., line segments so it can be calculated surface and leading plane cross section. In the past, beside development of machining strategies it was started on research in the field of tool path optimization so that free form surface machining could be done faster, better and cheaper. The worldwide used method for tool path optimization is federate scheduling which is commonly based on specific production (MRR – **Material Removal Rate**) [1, 2] or on cutting force prediction also called TWE – **Tool**

Workpiece Engagement [3, 4]. There are a few more methods which are also used like workpiece discretization and models with Z map for example.

In this paper is presented developed software for automatic tool part generation and optimization for milling of one parts class with free form surfaces on 3 axis milling machines with ball end mill cutter.

2. SYSTEM DEVELOPMENT

Research in the field of free form surface machining exist over than 20 years at the Department of Production Engineering at the University of Belgrade – Faculty of Mechanical Engineering. A few years ago, it was developed CAM software (figure 1) for automatic technology design for machining of parts with free form surfaces [5].

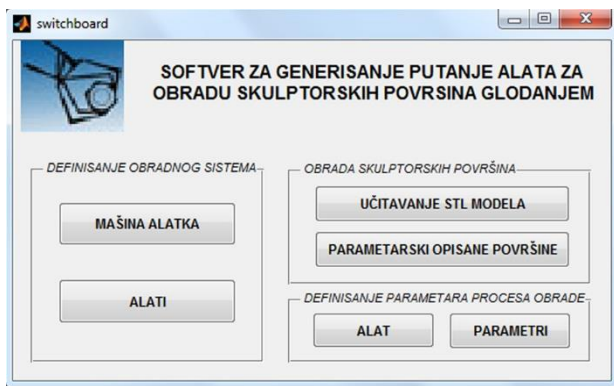


Figure 1. Developed CAD/CAM software [5]

The main system core is a module for cutting process simulation which allows exact calculations of machining parameters based on force prediction model [6-10] which is also developed and built in system.

Bellow, there will be given a short description of the main system components.

2.1 Free form surface CAD model loading

This CAM system is developed for loading CAD models from commercial CAD software which is saved in STL (Stereolithography) file format. Using of this file format allows to get approximate surface shape, figure 2 and based on that reduce the need for big numerical calculation of surface and leading plane cross

section. When the CAD model is loaded, system also calculates minimal curvature radius of the surface so it can be chosen tool from the software database which is also developed and described in [5].

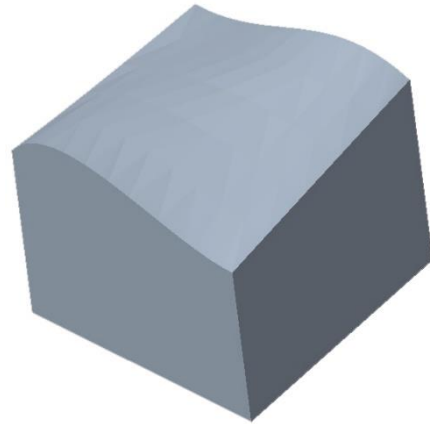


Figure 2. Approximated surface with triangles

In this step, software generates leading planes parallel to the coordinate axes with distances between them calculated based on demanded surface roughness defined by software used. For every leading plane it is calculated CL (Cutter Location) points which will be used to generate optimized tool path which allows machining with minimal needed time. Idea for machining strategies comes from detailed analysis of commercial CAM softwares which are described in [11-13]. For further procedures in this stage workpiece CAD model is also loaded in the same format as part which should be machined.

2.2 Cutting process simulations

After CAD model is loaded and appropriate tool is chosen, system calculate number of tool revolution and federate from [14, 15]. This federate is corrected by amount of material in every CL point so total cutting force will be the same value in every CL point. On this way, it is avoided tool breakage because for every tool loaded in software database is given the maximal value of allowed cutting force. Developed system has possibility for upgrade with new materials and tools because parameters for force model prediction are in direct correlation with chosen tool and workpiece geometry and material. Described

procedure allows rough machining with an approximate shape of surface directly in one pass from workpiece without previous pre-machining. If the direct machining with ball end mill cutter isn't possible, system gives message that pre-machining method is needed. In those cases, it is possible to get the NC code for rough machining with end mill or milling head described in [16, 17].

2.3 Tool path generation

After the CL points and machining parameters are calculated system chooses which of the implemented machining strategies gives minimal machining time. For now, system has 3 solutions for tool part: parallel, spiral and ZIG-ZAG topology. Generation of the NC code is automated and it is after calculation stored in installation folder of CAM software.

3. EXPERIMENTAL VERIFICATION

3.1 NC code generation

With the developed application is allowed automated tool path generation, figure 3.

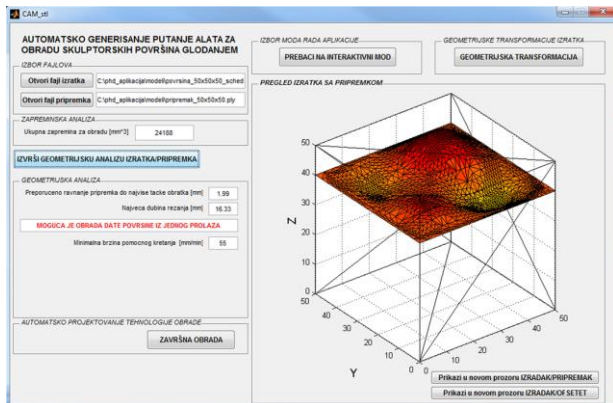


Figure 3. Developed CAD/CAM software [5]

It is not needed expert knowledge from user to work with software. At the beginning of technology design, user loaded CAD models of part and workpiece. After that it is needed to input required surface roughness and tolerance. Tool selection is automated by the geometry analysis of the loaded part, but it is also possible to manually choose tool for machining. User

can also choose a machining strategy if there is some special demand.

The final output from generated CAM software is NC code. That code is generated by multicriteria optimization and allows machining of loaded part in one pass with ball end mill cutter. For this purpose, all the machining parameters and tool part topology are generated in automatic software mode.

3.2 Machining

Automatically generated NC code is used for machining. Machining was performed on Horizontal working center ILR HMC500/40 at the University of Belgrade – Faculty of Mechanical Engineering, Department of Production Engineering.

Workpiece from aluminum AlMg4.5Mn was fastened on machine table with dynamometer, figure 4. Machining was done with ball end mill cutter without cooling because we wanted to tested generated force prediction model which doesn't predict the use of a cooling system, figure 4.

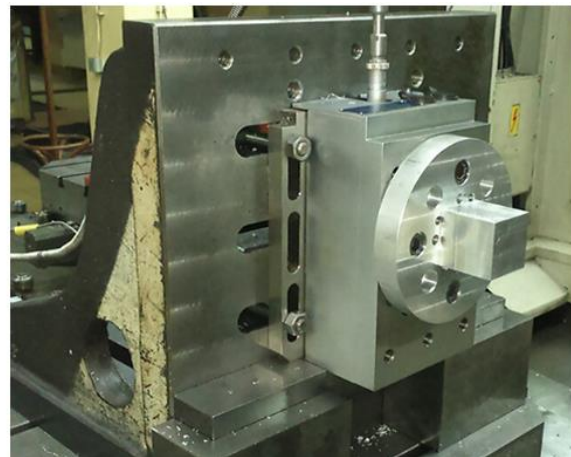


Figure 4. Machining on ILR HMC 500/40 [5]

4. CONCLUSION

By the described procedures in this paper it was presented one way for free form surface machining, especially NC technology design for this purposes. Use of the given procedures are justified only in rough machining where depth of cut is large and it is not needed to get exact shape of the surface, which will be conducted in finish machining where depth of cut is small.

ACKNOWLEDGEMENT

The author wishes to thank the Ministry of Science, Technological Development and Innovation of Republic of Serbia for providing financial support that made this work possible (by the contract: 451-03-47/2023-01/ 200105 from 03.02.2023).

REFERENCES

- [1] Ip R.W.L., Lau H.C.W., Chan F.T.S., An economical sculptured surface machining approach using fuzzy models and ball-nosed cutters. *Journal of Materials Processing Technology*, 138(1-3), pp. 579-585, 2003.
- [2] Li Z.Z., Zheng M., Zheng L., Wu Z.J., Liu D.C., A solid model-based milling process simulation and optimization system integrated with CAD/CAM. *Journal of Materials Processing Technology*, 138(1-3), pp. 513-517, 2003.
- [3] Altintas Y., *Manufacturing Automation – Metal Cutting Mechanics, Machine Tool Vibrations and CNC Design*, Cambridge University Press, Cambridge, 2000.
- [4] Layegh S.E.K., Lazoglu I., Offline Force Control and Feedrate Scheduling for Complex Free Form Surfaces in 5-Axis Milling. *Procedia CIRP*, Fifth CIRP Conference on High Performance Cutting 2012, 1, pp. 96-101, 2012.
- [5] Mladenovic G. Tool Path Optimization in Sculptured Surface machining, Doctoral Dissertation, University of Belgrade – Faculty of Mechanical Engineering, 2015. (in Serbian).
- [6] Mladenovic G., Tanovic Lj., Ehmann K.F.: Tool Path Generation for Milling of Free Form Surfaces with Feedrate Scheduling. *FME Transactions*, 43(1): pp. 9-15, 2015.
- [7] Mladenović G., Tanović Lj., Puzović R., Pjević M., Popović M.: The Development of Software Solution for Automatic Choice of Machining Parameters for Free Form Surfaces Parts, 41th JUPITER Conference, pp. 2.19-2.24, Belgrade, June, 2018. (in Serbian).
- [8] Goran M. Mladenovic, Marko J. Milovanovic, Ljubodrag M. Tanovic, Radovan M. Puzovic, Milos D. Pjevic, Mihajlo D. Popovic, Slavenko M. Stojadinovic: Development of Application Software for Automatic Manufacturing Technology Design of Free Form Surfaces, 3rd International Conference of Experimental and Numerical Investigations and New Technologies - CNN TECH 2019, pp. 65-65, Zlatibor, June, 2019.
- [9] Mladenović, G., Tanović, Lj., Milovanović, M., Popović, M., Puzović, R., Pjević, M., Development of a System for Automatic Technology Design for Pre-Machining of Parts with Free Form Surfaces, 42nd JUPITER Conference, pp.2.1-2.6, Belgrade, October, 2020. (in Serbian).
- [10] Jagos M. Stojanovic, Goran M. Mladenovic, Jovan D. Tanaskovic, Milos D. Pjevic, Force Prediction Models in Ball End Milling of Freeform Surfaces, 7th International Conference of Experimental and Numerical Investigations and New Technologies – CNN TECH 2023, pp.64-64, Zlatibor, July, 2023.
- [11] G. Mladenović, Lj. Tanović, R. Puzović, M. Popović, Analysis of Machining Strategies Using Commercial CAD/CAM Software, 35th International Conference On Production Engineering 2013, pp.307-310, Kopaonik, September, 2013.
- [12] Mladenović G., Tanović Lj., Pjević M., Free Form Machining – Comparison of Machining Strategies, 39th JUPITER Conference, pp.2.19-2.24, Belgrade, October, 2014. (in Serbian).
- [13] Jagos Stojanovic, Goran Mladenovic, Analysis of Methods for Tool Path Generation Using Commercial CAM Systems, 6th International Conference of Experimental and Numerical Investigations and New Technologies – CNN TECH 2022, pp.59-59, Zlatibor, July, 2022.
- [14] Kalajdzic, M. et al. *Cutting technology - a handbook*, FME, Belgrade, 2017 (in Serbian).
- [15] Kalajdzic, M. *Manufacturing technology*, FME, Belgrade, 2019 (in Serbian)
- [16] Goran Mladenović, Ljubodrag Tanović, Radovan Puzović, Marko Milovanović, Mihajlo Popović, Miloš Pjević, Vojislav Simonović, Development OF CAM System for Rough Machining in Free Form Surface Manufacturing, 5th International Scientific Conference COMETA2020, pp. 84-90, Jahorina, B&H, November 2020.
- [17] Goran Mladenović, Ljubodrag Tanović, Radovan Puzović, Mihajlo Popović, Milos Pjević, Software Upgrade for Automatic Rough Milling Technology Design for Parts with Free Form Surfaces, 38th International Conference on Production Engineering of Serbia- ICPE-S 2021, pp.57-57, Čačak, October, 2021.



Society of Production
Engineering

SPMS 2023

39. Savetovanje proizvodnog mašinstva Srbije

ICPES 2023

39th International Conference on Production Engineering of
Serbia



Faculty of Technical
Sciences
University of Novi Sad

Novi Sad, Serbia, 26. – 27. October 2023

OPTIMIZACIJA PRIPREME MAŠINE ZA OBRADU DRVETA PRIMENOM SMED METODE

Jovana PERIĆ¹, Milovan LAZAREVIĆ², Dragić TOMIĆ², Branko RADIČEVIĆ¹, Vladan GRKOVIĆ¹

¹ Fakultet za mašinstvo i građevinarstvo u Kraljevu, Srbija, peric.j@mfkv.kg.ac.rs,
radicevic.b@mfkv.kg.ac.rs, grkovic.v@mfkv.kg.ac.rs

² Fakultet tehničkih nauka, Srbija, laza@uns.ac.rs, drtomic81@hotmail.com

Apstrakt: U svetu neprekidnog razvoja tržišta i sve zahtevnijih potreba kupca, od ključne je važnosti uskladiti proizvodne procese. Kako bi se direktno odgovorilo na zahteve u pogledu smanjenja proizvodnog vremena, neophodna je primena SMED (Single Minute Exchange of Die) metode kao osnovnog alata unutar Toyota proizvodne filozofije. SMED metoda omogućava zamenu alata u kratkom vremenskom intervalu čime ostvaruje minimalne zastoje i omogućava proizvodnju različitih proizvoda. Na ovaj način pomenuta metoda dodatno povećava fleksibilnost i produktivnost kompanije. Cilj ovog istraživanja je smanjenje vremena zamene alata u proces obrade okvira vrata, koja obuhvata pet tehnoloških operacija koje zahtevaju tri izmene alata.

Ključne reči: SMED, Kaizen, Lean, Fleskibilnost, Efikasnost

UVOD

U današnjem globalnom poslovnom okruženju, kompanije su pod stalnim pritiskom zbog brzih tehnoloških promena i oštre konkurencije. Kupci, svesni prednosti savremenog tržišta, zahtevaju ne samo brze isporuke, već i besprekornu pouzdanost usluga isporuke [1]. Ovaj zahtevni spektar potreba postavlja kompanije pred složen izazov: kako povećati varijabilnost u proizvodnji, istovremeno smanjujući aktivnosti koje ne donose dodatnu vrednost proizvodima, a sve to uz održavanje kontinuiteta proizvodnje [2]. Ovaj paradoks naglašava važnost procesa zamene alata u proizvodnji. Pa se kompanije suočavaju s dilemom - da li minimizirati ukupan broj zamena alata ili smanjiti vreme trajanja samih zamena [3].

Kada se analiziraju gubici u kompanijama, vreme utrošeno na zamenu alata često se smatra jednim od najznačajnijih oblika nepotrebnog gubljenja vremena [4]. Smanjenje trajanja ovog procesa direktno vodi do smanjenja troškova [5]. Jedan od efikasnih načina za rešavanje ovog problema je prelazak na proizvodnju manjih serija, uz istovremenu primenu principa Lean proizvodnje kako bi se povećala produktivnost i održali niski troškovi [6]. S druge strane, dugotrajne i komplikovane zamene alata često teraju kompanije da izbegavaju zamene, što rezultira proizvodnjom velikih serija [7].

Svi navedeni razlozi jasno ukazuju na potrebu za smanjenjem vremena potrebnog za zamenu alata, što se postiže uvođenjem sistema brze zamene [8]. Jedan od najefikasnijih alata za implementaciju ovog sistema je poznat kao SMED metoda (Single

Minute Exchange of Die) [9]. Koji kroz postupne promene u organizaciji procesa zamene, standardizaciji procedura, primeni specijalnih pomagala i tehničke modifikacije mašina, omogućava radikalno skraćivanje vremena potrebnog za zamenu alata, smanjujući ga sa nekoliko sati na svega nekoliko minuta [10].

CHANGEOVER

U modernoj proizvodnji, posebno u okviru Lean proizvodne prakse, teži se smanjenju proizvodnog otpada i ispunjenju zahteva kupaca u željenim količinama i u pravom vremenu isporuke kako bi se postigla konkurentna prednost na tržištu [11]. Ključ za postizanje ovih ciljeva je povećanje fleksibilnosti kroz proizvodnju manjih serija [12]. Međutim, ovakav pristup obično dovodi do čestih promena sistema, poznatih kao "Changeover".

Changeover obuhvata vreme (Setup time), potrebno za izvođenje niza aktivnosti koje su neophodne prilikom prelaska sa jedne tehnološke operacije/procesa na drugu, uključujući zamenu alata ili opreme [13]. Ove aktivnosti uključuju zaustavljanje mašina, čišćenje, zamenu alata, podešavanje, testiranje i postizanje visokog kvaliteta proizvoda. Sve ove aktivnosti se mogu podeliti na eksterne i interne. Aktivnosti eksternog podešavanja se mogu izvoditi dok sistem radi, dok se aktivnosti internog podešavanja mogu izvoditi samo kada je sistem zaustavljen [14].

Važno je napomenuti da se ove aktivnosti često smatraju nepotrebnim gubicima jer ne doprinose vrednosti proizvodu, a istovremeno značajno povećavaju ukupne troškove proizvodnje [15]. Stoga je od suštinskog značaja optimizovati ih kako bi se smanjilo vreme potrebno za njihovo izvođenje. U tu svrhu, ključna je primena odgovarajućih metoda, kao što je SMED metod.

SMED METOD

SMED, skraćenica od "Single Minute Exchange of Dies," je moćna tehnika usmerena na smanjenje vremena potrebnog za zamenu i

podešavanje alata na manje od deset minuta [16]. Razvoj SMED tehnike započeo je 1950. godine, pod vodstvom Shigeo Shinga, istaknutog stručnjaka za kaizen, u kompaniji Mazda u Hirošimi. Prvi konkretni rezultati primene SMED-a pojavili su se u kompaniji Toyota u Nagoyi 1969. godine, da bi tek 1985. godine SMED metod pojavio i u zapadnim zemljama [17].

Cilj SMED metode je fokusirati se na smanjenje vremena potrebnog za zamenu i postavljanjem alata kako bi se smanjili zastoji mašina, gubitak vremena i troškovi proizvodnje [18]. Rezultat ovog pristupa je veća fleksibilnost i efikasnost u proizvodnji, ključna za optimizaciju vremena u proizvodnim procesima [19]. SMED je posebno koristan za proizvodnju različitih delova i za slučajeve čestih zamena alata pri proizvodnji manjih serija.

Očekivani rezultati primene SMED metode ogledaju se ne samo u ekonomskim koristima, kao što je povećan proizvodni kapacitet, već i u poboljšani ergonomski uslovi, standardizaciji, jačanju timskog rada i ravnoteži opterećenja. [20]. Razvojem ove tehnike omogućeno je brzo i efikasno izvođenje zamena alata, čime se olakšava rad proizvodnih radnika.

Implementacija SMED metode

Kako bi se SMED metoda pravilno implementirala u proizvodnom procesu, neophodno je sprovesti četiri glavna koraka (Slika 1) [21]:

1. Posmatranje procesa zamene alata:

Prvi korak u primeni SMED metode podrazumeva temeljnu analizu postojećeg sistema. Ovo uključuje pažljivo posmatranje procesa zamene alata i komunikaciju sa operaterima kako bi se bolje razumeo proces. Takođe, važno je dokumentovati sve korake koji su potrebni tokom zamene alata, uključujući i merenje vremena potrebnog za izvođenje svake od aktivnosti.

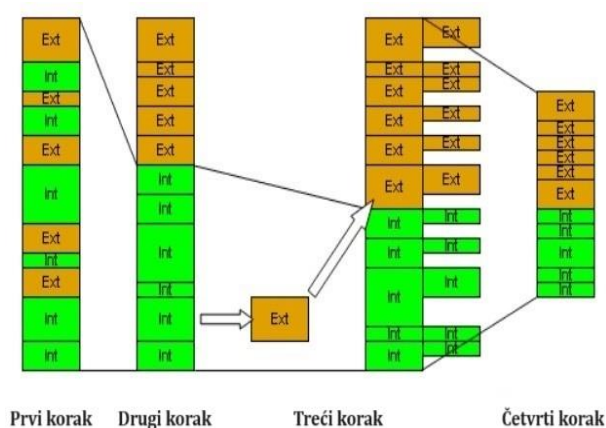
2. Razdvajanje internih i eksternih aktivnosti:

Nakon što se detaljno

analizira proces zamene alata, sledeći korak je precizno razdvajanje aktivnosti na interne (koje se obavljaju dok je mašina zaustavljena) i eksterne (koje se mogu izvoditi dok mašina radi). Takođe, neophodno je identifikovati ukupno vreme trajanja internih i eksternih aktivnosti.

3. Transformacija internih aktivnosti u eksterne aktivnosti: U ovom koraku, izvodi se transformacija internih aktivnosti kako bi se utvrdilo da li postoje interne aktivnosti koje bi se mogle transformisati u eksterne, tj. koji bi se obavljati dok mašina radi.

4. Optimizacija internih i eksternih aktivnosti: Poslednji korak je fokusiran na unapređenje procesa zamene alata kako bi se smanjila vremena potrebna za obavljanje internih i eksternih aktivnosti. Ovo može uključivati eliminaciju nepotrebnih koraka ili aktivnosti tokom zamene alata, optimizaciju ljudskih aspekata kroz bolju pripremu i organizaciju rada, tehnološke promene unutar procesa, uvođenje automatizacije, redizajn mašina i alata.



Slika 1. Koraci u implementaciji SMED-a [22]

PRIMENA SMED METODE U PROIZVODNOJ KOMPANIJI ZA PROIZVODNJU SOBNIH VRATA

U proizvodnoj kompaniji koja se bavi proizvodnjom sobnih vrata, uočen je problem prilikom zamene alata tokom procesa obrade

okvira vrata, kada je u pitanju obrada u pojedinačnoj proizvodnji sa malim serijama. Proces obrade okvira vrata koji se izvodi na glodalici obuhvata pet tehnoloških operacija, za koje je potrebna zamena tri različita alata. Konkretni problemi prilikom zamene alata obuhvataju dugo vreme potrebno za zamene i podešavanja alata. Dodatno, pri podešavanju alata na određenu dubinu i visinu prodiranja u materijalu, često se javljaju odstupanja od propisanih vrednosti. Sve ove poteškoće zajedno dovode do zastoja u proizvodnom procesu, gubitka vremena i dodatnih troškova, što rezultira smanjenjem fleksibilnosti i efikasnosti kompanije. Jedan od pristupa za rešavanje ovog problema je primena SMED metode, koja se sprovodi kroz četiri ključna koraka.

Posmatranje procesa zamene alata

Nakon detaljnog posmatranja i analize procesa zamene alata, zabeležene su sve aktivnosti koji su neophodne za zamenu alata u svakoj tehnološkoj operaciji, uključujući merenje vremena koje je potrebno za svaku od tih aktivnosti. Dobijeni rezultati su vizuelno ilustrovani kreiranjem Gantovog dijagram koji je prikazan na slici 2.

Razdvajanje internih i eksternih aktivnosti

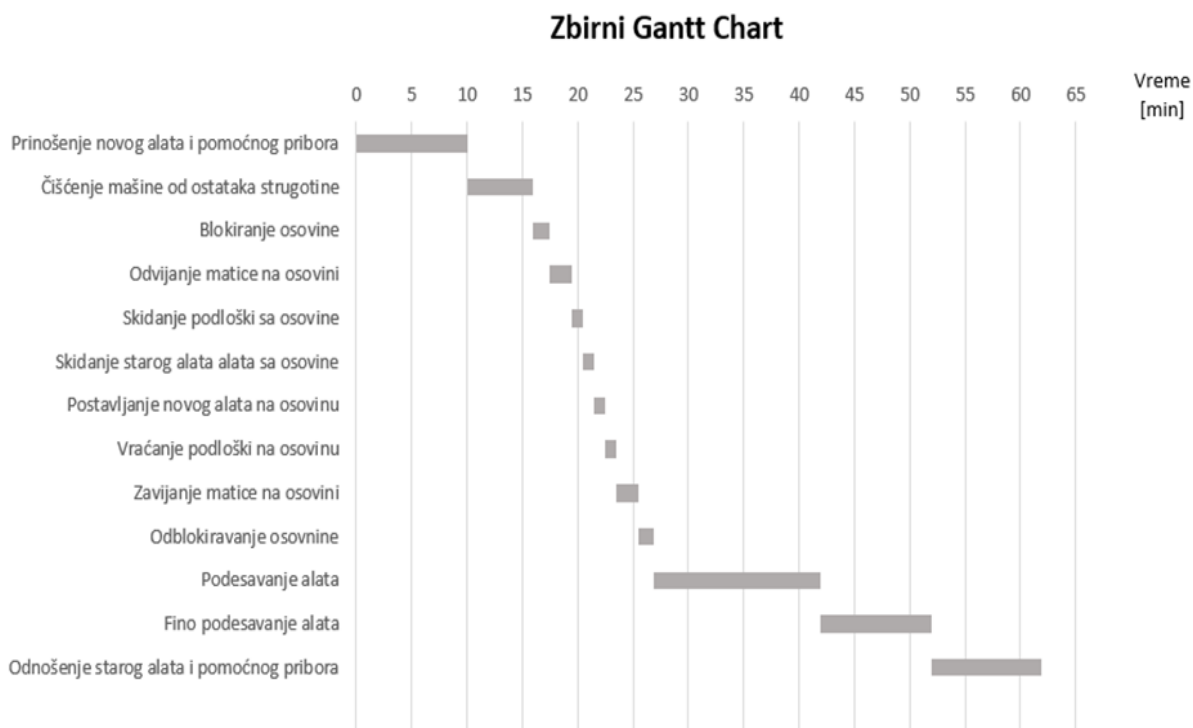
U drugom koraku ovog procesa, izuzetno važno je pažljivo i precizno razdvojiti interne od eksternih aktivnosti. Rezultate razdvajanja aktivnosti kao i vremena trajanja za svaku od njih jasno je prikazano na Gantovom dijagramu, koji se nalazi na slici 3. Ovaj dijagram pruža celovit pregled internih i eksternih aktivnosti, čime omogućava bolje razumevanje procesa zamene alata i identifikaciju potencijalnih oblasti za transformaciju i optimizaciju.

Transformacija internih aktivnosti u eksterne aktivnosti

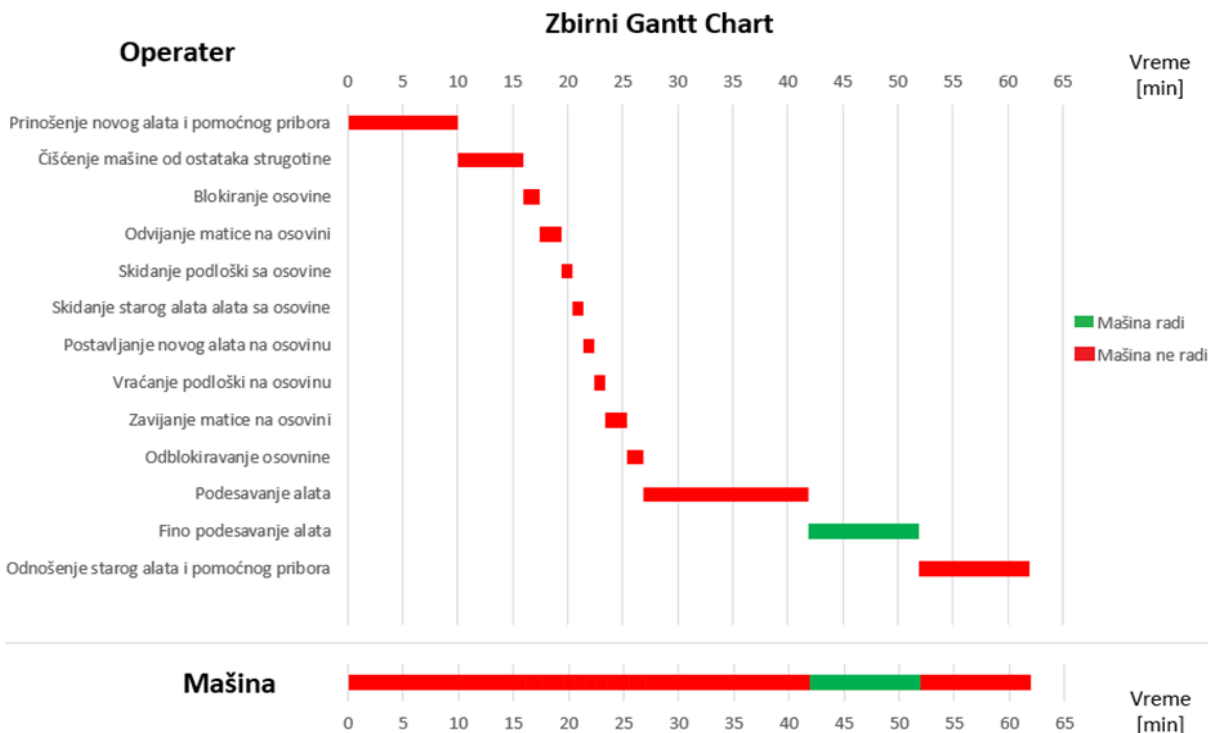
S obzirom na to da se radi o zamenama alata koji služi za obradu okvira vrata, sve zamene alata je neophodno obavljati onda kada mašina

ne radi, što bi predstavljalo interne aktivnosti. Razlog tome je prvenstveno radi sigurnosti radnika na tom radnom mestu, ali i zbog toga što te aktivnosti nije ni moguće obavljati dok mašina radi. Shodno tome mali je broj aktivnosti koje se mogu transformisati u

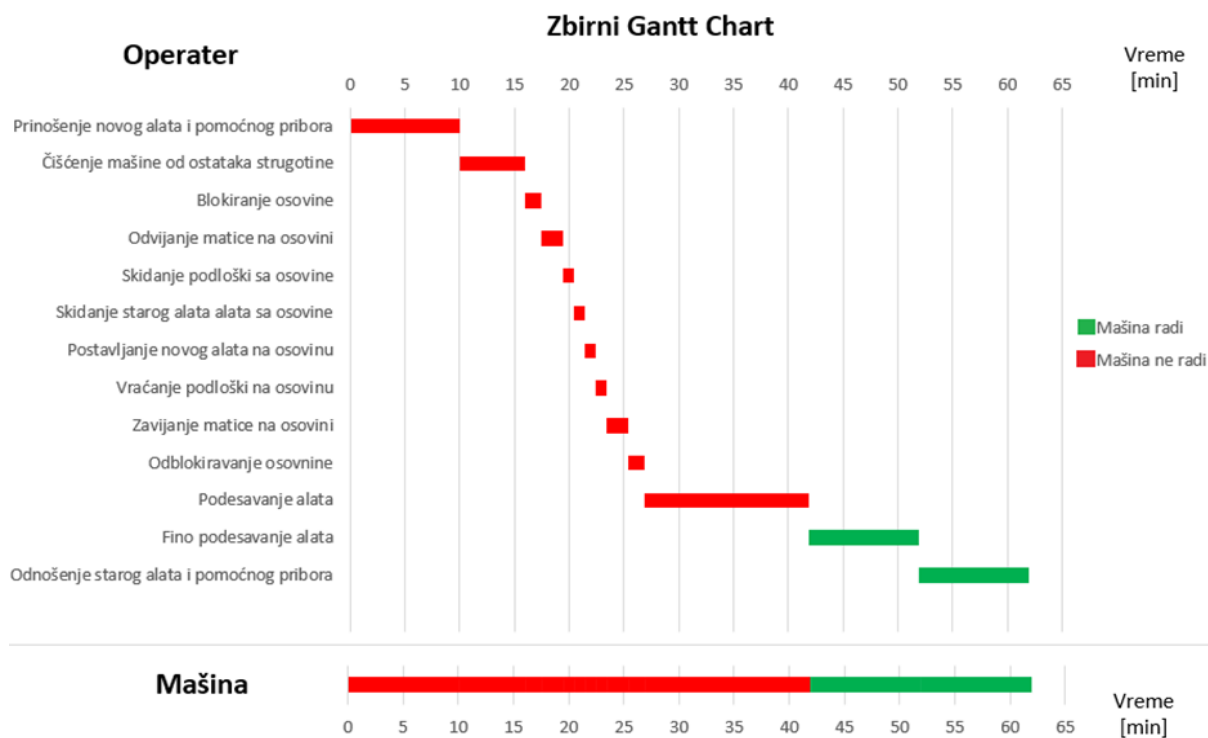
eksterne. Jedna od aktivnosti koja se nakon transformacije izvodi u toku rada mašine je "Odošenje starog alata i pomoćnog pribora", što je prikazan na Gantovom dijagramu ilustrovanom na slici 4.



Slika 2. Zbirni Gant-ov dijagram svih aktivnosti



Slika 3. Zbirni Gant-ov dijagram internih i eksternih aktivnosti



Slika 4. Zbirni Gant-ov dijagram transformacije internih u eksternih aktivnosti

Optimizacija internih i eksternih aktivnosti

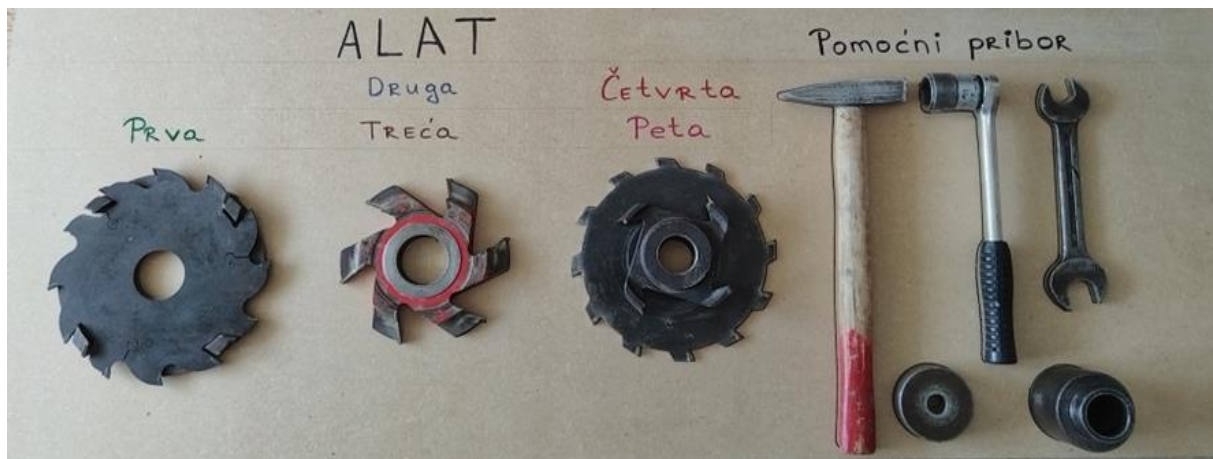
Na kraju, u poslednjem korak detaljnom analizom identifikovane su sledeće interne aktivnosti koje se ne mogu pretvoriti u eksterne, ali ih je moguće značajno ubrzati. Što se tiče eksternih aktivnosti, pronađen je način da se njihovo izvođenje ubrza, a čak neke od njih i potpuno eliminišu.

- Interna aktivnost označena kao "Prinošenje novog alata i pomoćnog pribora"/"Prinošenje pomoćnog pribora" ranije je zahtevala znatno vreme zbog loše organizacije alata za obradu i pomoćnog pribora. Da bi se to rešilo uvedena je "Shadow tool boards" (Slika 5), na kojima su svi neophodni alati i pomoćni pribor uredno smešteni. Primena ove table je omogućila i da se eksterna aktivnost "Oдноšenje starog alata i pomoćnog pribora"/"Oдноšenje pomoćnog pribora" znatno ubrza.
- Za izvođenje internih aktivnosti označenih kao "Odvijanje matice na

osovini" i "Zavijanje matice na osovini" prešlo je se sa običnog ključa (Slika 6), na nasadni ključ (Slika 7), čime se skratili vreme potrebno za ove aktivnosti.

- Interne aktivnosti označene kao "Skidanje podloški sa osovine" i "Vraćanje podloški na osovinu" ranije su zahtevale više vremena koje je skraćeno primenom čaure (Slika 9), umesto nekoliko podloški (Slika 10).
- Interna aktivnost označene kao "Podešavanje alata" unapređena je primenom Vizuelnog menadžmenta (Slika 11) umesto korišćenja šablona (Slika 10) što je omogućilo precizno štelovanje alata i time izbegla potreba za dodatnom eksternom aktivnošću "Fino podesavanje alata".

Primenom svega gore navedenog ukupno interno vreme sa 51,92 minuta je skraćeno na 33,5 minuta, dok ukupno eksterno vreme sa 10 minuta skraćeno je na 5 minuta.

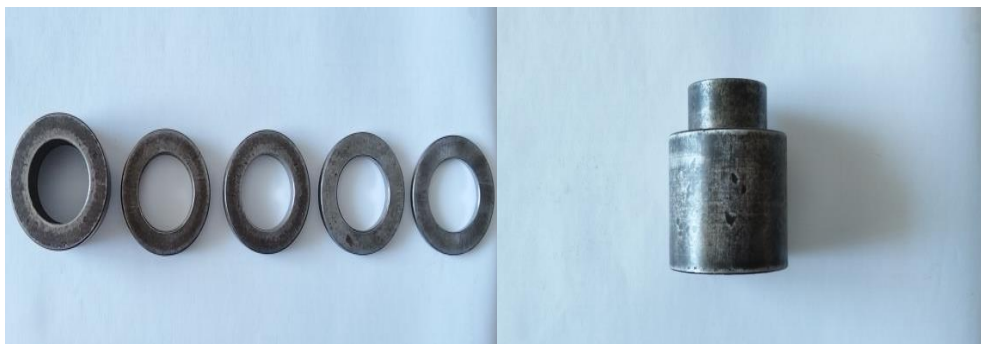


Slika 5. Shadow tool boards



Slika 6. Običan ključ

Slika 7. Nasadni ključ



Slika 8. Podloške

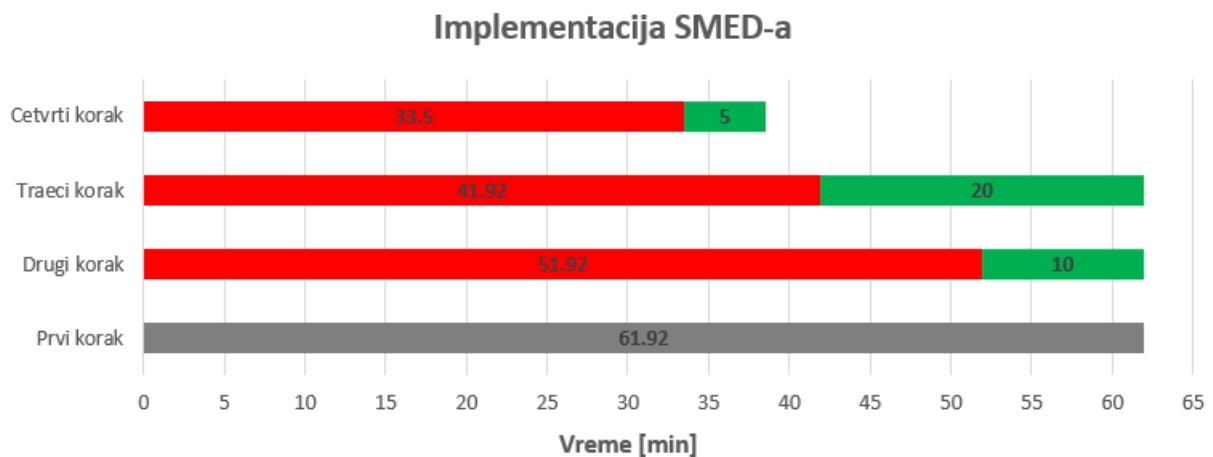
Slika 9. Čaura



Slika 10. Podešavanje alata šablonom



Slika 11. Podešavanje alata po širini i visini



Slika 12. Faze implementacije SMED-a u kompaniji za proizvodnju sobnih vrata

ZAKLJUČAK

Implementacijom SMED metode u kompaniji za proizvodnju sobnih vrata postignuto je značajno smanjenje vremena promene za 23,42 minuta, što predstavlja impresivan pad od 37,82% u odnosu na originalno vreme zamene alata, kako je prikazano na Slici 12. Ovo znatno smanjenje postignuto je putem modifikacije sedam različitih aktivnosti u procesu zamene alata. Osim što potvrđuje da primena SMED metode može doneti značajne uštede u vremenu zamene alata, ovo takođe jasno ukazuje na to da je SMED metoda ključni alat za kompanije poput spomenute u okviru ove studije slučaja koje se suočavaju sa čestim i dugotrajnim zamenama alata u procesu proizvodnje. Takođe, primena SMED metode je omogućila precizno podešavanje alata na određenu dubinu i visinu prodiranja u materijalu, čime su smanjena odstupanja od propisanih vrednosti. Ova

poboljšanja doprinose većoj preciznosti i kvalitetu proizvoda.

S ekonomske perspektive, ostvarene uštede u vremenu promene mogu se iskoristiti za dodatnu proizvodnju, što rezultira povećanjem proizvodnih kapaciteta kompanije. Ovo povećanje kapaciteta proizvodnje može se meriti kroz dodatne prihode generisane prodajom proizvoda. Ukratko, implementacija SMED metode donosi značajne finansijske uštede, skraćuje trajanje promene i pojednostavljuje postojeće aktivnosti kompanije.

ZAHVALNOST

Ovaj rad je sufinansiran od strane Ministarstva nauke, tehnološkog razvoja i inovacija Republike Srbije na osnovu ugovora čiji je broj evidencije 451-03-47/2023-01/200108. Autori se zahvaljuju Ministarstvu

nauke, tehnološkog razvoja i inovacija Republike Srbije na podršci ovom istraživanju.

LITERATURA

- N. Horňáková, L. Jurík, H. Hrablík Chovanová, D. Caganova, D. Babcanova: AHP method application in selection of appropriate material handling equipment in selected industrial enterprise, *Wireless Networks* 27, pp. 1683-1691, 2021.
- P. Rahayu, J. Supono, N. Anisa: SMED Implementation: Changeover Part Time Improvement at Seat Line Production PT. Selamat Sempurna, Tbk, *Journal Industrial Manufacturing*, Vol. 6, No. 2, pp. 105-114, 2021.
- R. Sahin, A. Kologlu: A Case Study on Reducing Setup Time Using SMED on a Turning Line, *Gazi University Journal of Science*, Vol. 35, No. 1, pp.60-71, 2022.
- T. Bidarra, R. Godina, J. C.O. Matias, S. G. Azevedo: SMED Methodology Implementation in an Automotive Industry Using a Case Study Method, *International Journal of Industrial Engineering and Management*, Vol. 9, No 1, pp. 1-16, 2018.
- M. Mulla, S. Bhatwadekar, S. Pandit: Implementation of Lean Manufacturing Through the Technique of Single Minute Exchange Oo Die (SMED) to Reduce Change Over Time, *International Journal of Innovative Research in Science*, Vol. 3, No 6, pp. 13069-13076, 2014.
- D. Guzel, A. Shahbazpour Asiabi: Improvement Setup Time by Using SMED and 5S (An Application In SME), *International Journal of Scientific & Technology Research*, Vo 9, No 1, pp. 3727-3732, 2020.
- A. Winatie, B. Perwitasari Maharani, V. Hangga Riksa, S. Hasibuan: Increasing Time Efficiency of Change over Process on Solid Product using SMED (Single Minute Exchange of Dies) Method in Pharmaceutical Industry, *International Journal of Innovative Science and Research Technology*, Vol. 4, No 6, pp. 639-644, 2019.
- E. Sousaa, F. J. G. Silvaa, L. P. Ferreiraa, M. T. Pereiraa, R. Gouveiaa, R. P. Silvab: Applying SMED Methodology in Cork Stoppers Production, *28th International Conference on Flexible Automation and Intelligent Manufacturing*, June 11-14, 2018, Columbus, OH, USA, pp. 611-622.
- D. Zimon, T. Gajewska, M. Malindzakova: Implementing the Requirements of ISO 9001 and Improvement Logistics Processes in Smes which Operate in the Textile Industry, *AUTEX Research Journal*, Vol. 18, No 4, pp. 392-397, 2018.
- M. V. N. Pinja, S. Shivakumar, G. V. Patil: Productivity Improvement through Single Minute Exchange of Die (SMED) Technique, *International Journal of Scientific and Research Publications*, Vol. 5, No. 7, pp.1-9, 2015.
- R. Pena, L.P. Ferreira, F.J.G. Silva, J.C. Sá, N.O. Fernandes, T. Pereira: Lean Manufacturing Applied to a Wiring Production Process, *30th International Conference on Flexible Automation and Intelligent Manufacturing*, 15-18 June, 2021, Athens, Greece, pp. 1387-1394
- M. J. R. Costa, R. M. Gouveia, F. J. G. Silva, R. D. S. G. Campilho: How to Solve Quality Problems by Advanced Fully-Automated Manufacturing Systems, *International Journal of Advanced Manufacturing Technology*, Vol. 94, pp. 3041–3063, 2018.
- G. Garcia-Garcia, Y. Singh, S. Jagtap: Optimising Changeover through Lean-Manufacturing Principles: A Case Study in a Food Factory, *Sustainability Journal*, Vol. 14, No. 14, pp.1-20, 2022.
- L. Jurík, N. Horňáková, V. Domčeková: The Application of SMED Method in the Industrial Enterprise, *International Scientific Journal about Logistics*, Vol. 7, No. 4, pp.269-281, 2020.
- R. Assaf, T. Haddad: An Application of Single Minute Exchange of Die Approach in an Aluminum Profiles Extrusion Production System: Case Study, *International Journal of Scientific Research and Innovative Technology*, Vol. 4 No. 7, pp. 14-22, 2017.
- Suhendra, F. E. Putra, K. B. Juliantoro, A. Fitra: Penurunan Change Over Time Automatic Machine Filling di PT XYZ Menggunakan Metode Single Minute Exchange of Dies (SMED), *Jurnal Teknik Industri*, Vol. 3, No. 2, pp. 72-82, 2022.
- S. Bhadea, S. Hegdea: Improvement of Overall Equipment Efficiency of Machine by SMED, *Materials Today: Proceedings*, Vol. 24, No. 2, pp. 463-472, 2020.
- R. Saputra, H. Arianto, L. Irianti: Usulan Meminimasi Waktu Set-up Dengan Menggunakan Metode Single Minute Exchange

Die (SMED) Di Perusahaan X, Jurnal Online Institut Teknologi Nasional, Vol.4, No.02, pp.206-2018, 2016.

A. Karam, M. Liviu, V. Cristina, H. Radu: The Contribution of Lean Manufacturing Tools to Changeover Time Decrease in the Pharmaceutical Industry. A SMED Project, *11th International Conference Interdisciplinarity in Engineering*, 5-6 October, 2017, Tirgu Mures, Romania, pp.886-892

A. Silva, J.C. Sá, G. Santos, F. J. G. Silva, L. P. Ferreira, M. T. Pereira: Implementation of SMED in a Cutting Line, *30th International Conference on Flexible Automation and Intelligent Manufacturing*, 15-18 June, 2021, Athens, Greece, pp. 1357-1362

A. P. Dillon, S. Shingo: *A revolution in manufacturing: the SMED system*. Tokyo, Japan: CRC Press, 1985.

Dostupno na:

<https://www.leansixsigmadefinition.com/glosary/smed/>, pristupljeno: 25.09.2023.

OPTIMIZATION OF WOOD PROCESSING MACHINE SETUP USING SMED METHOD

Abstract: *In a world of continuous market development and increasingly demanding customer needs, it is crucial to align production processes. To directly address the requirements for reducing production time, the application of the SMED (Single Minute Exchange of Die) method is essential as a fundamental tool within the Toyota production philosophy. The SMED method enables tool changeovers in a short time frame, minimizing downtime and allowing for the production of different products. This method further enhances a company's flexibility and productivity. The goal of this research is to reduce the tool changeover time in the door frame processing process, which involves five technological operations requiring three tool changes.*

Keywords: *SMED, Kaizen, Lean, Flexibility, Efficiency*



Society of Production
Engineering

SPMS 2023

39. Savetovanje proizvodnog mašinstva Srbije

ICPES 2023

39th International Conference on Production Engineering of
Serbia



Faculty of Technical
Sciences
University of Novi Sad

Novi Sad, Serbia, 26. – 27. October 2023

DEVELOPMENT OF A POSTPROCESSOR FOR MILLING WITH A ROTARY AXIS AND VERIFICATION ASSISTED BY VIRTUAL MACHINING ENVIRONMENT

Julija MALETIĆ¹, Saša ŽIVANOVIĆ²

¹LOLA Institute, Belgrade, julija.maletic@li.rs

²University of Belgrade, Faculty of Mechanical Engineering, Belgrade, szivanovic@mas.bg.ac.rs

Abstract: This paper presents the development of a postprocessor for a vertical milling machine with one rotary axis, commonly known as mill-turn. The subject of this analysis is the 4-axis machine MultiProDesk, whose kinematic structure formula is A'Y'OXZ. A postprocessor is a software that transforms the CL file into a machine-readable G-code. The CL file contains the universally formulated toolpath in sets of tool positions and orientations regarding the workpiece coordinate system. The inverse kinematic model method was used to derive the equations needed to transform the CL data into the displacement of the machine's axis. The displacements of the machine's axis are then implemented into a series of commands in the G-code. Machine kinematics can be designed as two unified kinematic chains with the same origin. The inverse kinematic equations were implemented in a postprocessing algorithm in the Matlab software. In order to test the derived equations, a virtual machining environment was developed. The proposed kinematic model was tested using several test workpieces with different machining strategies. The virtual simulation resulted in a virtual workpiece that matched the original workpiece used to calculate the toolpath, verifying the machine's developed postprocessor.

Keywords: post-processor, inverse kinematics, verification, simulation, virtual machine tools

1. INTRODUCTION

Adding a rotary axis to a conventional three-axis milling machine greatly increases the complexity of the potential parts manufactured on said machine. Machines with one rotary axis on the machine table are commonly known as mill-turn machines, as they combine both milling (*tool rotating*) and turning (*workpiece rotating*) motions. These machines are classified as multi-axis machines, given that the manufacturing process can be obtained by

simultaneously utilising all four of the machine's axes. In conventional three-axis milling, the tool orientation does not change during machining. In four- and five-axis machines, the additional rotary axes enable the control of the tools' orientation during the machining process. The alternating orientation of the tool requires a more complex approach to programming multi-axis machines. With complex parts requiring programs with many lines and the utilisation of the tools axis, multi-axis machines are almost exclusively

programmed using CAM systems. CAM software include postprocessors developed for a specific machine regarding its kinematic structure. A postprocessor is a software used to generate G-code for a specific machine by transforming the data in a general machining program. Typically, when developing a machining program, first, the toolpath is formed in a general machining program called the CL file, which contains data that describe the position and orientation of the tool regarding the workpiece coordinate system. The CL file is then converted into a G-code using a postprocessor, containing the specific machine kinematics and control functions.

Many approaches to developing kinematic models of machine tools for postprocessing were formed. As the complexity of machines grew, many researchers focused on developing the kinematic models of five-axis machine tools with orthogonal axes. Lee and She focused on developing an inverse kinematic model for three typical types of five-axis machines with orthogonal axes [1]. Based on that work, postprocessing software for specific types of machines were developed in [2-3]. Given the similar approach in the modelling of kinematic structures of five-axis machine tools, there were many attempts to unify the approach into a universal model for postprocessing, such as shown by Chen [4]. With the development of composite machine tools, meaning the machine tools combining milling and turning, there is a need for research for corresponding postprocessors, such as in the work of Tang et al. [5].

This paper focuses on developing a postprocessor for the machine MultiProDesk [6]. The machine is currently a vertical three-axis mill with additional rotary axes in preparation. The kinematic equations implemented into the software are derived using the inverse kinematic method. The software used in this paper is a revised version of the software developed in [7]. In order to verify the postprocessing program and the kinematic equations, a virtual machining simulation was carried out. The three-axis machine model was enhanced with the fourth

rotary axis A and used for creating a virtual machining simulation in the Vericut software.

2. INVERSE KINEMATIC TRANSFORMATION OF THE MACHINE

The kinematic equations that describe the machine axis motions regarding the workpiece coordinate system are obtained using the inverse kinematic model. In this method, machine tools are defined as two kinematic chains with the same origin, one carrying the tool and the other carrying the workpiece. On the machine, these kinematic chains represent serially connected translational and rotational joints. Deriving the kinematic equations of the machine starts with assigning each of the moving joints a coordinate system and defining the relative motions between these joints. When defined, these equations will provide a link between the tool position and orientation and the displacements of the axes of the machine. By defining each machine link with a coordinate system, the relative motions of the joints can be defined with elementary transformational matrices. The composition of the elementary transformational matrices yields a complex transformation which can include both translational and rotary transformations. An illustration of the machine's axes and the necessary transformation matrices is shown in Fig. 1.

As outlined above, the kinematic structure of the four-axis machine is defined using two open kinematic chains. The first chain contains

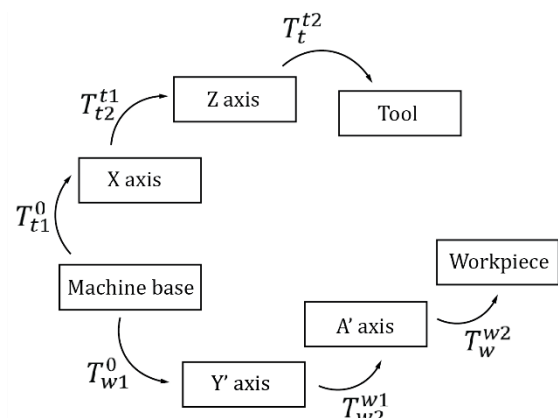


Figure 1. Schematic diagram of machine tool kinematic chains

the joints actuating the motions of the workpiece, called the workpiece coordinate chain. In compliance with the machine tool structure, A'Y'OXZ, the first kinematic chain includes the Y and A axes of the machine. The coordinate systems of the workpiece coordinate chain, $Ox_{w1}y_{w1}z_{w1}$ and $Ox_{w2}y_{w2}z_{w2}$, and the base coordinate system, $Ox_0y_0z_0$, are shown in Fig. 2. The first elementary transformational matrix, T_{w1}^0 , defines the translational displacement of the machine's Y axis.

$$T_{w1}^0 = \begin{bmatrix} 1 & 0 & 0 & x_{w1} \\ 0 & 1 & 0 & Y - y_{w1} \\ 0 & 0 & 1 & z_{w1} \\ 0 & 0 & 0 & 1 \end{bmatrix} \quad (1)$$

The adjacent machine axis is the rotary axis A. The elementary transformational matrix defines the relative displacements of the rotary axis to the Y-axis coordinate system.

$$T_{w2}^{w1} = \begin{bmatrix} 1 & 0 & 0 & x_{w2} \\ 0 & \cos(A) & -\sin(A) & 0 \\ 0 & \sin(A) & \cos(A) & z_{w2} \\ 0 & 0 & 0 & 1 \end{bmatrix} \quad (2)$$

In the previous matrices, values $x_{w1}, y_{w1}, z_{w1}, x_{w2}$ and z_{w2} are constant and represent the distances along the X and Z axes between the joint coordinate systems. The only variable values are Y and A, representing the necessary displacements of the machine's translation axis and the necessary rotation angle of the machine's rotary axis.

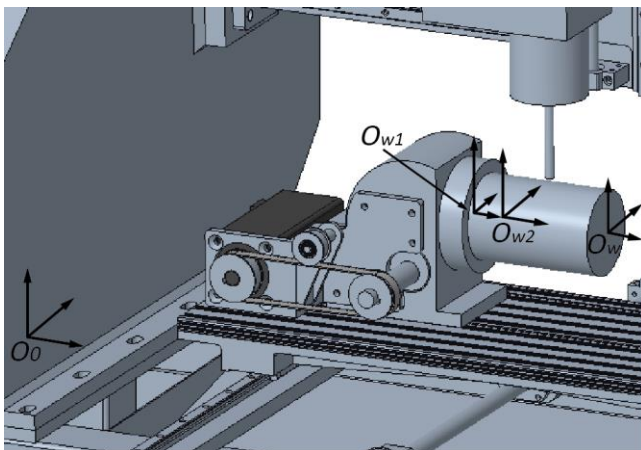


Figure 2. The position of the coordinate systems of the workpiece kinematic chain

A transformational matrix defining the workpiece coordinate system's position completes the workpiece kinematic chain, as shown below. This matrix does not have any variables, as the workpiece is fixed.

$$T_w^{w2} = \begin{bmatrix} 1 & 0 & 0 & x_w \\ 0 & 1 & 0 & y_w \\ 0 & 0 & 1 & z_w \\ 0 & 0 & 0 & 1 \end{bmatrix} \quad (3)$$

The second kinematic chain, or tool kinematic chain, defines the machine's X and Z axis displacements. The coordinate systems of the tool coordinate chain, $Ox_{t1}y_{t1}z_{t1}$ and $Ox_{t2}y_{t2}z_{t2}$, and $Ox_t y_t z_t$, are shown in Fig. 3. Defining the tool kinematic chain equations begins with the transformation matrix between the machine's X axis and the base coordinate system.

$$T_{t1}^0 = \begin{bmatrix} 1 & 0 & 0 & X - x_{t1} \\ 0 & 1 & 0 & y_{t1} \\ 0 & 0 & 1 & z_{t1} \\ 0 & 0 & 0 & 1 \end{bmatrix} \quad (4)$$

The relative displacement of the X and Z axis are defined with the following matrix:

$$T_{t2}^{t1} = \begin{bmatrix} 1 & 0 & 0 & x_{t2} \\ 0 & 1 & 0 & y_{t2} \\ 0 & 0 & 1 & Z - z_{t1} - H_t \\ 0 & 0 & 0 & 1 \end{bmatrix} \quad (5)$$

The last coordinate system, located at the tool tip, is defined to complete the tool

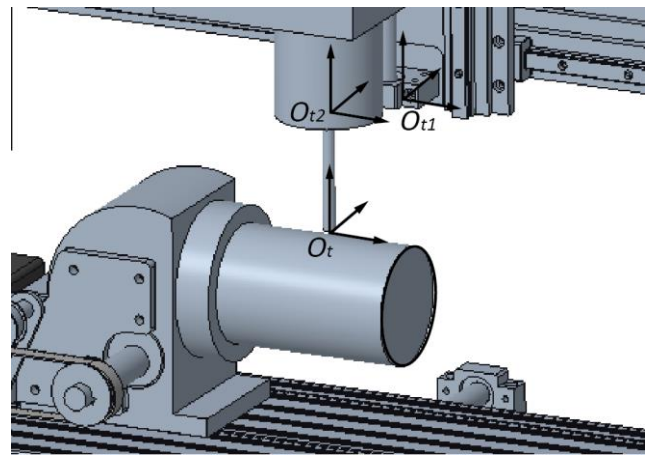


Figure 3. The position of the coordinate systems of the tool kinematic chain

kinematic chain. The transformation matrix that defines this coordinate system contains the tool length correction.

$$T_t^{t2} = \begin{bmatrix} 1 & 0 & 0 & 0 \\ 0 & 1 & 0 & 0 \\ 0 & 0 & 1 & H_t \\ 0 & 0 & 0 & 1 \end{bmatrix} \quad (6)$$

As defined above, the CL file contains information about the position and orientation of the tool in points along the toolpath. The position and orientation of the tool regarding the workpiece coordinate system can also be defined using a transformation matrix - T_t^w . The T_t^w matrix can be derived as a function of the machine's axis displacements using the above elementary transformation matrices.

First, the tooltip vector regarding the base coordinate system can be described in two ways, either using the workpiece kinematic chain or the tool kinematic chain, as stated below.

$$r_t^0 = T_{w1}^0 \cdot T_{w2}^{w1} \cdot T_w^{w2} \cdot T_t^w \quad (7)$$

$$r_t^0 = T_{t1}^0 \cdot T_{t2}^{t1} \cdot T_t^{t2} \quad (8)$$

The previous equations are equivalent and can be defined in the form shown in Eq. 9.

$$T_{w1}^0 \cdot T_{w2}^{w1} \cdot T_w^{w2} \cdot T_t^w = T_{t1}^0 \cdot T_{t2}^{t1} \cdot T_t^{t2} \quad (9)$$

Arranging Eq. 9 to get the matrix T_t^w in the form of a function is shown in Eq. 10.

$$T_t^w = (T_w^{w2})^{-1} \cdot (T_{w2}^{w1})^{-1} \cdot (T_{w1}^0)^{-1} \cdot T_{t1}^0 \cdot T_{t2}^{t1} \cdot T_t^{t2} \quad (10)$$

The transformation matrix is the result of the composition of all elementary transformation matrices and, as such, is a function of all of the defined displacements of the machine's axes: X, Y, Z and A. The derived matrix contains information on the position and orientation of the tool regarding the workpiece coordinate system. It can provide the equations needed to calculate the displacements of the machine's axes by equating the matrix element with CL data. The resulting matrix has the following form:

$$T_t^w = \begin{bmatrix} u_x & v_x & w_x & p_x \\ u_y & v_y & w_y & p_y \\ u_z & v_z & w_z & p_z \\ 0 & 0 & 0 & 1 \end{bmatrix} \quad (11)$$

The matrix shown in Eq. 11 represents the transformation between the workpiece and tool coordinate systems. In the third column are the cosines of the tool coordinate system that are used for deriving the equations for the rotary axis angle.

$$w_x = 0 \quad (12)$$

$$w_y = \sin(A) \quad (13)$$

$$w_z = \cos(A) \quad (14)$$

Solving the above equations results in the necessary angle of the rotary axis. The fourth column of the resulting matrix represents the displacements of the translational axis, with compensation to counteract the movements of the rotational axis.

$$p_x = a_1 \quad (15)$$

$$p_y = b_1 \sin(A) (Z + b_2) - b_3 \cos(A) (Y + b_4) \quad (16)$$

$$p_z = c_1 \sin(A) (Y + c_2) - c_3 \cos(A) (Z + c_4) \quad (17)$$

In the previous equations, a_i , b_i , and c_i ($i = 1..3$) are constant values resulting from the constant distances between the coordinate systems. Solving the system Eq. 15-17 results in the final values of the machine axis displacements.

3. POSTPROCESSOR IMPLEMENTATION

In order to test the derived kinematic model, the solutions to Eq. 12-17 were implemented into the postprocessing software developed in [7]. This program is based on an iterative algorithm, where each command in the CL file is read, calculated, and then translated into a separate file using the G-code syntax.

2.1 Rotary axis correction

The equation for the necessary rotary angle of the axis A is given in Eq. 18

$$A = \text{atan2}(w_y, w_z) \quad (17)$$

Given the origin of the trigonometric function, the resulting angle has constraints in the form of $A = [-\pi, \pi]$. In order to prevent errors during machining, an addition to the postprocessing software was made. At the beginning of the program for a given machining process, it is determined if the A axis moves clockwise or anticlockwise. As the calculated angles approach the limit, the values are controlled until that limit is surpassed. Suppose the angles surpass the limit during the machining process. In that case, a correction is made so that the tool continues the motion matches the one at the beginning of the machining, clockwise or anticlockwise.

4. KINEMATIC MODEL VERIFICATION

In order to verify the kinematic model of the four-axis machine, MultiProDesk, two test models were created, shown in Fig. 4. The manufacturing process for the test workpieces was created using the PTC Creo software, with the result being the CL file of both manufacturing processes. The CL toolpaths for both test pieces were then translated using the developed postprocessing program. Generated G-code programs were then tested on a virtual model using the Vericut software, where it is possible to simulate a material removal process. For the first experiment, a workpiece with a concave surface was formed to control the machine's axis motion simultaneously. The workpiece, the machining process, and the resulting virtual manufactured part are shown in Fig. 5. A cylinder workpiece with a spiral groove was formed for the second experiment to test the rotary axis correction. The

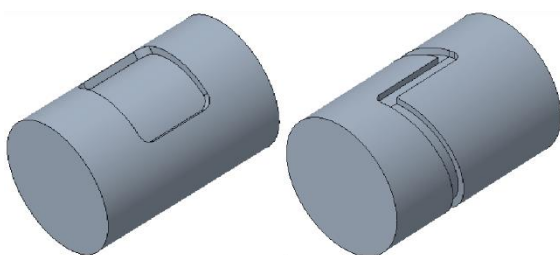


Figure 4. Test workpieces

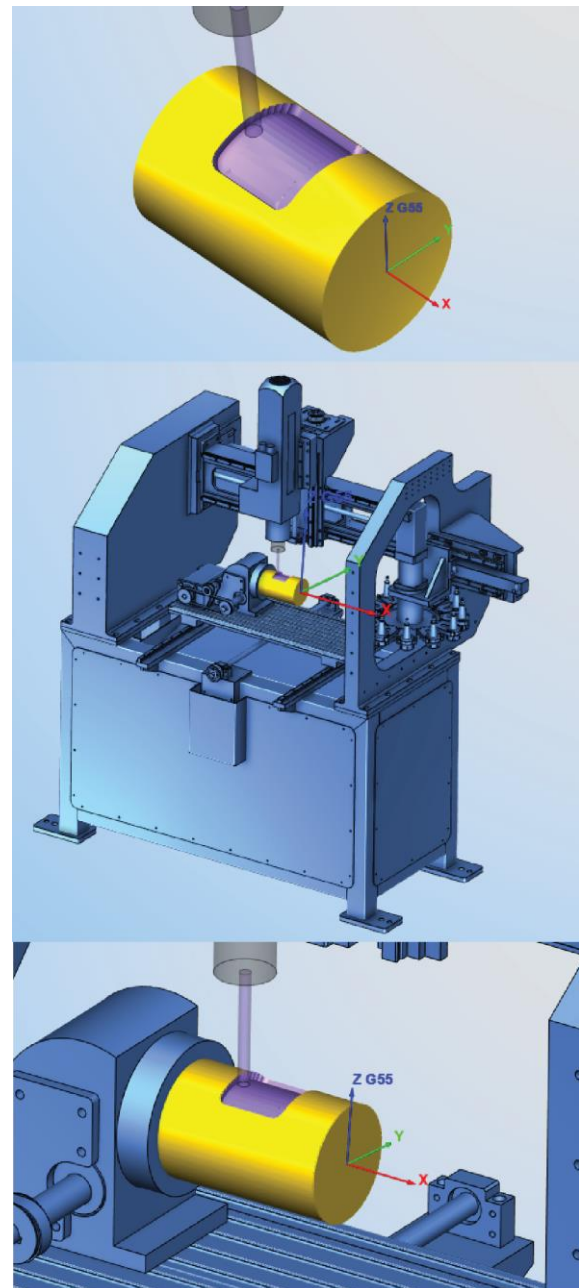


Figure 5. Testing the G-code in Vericut, first test

workpiece, the machining process, and the resulting virtual manufactured part for the second experiment are shown in Fig. 6.

Given that the material removal simulation was conducted using only the G-code program and that the virtual model of the machine corresponds to the real-life machine, both of these experiments can be classified as virtual machining. The virtual machined parts were saved in a standard CAD format and compared to the desired parts, where it was concluded that the experiments were successful.

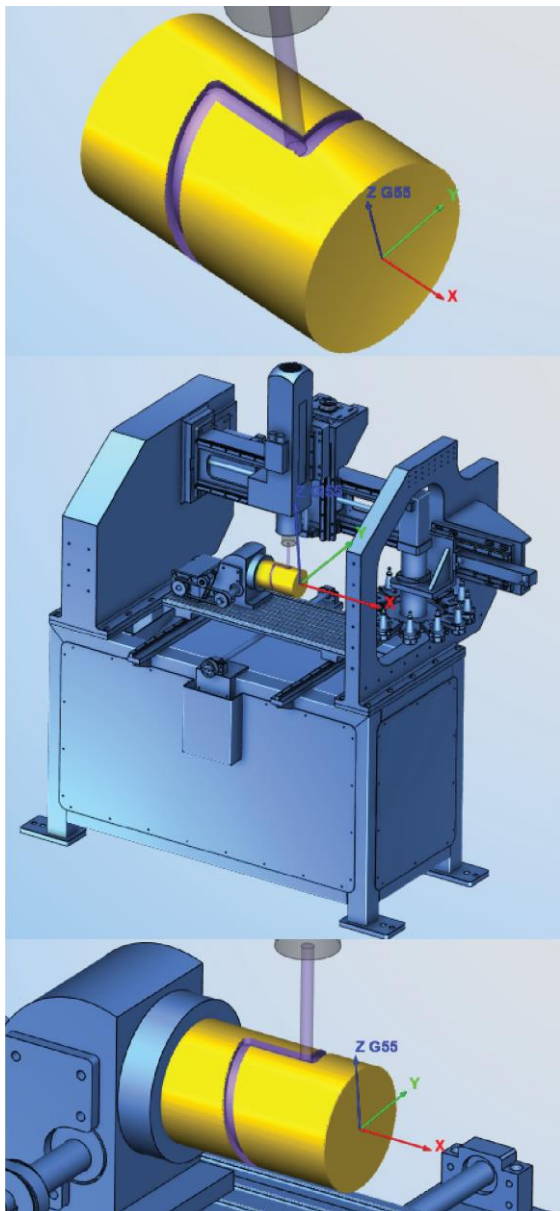


Figure 6. Testing the G-code in Vericut, second test

5. CONCLUSION

A method of developing a postprocessor used for converting a CL file into G-code was presented in this paper. The main objective is the kinematic modelling of a four-axis machine. The kinematic model of the machine was developed using the inverse kinematic method. The kinematic model was implemented into the postprocessing software with an addition of the rotary axis correction.

The results were tested in the form of virtual machining a virtual machine. The method for deriving the necessary equations can be utilised for various types of multi-axis machines, as it provides flexibility for various machine

configurations. Further research can be extended by developing postprocessing software for different configurations of the machine's rotary axis.

ACKNOWLEDGEMENT

This research has been supported by the Transfer of Technology grant of the Innovation Fund of the Republic of Serbia, project no. TT1129, and by the research grants of Serbian Ministry of Science, Technological Development and Innovations, grant No. 451-03-68/2023-14/200066 and 451-03-47/2023-01/200105 from 03.02.2023.

REFERENCES

- [1] R.S. Lee, and C.H. She: Developing a postprocessor for three types of five-axis machine tools, *International Journal of Advanced Manufacturing Technology*, Vol.13, pp. 658–665, 1997.
- [2] Y.H. Jung, D.W. Lee, J.S. Kim, H.S. Mok: NC Post-processor for 5-axis milling machine of table-rotating/tilting type, *Journal of Material Processing technology*, Vol.130-131, pp.641-646, 2002.
- [3] C.H. She, C.C. Chang: Development of a five-axis post-processor system with a nutating head. *Journal of Materials Processing Technology*, Vol.187-188(2), pp.60-64, 2007.
- [4] F.C. Chen: On the structural configuration synthesis and geometry of machining centres, *Proceedings of the Institution of Mechanical Engineers, Part C: Journal of Mechanical Engineering Science*, Vol. 215(6), pp.641-652. 2001.
- [5] Q.C. Tang, S.H. Yin, G.H. Zhang: Post-processor development for a turning and milling composite machine tool, *The International Journal of Advanced Manufacturing Technology*, Vol. 95, pp.131–141, 2018.
- [6] Project Multifunctional rapid prototyping desktop machine – MULTIPRODESK, Project ID 1129, Technology Transfer Program, Innovation Fund, Republic of Serbia, 2023.
- [7] J. Maletić, S. Živanović: Verification of inverse kinematic equations for a five-axis machine tool with a spindle tilting configuration. *Advanced Technologies & Materials*, Vol. 47, No. 1, pp.33-38, 2021.



Society of Production
Engineering

SPMS 2023

39. Savetovanje proizvodnog mašinstva Srbije

ICPES 2023

39th International Conference on Production Engineering of
Serbia



Faculty of Technical
Sciences
University of Novi Sad

Novi Sad, Serbia, 26. – 27. October 2023

VERIFICATION OF KINEMATIC JOINTS ON A PHYSICAL PROTOTYPE OF A NOVEL PARALLEL MECHANISM BASED ON CHEBYSHEV'S LINKAGE

Ljubomir NEŠOVANOVIĆ¹, Saša ŽIVANOVIĆ²,

¹ LOLA Institute, Serbia

² University of Belgrade, Faculty of Mechanical Engineering, Serbia

ljubomir.nesovanovic@li.rs

Abstract: *Developing a novel parallel mechanism design is a complex process, including multiple phases. Designing and analyzing the mechanism's physical prototype is one of the most important phases. The proposed mechanism is novel, with parallel kinematics with actuated translation joints. The considered mechanisms platform has three degrees of freedom (DOF) achieved with three independent kinematic chains representing the connection between the stationary base and the moving platform. The proposed mechanism has numerous connected linkages because of the parallel kinematic construction. The weakest parameter of the mechanisms with parallel kinematics compared to mechanisms with serial kinematics is the shape and size of the workspace. Because of this, the workspace is one of the main parameters in designing a mechanism with parallel kinematics. To achieve the optimal workspace, it is necessary to use the proper joints in the mechanism construction. The mechanism analysis and proper joint selection can be achieved in two ways. The first way is to build the virtual model and experiment on it, and the second is to build the physical prototype. The best way to select the proper joints for the mechanism construction is to compare the analysis results of virtual and physical mechanisms. If the results of comparing virtual and physical prototypes are the same, the physical prototype verifies the mechanism design.*

Keywords: *Parallel mechanism, Chebyshev's linkage, Physical prototype, Workspace, Verification.*

1. INTRODUCTION

Hexaglide and Triaglide mechanisms are examples of workspace extension achieved by extending one axis as a principal motion axis, a common feature of all serial kinematic machines. With the idea of extending one axis of motion, a new 3 DOF parallel kinematic mechanism has been developed with a specific passive translation rotary joint [1]. The mechanism with parallel kinematics shown in [2] presents the mechanism with an extended

horizontal axis. It has the ability to transform the rotary motion of the linkages into the rectilinear motion of the desired point. The proposed mechanism's main characteristic is the passive translation rotary joint [1, 2]. In the case of the proposed mechanism, Chebyshev's linkage has the function of a passive translation rotary joint. An example of a developed solution for an industrial machine with parallel kinematics is the LOLA pn101_4 [3], which uses a passive translation rotary joint in its kinematic chain. The mechanism concepts with specific

solutions of passive translation rotary joints were also considered for this machine [1].

The parallel construction of the mechanism and usage of Chebyshev's linkage, the proposed mechanism has numerous linkages connected with multiple joints. Because of the mechanism's complexity, the development of the mechanism design is a complicated process. The first thing in the developing process is choosing the right joints that can guarantee the mechanism's proper motion. The joints greatly impact the workspace, which is the main parameter of the mechanisms with parallel kinematics, and because of that, it is necessary to verify the mechanism's movements. For the verification of the mechanism's movements, it is essential to create the mechanism prototype. Construction of the required prototype can be expensive and time-consuming but of huge importance to the mechanism design [4, 5].

A virtual prototype of the proposed mechanism is created to verify the movements of joints. Also, for verification of the proposed mechanism is used physical prototype of the proposed mechanism. Fused deposition modelling (FDM) is used to fabricate the physical prototype. FDM is one of the most used additive technologies (AT). The advantage of AT is the ability to save time in the design and development process. AT is used for quickly fabricating functional models, physical prototypes and small series of parts directly from CAD models [6, 7].

This paper is dedicated to explaining the proposed mechanism's functionality with an accent on the kinematic connections between rigid components. Because of the mechanism complexity, every kinematic chain is explained separately, with special attention on Chebyshev's linkage. The mechanism movements are tested on created prototypes of the proposed mechanism. The final verification is accomplished by comparing the movements of the virtual and physical prototypes.

2. THE KINEMATIC STRUCTURE OF THE PROPOSED PARALLEL MECHANISM BASED ON CHEBYSHEV'S LINKAGE

The proposed mechanism has three kinematic chains which form the connection between the moving platform (MP) and stationary base (SB), shown in Fig. 1. The MP can achieve three degrees of freedom (3 DOF) in the mechanisms' workspace. Each kinematic chain is connected to the SB with one actuated translation joint (s_1 , s_2 and s_3). The connections between the kinematic chains and MP and between the links of each kinematic chain are connected with passive joints.

The movement of each translation joint has the direction of the mechanism's extended axis. The first and the second kinematic chain has the shape of a simple parallelogram. The active translation joint connects the first and the second kinematic chain to the SB. The connection between the first kinematic chain and MP, as well as the connection between the second kinematic chain and MP, is achieved with two spherical joints. Each spherical joint has 3 DOF. Each parallelogram is built with four rigid components connected with spherical joints.

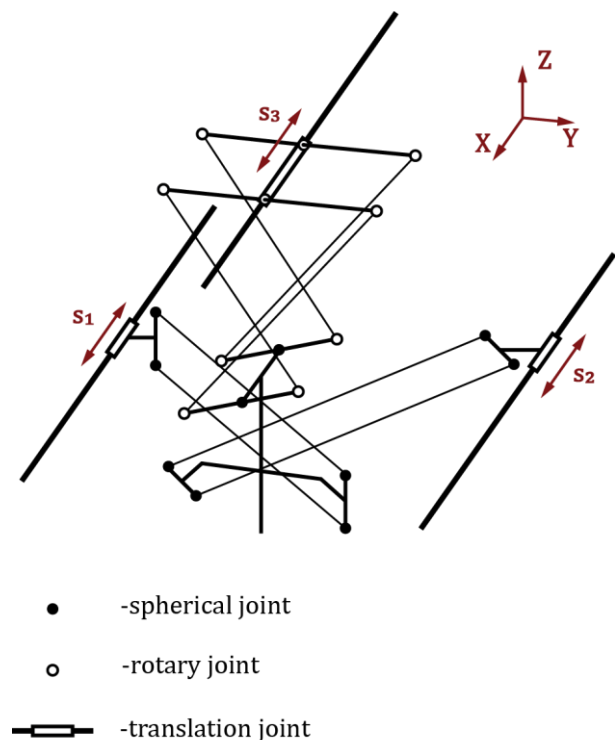


Figure 1. Kinematic model of the proposed mechanism [2]

The first rigid component has a specific shape, and it is used to connect the parallelogram and translation joint. The second and third rigid component are simple links, and the fourth rigid component of the parallelogram is part of the MP. The main difference between the first and the second kinematic chain is in the shape of the first and fourth rigid component.

The first and second kinematic chains are oriented to cross each other without collision. The second kinematic chain is rotated for 90 degrees in relation to the first kinematic chain. This arrangement of the first and second kinematic chains is why the chains are not in collision.

The third kinematic chain is based on Chebyshev's linkage and completes the 3D motion of the MP. This kinematic chain is also the four-bar mechanism, which has the shape of a parallelogram. The first component of the third kinematic chain is the translation joint. The second and third components of the third kinematic chain are Chebyshev's linkages. The connection between the translation joint and Chebyshev's linkages is provided with a simple rotary joint (1 DOF). The third kinematic chain's fourth component is the MP part. The MP and Chebyshev's linkages are connected with spherical joints.

3. VERIFICATION OF THE CHEBYSHEV'S LINKAGE

As already mentioned, the proposed mechanism is based on Chebyshev's linkage, shown in Fig. 2 and Fig. 3. In the mechanism construction, the Chebyshev's linkage is a part of the four-bar mechanism, but the Chebyshev's linkage is a four-bar mechanism itself. The main difference between the previously explained four-bar mechanisms and Chebyshev's linkage is the arrangement of the components. The Chebyshev's linkage does not have the shape of a parallelogram.

The Chebyshev's linkage is a Straight-line generator, which has the ability to transform the rotary motion of linkages into the rectilinear motion of the desired point (P) [8].

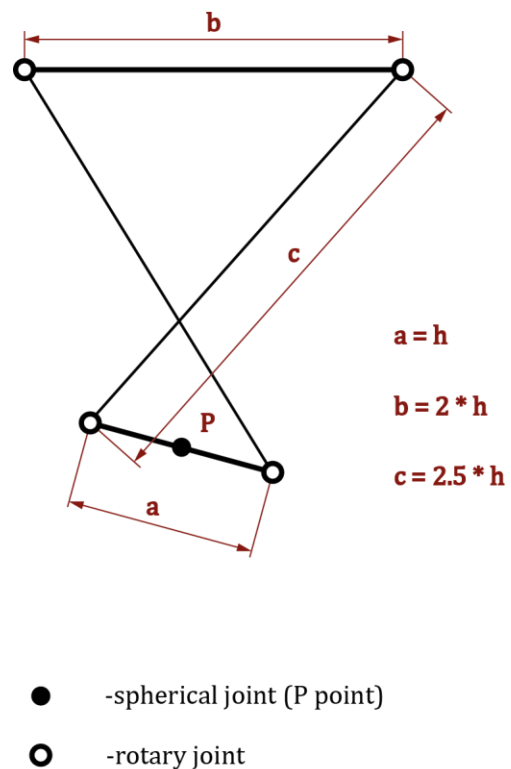


Figure 2. The Chebyshev's mechanism [2]

For the future explanation, the value h is the constant parametric variable. The first rigid component of Chebyshev's linkage has a length equal to $2h$ ($b = 2 * h$). The second and third components are crossed without collision and have the same length ($c = 2.5 * h$). The value of the last component of Chebyshev's linkage equals h ($a = h$). All connections between components of Chebyshev's linkage are rotary joints.

One simple design is produced using the 3D additive machine to test the functionality of the Chebyshev's linkage, shown in Fig. 3. PLA is the material used for additive manufacturing of the simple design of Chebyshev's linkage. The machine used for additive manufacturing is Velleman Vertex K8400, which possesses 3 DOF achieved with Cartesian serial kinematics [9].

This simple design of Chebyshev's linkage is produced to show that it is possible to generate a straight line with this mechanism. Fig. 3 shows that a straight line is generated by moving the pencil fixed in the P point of Chebyshev's linkage.

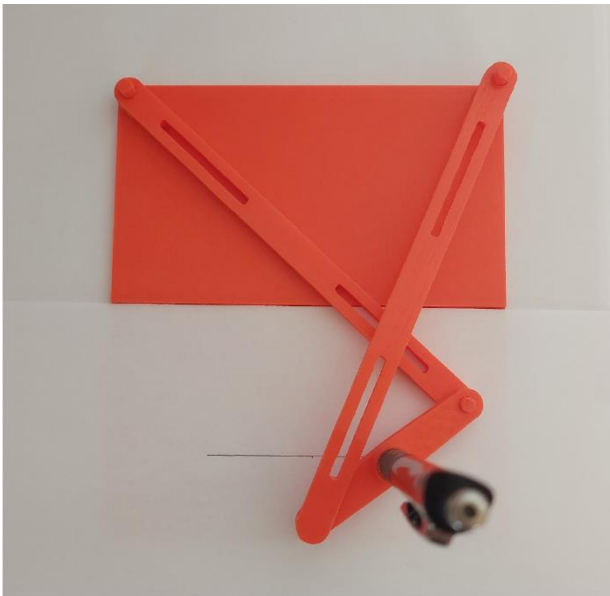


Figure 3. Verification of the Chebyshev's linkage

4. PROTOTYPES OF THE PROPOSED MECHANISM

As already mentioned, two prototypes are created to verify the functionality of the proposed mechanism, shown in Fig. 4 and Fig. 5. The first is a virtual prototype, and the second is a physical prototype.

4.1 The virtual prototype of the proposed mechanism

The virtual prototype of the proposed mechanism is designed using the PTC Creo Parametric software. A 3D model of the proposed mechanism created in this software is used for virtual tests of the mechanism. A created virtual prototype includes all previously explained connections between mechanisms components. The command Pin is used to define a simple rotary joint in a virtual model of the mechanism, which enables the rotation around the desired axis. The second used command is command Ball, which defines the spherical joint and enables rotation around the desired point. The last used command is Slider. This command enables the translation movement along the required axis in a defined movement range.

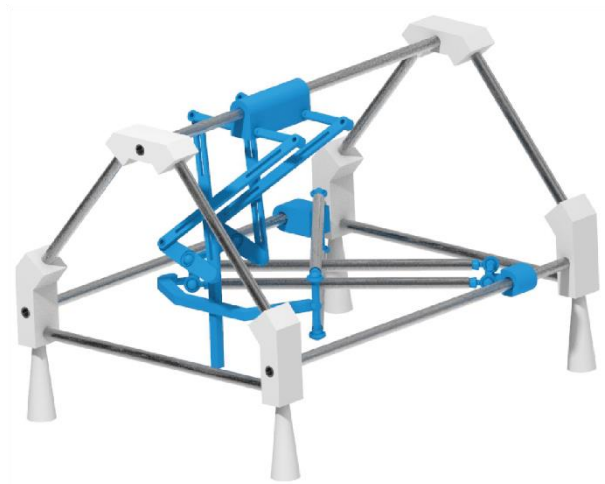


Figure 4. The virtual prototype

All relationships between mechanism components are tested using the created 3D model. The results of the virtual prototype tests show that the mechanism is working properly without breakdowns. The 3D model of the proposed mechanism created in PTC Creo Parametric is shown in Fig. 4.

The mechanism configured in this way can also be used to simulate the work of the mechanism according to the given program [10] to check the mechanism's possibility and potential collisions within the workspace's limits.

4.2 The physical prototype of the proposed mechanism

The second prototype is the physical prototype, shown in Fig. 5. This prototype is created using the information from the virtual prototype. Because of this, the physical prototype has the same dimensions as the virtual prototype.

The components of the physical prototype are steel tubes and plastic components manufactured using the Velleman Vertex K8400 3D printing machine. The physical prototype is built to allow all passive motions between components. Tests on a physical prototype are done by moving all mechanism components and observing the resulting movement of the machine. The result of the testing shows that the mechanism is working as expected.

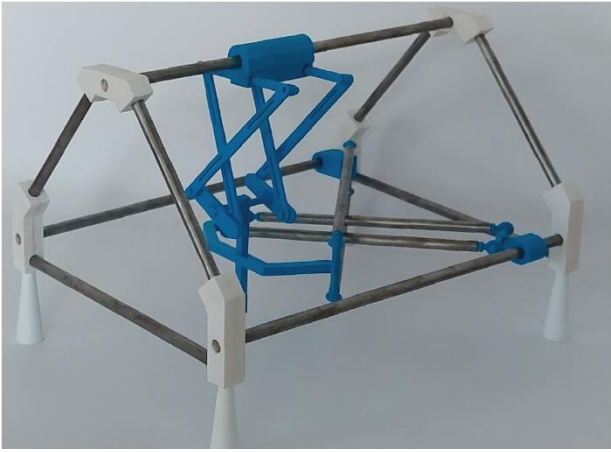


Figure 5. The physical prototype

The final verification of the proposed mechanisms is done by comparing the mechanism's virtual and physical prototypes, shown in Fig. 6. This comparison is made by moving the MP of both mechanisms to similar characteristic points and confirming that both mechanisms are moving in the same way.

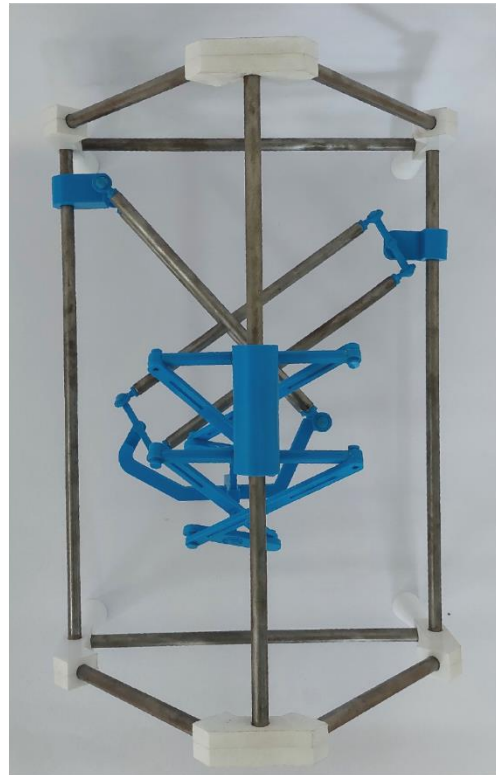
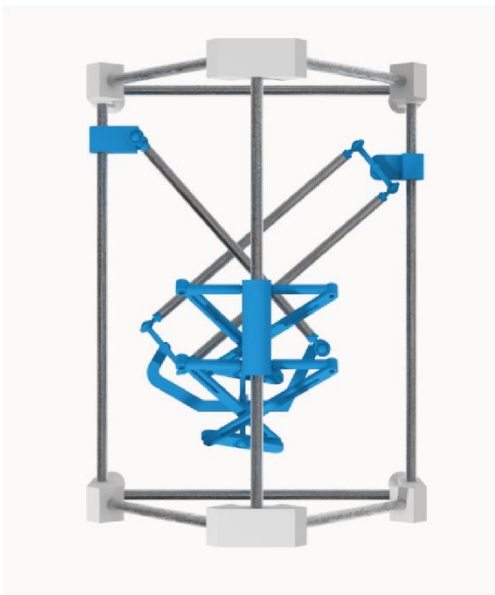
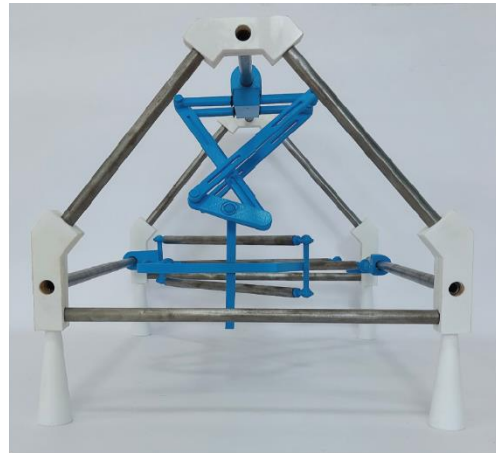
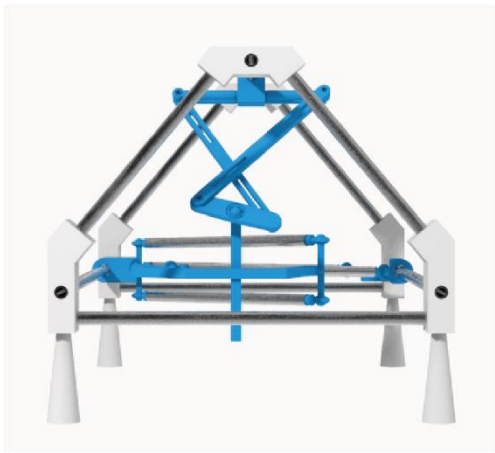


Figure 6. The virtual and physical prototypes

5. CONCLUSION

This paper has shown that the proposed mechanism is moving as expected, which is concluded with testing on virtual and physical prototypes. The tests are done separately on each prototype, and the results confirm that the used joints are correctly selected and positioned.

Also, the important point is that the virtual and especially physical prototype has shown some areas for improvement in the mechanism construction. The first point is the shape of the MP, which can be improved to enable the movement of the MP in a much larger workspace. The second one is the possibility of using the joints with 2 DOF on some points where the spherical joints (3 DOF) are now. This can also allow the bigger workspace of the mechanism. This procedure still needs to be implemented because the 2 DOF joints require much larger precision than the Used 3D printer can achieve.

The one point that needs to be considered is the links' dimensions, but it is essential first to solve the Inverse kinematic problem. Also, one of the main points in future research will be the proposed mechanisms orientation (horizontal or vertical guideways), which will greatly impact future mechanism construction. The main parameter that will define the mechanism's orientation is the workspace.

ACKNOWLEDGEMENT

The presented research was supported by the Ministry of Education, Science and Technological Development of the Republic of Serbia by contract no. 451-03-68/2023-14/200066 and 451-03-47/2023-01/ 200105 from 03.02.2023.

REFERENCES

- [1] M. Glavonjić, D. Milutinović, S. Živanović: 3-axis parallel mechanism with specific solutions of a passive translatory joint, in: *Proceedings of the 32nd JUPITER conference*, 05.2006, Belgrade, Zlatibor, SRB, pp. 3.1-3.4, (In Serbian).
- [2] Lj. Nešovanović, S. Živanović: Conceptual design of a novel mechanism with parallel kinematics based on Chebyshev's linkage, in: *Proceedings of the 16th International Conference on Accomplishments in Mechanical and Industrial Engineering*, 01-02.06.2023, Banja Luka, BIH pp. 35-40.
- [3] D. Milutinovic, M. Glavonjic, V. Kvrjic, S. Zivanovic: A New 3-DOF Spatial Parallel Mechanism for Milling Machines with Long X Travel, *CIRP Annals*, Vol 54, No. 1, pp. 345-348, 2005.
- [4] C.H. Amon, J.L. Beuth, L.E. Weiss, R. Merz, F.B. Prinz: Shape Deposition Manufacturing With Microcasting: Processing, Thermal and Mechanical Issues, *Journal of Manufacturing Science and Engineering*, Vol. 120, No. 3, pp. 656-665, 1998.
- [5] J.E. Beck, B. Fritz, D. Siewiorek, L. Weiss: Manufacturing Mechatronics Using Thermal Spray Shape Deposition, in: *Proceedings of the Solid Freeform Fabrication Symposium*, 03-05.08.1992, Austin, SAD, pp. 272-279.
- [6] D. Pham, S. Dimov: *Rapid Manufacturing: The Technologies and Applications of Rapid Prototyping and Rapid Tooling*, Springer Verlag, London, 2001.
- [7] D. Pham, S. Dimov: Rapid prototyping and rapid tooling – the key enablers for rapid manufacturing, *Proceedings of the Institution of Mechanical Engineers, Part C*, 217, pp 1–23, 2003.
- [8] J.E. Shigley, J. J. Uicker: *Theory of Machines and Mechanisms*, McGraw-Hill, 1980.
- [9] Vertex original 3d printer, available at: <https://www.velleman.eu/products/view/?id=417866>, accessed: 08.10.2023.
- [10] S. Zivanovic, M. Glavonjic, D. Milutinovic: Configuring A Mini-Laboratory and Desktop 3-Axis Parallel Kinematic Milling Machine, *Strojniški vestnik - Journal of Mechanical Engineering*, Vol.61, No1, pp. 33-42, 2015.



Society of Production
Engineering

SPMS 2023

39. Savetovanje proizvodnog mašinstva Srbije

ICPES 2023

39th International Conference on Production Engineering of
Serbia



Faculty of Technical
Sciences
University of Novi Sad

Novi Sad, Serbia, 26. – 27. October 2023

SIMULATION, ANALYSIS AND OPTIMIZATION OF FORGING PROCESS FOR AXISYMMETRIC PART

Mihajlo POPOVIĆ^{1,*}, Marko FURTULA¹, Miloš PJEVIĆ¹, Goran MLADENOVIĆ¹

¹University of Belgrade, Faculty of Mechanical Engineering, Belgrade, Serbia

*Corresponding author: mpopovic@mas.bg.ac.rs

Abstract: Forging, as a type of technological process based on metal forming, is widely used in the modern manufacturing industry. This paper is focused on the utilization of CAE software tools for simulating the forging process of an aluminium piston. The starting point for designing the technological process was a technical drawing of the machined piston. After determining forging tolerances, parting lines, forging angles, radii, and flash land, the forging part and forging dies were designed. The forging process in this particular case encompasses three metal-forming operations: upsetting, final forging, and trimming of the flash. The proposed technological solution was verified using the CAE software tool - QForm through various simulations of material behaviour during the forging process. The analysis included material flow, potential defects, as well as temperature and stress within the workpiece. After making a few adjustments to the forging design and parameters, the optimal solution was presented. Temperature and stress distributions in the best-case scenario were within an acceptable range, while the risk of surface defects and material flow abnormalities was very low. This paper demonstrates that the use of software tools for numerical simulations during the design of the forging technological process provides significant benefits, such as reducing production costs, improving product quality, minimizing scrap, saving time in product development, and reducing the number of required test samples.

Key words: Metal forming process, Forging, CAE system, Simulation, QForm

1. INTRODUCTION

The forging process is still being used in modern industrial production. This can be explained by the fact that forging, as a manufacturing technology based metal forming, i.e. plastic deformation of workpiece material, provides certain benefits compared to other technologies. The main advantages are the shorter cycle time in production and the quite good mechanical properties of the forged parts. Nowadays, complex problems during the product development process require the

application of engineering tools for numerical simulations based on FEM (Finite Element Method) [1].

The forging process can be carried out by using different equipment (machine tools): a hammer or a press. Also, the forging process is classified according to the dies [1]:

1. Open die forging (free forging)
2. Closed die forging
 - a. with flash (Figure 1)
 - b. without flash (Figure 2)

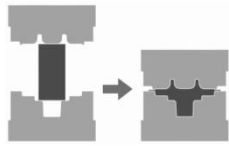


Figure 1. Closed die forging with flash [4]

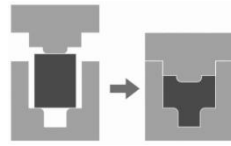


Figure 2. Closed die forging w/o flash [4]

2. DESIGN OF FORGED PART AND FORGING TOOL DIE

For the axisymmetric part – piston (Figure 3), a forged part and tooling die have been designed. The material of the piston is aluminum, AlSi1Mg (EN AW 6082). Figure 4 shows a 3D model of the piston, while a corresponding technical drawing can be found in Figure 5.



Slika 3. Aluminium piston (final shape after machining)



Figure 4. Aluminum piston – 3D CAD model

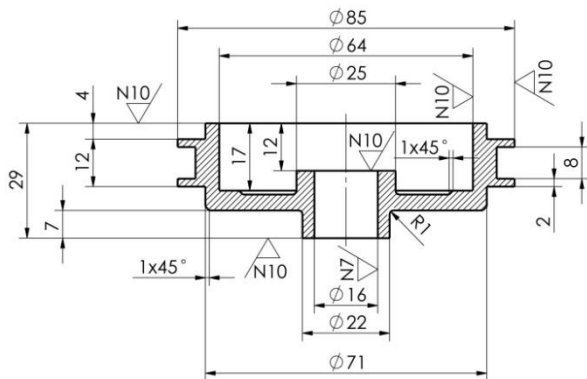


Figure 5. Aluminum piston – technical drawing

The design of forging technology begins with the determination of all relevant elements that are needed to define the drawing of the forged part:

1. Parting line,
2. Tolerances and machining allowances,
3. Forging draft angles (inner and outer),
4. Forging fillet radii (inner and outer),
5. Barrier plate.

The forged part has been designed according to the recommendations from the source [2, 3]. The parting line is placed in the middle of the part height on the largest diameter. The goal was to ensure better material flow and die filling during the forging process. All dimensions of the final machined part must be increased by the machining allowances of the forged part. All tolerances and allowances were selected according to the mass, nominal dimensions, and quality of the part [2, 3]. Due to the small value of the central hole diameter ($\varnothing 16$ mm), it's not feasible to perform additional operations, such as punching of the barrier plate. Simplification of the initial piston shape is also done in the case of the groove at the perimeter, which can't be formed by the forging process. In case of forging process on a hammer, the inner draft angles are 10° , while the outer draft angles are 7° . Radius is needed on every edge of the forged part in order to reduce stress concentration as well as to ensure better material flow. The inner radius is 4 mm, while the outer radius is 1 mm. Figure 6 shows a technical drawing of the forged part, where all forging dimensions have been defined. The technical drawing of the forged part is the basis for designing tool dies.

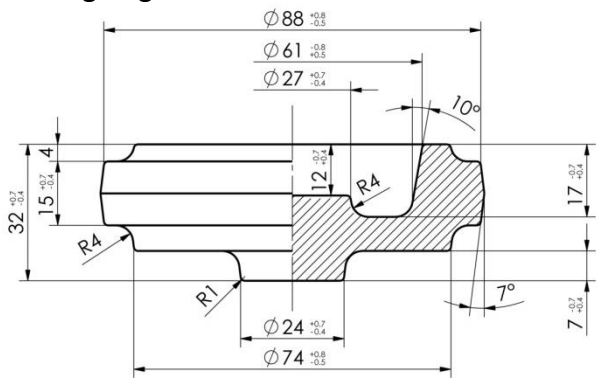


Figure 6. Forged part – technical drawing

To define the dimensions and shape of the tool dies for final forging, it is necessary to determine the dimensions of the hot forged part according to the following equations:

$$L_k = L_o (1 + \alpha t) = n L_o \quad (1)$$

$$l_k = l_o (2 - n) \quad (2)$$

where:

L_o, l_o [mm] – outer/inner dimensions of forged part in cold state,

L_k, l_k [mm] – outer/inner dimensions of forged part in hot state,
 $t = 420$ [°C] – forging temperature,
 $\alpha = 24$ [$10^{-6}/^{\circ}\text{C}$] – thermal expansion coefficient
 n – dimensional increase coefficient.

During the final forging, a flash is being formed along the perimeter of the forged part in the parting plane. For this purpose, it is necessary to design appropriate flash land (channels) in the tool die for excess material during the final forging process. In this particular case, the basic type of flash land was adopted according to the source [1, 2]. Figure 7 shows the dimensions and shape of the tooling dies for final forging.

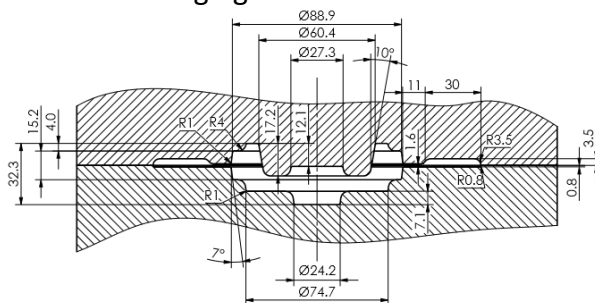


Figure 7. Tool dies for final forging

3. NUMERICAL SIMULATIONS OF THE FORGING PROCESS

The software tool QForm is used to build a simulation model and perform simulations of the forging process itself. Since the forged part is axisymmetric and the rotational part, during the simulation, the QForm problem is specified as "2D axisymmetric". This leads to a shorter processing time for the simulation and also means that the initial workpiece and tool die geometry are prepared as a 2D sketch. The forging process in this particular case contains the following phases:

1. Production of the initial workpiece $\varnothing 45 \times 77$ mm by cutting process on a mechanical saw (Figure 8). The dimensions of the initial workpiece are calculated according to the volume of the forged part with flash. It was also necessary to determine the ratio between workpiece height and diameter in order to ensure that there are no

buckling phenomena during the forging process.

2. Heating the workpiece up to the predefined forging temperature for aluminum alloys (420 °C)
3. Upsetting operation: deforming the initial workpiece to a height of 26 mm on a hammer in open tool dies (Figure 9).
4. Final forging process in closed tool dies. Forged parts get final shape with flash (Figure 10).
5. Removing excess material: trimming flash (Figure 11).



Figure 8. Initial workpiece $\varnothing 45 \times 77$ mm after cutting



Figure 9. Forged part after upsetting operation to height of 26 mm



Figure 10. Forged part with flash after final forging



Figure 11. Forged part after flash trimming

Figure 12 shows the general procedure for building a forging process simulation model as well as for generating simulation results in the software tool QForm.

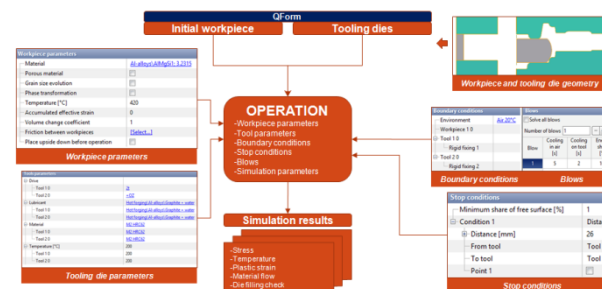


Figure 12. Procedure for building a simulation model of the forging process in QForm

At first, the initial workpiece and tool dies for each operation were imported into QForm.

Further steps in the creation of the forging process simulation model are related to the definition of workpiece parameters, tool parameters, boundary conditions, stop conditions, etc. After completion of simulation processing, the following results have been generated: temperature, stress, and plastic strain distribution at the workpiece during the forging process.

Figure 13 shows the temperature of the forged part after an upsetting operation. Initial workpiece $\varnothing 45 \times 77$ mm has been forged to a height of 26 mm. The target forging temperature was set to 420°C , while the temperature of the forged part after upsetting was within a range of 381°C to 467°C .

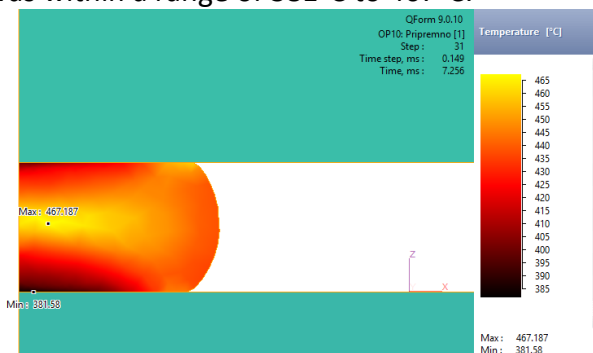


Figure 13. Temperature range after upsetting

Plastic deformation of material happens when stress in material exceeds tensile strength. Considering the previous statement, it is necessary to analyze the stress distribution and plastic strain of the forged part. Figure 14 shows the effective stress of the forged part after upsetting. Effective stress values are within a range of 74 to 98 MPa.

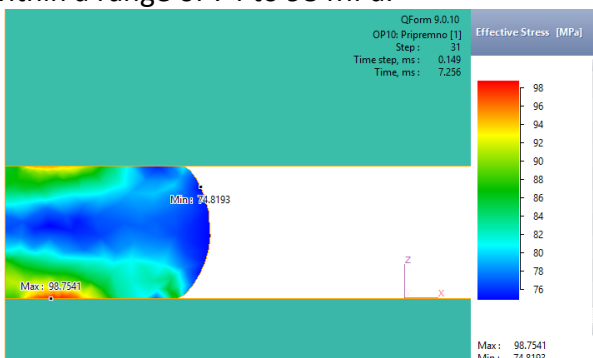


Figure 14. Effective stress after upsetting

Figure 15 shows plastic strain after a forged part is upsetting. Plastic strain takes values from 0.1 to 2.

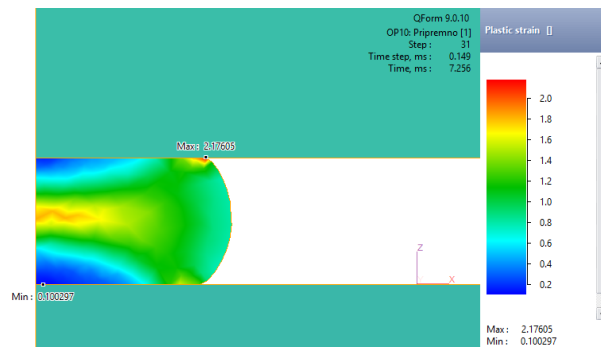


Figure 15. Plastic strain after upsetting

Load distribution during an upsetting operation is shown in Figure 16. Load increases over time and reaches its maximum value of 0.4 MN at the end of an upsetting operation. No abnormalities were detected during the evaluation of the simulation results related to the upsetting operation.

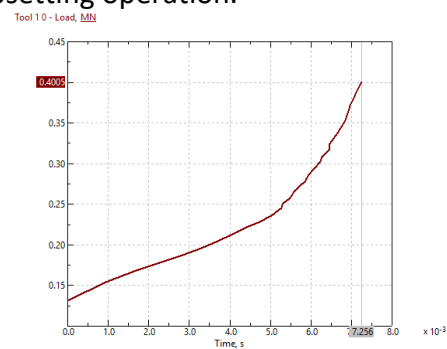


Figure 16. Load – Time graph during upsetting

In order to optimize the forging process, certain changes have been made regarding tooling dies geometry and process parameters. The technological solution that has been adopted as optimal is shown in this paper. Among other things, the flash land type has been changed, and this decision deviates from the recommendations given in the source [2]. The goal was to ensure better material flow and die filling, as well as to reduce the risk of overload in the tool. Figure 17 shows the contact nodes between tooling dies and workpiece after final forging. There were no unfilled areas in the tool dies, which indicates that the workpiece has been formed properly to its final shape.

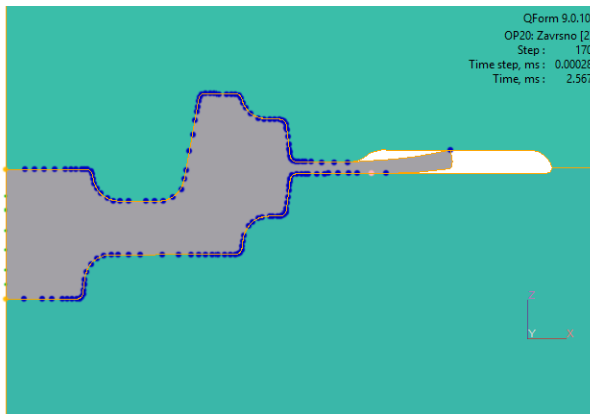


Figure 17. Contact nodes between tool die and workpiece after final forging

The temperature of the forged part after final forging is shown in Figure 18. The minimum temperature is 432°C, while the maximum temperature is 693°C. The maximum temperature is detected in the lower section of the flash due to the high friction that occurs during the material flow. This is not considered as critical, because flash needs to be removed by the trimming process anyway. The temperature of the forged part without flash is acceptable, so there is no risk to the thermal stability of the workpiece material.

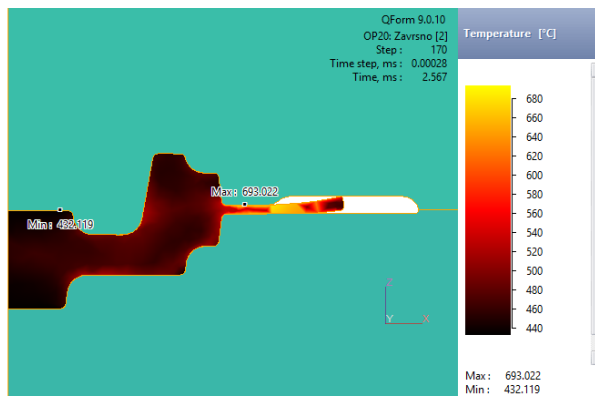


Figure 18. Temperature range after final forging

Effective stress after final forging is shown in Figure 19. The maximum effective stress is 104 MPa, while the minimum effective stress is 21 MPa. A higher stress concentration is noticed at the forged part nearby the flash land channel, as expected for this type of forging technology.

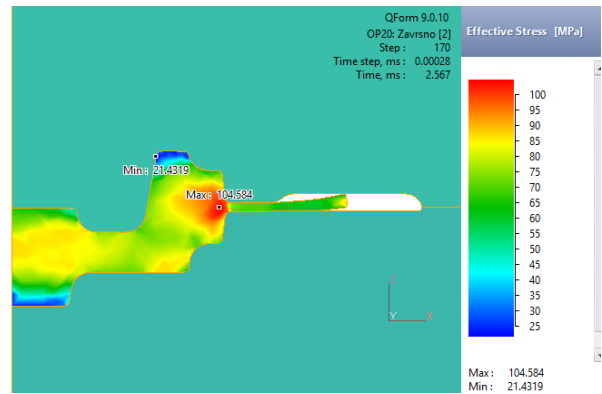


Figure 19. Effective stress after final forging

Figure 20 shows the plastic strain of the forged part after the final forging operation. The plastic strain is within the range of 0.1 to 6.8. Maximum plastic deformation is located at flash land. This is not a big issue since the flash has to be removed later. Minimum deformation is noticed at the bottom of the workpiece surface in the central area, as shown in Figure 20.

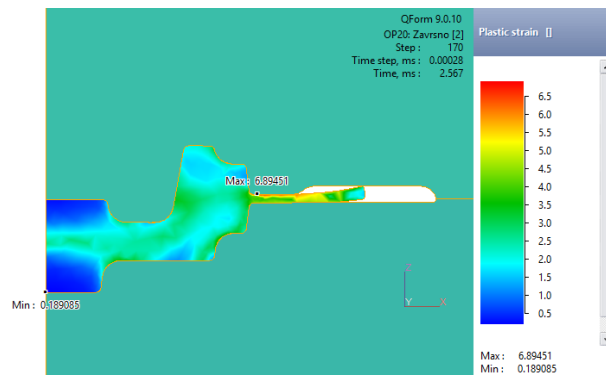


Figure 20. Plastic strain after final forging

Figure 21 shows load distribution over time for the final forging operation. Load increases during time and reaches its maximum value of 4.5 MN at the end of final forging.

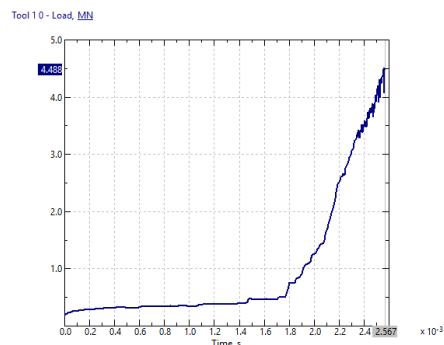


Figure 21. Load – Time graph after final forging

In order to check for potential defects in metal flow, an additional method has been applied: Minimum distance to surface The field

Minimum distance to surface can be used to analyze metal flow defects related to draw the metal from the surface of the workpiece into the depths. In this case, a forged part area up to a depth of 1.5 mm was in scope. Figure 22 shows the undersurface structure of the forged part before final forging. Figure 23 shows the undersurface structure of the forged part after final forging. The result has shown there was no significant displacement of the points on the traced lines, which could cause potential cracks.

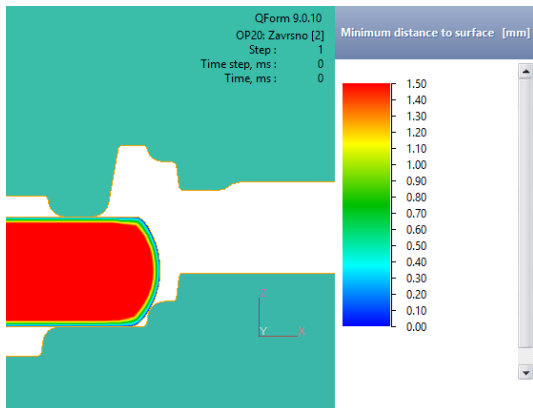


Figure 22. Undersurface flow lines before final forging

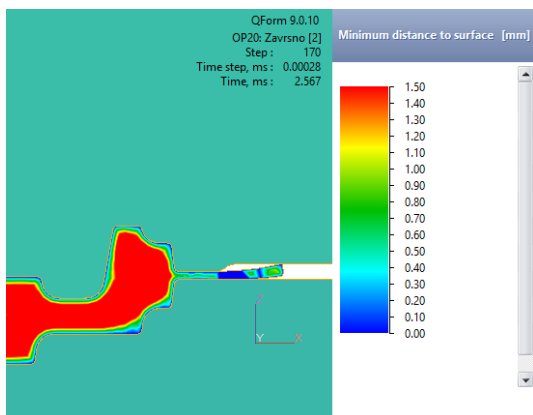


Figure 23. Undersurface flow lines after final forging

In addition to the analysis of the forged part, the behavior of the tooling die material during the final forging operation was also within the scope of the investigation. Figure 24 shows the temperature of the tool after the final forging. The tool has been pre-heated to 200°C before the final forging operation itself, in order to avoid any damage of the forging dies and to increase their longevity. Graphite mixed with water was used as a lubricant for tooling dies in order to reduce friction between the tool and the workpiece during the process of material

flow and die filling. The temperature of the tool after final forging is within the range of 200°C to 647°C, with the maximum temperature in the flash land area. There is no risk to the thermal stability of the tooling dies. In addition to analyzing the state of the forging, material tool behavior during the final forging operation has also been predicted.

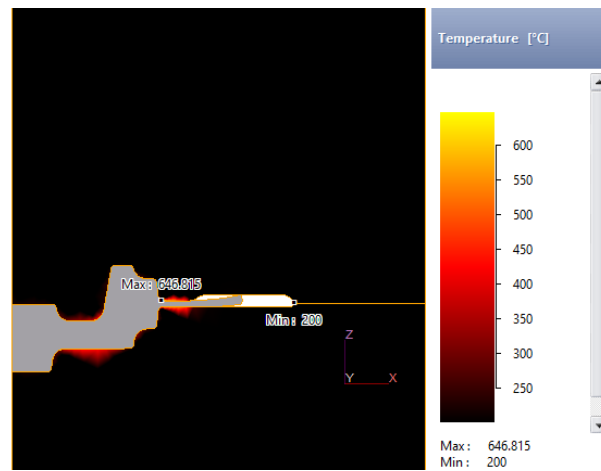


Figure 24. Temperature of tooling dies after final forging

Figure 25 shows the elastic strain of the tool after the final forging operation. Elastic strain has values from 0.000017 to 0.004, so there is no negative impact on the quality of the forged part.

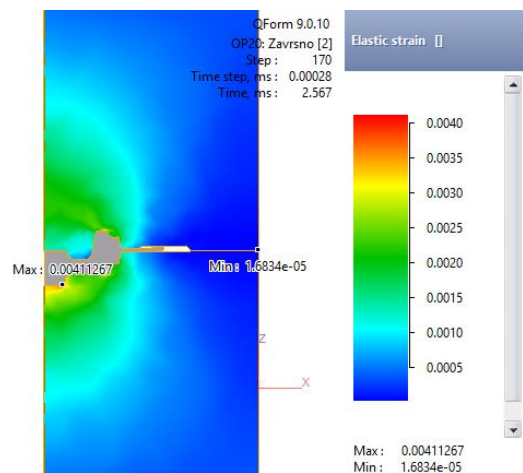


Figure 25. Elastic strain of tooling dies after final forging

4. CONCLUSION

This paper describes the process of designing the technological process of forging based on the drawing of the final machined part. For this purpose, an aluminum piston was

chosen as an example. The forging process is carried out in three operations. The first operation was upsetting, where the initial workpiece was deformed on a hammer up to a certain height. The second operation is related to the final forging in a closed tool die with a flash, where the final shape of the forged part was formed. The third operation is related to the removal of the excess material from the forged part, i.e., trimming the flash. For this purpose, it was necessary to define: tolerances and machining allowances; draft angles and radii of the forged part edges, parting line, the geometry of the flash land, as well as the dimensions of the initial workpiece. After the preparation of the geometry of the initial workpiece and the tool die, the building of the corresponding simulation model was started in the QForm software. During that procedure, all the relevant parameters of the forging process were defined: the material and temperature of the tooling dies and forged part, forging equipment, cooling and lubricating fluids, etc. The simulations in the mentioned software are based on the finite element method, and the goal was to predict the behavior of the material during the forging process itself and to detect potential irregularities. An analysis of the change in the structure of the forging material during the forging process itself was performed

in order to check for possible material flow defects, the appearance of internal or external cracks, etc. The obtained results in the form of temperatures, stresses, and deformations of the forged part are OK, so the proposed forging technology has been validated. On a certain example (the aluminum piston), it was shown that modern software packages for numerical simulations can provide significant support and benefits when designing the technological process of forging in terms of predicting the behavior of workpiece materials during the plastic deformation, optimizing the process, reducing production costs, improving product quality, reducing scrap, saving time during development of products, reducing the number of test samples, etc.

REFERENCES

- [1] Kalajdžić, M.: *Tehnologija mašinogradnje*, Mašinski fakultet, Beograd, 2008.
- [2] Jovičić, M.: *Alati za kovanje u kalupima, livenje pod pritiskom i presovanje plastičnih masa*, Mašinski fakultet, Beograd, 1979.
- [3] Kalajdžić, M., Tanović, Lj., Babić, B., i dr.: *Tehnologija obrade rezanjem – priručnik*, Mašinski fakultet, Beograd, 2012.
- [4] QForm, <https://www.qform3d.com/>, [August, 2023.]



Society of Production
Engineering

SPMS 2023

39. Savetovanje proizvodnog mašinstva Srbije

ICPES 2023

39th International Conference on Production Engineering of
Serbia



Faculty of Technical
Sciences
University of Novi Sad

Novi Sad, Serbia, 26. – 27. October 2023

ANFIS PLASMA ARC CUTTING SYSTEM OPTIMUM PARAMETERS ESTIMATION

Miloš MILOVANČEVIĆ^{1*}, Srećno ČURČIĆ²

¹Faculty of Mechanical Engineering, University of Nis, A. Medvedeva 14, 18000 Niš, Serbia

²Faculty of Technical Sciences in Čačak, University in Kragujevac, Svetog Save 65, 32102 Čačak, Serbia

*Corresponding author: milos.milovancevic@masfak.ni.ac.rs

Abstract: *Within the scope of this research, a data-driven optimization strategy was used in order to perfect the plasma arc cutting procedure. The quality of the cut is determined by these six output characteristics. Cutting current, cutting speed, and stand-off gap are the elements that go into the process. Material removal rate (MRR), surface roughness, chamfer, dross, kerf width, and heat impacted zone are the output answers (HAZ). Due to the fact that the process is quite complicated as a result of the many processing factors, it is necessary to develop an optimization model in order to acquire the structures that are free from deformation. The primary objective of this piece was to determine the factors that have the most impact on the circumstances that provide the best results during plasma arc cutting. This study's objective is to use an adaptive neural fuzzy inference system, or ANFIS for short, in order to categorise the various input parameters for the goal of maximising the efficiency of plasma arc cutting. The cutting current and stand-off distance, when combined, have the greatest impact on the material removal rate (MRR), surface roughness, chamfer, dross, kerf width, and heat affected zone (HAZ). In other words, the ideal combination for predicting material removal rate (MRR), surface roughness, chamfer, dross, kerf width, and heat affected zone is the combination of cutting current and stand-off gap (HAZ). It is claimed that this research is the first on a small scale to evaluate a variety of input factors concurrently. As a result, it has piqued the curiosity of everyone.*

Keywords: *plasma arc cutting; optimization; ANFIS.*

1. INTRODUCTION

The plasma arc cutting technique has seen widespread use, but it is not without its share of challenges and pitfalls, all of which must be carefully considered before beginning the procedure. The manufacturing industry makes use of the method for producing heavy-duty cycles. Nevertheless, traditional control procedures are not applicable to the

development of the technology since the many input parameters have been altered.

Because of its great productivity and its capacity to cut almost any material, plasma arc cutting, also known as PAC, is a method that is used extensively in the industrial sector. During the cutting process, the most significant challenge in PAC is the production of dross [1]. It was discovered that the key influencing factors in the PAC process are the

arc current, the standoff distance, and the cutting speed; in each of these cases, three levels are taken into consideration [2]. The heat-affected zone (HAZ) that is produced during the cutting of stainless steel (Grade 304) with a plasma arc has been researched in work [3]. Through the use of the response surface methodology (RSM), the best circumstances were determined to be a voltage of 240 volts, a current of 65 amps, and a speed of cut of 1.5 millimetres per second. The output values produced were the following: a material removal rate of 5.79 mm³/s, surface roughness of 65 m, and duration of cut of 246 s [4]. These values were acquired by adopting these values for the input process parameters. Following an investigation of the microstructure of the cut surface, the presence of micro striation, dross production, and recast layer was discovered [5]. The results of the experiments show that this control is superior to the conventional PI control in terms of the workpiece's precision, ripples, finish, and other comprehensive indexes. Furthermore, the plasma arc cutting power supply that is based on the fuzzy-neural network has excellent control performance [6].

The primary objective of this research is to determine which parameters have the most significant impact on the plasma arc cutting of stainless steel [7]. There are six output parameters that are examined and analysed in this process. When it comes to identifying and categorising input properties for the construction of the plasma arc cutting process,

the adaptive neuro fuzzy inference system, also known as ANFIS [8], performs well. A high normalisation and generalisation capability, noise immunity, resilience, and fault tolerance are all features that the ANFIS has. Because of this, it is not expected that changes to the process's different characteristics will have a substantial effect on the output of the plasma arc cutting process that is based on ANFIS.

2. METHODOLOGY

2.1 Experimental setup and data

For the cutting experiments stainless steel AISI 304 was used by samples 250×70×50mm. The input factors are cutting current, cutting speed and stand-off gap. The output responses are material removal rate (MRR), surface roughness, chamfer, dross, kerf width, heat affected zone (HAZ). MRR is calculated by an electronic weighing machine. Surface roughness is measured by a Talysurf device. A digital Vernier calliper is used for measurement of the other outputs. Figure 1 shows experimental setup of the plasma arc cutting system. Table 1 shows experimental data samples of the inputs and outputs [9].

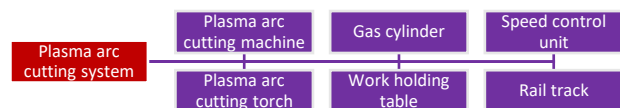


Figure 1. Experimental setup of plasma arc cutting system

Table 1. Input and output variables [9]

Input 1	Input 2	Input 3	Input 4	Output 1	Output 2	Output 3	Output 4	Output 5	Output 6
Cutting Current, A	Cutting Speed, mm/s	Gas Pressure, l/min	Stand-off Gap, mm	MRR, mm ² /min	Surface Roughness, lm	Chamfer, mm	Dross, mm ²	Kerf width, mm	HAZ, mm
100	2	15	2.5	1056.12	21.7	0.24	1.38	2.78	1.53
200	2	15	2.5	733.27	18.23	0.21	1.12	2.66	2.4
100	4	15	2.5	1049.5	23	0.31	1.36	2.75	2.02
200	4	15	2.5	890.65	19.96	0.22	1.3	2.7	1.86
150	3	12	2	979.92	20.88	0.22	1.36	2.68	1.79
150	3	18	2	1219.03	23.63	0.29	1.47	2.86	1.69
150	3	12	3	931.24	20	0.21	1.29	2.75	2.03
150	3	18	3	880.36	18.98	0.19	1.26	2.64	2.11
100	3	15	2	1270.86	25.85	0.32	1.57	2.87	1.34

Input 1	Input 2	Input 3	Input 4	Output 1	Output 2	Output 3	Output 4	Output 5	Output 6
Cutting Current, A	Cutting Speed, mm/s	Gas Pressure, l/min	Stand-off Gap, mm	MRR, mm ² /min	Surface Roughness, lm	Chamfer, mm	Dross, mm ²	Kerf width, mm	HAZ, mm
200	3	15	2	1087.42	23.69	0.3	1.4	2.79	1.84
100	3	15	3	1134.58	24.19	0.31	1.41	2.8	1.82
200	3	15	3	836.33	19.83	0.21	1.28	2.71	2.02
150	2	12	2.5	609.54	15.77	0.14	1.07	2.61	2.2
150	4	12	2.5	1001.8	19.77	0.22	1.34	2.69	2.01
150	2	18	2.5	1020.53	19.12	0.21	1.3	2.72	2.03
150	4	18	2.5	779.04	18.15	0.2	1.19	2.65	2.16
100	3	12	2.5	948.27	20.55	0.24	1.32	2.71	1.95
200	3	12	2.5	865.77	19.64	0.21	1.27	2.7	1.87
100	3	18	2.5	1200.73	23.76	0.29	1.47	2.82	1.51
200	3	18	2.5	801.54	18.15	0.21	1.2	2.65	2.29
150	2	15	2	1367.02	25.37	0.34	1.56	2.85	1.5
150	4	15	2	788.54	19.53	0.2	1.22	2.7	2.07
150	2	15	3	519.48	15.26	0.11	1	2.62	2.43
150	4	15	3	1248.72	24.13	0.32	1.5	2.79	1.8
150	3	15	2.5	773.53	17.38	0.15	1.23	2.57	2.13
150	3	15	2.5	773.61	17.39	0.16	1.25	2.56	2.13
150	3	15	2.5	773.33	17.38	0.16	1.22	2.55	2.12

2.2 ANFIS methodology

As shown in Figure 2, the ANFIS network contains five levels. The fuzzy inference system lies at the heart of the ANFIS network. Layer 1 accepts the inputs and uses membership functions to convert them to fuzzy values. The bell-shaped membership function is employed in this study because it has the best capability for nonlinear data regression.

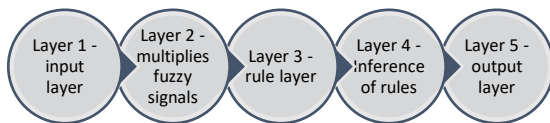


Figure 2. ANFIS layers

Bell-shaped membership functions is defined as follows:

$$\mu(x) = \text{bell}(x; a_i, b_i, c_i) = \frac{1}{1 + \left[\frac{x - c_i}{a_i} \right]^{2b_i}} \quad (1)$$

where $\{a_i, b_i, c_i\}$ is the parameters set and x is input.

The second layer multiplies the first layer's fuzzy signals and produces the rule's firing

strength. The rule layers are the third layer, and they normalize all of the signals from the second layer. The fourth layer does rule inference and converts all signals to crisp values. The last layers summed all of the signals and provided a clean output value.

3. RESULTS

The best predictors for the different types of defects were chosen using the ANFIS approach. The selection is crucial, as is the preprocessing of the input parameters to eliminate irrelevant inputs. Following the command in MATLAB Software, the dataset is partitioned into a training set (odd-indexed samples) and a checking set (even-indexed samples):

```

>>[data] = plasma;
>>trn_data = data(1:2:end,:);
>>chk_data = data(2:2:end,:);
  
```

The function "exhsrch" conducts an exhaustive search of the available inputs to identify the set of inputs that have the greatest impact on the six output variables. The function's first parameter defines the

number of input combinations that will be tested during the selection process. In essence, "exhsrch" creates an ANFIS model for each combination, trains it for one epoch, and then publishes the results. The command line below is used to find the one and two most important attributes in forecasting outputs:

```
>> exhsrch(1,trn_data,chk_data);
>> exhsrch(2,trn_data,chk_data);
```

Table 2 shows the correlations of the influence of single and two input combinations on the MRR. The influence is determined based on RMSE training and checking errors.

Input attribute stand-off gap has the smallest training error hence the highest influence on the MRR. In other words, any small changes of the stand-off gap would provide large oscillations of the MRR.

Combination of cutting current and stand-off gap has the smallest training error hence the highest influence on the MRR. In other words, if cutting current and stand-off gap are changing in the same time it would produce the highest changing of the MRR. Figure 3 shows ANFIS decision surface based on the two optimal inputs.

Table 2. Correlation matrix between input parameters and MRR

MRR	Cutting Current, A	Cutting Speed, mm/s	Gas Pressure, l/min	Stand-off Gap, mm
Cutting Current, A	trn=200.4070, chk=266.0967			
Cutting Speed, mm/s	trn=198.5691, chk=265.8494	trn=227.9316, chk=185.7137		
Gas Pressure, l/min	trn=189.1326, chk=270.5929	trn=200.4373, chk=413.1904	trn=218.9203, chk=206.6505	
Stand-off Gap, mm	trn=140.9772, chk=310.8652	trn=148.4954, chk=197.2559	trn=157.0890, chk=282.0749	trn=196.6478, chk=186.2681

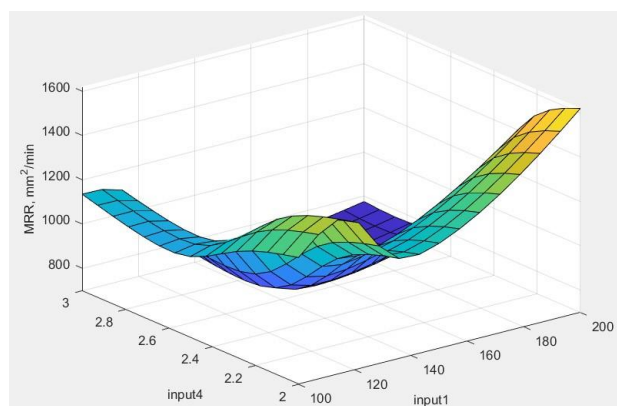


Figure 3. Optimal ANFIS decision surface for MRR

Table 3 shows the correlations of the influence of single and two input combinations on the surface roughness. Input attribute

cutting current has the smallest training error hence the highest influence on the surface roughness. In other words, any small changes of the cutting current would provide large oscillations of the surface roughness.

Combination of cutting current and stand-off gap has the smallest training error hence the highest influence on the surface roughness. In other words, if cutting current and stand-off gap are changing in the same time it would produce the highest changing of the surface roughness. Figure 4 shows ANFIS decision surface based on the two optimal inputs.

Table 3. Correlation matrix between input parameters and surface roughness

Surface Roughness	Cutting Current, A	Cutting Speed, mm/s	Gas Pressure, l/min	Stand-off Gap, mm
Cutting Current, A	trn=2.5681, chk=4.3947			
Cutting Speed, mm/s	trn=2.5276, chk=4.4007	trn=3.1573, chk=2.8265		
Gas Pressure, l/min	trn=2.4495, chk=4.3424	trn=2.8351, chk=6.6431	trn=3.2032, chk=2.4485	
Stand-off Gap, mm	trn=1.5345, chk=4.5983	trn=2.1837, chk=3.4789	trn=2.5032, chk=3.3776	trn=2.8467, chk=2.0403

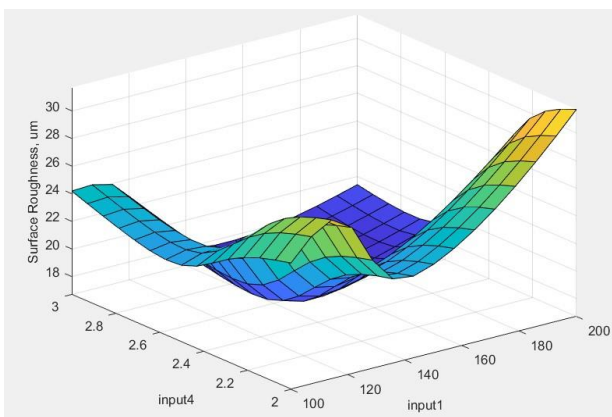


Figure 4. Optimal ANFIS decision surface for surface roughness

Table 4 shows the correlations of the influence of single and two input combinations

Table 4. Correlation matrix between input parameters and chamfer

Chamfer	Cutting Current, A	Cutting Speed, mm/s	Gas Pressure, l/min	Stand-off Gap, mm
Cutting Current, A	trn=0.0548, chk=0.0558			
Cutting Speed, mm/s	trn=0.0527, chk=0.0625	trn=0.0667, chk=0.0666		
Gas Pressure, l/min	trn=0.0530, chk=0.0548	trn=0.0614, chk=0.1303	trn=0.0689, chk=0.0482	
Stand-off Gap, mm	trn=0.0367, chk=0.0739	trn=0.0453, chk=0.0871	trn=0.0569, chk=0.0834	trn=0.0638, chk=0.0439

on the chamfer. Input attribute cutting current has the smallest training error hence the highest influence on the chamfer. In other words, any small changes of the cutting current would provide large oscillations of the chamfer.

Combination of cutting current and stand-off gap has the smallest training error hence the highest influence on the chamfer. In other words, if cutting current and stand-off gap are changing in the same time it would produce the highest changing of the chamfer. Figure 5 shows ANFIS decision surface based on the two optimal inputs.

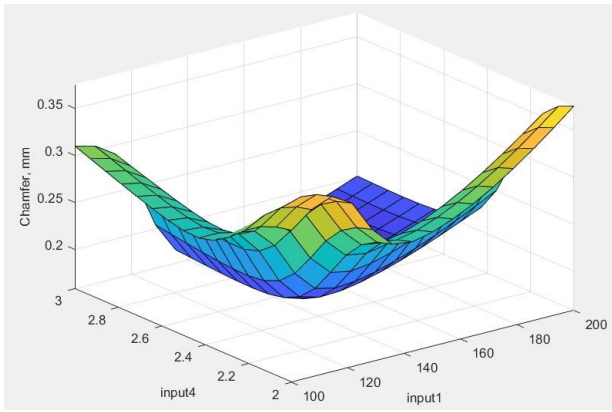


Figure 5. Optimal ANFIS decision surface for chamfer

Table 5 shows the correlations of the influence of single and two input combinations

Table 5. Correlation matrix between input parameters and dross

Dross	Cutting Current, A	Cutting Speed, mm/s	Gas Pressure, l/min	Stand-off Gap, mm
Cutting Current, A	trn=0.1333, chk=0.3058			
Cutting Speed, mm/s	trn=0.1303, chk=0.3174	trn=0.1491, chk=0.1134		
Gas Pressure, l/min	trn=0.1290, chk=0.3054	trn=0.1334, chk=0.2615	trn=0.1501, chk=0.1264	
Stand-off Gap, mm	trn=0.0855, chk=0.3197	trn=0.0931, chk=0.1117	trn=0.1039, chk=0.1768	trn=0.1254, chk=0.1286

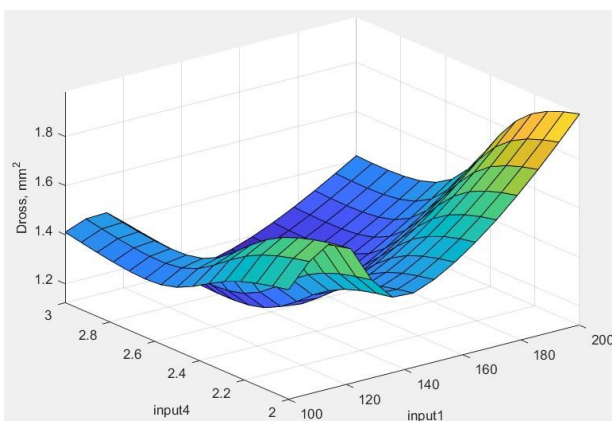


Figure 6. Optimal ANFIS decision surface for dross

Table 6 shows the correlations of the influence of single and two input combinations on the kerf width. Input attribute cutting

on the dross. Input attribute stand-off gap has the smallest training error hence the highest influence on the dross. In other words, any small changes of the stand-off gap would provide large oscillations of the dross.

Combination of cutting current and stand-off gap has the smallest training error hence the highest influence on the dross. In other words, if cutting current and stand-off gap are changing in the same time it would produce the highest changing of the dross. Figure 6 shows ANFIS decision surface based on the two optimal inputs.

current has the smallest training error hence the highest influence on the kerf width. In other words, any small changes of the cutting current would provide large oscillations of the kerf width.

Combination of cutting current and stand-off gap has the smallest training error hence the highest influence on the kerf width. In other words, if cutting current and stand-off gap are changing in the same time it would produce the highest changing of the kerf width. Figure 7 shows ANFIS decision surface based on the two optimal inputs.

Table 6. Correlation matrix between input parameters and kerf width

Kerf Width	Cutting Current, A	Cutting Speed, mm/s	Gas Pressure, l/min	Stand-off Gap, mm
Cutting Current, A	trn=0.0790, chk=0.5970			
Cutting Speed, mm/s	trn=0.0744, chk=0.5748	trn=0.0983, chk=0.0808		
Gas Pressure, l/min	trn=0.0731, chk=0.5837	trn=0.0881, chk=0.1919	trn=0.0953, chk=0.0855	
Stand-off Gap, mm	trn=0.0577, chk=0.5746	trn=0.0767, chk=0.1121	trn=0.0702, chk=0.1311	trn=0.0884, chk=0.0594

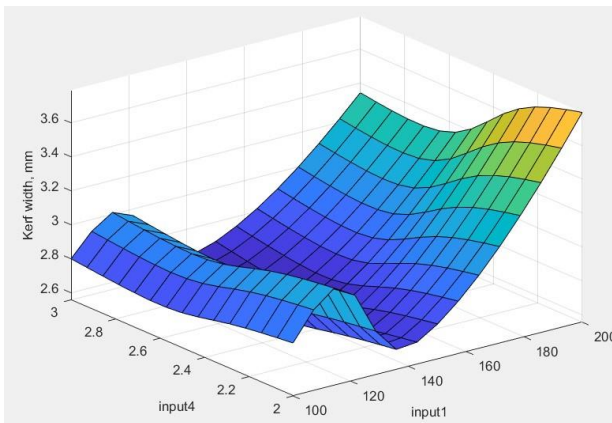


Figure 7. Optimal ANFIS decision surface for kerf width

Table 7 shows the correlations of the influence of single and two input combinations on the HAZ. Input attribute stand-off gap has

Table 7. Correlation matrix between input parameters and HAZ

HAZ	Cutting Current, A	Cutting Speed, mm/s	Gas Pressure, l/min	Stand-off Gap, mm
Cutting Current, A	trn=0.2562, chk=0.4912			
Cutting Speed, mm/s	trn=0.2359, chk=0.4818	trn=0.2988, chk=0.2375		
Gas Pressure, l/min	trn=0.2415, chk=0.4920	trn=0.2674, chk=0.6201	trn=0.2957, chk=0.2767	
Stand-off Gap, mm	trn=0.1594, chk=0.5895	trn=0.2102, chk=0.3228	trn=0.2084, chk=0.3930	trn=0.2390, chk=0.2663

the smallest training error hence the highest influence on the HAS. In other words, any small changes of the stand-off gap would provide large oscillations of the HAZ.

Combination of cutting current and stand-off gap has the smallest training error hence the highest influence on the HAZ. In other words, if cutting current and stand-off gap are changing in the same time it would produce the highest changing of the HAZ. Figure 78 shows ANFIS decision surface based on the two optimal inputs.

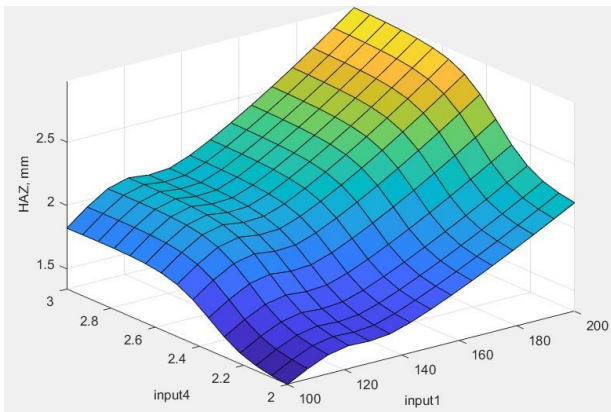


Figure 8. Optimal ANFIS decision surface for HAZ

4. CONCLUSION

In the manufacturing industry, heavy-duty cycles often call for the usage of plasma arc cutting. Nevertheless, traditional control procedures are not applicable to the development of the technology since the many input parameters have been altered. Within the scope of this research, a data-driven optimization strategy was used in order to perfect the plasma arc cutting procedure. The quality of the cut is determined by these six output characteristics. Cutting current, cutting speed, and stand-off gap are the elements that go into the process. Material removal rate (MRR), surface roughness, chamfer, dross, kerf width, and heat impacted zone are the output answers (HAZ).

The primary objective of this piece was to determine the factors that have the most bearing on creating the ideal circumstances for plasma arc cutting. The objective of this study is to identify the various input parameters of plasma arc cutting by using an adaptive neural fuzzy inference system, or ANFIS for short. According to the results of an ANFIS prediction, the combination of cutting current and stand-off gap has the most significant impact on the material removal rate (MRR), surface roughness, chamfer, dross, kerf width, and heat impacted zone (HAZ). In other words, the ideal combination for predicting material removal rate (MRR), surface roughness, chamfer, dross, kerf width, and heat affected

zone is the combination of cutting current and stand-off gap (HAZ).

REFERENCES

- [1] Sharma, D. N., & Kumar, J. R. (2020). Optimization of dross formation rate in plasma arc cutting process by response surface method. *Materials Today: Proceedings*, 32, 354-357.
- [2] Rajeshkannan, A., Ali, M., Prakash, R., Prasad, R., Jeevanantham, A. K., & Jayaram, K. (2020). Optimizing the process parameters in plasma arc cutting using Taguchi approach for the case industry in Fiji. *Materials Today: Proceedings*, 24, 1122-1131.
- [3] Singh, D., & Shrivastava, Y. (2021). Identification of suitable machining zone during the plasma arc cutting of SS-304. *Materials Today: Proceedings*, 38, 413-417.
- [4] Suresh, A., & Diwakar, G. (2021). Optimization of process parameters in plasma arc cutting for TWIP steel plates. *Materials Today: Proceedings*, 38, 2417-2424.
- [5] Ananthakumar, K., Rajamani, D., Balasubramanian, E., & Davim, J. P. (2019). Measurement and optimization of multi-response characteristics in plasma arc cutting of Monel 400™ using RSM and TOPSIS. *Measurement*, 135, 725-737.
- [6] Deli, J., & Bo, Y. (2011). An intelligent control strategy for plasma arc cutting technology. *Journal of Manufacturing Processes*, 13(1), 1-7.
- [7] Kumar Naik, D., & Maity, K. P. (2018). An optimization and experimental analysis of plasma arc cutting of Hardox-400 using Taguchi based desirability analysis. *Materials Today: Proceedings*, 5(5), 13157-13165.
- [8] Jang, J.-S.R, ANFIS: Adaptive-Neuro-based Fuzzy Inference Systems, *IEEE Trans. On Systems, Man, and Cybernetics* (1993), Vol.23, 665-685.
- [9] Mangaraj, S. R., Bagal, D. K., Parhi, N., Panda, S. N., Barua, A., & Jeet, S. (2022). Experimental study of a portable plasma arc cutting system using hybrid RSM-nature inspired optimization technique. *Materials Today: Proceedings*, 50, 867-878.



Society of Production
Engineering

SPMS 2023

39. Savetovanje proizvodnog mašinstva Srbije

ICPES 2023

39th International Conference on Production Engineering of
Serbia



Faculty of Technical
Sciences
University of Novi Sad

Novi Sad, Serbia, 26. – 27. October 2023

ANFIS CHIP-TOOL INTERFACE TEMPERATURE EVALUATION

Miloš MILOVANČEVIĆ^{1*}, Srećno ĆURČIĆ²

¹Faculty of Mechanical Engineering, University of Nis, A. Medvedeva 14, 18000 Niš, Serbia

²Faculty of Technical Sciences in Čačak, University in Kragujevac, Svetog Save 65, 32102 Čačak, Serbia

*Corresponding author: milos.milovancevic@masfak.ni.ac.rs

Abstract: *The primary objective of the research is to develop an optimization technique for determining the temperature at the chip-tool interface using an adaptive neural fuzzy inference system (ANFIS). ANFIS is a representation of a heuristic optimization approach that utilizes back propagation training in one direction and a gradient desc ANFIS chip-tool interface temperature evaluation algorithm in the other way. The experimental training data samples are collected for publication in the relevant academic journals. There are operational factors which may have an effect on the temperature of the chip-tool contact. Input attribute The environment has the least amount of variance in its training, giving it the greatest impact on the temperature. The interaction of cutting speed and environment results in the least amount of temperature variation and, hence, the greatest temperature effect. Therefore, the combination of cutting speed, feed rate, and environment has the greatest impact on the etch rate since it has the fewest amount of training error. It is thought to be the first research on a small scale to evaluate several operational factors concurrently, and it has attracted the curiosity of everyone.*

Keywords: *chip-tool interface; temperature; optimization; ANFIS.*

1. INTRODUCTION

The quality of the machining process could be able to be inferred from the shapes of the chips. Even though the chip may be regarded a waste item, the shapes the chip takes could be extremely essential. This is because the forms can have a significant impact not only on the machining process but also on the quality of the product that is machined. The chip shapes may be a crucial characteristic that has a significant influence on the stability of the cutting process. The temperature distribution that occurs in the cutting zone as a result of

contact between the cutting tool and the working material is one of the most critical aspects that determine the chip shapes [1]. Because of this, the industrial research community has shown a significant amount of interest in the process of assessing the chip shapes and temperature distribution in the cutting zone [2]. Because of the potential influence that chip shapes creation and temperature distribution in the cutting zone might have on surface roughness, tool life, force components of the cutting process, and overall product quality, conducting an analysis

of these phenomena is of the utmost importance.

The generation of chips and the total size of the cutting zone are both significant elements that have received inadequate attention. Cutting zone area developed sluggishly with increasing cutting speed and levelled out at high cutting speed; nevertheless, it climbed dramatically with increased feed [3]. Cutting zone area grew level at high cutting speed. In the study [4], both experimental research and modelling using finite elements were carried out in order to get a comprehensive knowledge of the chip temperature and how it affects chip morphology, cutting forces, and surface roughness. There has been a great deal of theory research done in terms of chip production and chip breaking characteristics under conventional cutting and high speed cutting conditions. However, there hasn't been nearly enough research done on the chip formation mechanism or its influence on the cutting state when it comes to large workpieces that are being cut under extreme loads [5]. Cutting at high speeds is used often in a variety of sectors, including aircraft, automobile, die, and others. On the other hand, a thorough understanding of the mechanism behind the high-speed cutting behaviour has not yet been achieved. For the purpose of analysing the thermal equilibrium that exists between the formation of heat and the consumption of energy during high-speed dry cutting [6], models of thermal sources and fields of cutting temperature have been presented. It was shown in article [7] that the temperature in the shear zone drops when there is a corresponding reduction in the chip thickness. Because of this, the material undergoes less thermal softening, and as a result, larger specific cutting forces may be achieved. A theoretical technique for the prediction of tool temperatures in intermittent turning was suggested in article [8] to disclose the impacts of cutting parameters on tool temperatures. This method took into consideration the creation of serrated chip and was designed to forecast tool temperatures. To achieve the lowest possible tool

temperature, it is recommended to use a relatively high feed rate in conjunction with a relatively shallow depth of cut. When end milling, a significant shift in the temperature of the tool may produce excessive tool wear and limit its life, which is particularly problematic in the machining of materials that are tough to work with [9]. An approach that is based on artificial neural networks (ANN) was proposed in study [10] to predict the experimental cutting temperatures generated in orthogonal turning of AISI 316L stainless steel, and it was demonstrated that the established ANN model is a powerful one for predicting the experimental cutting temperatures. This was accomplished by demonstrating that the established ANN model is a powerful one. Since there are numerous machining characteristics that may be altered in order to achieve ideal machining conditions, the primary goal of this research was to identify the most essential elements of the process, with a particular emphasis on the temperature distribution in the cutting zone. The neuro-fuzzy technique was used because it is a method that is very well-suited for the analysis of nonlinear systems that include a wide variety of parameters [11].

2. METHODOLOGY AND MATERIALS

2.1 Experimental setup

Experimental tests were performed during turning on the machine Model VDF-D480 10KW. Cutting zone temperature was measured during machining as can be seen in Figure 1a. Thermal camera was used for the temperature measurement in the cutting zone. The camera FLIR E50 which is thermal sensitive is shown in Figure 1b. The main features of the camera are:

- Class II laser product, 1mW power output.
- IR resolution - 43,200 (240x180) pixels,
- Measurement modes include 3 Spots, 3 Area Box, Isotherm, Auto Hot/Cold spots
- Bluetooth links camera to mobile devices,
- Picture-in-Picture,
- Auto Orientation.

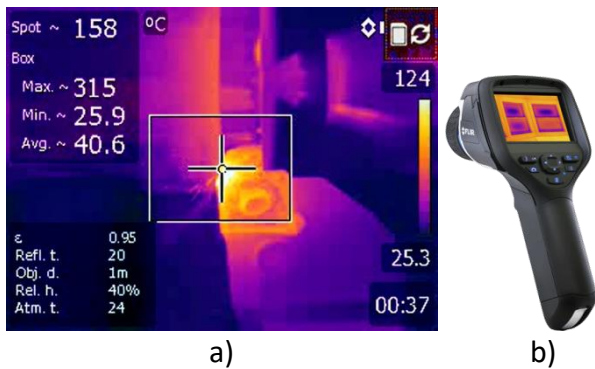


Figure 1. (a) Temperature measurement in cutting zone and (b) thermal camera FLIR E50

Surface roughness was measured by roughness meter, Perthometer M1 by Mahr Company. Roughness recordings were performed in Perthometer software. As the surface roughness measure, arithmetical average roughness Ra was used. The average values were evaluated for each of the specimens. The surface roughness was measured on the three specimen's sections – upper, lower and middle section and average values were determined. The roughness was measured 0.1 mm from the upper and lower edges of the specimen. The experimental procedure of surface roughness measurement was performed on the Talysurf 6 (*Taylor Hobson*) system. This system could measure micro-geometric characteristics of the surface.

The cutting forces were measured experimentally. The experiment was composed of a dynamometer KISTLER type 9265A1, an amplifier KISTLER tip Ca5001, an AD converter Burb Brown type 2000 and a computer PC/AT 486 33MHz. For the signal acquisition software LT/CONTROL version 5.02 was used through a virtual instrument in order to track the cutting forces graphically.

After the experimental investigation for different cutting condition based on the experimental plan, the acquired signals of the cutting forces were analyzed. The name of the cutting tool was PTG NR 2525 M16 with TNMG 160404-CM 4C15 P15. Figure 2 shows the thermal camera in action and the cutting process.

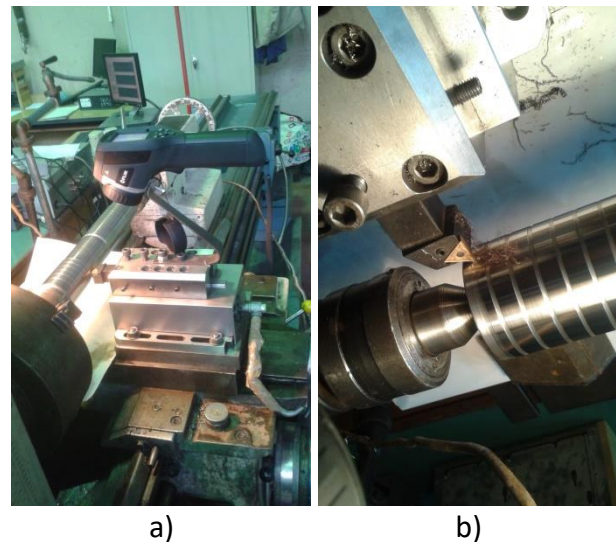


Figure 2. (a) Temperature measures in the cutting zone and (b) the cutting process

In order to have the full control on the tool life and on the surface roughness as the main indicator of the machining process quality it is essential to measure the temperature in the cutting tool and in the chip as well. It is very important to know the temperature distribution in the cutting zone in order to understand and to control the machining process. Figure 3 shows the experimental setup scheme of the machining process and the temperature measurement in the cutting zone.

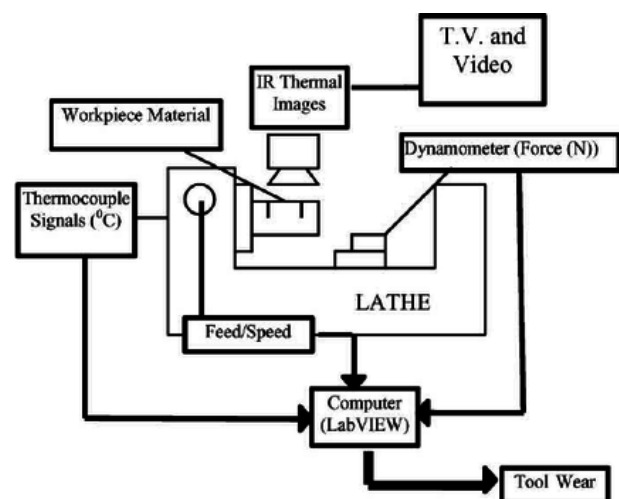


Figure 3. Experimental setup scheme

In the present study, the role of high-pressure coolant jet by water-insoluble mineral oil VG-68 on cutting temperature and tool life in turning C-60 steel, 17CrNiMo6 steel, and 42CrMo4 steel by uncoated SNMG and SNMM carbide inserts is experimentally

investigated. To evaluate the effects of cutting speed, feed rate, environment (dry and HPC-assisted machining), materials, and cutting inserts on chip-tool interface temperature, mathematical models are formed based on response surface methodology and validity of the models are confirmed by employing various statistical evaluation techniques. Tables 1 and 2 shows the input or operating parameters which are varied in the design [12].

Table 1. Numerical values of the input variables [12]

Environment	Material	Cutting tool
Dry - 1	C-60 - 1	SNMG - 1
HPC - 2	17CrNiMo6 - 2	SNMM - 2
	42CrMo4 - 3	

Table 2. Input and output variables [12]

Input 1	Input 2	Input 3	Input 4	Input 5	output
Cutting speed m/min	Feed rate mm/rev	Environment	Material	Cutting tool	Temperature
93	0.1	1	1	1	592
93	0.14	1	1	1	662
93	0.18	1	1	1	694
93	0.22	1	1	1	698
133	0.1	1	1	1	652
133	0.14	1	1	1	694
133	0.18	1	1	1	709
133	0.22	1	1	1	736
186	0.1	1	1	1	714
186	0.14	1	1	1	769
186	0.18	1	1	1	782
186	0.22	1	1	1	790
266	0.1	1	1	1	773
266	0.14	1	1	1	821
266	0.18	1	1	1	826
266	0.22	1	1	1	843
93	0.1	2	1	1	453
93	0.14	2	1	1	534
93	0.18	2	1	1	563
93	0.22	2	1	1	584
133	0.1	2	1	1	566
133	0.14	2	1	1	595
133	0.18	2	1	1	617
133	0.22	2	1	1	640
186	0.1	2	1	1	595
186	0.14	2	1	1	644
186	0.18	2	1	1	678
186	0.22	2	1	1	701
266	0.1	2	1	1	697
266	0.14	2	1	1	717
266	0.18	2	1	1	757
266	0.22	2	1	1	784
93	0.1	1	2	1	690
93	0.14	1	2	1	564

Input 1	Input 2	Input 3	Input 4	Input 5	output
Cutting speed m/min	Feed rate mm/rev	Environment	Material	Cutting tool	Temperature
93	0.18	1	2	1	708
93	0.22	1	2	1	591
133	0.1	1	2	1	730
133	0.14	1	2	1	646
133	0.18	1	2	1	743
133	0.22	1	2	1	671
186	0.1	1	2	1	780
186	0.14	1	2	1	706
186	0.18	1	2	1	791
186	0.22	1	2	1	724
266	0.1	1	2	1	826
266	0.14	1	2	1	757
266	0.18	1	2	1	839
266	0.22	1	2	1	770
93	0.1	2	2	1	566
93	0.14	2	2	1	468
93	0.18	2	2	1	581
93	0.22	2	2	1	491
133	0.1	2	2	1	606
133	0.14	2	2	1	549
133	0.18	2	2	1	624
133	0.22	2	2	1	590
186	0.1	2	2	1	679
186	0.14	2	2	1	628
186	0.18	2	2	1	680
186	0.22	2	2	1	644
266	0.1	2	2	1	710
266	0.14	2	2	1	651
266	0.18	2	2	1	738
266	0.22	2	2	1	701
93	0.1	1	3	1	671
93	0.14	1	3	1	688
93	0.18	1	3	1	707
93	0.22	1	3	1	713
133	0.1	1	3	1	692
133	0.14	1	3	1	732
133	0.18	1	3	1	736
133	0.22	1	3	1	749
186	0.1	1	3	1	712
186	0.14	1	3	1	746
186	0.18	1	3	1	767
186	0.22	1	3	1	786
266	0.1	1	3	1	739
266	0.14	1	3	1	769
266	0.18	1	3	1	799
266	0.22	1	3	1	823

Input 1	Input 2	Input 3	Input 4	Input 5	output
Cutting speed m/min	Feed rate mm/rev	Environment	Material	Cutting tool	Temperature
93	0.1	2	3	1	510
93	0.14	2	3	1	523
93	0.18	2	3	1	573
93	0.22	2	3	1	613
133	0.1	2	3	1	547
133	0.14	2	3	1	586
133	0.18	2	3	1	633
133	0.22	2	3	1	667
186	0.1	2	3	1	577
186	0.14	2	3	1	619
186	0.18	2	3	1	667
186	0.22	2	3	1	715
266	0.1	2	3	1	621
266	0.14	2	3	1	669
266	0.18	2	3	1	727
266	0.22	2	3	1	757
93	0.1	1	1	2	565
93	0.14	1	1	2	641
93	0.18	1	1	2	682
93	0.22	1	1	2	691
133	0.1	1	1	2	618
133	0.14	1	1	2	670
133	0.18	1	1	2	697
133	0.22	1	1	2	713
186	0.1	1	1	2	680
186	0.14	1	1	2	744
186	0.18	1	1	2	757
186	0.22	1	1	2	790
266	0.1	1	1	2	727
266	0.14	1	1	2	788
266	0.18	1	1	2	813
266	0.22	1	1	2	822
93	0.1	2	1	2	470
93	0.14	2	1	2	540
93	0.18	2	1	2	566
93	0.22	2	1	2	578
133	0.1	2	1	2	526
133	0.14	2	1	2	568
133	0.18	2	1	2	587
133	0.22	2	1	2	634
186	0.1	2	1	2	582
186	0.14	2	1	2	638
186	0.18	2	1	2	681
186	0.22	2	1	2	703
266	0.1	2	1	2	631
266	0.14	2	1	2	697

Input 1	Input 2	Input 3	Input 4	Input 5	output
Cutting speed m/min	Feed rate mm/rev	Environment	Material	Cutting tool	Temperature
266	0.18	2	1	2	711
266	0.22	2	1	2	755
93	0.1	1	2	2	645
93	0.14	1	2	2	672
93	0.18	1	2	2	709
93	0.22	1	2	2	728
133	0.1	1	2	2	707
133	0.14	1	2	2	741
133	0.18	1	2	2	760
133	0.22	1	2	2	777
186	0.1	1	2	2	771
186	0.14	1	2	2	803
186	0.18	1	2	2	812
186	0.22	1	2	2	826
266	0.1	1	2	2	823
266	0.14	1	2	2	846
266	0.18	1	2	2	858
266	0.22	1	2	2	865
93	0.1	2	2	2	522
93	0.14	2	2	2	551
93	0.18	2	2	2	588
93	0.22	2	2	2	612
133	0.1	2	2	2	573
133	0.14	2	2	2	600
133	0.18	2	2	2	638
133	0.22	2	2	2	660
186	0.1	2	2	2	655
186	0.14	2	2	2	675
186	0.18	2	2	2	690
186	0.22	2	2	2	743
266	0.1	2	2	2	691
266	0.14	2	2	2	728
266	0.18	2	2	2	746
266	0.22	2	2	2	770
93	0.1	1	3	2	673
93	0.14	1	3	2	686
93	0.18	1	3	2	700
93	0.22	1	3	2	713
133	0.1	1	3	2	703
133	0.14	1	3	2	720
133	0.18	1	3	2	735
133	0.22	1	3	2	745
186	0.1	1	3	2	736
186	0.14	1	3	2	746
186	0.18	1	3	2	753
186	0.22	1	3	2	771

Input 1	Input 2	Input 3	Input 4	Input 5	output
Cutting speed m/min	Feed rate mm/rev	Environment	Material	Cutting tool	Temperature
266	0.1	1	3	2	764
266	0.14	1	3	2	780
266	0.18	1	3	2	797
266	0.22	1	3	2	811
93	0.1	2	3	2	505
93	0.14	2	3	2	528
93	0.18	2	3	2	560
93	0.22	2	3	2	606
133	0.1	2	3	2	534
133	0.14	2	3	2	576
133	0.18	2	3	2	595
133	0.22	2	3	2	671
186	0.1	2	3	2	581
186	0.14	2	3	2	612
186	0.18	2	3	2	663
186	0.22	2	3	2	694
266	0.1	2	3	2	634
266	0.14	2	3	2	654
266	0.18	2	3	2	733
266	0.22	2	3	2	754

2.2 ANFIS methodology

As shown in Figure 4, the ANFIS network contains five levels. The fuzzy inference system lies at the heart of the ANFIS network. Layer 1 accepts the inputs and uses membership functions to convert them to fuzzy values. The bell-shaped membership function is employed in this study because it has the best capability for nonlinear data regression.

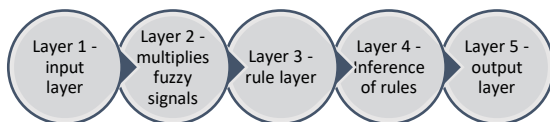


Figure 4. ANFIS layers

Bell-shaped membership functions is defined as follows:

$$\mu(x) = \text{bell}(x; a_i, b_i, c_i) = \frac{1}{1 + \left[\frac{x - c_i}{a_i} \right]^{2b_i}} \quad (1)$$

where $\{a_i, b_i, c_i\}$ is the parameters set and x is input.

The second layer multiplies the first layer's fuzzy signals and produces the rule's firing strength. The rule layers are the third layer, and they normalize all of the signals from the second layer. The fourth layer does rule inference and converts all signals to crisp values. The last layers summed all of the signals and provided a clean output value.

3. RESULTS

The best predictors for the different types of defects were chosen using the ANFIS approach. The selection is crucial, as is the preprocessing of the input parameters to eliminate irrelevant inputs. Following the command in MATLAB Software, the dataset is partitioned into a training set (odd-indexed samples) and a checking set (even-indexed samples):

```

>>[data] = temperature;
>>trn_data = data(1:2:end,:);
>>chk_data = data(2:2:end,:);
  
```

The function "exhsrch" conducts an exhaustive search of the available inputs to

identify the set of inputs that have the greatest impact on the temperature. The function's first parameter defines the number of input combinations that will be tested during the selection process. In essence, "exhsrch" creates an ANFIS model for each combination, trains it for one epoch, and then publishes the results. The command line below is used to find the one and two most important attributes in forecasting outputs:

```
>> exhsrch(1,trn_data,chk_data);
>> exhsrch(2,trn_data,chk_data);
```

Figures 5-7 show the correlations of the influence of single, two and three input combinations on the temperature. The influence is determined based on RMSE training (trn) and checking (chk) errors. Input attribute **Environment** has the smallest training error hence the highest influence on the temperature. In other words, any small changes of the **Environment** would provide large oscillations of the temperature.

Figure 6 shows the optimal combination of two input attributes based on the temperature. Combination of **cutting speed** and **environment** has the smallest training error hence the highest influence on the temperature. In other words, if **cutting speed** and **environment** are changing in the same time it would produce the highest changing of the temperature.

Figure 7 shows the optimal combination of three input attributes based on the temperature. Combination of **cutting speed**, **feed rate** and **environment** has the smallest training error hence the highest influence on the etch rate. In other words, if **cutting speed**, **feed rate** and **environment** are changing in the same time it would produce the highest changing of the temperature.

Tables 3-5 shows numerical values of RMSE based on the prediction of temperature for one, two and three input attributes.

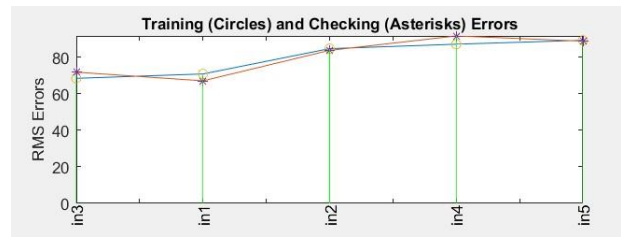


Figure 5. Correlations of one input attribute with response

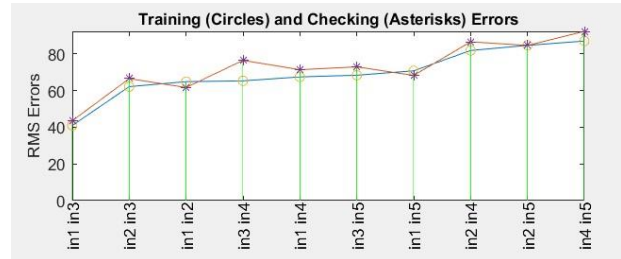


Figure 6. Correlations of two inputs attribute with response

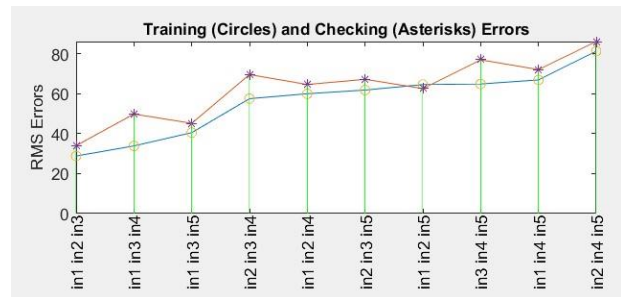


Figure 7. Correlations of three inputs attribute with response

Table 3. Correlations of one attribute with response

ANFIS model 1: in1 --> trn=70.9333, chk=67.1488
ANFIS model 2: in2 --> trn=84.7981, chk=83.8550
ANFIS model 3: in3 --> trn=68.5321, chk=71.9043
ANFIS model 4: in4 --> trn=87.2305, chk=91.7571
ANFIS model 5: in5 --> trn=89.3803, chk=88.8896

Table 4. Correlations of two attributes with response

ANFIS model 1: in1 in2 --> trn=64.8226, chk=61.6328
ANFIS model 2: in1 in3 --> trn=40.9577, chk=43.5176
ANFIS model 3: in1 in4 --> trn=67.4106, chk=71.3364
ANFIS model 4: in1 in5 --> trn=70.7269, chk=68.2225
ANFIS model 5: in2 in3 --> trn=62.1072, chk=66.4773
ANFIS model 6: in2 in4 --> trn=81.8142, chk=86.5173
ANFIS model 7: in2 in5 --> trn=84.5962, chk=84.5537
ANFIS model 8: in3 in4 --> trn=65.2682, chk=76.4268
ANFIS model 9: in3 in5 --> trn=68.3311, chk=72.8869
ANFIS model 10: in4 in5 --> trn=86.9476, chk=92.2298

Table 5. Correlations of three attributes with response

ANFIS model 1: in1 in2 in3 --> trn=28.8028, chk=34.0016
ANFIS model 2: in1 in2 in4 --> trn=59.9626, chk=64.5875
ANFIS model 3: in1 in2 in5 --> trn=64.5303, chk=62.5517
ANFIS model 4: in1 in3 in4 --> trn=33.8589, chk=49.8112
ANFIS model 5: in1 in3 in5 --> trn=40.4942, chk=45.1703
ANFIS model 6: in1 in4 in5 --> trn=66.8746, chk=72.0426
ANFIS model 7: in2 in3 in4 --> trn=57.5043, chk=69.5606
ANFIS model 8: in2 in3 in5 --> trn=61.8193, chk=67.1821
ANFIS model 9: in2 in4 in5 --> trn=81.2755, chk=86.0852
ANFIS model 10: in3 in4 in5 --> trn=64.8590, chk=76.9501

For further analyzing the optimal two-attributes is extracted and analyzed. There is always preferable to use models with small number of inputs. Figure 8 shows the ANFIS decision surface for the minimal checking error.

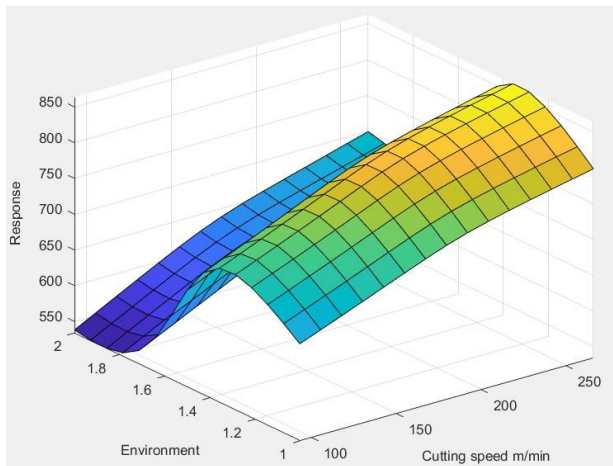


Figure 8. Relationship between the optimal two-attributes and the temperature

4. CONCLUSION

The research presented an illustration of a neuro-fuzzy-based approach for monitoring chip morphologies and surface roughness based on temperature distribution in the cutting zone for various machining settings. This method monitors the chip forms and surface roughness. The quality of the machining process is determined in large part by the form of the chips and the roughness of the surfaces. A good chip shape guarantees the highest quality end products with the smoothest possible surfaces. Within the scope of this study, we investigated the effect that the temperature distribution in the cutting

zone had on the chip forms and the surface roughness.

The neuro-fuzzy technique was used because it is an exceptionally well-suited method for dealing with nonlinear systems that include a wide variety of parameters. During the machining process, it was discovered that the temperature at a specific area has a greater impact than the temperature at its highest point.

REFERENCES

- [1] Hwang, J., & Chandrasekar, S. (2011). Contact conditions at the chip-tool interface in machining. *International Journal of Precision Engineering and Manufacturing*, 12(2), 183-193.
- [2] Maruda, R. W., Krolczyk, G. M., Nieslony, P., Wojciechowski, S., Michalski, M., & Legutko, S. (2016). The influence of the cooling conditions on the cutting tool wear and the chip formation mechanism. *Journal of Manufacturing Processes*, 24, 107-115.
- [3] Ke, Q., Xu, D., & Xiong, D. (2017). Cutting zone area and chip morphology in high-speed cutting of titanium alloy Ti-6Al-4V. *Journal of Mechanical Science and Technology*, 31(1), 309-316.
- [4] Cui, X., Guo, J., Zhao, J., & Yan, Y. (2015). Chip temperature and its effects on chip morphology, cutting forces, and surface roughness in high-speed face milling of hardened steel. *The International Journal of Advanced Manufacturing Technology*, 77(9-12), 2209-2219.
- [5] Xianli, L. I. U., Genghuang, H. E., Fugang, Y. A. N., Yaonan, C. H. E. N. G., & Li, L. I. U. (2015). Large chip production mechanism under the extreme load cutting conditions. *Chinese Journal of Mechanical Engineering*, 28(02), 1.
- [6] An, H. P., Rui, Z. Y., Wang, R. F., & Zhang, Z. M. (2014). Research on cutting-temperature field and distribution of heat rates among a workpiece, cutter, and chip for high-speed cutting based on analytical and numerical methods. *Strength of Materials*, 46(2), 289-295.
- [7] Denkena, B., de Leon, L., & Köhler, J. (2010). Influence of scaled undeformed sections of cut on strain rate, cutting force and temperature. *Production Engineering*, 4(5), 457-464.

- [8] Cui, X., & Guo, J. (2017). Effects of cutting parameters on tool temperatures in intermittent turning with the formation of serrated chip considered. *Applied Thermal Engineering*, 110, 1220-1229.
- [9] Baohai, W., Di, C., Xiaodong, H., Dinghua, Z., & Kai, T. (2016). Cutting tool temperature prediction method using analytical model for end milling. *Chinese Journal of Aeronautics*, 29(6), 1788-1794.
- [10] Kara, F., Aslantaş, K., & Cicek, A. (2016). Prediction of cutting temperature in orthogonal machining of AISI 316L using artificial neural network. *Applied Soft Computing*, 38, 64-74.
- [11] Jang, J. S. (1993). ANFIS: adaptive-network-based fuzzy inference system. *IEEE transactions on systems, man, and cybernetics*, 23(3), 665-685.
- [12] Kamruzzaman, M., Rahman, S. S., Ashraf, M., Ibne, Z., & Dhar, N. R. (2017). Modeling of chip-tool interface temperature using response surface methodology and artificial neural network in HPC-assisted turning and tool life investigation. *The International Journal of Advanced Manufacturing Technology*, 90(5), 1547-1568.



Society of Production
Engineering

SPMS 2023

39. Savetovanje proizvodnog mašinstva Srbije

ICPES 2023

39th International Conference on Production Engineering of
Serbia



Faculty of Technical
Sciences
University of Novi Sad

Novi Sad, Serbia, 26. – 27. October 2023

VARIANTS OF HYBRID KINEMATICS MACHINE TOOLS BASED ON O-X GLIDE MECHANISM WITH ADDITIONAL ROTARY AXES

Sasa ZIVANOVIC¹, Slobodan TABAKOVIC^{2,*}, Zoran DIMIC³, Milan ZELJKOVIC²

¹University of Belgrade, Faculty of Mechanical Engineering, Belgrade, Serbia

²University of Novi Sad, Faculty of Technical Sciences, Novi Sad, Serbia

³Lola Institute, Belgrade, Serbia

*Corresponding author: tabak@uns.ac.rs

Abstract: *The paper discusses the variants of upgrading the basic concept of the machine with hybrid kinematics based on the O-X glide mechanism, by adding one or two rotating axes on the work table. The variant project was realized at the level of virtual prototypes, which were used to simulate the operation of the machine according to the given program. In this way, the programming environment was created and programming verification was performed on the virtual machining system. The simulations were carried out on selected workpieces of certain dimensions, taking into account the available working space of the machine. In this way, machining simulations on a virtual prototype of four-axis and five-axis machining demonstrated and verified the possibility of machining with additional rotating axes.*

Keywords: *Hybrid kinematics machine, rotary axes, CAD/CAM, simulation.*

1. INTRODUCTION

Due to the constant change in the type and volume of production, machine tool users constantly demand the development of new machine tools improved with the characteristics of accuracy, rigidity, speed, compactness, and a greater number of control axes (four, five and more). The appearance of machines with parallel kinematics (in 1984) opened up new directions of research in order to fulfill the set requirements and caused a significant research momentum at that time. With the development of machines with parallel kinematics, a new approach was adopted in the design of machine tool mechanisms, where the emphasis was placed on the analysis and improvement of existing ones, but also on the development of

completely new machines with parallel kinematics (PKM). The reason for analyzing and studying PKM is the advantages provided by parallel compared to serial mechanisms: i) smaller mass of moving parts; ii) better ratio of mass and stiffness of parts; iii) greater flexibility; iv) good dynamic characteristics [1,2]. In addition to the mentioned advantages, PKM is also characterized by disadvantages such as: i) an irregularly shaped workspace; ii) useful working space of small dimensions; iii) complex solutions to kinematic problems; iv) complex construction of the mechanism [3]. Hybrid mechanisms, which represent a combination of serial and parallel mechanisms, contain the advantages of both types of mechanisms with a significant reduction in disadvantages.

Hybrid mechanisms can be very different. Here the addition of 1 or 2 degrees of freedom series mechanisms to a parallel mechanism will be considered. The main reasons for combining mechanisms are as follows: (1) to increase the number of degrees of freedom, such as in the case of a DELTA or TRICEPT mechanism [4], (2) to translate machining from three-axis to four-axis or five-axis, and (3) to increase the range of tool orientation which is small in purely parallel mechanisms with 6 degrees of freedom (e.g. Geodetic Hexapod [5]), (4) to increase the working space.

2. HYBRID KINEMATIC MACHINES

The machine tool based on the O-X glide mechanism in the basic version enables three-axis machining. With the addition of one rotary axis, four-axis machining can be achieved. This type of machining can be of two types: index and continuous. Continuous machining enables simultaneous interpolation of all available axes. Index machining implies a rotary axis as a positional one, that is, it enables the workpiece to be correctly positioned and processed on 4 different sides, without the need for special auxiliary screening and basing, which are necessary when the machine is three-axis.

In addition to three translational movements (X, Y, Z), five-axis machining also has two rotary ones, which enables the machine to perform simultaneous interpolation along several axes. Machining on such machines can be continuous with a 5-axis or positional with a 3+2-axis. With 3+2 axis machining, the desired orientation of the workpiece is taken with two rotary axes, after which the machining is carried out with the remaining translator axes.

This paper plans to analyze the possibility of upgrading the basic machine, with one [6, 7,8] or two rotating axes [6,9], taking into account the limitations that come from the shape and dimensions of the working space. Simulations of four- and five-axis machining on virtual prototypes of the machine, in the various considered variants, were used for the analysis.

3. VARIANTS ANALYSIS OF O-X GLIDE MECHANISM

The development of the basic configuration of the machine tool with hybrid kinematics, the variants of which are discussed in this paper, was presented to the scientific and professional public in papers [10,11], Fig.1.

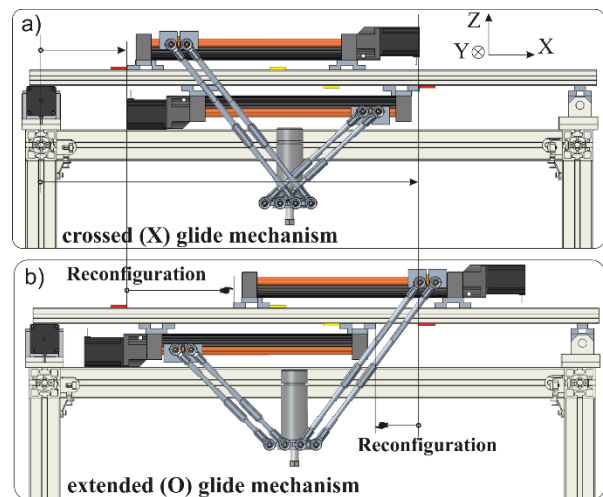


Figure 1. Basic configurations of O-X glide hybrid machine tools [10]

The three-axis machine with hybrid kinematics is based on a hybrid O-X mechanism, which was created by combining a plane parallel mechanism and a serial translator axis (HMO), which are mounted on the supporting structure of the machine. Conceptual solutions of multi-axis machine tools defined by upgrading the basic machine concept with one more (HM1) or two serial (HM2) rotary axes are considered here. The basic conceptual solution and upgrade variants are shown in Table1.

Table 1. Variants of O-X glide hybrid mechanism

Type	HMO	HM1	HM2
Description	Hybrid mechanism Basic	1 additional rotational axis	2 additional rotational axis
Kinematic structure	OYXZC _v	A'OYXZC _v B'OYXZC _v	A'C'OYXZC _v B'C'OYXZC _v
Serial	1	1	1
Parallel	2	2	2
Serial	-	1	2
DOF	3	4	5

The table also shows the kinematic structure of the considered machine tool variants, the defined number of degrees of freedom of the

serial and parallel parts of the mechanism, as well as the total number of CNC axes.

For further analysis of the upgrade of the basic machine, adequate CAD models have been prepared for the purpose of checking the placement and basing of these rotary axes on the supporting structure of the machine in the selected coordinate directions, in the direction of the X or Y axis, Fig.2.

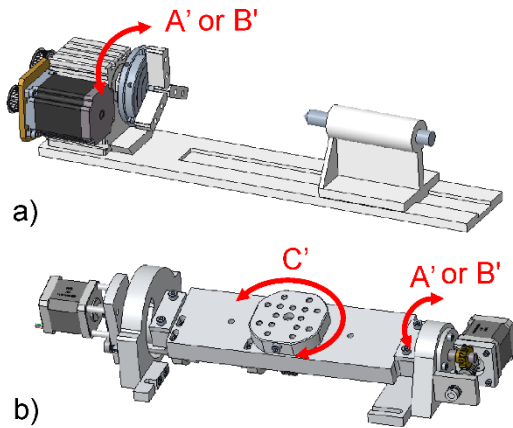


Figure 2. Variants of kinematic modules with rotary

Fig. 3a shows the basic variant of the O-X glide of the hybrid mechanism in the X configuration (HM0) in the reference and arbitrary position with the contours of the working space of the parallel mechanism in the XZ plane. At this stage of the research, the analysis is not performed on the O variant of the mechanisms, although all this may also apply to that configuration of the mechanism.

Respecting the shape and dimensions of the working space, it is necessary to check the possibility of installing additional serial rotary axes. In the HM1 variant, a rotary axis A' was added, as a rotation around the X axis, Fig.3b. This axis of rotation can be set in the other direction as well. If this axis is rotated by 90° so that the rotation axis is parallel to the Y axis, the rotation axis B' is obtained.

In the HM2 variant, two rotary axes are added as a rotary tilting table with rotations A' and C', Fig.3c. Here, a variant of rotating the two-axis rotary table by 90° is also possible, so that the rotary axes in this case become B' and C'.

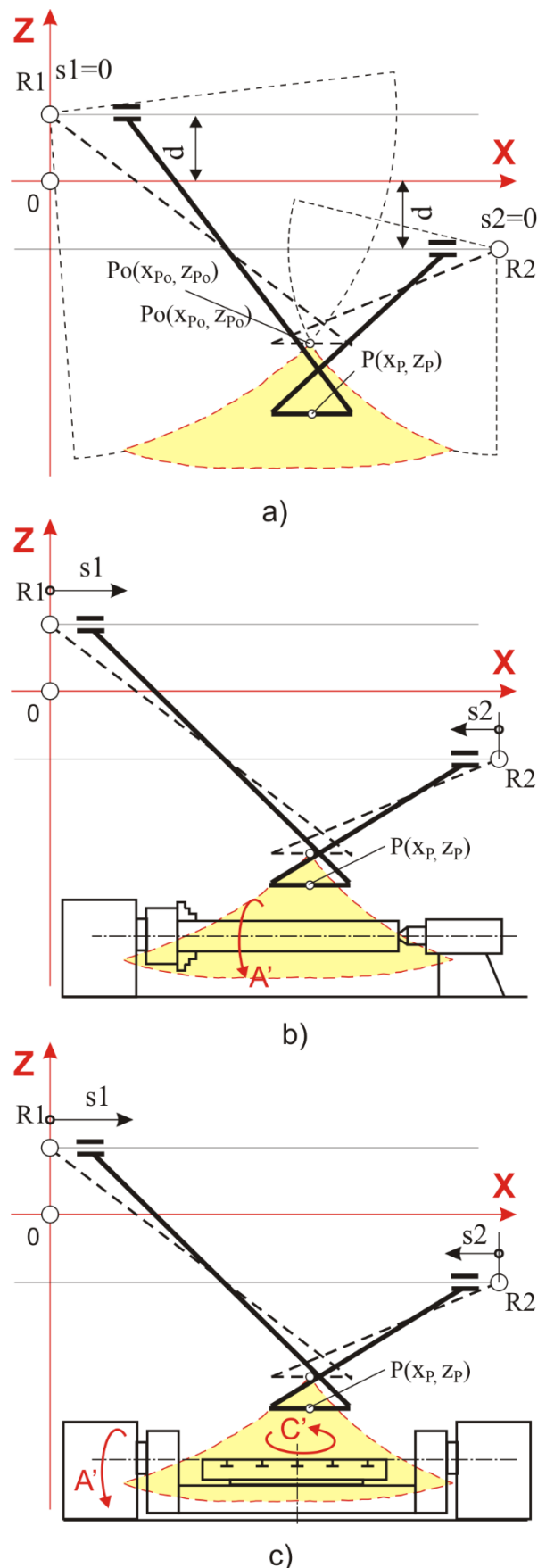


Figure 3. Basic kinematic variants of O-X glide hybrid machine tools

Prepared prototypes of the machine with added rotary axes are shown in Fig. 4. The CAD

model of the machine with the folded fourth axis, i.e. axis A' is given in Fig. 4 a), while the variant with rotating axis B' is given in Fig. 4b). The model of the added two-axis rotary table on the virtual prototype of the machine with rotations A'C' is given in Fig. 4c), while the variant when this table is rotated by 90°, i.e. it has rotations B'C', is given in Fig. 4d).

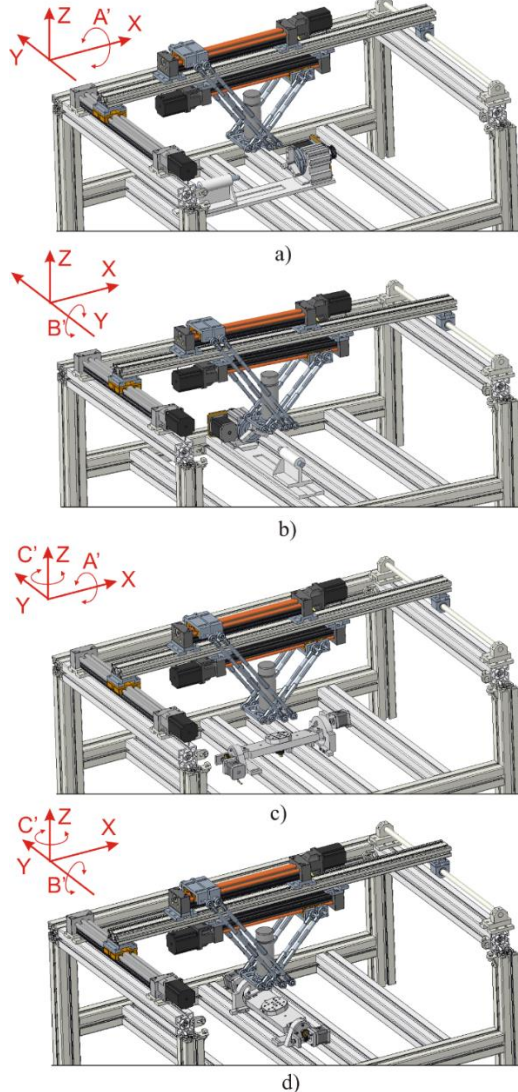


Figure 4. CAD variants of O-X glide hybrid machine tools with rotary axes

In order to check the possibility of using rotary axes within the limits of the available working space, a simulation of the selected workpiece machining was performed, which was shown in chapter 4.

4. MACHINE SIMULATION OF O-X GLIDE MECHANISM WITH ROTARY AXES

The verification of the operation of the machine with added rotating axes from Fig.2

was realized on a virtual prototype of the machine in the environment of the CAD/CAM system PTC Creo, which was used both for the development of the machines and for their programming.

During the development of the virtual prototype, a hybrid mechanism was modeled with all kinematic connections between the components, which give the possibility of moving the elements of the virtual prototype as a system of rigid bodies. Examples of such simulations can be seen in papers [7,10,11].

Fig. 5, presented the characteristic markings of the used kinematic connections, such as Pin, Slider, and Ball. This configuration of the machine assembly enables the movement of its moving components within the limits defined by the kinematic links, which is of particular importance for detecting possible collisions during the movement of the mechanism elements.

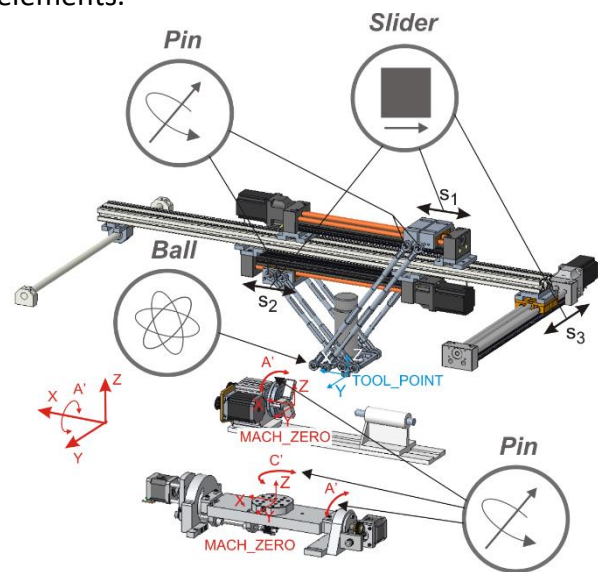


Figure 5. Coordinate systems

In the environment used for configuring the virtual prototype, it is possible to run a simulation of the operation of the virtual prototype that works according to the given control program, i.e. according to the defined path of the tool (Cutter Location File - CLF), in order to check the kinematics of the machine and possible collisions, as well as the feasibility and possibility of machining in the boundaries of the workspace.

On the virtual model of the workpiece, it is necessary to define the coordinate system MACH_ZERO. The coordinate system of the

same name needs to be defined on that part of the virtual prototype of the machine that will carry the virtual workpiece, the chuck of the rotating axis or the work table of the two-axis rotating-tilting module (Fig. 5). The tool coordinate system is also defined on the virtual prototype of the machine, which is marked with TOOL_POINT and is located on the front surface of the main spindle. The Z axis of this coordinate system is directed in the direction of the tool axis, according to the rules for marking CNC axes.

Programming experiences with one horizontal axis of rotation can be seen in works [7,8], and here they are shown on the example of the considered machine with hybrid kinematics.

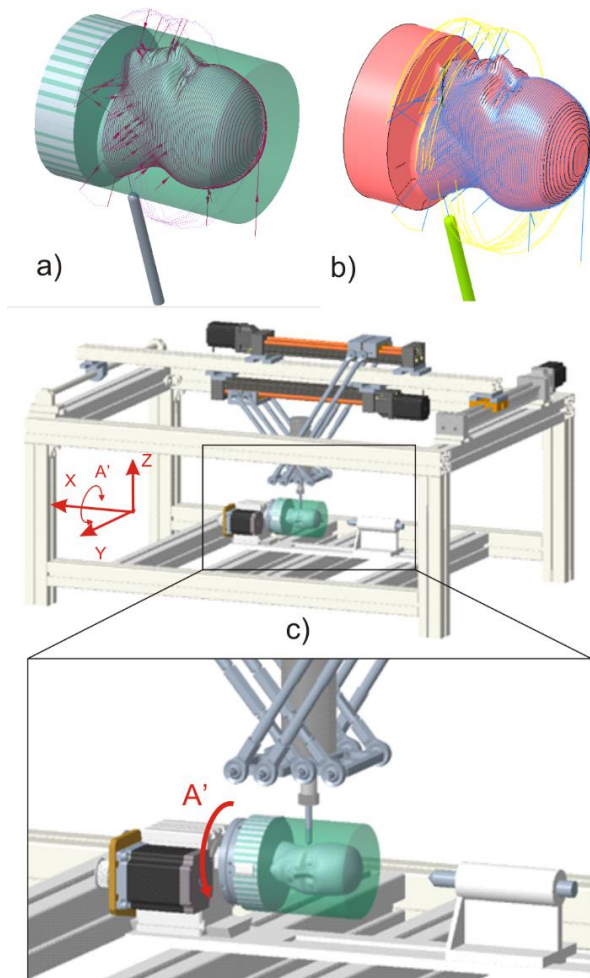


Figure 6.Machine simulation with rotary axis A'

Fig. 6 shows an example of the verification of the program for machining the model of the human head, which includes the simulation of the tool path (Fig. 6a), the simulation of material removal (Fig. 6b), and the simulation

of the operation of the machine according to the given program with the rotary axis A' (Fig. 6c).

In Fig. 7 shows an example of simulation of five-axis machining of a convex calotte with rotating axes A' and C'.

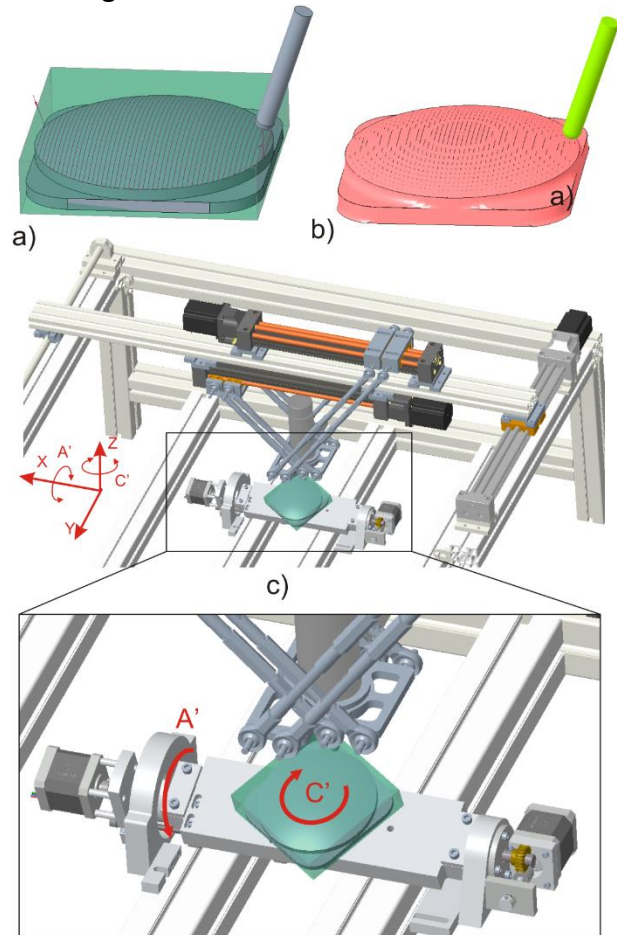


Figure 7.Machine simulation with rotary axes A'C'

Simulations of four-axis and five-axis machining in Figs. 5 and 6, the possibility of machining with additional rotary axes on the considered machine with hybrid kinematics was demonstrated and verified.

5. CONCLUSION

The paper shows the analysis of the upgrade of a three-axis machine with hybrid kinematics with additional serial rotary axes, so that the machine can be either 4-axis or 5-axis. Possible variants of adding rotary axes were considered with the analysis of machining simulations and the placement and basing of rotary axes, so as to check the possibility of machining within the limits of the available working space. The possibility of such machining was verified on a

virtual prototype by simulations of the machine's operation when it works according to the set tool path (CLF). Experimental verification on a real machine is also planned in further research.

ACKNOWLEDGEMENT

The presented research was supported by the Ministry of Education, Science and Technological Development of the Republic of Serbia through the projects: "Integrated research in macro, micro, and nano mechanical engineering" (contract no. 451-03-47/2023-01/200105 dated 3 February 2023) and "Innovative scientific and artistic research in the field of FTN activities", supported by the Ministry of Science, Technological Development and Innovation of the Government of the Republic of Serbia

REFERENCES

- [1] T.K. Tanev: Kinematics of a hybrid (parallel-serial) robot manipulator, *Mechanism and Machine Theory*, Vol. 35, No.9, pp. 1183-1196, 2000.
- [2] J. Wu, J. Wang, T. Li, L. Wang: Dynamic analysis of the 2-DOF planar parallel manipulator of a heavyduty hybrid machine tool, *International Journal of Advanced Manufacturing Technology*, Vol. 34, No.3-4, pp. 413-420, 2007.
- [3] J. Wu, T. Li, X. Liu, L. Wang: Optimal kinematic design of a 2-DOF planar parallel manipulator, *Tsingua Science & Technology*, Vol. 12, No.3, pp.269-275, 2007.
- [4] Z. Pandilov, V. Dukovski: Parallel kinematics machine tools: Overview- from history to the future, *Annals of faculty engineering Hunedoara – International Journal Of Engineering*, Vol. 10, No. 2, pp.111-124, 2012.
- [5] F. Joseph: Simulation Tools for Collaborative Exploration of Hexapod Machine Capabilities and Applications, National Institute of Standards and Technology, 2023.
- [6] F. Pierrot: Towards non-hexapod mechanisms for high performance parallel machines, in: *Proceedings of 26th Annual Conference of the IEEE, IECON 2000*, 22-28.10. 2000, Nagoya, vol. 1, pp. 229 – 234.
- [7] N. Vorkapić, S. Živanović, Z. Dimić: Development of an educational 3-axis CNC machine tool for rapid prototyping with two translational and one rotary axis, *Tehcnics*, Vol. 68, No.6, pp.725-732, 2020. (in Serbian)
- [8] N. Vorkapić, S. Živanović, B. Kokotović, N. Slavković, Z. Dimić: Programming of 3-axis CNC milling machines with two translatory and one rotary axes, in: *Proceedings of 42. JUPITER conference*, 06-07. 10. 2020, Belgrade, Serbia, pp. 3.122-3.128. (in Serbian)
- [9] M. Terrier, M., Giménez, J.-Y. Hascoët: VERNE - a five-axis parallel kinematics milling machine, *Proceedings of the Institution of Mechanical Engineers, Part B: Journal of Engineering Manufacture*, vol. 219, No.3, pp. 327–336, 2005.
- [10] S. Zivanovic, S. Tabakovic, M. Zeljkovic, Z. Dimic: Modelling and analysis of machine tool with parallel–serial kinematics based on O-X glide mechanism, *Journal of the Brazilian Society of Mechanical Sciences and Engineering*, Vol. 43, No.456, 2021.
- [11] Tabakovic, S. Zivanovic, Z Zeljkovic, Z. Dimic: Configuring a new educational machine tool based on hybrid kinematic mechanism, *Tehcnics*, Vol. 71, No.5, pp. 603-612, 2021. (in Serbian)



Society of Production
Engineering

SPMS 2023

39. Savetovanje proizvodnog mašinstva Srbije

ICPES 2023

39th International Conference on Production Engineering of
Serbia



Faculty of Technical
Sciences
University of Novi Sad

Novi Sad, Serbia, 26. – 27. October 2023

ANALIZA DINAMIČKIH KARAKTERISTIKA DRŽAČA ALATA ZA OBRADU STRUGANJEM

**Dejan MARINKOVIĆ^{1*}, Miloš KNEŽEV¹, Aleksandar ŽIVKOVIĆ¹, Cvijetin MLAĐENOVIĆ¹,
Luka MEJIĆ¹**

¹Univerzitet u Novom Sadu, Fakultet tehničkih nauka Novi Sad, Srbija,

*Corresponding author: dejan.marinkovic@uns.ac.rs

Apstrakt: Mašinska obrada predstavlja složen proces pri kojem se javlja više različitih faktora koji utiču na tačnost i kvalitet obrade. Pojava vibracija alata predstavlja jedan od najuticajnijih parametara koji se negativno odražava na životni vek alata za rezanje, kvalitet obrađenih delova i tačnost obrade. Ovaj prepoznatljivi fenomen javlja se u mnogim operacijama mašinske obrade uključujući struganje, glodanje, bušenje itd. Faktori koji uzrokuju pojavu vibracija alata povezani su sa samom mašinom, načinom stezanja alata, dužinom i prečnikom držača alata i odabranim režimima rezanja. Jedan od načina da se izbegne problem pojave vibracija tokom procesa obrade struganjem jeste promena dužine stezanja držača u nosač alata. U ovom radu cilj je bio ispitati uticaj prepusta na statičko i dinamičko ponašanje držača alata za struganje PTGNL 2020K 16 kao i poređenje dobijenih računarskih i teorijskih rezultata.

Ključne reči: obrada struganjem, držač alata, vibracije, modalna analiza, dinamika mašina alatki

UVOD

Moderna mašinska industrija pretežno je fokusirana na postizanje visokog kvaliteta obrade, visoke tačnosti radnih predmeta, visoke produktivnosti i ekonomičnosti. Pri obradi struganjem česta je pojava vibracija što dovodi do opadanja kvaliteta i tačnosti obrađene površine, oštećenja reznog alata i iritirajuće buke. Pod određenim opterećenjem alata, amplituda vibracija kontinuirano raste, što dovodi do pojave samopobudnih vibracija. Praksa za izbegavanje samopobudnih vibracija svodi se na upotrebu optimalnih režima obrade kao i dužinu prepusta držača alata pri struganju [1].

Pojava vibracija kod alata ispitivana je i analizirana u velikom broju naučnih istraživanja. Detektovanje samopobudnih vibracija u procesu obrade struganjem uz varijacije režima obrade, predstavili su Yao, Mei i Chen [2]. Kako bi se izbegla pojava samopobudnih vibracija za njihovo prepoznavanje korišćeni su alati talasne transformacije (Wavelet transformation), koja omogućava prikaz prikupljenih informacija u vremenskom i frekventnom domenu, kao i alat SVM (Support Vector Machine) koji se koristi za prepoznavanje stabilnog, prelaznog ili nestabilnog perioda kada se pojavljuju samopobudne vibracije.

Chiou i saradnici [3], predstavili su novi dinamički model procesa rezanja kako bi se istražio mehanizam pojave samopobudnih

vibracija koje se javljaju uporedo sa habanjem na leđnoj površini alata. Model prikazuje uticaj sile rezanja na pojavu habanja alata. Analiza Laplasovog domena pruža analitičko rešenje za granice stabilnosti u pogledu glavnih karakteristika mašine i režima rezanja. Izvedeni su ekperimenti pri različitim režimima rezanja da bi se identifikovali parametri uticajni na pojavu vibracija i da bi se verifikovale granice analitičke stabilnosti.

RAČUNARSKA ANALIZA DRŽAČA ALATA

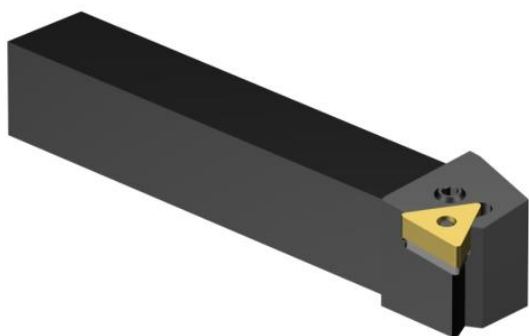
Za računarsku analizu korišćen je model držača alata oznake PTGNL 2020K 16, sa kvadratnim poprečnim presekom dimenzija 20x20 mm i dužine 125 mm. Materijal držača alata je čelik.

Tabela 1. Karakteristike držača i alata

	Materijal	Gustina [kg/m ³]	Modul elastičnosti [N/m ²]
Držač alata	legirani čelik	7850	2,09x10 ¹¹
Rezna pločica	volfram karbid	15800	5,5x10 ¹¹

Geometrijski model držača alata

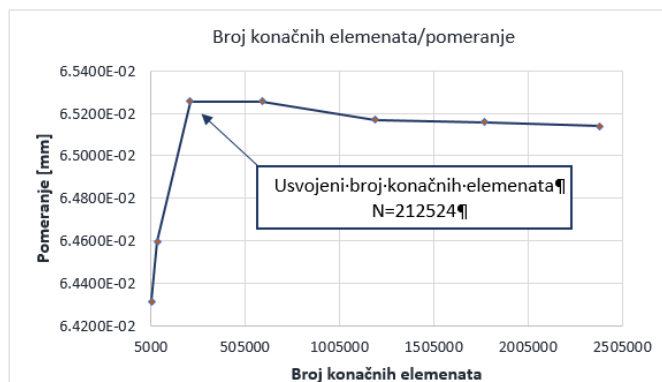
Na slici 1 prikazan je CAD model držača alata sa umetnutom reznom pločicom. Prethodno pomenuti kvadratni poprečni presek drške alata, kasnije će imati uticaj na teorijsku analizu pomeranja vrha reznog alata.



Slika 1. Model držača alata PTGNL 2020K 16

Konvergencija mreže konačnih elemenata

Broj konačnih elemenata koji treba izabrati za diskretizaciju modela povezan sa željenom tačnošću. Iako povećanje broja konačnih elemenata u opštem slučaju znači i dobijanje tačnijih rezultata, za određene slučajeve povećanje broja konačnih elemenata neće dati bolji rezultat. U ovom slučaju broj konačnih elemenata određen je pomoću konvergencije mreže. Konvergencija mreže konačnih elemenata je sprovedena da bi se dobio odgovarajući broj konačnih elemenata, čijim povećanjem bi uticaj na tačnost rezultata bila zanemarljivo mala. Broj konačnih elemenata se postepeno povećavao i na određenoj granici je utvrđeno se ustalio, kao što je prikazano na slici 2.



Slika 2. Konvergencija mreže konačnih elemenata za razmatrani držač alata

Statička analiza

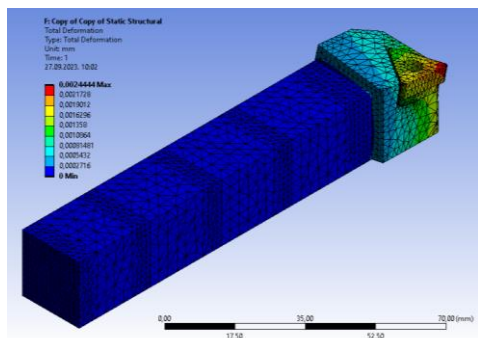
Statička analiza je izvedena korišćenjem softvera za primenu metode konačnih elemenata kako bi se dobile vrednosti pomeranja vrha alata za različite vrednosti prepusta. U ovom istraživanju korišćeni su konačni elementi tipa 10 node Solid 187 za diskretizaciju i Conta 174 za definisanje kontakta. Imajući u vidu da se držač alata ponaša kao konzolna greda, svi stepeni slobode su oduzeti uklještenjem za različite dužine prepusta. Za analizu pomeranja vrha alata korišćene su četiri različite vrednosti prepusta (25 mm, 50 mm, 75 mm i 100 mm). Prepust nije smanjivan ispod 25 mm jer praktično nije moguće izvesti operaciju struganja na manjem

prepustu. Opterećenje u obliku sile iznosilo je 500 N, zadata je na poziciji površine reznog alata vertikalno nadole. Statička analiza je izvršena za različite pozicije prepusta posebno i zabeležena su odgovarajuće maksimalne vrednosti pomeranja vrha alata.

U tabeli 2 prikazane su različite dužine prepusta i vrednosti pomeranja vrha alata, za svaki od njih. Iz prikazanih rezultata može se videti da pomeranje vrha alata opada kada se dužina prepusta smanji. Pomeranje vrha alata je minimalno kada je prepust držača alata dužine 25 mm kao što je prikazano na slici 3.

Tabela 2. Vrednosti pomeranja držača alata za odgovarajuće vrednosti prepusta

Redni broj	Vrednost prepusta [mm]	Pomeranje [mm]
1	25	0,00244
2	50	0,01002
3	75	0,02878
4	100	0,06459



Slika 3. Pomeranje pri vrednosti prepusta 25 mm

Modalna analiza

Modalna analiza predstavlja proučavanje dinamičkih svojstava posmatranog sistema u frekvencijskom domenu. Primenom modalne analize u odgovarajućem softveru na bazi metode konačnih elemenata omogućeno je da se različiti sistemi testiraju, optimizuju i validiraju [4] [5]. Široko je primenjena u automobilske industriji, vazduhoplovstvu, građevini, mašinstvu, čak i u industriji izrade muzičkih instrumenata, itd. U ovom radu izvedena je modalna analiza i maksimalna frekvencija dobijena pri vrednosti prepusta od

25 mm iznosila je 48900 Hz, kao što je prikazano vrednostima u tabeli 3 [1].

Tabela 3. Modalna analiza za vrednosti prepusta 25 mm

Redni broj	Frekvencija [Hz]
1	27
2	73
3	6169
4	10915
5	15082

Teoretska analiza

Kako bi prethodno dobijeni rezultati bili verifikovani, za vrednost prepusta držača alata od 25 mm, izvedena je provera korišćenjem sledeće matematičke formule:

$$\varphi = \frac{Fl^3}{3EI} = \frac{12Fl^3}{Ea^4} \quad (1)$$

gde oznaka φ predstavlja pomeranje (mm), F predstavlja silu opterećenja držača alata i iznosi 500 N, E predstavlja Jungov modul elastičnosti (N/mm^2), I moment inercije (mm^4) i l predstavlja dužinu prepusta od 25 mm za konkretni slučaj. Moment inercije računa se po sledećoj formuli, jer se radi o kvadratnom poprečnom preseku držala alata:

$$I = \frac{a^4}{12} = \frac{0,02^4}{12} = 13333,3 \text{ mm}^4 \quad (2)$$

gde veličina a predstavlja dužinu stranice kvadratnog poprečnog preseka držača alata, kada su sve promenljive poznate, može se izračunati i teoretska vrednost pomeranja φ :

$$\varphi = \frac{12 \times 500 \times 0,025^3}{2100 \times 0,02^4} = 0,0028 \text{ mm} \quad (3)$$

nakon dobijene teorijske vrednosti pomeranja izračunata je vrednost greške eksperimenta po sledećoj formuli:

$$\Delta_{ukupno} = \left| \frac{\Delta_1 - \Delta_2}{\Delta_1} \times 100\% \right| \quad (4)$$

$$\Delta_{ukupno} = \left| \frac{0,00244 - 0,0028}{0,00244} \times 100\% \right|$$

$$\Delta_{ukupno} = 14,75\%$$

Δ_{ukupno} predstavlja ukupnu grešku eksperimenta, a Δ_1 i Δ_2 računarsku i teorijsku vrednost pomeranja vrha alata. Iz dobijenih rezultata može se zaključiti da je su eksperimentalna i teoretska vrednost pomeranja veoma bliske, što govori da je i greška eksperimenta minimalna.

ZAKLJUČAK

Sumirajući prikazano istraživanje u ovom radu, može se konstatovati da je predstavljen matematički model, na bazi metode konačnih elemenata, za predviđanje statičkog i dinamičkog ponašanja držača alata. Prednost ovakvih modela je mogućnost predviđanja ponašanja držača alata pri eksploataciji, u fazi projektovanja. Odziv je pokazao da povećanje dužine prepusta držača alata povećava i vrednost pomeranja vrha reznog alata. Modalnom analizom je pokazano da prva sopstvena frekvencija iznosi 27 Hz, što odgovara 1620 o/min. Pri obradi sa ovim alatom tu vrednost broja obrtaja treba izbegavati zbog postojanja mogućnosti pojave samopobudnih vibracija. Sledeća vrednost 73 Hz prelazi tehničke mogućnosti mašine alatke. Takođe, razlika između simuliranih i teorijskih rezultata je manja od 20%, što potvrđuje adekvatnost razvijenog modela.

ZAHVALNOST

Ovo istraživanje je podržano od strane Ministarstva prosvete, nauke i tehnološkog razvoja kroz projekat broj 451-03-68/2022-14/200156 „Inovativna naučna i umetnička istraživanja iz domena delatnosti FTN-a“.

LITERATURA

- [1] Sam Paul, P., Lawrence, G., Yadav, R.K., Mohankrishnan, N.V., Nair, N., Vasanth, X.A. Analysis of dynamic characteristics of boring tool holder, *International Conference on Advances in Manufacturing and Materials Engineering, AMME 2014*, pp. 2283-2292.
- [2] Yao, Z., Mei, D., Chen, Z. On-line chatter detection and identification based on wavelet and support vector machine, *Journal of Materials Processing Technology* (2010), pp. 713-719.
- [3] Chiou, Y. S., Chung, E. S., Liang, S. Y. Analysis of tool wear effect on chatter stability in turning, *International Journal of Mechanical Sciences* (1995), 37(4), pp. 391-404.
- [4] Knežev, M., Živković, A., Mladenović, C., Marinković, D., Ilić, V., Moravec, M.: Finite element and experimental modal analysis of high speed spindle, *16th International Conference on Accomplits in Mechanical and Industrial Engineering Demi 2023, (2023)*, pp. 60-63.
- [5] Knežev, M., Živković, A., Marinković, D., Mladenović, C., Calin, A., Ilić, V.: Modal analysis of motorized spindle using finite element method, *Journal of Production Engineering*, (2023), 26(1), pp. 9-12.

ANALYSIS OF THE DYNAMIC CHARACTERISTICS OF THE TOOL HOLDER FOR TURNING PROCESS

Abstract: *Machining is a complex process in which many different factors affect the accuracy and quality of processing. The occurrence of tool vibrations is one of the most influential parameters that negatively affects the life of the cutting tool, the quality of the processed parts and the accuracy of processing. This distinctive phenomenon occurs in many machining operations including turning, milling, drilling, etc. The factors that cause tool vibrations are related to the machine itself, the way the tool is clamped, the length and diameter of the tool holder and the selected cutting modes. One way to avoid the problem of vibrations during the turning process is to change the clamping length of the holder in the tool holder. In this work, the aim was to examine the influence of the overhang on the static and dynamic behavior of the turning tool holder PTGNL 2020K 16, as well as the comparison of the obtained computer and theoretical results.*

Keywords: *turning, tool holder, vibrations, modal analysis, dynamics of machine tools.*



Society of Production
Engineering

SPMS 2023

39. Savetovanje proizvodnog mašinstva Srbije

ICPES 2023

39th International Conference on Production Engineering of
Serbia



Faculty of Technical
Sciences
University of Novi Sad

Novi Sad, Serbia, 26. – 27. October 2023

THE INFLUENCE OF TRAVERSE SPEED ON THE APPEARANCE OF INCOMPLETE CUT

Jelena Baralić^{1,*}, Bogdan Nedić², Anđelija MITROVIĆ¹

¹Faculty of Technical Sciences, Čačak, Serbia

²Faculty of Engineering, Kragujevac, Serbia

*Corresponding author: jelena.baralic@ftn.kg.ac.rs

Abstract: Abrasive water jet machining is an universal and effective cutting method that uses a high-pressure water jet mixed with abrasive particles to cut various materials. In some cases, there may be incomplete cuts and increased roughness values of the machined surface. In some cases, an incomplete cut and increased values of the roughness of the machined surface may occur. Traverse speed is a parameter that has a significant impact on the occurrence of incomplete material cutting. In this work, the influence of cutting speed on the occurrence of incomplete tearing during cutting of material C45 (Č 4732) was investigated. The samples were cut at different traverse speeds, from 100 mm/min to 280 mm/min. For each machined surface, the obtained slices were analyzed. At traverse speeds of up to 200 mm/min, complete cut was achieved. When cutting at higher speeds, an incomplete cut appeared. On the surfaces where the material was not completely cut, the uncut triangle, i.e. its height and angles, was measured. Based on the samples, it was concluded that with the increase of traverse speed, the height of the uncut triangle increases, while the angle at the top decreases.

Keywords: Abrasive water jet, traverse speed, uncomplete cut, uncut triangle

1. INTRODUCTION

Abrasive water jet machining is one of the newer unconventional methods, which has recently been increasingly used in the industry for cutting metal materials such as aluminum, bronze, steel, nickel-based alloys and titanium, as well as for cutting brittle materials such as glass, stone and ceramics. It is most often used for contour cutting of sheet materials. In addition to this basic purpose, the abrasive water jet is increasingly used for polishing, cleaning and drilling. It is characteristic of this

processing that there is no increase in temperature in the cutting zone, complex contours can be easily made and there is no appearance of residual stresses in the cutting zone. Cutting with an abrasive water jet is based on the process of erosion as the basic machining mechanism. The removal of workpiece material is a continuous process that begins with the removal of a small volume of workpiece material due to the impact of a single abrasive particle. The number of abrasive particles that hit the workpiece material in one second is several tens of thousands [1].

Modern installations for the abrasive water jet machining work with water pressure over 5000 bar, where the water jet reaches speed up to 1400 m/s. The water that enters the cutting head (nozzle) is usually under a pressure of 1300 to 5000 bar and passes through a diamond nozzle. The diameter of the diamond nozzle hole, ranges from 0.18 to 0.4 mm. This jet further reaches the mixing chamber, where, due to the Venturi effect, a vacuum is created. This vacuum is sufficient to suck a certain amount of abrasive. In addition to the abrasive, a certain amount of air is also sucked in. The water jet accelerates the abrasive particles and together with them passes through the focusing tube. In the focusing tube, the kinetic energy is transferred from the water jet to the abrasive particles. Schematic of abrasive water jet cutting head is shown in Figure 1.

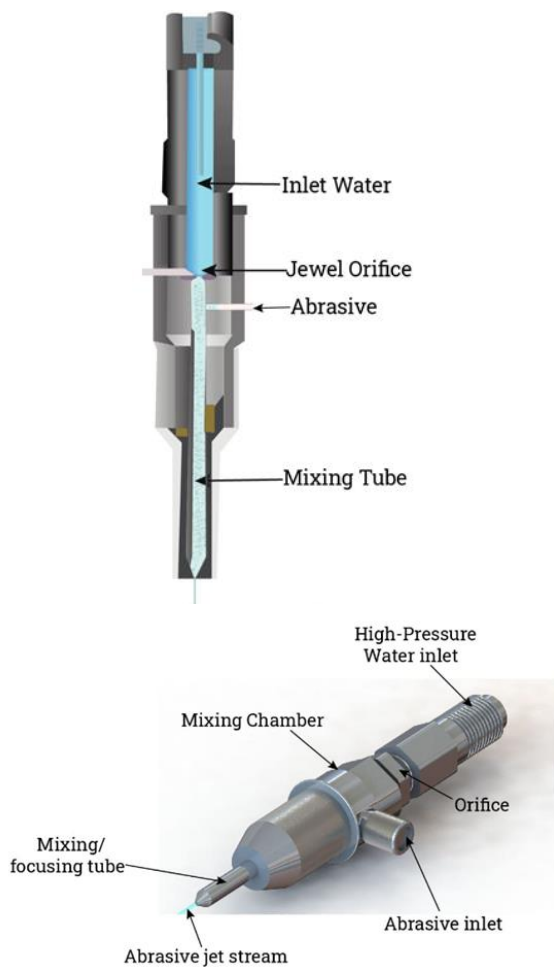


Figure 1. Schematic of abrasive water jet cutting head [2]

2. APPEARANCE OF INCOMPLETELY CUT SURFACE

Hashish [2] was the first to systematically investigate macroscopic phenomena during abrasive water jet processing, as well as the phenomenon of incomplete cutting. Based on quick photographs in transparent materials (Plexiglass, Lexan), he presented the abrasive water jet machining process in Figure 2.

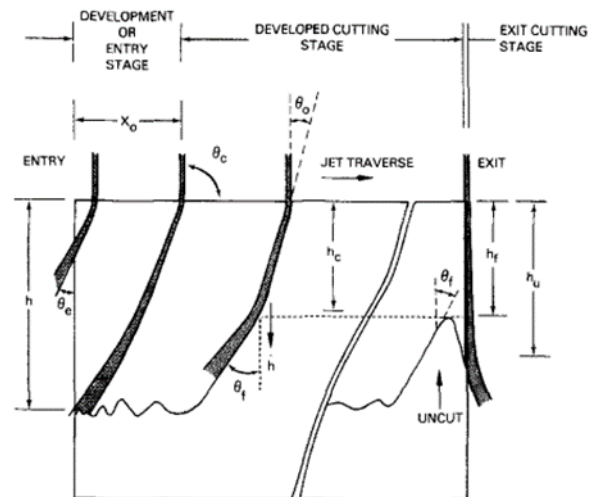


Figure 2. The abrasive water jet machining process [3]

The picture shows three characteristic areas-phases in the cutting process: the initial cutting phase, the continuous cutting phase and the cutting phase at the exit of the abrasive water jet from the workpiece. The first phase - the initial phase of cutting occurs in cases where the depth of cut is less than the maximum possible depth of cut, that is, when the thickness of the workpiece is less than the maximum depth of cut. When the maximum cutting depth is reached, that is, when the thickness of the workpiece is greater than the maximum cutting depth, the phase of continuous cutting begins. This phase is presented as a cyclic material removal phase. When the cutting phase at the exit occurs, the abrasive water jet is deflected from the treated surface and deflects to the opposite side, which leads to the appearance of an uncut triangle, which is characteristic of incomplete cutting of the material. In further research, Hashish [4] divided the surface treated with an abrasive water jet into two areas, the fine machining

zone or cutting wear zone and the rough machining zone or deformation wear zone. Cutting wear zone reaches the depth h_c . When this depth is reached, the formation of characteristic steps and jet lagging occurs, Figure 3.

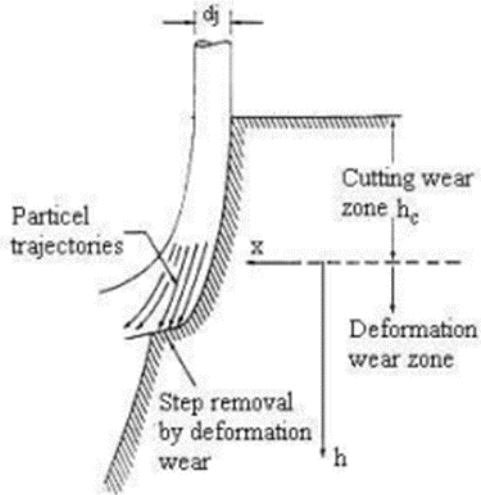


Figure 3. The cutting wear and deformation wear zones [4]

Studying the results of cutting polycrystalline ceramics with AWJ, Zeng and Kim [5] proposed a two stage impact zone model. Unlike Hashish's two-dimensional model [4], Zeng and Kim determined that in the two stage model, the entire cutting process is related to the angle at which the abrasive particles strike the surface of the workpiece. Ohlsson et al. [6] measured cyclic changes in cutting forces acting on the cutting front in both vertical and horizontal directions. Analyzing the results, he came to similar conclusions as Zeng and Kim [5].

2.1 Effect of traverse speed on depth of cut

The optimal traverse speed for abrasive water jet machining depends on several parameters, including the material type and thickness, desired surface roughness, kerf requirements, and the specific abrasive water jet system being used. In practice, the optimal traverse speed is most often determined experimentally or adopted from the speed calculator that comes with the equipment (it was made based on experiments). Generally,

higher traverse width results in shallower depths of cut, picture 4 [7].

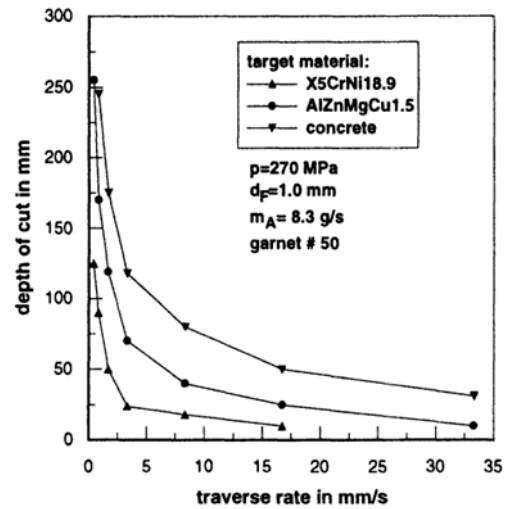


Figure 4. Influence of traverse speed on depth of cut [7]

3. EXPERIMENTAL PROCEDURE

Experimental investigations were performed on C45 steel, which chemical composition is given in Table 1. Tensile strength of C45 is 650 N/mm².

Table 1. Material composition C45 expressed as a percentage (%)

	C	Si	S	P
[%]	0.37089	0.23707	0.00179	0.00732
	Mn	Ni	Cr	Mo
[%]	0.56557	0.06974	0.16295	0.03965

During the experiment, the traverse speed was varied, while the operating pressure was constant and its value was 4130 bar. The abrasive type was garnet mesh size 80, the abrasive mass flow rate was 350 g/min and the distance of the cutting head from the workpiece x_0 was 3 mm. In the experiment, 10 samples, 15 mm thick were cut with different traverse speeds. Also, two samples of 50 mm thick material were cut with traverse speeds of 20 mm/min and 40 mm/min. The first five samples were not cut through, because there was no incomplete cut. The next five samples were cut all the way through, but due to the appearance of an incomplete cut, the surfaces were not completely separated. After cutting with abrasive water jet, samples were cut

through on Wire EDM machine. Figure 5. shows the machined surfaces of the samples.

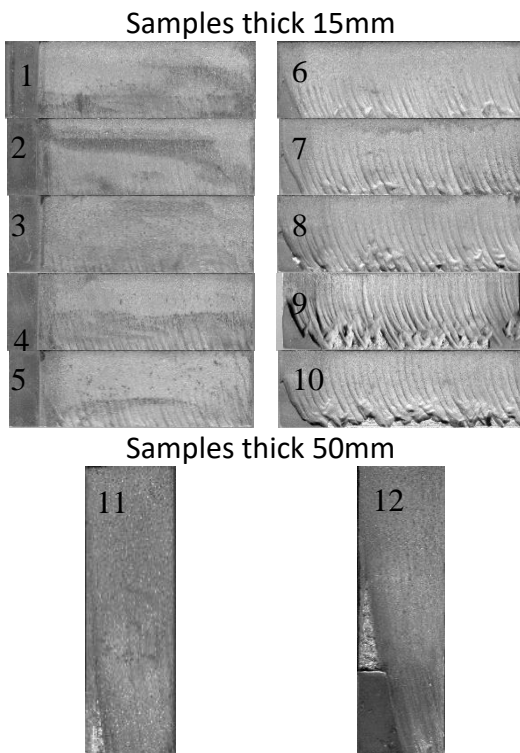


Figure 5. The appearance of the machined surfaces

Samples 11 and 12 were test samples, to determine the existence of an uncut triangle and whether there is an influence of traverse speed. By analyzing samples from 1 to 10, it was concluded that the uncut triangle is clearly visible on samples from 6 to 10. The geometric parameters shown in Figure 6 were measured for these samples.

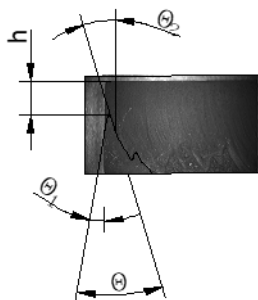


Figure 6. Geometric parameters of an uncut triangle

Measurements of uncomplete cut, that is uncut triangle, was realized an optical microscope with an accuracy of 0.01 mm. The results of measurements are given in Table 2.

Table 2. Values of geometric parameters

Sample no.	Thickness [mm]	Vc [mm/min]	θ	θ_1	θ_2	h [mm]
6	15	200	58.5	35.44	23.06	7.69
7	15	220	54.24	27.84	26.41	6.83
8	15	240	53.14	32.48	20.67	6.52
9	15	260	44.25	24.05	20.2	5.16
10	15	280	27.23	9.96	17.27	4.22
11	50	20	13.95	5.94	8.00	38.33
12	50	40	11.19	3.9	7.25	18.07

Based on the measured values, diagrams of the dependence of the characteristic angles of the uncut triangle and the minimum depth to which the abrasive water jet reaches (above the top of the uncut triangle) from the traverse speed were drawn, Figure 7 and Figure 8.

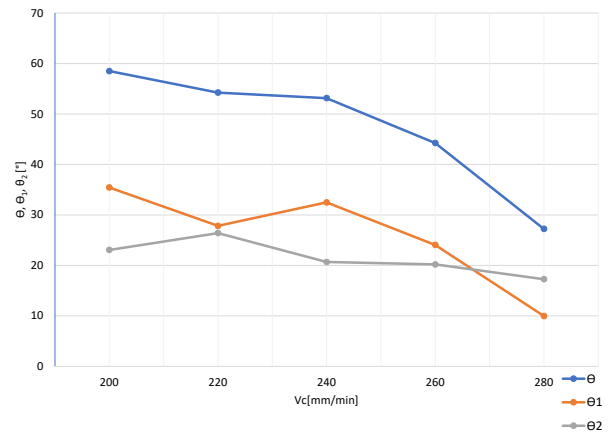


Figure 7. Influence of traverse speed on uncut triangle angles

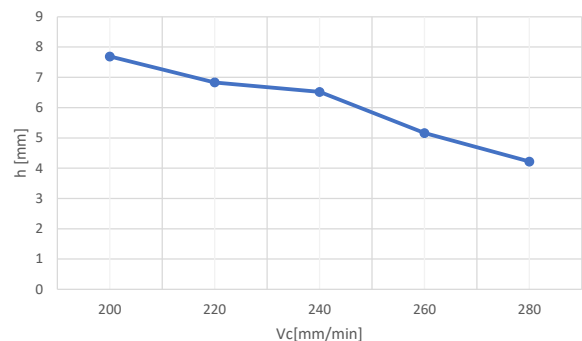


Figure 8. Influence of traverse speed on minimum depth of cut

4. CONCLUSION

The basic goal in every production, today, is to produce the largest possible quantity of products, of the appropriate quality, in the

shortest possible time. When processing with an abrasive water jet, this means that the material should be cut with the highest possible traverse speed, and the desired processing quality should be achieved. Abrasive water jet processing is often used for cutting preparations from plate materials, for further machining. In this case, the quality of the machined surface is not of crucial importance for the choice of traverse speed, but the cutting is done at maximum speed. When cutting material in this way, very often there is an incomplete cut and the appearance of an uncut triangle. Based on the conducted experimental research, it can be concluded that with the increase of traverse speed, there is a decrease in the value of the angle at the top of uncut triangle as well as a decrease in the minimum depth to which the abrasive water jet reaches - h. This means that the uncut triangle has an increasing height and the angle at the top is sharper. Also, with the increase of traverse speed, the incomplete cut occurs along the entire surface of the sample. The uncut triangles that appear along the machined surface have larger surface as the traverse speed increases. On the basis of these studies, the traverse speed at which complete separation of the material occurs and what is the critical value of traverse speed, at which the occurrence of incomplete cut begins can be determined. Based on the surfaces of the uncut triangles, it is possible to approximately determine the required force for separating the workpiece from the rest of the material.

ACKNOWLEDGEMENT

This study was supported by the Ministry of Science, Technological Development and Innovation of the Republic of Serbia, and these results are parts of the Grant No. 451-03-47/2023-01/200132 with University of Kragujevac - Faculty of Technical Sciences Čačak.

REFERENCES

- [1] M. Hashish: A modelling study of metal cutting with abrasive waterjets, *J. Eng. Mater. Technol.*, Vol. 106, pp. 88-100, 1984.
- [2] Water Jet Cutting: What Is It? How Does It Work? Types, Uses, available at: <https://www.iqsdirectory.com/articles/water-jet-cutting.html>, accessed: 25.08.2023.
- [3] M. Hashish: Visualization of the abrasive waterjet cutting process, *Expl. Mech.*, pp.159-169, 1988.
- [4] M. Hashish: On the modelling of abrasive-waterjet cutting, *Proceedings of 7th International Symposium on Jet Cutting Technology*, 1984, Ottawa, Canada, Bedford, BHR Group, pp. 249-265.
- [5] J. Zeng, T.J.Kim: Development of an abrasive waterjet kerf cutting model for brittle materials, *Proceedings of 11th International Conference on Jet Cutting Technology*, 1992, St Andrews, Scotland, Kluwer Academic Publishers, pp. 483-501.
- [6] L.Ohlsson, J. Powell, C. Magnusson: Mechanisms of striation formation in abrasive waterjet cutting, *Proceedings 12th International Conference on Jet Cutting Technology*, 1994, Rouen France, Mechanical Engineering Publication Limited, pp. 151-164.
- [7] A. Mombert, R. Kovacevic: *Principles of abrasive waterjet machining*, Springer, Berlin, 1998.
- [8] M. Hashish: Characteristics of surfaces machined with abrasive waterjets, *J. Eng. Mater. Technol. Trans. ASME*, Vol. 113, No. 3, pp.336-354, 1991.
- [9] J. Baralić, B. Nedić, P. Janković: The traverse speed influence on surface roughness in abrasive waterjet cutting applications, *Proceedings of the 12th International Conference on Tribology, SERBIATRIB*, 11-13.05.2011, Kragujevac, Serbia, pp. 349-353.

SPMS/ICPES 2023

**39TH INTERNATIONAL CONFERENCE ON
PRODUCTION ENGINEERING OF SERBIA**

**SESSION 5:
ADDITIVE MANUFACTURING TECHNOLOGIES**

Novi Sad, 26 – 27 October 2023



Society of Production
Engineering

SPMS 2023

39. Savetovanje proizvodnog mašinstva Srbije

ICPES 2023

39th International Conference on Production Engineering of
Serbia



Faculty of Technical
Sciences
University of Novi Sad

Novi Sad, Serbia, 26. – 27. October 2023

INFLUENCE OF INJECTION MOLDING PROCESS PARAMETERS ON THE MECHANICAL PROPERTIES OF POLYPROPYLENE AND POLYETHYLENE PARTS

Ljiljana STEFANOVIĆ^{1*}, Dejan MOVRIN¹, Mladomir MILUTINOVIĆ¹, Mihajlo POPOVIĆ²,
Miloš PJEVIĆ²

¹ University of Novi Sad, Faculty of Technical Sciences,
Department of Production Engineering, Serbia,

² University of Belgrade, Faculty of Mechanical Engineering,
Department of Production Engineering, Serbia,

*Corresponding author: ljiljanastefanovic@uns.ac.rs

Abstract: Polypropylene (PP) and high-density polyethylene (HDPE) are the most common polymers in modern industrial plastic part production. Both materials can be easily shaped through injection molding, which is one of the most widespread processing methods for polymer materials. When manufacturing parts from PP and HDPE, it is necessary to achieve the required mechanical characteristics that depend on processing parameters (melt temperature, tool temperature, cooling time, etc.). This paper presents research on the impact of tool temperature on the tensile strength of injection-molded test specimens made from PP and HDPE. Since both materials contain amorphous and crystalline phases, changes in the ratio of phases are possible depending on the tool temperature, which leads to mechanical properties (tensile strength) changes. In the experimental assessment of tensile strength for polypropylene (PP) and high-density polyethylene (HDPE) specimens, conducted at varying tool temperatures (20°C, 50°C, and 80°C), notable disparities in tensile strength values were observed. These variations were attributed to alterations in the crystalline phase content within the materials, instigated by disparate cooling rates resulting from utilizing distinct tool temperatures.

Keywords: Polypropylene, high-density polyethylene, injection molding, mechanical characteristics, tensile testing, tensile strength

1. INTRODUCTION

Polymers are categorized as engineering materials due to their versatile utility alongside other materials, such as metals, ceramics, glass,

and rubber. Their advantageous properties and processing capabilities have facilitated their application across various industrial sectors. Polypropylene and high-density polyethylene are among the most used materials for plastic part

production through injection molding. Polypropylene, characterized by its low density and excellent high-temperature stability, enables various applications in diverse temperature conditions. Although it shares some properties with polyethylene, polypropylene exhibits greater hardness and strength, making it relatively rigid compared to polyethylene, which offers a higher degree of flexibility and elasticity [1].

In the conventional injection molding process, the polymer material is first melted and then injected into a mold under pressure, where the molded part solidifies through cooling. Subsequently, the mold is opened, and the finished part is ejected. In the context of injection molding, it is crucial to accurately define and control process parameters to ensure the production of workpieces with satisfactory mechanical characteristics. Influential parameters, such as melt temperature, tool temperature, and cooling time, must be carefully specified and monitored throughout the process [2, 3].

A frequent area of interest for numerous researchers is the analysis of the mechanical characteristics of parts obtained through injection molding using metallic tools. Rashid and colleagues, in their study [4], demonstrated that the high thermal conductivity of aluminum reduces cooling time by 30% compared to steel tools. It is well-known that accelerated cooling may lead to increased part shrinkage; however, research findings [4, 5] indicate relatively similar mechanical properties for parts molded using aluminum tools when compared to those molded in steel tools.

The crystalline structure plays a significant role in the mechanical properties of parts, in the way to enhance its tensile strength [6]. In the study by [7], the influence of heating rate on crystallinity in PP was analyzed, and it was concluded that a slower heating rate improves crystalline perfection through the reorganization of the crystal structure. Through ANOVA analysis

in [8], it was determined that mold temperature, along with injection pressure, represents the most influential parameters on the mechanical characteristics of parts after injection molding. Authors in [9] demonstrated that a higher melting temperature has the potential to enhance the crystallization rate and impact strength of HDPE parts but concurrently reduces tensile and flexural strength. Conversely, in research [10], it was observed that an increase in mold temperature augments tensile and flexural resistance while decreasing impact strength.

In this study, samples from polypropylene and high-density polyethylene were produced by injection molding, aiming to analyze the influence of varying tool temperatures during the injection molding process on the mechanical properties of the materials, specifically the tensile strength.

2. EXPERIMENTAL PROCEDURE

The research presented in this paper encompasses the fabrication of test specimens from PP and HDPE, following the ISO 527/2-5A standard (Figure 1), using an injection molding machine. The study aims to determine the influence of tool temperature on the tensile properties of the materials [11].

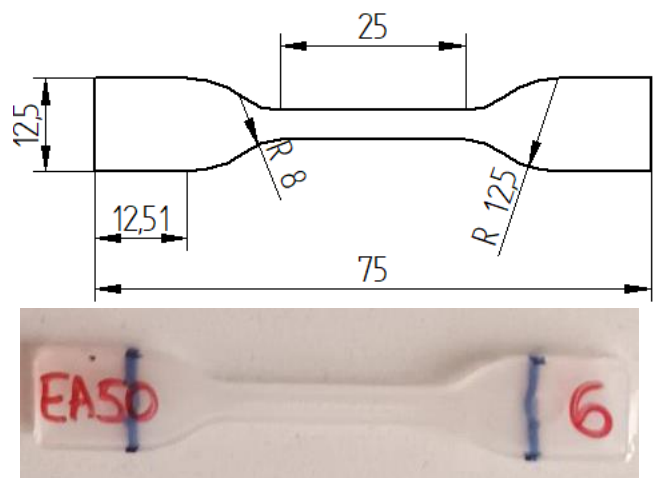


Figure 1. Test specimen according to ISO 527/2-5A standard [11] and injection molded specimen

For experimental research, an Engel Victory 50 injection molding machine was used. The injection molding process was carried out using a tool with two aluminum inserts situated in one half of the mold, while the other half of the mold remained flat (Figure 2).

The parameters used in the injection molding process are presented in Table 1. As indicated in Table 1, the specimens were produced at varying tool temperatures (20, 50, and 80°C), while the remaining parameters were optimized through an iterative process based on recommendations from the literature [12] for the specified materials and wall thickness.

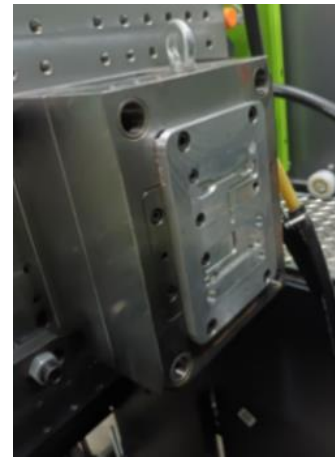


Figure 2. Injection molding tool with aluminum inserts

Table 1. The values of the parameters used in the injection molding process.

	Polypropylene	High-density polyethylene
T_a (tool temperature [°C])	20, 50, 80	20, 50, 80
T_t (melting temperature [°C])	190	230
t_h (cooling time [s])	30	30
p_u (first-stage pressure [bar])	800	1000

2.1 Specimens testing

A total of 18 test specimens were produced through injection molding, with three specimens from each material for every tool temperature. Tensile strength testing was conducted using an INSTRON 34SC-2 tensile testing machine (figure 3).



Throughout the tensile testing, force values were continuously recorded as a function of displacement, along with the tensile strength values for each tested specimen.

3. RESULTS AND DISCUSSION

A graphical representation of the tensile strength testing results for HDPE and PP is provided in Figure 4. The diagrams marked as EA20H, EA50H, and EA80H represent high-density polyethylene, while diagrams marked as EA20, EA50, and EA80 correspond to polypropylene characteristics. The values 20, 50, and 80 refer to the tool temperatures used in sample fabrication.

Figure 3. INSTRON 345C-2 testing machine

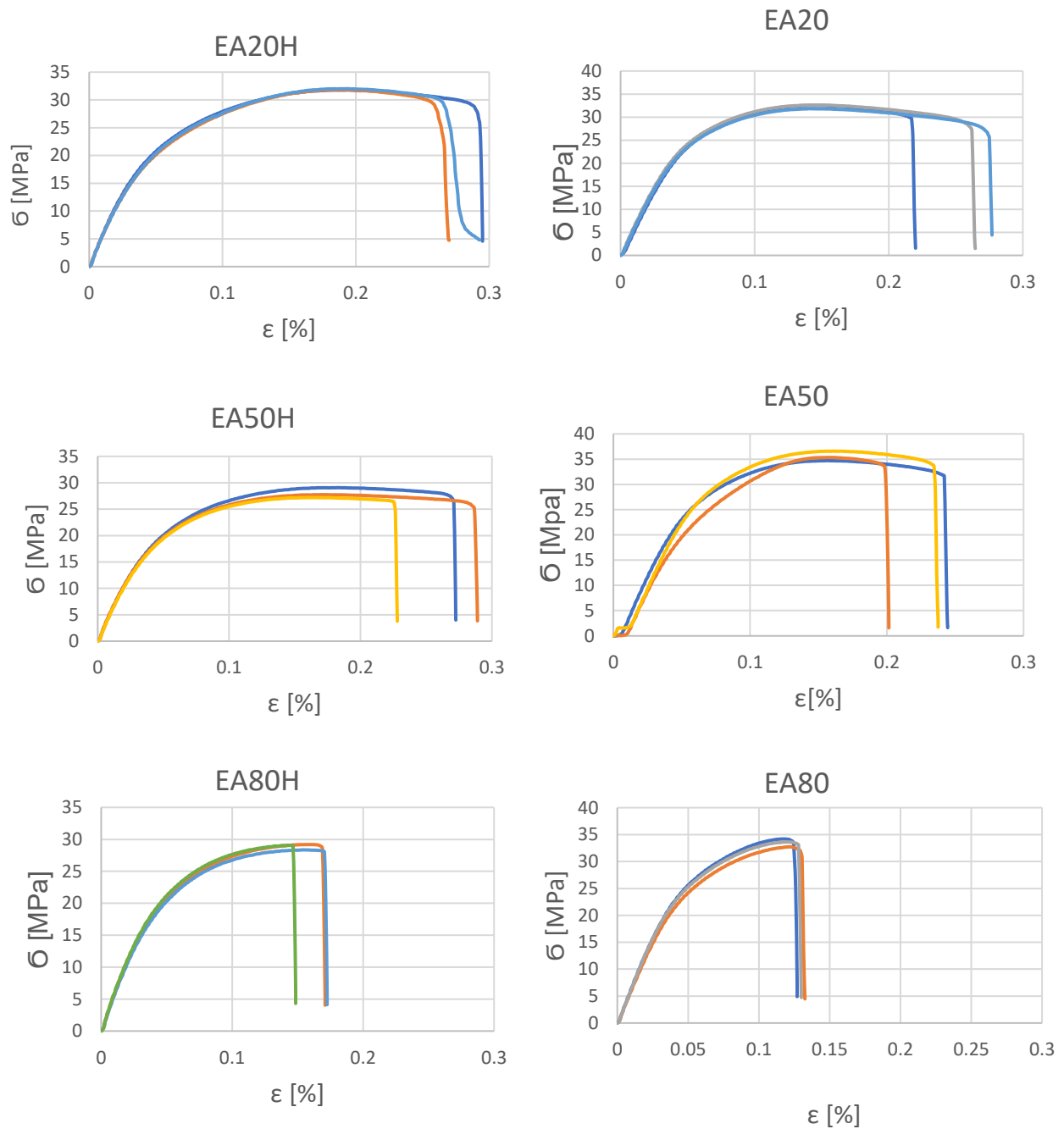


Figure 4. Tensile testing diagrams for HDPE and PP.

Table 2. The average values of tensile strength for HDPE and PP specimens

Specimen	EA20H	EA50H	EA80H	EA20	EA50	EA80
Average values of R_m [MPa]	31,86	28,01	28,88	32,32	35,53	33,51

The average tensile strength (R_m) values of the tested HDPE and PP specimens are presented in Table 2.

The higher tensile strength in polymeric materials is achieved through a higher share of the crystalline region. Crystallization represents the process of transforming the molecular structure of polymers into a specific form. A high degree of crystallization contributes to increased strength, hardness, and rigidity of the material. The degree of crystallization primarily depends on the material's molecular structure and the defined processing parameters. Mold temperature influences crystallization, as high cooling rates and low temperatures reduce material crystallinity [13]. In addition to the degree of crystallinity, the orientation of polymer chains has a significant impact on the tensile properties of materials.

During the testing of HDPE specimens, it was observed that material strength decreases as the tool temperature increases. In contrast, with PP specimens, an initial increase in tensile strength was noted as the tool temperature rose to 50°C, followed by a decrease in strength when the tool temperature reached 80°C (Table 2). This behavior in the specimens results from the formation of different material structures at different tool temperatures, primarily due to changes in crystallinity. Furthermore, the tensile strength value is also affected by residual stresses, which arise due to the varying mobility of molecules during the cooling and melting phases of the material.

Analyzing the tensile stress-strain diagrams (Figure 4), it can be concluded that the variation in tool temperature significantly impacts the achieved elongation at break and tensile strength. Notably, both materials exhibited substantial tensile strength values in accordance with the reference values specified by the manufacturers of the materials used [14, 15].

4. CONCLUSION

The significant utilization of polymeric materials across various industrial sectors arises from their favorable properties, which enable optimal performance under demanding operating conditions. When industrial components are made from polymeric materials, achieving the necessary mechanical characteristics is of paramount importance.

This research shows that the applied parameters during the injection molding process facilitate the production of high-quality workpieces. The variation in mold temperature during injection molding significantly influences the formation of the material's microstructure, thereby directly impacting the mechanical properties of the component. It has been shown that fluctuations in tool temperature affect the tensile strength value, which may be a result of combinations in crystallinity and the size of crystalline as well as residual stresses after injection molding. The materials achieved a notable tensile strength value, exhibiting substantial plastic deformation prior to fracture.

5. REFERENCES

- [1] Čatić I., Johannaber F.: Injekcijsko prešanje polimera i ostalih materijala, Fakultet strojarstva i brodogradnje, Zagreb, 2004.
- [2] Lukić D.: Razvoj sistema za automatizovano projektovanje tehnoloških procesa izrade alata za brizganje plastike - magistarska teza, Fakultet tehničkih nauka, Novi Sad, 2007.
- [3] Kusić D., Hančić A.: Influence of molding conditions on the shrinkage and warpage behavior of standardized test specimens, AIP Conference Proceedings 1779, Graz, Austria, 2016.
- [4] Rashid O., Low K., Pittman J.: Mold cooling in thermoplastics injection molding: Effectiveness and energy efficiency, Journal of Cleander Production, Vol.264, p.264, 2020.

- [5] Ozcelik B., Ozbay A., Demirbas E.: Influence of injection parameters and mold materials on mechanical properties of ABS in plastic injection molding, *International Communications in Heat and Mass Transfer*, Vol.37, No.9, 2010.
- [6] Mendible G., Saleh N., Barry C., Johnston P.: Mechanical properties and crystallinity of polypropylene injection molded in polyjet and aluminium tooling, *Rapid Prototyping Journal*, 28/4, 2022.
- [7] Scawe J.: Measurement of the thermal glass transition of polystyrene in a cooling rate range of more than six decades, *Thermochimica Acta*, Vol.603, p.85, 2015.
- [8] Farotti E., Natalini M.: Injection molding. Influence of process parameters on mechanical properties of polypropylene polymer. A first study, *International Conference on Stress Analysis, AIAS 2017, Italy*.
- [9] Karagoz I., Tuna O.: Effect of melt temperature on product properties of injection-molded high-density polyethylene, *Polymer Bulletin* 78,2021.
- [10] Karagoz I.: An effect of mold surface temperature on final product properties in the injection molding of high-density polyethylene materials, *Polymer Bulletin* 78,2021.
- [11] *Plastics — Determination of tensile properties — Part 2: Test conditions for moulding and extrusion plastics*, BS EN ISO 527-2:1996 BS 2782-3: Method 322: 1994.
- [12] Perošević B.: Kalupi za injekciono presovanje plastomera (termoplasta), *Naučna knjiga*, 1995.
- [13] Vilotić D.: *Mašine za injekciono presovanje*, skripta sa predavanja, Fakultet tehničkih nauka, Novi Sad, 2008.
- [14] <https://www.hipol.rs/wp-content/uploads/2022/10/tds-ma-21.pdf> - 30.6.2023..
- [15] http://www.lookpolymers.com/polymer_Borealis-Borcell-HE1346-High-Density-Polyethylene.php - 30.06.2023.



Society of Production
Engineering

SPMS 2023

39. Savetovanje proizvodnog mašinstva Srbije

ICPES 2023

39th International Conference on Production Engineering of
Serbia



Faculty of Technical
Sciences
University of Novi Sad

Novi Sad, Serbia, 26. – 27. October 2023

IMPACT OF POLYMER TYPES ON APPLICABILITY IN RAPID TOOLING

Miloš PJEVIĆ^{1, *}, Mihajlo POPOVIĆ¹, Mladomir MILUTINOVIĆ², Dejan MOVRIN²,
Ljiljana STEFANOVIĆ²

¹University of Belgrade, Faculty of Mechanical Engineering, Department of Production
Engineering, Serbia, mpjevic@mas.bg.ac.rs, mpopovic@mas.bg.ac.rs

²University of Novi Sad, Faculty of Technical Sciences, Department of Production Engineering,
Serbia, mladomil@uns.ac.rs, movrin@uns.ac.rs, ljiljanastefanovic@uns.ac.rs

*Corresponding author: mpjevic@mas.bg.ac.rs

Abstract: *In the last decade, owing to its accessibility, additive technologies have been occupying an increasingly significant percentage share in the production of new components. Whether it pertains to the creation of prototypes, test or final tools, and even direct manufacturing, additive technologies can be found in all spheres of product development. One of the key advantages of additive technologies is reducing the final cost due to the relatively low cost of implementing said technology. For this reason, it's not surprising that recent research in the field of additive technologies frequently focuses on rapid tooling, specifically on injection molding parts. By reducing the cost of tools, a substantial impact can be made on the final product's cost and, consequently, on market competitiveness. However, the application of additive technologies in the realm of polymer injection molding is not straightforward and presents numerous challenges. Given that this involves creating polymer parts within a tool that is also made of polymer, the task can be exceptionally complex. Physical properties such as material density or the interaction between two polymers can adversely influence the polymer injection molding process within a polymeric insert. This paper will present the influence of two types of polymers (PP and HDPE) on manufacturing (injection molding) parameters and the potential of their application in the rapid tooling.*

Keywords: *Rapid Tooling, Injection Molding, Polymer, 3D Printing, Additive Manufacturing*

1. INTRODUCTION

In addition to well-established machining technologies, including cutting, plastic deformation, unconventional methods, etc., additive manufacturing technologies are gaining increasing use, from product development to mass production.

Additive manufacturing technologies offer several benefits, including:

- **Design Flexibility [1]:** Additive manufacturing allows for complex and intricate designs that would be challenging or impossible to create using traditional manufacturing methods. This flexibility in design can lead to improved product performance and functionality.
- **Reduced Material Waste [2]:** Traditional subtractive manufacturing processes often result in significant material waste, as excess material is cut away. Additive manufacturing builds parts layer by layer, minimizing material wastage and reducing environmental impact.
- **Rapid Prototyping [3]:** Additive technologies enable rapid prototyping, allowing for the quick and cost-effective production of prototypes and iterative design changes. This speeds up the product development cycle.
- **Customization [4]:** Additive manufacturing enables the easy customization of products. This is particularly valuable in industries like healthcare, where personalized medical devices and prosthetics can be created.
- **Complex Geometries [5]:** Additive manufacturing can produce parts with intricate internal structures, such as lattice structures, which can reduce weight while maintaining strength. These structures are difficult to achieve with traditional manufacturing methods.
- **Reduced Tooling Costs [6]:** Unlike traditional manufacturing, which often requires expensive molds, dies, or tooling, additive manufacturing does not rely on these costly components. This can result in

cost savings for low-volume or highly customized production runs.

- **Lightweighting [7]:** Additive manufacturing can optimize part designs for lightweighting, which is essential in industries like aerospace and automotive for improving fuel efficiency and performance.
- **Reduced Lead Times [8]:** The ability to quickly produce parts and components can significantly reduce lead times, which is beneficial for meeting tight production schedules and responding to changing market demands.
- **Complex Assemblies [9]:** Additive manufacturing can consolidate multiple components into a single, more complex part, reducing the need for assembly and fasteners. This simplifies the manufacturing process and can enhance product reliability.
- **Material Variety [10]:** Additive manufacturing can use a wide range of materials, including metals, plastics, ceramics, and composites, allowing for compatibility with diverse applications and industries.

The mentioned advantages not only put additive manufacturing among the leaders when it comes to rapid prototyping but also when it comes to applications for rapid tool manufacturing.

2. RAPID TOOLING

Rapid tooling, as a classification of additive manufacturing technologies, is becoming more prevalent thanks to recent advancements and the accessibility of additive manufacturing technologies. While its primary application used to be in the production of end-effectors for manipulators, recently, it has gained importance in the production of component parts for plastic injection molds.

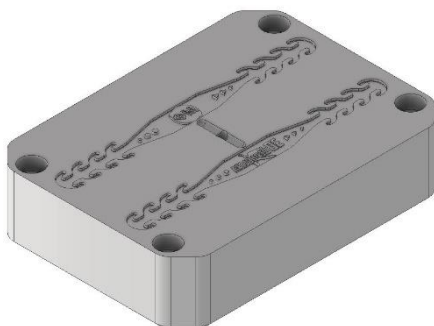
One of the main reasons for this shift is the capability offered by additive manufacturing technologies in the field of creating complex systems of cooling channels. Previous

applications were limited to metallic materials, which could guarantee larger production batches. However, due to its accessibility, recent research has shifted towards creating polymeric tools (mold cavities) for limited production runs, where the emphasis is placed on the speed of tool making.

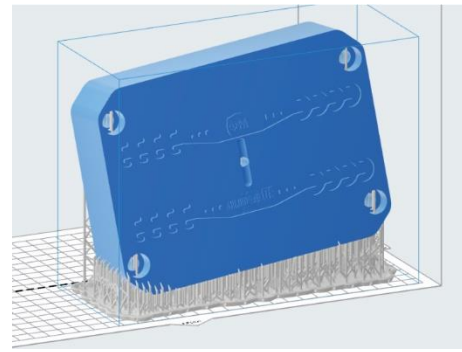
One of the main challenges in the use of polymeric tools obtained through the application of additive manufacturing technologies is the interaction between the polymeric tool and the polymer from which the part is obtained, as well as the temperature resistance of the polymeric tool and its ability to withstand increased pressures. Based on this, this paper presents an experimental investigation into the applicability of PP and HDPE materials in plastic injection molding using a polymeric tool.

3. EXPERIMENTAL SETUP

For initial investigations in this field, a simple flat part was chosen, which does not require a large amount of material and has a short production cycle time. Additionally, one of the requirements is that the part should be functional. Therefore, a respirator mask holder was selected as the test part. The insert with the mold core was produced using SLA technology on a Formlabs device, as shown in Fig. 1 and 2. The material used for the insert is Rigid 4000.

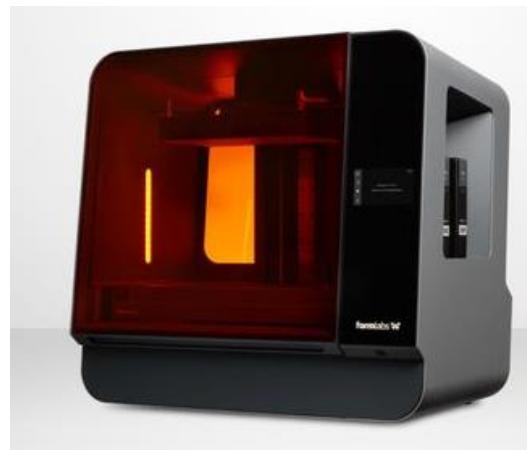


a)



b)

Figure 1. a) CAD model of the mold and b) production preparation [11]



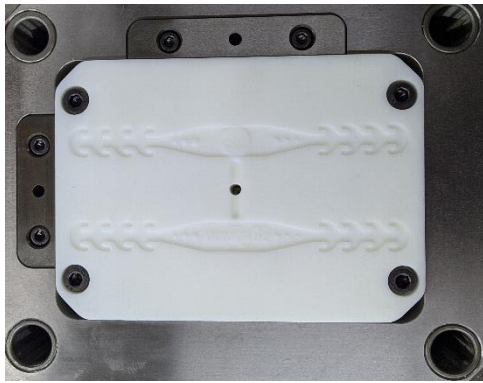
a)



b)

Figure 2. a) 3D printer Form 3L and b) printed part [11]

The tool is designed in such a way that the movable part contains an insert with a mold core made of polymer using additive technologies, while the stationary part of the tool is made of aluminum, forming the flat side of the part (no mold cavities are present), Fig 3. To ensure the shortest possible cycle time and increase the durability of the polymeric tool, cooling channels have been formed through the insert itself, allowing the flow of cooling fluid.



a)

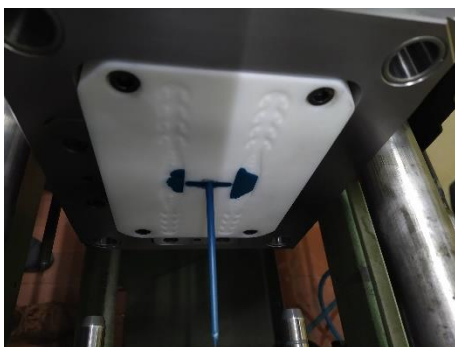


b)

Figure 3. a) Core and b) cavity side of the molding tool [11]

4. RESULTS AND CONCLUSIONS

Initial experiments were conducted using PP material. In order to establish optimal parameters in terms of injection pressure, these initial experiments either resulted in incomplete filling of the mold cavity or plastic flash, Fig 4.



a)



b)

Figure 4. a) Insufficient filling of the mold cavity and b) flashing on the parting surface [11]

However, very quickly, it became possible to produce a part without the visual irregularities that occur during plastic injection molding, Fig 5. As an additional verification, consecutive injection molding over 100 cycles was performed. It was determined that in none of these cycles did any undesirable interaction occur between the tool material and the part, with each produced part meeting the desired quality. Additionally, no damage to the polymeric tool was observed.

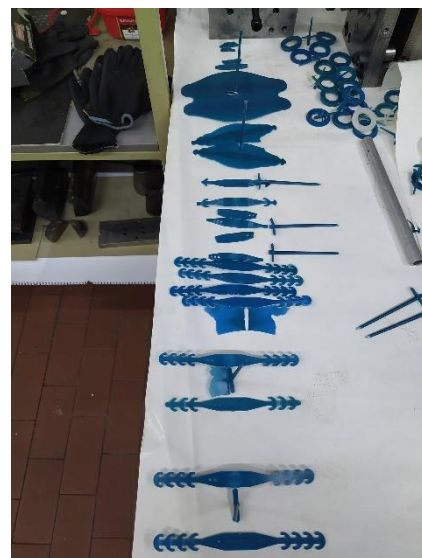
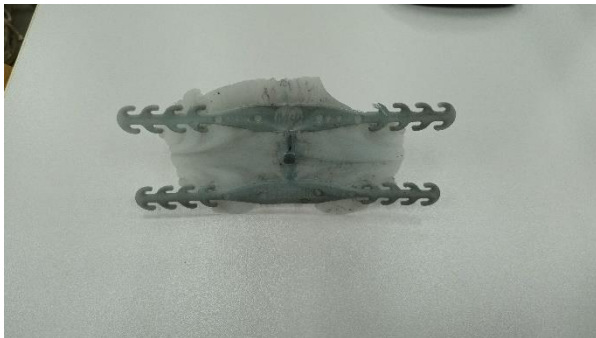


Figure 5. Iterative reporting of obtained parts during the experiment [11]

On the other hand, when using HDPE as the raw material, the issue arose even during the definition of the injection pressure. Regardless of its variation, which was accompanied by a change in melt temperature from 180 to 260°C, it was not possible to achieve complete filling of the mold cavity, Fig 6.



a)



b)

Figure 6. Iterative reporting of obtained parts during the experiment

In an attempt to achieve complete filling of the mold cavity with the raw material while avoiding material flash, a gradual increase in the tool's clamping force was implemented. However, after several iterations, the polymeric insert cracked, Fig 7.

In conclusion, it can be stated that additive manufacturing technologies can be successfully used for the production of component parts for injection molding tools. Although these are polymeric inserts, with the proper choice of raw material, a satisfactory production volume can be achieved, especially for parts with simpler geometries. However, when using materials with physical

and mechanical properties that demand the use of significantly higher-quality materials, the creation of mold cavities in polymeric inserts is not feasible, even for simpler parts.

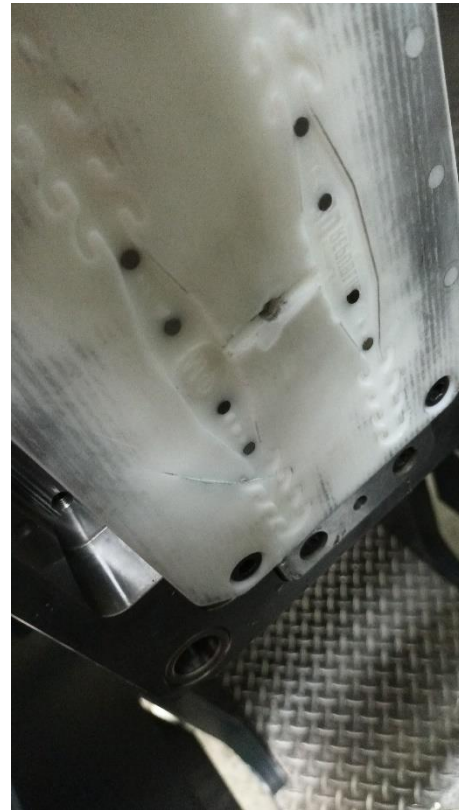


Figure 7. Iterative reporting of obtained parts during the experiment

ACKNOWLEDGEMENT

The results shown here are the result of research supported by the Ministry of Science, Technological Development and Innovation of the RS under Contract 451-03-47/2023-01/200105 dated 02/03/2023.

REFERENCES

- [1] Attaran, M. (2017). The rise of 3-D printing: The advantages of additive manufacturing over traditional manufacturing. *Business Horizons*, 60(5), 677-688.
- [2] Huang, S. H., & Liu, P. (2012). The impact of additive manufacturing in the aircraft spare parts supply chain: Supply chain operation reference (SCOR) model. *Rapid Prototyping Journal*, 18(6), 451-467.
- [3] Campbell, I., Bourell, D., & Gibson, I. (2012). Additive Manufacturing: Rapid Prototyping Comes of Age. *Rapid Prototyping Journal*, 18(4), 255-258.

- [4] Murr, L. E., et al. (2010). Metal fabrication by additive manufacturing using laser and electron beam melting technologies. *Journal of Materials Science & Technology*, 26(12), 909-915.
- [5] Guo, N., Leu, M. C. (2013). Additive manufacturing: Technology, applications and research needs. *Frontiers of Mechanical Engineering*, 8(3), 215-243.
- [6] Chua, C. K., Leong, K. F., & Lim, C. S. (2017). *Rapid prototyping: principles and applications* (3rd ed.). World Scientific.
- [7] Wong, K. V., & Hernandez, A. (2012). A review of additive manufacturing. *ISRN Mechanical Engineering*, 2012, 208760.
- [8] Gao, W., Zhang, Y., & Ramanujan, D. (2015). Recent Advances in 3D Printing of Alloys and Composites. *Progress in Materials Science*, 74, 401-477.
- [9] Huang, S. H., & Liu, P. (2014). Mainstreaming of additive manufacturing for engineering design and education. *Journal of Mechanical Design*, 136(12), 121010.
- [10] Chua, C. K., Leong, K. F., & Lim, C. S. (2010). *Rapid Prototyping: Principles and Applications*. World Scientific Publishi
- [11] Pjević, M., Popović, M., Milutinović, M., Movrin, D., Stefanović, Lj., EXPERIMENTAL EXAMINATION OF THE APPLICABILITY OF ADDITIVE TECHNOLOGIES IN THE FIELD OF RAPID TOOLING - INJECTION MOLDING, 6th International Scientific Conference - COMETA2022, Proceedings, ISBN 978-99976-947-6-8, pp.241-247, University of East Sarajevo, Faculty of Mechanical Engineering East Sarajevo, B&H, RS, 17th-19th November, 2022



Society of Production
Engineering

SPMS 2023

39. Savetovanje proizvodnog mašinstva Srbije

ICPES 2023

39th International Conference on Production Engineering of
Serbia



Faculty of Technical
Sciences
University of Novi Sad

Novi Sad, Serbia, 26. – 27. October 2023

APPLICATIONS AND ECONOMICS OF ADDITIVE METAL PRODUCTION TECHNOLOGIES

Slobodan MALBAŠIĆ^{1,*}, Bogdan NEDIĆ², Aleksandar ĐORĐEVIĆ²,
Srdjan ŽIVKOVIĆ³, Aleksa GRUBIĆ³

¹Department for Defence Technologies, Belgrade, Serbia

²Faculty of Engineering University of Kragujevac, Serbia

nedic@kg.ac.rs, adjordjevic@kg.ac.rs

³Military Technical Institute, Belgrade, Serbia

srdjan.zivkovic@mod.gov.rs, aleksa.grubic@mod.gov.rs

*Corresponding author: slobodan.malbasic@mod.gov.rs

Abstract: Additive manufacturing (AM) is on the path from changing its early application in prototyping and low-volume production to serial production. Researchers, potential users, and companies from different industrial segments still raise questions and doubts about whether to accept this technology and which advantages AM technologies can provide compared to traditional production techniques. This work will try to give some reasonable explanations and answers in order to resolve some concerns about AM.

Also, the economic benefits of AM compared to traditional manufacturing are explained. Besides, special attention is given to the explanation of the current state in the field of Metal Additive Manufacturing production technologies.

In order to provide an adequate answer on whether AM can substitute some traditional production techniques and consequently save time, labor, and cost, the case study of the metal part production of complex part, through the application of the L-PBF (Laser Powder Bed Fusion) metal additive technology is presented and analyzed.

Keywords: Metal's additive manufacturing, L-PBF technology, economics of additive manufacturing.

1. INTRODUCTION

Market demands for personalized products, products with complex geometries and internal structures, as well as quality in manufacturing, represent a significant motivation for manufacturing technology advancement.

Traditional technologies (casting, forming, machining, forging and welding) have their position on the market and certainly plan to keep it.

However, when it comes to meeting the complex requirements of the market/clients, the answers are increasingly found in the application of different technologies of additive manufacturing.

However, despite the indisputable advantages of additive technologies, judging by the statements in [1], a justified question is being asked more and more often - whether and what effect and advantage additive technologies have in comparison to traditional production technologies: on the production

line itself, how does it facilitate production cycle and eliminates some operations, impact on product assembly or the possibility of integrating complex geometries, reduction of manufacturing time and costs, elimination of certain operations.

In his article [2], the author asks a new question - whether traditional production techniques need additive techniques. One answer is that it is necessary to find production scenarios that justify it.

The third question that arises is whether the replacement of traditional additive manufacturing should be carried out at the level of the entire factory or at some production line, or it can be done through certain scenarios.

There is no universal answer to the above questions. In the following text, we will try to give answers to some of the questions.

However, what is known so far and which additive technologies have gained advantages over traditional production technologies and how they can improve classical processes is that AM has successfully solved the "prototyping problem" and that they can be used for the rapid production of functional prototypes.

As an aid to traditional production, various auxiliary tools can be additively produced for less time and costs. For example, AM technology can be used to create any or all of the following components often at less time and cost [2]: jigs and fixtures, tooling and work holding, assembly/disassembly jigs, custom assembly tools, alignment tools and ergonomic grips, soft jaws and custom chucks, welding fixtures and bonding jigs, drill guides, Go/No Go gauges and other inspection fixtures.

In [3] a comprehensive systematization of the advantages of additive technologies in relation to traditional production technologies was presented. Authors depicted several areas as follows: (1) shortened product development lead time (the absence of tooling fabrication and quick physical prototypes); (2) design performance gains (weight and cost reduction and multifunctionality); (3) logistical savings (simplification of assemblies through design

integration); (4) product differentiation through clever designs can yield marketing benefits; (5) customized material solutions that take advantage of inherent AM processing physics; (6) software solutions (enhance the design, build, and verify aspects of the technology).

Among the so far developed additive technologies, technologies for the production of metal parts (MAM – Metal Additive Manufacturing) stand out. MAM technologies enable the production of complex structures with near-net shape capabilities from different types of metal powders, [4].

They find their application in specialized industries such as the aviation and automotive industries, medicine, electronic and military industries.

According to [3] there are three primary technologies relevant for metal-based AM: directed energy deposition (DED), PBF, and binder jetting. All of these technologies have their relative advantages to certain applications based on material compatibility and manufacturing limitations.

Since the PBF technology has been at the AM scene for quite long time, this led to mature stage and huge ecosystem of software's, materials and post processing around this technology. This is reason why PBF technology has breached into different industrial areas, and why the first MAM wave is linked primary to PBF.

The forerunner of the second MAM wave is Binder Jetting. This technology currently profiting because of close link to the MIM (Metal Injection Molding) technology in the form of material developments, sintering expertise and customer base.

After the introduction in the first chapter, economically optimal AM scenarios are presented at 2nd chapter. In the 3rd chapter, the basic characteristics of additive technologies for the production of metal parts are stated, with special reference to L-PBF technology. After that a case study based on a real example from practice is presented. At the end of the paper, a conclusion is given.

2. ECONOMICALLY OPTIMAL AM SCENARIOS

A comparison of traditional and additive production can be made from an economic point of view. This further means that some specific economically justified and optimal scenarios can be defined. These scenarios were in details elaborated and explained by [5].

According to [5], three key regions/scenarios are recognized (Figure 1): Batch-enabled scenarios (zone 1), Complexity-enabled scenarios (zone 2), Ultra-high complexity scenarios (zone 3).

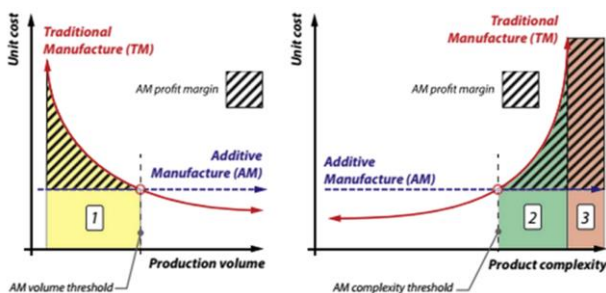


Figure 1. Economical optimal AM scenario, [5].

Key assumption is that AM part cost is independent of production volume and product complexity (or have very small influence to the overall unit cost). This helps us to get useful insights into the relative economic merit of AM and traditional methods.

Batch-enabled scenarios: Production volumes are below the AM volume threshold, unit costs associated with AM are less than for traditional manufacturing. From technical point of view this relates to the pre-production development of some tools, models or functional prototypes or single unit-production; and short volume serial production.

Complexity-enabled scenarios: This zone comes after the complexity threshold lines where AM methods enable lower cost than competing traditional manufacturing methods. Topologically optimized parts, functionally integrated systems and serial production of highly complex geometries belong under this scenario.

Ultra-high complexity scenarios: These scenarios provide a unique commercial design opportunity for AM. Under this scenario traditional manufacturing methods are

technically unable to provide the required complexity at any cost, thus giving a unique commercial design opportunity for AM.

3. METAL ADDITIVE MANUFACTURING PROCESSES

So far MAM technology has been often associated with Laser or Electron Beam Powder Bed Fusion. In meanwhile, some new processes have been emerged in the MAM industry. According to [6], there is more than 18 different additive metal technology principles identified today.

However, in MAM the precision and reliability of the components largely depend upon the good quality of powder characterization, thorough understanding of process parameters, metallurgical bonding mechanism between layers and mechanical properties, [4].

According to [6], metal additive technologies are divided into two groups:

1) direct technologies (create a finished product by directly melting metal powders, use powder or wire to directly produce the part), there are distinction of the material deposition method (direct or powder bed) and by energy source.

2) indirect technologies (sinter-based, require a minimum of two processes to form the finished product, the so-called green product as an intermediate phase and sintering step and therefore have heat as the main energy source in common). Sintering always comes with a binder component and a two-step manufacturing process.

Indirect technologies have been gaining momentum in the last few years. They are characterized by a faster printing process compared to direct technologies, so a reduction in the price of the finished product is expected. Because of the above characteristics, the suppliers of these printers are trying to get a larger marketing share and tend towards their application in serial production.

Every technology has its specific advantages and limitations regarding part design, mechanical properties and costs. This leads to

a more and more complex decision when it comes to the choice of technology for a given application.

The classification of additive technologies for metal production based on the energy source used to melt metal powders is presented in [7]. The two basic groups of processes refer to processes that require a directed source of energy (laser or electric beam) and processes that do not use a directed source of energy (mechanical deformation, material injection, heat in the sintering process).

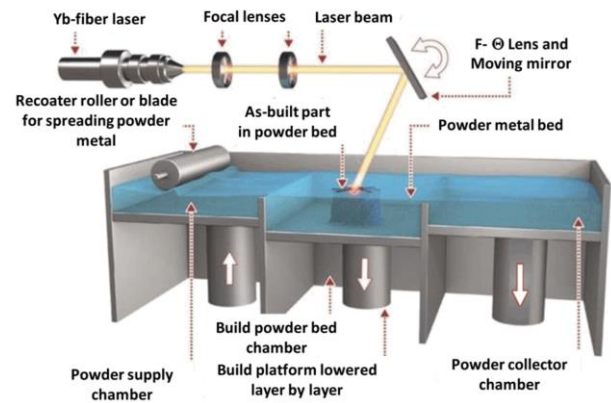


Figure 3. L-PBF principle, [8]

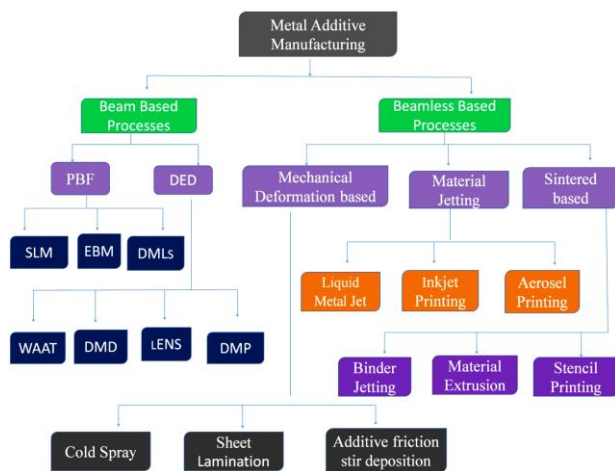


Figure 2. Metal AM Classifications, [7]

3.1 Laser sintering Powder bed fusion (L-PBF)

PBF is the processes where electron beam or laser beam is used to fuse the metal powder particles on the powder bed, [4].

PBF machine has several computer-controlled chambers aimed to help with powder manipulation. Supply chamber acting as delivery system of powder, re-coater spread this powder over the working surface build powder bed chamber where through the system of mirrors laser/energy beam is focused on the surface to form one layer. After one layer is formed this process is repeated until the whole part is not finished. Powder that is not fused during the process is moved (during the re-coater movement) to the powder collector chamber for further sintering process. This process is illustrated at Figure 3, and further explained in [8].

Electron beam melting (EBM) process uses an electron beam as an energy source, whereas laser beams are used in selective laser sintering (SLS) and direct metal laser sintering (DMLS) process [9]. However, in the SLS process, powder material is heated below the melting point, whereas complete melting takes place to make full density components in the DMLS process.

PBF process is used to produce near net shape components (processes that aim to produce products which are close to the final shape) that can reduce production steps and costs. Mechanical, chemical, physical, and thermal properties and subsequently the overall quality of printed components are directly related to the quality of the raw material put into an AM machine.

Good materials are crucial for effective AM, and different processes require these materials to be prepared in different ways. Some AM processes are capable of processing a wider range of materials than others. PBF process polymer, ceramic, composite, or metallic material feedstocks.

At Figure 4. the basic principles in the application of metal materials (state of the fusion, variant of metal feedstock, distribution process, etc...) during the additive printing process is displayed.

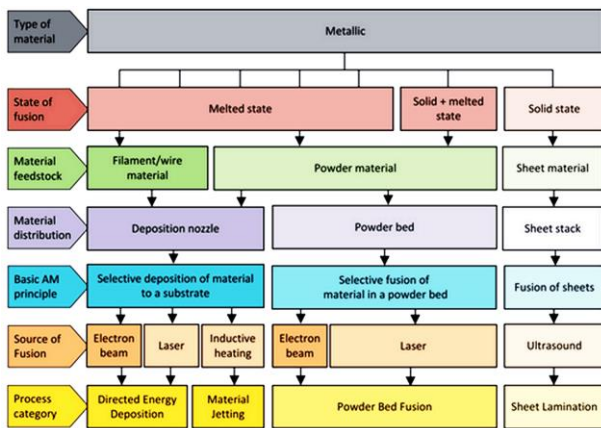


Figure 4. Overview of single-step AM processing principle for metallic materials, [9]

4. CASE STUDY

In this chapter, the production of the chosen model (machine gun barrel stand, Fig. 5) will be analyzed using traditional and additive technology (fusion of metal powder with a laser beam, L-PBF). Bearing in mind that prototyping stage is in question (total 3 pieces to be produced), that the production of the "0" series and serial production is expected only after the acceptance of the prototype model, it is expected that at this stage of production (a small number of pieces, the need to modify and refine parts regarding functionality is evident) producer of the part consider the possibility of reducing costs and optimizing their production.

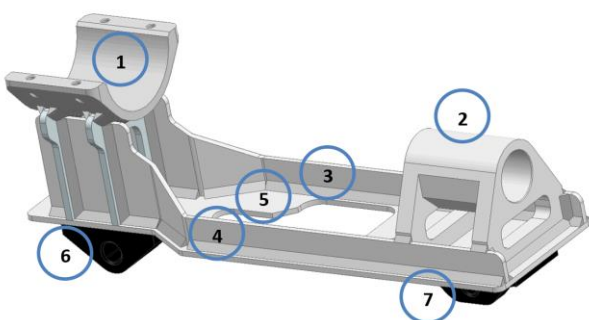


Figure 5. Machine Gun Barrel Stand

Main parts of the stand are (Figure 5):

1. Holder with ribs (2 pieces of ribs)
2. Guider
3. Rib longitudinal (left)
4. Rib longitudinal (right)
5. Base plate
6. Fixing part (front)

7. Fixing part (rear)

An analysis of the traditional manufacturing methodology and costs show the following parameters:

- Material costs per part (8 kg – alloy steel) + labor costs (15 hours) in total is about 30,000 RDS (about 250 €), without prices for additional processing and finishing (phosphating, sandblasting and final painting). For the whole prototype lot (3 pieces) the total cost is 750€.
- The production time: 3 pcs * 15 hours = 45 hours/part, it is 6 working days (for an 7.5 hours working time). This can be reduced to a total production time of 2 working days by hiring 3 workers to work in parallel.

Evident problems in traditional production:

- Materials are different types of alloy steel, the production time is quite long, main part (stand) is consisting of a large number of parts (7 positions) as well as a large number of technological operations.
- Some operations (phosphating, sandblasting) are performed at the subcontractor what introduce additional waiting times (transport, delivery, return back from the subcontractor).
- Operations of joining parts by welding ask for designing and manufacturing of auxiliary tools and accessories, which additionally increases the unit price.
- Within the prototype lot, changes and modifications to the construction are possible, so the issue of making auxiliary tools and accessories becomes even more important.
- A total of up to 5 workers are hired, what is also quite big.
- The percentage of unused material is extremely high 67% (the mass of the preparations is 8 kg and the mass of the finished part is 2.5kg),

There are several areas (questions) for consideration in order to optimize the process:

- Is it possible to reduce the number of parts?
- Consider the possibility of reducing production time?

- Analyzing the total number of machining operations as well as labor force in order to optimize it. Multiple steps in the production process cumulatively affect the final quality and tolerances of the finished part.
- Consider the possibility of eliminating the additional costs of making auxiliary tools (for welding and control).

The optimization of the production process can be carried out through the application of additive technology methods (L-PBF method on an available industrial 3D machine made of 316L stainless steel).

The costs of making a part with L-PBF technology refer to the total costs of materials, hired labor, electricity consumption and amortization (depreciation cost) of equipment. The total cost is about 1,900€ (633€/ piece), all 3 pieces are manufactured in one process, which corresponds to the size of the prototype batch, and at the same time, the working plate of the machine is filled to the maximum.

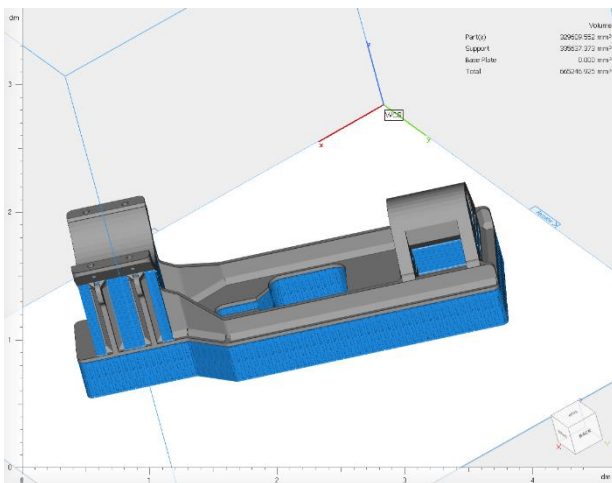


Figure 6. AM process planning (supports)

Benefits of using additive manufacturing technique:

- Consolidation of parts was carried out (from 7 parts it was reduced to 1 part), Figure 7.
- Total production time has been reduced (the production time of all 3 parts is 106 continuous working hours, 4.4 continuous working days).

- Number of manufacturing operations (without subsequent machining operations) are reduced to one operation.
- No additional tools and accessories are required.
- The consumption of materials in additive manufacturing (5.2 kg/piece of metal powder) is drastically lower compared to the consumption of materials in classical production (8 kg/piece of plate preparations of alloy steel).

Some of the disadvantages and possible solutions:

- The production of parts from metal requires a support structure, which additionally increases costs (Figure 6).
- Optimization of the structure was not performed if this were applied the total price would be reduced.
- The applied technology also requires subsequent machining of the manufactured parts and it was not taken into account in this case study.
- The L-PBF technology itself requires the engagement of several operators for the manipulation of the work plate and powder, which also increases costs.

It is necessary to point out that the presented example was made during the initial research and determination of the possible range of application of additive technology in the production of metal parts (through the time of making parts, realized costs, number of engaged persons, positive effects from the aspect of design of integrated functionalities - direct production of assemblies...) and for the purposes of making a prototype batch of individual elements.

The chosen example does not fully depict all the advantages of the applied method of additive technology, especially from the cost aspect (price of 633 euros / piece for additive technology compared to 250 euros / piece for traditional technology). However, PBF technology, and especially the use of industrial-scale 3D printers, have high initial costs for several reasons:

- The initial price of the machine is affected by the large amortization price, which is reflected in the price of the part.
- The need for additional machining and subsequent treatment.

Other benefits of PBF technology in contrast to traditional techniques are:

- Material consumption in classic production cannot be drastically reduced. The consumption of materials for the production of auxiliary tools and accessories, averaged per piece for the entire series, should be added.
- If classic production involves the hiring of subcontractors, it increases the waiting time for the assembly of the assembly.
- Material consumption in additive manufacturing can be drastically lower if topological optimization is performed, which is the next step in this research.

However, in the prototyping stage, when the uncertainty in the design is high, and the need for rapid production of parts to test functional capabilities is high, the application of additive technologies has its advantages, although the price does not always justify it in every case.



Figure 7. Finished (printed) part

Even if the economic indicators in the prototype lot do not justify it, it is possible to consider that one or more traditional production technologies can be applied in serial production (fulfillment of the economy of scale). By analyzing the application of PBF additive technology for the production of metal parts, it was concluded that there are certain hidden costs that, if not identified in a timely and correct manner, can significantly increase the total final costs.

5. CONCLUSION

This paper presents one possible approach to the analysis of the costs of manufacturing parts by fusion of metal powder using a laser (L-PBF). The obtained results were compared with traditional and well-established technological production process. For small series and especially for prototype batches, while the development phase of the entire assembly has not yet been completed, additive manufacturing shows its undoubted advantage over traditional technological process. In medium and large-scale serial production the unit price of parts made by traditional technological process would be significantly lower than the production of parts by additive technology.

Certainly, costs are the biggest challenge when analyzing additive manufacturing. The total cost of the finished product depends on many variables (material, production time, depreciation price, labor force), which is also shown in this paper. Post processing activities, which are carried out to improve the quality and mechanical characteristics of the finished product, also entail certain costs.

How do we overcome this challenge? Aside from continuous improvements in process efficiency (application of higher power lasers, multi-laser systems, lower layer thickness, larger volume of the working chamber, ensuring continuity in the manufacturing process - more streamlined workflows), it is also necessary to educate staff for additive manufacturing and later especially for specific AM technologies, [10].

It is to be expected that a stable and sustainable base of technologically educated personnel will be created in due time.

One of the answers to the question posed at the beginning of this paper is: In essence, if classic production provides economically justified production of parts, delivery of parts on time and within deadlines, if there is an economy of scale or ROI is achieved - financial return through investments, if there is no disruptions in supply chains, as there is no need for product personalization and clients

are satisfied with the offered product (no striving for lighter parts, better performance), then there is no need for changes in production technologies.

After analyzing the additive technologies for the production of metal parts and the materials that provide it, the following conclusions can be drawn regarding the current level of representation of these technologies:

- Of all the represented additive technologies for the production of metal parts, only Powder Bed Fusion and Direct Energy Deposition are represented at the industrial level. Binder Jetting is expected to reach the level of industrial application soon.
- In comparing L-PBF technology with traditional technologies in possible application in serial production, this technology is still characterized by high costs of machines and materials, as well as low production speed. In connection with the above, it is also concluded that not every machine part is suitable for production with PBF technology.
- Sinter-based metal AM technologies provide a good basis for reducing the cost of manufacturing parts and applying them in serial production. OEMs of these technologies are doing everything to make this technology available to users and to take more market share.

The application of additive technological procedures in certain stages of research and development of prototyping batches of complex products, with the easy and quick change of shape as well as the possibilities of making lattice structures, fully justify their use.

REFERENCES

- [1] *Saving Time and Money on the Shop Floor with AM*, on-line: <https://www.additivemanufacturing.media/articles/saving-time-and-money-on-the-shop-floor-with-am>, accessed: 02.08.2023.
- [2] *Does Manufacturing Need Additive?* on-line: <https://www.additivemanufacturing.media/articles/why-manufacturing-needs-additive>, accessed: 02.08.2023.
- [3] D.M. Dietrich, M. Kenworthy, E.A. Cudney, *Additive Manufacturing Change Management - Best Practices*, CRC Press. Taylor & Francis Group, 2019.
- [4] H. Wang, J. Ying, H. Fuh: *Metal Additive Manufacturing and Its Post-Processing Techniques*. *J. Manuf. Mater. Process.* 2023, 7, 47; <https://doi.org/10.3390/jmmp7010047>
- [5] M. Leary: *Design for Additive Manufacturing (Additive Manufacturing Materials and Technologies)*, 2020 Elsevier Inc.; <https://doi.org/10.1016/C2017-0-04238-6>
- [6] *Additive Manufacturing - New metal technologies*, available at: www.am-power.de/insights, accessed: 10.03.2023.
- [7] M. Pant, L. Nagdeve, H. Kumar, G. Moona: *A contemporary investigation of metal additive manufacturing techniques*. *Sadhana* (2022) 47:18. Indian Academy of Sciences.
- [8] A. Altay, B. Kaftanoglu, R. Leach, N. Senin, A. Donmez: *Focus Variation Measurement and Prediction of Surface Texture Parameters Using Machine Learning in Laser Powder Bed Fusion*, *Journal of Manufacturing Science and Engineering JAN.* 2020, Vol. 142 / 011008-1
- [9] I. Gibson, D. Rosen, B. Stucker, M. Khorasani: *Additive Manufacturing Technologies*. Third Edition, Springer Nature Switzerland AG 2021.
- [10] *Pathway to Metal AM Adoption: Overcoming Metal AM's Core Challenges* available at <https://velo3d.com/overcoming-challenges-in-metal-am-ebook/>, accessed: 12.08.2023



Society of Production
Engineering

SPMS 2023

39. Savetovanje proizvodnog mašinstva Srbije

ICPES 2023

39th International Conference on Production Engineering of
Serbia



Faculty of Technical
Sciences
University of Novi Sad

Novi Sad, Serbia, 26. – 27. October 2023

A MULTI-CRITERIA DECISION-MAKING APPROACH FOR ENHANCING MECHANICAL PROPERTIES OF FDM 3D-PRINTED PARTS

Rajko TURUDIJA^{1*}, Jelena R. STOJKOVIĆ¹, Miloš STOJKOVIĆ¹, Jovan ARANĐELOVIĆ¹, Nikola KORUNOVIĆ¹

¹Faculty of Mechanical Engineering, University of Niš, 18000 Niš, Serbia

*Corresponding author: rajko.turudija@masfak.ni.ac.rs

Abstract: *The quest for optimizing 3D printing processes to meet industrial demands for improved mechanical properties and dimensional stability is an ongoing challenge. This study delves into the task of determining the optimal 3D printing parameter (material and layer height) and annealing parameter (annealing time and annealing temperature) combinations for FDM 3D-printed parts through a systematic and objective approach. By utilizing Multi-Criteria Decision-Making (MCDM) methods, specifically the Analytic Hierarchy Process (AHP) for criteria weighting and the Technique for Order of Preference by Similarity to Ideal Solution (TOPSIS) for ranking, the study endeavours to address this challenge effectively. The primary aim of this research is to identify the most suitable 3D printing and annealing parameter combination that maximizes tensile strength and Young's modulus of elasticity while minimizing change in width, change in thickness, and change in length of the specimen after annealing. To achieve this, a comprehensive dataset stemming from the experimental analysis of three distinct materials (Polylactic acid - PLA, Polyethylene terephthalate glycol - PETG, carbon fiber reinforced PETG - PETGCF), three layer heights (0.1 mm, 0.2 mm, 0.3 mm), five annealing temperatures (60°C, 70°C, 80°C, 90°C, 100°C), and three annealing times (30 minutes, 60 minutes, 90 minutes) is employed. These criteria were determined based on the requirements of a specific industrial case study, highlighting their relevance and significance in real-world applications. The results show that the best combinations are the ones from PETGCF material with 0,1 mm layer height, with long annealing times (90 minutes) and low to mid annealing temperatures (60 - 70°C). The worst alternatives are the ones annealed at high temperatures (90 - 100°C), and with PETG material, as the dimensional change of this material are significant at high temperatures.*

Keywords: Multi-criteria decision making, AHP, TOPSIS, FDM 3D printing, annealing.

1. INTRODUCTION

3D printing, also known as additive manufacturing (AM), has transformed the landscape of modern industry, offering unmatched versatility and efficiency for crafting intricate parts. As industries

increasingly adopt this technology, the need to optimize 3D printing processes becomes more vital than ever. Among the many challenges in this quest, two stand out: improving the mechanical performance of 3D-printed parts and achieving greater dimensional accuracy. The study takes on this dual challenge by

systematically and objectively identifying the best combinations of printing parameters, with both goals in mind. To achieve this, the study uses well established Multi-Criteria Decision-Making (MCDM) methods, specifically the Analytic Hierarchy Process (AHP) and the Technique for Order of Preference by Similarity to Ideal Solution (TOPSIS). The widespread applicability and global significance of MCDM methods are underscored by their extensive utilization in resolving real-world challenges, as evidenced by numerous studies [1, 2, 3]. Furthermore, the adaptability of this approach to diverse problems is a testament to its flexibility in accommodating variations in criterion weights [4, 5]. The determination of weighting coefficients emerges as a pivotal element in the process of selecting the optimal alternative and ranking research findings, as evidenced by the studies conducted by [6] and [7]. Furthermore, the works of [8] and [9] underscore the significance of preserving subjective viewpoints when establishing initial weights, a practice that enhances the relevance of results and their applicability to specific scenarios. It is imperative to recognize that the assignment of criterion weights exerts a direct and profound influence on the research outcomes, thereby highlighting the inherent interplay between weight allocation and decision-making results. Extensive research within the domain of MCDM consistently advocates the adoption of robust models for the selection of optimal alternatives within the decision-making framework, aligning with the recommendations put forth by a majority of authors, including [10] and [7]. Because of this, the primary objective of the study is to introduce a robust and hybrid MCDM approach, which encompasses the assessment of the collective influence of printing and annealing parameters in the context of 3D printing.

The utilization of the Multi-Objective Optimization using Ratio Analysis (MOORA) method for optimizing 3D printing process parameters, accommodating diverse criteria, both quantitative and qualitative, and providing an accessible computational approach, is noteworthy [11]. This study's

exploration of FDM 3D printer parameters, specifically layer thickness, build pattern, and fill pattern, with a focus on their impact on surface roughness and build time, adds valuable insights to the field. The study [12] contributes to understanding the influence of process parameters on the mechanical properties of FDM printed parts, with a focus on optimizing these parameters to achieve reduced surface roughness and maximum strength. The research employs diverse optimization techniques, including the TOPSIS, the response surface methodology (RSM), the Non-dominated Sorting Genetic Algorithm (NSGA-II), and Grey Relational Analysis (GRA), to identify the optimal FDM process parameters. The hybrid optimization approach, combining a genetic algorithm with RSM, demonstrates enhanced prediction accuracy. Notably, the study identifies the optimal parameters, including an infill density of 61.02%, a layer thickness of 0.26 mm, a print speed of 37.77 mm/s, and an extrusion temperature of 191.1 °C, for achieving the lowest surface roughness and maximum strengths in FDM parts. The study [13] presents an endeavour to discern the most suitable AM process with a focus on sustainability considerations. The research encompasses a comprehensive assessment of key dimensions within the realm of sustainable AM, encompassing aspects such as material and product quality, machine performance, market stability, total cost, and ecological values. To facilitate this decision-making process, a hybrid multi-criteria approach, combining stepwise weight assessment ratio analysis and complex proportional assessment methods, is applied. Among the four AM processes evaluated, namely FDM, laminated object manufacturing (LOM), stereolithography apparatus (SLA), and selective laser sintering (SLS), the study identifies FDM as the most favourable alternative. In the work [14], authors delve into the analysis of process parameters within the context of the FDM process, employing an integrated MCDM approach that combines modified fuzzy and Analytic Network Process (ANP) methods. The experimental investigation

centres on three pivotal process parameters: layer height, shell thickness, and fill density, alongside their corresponding response parameters, encompassing ultimate tensile strength, dimensional accuracy, and manufacturing time. Subsequently, the research undertakes the optimization of FDM process parameters utilizing the proposed methodology. The results highlight that experiment recommend a configuration with a layer height of 0.08 mm, shell thickness of 2.0 mm, and fill density of 100%. This optimized setting not only enhances ultimate tensile strength but also improves dimensional accuracy while reducing manufacturing time, thereby enhancing the overall performance and efficiency of the FDM process. The article [15] introduces an efficient decision support system designed for the purpose of selecting the most suitable AM process. To achieve this, a novel hybrid MCDM technique is proposed, featuring the utilization of the Best Worst Method (BWM) to determine optimal criteria weights and the Proximity Indexed Value (PIV) method for ranking available AM processes. The study benchmarked the capabilities of four AM processes, including Vat Photopolymerization (VatPP), Material Extrusion (ME), Powder Bed Fusion (PBF), and Material Jetting (MJ), by fabricating a conceptual model of a spur gear. Key criteria under consideration encompassed dimensional accuracy, surface roughness, tensile strength, percentage elongation, heat deflection temperature, process cost, and build time. Sensitivity analysis was further conducted to validate the reliability of the results. The findings indicate that the Material Jetting (MJ) process consistently produces dimensionally accurate and high-quality parts, as corroborated by the ranking derived through the PIV method, which is noted for its reliability and consistency.

The literature review underscores the frequent and successful utilization of MCDM techniques within the additive manufacturing domain. However, it is worth noting that, to the best of the authors' knowledge, none have applied MCDM techniques to the context of

FDM 3D printing in conjunction with an annealing process. Within the academic realm, this study contributes significantly to the ever-expanding body of knowledge surrounding additive manufacturing and the practical implementation of MCDM methodologies. It advances our comprehension of optimizing 3D printing, specifically addressing a pivotal challenge: the enhancement of both the strength and quality of 3D-printed components, through annealing process. Extending beyond academia, in today's fiercely competitive industrial landscape, where efficiency, product, and environmental considerations take precedence, the optimization of 3D printing processes assumes critical importance. The capacity to fabricate 3D-printed parts boasting superior mechanical properties without compromising precision holds far-reaching implications across diverse industries.

2. METHODOLOGY

The objective of this study is to identify the optimal combinations of 3D printing and annealing parameters that maximize mechanical properties (e.g., tensile strength and Young's modulus of elasticity) while minimizing dimensional changes (width, thickness, and length after annealing). To achieve this objective, a two-step approach was adopted. Firstly, the Analytic Hierarchy Process (AHP) method was employed to establish objective weights for the evaluation criteria, considering the relative importance of mechanical properties and dimensional changes. Subsequently, the Technique for Order of Preference by Similarity to Ideal Solution (TOPSIS) method was applied to rank the optimized parameter combinations based on their performance across the defined criteria. This comprehensive methodology enables a systematic and efficient evaluation of parameter combinations, facilitating well-informed decision-making in the context of 3D printing and annealing processes. The best solutions (based on the MCDM analysis) are then used for real world case study.

2.1 AHP method

The Analytic Hierarchy Process (AHP) method, developed by Saaty [16, 17], is a robust tool widely employed in MCDM to establish objective weights for evaluating criteria. AHP provides a structured approach to decision-making by breaking down complex problems into a hierarchical structure comprising a goal, criteria, and alternatives. In the context of the study, the goal is to optimize 3D printing and annealing parameters for enhancing mechanical properties and minimizing dimensional change after annealing. The criteria include factors such as tensile strength, Young's modulus of elasticity, and dimensional changes after annealing process (width, thickness, and length after annealing). AHP employs pairwise comparisons to assess the relative importance of these criteria. These pairwise comparison matrices can be established using expert opinions or data-driven techniques. To quantify preferences, Saaty's scale (refer to Table 1) was utilized to populate the matrices with numerical values. Subsequently, through the calculation of eigenvectors and eigenvalues, the weights for each criterion were derived, indicating their relative importance in the parameter optimization process.

Table 1. Saaty's scale

Saaty's scale	Meaning
1	Equally preferred
3	Moderate preference of one over the other
5	Strong preference of one over the other
7	Very strong preference of one over the other
9	Extreme preference of one over the other
2,4,6,8	Intermediate values, indicating the degree of preference between adjacent values

To maintain the robustness of the analysis, evaluation of the consistency of pairwise

comparisons using the consistency ratio (CR) was employed. A CR value close to 0 signifies a high level of consistency, while higher CR values prompt a reassessment and adjustment of the comparisons. The flexibility of the AHP method permits its application across diverse processes, as the CR ensures the consistency of criteria weights. This adaptability makes the hybrid approach, which combines AHP with TOPSIS method, a robust and dependable decision-making tool for optimizing 3D printing and annealing parameters to achieve the research objectives.

2.2 TOPSIS method

The Technique for Order of Preference by Similarity to Ideal Solution (TOPSIS) method, a widely recognized MCDM method, plays a pivotal role in the study, facilitating the ranking of optimized alternatives for 3D printing and annealing operations. TOPSIS is a distance-based method that assesses alternatives based on their proximity to the ideal and anti-ideal solutions. In this context, the ideal solution represents the optimal achievement of desired criteria (e.g., maximum tensile strength, maximum Young's modulus of elasticity, minimum dimensional changes) while the anti-ideal solution represents the least favourable scenario.

To compute the TOPSIS rankings, one first represents the alternatives as a decision matrix. Each row in the matrix corresponds to an alternative, while each column corresponds to a specific criterion. To ensure fairness in the evaluation, normalizing the decision matrix to eliminate the influence of scale differences among the criteria is needed. Subsequently, the ideal and anti-ideal solutions are identified based on the maximum and minimum values for each criterion, respectively. After that, distance metrics is employed (such as the Euclidean distance or other suitable measures), to gauge the proximity of each alternative to these reference solutions. The relative closeness of each alternative to the ideal solution is quantified using relative closeness coefficients. Finally, the alternatives are ranked

based on these coefficients. The TOPSIS method offers a robust and intuitively comprehensible approach to prioritize the alternatives, facilitating the selection of the most promising combination of 3D printing and annealing parameters.

By incorporating the TOPSIS method into the hybrid MCDM framework, one can enhance the overall decision-making process, rendering it more comprehensive and effective in optimizing 3D printing and annealing operations for superior mechanical performance and dimensional stability.

3. CASE STUDY

The case study presented in the paper centres on the fabrication of a camera holder for mounting on a simple drone design. This camera mount production was undertaken using FDM 3D printing, as part of a Do-It-Yourself (DIY) drone project (Figure 1). To meet the specific requirement of keeping the camera mount as lightweight as possible, but also to have exceptional mechanical properties, unconventional approaches were explored. One approach involved the production of the camera mount with minimal dimensions and weight through 3D printing, followed by a subsequent annealing process to enhance its mechanical properties. Because of this, the need for determining the best combination of printing parameters and annealing parameters was born. In addition, because the material of the camera mount was not specifically determined, different materials could also be tested, which just added more depth to the research.



Figure 1. DIY drone design with the camera mount

The data employed in this study originates from a prior research investigation conducted

by the authors, as documented in a previous research paper [18]. In that study, the primary focus was to explore the effects of annealing time, temperature, and layer height on the tensile strength, modulus of elasticity and dimensional change characteristics of three distinct 3D printing materials, namely PLA, PETG, and carbon fiber-reinforced PETG. A comprehensive series of experiments was executed, involving variations in layer heights (0.1 mm, 0.2 mm, and 0.3 mm) and annealing processes conducted within a temperature range of 60–100 °C, spanning time intervals of 30, 60, and 90 minutes. The utilization of data from the prior research paper is justified by the specific requirements and constraints associated with the camera mount's design and function. The camera mount, due to its position and structural characteristics, is primarily subjected to tensile forces resulting from the weight of the camera it supports. Consequently, the tensile strength and modulus of elasticity of the chosen material for the camera mount emerge as paramount considerations. Furthermore, beyond its mechanical attributes, it is essential for the camera mount to exhibit a reasonable degree of dimensional accuracy. While exacting tolerances are not obligatory for this application, the avoidance of significant warping or substantial dimensional variations is crucial. In this context, the utilization of FDM 3D printing, complemented by annealing processes, offers an effective means to strike a balance between mechanical integrity and dimensional stability.

By leveraging the previously discussed dataset and considering the case study involving the camera mount, we encounter a MCDM challenge as follows:

A total of 144 alternative combinations have been formulated, each encompassing distinct attributes related to 3D printing layer height, material type, annealing time, and temperature [18]. The objective is to discern the optimal combination from this vast array of possibilities, guided by a set of well-defined criteria. The criteria identified for evaluation encompass maximal tensile strength, maximal modulus of elasticity, minimal dimensional changes in

terms of thickness, minimal dimensional changes in terms of width, and minimal dimensional changes in terms of length of the specimen. These criteria form the foundation for determining the most favourable combination amidst the multitude of choices, aligning with the overarching aim of enhancing the camera mount's mechanical properties and dimensional accuracy after annealing process.

The AHP method was used to determine the weight coefficients. The pairwise comparison matrix was formulated to establish the relative importance of the criteria. In this case, the matrix indicates that tensile strength (TS) was considered two times more important than Young's modulus of elasticity (YM), six times as important as dimensional change in terms of width (ΔW_c) and thickness (ΔT), and four times as important as dimensional change in terms of length (ΔL_0), as can be seen in Table 2.

Table 2. Pairwise comparison matrix

	TS	YM	ΔW_c	ΔT	ΔL_0
TS	1	2	6	6	4
YM	0.5	1	3	3	2
ΔW_c	0.16667	0.33333	1	1	0.6667
ΔT	0.16667	0.33333	1	1	0.6667
ΔL_0	0.25	0.5	1.499925	1.499925	1

The weight coefficients obtained as the result of the AHP analysis are as follows:

- w_1 (weight coefficient for TS) = 0.480000384
- w_2 (weight coefficient for YM) = 0.240000192
- w_3 (weight coefficient for ΔW_c) = 0.080000864
- w_4 (weight coefficient for ΔT) = 0.080000864
- w_5 (weight coefficient for ΔL_0) = 0.119997696

Furthermore, the consistency of criterion importance was verified, confirming that the criteria were adequately compared in terms of importance, with a consistency ratio (CR) of 0.000000000892812.

Following the assessment of MCDM rankings, the two top-ranked alternatives were selected

for the production of the camera mount. The 3D printing process was executed using the Wanhao Duplicator i3 Plus 3D printer (Figure 2a), while the annealing process was conducted within an industrial-grade oven (Figure 2b). Subsequently, a tensile strength analysis was performed on these two camera mounts, in comparison with the base camera mount which did not undergo the annealing process. The evaluation was conducted utilizing the Shimadzu Table-top AGS-X 10kN universal testing machine (Figure 3). It's important to note that the camera mount does not conform to a standardized shape for testing, thus the results may not be considered entirely precise or universally applicable. However, the consistency in testing methodology across all camera mounts allows for meaningful comparisons and serves as a reference point to assessing if any potential improvements in mechanical properties were achieved, and if the presented MCDM method was successful.

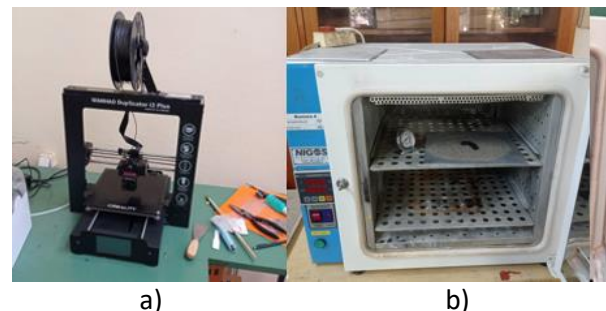


Figure 2 presentations of a) Wanhao Duplicator i3 Plus 3D printer, and b) industrial-grade oven



Figure 3 Shimadzu Table-top AGS-X 10kN universal testing machine

4. RESULTS AND DISCUSSION

Identifying the optimal combination of 3D printing and annealing parameters based on the criteria of minimizing dimensional changes, maximizing tensile strength and modulus of elasticity is inherently a multi-criteria decision-making challenge. Within this context, the criteria encompass minimizing changes in width, thickness, and length (dimensional stability), while maximizing tensile strength and modulus of elasticity (mechanical performance). The outcomes of this investigation yield valuable insights into the recommendations put forth by the TOPSIS method. Upon examining Figure 4, a notable trend emerges: PETG material consistently exhibits inferior rankings among the various alternatives, with the exceptions being those employing a 0.3 mm layer height, which demonstrate comparably good results when compared to the other materials with the same layer height. In contrast, PLA material showcases a remarkable level of consistency across different parameter combinations, with only the variants featuring a 0.1 mm layer height marginally deviating from the otherwise stable performance. As for PETGCF, the outcomes are notably favourable, with the alternatives employing a 0.1 mm layer height showcasing significantly superior performance in comparison to other parameter combinations.

Based on the findings derived from the TOPSIS analysis, the optimal methods predominantly originate from the PETGCF material, evident in the top four alternatives that emerge as the highest-ranked (as presented in Table 3). Additionally, a preference for lower layer heights is discernible, as they appear to yield superior tensile strength, likely attributed to enhanced interlayer bonding. Furthermore, with respect to annealing parameters, lower temperatures are favoured (60°C and 70°C), primarily due to their tendency to induce lesser dimensional changes in the specimens, as well as longer annealing times (60 and 90 minutes).

Table 3. Best alternatives according to TOPSIS method

#	Material	Layer height (mm)	Annealing time (min)	Annealing temperature (°C)
108	PETGCF	0.1	90	60
103	PETGCF	0.1	60	60
109	PETGCF	0.1	90	70
98	PETGCF	0.1	30	60

Conversely, the least favourable alternatives tend to be associated with the PETG material, particularly those involving extended annealing

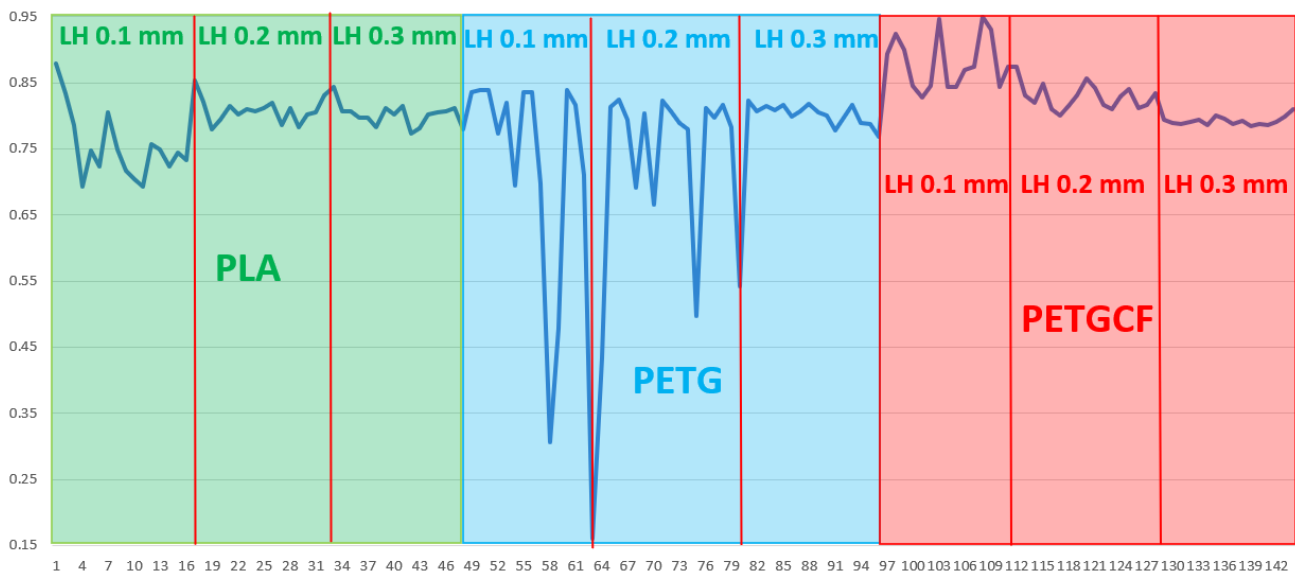


Figure 4 Results of TOPSIS analysis with LH depicting layer height of the alternative

times and higher temperatures (90°C and 100°C), as indicated in Table 4. This observation can be attributed to PETG's suboptimal mechanical properties following annealing, along with its pronounced dimensional instability.

Table 4. Worst alternatives according to TOPSIS method

#	Material	Layer height (mm)	Annealing time (min)	Annealing temperature (°C)
63	PETG	0.1	90	90
58	PETG	0.1	60	90
75	PETG	0.2	60	100
80	PETG	0.2	90	100

Following the analysis of MCDM results, two of the highest-rated alternatives were selected to produce camera mounts, enabling subsequent testing and comparison with the base camera mount (which underwent no annealing process). The base camera mount model, printed with a 0.1 mm layer height but without annealing, exhibited a maximum strain force of 253 N, roughly equivalent to a tensile strength of 5 MPa. In contrast, the model printed with a 0.1 mm layer height and annealed at 60°C for 60 minutes achieved a force of 266 N, approximately corresponding to a tensile strength of 5.3 MPa. Lastly, the model printed with a 0.1 mm layer height and annealed at 60°C for 90 minutes resulted in a force of 270 N, representing an estimated tensile strength of 5.4 MPa. Again, it should be noted that the testing method was not standard, and one cannot be certain about the results of the testing, nor should the results be used for universal comparison. However, due to the experiments being done in the same way every time, the results can be compared with each other, and it can be concluded that by following the recommendations from presented MCDM method, the enhancement of mechanical properties of the camera mount was achieved.

5. CONCLUSION

This paper explores the application of established MCDM methods to determine the optimal parameter combinations for enhancing the mechanical properties of FDM 3D-printed parts and minimizing dimensional changes following the annealing process. MCDM methods offer valuable insights, particularly when dealing with extensive databases and numerous alternative combinations. The combined use of AHP and TOPSIS methods provides a comprehensive and robust analytical framework adaptable to various applications. According to the analysis, the most favourable alternatives in the presented case study are those produced with PETGCF material, with low layer heights (0.1 mm), low annealing temperatures (60 and 70°C), and long annealing times (60 and 90 minutes). Conversely, the least favourable alternatives tend to originate from PETG material, annealed at higher temperatures (90 - 100°C) and for longer durations (60 – 90 minutes).

Camera mounts were fabricated for the DIY drone using the top two alternatives identified through the MCDM analysis. These mounts were subsequently compared with the base mount, which had not undergone the annealing process. The results indicated a notable improvement in achieved tensile force, ranging from 13 to 22 N.

ACKNOWLEDGEMENT

This research was financially supported by the Ministry of Science, Techno-548 logical Development and Innovation of the Republic of Serbia (Contract No. 451-03-47/2023-01/ 549 200109).

REFERENCES

- [1] Zavadskas, E.K., Turskis, Z., Stević, Ž., Mardani, A.: Modelling Procedure for the Selection of Steel Pipes Supplier by Applying Fuzzy AHP Method. *Oper. Res. Eng. Sci. Theory Appl.*, 3, 39–53 (2020).
- [2] Stanković, A., Petrović, G., Marković, D., & Čojbašić, Ž.: Solving Flexible Job Shop

- Scheduling Problem with Transportation Time Based on Neuro-Fuzzy Suggested Metaheuristics. *Acta Polytechnica Hungarica*, 19(4) (2022).
- [3] Stanković, A., Petrović, G., Čojbašić, Ž., Marković, D.: An application of metaheuristic optimization algorithms for solving the flexible job-shop scheduling problem. *Operational Research in Engineering Sciences: Theory and Applications*, 3(3), 13-28 (2020).
- [4] Žižović, M., Miljković, B., Marinković, D.: Objective methods for determining criteria weight coefficients: A modification of the CRITIC method. *Decis. Mak. Appl. Manag. Eng.* 3, 149–161 (2020).
- [5] Mukhametzyanov, I.: Specific character of objective methods for determining weights of criteria in MCDM problems: Entropy. *CRITIC and SD. Decis. Mak. Appl. Manag. Eng.*, 4, 76–105 (2021).
- [6] Pamučar, D., Žižović, M., Biswas, S., Božanić, D.: A new logarithm methodology of additive weights (LMAW) for multi-criteria decision-making: Application in logistics. *Fact. Univ. Ser. Mech. Eng.* (2021).
- [7] Petrović, G.S., Madić, M., Antucheviciene, J. An approach for robust decision making rule generation: Solving transport and logistics decision making problems. *Expert Syst. Appl.*, 106, 263–276 (2018).
- [8] Keshavarz-Ghorabae, M., Amiri, M., Zavadskas, E., Turskis, Z., Antucheviciene, J. Determination of Objective Weights Using a New Method Based on the Removal Effects of Criteria (MERECE). *Symmetry*, 13, 525 (2021).
- [9] Petrović, G., Pavlović, J., Madić, M., Marinković, D.: Optimal Synthesis of Loader Drive Mechanisms: A Group Robust Decision-Making Rule Generation Approach. *Machines*, 10, 329 (2022).
- [10] Brauers, W.K.M.; Zavadskas, E.K. Robustness of MULTIMOORA: A Method for Multi-Objective Optimization. *Informatica*, 23, 1–25 (2012).
- [11] Vinodh, S., Shinde, P.: Parametric Optimization of 3D Printing Process Using MCDM Method. In: Pande, S., Dixit, U. (eds) *Precision Product-Process Design and Optimization. Lecture Notes on Multidisciplinary Industrial Engineering*. Springer, Singapore (2018).
- [12] Chinchankar, S., Shinde, S., Shaikh, A. et al. Multi-objective Optimization of FDM Using Hybrid Genetic Algorithm-Based Multi-criteria Decision-Making (MCDM) Techniques. *J. Inst. Eng. India Ser. D* (2023).
- [13] Chandra, M., Shahab, F., KEK, V. and Rajak, S.: Selection for additive manufacturing using hybrid MCDM technique considering sustainable concepts, *Rapid Prototyping Journal*, Vol. 28 No. 7, pp. 1297-1311, 2022.
- [14] Jagadish, Bhowmik, S. Parameters Optimization of FDM for the Quality of Prototypes Using an Integrated MCDM Approach. In K. Kumar, D. Zindani, & J. Davim (Eds.), *Additive Manufacturing Technologies From an Optimization Perspective*, pp. 199-220, 2019. IGI Global.
- [15] Raigar, J., Sharma, V.S., Srivastava, S. et al.: A decision support system for the selection of an additive manufacturing process using a new hybrid MCDM technique. *Sādhanā* 45, 101, 2020.
- [16] Saaty, T.L.: A scaling method for priorities in hierarchical structures. *J Math Psychol* 15(3):234–281 (1977).
- [17] Saaty, T.L. *The analytic hierarchy process*. McGraw-Hill Company, New York (1980).
- [18] Stojković, J.R.; Turudija, R.; Vitković, N.; Górski, F.; Păcurar, A.; Pleșa, A.; Ianoși-Andreeva-Dimitrova, A.; Păcurar, R. An Experimental Study on the Impact of Layer Height and Annealing Parameters on the Tensile Strength and Dimensional Accuracy of FDM 3D Printed Parts. *Materials* 2023, 16, 4574.



Society of Production
Engineering

SPMS 2023

39. Savetovanje proizvodnog mašinstva Srbije

ICPES 2023

39th International Conference on Production Engineering of
Serbia



Faculty of Technical
Sciences
University of Novi Sad

Novi Sad, Serbia, 26. – 27. October 2023

EFFECTS OF AGING AND REFRESHMENT RATIO ON THE STRENGTH PROPERTIES OF SELECTIVELY LASER SINTERED POLYAMIDE 12

Igor DRSTVENŠEK^{1*}, Rembert DHONDT², Snehashis PAL¹, Tomaž BRAJLIH¹

¹Faculty of Mechanical Engineering, University of Maribor, Smetanova ulica 17, 2000 Maribor, Slovenia, igor.drstvensek@um.si; snehashis.pal@um.si; tomaz.brajlih@um.si

²Jan De Nul nv, Tragel 60, 9308 Hofstade-Aalst, Belgium

*Corresponding author: igor.drstvensek@um.si

Abstract: This study investigated how the tensile properties of selectively laser-sintered polyamide 12 (PA12) specimens are affected by aging and refresh ratio. Starting with a new powder, printing cycles of approximately ten hours were performed, during which tensile and density specimens were printed. After each cycle, the powder was tested for melt flow index (MFI). In the first part, the best processing direction was determined. It was found that tensile strength, modulus of elasticity, elongation at break and MFI showed a linear trend, with the independent variable being the number of hours at elevated temperature. This was analyzed by linear regression. MFI increased with the number of hours at elevated aging, while all other properties mentioned decreased.

Keywords: Polyamide 12, aging, refresh ratio, density, tensile strength, selective laser sintering

1. INTRODUCTION

Selective laser sintering produces a large amount of excess powder. To reuse it, it must be mixed in the correct ratio with the new, unused powder. After several passes of selective laser sintering, the excess powder begins to accumulate, which is associated with a significant cost. The objective of this

study is to economically evaluate the SLS process based on powder utilization efficiency. Optimal utilization of this technology can only be achieved with good powder control.

In the market, SLS is very promising and competitive because it offers great freedom in design and high consistency of mechanical

properties. After each layer is sintered, another layer of powder is applied with a recoater. This new layer is sintered again, leaving the unsintered powder of the previous layers as a support powder [2]. This makes the process a quasi-isothermal process [3]. The surrounding unsintered powder also serves as an insulating layer to ensure uniform cooling and homogeneous crystallization. In this way, the process allows undercuts, holes, and more complex shapes in the products. An important feature of this process is that the unsintered powder can be reused for the next process cycle after sieving. The limitations of this process are the relatively small variety of polymer powders that can be used [4].

Polyamide 12 (PA12) is by far the most commonly used and makes up the bulk of the available literature on SLS printing [5]. This in pure form of PA12 or PA12 compounds, which are almost always used for commercial purposes. In addition, progress and results have been made with other polyamides, elastomeric polymers, and more "exotic" polymers, but these are inherently more limited. Compared to injection molding, the required granulation is much higher, which increases the initial cost of the process [6].

The mechanical properties of SLS products depend on a variety of parameters such as granulation, ageing, degree of refreshment, power density, etc [7]. In this study, the influence of ageing and refreshment ratio is investigated by measuring the melt flow index (MFI) of PA12 powder, tensile strength, elastic modulus, density and to a limited extent dimensional deviation. The focus of this study is more on the ageing process of the powder.

2. EXPERIMENTAL RESEARCH

2.1. Materials

PA12 smooth V2 powder with excellent surface resolution and navy grey in colour has been used to prepare the samples in this study. The powder particle size was 18-90 μm (Mean particle size 38 μm and ISO 13320) which was provided by Sinterit S.P.

2.2. Methods

The cubes and tensile samples were fabricated using Sinterit Lisa PRO SLS machine. The machine is fitted with an infrared laser diode with a power of 5W, the wavelength of the emitted light is 808 nm. The laser scanner type is of the form XY. The important processing parameters are depicted in table 1. Three cubes having a dimension of 1000 mm^3 were fabricated for each testing condition. Three tensile specimens were fabricated for each testing condition and dimensions of a tensile specimen is provided in Fig. 1 which is ISO slandered with number ISO-527-2-5A. The fresh powder undergone multiple print cycles until the mechanical properties are relatively poor.

Table 1. Manufacturing parameters

Layer Height	0.125 mm
Refresh ratio	25%
Print bed temperature	177.5 °C
Print chamber temperature	140°C
Laser power ratio	1.00
Energy scale laser power	1.30
Max energy / cm^3 , infill	250.0
Cooldown time	5400 s

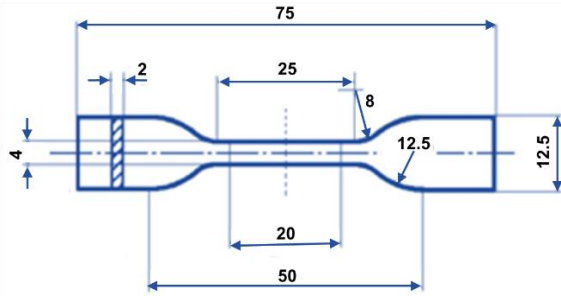


Figure 1. Dimensions of the tensile specimen. All the dimensions are in mm.

Three different orientations were chosen: 0 ° (horizontal), 45 ° (oblique) and 90 ° (vertical), keeping the main axis of the tensile specimens horizontal (see Fig. 2). However, after each printing cycle, the parts are manually cleaned and glass bead blasted to remove loosely bound, unsintered PA12 particles adhering to the surfaces of the specimens. The remaining powder from the overflow container, the conveyor bed and the support powder around the specimens is sieved for eighteen minutes with a sinterite powder sieve.

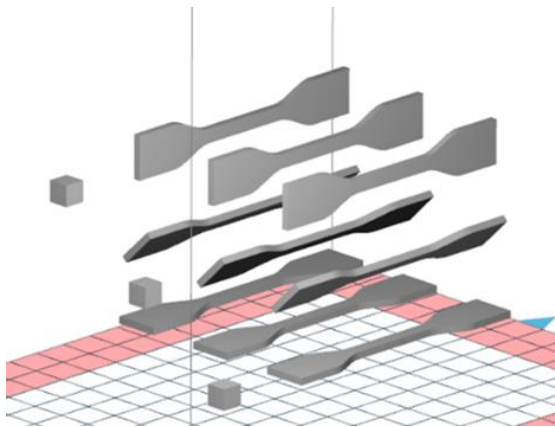


Figure 2. Tensile specimen orientation

A test apparatus according to the standard SIST EN ISO 1133-2012 was used to measure the mass flow rate. The temperature was set at 210°C and a weight of 5 kilograms was used. MFR could be calculated by measuring the elapsed time of extrusion of 0.711 cm³ of compressed PA12,

which was in the barrel for five minutes to ensure homogeneous melt. The MFI was calculated by using equation (1) expressed in cm³ per ten minutes. Where A is the volume of that is extruded by the piston, a correction factor of 600 to transform the equation to cm³ per ten minutes, l is the length of the cylinder and t the elapsed time.

$$MVRT(T, m_{nom}) = \frac{A * 600 * l}{t} \quad (1)$$

After each completion of fabrication, all the above measurements were taken and recorded. Once the exhaustion point was determined, a nominal operating point was defined with a specific MFI. The data from the MFI was then used to apply a refresh ratio to the aged and exhausted powder to achieve the nominal operating point. A tumbler was used to homogeneously mix virgin and aged powder for up to two hours and retest which was done incrementally. After the nominal MFI was reached, a new print cycle of ten hours was performed to determine if the mechanical properties are back to the same values. To reach this nominal point with the MFI, incremental steps of the refresh ratio were applied, with tumbling mixing between each step. After fabricating with the refreshed powder, another final production cycle was processed by applying a refresh ratio of 30 % to the last mixed powder and hence, another ten more hours of aging was applied.

3. RESULTS AND DISCUSSION

3.1 Fabricating orientation

Table 2 listed the values of ultimate tensile strength (UTS) and elongation at break (EaB) of the tensile specimens which were fabricated in the first step of the study where their stress-strain curves are given in Fig. 3. The absolute deviation of the

dimensions in thickness was on average 5.1 % from the desired dimension, which was similar for the other orientations. With an average deviation of 4.1 % for the horizontal print and 8.6 % for the vertical samples (rotated 90 °). The absolute deviation of the 45 ° rotated samples for width was on average only 0.3 %, while for the horizontal and vertical samples it was on average 6.1 % and 1 % respectively. Eventually, in the first step, the best orientation with the best mechanical properties was found to be an angular orientation of 45 ° rotation.

Table 2. Ultimate tensile strength (UTS) and elongation at break (EaB) of the tensile specimens in the first step of the study

Samples	UTS (in MPa)	EaB (in %)
1. Horizontal	46.9	11.1
2. Horizontal	51.4	7.6
3. Horizontal	41.3	6.8
4. Vertical	50.3	8.7
5. Vertical	45.9	8.6
6. Vertical	45.5	9.6
7. 45° angled	50.5	10.5
8. 45° angled	54.6	8.4
9. 45° angled	57.1	9.7

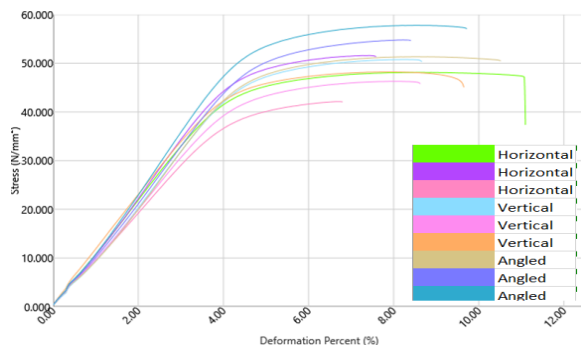


Figure 3. Stress-strain curves of the tensile specimens fabricated in the first step of the study.

3.2. Aging effect

Table 3 provided an overview of aging exposed hours and their effects on the metallurgical properties. A total of ten fabricating runs were made with a fabricating time of about nine to ten hours each. It is important to note that each cycle includes a warm-up time and a cool-down time, so the exposure time reported here is not at an elevated temperature of a constant 177.5 ° C, the printing temperature, and that each column represents the average of several measurements. Density, tensile strength, and Young's modulus show a clear downward trend. The MFI measurements show a clear upward trend.

Each data set can be analyzed with linear regression models to determine significance and trend. It should be noted that this model assumes a direct correlation between the two variables, with the x-values representing the independent variable and the y-values representing the dependent values. Linear relationship, normally distributed dispersion, homoscedasticity, independent observations and no uncertainty in predictors are other assumptions of linear regression. The coefficient of determination (r^2) indicates how much of the trend in the data set can be correctly predicted by the linear regression model. It is a value between 0 and 1, with lower values representing a worse fit and higher values representing a better fit. Using the goodness of fit section can be an indication how close the relationship is. R-squared quantifies the percentage of variation in Y that can be explained by the value of X. If the slope is significantly non-horizontal, there is reason to believe that X can be used to predict Y, referring specifically to the slope parameter or tangent. If it is not, the line of the model is no better than no line at all, so the model will not be very useful. The P-values also help

with interpretation. Here, if it is smaller than a certain threshold, the model indicates a statistically significant relationship [8]. The threshold here is set at 5% or 0.05. Linear

regression of the density, UTS, and Young's moduli data sets with the number of hours of exposure for each set as x-values gives the following results.

Table 3. Aging exposed hours and their effects on the metallurgical properties.

Exposed (hours)	Density (g/cm ³)	MFI	tensile strength (MPa)	young's modulus (MPa)	Elongation at Break (%)	absolute deviation thickness (%)	absolute deviation width (%)
0	-	13.11	-	-	-	-	-
11	1.026	13.73	50.13	1656.38	9	5.17	0.34
22.5	0.999	13.91	40.16	1391.43	7.56	2.33	1.08
31.5	0.978	16.56	38.96	1192.18	8.26	2.33	1.08
40.333	0.960	18.88	34.1	1116.19	8.2	2.17	0.83
50	0.977	18.49	35.26	1142.98	7.4	3.5	1
59	1.001	18.9	40.93	1258.65	7.96	3.5	2.33
68	0.978	21.15	34.6	1016.55	8.3	5.5	2,17
77	0.964	21.37	31.06	1016.8	7.45	4.5	1.08
85	0.955	21.95	29.2	962.73	7.26	3.33	2.58
95	0.963	22.89	30.3	947.55	7.4	2.67	1.92

Fig. 4 shows the linear regression model from the hours exposed-density data set, the graph shows a significant deviation from a horizontal line. The model is defined as $Y = -0.0005758 \times X + 1.012$, with an r^2 value of 0.5113, indicating that the fit is neither good nor bad, which could be explained by the small deviations in the data. A p -value of 0.0201 indicates a statistically significant relationship.

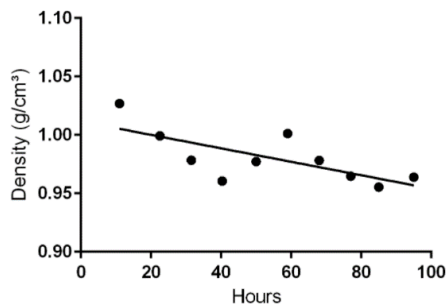


Figure 4. Linear regression hours exposed vs. density

Fig. 5 shows the linear regression model of the ultimate tensile strength defined as $Y = -0.1915 \times X + 46.80$ with an r^2 coefficient of 0.7126 which implies a reasonably good fit. A significant deviation from the horizontal can also be seen. A p -value of 0.0021 strongly suggests a statistically significant relationship.

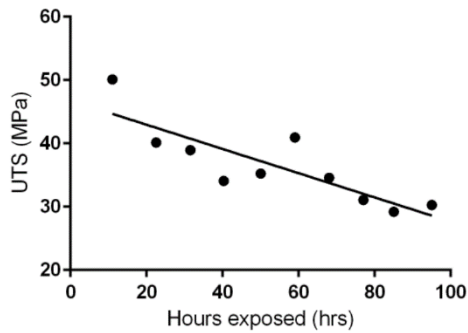


Figure 5. Linear regression hours exposed vs. UTS

The linear regression model for the Young's modulus is shown in Fig. 6 and is defined as $Y = -6.960 \times X + 1546$ with an r^2 value of 0.7695. The deviation from horizontal is significant. A p -value of 0.009 strongly suggests a statistically significant relationship.

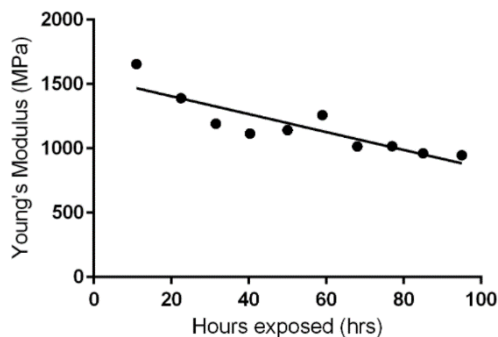


Figure 6. Linear regression hours exposed vs. Young's modulus

For the melt flow index the model is shown in Fig. 7 and defined by $Y = 0.1104 \times X + 12.85$. The deviation from the horizontal is significant and the r^2 value is 0.9520. A p -value of less than 0.0001 strongly suggests a statistically significant relationship.

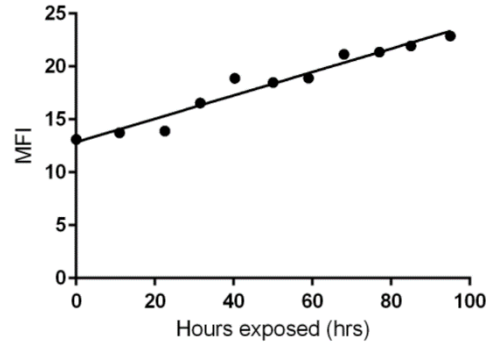


Figure 7. linear regression hours exposed vs. MFI

3.3. Refresh ratio

These values imply that these models acceptably correlate the exposed hours and the MFI value, UTS, Young's modulus, and density as linear dependent variables. The elongation at break and absolute deviations for thickness as well as for width do not initially give the impression of a downward or upward trend, but seem to be rather constant in general, but the linear regression suggests otherwise. For EaB and absolute deviation for width, the models are defined as $Y = -0.01353 \times X + 8.671$, $r^2 = 0.4979$, $p=0.0338$ and $Y = 0.01887 \times X + 0.3718$, $r^2=0.5405$, $p=0.02450$, respectively, indicating that there is a correlation. However, the absolute deviations of the thickness show a non-significant curve with an r^2 value of 0.0049, which is too low to speak of a correlation. In addition, the MFI was measured of the Sinterit PA12 Smooth starter powder as a reference. This powder is supplied by Sinterit for mixing with virgin material for the first print after which the normal refreshing ratios can be applied. The MFI was measured at 20.25, which, if the other data is consulted, suggests an aging time or exposure time of about 60 hours at elevated temperatures. This is not stated in the Sinterit data sheet. Here, a nominal operating point of UTS of 35 MPa is chosen.

This gives an EaB of 7.5 to 8 percent and an MFI between 18.5 and 19. By gradually refreshing the aged powder, as mentioned earlier, this MFI value is approximated and then tested. It resulted in a stop of adding virgin powder when this point was reached and Table 3 is provided after recalculating the refreshing ratio.

Table 3. Refreshing ratio

Applied refreshing ratio (in%)	MFI
9.09	22.97
16.65	21.61
23.07	20.50
28.58	20.15
33.33	19.13

4. CONCLUSION

In this study, the influence of aging and refreshing ratio on the mechanical properties of PA12 was investigated. An angled orientation of 45° degrees rotated by keeping the major axis horizontal of the tensile specimens was obtained as the best orientation.

Linear regression analyzes of the results yielded models that can relate the number of hours the powder is exposed to elevated temperatures to a number of properties. Since ultimate tensile strength and melt flow index show a credible linear dependence on the number of hours the powder has been aged, it can be said that these two values can be indicative of each other.

The melt flow index, ultimate tensile strength and the Young's modulus show a clear trend with acceptable probability. Density, elongation at break and absolute dimensional deviation in width show a plausible linear dependence on the hours the powder was exposed to elevated temperatures.

By applying a refresh ratio to the aged powder, the melt flow index of this working point was approximated by intermediate measurements of the melt flow index of the powder. The linear regression model suggests a linear dependence with high plausibility, with the refreshing ratio as the independent variable and the melt flow index as the dependent variable.

When the melt flow index of the working point was reached, a new print cycle was performed and the same measurements as before were recorded. This showed that it is possible to obtain good mechanical properties if a sufficient refreshing ratio is applied.

In a final test, another refresh ratio was applied to this refreshed powder, which now had an additional aging time. The mechanical properties of this last printout showed that by applying a refreshing ratio after each cycle, the properties slightly decrease. It can be said that the powder has changed from virgin to reused polyamide 12 powder.

ACKNOWLEDGEMENT

The authors acknowledge the financial support from the Slovenian Research Agency (Research Core Funding No. P2-0157, Research Project J1-2470 Biofunctionalization of 3D-printed metal alloys as a newly emerging strategy to diminish undesired effects of orthopedic implants, Research project J3-9262 Advanced surface finishing technologies for antibacterial properties of patient-specific 3D-printed implantable materials). This project has also received funding from the European Union's Horizon 2020 research and innovation program under grant agreement No. 788361.

REFERENCES

- [1] Van Hooreweder, B.; De Coninck, F.; Moens, D.; Boonen, R.; Sas, P. Microstructural Characterization of SLS-PA12 Specimens under Dynamic Tension/Compression Excitation. *Polym. Test.* 2010, 29, 319–326, doi:10.1016/j.polymertesting.2009.12.006.
- [2] Schneider, J.; Kumar, S. Multiscale Characterization and Constitutive Parameters Identification of Polyamide (PA12) Processed via Selective Laser Sintering. *Polym. Test.* 2020, 86, 106357, doi:10.1016/j.polymertesting.2020.106357.
- [3] Zhao, M.; Wudy, K.; Drummer, D. Crystallization Kinetics of Polyamide 12 during Selective Laser Sintering. *Polymers (Basel)*. 2018, 10, doi:10.3390/polym10020168.
- [4] Goodridge, R.D.; Hague, R.J.M.; Tuck, C.J. Effect of Long-Term Ageing on the Tensile Properties of a Polyamide 12 Laser Sintering Material. *Polym. Test.* 2010, 29, 483–493, doi:10.1016/j.polymertesting.2010.02.009.
- [5] Rosso, S.; Meneghello, R.; Biasetto, L.; Grigolato, L.; Concheri, G.; Savio, G. In-Depth Comparison of Polyamide 12 Parts Manufactured by Multi Jet Fusion and Selective Laser Sintering. *Addit. Manuf.* 2020, 36, 101713, doi:10.1016/j.addma.2020.101713.
- [6] Van Hooreweder, B.; Moens, D.; Boonen, R.; Kruth, J.P.; Sas, P. On the Difference in Material Structure and Fatigue Properties of Nylon Specimens Produced by Injection Molding and Selective Laser Sintering. *Polym. Test.* 2013, 32, 972–981, doi:10.1016/j.polymertesting.2013.04.014.
- [7] Caulfield, B.; McHugh, P.E.; Lohfeld, S. Dependence of Mechanical Properties of Polyamide Components on Build Parameters in the SLS Process. *J. Mater. Process. Technol.* 2007, 182, 477–488, doi:10.1016/j.jmatprotec.2006.09.007.
- [8] Draper, N.R.; Smith, H. *Applied Regression Analysis*; 3rd ed.; Wiley, 1998; ISBN 978-0-471-17082-2.



Society of Production
Engineering

SPMS 2023

39. Savetovanje proizvodnog mašinstva Srbije

ICPES 2023

39th International Conference on Production Engineering of
Serbia



Faculty of Technical
Sciences
University of Novi Sad

Novi Sad, Serbia, 26. – 27. October 2023

CHARACTERISTICS OF PARTIALLY MELTED POWDER PARTICLES IN LASER POWDER BED FUSION

Snehashis PAL^{1,*}, Matjaž FINŠGAR², Janez GOTLIH¹, Tomaž BRAJLIH¹, Prabas BANERJEE³,
Özkan YAPAR¹, Gorazd LOJEN¹, Tonica BONČINA¹, Igor DRSTVENŠEK¹

¹Faculty of Mechanical Engineering, University of Maribor, Slovenia

²Faculty of Chemistry and Chemical Engineering, University of Maribor, Maribor, Slovenia

³Department of Mechanical Engineering, National Institute of Technology Durgapur, Durgapur,
India

*Corresponding author: snehashis.pal@um.si

Abstract: This study investigated the properties of the partially melted powder particles and their plausible effects on the mechanical and corrosive properties of a product fabricated by the Laser Powder Bed Fusion process. Scanning electron microscopy images of the surfaces and pores analysed when particles were adherent and their microstructures even when a particle was fully enclosed in the melt pool. In this study, Ti-6Al-4V was considered, where the range of powder particles was between 10–45 μm and the thickness of the built-up layer was 25 μm . Different combinations of laser powers and scanning speeds were chosen according to the melting, mixing and solidification characteristics. Several partially melted powder particles created microcracks and increased the corrosive surface area. Moreover, their microstructures differed from those of the core area of the product. Fully integrated particles and mostly melted particles were also found using microstructure analysis. The results suggest potential innovative applications for complex designed products where these particles are difficult to remove and for bone implantation to improve osseointegration.

Keywords: Adhered powder particle; partially melted particle; Ti-6Al-4V; porosity; microcrack; microstructure; surface; selective laser melting

1. INTRODUCTION

Additive Manufacturing (AM) is considered the best manufacturing process in Industry 4.0 [1]. AM offers high manufacturing flexibility for custom production [2]. It can replicate a Computer-Aided Design (CAD) model into a real product by making it layer by layer fabrication process [3]. A wide range of materials can be produced. Even refractory and highly flammable metals can be easily produced with

AM [4]. Moreover, it is possible to alloy metals with high melting points and chemical affinity in-situ [5]. This makes it particularly attractive for manufacturers to produce their components for aerospace, automotive, mould making and biomedical applications [6], [7]. Although several AM technologies are available for the production of metal parts, Laser Powder Bed Fusion (LPBF), also known as selective laser melting, is the most preferred process by manufacturers [8].

In the LPBF process, metallic powder particles are fused together after melting, mixing and solidifying, track by track and layer by layer, to form a component [9]. Many powder particles adhere to the surface of the product as well as in the pores of the product during fabrication [8]. Since the powder particles adhere to the component by partial melting, they are difficult to remove, especially from parts with complex designs [10]. On the other hand, they must remain on the implant surface in this way to improve osseointegration [11]. However, these particles contribute to surface corrosion broadly and create microcracks [9]. As they partially melt, their bond to the part and their microstructure are different from that of the core part [12].

Titanium alloys such as Ti-6Al-4V are one of the most attractive alloy groups whose materials can be easily machined and processed into the desired product using LPBF. The Ti-6Al-4V alloy has a high strength to weight ratio and high corrosion resistance [13]. It is also considered highly biocompatible and is therefore widely used in biomedical prostheses, especially for load bearing and permanent bone implantation [14]. The LPBF process is considered the best process for manufacturing parts from the Ti-6Al-4V alloy because of its high melting temperature, high chemical affinity and low thermal conductivity [15]. On the other hand, the LPBF process offers some better and controllable metallurgical properties compared to the casting process [16].

There is a large body of research in the literature on mechanical and corrosion properties, including density, porosity and metallography for the same material fabricated by LPBF. However, there is only a limited amount of literature dealing with adherent and partially melted powder particles and their effects on these properties. Therefore, this study investigated the properties of powder particles adhering to the product by partial melting and their plausible effects on mechanical and corrosive properties.

2. MATERIALS AND METHODS

2.1 Material

Completely dense Ti-6Al-4V powder of grade 23 with a diameter between 5 and 45 μm , which was provided by Dentaurum GmbH & Co. KG (Germany), was used to fabricate the samples. The chemical composition of the supplied material was 90% Ti, 6% Al, 4% V and less than 1% N, C, H, Fe, O, together. The Scanning Electron Microscopy (SEM) images of the powder particles can be seen in Figure 1, where different sizes of the particles can be observed.

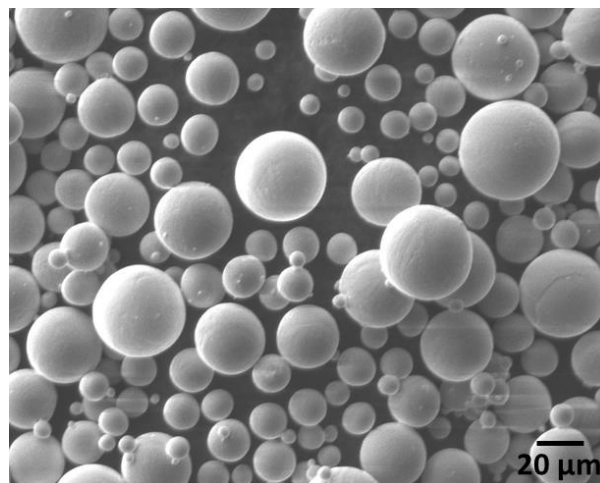


Figure 1. SEM image of Ti-6Al-4V powder.

2.2 Methods

2.2.1. Sample preparation

Several cubic specimens with a size of 8×8×8 mm³ were fabricated with different laser powers, scanning speeds, hatch spacings and volumetric energy densities. Laser power varied between 55 W and 95 W and scanning speed between 150 mm/s and 1000 mm/s. The hatch spacing varied considering the web overlap. While the web overlap increased from 10% to 55%, the hatch space decreased from 0.099 mm to 0.0495 mm. The diameter of the laser beam was 0.110 mm. The volumetric energy density varied from 39 J/mm³ to 260 J/mm³. The Yb:glass fiber laser from IPG, Germany, was used and the laser was focused perpendicular to the working plane using a telecentric f-theta lens. However, all these parameters showed that the powder particles were partially melted and adhered to the vertical surface. However,

when the laser power was lowered to 65 W and 55 W, the partially melted particles in the pore had decreased significantly. The samples were set up with a 2 mm high support, keeping the base plane horizontal. Therefore, the four vertical surfaces are where most of the partially melted particles can adhere.

2.2.2. Porosity and microstructure performances

The porosity of the sample was checked using SEM images. The samples were ground 2 mm and then polished to expose the surface for conducting the test. After taking the porosity images, the polished surfaces were etched with Kroll's reagent. 100 mL of Kroll's reagent was prepared from 2 mL HF, 6 mL HNO₃ and 92 mL distilled water and the exposed surface was immersed in it for 30 seconds. The etched surfaces of the sample were examined with field emission scanning electron microscopes (FE-SEM).

3. RESULTS AND DISCUSSION

3.1 Classification of partially melted powder particles

The characteristics of melting of the powder particles and their amount of melting differ considerably. Taking into account the degree of melting, they have been classified here into three categories, namely 'less melted', 'medium melted' and 'mostly melted' powder particles. 'Less melted' refers to the partially melted powder particles, of which only a small part is melted. In the case of moderately melted powder particles, about half of the powder is melted. 'Mostly melted' powder particles belong to those particles that are largely or almost completely melted, but have not mixed well with the melt pool. An example of all these partially melted powder particles is shown in Figure 2. All these particles adhered strongly to the surface or remained in the pores of a product. The particles with a very small amount of melting were not considered in this study

because they can be easily removed from the surface. When these particles remain in the pores, they mainly contribute to the weight of the sample but not to the mechanical or corrosive properties, unless they have been touched by the corrosive agent after the corrosion of the large amount of the component.

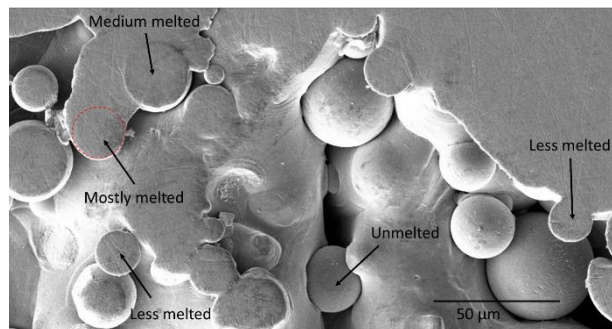


Figure 2. An ideal example of a pore containing all kinds of partially melted powder particles.

In Figure 2, two less molten particles are marked, one attached to the side of the main consolidation area and the other seen at the bottom. However, neither of these were removed when the sample was ground and polished. Although the particles attached to the side were less likely to detach, the other particle was more likely to lose the bond. So the less molten particles also had a strong bond with the solidified melt pool.

3.2 Inside pores

All kinds of the above-mentioned partially melted powder particles are observed in various pores. Some of them have not caused cracking and may or may not affect in crack initiation under mechanical loading. On the other hand, some of them have already created a microcrack. Some of them can be observed to act as stress concentrators under load. Figure 3 shows two types of mostly melted powder particles, one of which has created a microcrack and the other of which has not created a crack but has a high probability of accumulating stress under mechanical loading [15]. On the other hand, Figure 2 shows that a mostly melted particle has neither produced a crack nor is likely to form a stress concentration zone. Figure 4 shows a less melted particle that does not contribute to the formation of microcracks

and also does not initiate a crack that will affect the product when loaded.

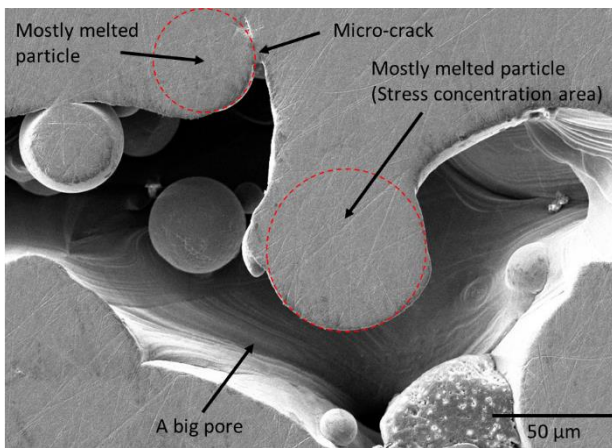


Figure 3. A pore containing mostly melted powder particles, one of which has produced a microcrack, while the other can accumulate stress under mechanical loading.

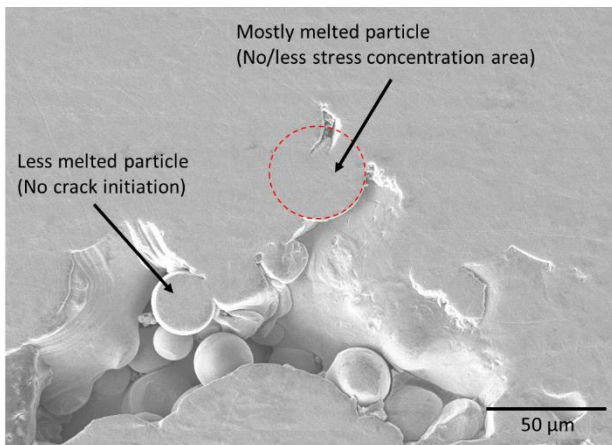


Figure 4. A pore containing a mostly melted and a less melted powder particle without a crack.

There are several different mechanisms for the formation of such partially melted powder particles. One of these mechanisms is shown in Figure 5. If two successive melt pools belonging to two successive tracks are smaller than the sufficient melting of all the powder needed, some particles may partially melt and adhered to one melt pool. This insufficient melting zone creates an irregularly shaped pore and contains some partially melted particles. If a mostly melted or medium melted particle is at the top of this pore, there is a good chance that a microcrack will form. A medium-melted particle was melted and bonded strongly with the melt pool. During the rapid cooling of the melt pools, they shrink much faster than the particle and so a stress is created at the contact

surface of the melt pool and the particle. While a particle melts most of its volume, it may increase its volume due to thermal expansion. However, the same situation can also occur during solidification and rapid cooling. These particles also form a corner point in the pore that causes creaking under load.

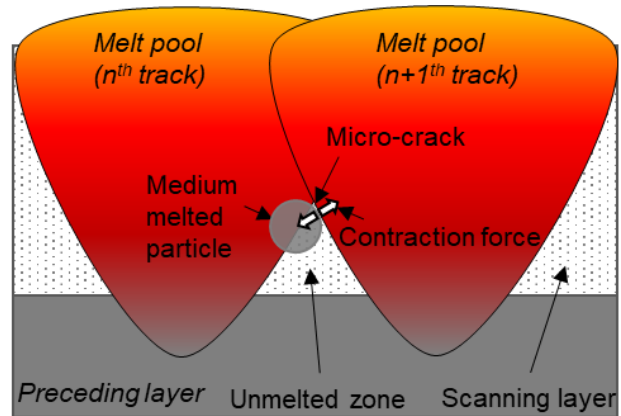


Figure 5. Formation of microcracks by a medium melted powder particle.

Figure 6 shows another mechanism of the formation of mostly melted powder particles. While a powder particle has recently entered the melt pool, it may not yet have melted enough to mix with the melt pool. This particle appears to be fully melted and mixed with the melt pool, but it remains in the melt pool and contributes to different metallurgical properties. Figure 6(d) shows the microstructure of one of these mostly melted particles, and it can be observed that the microstructure is different from the other areas of the part. Therefore, different mechanical properties as well as different corrosion behaviour can be seen. The mechanism of mixing these types of mostly melted particles with the melt pool is depicted in Figure 6(a)-(c). Figure 6(a) shows a particle adhering to the melt and entering the melt pool. On the other hand, the vortex inside the melt pool is known to flow down at the verticle surface areas of the pool as shown in Figure 6(a) [17]. As the particle enters, it flows downwards with the help of the vortex, as shown in Figure 6(b). On the other hand, the melt pool solidifies rapidly from the bottom to the top [18]. Therefore, the particle may not get enough time to melt and mix with the melt pool. Therefore, it remains as a mostly melted particle, as shown in Figure 6(c). Since it does not mix with the

molten material in the melt pool, it is left with a different microstructure. A cellular microstructure can be observed on the surface region. However, the microstructure and grain formation are not associated with the melt pool materials.

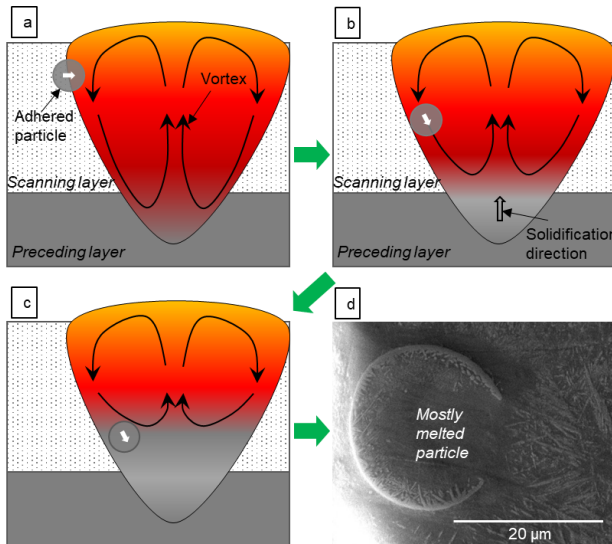


Figure 6. Mostly melted powder particles entrapment by the melt pool, (a) adhesion of a particle to the melt pool, (b) downward flow of the melt pool with the aid of vortex, (c) cooling due to rapid solidification of the melt pool from the bottom to the top, and (d) microstructure image of a mostly melted powder particle trapped by the melt pool.

3.3 On the surface

Numerous adherent partially melted powder particles were observed on the vertical surface of the samples. The vertical surface refers to the surfaces that are perpendicular to the XY plane, where Z is the built up direction of the samples. However, all types of partially melted particles can be observed adhering to the vertical surface as shown in Figure 7. While scanning the contours, the outer surface was filled with powder, so the particles could easily stick to the surface. After adhering, the particles started to melt due to the heat of the corresponding melting bath. However, depending on how long the adhesion took from the formation of the melt pool to solidification, a particle was melted. So if a particle adhered to the melt pool at the beginning, it most likely melted most of the volume. If a particle adheres later, it may be

medium or less melted. In addition, these phenomena may also depend on the time of cooling. The cooling time also depends on the scanning speed and less on the laser power. Thus, when the laser power and scanning speed decrease, the porosity of the partially melted powder particles decreases. Although the surface absorbed a similar amount of partially melted powder particles under these conditions, a higher amount of mostly melted particles was observed. This is due to the fact that there was sufficient time to melt most portion of the particles.

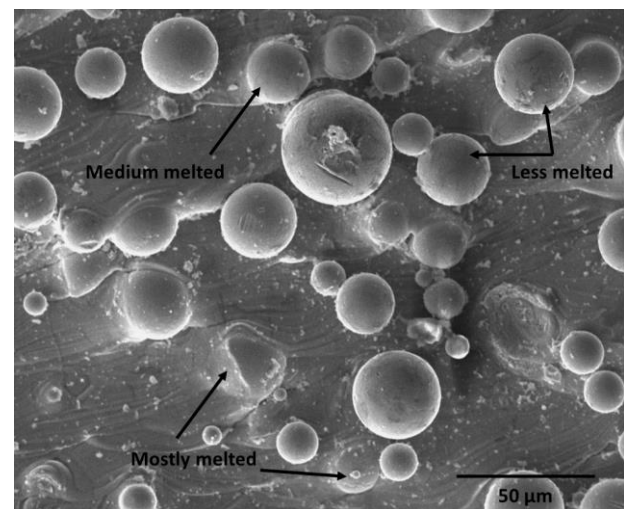


Figure 7. Several types of partially melted powder particles adhering to the vertical surface of a sample.

Several micro-cracks have developed among the mostly melted particles, as can be seen in Figure 8 (d). A crack is located between the connecting surface between the particles and the melt pool. The mechanism for the formation of such cracks is shown in Figure 8(a)-(c). As a particle adheres to the melt or enters the melt pool, the particle is pulled by the vortex flow as shown in Figure 8(a). As the vortex flows downwards at the surface of the melt pool, the particles also move downwards. On the other hand, solidification occurs from the bottom to the top of the melt pool. Therefore, the bottom cools faster than the partially melted particles. Therefore, a contraction force occurs from the bottom of the melt pool and the particles remain mostly the same. This contraction force separates the molten materials from the surface of the particles [8], as shown in Figure

8(b), a side view. However, the front view of the crack can be seen in Figure 8(c) and a SEM image of such a micro-crack can be observed in Figure 8(d).

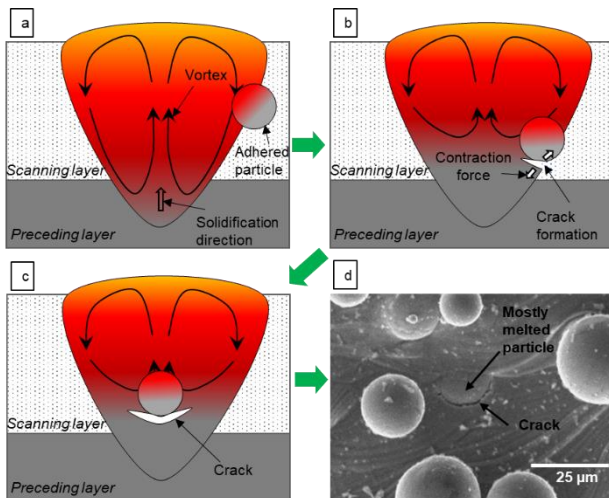


Figure 8. Mechanism of micro-crack formation by the mostly melted powder particles, (a) adhesion of a powder particle to a melt pool, (b) crack formation – side view, (c) a crack – front view, (d) SEM image of a crack by the mostly melted particles on the vertical surface of a sample.

As already shown, the microstructures of the partially powder particles differed from those of the main part of the product, they contribute to a different corrosion resistance [12]. The cooling rate between less melted and mostly melted particles is very different. Therefore, their microstructure also varied depending on the amount of melting and the amount that enters the melt pool. Thus, both their microstructure and their corrosion properties vary over a wide range. Furthermore, they also have different surface areas, which also changes the area in which they are exposed to the corrosive environment.

4. CONCLUSIONS

Additive The formation of partially melted powder particles in the Laser Powder Bed Fusion (LPBF) process and their functions are explained elaborately in this article. Three types of partially melted particles were identified for the fabrication of Ti-6Al-4V alloys and their properties were observed from cross-sectional images, surface images and microstructures. These partially fused powder

particles are referred to as less melted, medium melted and mostly melted powder particles. The following conclusions can be drawn from the current study.

- i. The partially melted particles are mainly located in the pores and on the vertical surface of the product.
- ii. The medium and mostly melted particles can create micro-cracks during manufacturing.
- iii. These partially melted particles can be responsible for the initiation of microcracks during mechanical stress.
- iv. The mostly melted particles can enter the melt pool, but they cannot mix completely with the molten metal and therefore their microstructure is also different from the surrounding metal.
- v. The microstructures of the different types of partially melted particles are different and therefore their corrosion resistance is also different.

ACKNOWLEDGEMENT

The Slovenian Research and Innovation Agency provided funding for the study in the form of grants (P2-0118, P2-0137, P2-0157, P2-0120, J1-2470, and I0-0029).

REFERENCES

- [1] B. Elhazmiri, N. Naveed, M. N. Anwar, and M. I. U. Haq, "The role of additive manufacturing in industry 4.0: An exploration of different business models," *Sustain. Oper. Comput.*, vol. 3, pp. 317–329, 2022, doi: 10.1016/j.susoc.2022.07.001.
- [2] A. A. Alogla, M. Baumer, C. Tuck, and W. Elmadih, "The impact of additive manufacturing on the flexibility of a manufacturing supply chain," *Appl. Sci.*, vol. 11, no. 8, 2021, doi: 10.3390/app11083707.
- [3] S. Pal, G. Lojen, V. Kokol, and I. Drstvensek, "Evolution of metallurgical properties of Ti-6Al-4V alloy fabricated in different energy densities in the Selective Laser Melting technique," *J. Manuf. Process.*, vol. 35, pp. 538–546, Oct. 2018, doi: 10.1016/j.jmapro.2018.09.012.
- [4] C. Wang *et al.*, "Effect of pore geometry on

- properties of high-temperature oxidized additively manufactured magnesium scaffolds," *J. Magnes. Alloy.*, 2023, doi: 10.1016/j.jma.2023.08.016.
- [5] S. Pal *et al.*, "Mechanisms of defect formation in Ti-6Al-4V product during re-melting of layers in selective laser melting," *J. Manuf. Process.*, vol. 105, pp. 260–275, 2023, doi: 10.1016/j.jmapro.2023.09.044.
- [6] A. H. Alami *et al.*, "Additive manufacturing in the aerospace and automotive industries: Recent trends and role in achieving sustainable development goals," *Ain Shams Eng. J.*, vol. 14, no. 11, p. 102516, 2023, doi: <https://doi.org/10.1016/j.asej.2023.102516>.
- [7] I. Drstvenšek, F. Zupanič, T. Bončina, T. Brajljih, and S. Pal, "Influence of local heat flow variations on geometrical deflections, microstructure, and tensile properties of Ti-6Al-4 V products in powder bed fusion systems," *J. Manuf. Process.*, vol. 65, pp. 382–396, 2021, doi: <https://doi.org/10.1016/j.jmapro.2021.03.054>.
- [8] S. Pal *et al.*, "As-fabricated surface morphologies of Ti-6Al-4V samples fabricated by different laser processing parameters in selective laser melting," *Addit. Manuf.*, vol. 33, p. 101147, Mar. 2020, doi: 10.1016/j.addma.2020.101147.
- [9] S. Pal, G. Lojen, N. Gubelj, V. Kokol, and I. Drstvenšek, "Melting, fusion and solidification behaviors of Ti-6Al-4V alloy in selective laser melting at different scanning speeds," *Rapid Prototyp. J.*, vol. 26, no. 7, pp. 1209–1215, Jun. 2020, doi: 10.1108/RPJ-07-2019-0206.
- [10] R. Ramadani *et al.*, "Topology optimization and additive manufacturing in producing lightweight and low vibration gear body," *Int. J. Adv. Manuf. Technol.*, vol. 113, pp. 3389–3399, 2021, doi: 10.1007/s00170-021-06841-w.
- [11] S. Pal, Z. Peršin, T. Vuherer, I. Drstvenšek, and V. Kokol, "The Effect of Ti-6Al-4V Alloy Surface Structure on the Adhesion and Morphology of Unidirectional Freeze-Coated Gelatin," *Coatings*, vol. 10, no. 5, p. 434, Apr. 2020, doi: 10.3390/coatings10050434.
- [12] S. Pal, M. Finšgar, T. Bončina, G. Lojen, T. Brajljih, and I. Drstvenšek, "Effect of surface powder particles and morphologies on corrosion of Ti-6Al-4 V fabricated with different energy densities in selective laser melting," *Mater. Des.*, vol. 211, p. 110184, 2021, doi: <https://doi.org/10.1016/j.matdes.2021.110184>.
- [13] J. Zhao *et al.*, "Study on mechanical properties of Ti-6Al-4 V titanium alloy with different microstructures under combined tension-bending load," *J. Alloys Compd.*, vol. 936, p. 168201, 2023, doi: 10.1016/j.jallcom.2022.168201.
- [14] A. N. Aufa, M. Z. Hassan, and Z. Ismail, "Recent advances in Ti-6Al-4V additively manufactured by selective laser melting for biomedical implants: Prospect development," *J. Alloys Compd.*, vol. 896, p. 163072, 2022, doi: 10.1016/j.jallcom.2021.163072.
- [15] S. Pal *et al.*, "Tensile properties of selective laser melting products affected by building orientation and energy density," *Mater. Sci. Eng. A*, vol. 743, pp. 637–647, Jan. 2018, doi: 10.1016/J.MSEA.2018.11.130.
- [16] W. Zhang, X. Shang, S. Chen, and L. Zhang, "Comparison of microstructural characteristics and mechanical properties of the high-strength low-alloy steels fabricated by wire arc additive manufacturing versus conventional casting," *Mater. Sci. Eng. A*, vol. 885, p. 145593, 2023, doi: 10.1016/j.msea.2023.145593.
- [17] E. Li, Z. Zhou, L. Wang, H. Shen, R. Zou, and A. Yu, "Particle scale modelling of melt pool dynamics and pore formation in selective laser melting additive manufacturing," *Powder Technol.*, vol. 397, p. 117012, 2022, doi: 10.1016/j.powtec.2021.11.056.
- [18] S. Pal, T. Brajljih, and I. Drstvenšek, "Physical Behaviors of Materials in Selective Laser Melting Process," in *DAAAM International Scientific Book 2018*, 2018, pp. 239–256. doi: 10.2507/daaam.scibook.2018.21.



Society of Production
Engineering

SPMS 2023

39. Savetovanje proizvodnog mašinstva Srbije

ICPES 2023

39th International Conference on Production Engineering of
Serbia



Faculty of Technical
Sciences
University of Novi Sad

Novi Sad, Serbia, 26. – 27. October 2023

RAZVOJ 3D ŠTAMPAČA TIPRA FGF

Milan KOLAREVIĆ¹, Stefan PAJOVIĆ¹, Vladan GRKOVIĆ¹, Boško NIKOLIĆ¹, Milan PEROVIĆ¹

¹ Fakultet za mašinstvo i građevinarstvo u Kraljevu Univerziteta u Kragujevcu, Srbija,
kolarevic.m@mfkv.kg.ac.rs, pajovic.s@mfkv.kg.ac.rs, grkovic.v@mfkv.kg.ac.rs,
nikolicbosko01@gmail.com, milan.perovic01@gmail.com

Apstrakt: U radu je prikazan razvoj 3D štampača tipa FGF dimenzija radnog prostora 500x500x500 mm. Štampač je razvijen u Studentskoj radionici Fakulteta za mašinstvo i građevinarstvo u Kraljevu u okviru studentskih aktivnosti i izrade završnih radova na studijskom programu Mašinsko inženjerstvo. Detaljan plan projekta je urađen uz korišćenje softvera Microsoft Project. Definisana je redosled neophodnih aktivnosti, njihove međuzavisnosti, potrebni resursi i analiza troškova projekta.

Idejno rešenje je urađeno na osnovu uporedne analize već postojećih tehničkih rešenja 3D štampača i njihovih prednosti i nedostataka. Na osnovu donetih zaključaka formiran je niz zahteva koje je potrebno implementirati prilikom projektovanja novog tehničkog rešenja. U okviru razvoja sprovedene su sledeće aktivnosti: definisanje kinematske strukture mašine, detaljno projektovanje, upravljanje mašine zasnovano na „Arduino“ platformi, specifikacija mehaničkih delova i elektronskih komponenti, kao i način konfigurisanja i unošenja osnovnog upravljačkog programa.

Na kraju rada je prikazan izgled napravljenog 3D štampača kao i jedan od probnih primera korišćen pri testiranju rada mašine.

Ključne reči: Projektovanje, Upravljanje, Aditivne tehnologije, 3D štampa, Fused Granulate Fabrication-FGF.

1. UVOD

U okviru studijskog programa Mašinsko inženjerstvo na Katedri za proizvodno mašinstvo Fakulteta za mašinstvo i građevinarstvo u Kraljevu Univerziteta u Kragujevcu formirana je Studentska radionica u kojoj studenti realizuju svoje praktične projekte. Jedan od projekta koji je realizovan u ovoj radionici je razvoj 3D štampača koji kao ulazni materijal koristi granulatu plastike.

1.1 Studentska radionica

Studentska radionica, na Fakultetu za mašinstvo i građevinarstvo u Kraljevu, je

nastala 2018. godine kao zajednička ideja nastavnika i studenata kako bi se kreativni i inženjerski nadareni studenti podstakli da praktično realizuju svoje ideje kroz primenu savremenih tehnologija. Cilj je da studenti sami projektuju i naprave razne mikro i mini mašine i sisteme uz pomoć asistenata i profesora, u svoje slobodno vreme ili kroz svoje projektne zadatke i diplomske radove.

Radionica je u početku imala jedan manji 3D štampač uz pomoć kog su studenti projektovani i napravili nekolicinu pomoćnih nastavnih sredstava, kao i puno inovativnog promotivnog materijala za potrebe fakulteta. Osim toga, do sada su uspešno napravljene tri različite mini

CNC mašine savremenog tipa koje su potpuno automatizovane i kompjuterski upravljane i to:

1. CNC laser za graviranje drveta i mekših materijala sa dimenzijom radnog prostora 400x500 mm;
2. Unapređeni FDM (Fused deposition modeling) 3D štampač sa dimenzijom radnog prostora 320x320x450 mm. Kod njega su studenti otklonili sve nedostatke uočene korišćenjem postojećeg 3D štampača i znatno popravili kvalitet 3D štampe. Ukupno je napravljeno 5 takvih 3D štampača sa poboljšanim karakteristikama;
3. CNC mašina za 3-osno savijanje žice prečnika do 4 mm.

Zadatak studenata pri izradi ovih mašina bio je da naprave sve komponente, koje je moguće napraviti, na postojećoj opremi sa kojom raspolaže Studentska radionica, Centar i laboratorija za proizvodne tehnologije. Ostale komponente, kao što su: elementi linearne mehanike i elektronika su kupljeni kao standardne komponente. Za upravljanje mašina korišćena su komercijalno dostupna rešenja zasnovana na Arduino platformi.

Uspešna realizacija projekata iz oblasti aditivne proizvodnje je motivisala projektni tim da započne projekat izrade 3D štampača tipa FGF sa radnim prostorom dimenzija 500x500x500 mm. Razlog za realizaciju ovog projekta bila je potreba Studentske radionice za većom produktivnosti, izradom komada većih dimenzija, smanjenjem troškova materijala štampe, kao i reciklažom već postojećih škart delova izrađenih FDM tehnologijom. Projektni tim ima ideju da u budućnosti, na osnovu ovog principa, projektuje i sistem za proizvodnju granulata od PET ambalaže čime bi se doprinelo zaštiti životne sredine.

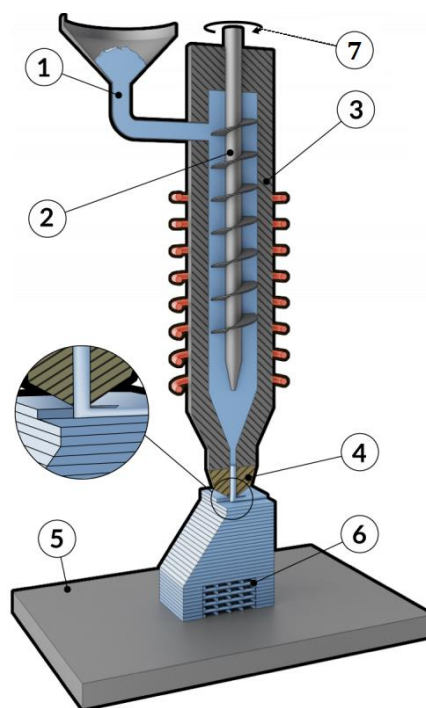
1.2 Fused Granulate Fabrication – FGF

„Fused Granulate Fabrication“ – FGF postupak spada u grupu aditivnih postupaka, pri čemu se kao ulazni materijal koristi granulati plastike, koji koriste i mašine za brizganje plastike (Slika 1) [1].



Slika 1. Materijal za FGF postupak 3D štampe [2]

Princip rada FGF postupka se zasniva na nanošenju odnosno, taloženju istopljenog materijala iz ekstrudera (Slika 2). Granulat se najpre dovodi na zavojno vreteno (2) u telo ekstrudera kroz dovodni levak (1) nakon čega se granulat topi kroz zagrejano kućište (3). Pri samom dnu kućišta, u zoni dizne, ostvaruje se potrebni pritisak pomoću obrtnog kretanja zavojnog vretena koji je dovoljan da istisne istopljeni materijal kroz diznu (4). Materijal se deponuje prema unapred generisanom kodu prvo na radnu platformu (5) a zatim se sloj po sloj formira objekat (6). Pogon zavojnog vretena koji obezbeđuje dovod potrebne količine materijala kroz diznu se dobija od pogonskog sistema (7) koji je sačinjen od motora, reduktora i spojnice.



Slika 2. Princip rada FGF postupka [3]

Nekoliko osnovnih karakteristika direktno utiče na kvalitet gotovog dela, i to su [4]:

1. Veličina i geometrija granulata;
2. Održavanje određenog nivoa vlage materijala granulata;
3. Temperature u grejnom bloku i glavi ekstrudera kako bi se ostvario kontinualan protok materijala;
4. Brzine zavojnog vretena kako bi se ostvarila potrebna debljina nanetog sloja materijala;
5. Synchronizacija svih brzina kretanja kako bi se ostvario zahtevan oblik i dimenzije gotovog dela;
6. Sistem kontrole koji direktno utiče na neželjene vibracije prilikom velikih brzina štampe.

Ovaj postupak 3D štampe ima brojne prednosti u odnosu na FDM postupak [2]:

1. Kao ulazni materijal se koristi plastični granulati, koji je pristupačniji i jeftiniji od filameta u obliku žice, jer se eliminiše korak pretvaranja granulata u žicu;
2. Materijali koji se često koriste sadrže određene primese koje direktno utiču na mehanička svojstva gotovog dela;
3. Produktivniji je od FDM postupka jer ima veliki dotok rastopljenog materijala i deblji sloj štampe;
4. Moguće je korišćenje granulata dobijenog recikliranjem delova dobijenih brizganjem plastike ili 3D štampom.

2. METODOLOGIJA RAZVOJA 3D ŠTAMPAČA

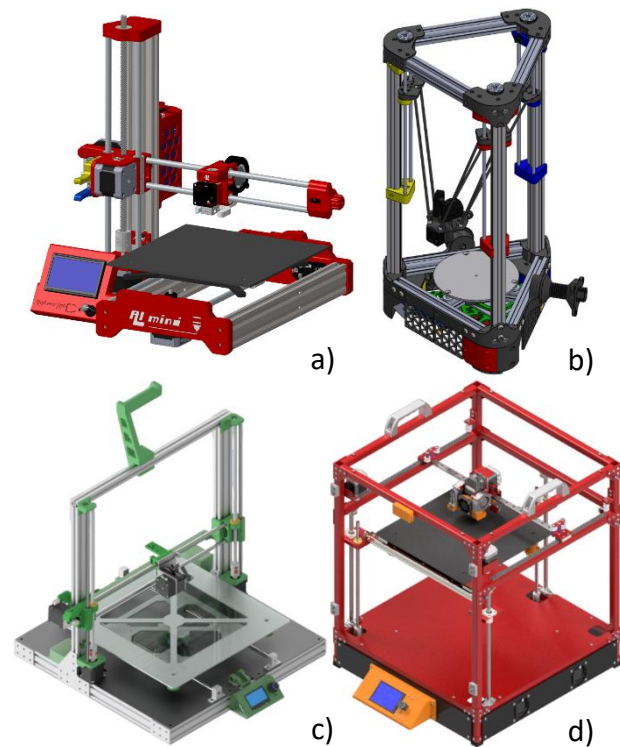
Projekat razvoja 3D štampača tipa FGF je realizovan kroz sledećih 7 faza:

- Faza 1: Idejni razvoj proizvoda,
- Faza 2: Detaljno projektovanje mašine,
- Faza 3: Nabavka materijala i gotovih komponenti,
- Faza 4: Razrada tehnologije izrade i montaže,
- Faza 5: Izrada delova i montaža proizvoda,
- Faza 6: Razvoj i programiranje upravljačkog sistema i
- Faza 7: Testiranje proizvoda.

Kako je faza 2 (detaljno projektovanje mašine) bila najvažnija i najobimnija u nastavku ovog poglavlja će biti detaljnije objašnjena.

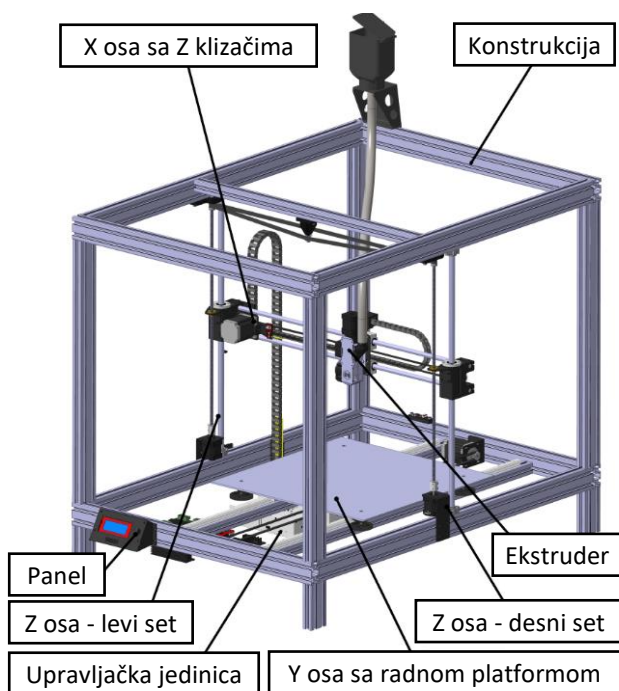
2.1 Analiza i izbor konceptualnog rešenja

Na početku projektovanja urađena je analiza postojećih konceptualnih rešenja 3D štampača (Slika 3).



Slika 3. Pregled konceptualnih rešenja 3D štampača: a) Konzolni tip, b) „Delta“ tip, c) „Prusa“ tip i d) „CoreXY“ tip [5]

Na osnovu uporedne analize, bazirane kako na teorijskim pretpostavkama tako i na empirijskim i iskustvenim činjenicama, doneti su određeni zaključci u smislu izbora tehničko-tehnoloških i geometrijskih rešenja za svaki od osnovnih podsklopova odnosno modula mašine. Prikaz usvojene koncepcije prikazan je na slici 4.



Slika 4. Prikaz usvojene koncepcije mašine [1]

Konačno tehničko rešenje mašine usvojeno je na osnovu sledećih zaključaka:

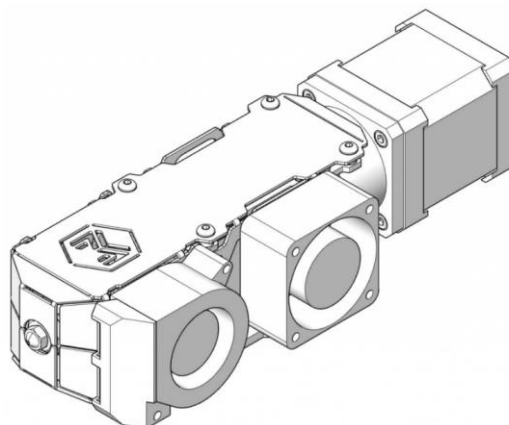
1. *Konstrukcija* – Na osnovu zahteva projektnog zadatka, neophodno je da konstrukcija obezbeđuje dinamičku krutost i stabilnost sistema za radnu zapreminu 500x500x500 mm, te je zato, kao tehnički prihvatljivo rešenje, izabran tip konstrukcije „CoreXY“.
2. *Modul X ose* – Kao tehnički prihvatljivo rešenje izabran je tip grede identičan „Prusa“ mašinama.
3. *Modul Y ose* – Kinematika radne platforme treba da je nezavisna u odnosu na kinematiku modula X ose, kako bi se obezbedila dinamička krutost i stabilnost mašine. Tehničko rešenje koje je primenjeno na mašinama konzolnog, kao i „Prusa“ tipa u potpunosti odgovara zahtevima ovog projektnog zadatka.
4. *Modul Z ose* – U okviru sklopa konstrukcije simetrično su ugrađene dve vertikalne indukcione kaljene cilindrične vođice prečnika 16 mm, koje obezbeđuju oslonac za linearno kretanje u pravcu Z ose i povećavaju krutost konstrukcije. Klizni ležajevi, tj. klizači koji se kreću u navedenom pravcu implementirani su u okviru sklopa X ose.

5. *Upravljanje i pogonski elementi* – Sa aspekta upravljanja najpogodnije rešenje je svakako upravljanje bazirano na „Arduino“ platformi. Pogonske elemente predstavljaju koračni motori NEMA17 i NEMA23, čija se manipulacija obavlja preko frekventnih koračnih regulatora, odnosno tzv. „Driver-a“. „Arduino“ platforma omogućava relativno jednostavno upravljanje motorima, komunikacijom preko navedenih uređaja („Driver-a“).

6. *Modul alata za nanošenje istopljenog materijala (ekstruder)* – Na osnovu projektnog zadatka odabran je „**Pellet ekstruder v4**“ proizvođača „**Mahor XYZ**“ iz Španije (Slika 5). Osnovne tehničke karakteristike odabranog ekstrudera date su u tabeli 1.

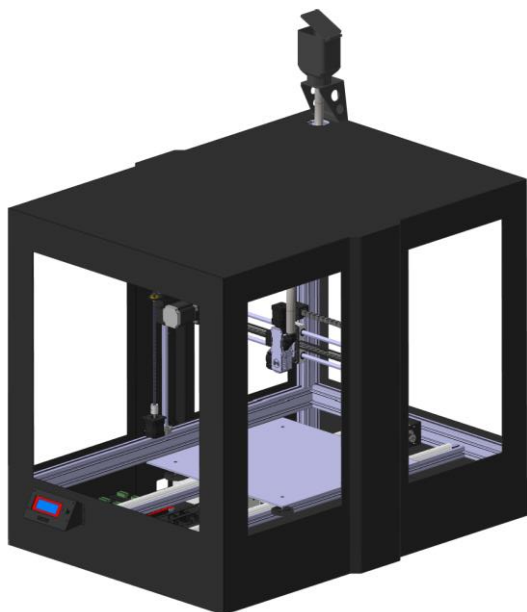
Tabela 1. Pellet ekstruder v4-tehničke karakteristike

Pogon	Koračni NEMA17 motor (jačina struje u pik-u 1.7A)
Prenos	Planetarni reduktor 5:1
Podržani materijali za štampu	PLA, PETG, ABS, ASA, TPE, TPU, EVA...
Senzor temperature	Termistor NTC 100k
Hlađenje ekstrudera	Aksijalni ventilator 24V
Hlađenje štampanog dela	Centrifugalni ventilator 24V
Grejanje bloka ekstrudera	Cevni grejač 24V 50W
Prečnik dizne	0.8 mm
Zavojno vreteno	Spirala prečnika 10 mm sa korakom od 7.5 mm
Masa ekstrudera	600 g



Slika 5. „Pellet ekstruder v4 Mahor XYZ“ [6]

Mašina je zatvorenog tipa (oklopljena) zbog: eliminisanja bilo kakvog vida povređivanja prouzrokovanog pokretnim delovima ili toplotnim dejstvom, smanjenja toplotnih gubitaka, zaštite od prašine i strujanja vazduha, kao i poboljšanja estetskog izgleda štampača. Zaštita mašine (oklop) je izvedena od čeličnog lima debljine 2 mm, dok su providne površine zatvorene pleksiglasom (Slika 6).



Slika 6. Prikaz 3D modela projektovane mašine sa okloпом [1]

Sa gornje strane mašine jasno je uočljiv dovod, odnosno skladištenje granulata za štampu tzv. levak. Iz skladišnog levka se odvodnim crevom plastika distribuira u dovodni levak na ulazu ekstrudera. Zapremina levka bez uračunate zapremine dovodnog creva iznosi 820 g, što je približno 1 kg granulata, zavisno od gustine granulata koji se koristi.

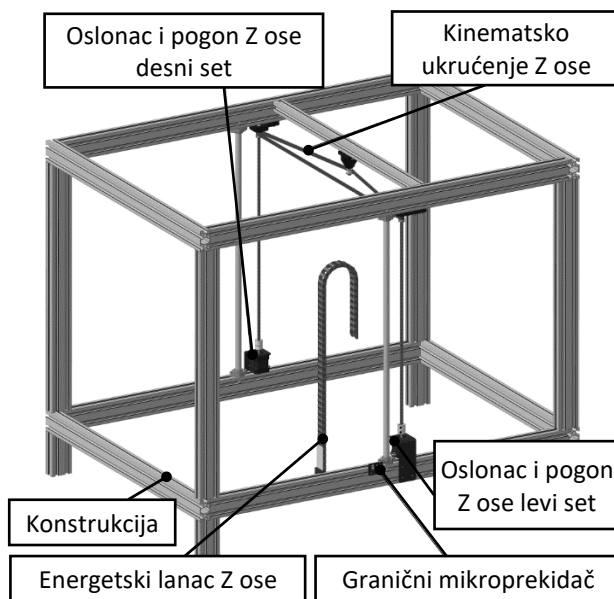
2.2 Prikaz razvijenog rešenja

Usvojeno rešenje se sastoji od 5 modula:

1. Modul Z ose sa nosećom strukturom;
2. Modul X ose sa ekstruderom za nanošenje istopljenog materijala;
3. Modul Y ose sa radnom platformom;
4. Periferna oprema;
5. Upravljački modul.

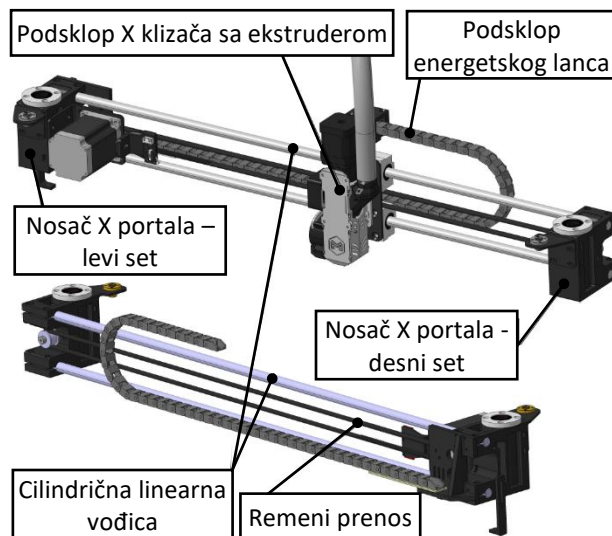
Modul Z ose sa nosećom strukturom: Noseća konstrukcija je formirana od aluminijumskih profila 3030 i 3060 koji se

spajaju pomoću odgovarajućih ugaonika i 3D štampanih komponenti. Konstrukciono rešenje modula Z ose prikazano je na slici 7.



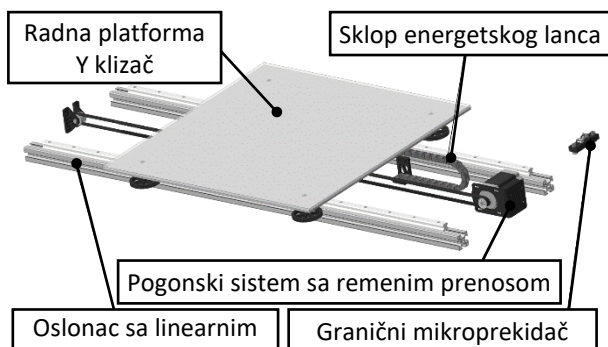
Slika 7. Prikaz tehničkog rešenja modula Z ose [1]

Modul X ose sa ekstruderom: Tehničko rešenje modula X ose je izvedeno pomoću cilindričnih vođica i oslonaca koji obezbeđuju kretanje u pravcu X ose, uključujući i ekstruder za nanošenje istopljenog materijala (Slika 8). Projektovana X osa se zapravo sastoji od dve cilindrične vođice prečnika 12 mm koje obezbeđuju precizno kretanje i oslanjanje X klizača prilikom kretanja u pravcu X ose. Na krajevima vođica nalaze se nosači X portala, koji predstavljaju klizače u pravcu Z ose. Kretanje ekstrudera u pravcu X ose je obezbeđeno pogonskim sistemom koji se sastoji od koračnog motora NEMA23 i remenog prenosa (tipa HTD3M).



Slika 8. Prikaz sastavnih delova modula X ose sa ekstruderom [1]

Modul Y ose sa radnom platformom: Tehničko rešenje modula Y ose sa radnom platformom je prikazano na slici 9. Horizontalni nosači izrađeni su od aluminijumskih profila 3030 na kojima se nalaze šinske linearne vođice tipa HGR15CA, dok su klizni ležajevi koji nose sklop radne platforme oznake HGW15CA. Kretanje radne platforme u pravcu Y ose je obezbeđeno pogonskim sistemom koji se sastoji od koračnog motora NEMA23 i remenog prenosa (tip HTD3M).



Slika 9. Prikaz tehničkog rešenja modula Y ose sa radnom platformom [1]

Modul periferne opreme: Periferna oprema mašine uključuje sklop levka i sklop zaštitne oplata od lima. Levak je izrađen postupkom 3D štampe od PETG materijala. Pored zaštitne oplata mašine, bilo je neophodno na adekvatan način zaštititi elektro ormar, displej kao i ostale komponente upravljanja. Zaštita elektro ormara je izvedena od šperploče, dok je nosač displeja izrađen 3D štampom od PETG materijala. Prikaz modul periferne opreme se može videti na slici 6.

2.3 Upravljanje mašine

Shodno već definisanim podsistemima i zahtevima, projektovani sistem automatskog upravljanja je podeljen na tri osnovne jedinice: upravljačka jedinica sa napajanjem, postprocesor na osnovu kog mašina prepoznaje i vrši upravljanje ostalim komponentama, kao i program pripreme G-koda za izradu objekata, odnosno obrada CAD podataka u CAM podatke (izrada G koda).

Upravljačka jedinica ima zadatak da sprovede željeno ponašanje zadato programom ka izvršnim organima, odnosno da obezbedi

sinhronizovanu, ispravnu komunikaciju i upravljanje između pogonskih sistema X, Y, Z i ekstruder ose, automatsku regulaciju grejača radne platforme i uređaja za merenje temperature, automatsko upravljanje sistema za nanošenje istopljenog materijala i slično. Elektronske komponente upravljačke jedinice smeštene u okviru elektro ormara su:

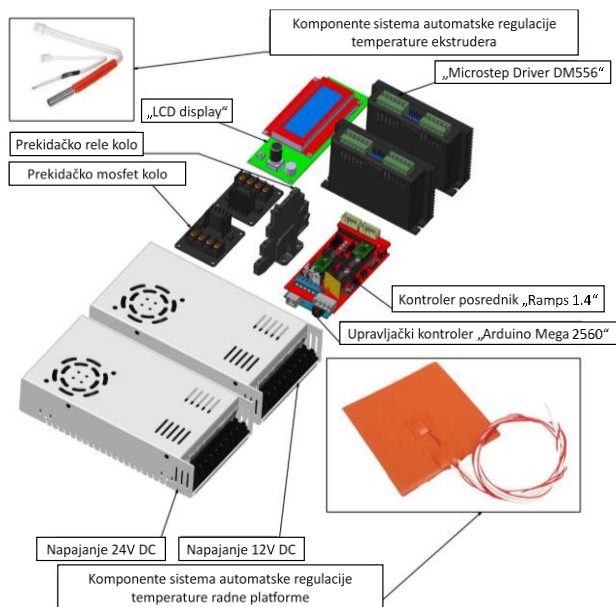
- Programabilni kontroler Arduino platforme - upravljački mikrokontroler tipa „Arduino Mega 2560“ u kome je sačuvan postprocesor za prepoznavanje, čitanje i upravljanje procesima prilikom izrade objekata - 1 komad.
- Kontroler posrednik „Ramps 1.4“ - predstavlja kontroler koji obezbeđuje jednostavniju komunikaciju i raspored signala između programabilnog kontrolera, ostalih upravljačkih komponenti i izvršnih organa - 1 komad.
- Prekidačka radna mosfet kola - predstavljaju vid upravljačke zaštite, odnosno posrednik pri regulaciji temperature radne platforme i ekstrudera - 2 komada.
- Prekidačko radno rele kolo - predstavlja vid upravljačke zaštite zajedno sa mosfet kolom, tj. posrednik pri regulaciji temperature radne platforme 220V - 1 komad.
- Napajanje jednosmernom strujom 12V - napajanje „Arduino“ kontrolera i ostalih komponenti sa navedenim radnim naponom - 1 komad.
- Napajanje jednosmernom strujom 24V - napajanje grejača ekstrudera, regulatora koračnih motora NEMA23 „Driver-a“, napajanje prekidačkih radnih rele kola i prekidačkih radnih mosfet kola - 1 komad.
- „Microstep Driver DM556“ - uređaj koji obezbeđuje upravljanje koračnih motora NEMA23 koji predstavljaju pogon X i Y ose - 2 komada.
- „Microstep Driver A4988“ - uređaj koji obezbeđuje upravljanje koračnih motora NEMA17 koji predstavljaju pogon Z i ekstruder ose - 2 komada.

- „LCD display“ - predstavlja upravljački panel pomoću koga se zadaju komande pomeranja, zagrevanja, učitavanja programa i slično. Sadrži u sebi modul za očitavanje kartice - 1 komad.

Pored navedenih komponenti, u modul upravljačke jedinice kao eksterne komponente van elektro ormara neophodne za obavljanje procesa upravljanja i automatske regulacije su:

- Granični mikroprekidači - uređaji koji obezbeđuju pozicioniranje ekstrudera u početnu poziciju i na taj način definiše se koordinatni početak, odnosno položaj od koga se zadaju apsolutne koordinate u pravcu X, Y i Z ose - 3 komada.
- Termistor „100k Beta 3950“ - uređaj koji predstavlja merač trenutne temperature. Zajedno sa grejačem učestvuje u sistemima automatske regulacije temperature radne platforme i ekstrudera - 2 komada.

Prikaz upravljačke jedinice dat je na slici 10 na kojoj se jasno mogu videti navedene hardverske komponente. Većina komponenti sa slike 10 (osim displeja, grejača radne platforme i ekstrudera, kao i termistora) se nalaze u elektro ormaru.



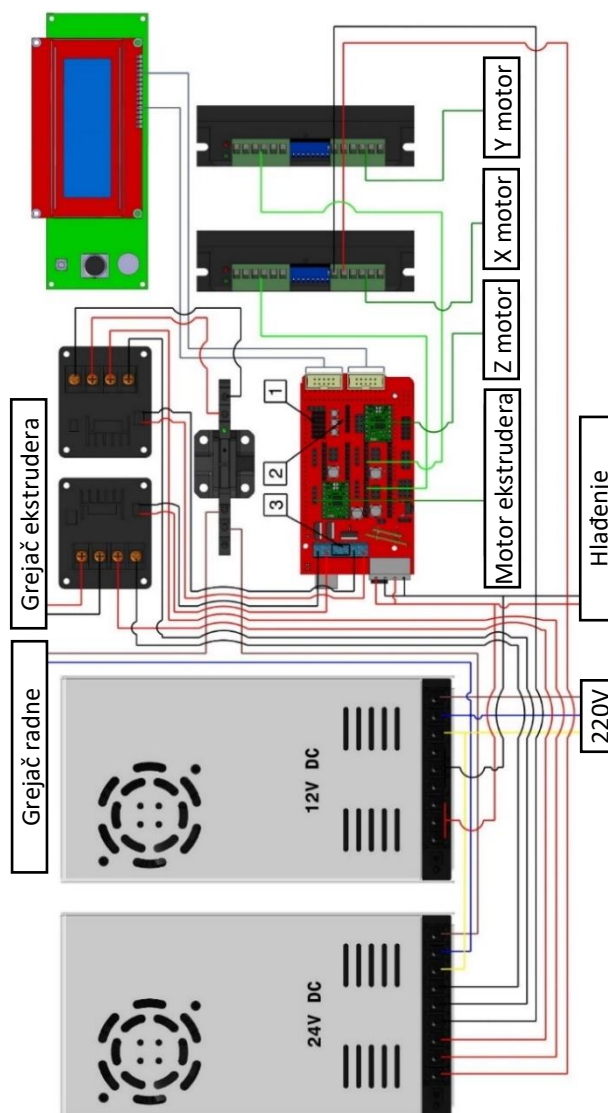
Slika 10. Prikaz sastavnih komponenti upravljačke jedinice [1]

Pored prikazanih napajanja 12V i 24V jednosmerne struje, upravljačka jedinica koristi

i napon od 220V, ne samo kao izvor naizmenične struje za generisanje jednosmerne, već i kao izvor naizmenične struje za napajanje grejača radne platforme karakteristika 220V 750W.

Šema povezivanja je data na slici 11. Slobodni konektori se povezuju na sledeći način:

1. Konektori za granične mikroprekidače X, Y i Z ose;
2. Konektori za termistore radne platforme i ekstrudera;
3. Konektori za hlađenje istopljenog materijala prilikom izrade objekata.



Slika 11. Šema povezivanja komponenti upravljačke jedinice [1]

Programabilni mikrokontroleri predstavljaju „miko“ upravljačke jedinice pomoću kojih je omogućeno upravljanje različitim procesima, motorima i drugim uređajima. Za potrebe ovog

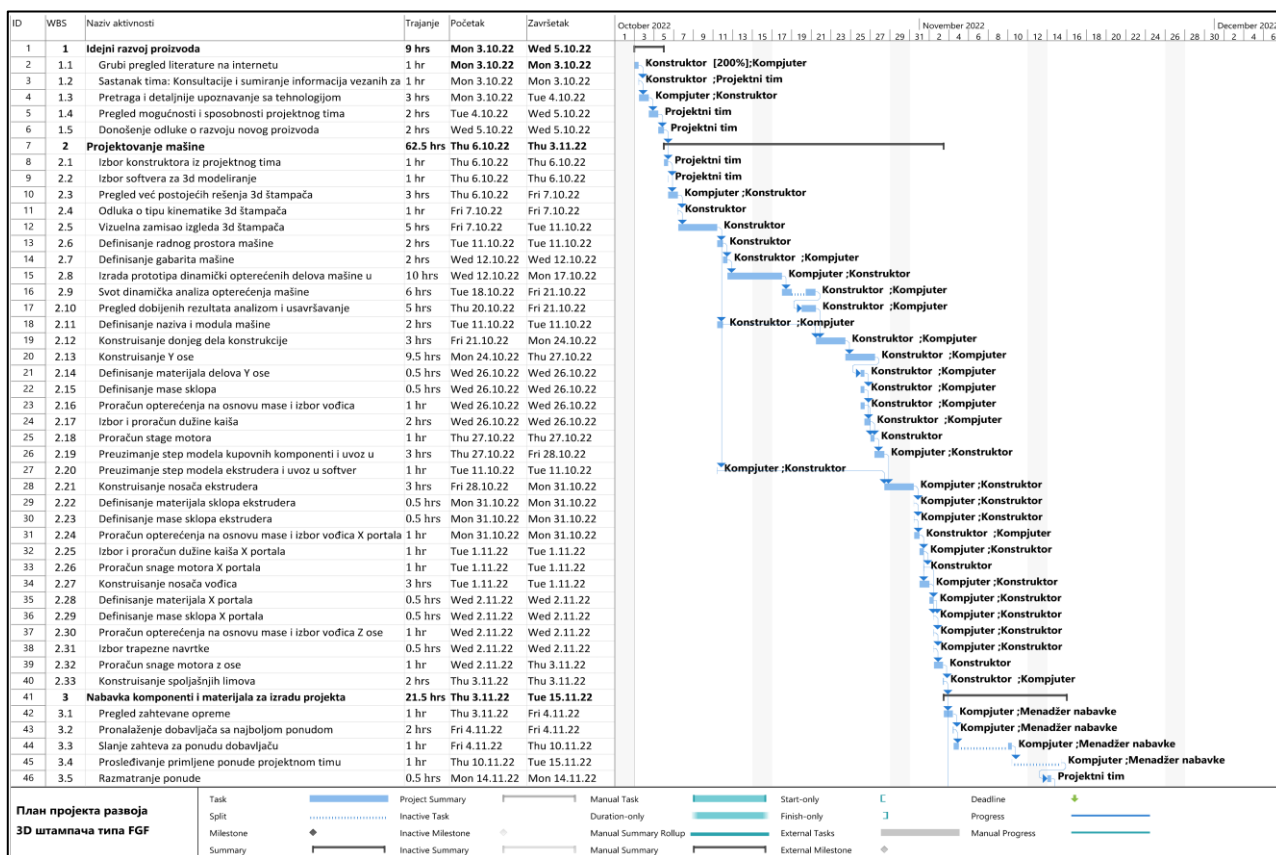
projekta izabran je programabilni kontroler „Arduino Mega 2560“. „Arduino Mega 2560“ predstavlja integrisano elektronsko programabilno kolo sa internom memorijom, na kojoj se čuva određeni programski kod koji na osnovu naredbi ili određenih ulaznih signala izvršava određene komande ili zadaje izlazne signale.

Softverski paket „Arduino“ platforme je izrađen na bazi C programskog jezika, tako da sam program i potprogrami imaju identičnu

strukturu i naredbe kao u navedenom C programskom jeziku.

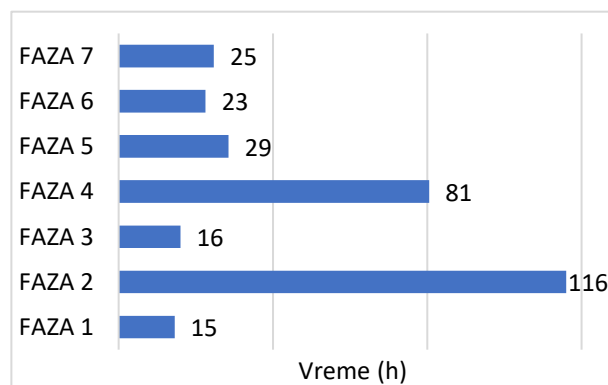
3. REZULTATI

Realizacija celog projekta je predstavljena detaljnim planom projekta koji je urađen u MS Project-u. Izradom plana projekta dobijeni su vreme trajanja projekta, troškovi projekta kao i potrebni resursi. Projekat se sastojao od 114 aktivnosti grupisanih u 7 faza. Na slici 12 je prikazan segment Gantovog dijagrama.



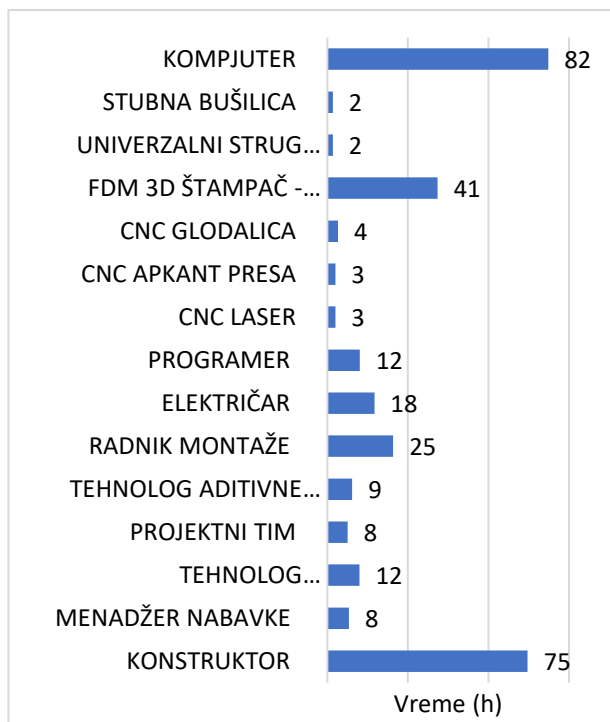
Slika 12. Segment plana projekta u MS Project-u [7]

Ukupno vreme rada potrebno za realizaciju projekta je 302,7 sati. Na slici 13 prikazana je struktura potrebnog vremena po fazama projekta. Može se primetiti da je najveći utrošak vremena u fazi detaljnog projektovanja mašine, jer detaljna analiza i sagledavanje mogućih problema pri izradi delova, montaži, testiranju i ekplataciji proizvoda je doprinela znatnoj uštedi vremena i troškova u narednim fazama projekta.



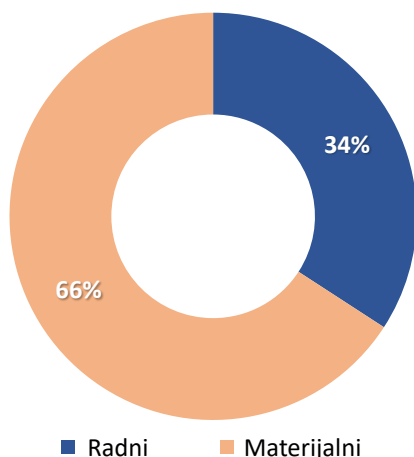
Slika 13. Grafički prikaz utrošenog vremena po fazama projekta [7]

Struktura vremenskog angažovanja radnih resursa je prikazana na slici 14. Analizom ovog grafika može se utvrditi da su najviše angažovani resursi kompjuter i konstruktor. Kompjuter iz razloga što je korišćen u više grupa aktivnosti i od strane više resursa: konstruktor, menadžer nabavke, tehnolog itd. Konstruktor jer je on zadužen za najobimniju fazu projekta (faza detaljnog projektovanja mašine).



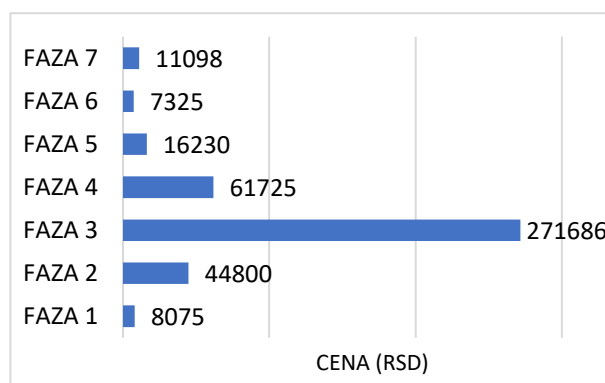
Slika 14. Grafički prikaz vremenskog angažovanja radnih resursa projekta [7]

Ukupni troškovi projekta iznose 420.939,00 RSD. Od toga se 66% odnosi na materijalne troškove a 34% na radne troškove (Slika 15).

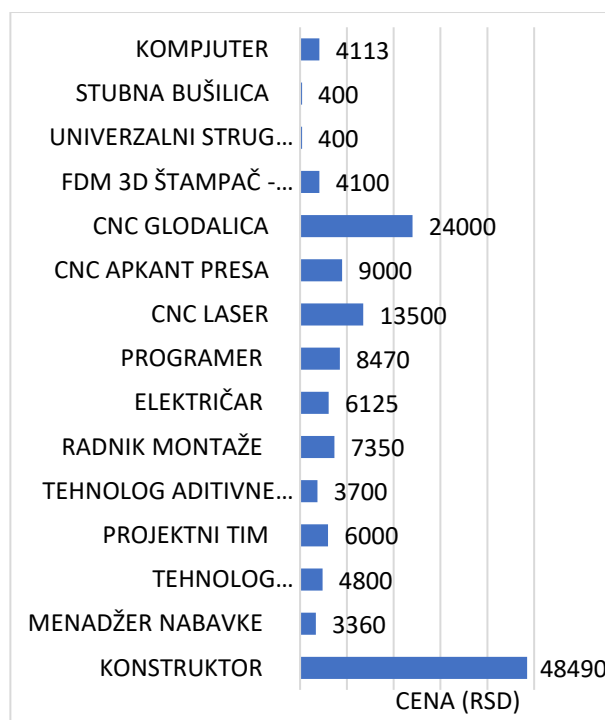


Slika 15. Struktura troškova projekta - odnos radnih i materijalnih troškova [7]

Struktura troškova po fazama projekta je prikazana na slici 16. dok je struktura troškova po radnim resursima prikazana na slici 17. Najveći trošak u ovom projektu je nabavka materijala i potrebnih komponenti. Troškovi radnih resursa su rađeni prema realnim uslovima, pa je tako trošak FDM 3D štampača relativno nizak (obzirom da je dosta korišćen) jer taj štampač poseduje Studentska radionica. Dok je trošak resursa CNC glodalica veći jer je to plaćeno eksternoj firmi da uradi za potrebe projekta.

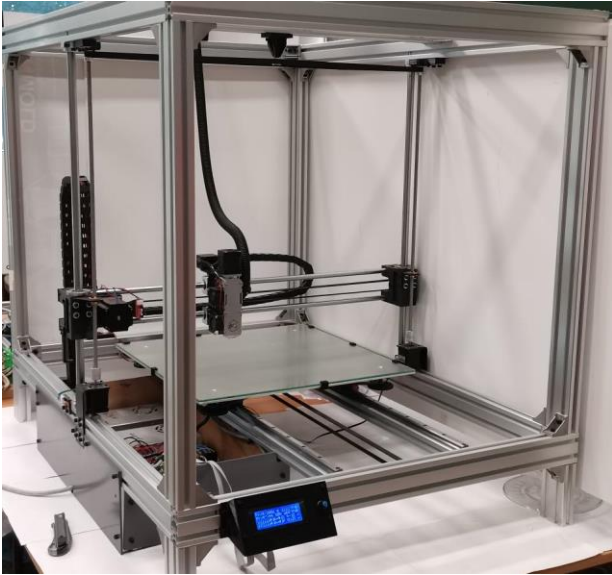


Slika 16. Struktura troškova projekta po fazama projekta [7]



Slika 17. Struktura troškova radnih resursa [7]

Izgled napravljenog 3D štampača je dat na slici 18. dok je na slici 19. dat prikaz jednog od probnih delova koji su štampani pri testiranju 3D štampača.



Slika 18. Izgled napravljenog 3D štampača



Slika 19. Probni deo oštampan pri testiranju 3D štampača

4. ZAKLJUČAK

Prilikom projektovanja 3D štampača tipa FGF analizirana su tehničko-tehnološka rešenja postojećih tipova 3D štampača sa aspekta konstrukcije, kinematske strukture, tehnologije koju koriste, dimenzija radne zapremine i naravno cene koštanja.

Analizom je zaključeno da ne postoji univerzalno tehničko-tehnološko rešenje štampača sa većim radnim prostorom, stabilnom konstrukcionom strukturom i niskom cenom koštanja koje uz to ima mogućnost brzog podešavanja parametara, visine radne

platforme i puštanja u rad. Projektovanje 3D štampača teklo je u pravcu implementiranja tehničkih rešenja za koja je analizom zaključeno da najbolje zadovoljavaju potrebe i zahteve projektnog zadatka.

Prilikom izrade i testiranja proizvoda, pojavio se problem neusaglašenosti okretanja koračnih motora Z ose kada je mašina isključena. To je direktno uticalo na pojavu zakošenja X portala, što je dovelo do nepravilne geometrije i oblika delova pri štampanju. Navedeni problem je rešen ugradnjom dopunskog ukrućenja Z ose.

Osim toga, uočena su moguća unapređenja mašine i to:

- Implementacija dodatnog ekstrudera kako bi se ubrzao proces izrade na tako velikom radnom prostoru;
- Razvoj uređaja za dodavanje određenog procenta dodatnog granulata u boji u određenim intervalima kako bi se izradio deo u više boja;
- Unapređenje dovoda granulata - pod pretpostavkom da može doći do toga da trenutno rešenje dovoda granulata ne funkcioniše ispravno;
- Sistem za automatsku regulaciju temperature i strujanja vazduha u radnom prostoru.

Na kraju treba dodati i sledeću činjenicu: u strukturi ukupne cene koštanja realizovane mašine (420.939,00 RSD) su radni troškovi koji se odnose na angažovanje fakultetske opreme i rad studenata i nastavnika angažovanih na projektu tako da su stvarni troškovi projekta iznosili oko 300.000,00 RSD. S obzirom na činjenicu da je od privrednog društva INMOLD PLAST D.O.O. - Požega dobijen na poklon ekstruder i da je privredno društvo BANIM REKLAME D.O.O. Kraljevo besplatno uradilo neke od operacija sečenja, savijanja i farbanja, to su realni troškovi Fakulteta bili manji od 200.000,00 RSD.

5. ZAHVALNICA

Ovaj rad sufinansira Ministarstvo prosvete, nauke i tehnološkog razvoja Republike Srbije na osnovu ugovora čiji je evidencijski broj 451-03-

47/2023-01/200108. Autori se zahvaljuju Ministarstvu prosvete, nauke i tehnološkog razvoja Republike Srbije na podršci ovom istraživanju. Takođe autori se zahvaljuju i privrednim društvima INMOLD PLAST D.O.O. Požega i BANIM REKLAME D.O.O. Kraljevo na materijalnoj podršci ovom projektu.

LITERATURA

- [1] B. Nikolić: *Projektovanje i programiranje 3D štampača tipa FGF*, Diplomski rad, Fakultet za mašinstvo i građevinarstvo u Kraljevu, Univerzitet u Kragujevcu, 2023.
- [2] FGF Printing Advances May Be a Game Changer, available at: <https://www.engineering.com/story/fgf-printing-advances-may-be-a-game-changer/>, accessed: 10.09.2023.
- [3] M. Stopka, R. Kohár, P. Weis, J. Šteinger: Concept of modular 3D printer construction, in: *IOP Conf. Series: Materials Science and Engineering*, vol 393, No. 1, pp. 1-7, 2018. doi:10.1088/1757-899X/393/1/012092
- [4] S. Ćirić Kostić, N. Bogojević: *Principi i primena aditivne proizvodnje*, Fakultet za mašinstvo i građevinarstvo u Kraljevu, Univerziteta u Kragujevcu, Kraljevo, 2020.
- [5] GrabCad community library, available at: <https://grabcad.com/library/>, accessed: 13.09.2023.
- [6] Pellet Extruders for 3D printing – Why Use Them and Which Ones Should I Buy, available at: <https://bitfab.io/blog/pellet-extruders-3d-printing/>, accessed: 17.03.2023.
- [7] M. Perović: *Plan projekta razvoja 3D štampača tipa FGF*, Diplomski rad, Fakultet za mašinstvo i građevinarstvo u Kraljevu, Univerzitet u Kragujevcu, 2023.

DEVELOPMENT OF FGF TYPE 3D PRINTER

Abstract: *The paper presents the development of a 3D printer of the FGF type with a working area of 500x500x500 mm. The printer was developed in the Student Workshop of the Faculty of Mechanical Engineering and Civil Engineering in Kraljevo as part of student activities and the preparation of final papers on the Mechanical Engineering study program. A detailed project plan was created using Microsoft Project software. The sequence of necessary activities, their interdependencies, required resources and analysis of project costs are defined.*

The conceptual solution was made on the basis of a comparative analysis of already existing technical solutions of 3D printers and their advantages and disadvantages. Based on the conclusions reached, a series of requirements were formed that need to be implemented when designing a new technical solution. As part of the development, the following activities were carried out: defining the kinematic structure of the machine, detailed construction, control of the machine based on the "Arduino" platform, specification of mechanical parts and electronic components, as well as the way to configure and enter the basic control program. At the end of the work, the appearance of the built 3D printer was shown, as well as one of the test examples used in testing the operation of the machine.

Keywords: *Design, Management, Additive technologies, 3D printing, Fused Granulate Fabrication-FGF.*

SPMS/ICPES 2023

**39TH INTERNATIONAL CONFERENCE ON
PRODUCTION ENGINEERING OF SERBIA**

**SESSION 6:
METROLOGY, QUALITY, FIXTURES, CUTTING TOOLS AND TRIBOLOGY**

Novi Sad, 26 – 27 October 2023



Society of Production
Engineering

SPMS 2023

39. Savetovanje proizvodnog mašinstva Srbije

ICPES 2023

39th International Conference on Production Engineering of
Serbia



Faculty of Technical
Sciences
University of Novi Sad

Novi Sad, Serbia, 26. – 27. October 2023

INDUCTIVE HEATING AND QUENCHING OF PLANETARY SHAFTS FOR DIESEL ENGINE STARTERS

**Borut KOSEC^{1,*}, Blaž KARPE¹, Mirko GOJIĆ², Zorana TANASIĆ³, Gorazd KOSEC⁴,
Aco ANTIĆ⁵, Aleš NAGODE¹**

¹University of Ljubljana, Faculty of Natural Sciences and Engineering, Ljubljana, Slovenia

²University of Zagreb, Faculty of Metallurgy, Sisak, Croatia

³University of Banja Luka, Faculty of Mechanical Engineering, Banja Luka, Rep. Srpska, BiH

⁴ACRONI d.o.o., Jesenice, Slovenia

⁵University of Novi Sad, Faculty of Technical Sciences, Novi Sad, Serbia

*Corresponding author: borut.kosec@ntf.uni-lj.si

Abstract: High mechanical and temperature cyclic loading of the final products for automotive, transport, construction and agriculture mechanization industry, demands sufficient mechanical properties of all of their components during its exploitation. Majority of the components is made of steel, by different cold forming processes. Their main demanded characteristics are surface wear resistance and fatigue strength under pulsating stress in combination with cyclic temperature loading, which could be achieved only by appropriate heat treatment. The efficiency of the combined inductive heating and water quenching heat treatment and quality of the planetary shafts were analyzed, with the use of thermographic analysis, hardness measurements, and metallographic examination. Combination of inductive heating and water quenching is the most effective heat treatment process of carbon steel planetary shafts for the diesel engine starters. Long life span of carbon steel planetary shafts it's essential for their economical production. The replacement of starter is expensive from both: money and working time point of view. Surface temperature measurements during the inductive heating process were performed in the industrial environment. The intensity and homogeneity of the planetary shaft surface temperature field was measured by thermographic camera. On the base of theoretical knowledge and measurements, a mathematical model for temperature conditions determination in the shaft during the entire process of heating and quenching was carried out, and used for analyses and optimization of planetary shafts induction hardening process.

Keywords: Planetary Shaft, Carbon Steel, Heat Treatment, Inductive Heating, Quenching, Temperature.

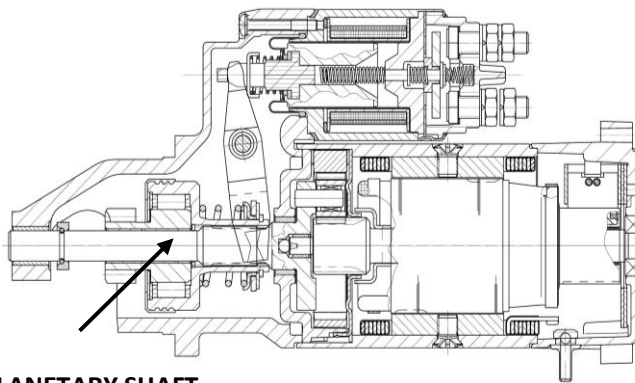
1. INTRODUCTION

Company MAHLE Electric Drivers Slovenia d.o.o., Šempeter near Gorica is one of the largest European producers of electrical components and equipment for automotive, construction, transport and agriculture

mechanization industry. High mechanical and temperature cyclic loading of the final product, during its exploitation, demands sufficient mechanical properties of all of its components.

Majority of the components is made from steel, by different cold forming processes [1]. Their main demanded characteristics are

surface wear resistance and fatigue strength under pulsating stress in combination with cyclic temperature loading, which could be achieved only by appropriate heat treatment [2,3]. Combination of inductive heating and water quenching is the most effective heat treatment process [4-7] of carbon steel planetary shafts for the diesel engine starters (Figure 1).



PLANETARY SHAFT

Figure 1. Diesel engine starter with planetary shaft (Ø14 mm × 155 mm)

The planetary shaft is made from the well known CK 45 steel [8], which is one of the most applied materials for this kind of mechanical parts.

2. EXPERIMENTAL WORK

The inductive spin-hardening device 3KTC (100 kW; 100 kHz) (Figure 2), which is used in company MAHLE Electric Drivers Slovenia d.o.o. for induction spin-hardening thermal treatment of different mechanical parts and components was made by Italian company SAET from Turin. Device is designed for spin case-hardening treatment of cylindrical shape products from 12 to 32 mm in diameter and 100 to 500 mm length.

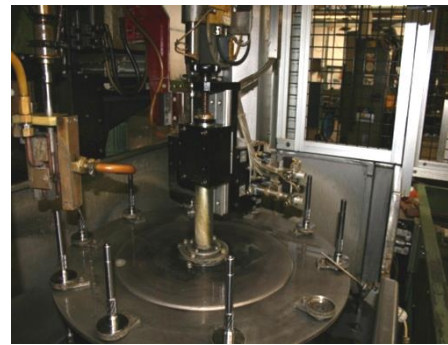


Figure 2. The spin case-hardening device 3KTC (above). Inductor and manipulation system detail (below)

Heat treatment and device parameters are collected in Table 2.

Table 1. Processing and device parameters

Parameter	
Theoretical power (kW)	93
Actual power (kW)	72.8
Frequency (kHz)	83
Voltage (V)	508
Heating time (s)	2.5
Quenching time (s)	1.5
Total time of the cycle (s)	15

During induction heat treatment process the planetary shaft turns around its axis, which ensures uniform heating all over the surface and through the cross section.

Temperature of the surface changes extremely rapidly between room temperature and 1120 °C. Rotational speed is approximately 10 rev/sec. Optimal heating time for required planetary shaft properties is 2.5 seconds, followed by 1.5 second quenching period with oil-water emulsion (Figure 3). After that, planetary shaft is ejected from manipulating system and cooled down in surrounding air.

For planetary shaft surface temperature determination we used thermographic camera ThermoCAM PM675 FLIR System. Measurements were made in cooperation with TERMING d.d. company from Ljubljana.

Because automatic predetermination of emissivity in thermographic camera as thermal

black body ($\epsilon = 1$), real emissivity value must be determined before temperature measurements. As is well known, emissivity is dependent upon material, surface condition and temperature [9,10]. According to literature data for CK 45 steel, emissivity value varies between 0.6 and 0.9, depending upon temperature and surface conditions [11]. In our case of induction heating process, surface temperature varies between room temperature and 1120 °C. Furthermore, quality of surface changes from polished to heavily oxidized, which has significant influence on emissivity value. Because induction heating is a very fast process, we had to determine emissivity as engineering correct constant for the whole temperature range and surface mutation.

For determination of real value of emissivity, we made comparative temperature measurements with Isotech T.T.I.-7 thermograph and thermographic camera of the same planetary shaft, heated in electro-resistance furnace. Best fitting emissivity value for thermographic camera was approximately 0.7.

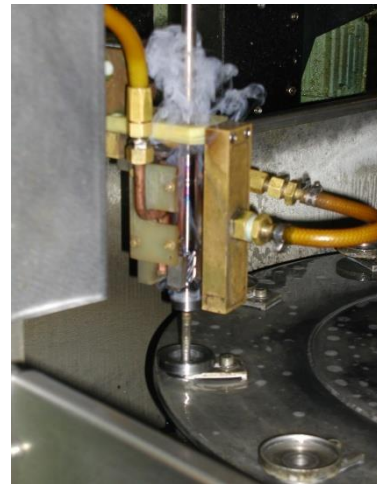
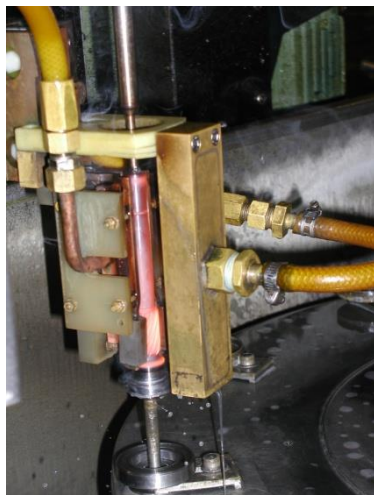


Figure 3. Chronological review of induction case-hardening process

Several thermographic snapshots were recorded at regular intervals of induction heating (entire heating time is approximately 2.5 sec.) Thermographic recording (Figure 4 - above) is showing temperature profile on a surface of planetary shaft after 0.5 second and thermographic recording (Figure 4 - below) after 2.5 second of induction heating. Maximum measured temperature on bevel gear surface was 1120°C.

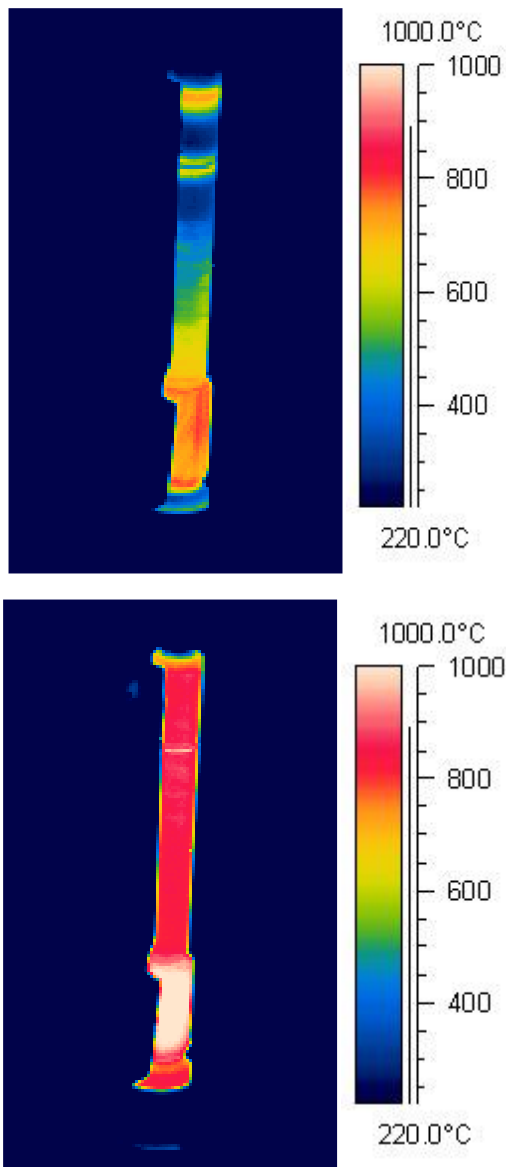


Figure 4. Thermograph records: At the beginning of induction heating (0.5 sec) (above). At the end of induction heating (2.5 sec) (below)

3. MATHEMATICAL MODEL

Primary task of our work was to develop a mathematical model for thermal field calculation inside the planetary shaft during inductive heating and quenching, which would enable examination of temperature distribution at any time of induction heat treatment [12]. Mathematical model based upon ten different assumptions and boundary conditions:

- planetary shaft is approximated as constant cross section cylinder
- material of the shaft is homogeneous and isotropic

- starting temperature field in the shaft is homogeneous and equal to the surrounding temperature
- mathematical model doesn't consider released or consumed latent heat at the allotropic phase changes
- thermal properties are temperature dependant
- density is assumed as a constant during entire induction spin case-hardening process
- surface temperature during induction heating is determined with thermographic camera measurements
- because of "skin effect" phenomenon at the inductive heating, temperature at 0.2 mm below the surface has the same temperature as surface
- during induction heating period, surface temperature rises between separate intervals monotonically to the measured temperatures for those particular intervals
- average heat transfer coefficient in quenching period with oil-water emulsion is determined backwards, after microstructure observations of trial precursors.

Temperature field in any solid body is monotonous function of location and time. For temperature distribution calculation inside planetary shaft we used cylindrical coordinate system. General form of heat conduction equation in cylindrical coordinate system in three dimensional (3D) forms is given by:

$$\frac{1}{r} \cdot \left(\lambda \cdot \frac{\partial T}{\partial r} \right) + \frac{\partial}{\partial r} \cdot \left(\lambda \cdot \frac{\partial T}{\partial r} \right) + \frac{1}{r^2} \cdot \frac{\partial}{\partial \varphi} \cdot \left(\lambda \cdot \frac{\partial T}{\partial \varphi} \right) + \frac{\partial}{\partial z} \cdot \left(\lambda \cdot \frac{\partial T}{\partial z} \right) + q''' = \rho \cdot c \cdot \frac{\partial T}{\partial t} \quad (1)$$

where:

- r, ϕ, z cylindrical coordinate system [m; rad; m]
- T temperature [K]
- $\rho = \rho(T)$ density [kg/m³]
- $\lambda = \lambda(T)$ thermal conductivity [W/(m·K)]
- $c = c(T)$ specific heat [J/(kg·K)]
- q''' volumetric heat generation rate [W/m³]

Because planetary shaft turns around its axis during entire induction spin case-hardening

process, surface temperature is homogenous ($\frac{\partial T}{\partial \varphi} = 0$), and we could make an assumption of two-dimensional (2D) transient heat transfer. Assuming 2D transient heat transfer with variable thermal properties and no internal heat generation or consumption, general partial differential equation reduces to:

$$\frac{1}{r} \cdot (\lambda \cdot \frac{\partial T}{\partial r}) + \frac{\partial}{\partial r} \cdot (\lambda \cdot \frac{\partial T}{\partial r}) + \frac{\partial}{\partial z} \cdot (\lambda \cdot \frac{\partial T}{\partial z}) = \rho \cdot c \cdot \frac{\partial T}{\partial t} \quad (2)$$

For calculation of temperature distribution inside planetary shaft we used explicit finite difference method (FDM), where thermal properties (thermal conductivity, specific heat) at given temperature are calculated for every time step with Lagrange interpolation.

4. RESULTS

Figure 5 shows numerical results of temperature distribution through the cross-section 5 mm beneath upper groove (see Figure 8) for the case of induction heating (2.5 second) and quenching (1.5 second) with water-emulsion. Average heat transfer coefficient in quenching period was determined on the basis of microstructure observation of trial precursors. Best fit value of heat transfer coefficient was 35000 W/m²K.

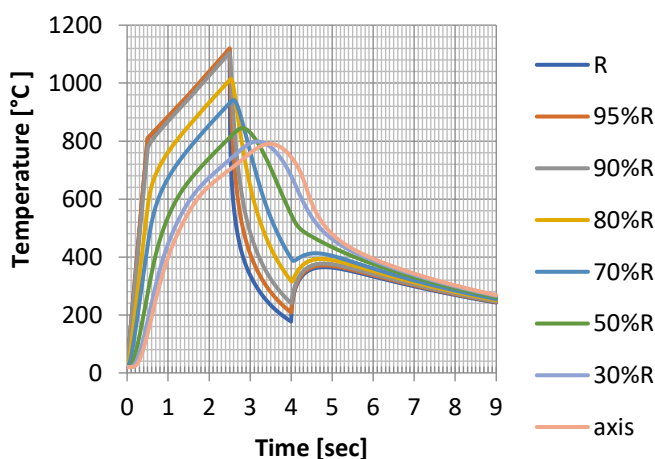


Figure 5. Calculated temperature field in planetary shaft during induction hardening process (htc = 35000 W/m²K)

Figure 6 shows photographs of heat treated planetary shaft (above) and its longitudinal

cross-section with clearly visible hardened case (below). Thickness of the hardened case is approximately 1.4 mm. Cutting was made with the water jet cutting machine.



Figure 6. Heat treated shaft (above). Longitudinal cross-section of the planetary shaft (below). Cutting was made with water jet cutting machine. Thickness of hardened case is approximately 1.4 mm

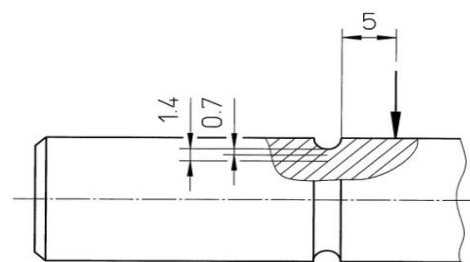


Figure 7. Cross-section line - microstructure analysis

Microstructures at different depths underneath the surface on cross section line are presented in Figure 8. Surface of the shaft is completely martensitic (A). At depth 0.7 mm under the surface, microstructure (B) is composed from martensite and ferrite, which was not completely transformed into austenite during induction heating period. Thickness of hardened case is approximately 1.4 mm (C), where constituents of microstructure are martensite, pearlite and ferrite. Beneath that depth microstructure is composed from pearlite and ferrite.

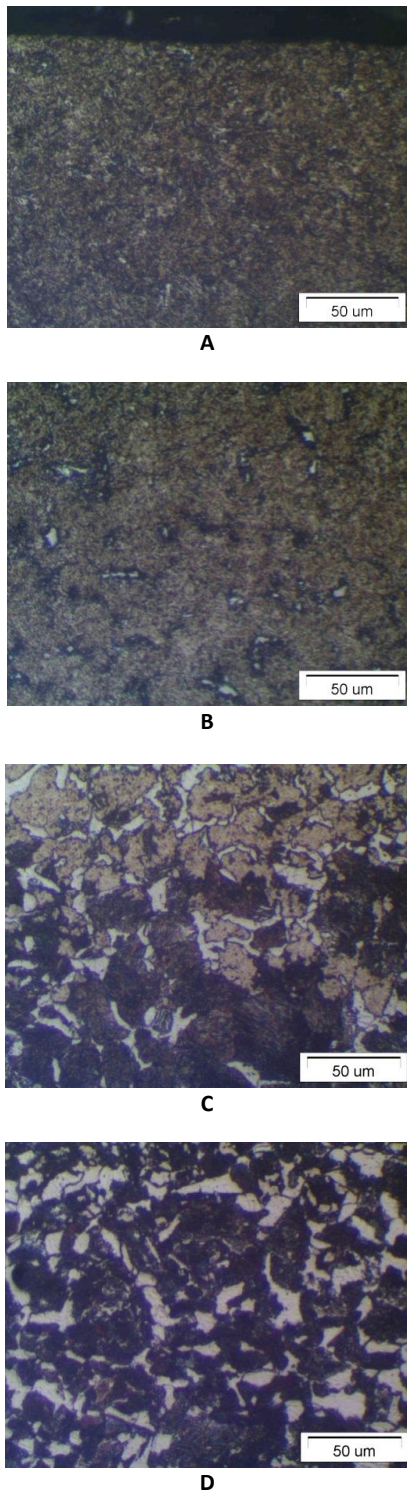


Figure 8. Steel microstructures at different depths under the surface: A) surface; B) 0.7 mm; C) 1.4 mm; D) 2.1 mm

5. CONCLUSIONS

In our research work, we analyzed induction spin hardening process of carbon steel planetary shafts for diesel engine starters.

Surface temperature thermographic camera measurements of planetary shaft during

induction spin-heating period were carried out in industrial environment of Slovenian company Iskra Avtoelektrika d.d.. For accurate temperature measurement with thermographic camera, we made comparative temperature measurements with thermograph and thermographic camera of the same planetary shaft, heated in electro-resistant furnace. Best fit emissivity value for thermographic camera was 0.7.

On the basis of our mathematical model we developed a computer program for temperature distribution calculation inside planetary shaft. Boundary condition for numerical calculations ($h_{tc} = 35000 \text{ W/m}^2\text{K}$) was determined backwards, after microstructure observation of test precursors.

On the basis of the numerical results we optimized heating and quenching time for induction hardening process of planetary shaft.

Induction spin hardened planetary shaft was substantially deformed during water jet cutting. Therefore next reasonable step would be calculation of stress-strain state in planetary shaft.

Acknowledgement

The authors want to thank Prof. Ladislav Kosec⁺ (University of Ljubljana) for information, instructions at SEM and OM analysis, and Mr. Metod Ličen⁺ (ISKRA Avtoelektrika d.d.) and Prof. Mirko Soković (University of Ljubljana) for technical information and discussions.

The authors want to thank Mr. Bojan Težak (Terming d.o.o.) for technical support at thermographic measurements.

REFERENCES

- [1] B. Kosec, M. Brezigar, G. Kosec, J. Bernetič, M. Bizjak: Heat Treatment of Cold Formed Steel Forgings for the Automotive Industry, *Journal of Achievements in Materials and Manufacturing Engineering*, 22 (87 – 90) 2, 2007.
- [2] G.E.Totten, M.A.H. Howes, *Steel Heat Treatment*, Marcel Dekker, New York, 1997.
- [3] M.L.C.F. Cannale, R.A. Mesquita, G.E. Totten, *Failure Analysis of Heat Treated Steel Components*, ASM International, Materials Park, Ohio, 2008.

- [4] C.R. Brooks, The Metallurgy of Induction Surface Hardening, *Advanced Materials & Processes*, 5 (2000) 12, 19 – 23.
- [5] V. Rudnev, *Handbook of Induction Heating*, Marcel Dekker, New York – Basel, 2003.
- [6] J.R. Davis, *Surface Hardening of Steels – Understanding the Basics*, ASM International, Materials Park, Ohio, 2002.
- [7] G.E. Totten, M.A. Howes, I. Tatsuo, *Handbook of Residual Stress and Deformation of Steel*, ASM International, Materials Park, Ohio, 2002.
- [8] B. Jocić, *Steels and Cast Irons*, BIO-TOP, Dobja Vas, 2008.
- [9] B. Kosec, G. Kosec, *Temperature Field Analysis on Active Working Surface of Die-Casting Die*, *Metall*, 57 (2003) 3, 134 – 136.
- [10] L. Machalski, K. Eckersdorf, K. McGhee, *Temperature Measurement*, John Wiley and Sons, Chichester, 1991.
- [11] M. Kaviany, *Principles of Heat Transfer*, John Wiley & Sons, New York, 2002.
- [12] M. Gojić, B. Kosec, I. Anžel, L. Kosec, A. Preloščan, *Hardenability of steels for oil industry*, *Journal of Achievements in Materials and Manufacturing Engineering*, 22 (2007) 2, 23-26.



Society of Production
Engineering

SPMS 2023

39. Savetovanje proizvodnog mašinstva Srbije

ICPES 2023

39th International Conference on Production Engineering of
Serbia



Faculty of Technical
Sciences
University of Novi Sad

Novi Sad, Serbia, 26. – 27. October 2023

APPLICATION OF CONTROL CHARTS IN THE ANALYSIS OF MEASUREMENT SYSTEMS

Predrag JANKOVIĆ¹, Miloš MADIĆ¹, Miodrag HADŽISTEVIĆ², Branko ŠTRBAC²

¹University of Niš, Faculty of Mechanical Engineering, Serbia,
predrag.jankovic@masfak.ni.ac.rs, milos.madic@masfak.ni.ac.rs

²University of Novi Sad, Faculty of Technical Science, Serbia,
miodrags@uns.ac.rs, strbacb@uns.ac.rs

Abstract: Control charts, also known as process control charts or Shewhart charts, are widely used in manufacturing and production industries to monitor and improve the production process. They play a vital role in monitoring, controlling, and improving the production process, allowing organizations to maintain process stability, identify problems, improve processes, make informed decisions, and ensure the consistent production of high-quality products. At the same time, control charts are commonly used for analyzing measurement systems as part of the Measurement System Analysis (MSA) process. MSA is a critical component of quality control and ensures that the measurement instruments used in manufacturing or testing processes are reliable and accurate. By identifying and addressing measurement system errors, organizations can enhance product quality, reduce variability, and improve overall quality control processes. The paper will present an example of the creation and interpretation of control charts in the measurement system analysis.

Keywords: Measuring, Measuring System Analysis, Control Charts, Measurement value variation, Quality Assurance.

1. INTRODUCTION

The production process is a complex interplay of various factors, tools, and methodologies aimed at creating a final product or service. Ensuring the consistent quality of this output is paramount for both the reputation of the producing entity and the satisfaction of the end consumer. This paper delves into the critical role of using control charts for Quality Assurance (QA) in the production process and Measurement system analysis (MSA), highlighting its significance in

maintaining product integrity, enhancing consumer trust, and ensuring regulatory compliance.

The measurement system is a crucial element of production systems. Its efficiency directly impacts the quality of decisions made by managers regarding the production process. A good measurement system should be consistent, reliable, efficient, and streamlined. It's essential to monitor and manage its capability and be aware of the uncertainties in the results it produces. Shewhart's method incorporates the theory of stochastic processes,

where the process model depends on its measurement variability and distribution [1]. A primary tool in this approach, known as statistical process control (SPC), is the control charts. These charts evaluate the consistency of the manufacturing process, ensuring that monitored statistics remain within set boundaries. Proper interpretation of these charts is vital. It is important to note that the chart displays the combined variation from both the manufacturing and measurement processes [2]. Therefore, the variability of the measurement system should be understood and should be significantly less than the manufacturing process's natural variation. This ensures accurate decisions about the stability of the process and the quality of the product. In essence, assessing the measurement system aims to determine if it's suitable for overseeing the production process and the final product.

A measurement system analysis initially aims to verify if the right measurement is being applied to the system. It evaluates if the chosen method is appropriate considering all potential variables. Next, it assesses the measuring instruments. Often, tools like gages and fixtures deteriorate or malfunction, compromising their efficiency. The MSA checks whether these tools require calibration, replacement, or an upgrade.

Furthermore, the MSA evaluates the staff's proficiency in implementing the measurement system's guidelines and any environmental elements that could impact the procedure. Inconsistencies in the process can lead to inaccurate outcomes and potentially defective products. The primary objective of the MSA is to pinpoint and reduce these inconsistencies [3].

A comprehensive review of different methods and techniques used for measuring system analysis is given as an in-depth analysis in many scientific articles. In [4] the authors discuss the sources of measurement variation, such as bias, linearity, and stability, and provide insights into how to assess and improve measurement systems. In a review article [5] authors provide a broader perspective on MSA and highlight the role of control charts as a tool

for assessing measurement system performance.

There are also studies in which it is examined, and the impact of various factors on the quality of measurement results from a coordinate measuring machine (CMM) was explored, with a particular focus on the role of temperature [6].

Control charts stand as an invaluable tool within Measurement system analysis, offering a visual and analytical means to ensure the reliability of measurement systems. Their ability to provide real-time insights, coupled with their utility in anomaly detection and continuous improvement, underscores their significance in the broader landscape of quality control. The paper will present an example of the creation and interpretation of control charts in the measurement system analysis.

2. THE IMPORTANCE OF CONTROL CHARTS IN QUALITY ASSURANCE

At the heart of every successful operation, be it in manufacturing, services, or technology, lies a commitment to quality. Quality assurance (QA) stands as the guardian of this commitment, ensuring that products, services, and systems meet or exceed predefined standards and expectations. It is not only a reactive process of identifying and rectifying defects but is a proactive approach that integrates quality into every phase of production or service delivery. Figure 1 shows the relationship and position of quality assurance, its improvement, and quality control in the Quality Management System.



Figure 1. Quality Management System

The essence of QA lies in its systematic approach to preventing errors. Instead of merely detecting faults after they occur, QA aims to establish processes that inherently minimize the chances of mistakes. This proactive stance not only reduces costs associated with rework and waste but also bolsters the reputation of an organization, fostering trust among its stakeholders.

In the world of quality control and process improvement, control charts stand as a cornerstone tool, offering a visual representation of process variation over time. Originally developed by Walter A. Shewhart in the 1920s, control charts have since found applications in a lot of industries, from manufacturing to healthcare, aiding professionals in monitoring and improving the consistency of processes.

By plotting measurements sequentially, these charts allow analysts to notice patterns, trends, and potential outliers in the data [7]. Any deviations from the established control limits can indicate inconsistencies or errors in the production process, necessitating further investigation.

A sample of a typical control chart is given in Figure 2.

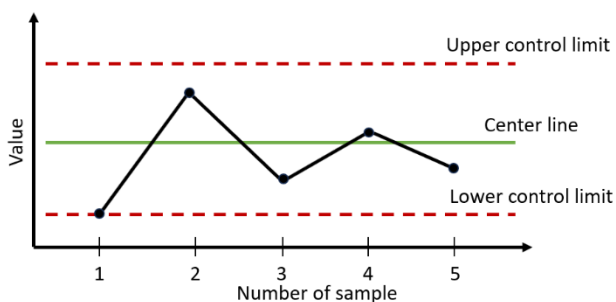


Figure 2. Typical control chart with its main elements

Control charts are essential tools in statistical quality control that play a crucial role in enhancing the overall quality of a process. Over the past decade, there has been a growing emphasis on quality improvement methods, which has led to an increased recognition of the significance of control charts [8].

Gathering data to prepare a control chart is done according to many national and international standards like British Standards

(BS), American Standards (ASTM), German Standards (DIN), Turkish Standards (TSE), etc. Variations in due time or sample order are examined by control charts to keep production under control according to the product's desired properties.

3. ROLE OF CONTROL CHARTS IN MSA

Every manufacturing company collects plentiful amounts of data on systems and processes them daily. This data then informs decisions across all areas of the company, including hiring, equipment needs, and even environmental elements. With so many critical factors at stake, data collection must be reliable. The only way to know this is to use a measurement system. In this sense, to effectively control and improve production processes and product quality, modern production systems require reliable measurement results [9].

In the vast and complex world of quality assurance, where every detail matters, measurement system analysis emerges as the precision tool, ensuring that every measurement, every data point, is accurate and reliable.

The task of MSA is to analyze the variation present in each type of inspection, measurement, and test equipment. Control charts can be applied in the analysis of measurement systems to monitor and evaluate the variation present in the measurement processes. By using control charts, organizations can ensure that the variation in measurement is minimal compared to the variation in the overall process. This helps in identifying and rectifying any inconsistencies or unpredictability in the measurement data. For example, let's say a manufacturing company wants to analyze the accuracy and precision of a measurement device used to measure the length of its products. They can collect a sample of measurements over time and plot them on a control chart. By analyzing the control chart, they can identify any out-of-control signals or patterns that suggest issues with the measurement device. This enables them to

take corrective actions and improve the measurement process to enhance overall quality control [1].

Control charts are employed in various contexts, including controlling production processes, and analyzing measurement systems. While they are a fundamental tool in both contexts, their application, objectives, and outcomes differ significantly. Here are the primary differences between their application in these two contexts:

1. Objective:

- **Process Control (PC):** The primary objective is to monitor and control the production process to ensure that it remains stable and operates at its full potential. Any variations detected beyond the control limits indicate that the process is out of control, prompting corrective actions.
- **Measurement System Analysis (MSA):** The objective is to assess the precision and accuracy of the measurement system. It helps in understanding if the variation in measurements is due to the measurement system itself or the actual variation in the process.

2. Type of Data:

- **PC:** Typically involves data related to product characteristics, such as dimensions, weight, strength, etc.
- **MSA:** Involves repeated measurements of the same item to assess the variability of the measurement system.

3. Outcome:


- **PC:** Identifies special causes of variation that need intervention. Helps in maintaining a consistent quality of the product.
- **MSA:** Determines if a measurement system is suitable for its intended purpose. It identifies sources of measurement variation, such as repeatability and reproducibility.

4. Application:


- **PC:** Used in real-time or near-real-time to monitor ongoing production processes.
- **MSA:** Typically conducted as a separate study, not in real-time. It's often a prerequisite before conducting other quality studies to ensure that the measurement system itself isn't a significant source of variability.

Considering the previously mentioned differences, as well as the fact that time does not figure on the abscissa x-axis, the interpretation of control charts in the analysis of measurement systems differs from the classic application of control charts for statistical process control [10]. In MSA, a combination of control charts is most often used, such as the mean value chart (\bar{X} -chart) and the range chart (R-chart). Measurements are made for k subgroups (number of samples/parts) of n observations (repeated measurement) and, first, a data table is formed. The same data can now be used both for monitoring the production process and the behavior of the measuring system (Figure 3).

Number of observations	Subgroup number									
	1	2	3	4	5	6	7	8	9	10
1	0.826	0.831	0.812	0.806	0.805	0.803	0.805	0.813	0.818	0.808
2	0.826	0.831	0.814	0.805	0.808	0.806	0.803	0.812	0.818	0.803
3	0.826	0.831	0.814	0.805	0.807	0.804	0.807	0.812	0.819	0.803



Statistical parameters for measurement system variation



Statistical parameters of process variation

Figure 3. Data table with measurement values for further processing

After the calculations were carried out and the creation of control charts, it was possible to display the differences between the statistical parameters of the subgroups (variation within the production process) and observations within the subgroups themselves (the result of the variation of the measurement system). By using the measurement data given in the table from Fig. 3, control charts are formed, and their interpretation is performed in the analysis of measurement systems. The R-chart is shown in Figure 4, while the \bar{X} -chart is shown in Figure 5.

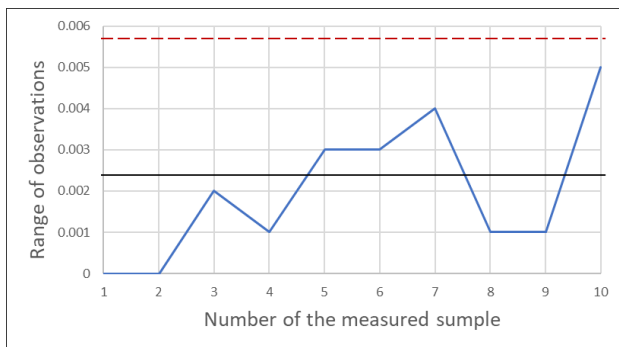


Figure 4. Range value control chart

As can be seen from the range control chart, since there are no out-of-control observations, it can be concluded that the measurement system is stable and that we are making consistent (uniform) measurements. Any observations outside the control limits may indicate the existence of special sources of variation.

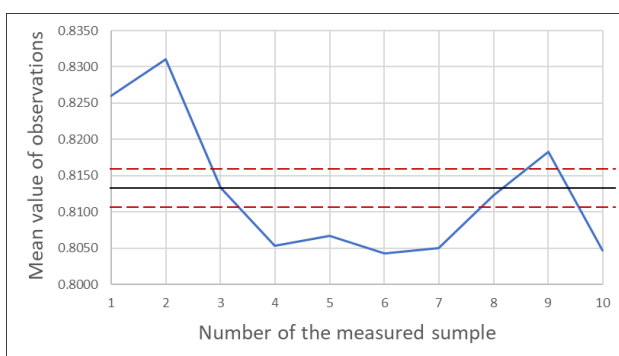


Figure 5. Control chart of mean values

As, in Figure 5, most of the observations (measurements) are outside the control limits on the map of mean values, it can be concluded that the measurement system can easily detect the variations of the measurement objects, independently of the variation of the measurement system. These results show that

the variation due to differences between the measurement items is greater than the variation of the measurement system due to repeatability and reproducibility, which is a favorable case.

Additionally, by combining the charts and the measurement results, the discrimination of the measurement system can be checked, that is, whether it is acceptable or not.

4. CONCLUSION

Measurement system analysis plays a key role in ensuring the reliability and accuracy of measurement systems in various industries. In the realm of quality control and assurance, measurement system analysis stands as a cornerstone methodology to evaluate the precision and accuracy of measurement systems. One of the fundamental tools employed in MSA is the control chart, which offers a visual representation of process variations over time. Among these, control charts emerge as a powerful tool, offering insights into process variations and potential areas of improvement.

There are several benefits of using control charts in MSA, including:

1. *Monitoring process stability and capability:* Control charts help monitor the stability and capability of a process, which allows for early detection of any special causes of variation.
2. *Separating common cause variations from special cause variations:* Control charts are a great way to separate common cause variations from special cause variations, which helps to understand the variations that are always present in processes.
3. *Ensuring measurement system reliability:* MSA is used to ensure that the measurement system used in SPC is reliable and produces consistent and accurate results.
4. *Assessing the quality of the measurement system:* MSA allows us to assess the quality of the measurement system and ensure that the variation in our

measurement is minimal compared to the variation in our process.

In essence, control charts are a reliable tool for evaluating the performance of measurement systems, ensuring that they provide accurate and consistent data. By systematically analyzing measurement data over time, organizations can identify, and address issues related to bias, precision, and stability, ultimately improving the reliability of their measurement processes.

ACKNOWLEDGEMENT

This research was financially supported by the Ministry of Science, Technological Development and Innovation of the Republic of Serbia (Contract No. 451-03-47/2023-01/200109)

REFERENCES

- [1] AIAG-Work Group, *Measurement Systems Analysis*, MSA 4th Edition – Reference manual, Daimler Chrysler Corporation, Ford Motor Company, General Motors Corporation, June 2010.
- [2] M. Diering: *The method of the current evaluating the suitability of the measurement system in the manufacturing process*, doctoral thesis, Faculty of Mechanical Engineering and Management, Poznan University of Technology, Poland, 2010.
- [3] What Is Measurement System Analysis: Understanding Process Variation, posted by Simplilearn, available at: <https://www.simplilearn.com/measurement-system-analysis-article>, accessed: Aug 30, 2023
- [4] M. A. Al-Dahidi, A. G. Fowler: *Measurement Systems Analysis - A Comprehensive Review*, *Procedia CIRP*, 2013.
- [5] A. Aggarwal and N. Aggarwal: *A Review on Measurement System Analysis and Its Importance for Quality Assurance*, in: *International Journal of Advanced Manufacturing Technology*, 2016.
- [6] Štrbac, B., Ačko, B., Havrišan, S., Matin, I., Savković, B., & Hadžistević, M: *Investigation of the effect of temperature and other significant factors on systematic error and measurement uncertainty in CMM measurements by applying design of experiments*, in: *Measurement*, 158, 2020.
- [7] C. P. Keferstein, M. Marxer: *Fertigungsmesstechnik Praxisorientierte Grundlagen, moderne Messverfahren*, Springer, 2014.
- [8] NG. Şengöz: *Control Charts to Enhance Quality. Quality Management Systems - a Selective Presentation of Case-studies Showcasing Its Evolution*, in: *InTech*. 2018.
- [9] P. Janković, M. Madić, B. Štrbac, M. Hadžistević, P. Mladenović: *Application of gage R&R for evaluation measurement system precision: case study*, 14th *International scientific conference – MMA 2021*, University of Novi Sad, Serbia, 2021.
- [10] P. Janković, M. Madić: *Basics of metrology and analysis of measuring systems* (in Serbian), University of Niš, 2020.



Society of Production
Engineering

SPMS 2023

39. Savetovanje proizvodnog mašinstva Srbije

ICPES 2023

39th International Conference on Production Engineering of
Serbia



Faculty of Technical
Sciences
University of Novi Sad

Novi Sad, Serbia, 26. – 27. October 2023

SMART ORTHOPEDIC IMPLANT: CONCEPTUAL SOLUTION

Vladimir ANTIĆ^{1,*}, Dragan MIŠIĆ², Miodrag MANIĆ², Milan MITKOVIĆ³

¹Center of Applied Mathematics and Electronics, Belgrade, Serbia

²University of Nis, Faculty of Mechanical Engineering, Nis, Serbia

³University of Nis, Medical Faculty, Nis, Serbia

*Corresponding author: vladimirantic2013@gmail.com

Abstract: SMART implants, which use measurement data related to physical stimuli such as pressure, force and strain, improve the diagnostic and surgical treatment of bone healing significantly. Strain sensors in SMART orthopedic devices may detect small resistance changes to indicate deformation. Advanced smart implants reduce the quantity of additional burdening activities, such as frequent X-ray imaging, which is the base for determining the degree of healing during the patient's recovery. Upgrading the existing model of the external fixator to a higher degree functionally would make the recovery more compliant and safer, considering that X-ray imaging would be reduced to a minimum. The design is based on piezoelectric sensors, which do not require electricity, making the construction and implementation of the improved external fixation substantially easier. The design and manufacturing of a model of the improved fixator would be followed by testing and verification in a laboratory setting. Based on the construction of the existing model, this article describes the conceptual design of an upgraded strain sensor system designed for the healing of fractures of the low extremities.

Keywords: SMART orthopedic devices, bone fractures, strain sensors

1. INTRODUCTION

The Self-Monitoring Analysis and Reporting Technology (SMART) has the potential to be used to support the medical devices – implants, and to enable personalized treatment of the patient. Often used as a diagnostic tool, SMART implants can be applied in therapeutic purposes too. The implants provide real-time information about number of factors that can vary during the period of patient's healing. This paper provides a conceptual design of the SMART implant based on piezo-electrical strain sensor technology. The basic of this topic is understanding the biomechanics and physical

parameter measurements that can aid in the evaluation of broken lower extremities bones (femur, tibia and fibula) healing process, especially considering that the highest nonunion rate occurs there [1].

Although external fracture fixation devices were developed earlier than more comfortable internal fixation devices, external fixation still has its importance in some types of bone fractures due to the better preventing of deep infection, better control of the fracture position after surgery, and many others. Implanted monitoring devices with an own power supply and measuring instruments have been used in continuous and wireless monitor of

interfragmentary movements, as well as to correlate these data on patient activity.

When a long bone fracture is treated by external fixation device, fracture stiffness can be measured by applying a force across the bone and measuring the resulting deflection of the implant.

To achieve better surgical results in the healing of bone fractures, it is necessary to monitor postoperative bone and other tissue changes as well as the mechanical properties of the injured limb.

Data collection and manipulation of sensor packages instrumentation has long been a challenge to be applied in bone fractures treatment due to the sensor size, low power consumption, and many other factors [2], [3]. The main issue was that sensor packages (microcontroller units and battery sources) were too large to be built into smaller components of orthopedic implants and devices [4-7].

Upgrading the external fixators functions to a higher degree could make the bone fracture treatment more compliant and safer. The design based on piezoelectric sensors (PES) does not require electricity, which makes the construction and its implementation to the fixation device substantially easier.

As diagnostic tools, SMART implants give information about the environment in the human body that cannot be obtained in another way. They can also continually monitor crucial intracorporeal parameters, enabling improvement of the rehabilitation in real time. This quantitative information can be used to change treatment options, initiate changes in the treatment, and prevent some adverse events.

This paper covers the conceptual design of one piezoelectric sensor system that is used as a key component of the SMART implant for assisting in fractured bone healing treatment.

2. SMART IMPLANTS: PIEZOELECTRIC RESPONSE TO THE BONE HEALING

Orthopedic implants are special mechanical devices that are surgically put inside the body

to restore loosed function of some bone structures.

SMART orthopedic implants are small and compact electrodynamic systems used for diagnosis, monitoring, and treatment [8].

Measuring SMART implant parameters related to the biomechanical and physical characteristics of the human body can contribute to broken bone treatment and patient care.

2.1 SMART implants in surgical fixation of fractures

Radiological and clinical examinations are currently the most commonly used tools for monitoring bone healing, although they are subjective and non-quantitative methods. Therefore, there is a need for a reliable and objective method capable of quantitatively determine bone healing status. Monitoring the stability of the implant may avoid further surgical interventions related to refractive non-union problems. In addition, a precise knowledge of the stages and end points in fracture healing may allow the development of patient-specific rehabilitation protocols [9].

In the surgical fixation of long bone fractures, implants are attached to the bone both proximal and distal to the fracture to act as a support, stabilize the bone fragments and allow for correct and faster healing. Fracture plates, intramedullary nails and external fixators are available for fixation of fractures. When the bone is loaded, the load is transferred through both the bone and the fixator (fixation device).

Since the fracture cannot bear the load in the acute postoperative period, the force when the limb is loaded is transmitted only to the fixator and not to the bone. As the fracture heals and a bone callus forms, the bone gets able to support some load and the forces on the fixator are reduced. Once a bone is firmly bridged, the fracture site can withstand greater loads and less force is transmitted through the fixator [10].

2.2 Piezoelectric materials and piezoelectric effect

The ability of certain materials to generate an electrical charge/potential in response to applied mechanical stress is known as the piezoelectric effect or piezoelectricity. The surface charge is generated by the distortion of the internal dipole caused by the applied mechanical force.

Piezoelectric materials can transmit electrical signals without the need for an external stimulator. They act like a tiny battery with a positive charge on one face and a negative charge on the opposite face. To make it as complete circuit, two faces are connected and current is passed through it [11].

Piezoelectric materials can be used as self-powered, battery-free sensors with inherent mechano-electric energy capabilities, making them a promising option for sensor systems.

It should be noted that piezoelectricity has also been found in bones, indicating the presence of important signals involved in tissue function [12].

2.3 Piezoelectric sensor

A piezoelectric sensor is a device that uses piezoelectricity to measure physical stimuli such as pressure, force, temperature and strain. It is used only to measure a dynamic pressure and cannot be used to measure static pressure. At the constant pressure, the output signal is zero. In addition, the piezoelectric sensors are insensitive to radiation and electromagnetic fields. Some of piezoelectric sensors are stable at high temperatures.

The piezoelectric sensor circuit consists of internal resistance, an inductor connected to produce inductance due to inertia of sensor, and capacitance that is inversely proportional to the elasticity of sensor material.

When a force is applied to the piezoelectric diaphragm, an electric charge is generated across the crystal faces. The output is measured as voltage proportional to the applied pressure.

2.4 Piezoelectric response to the fracture healing

The basic idea of the SMART implant presented here is that its integral part, the piezoelectric sensor, generates a signal based on the detected force. The load on the piezoelectric sensor is actually a response to the weight of the patient leaning against the fractured bone.

By monitoring the mechanical response of the external fixation device relative translation and rotation of the external fixation pin scan be detected in order to determine bone healing status i.e., indirectly measure fracture stiffness and bone union [13-15]. When the bone is subjected to external load, the external fixator deforms. As the stiffness of the bone callus increases, deformation decreases [16], [17].

At the beginning of the treatment, there is a gap between the fractured parts of the bone. As the healing process progresses, a callus forms and the gap becomes smaller. When the gap allows the patient to lean on the injured leg, the reaction force against the floor causes the broken bone parts to move closer together. The axis of the reaction is not aligned with the axis of the SMART implant resulting in compression and bending. This means that the piezoelectric sensor generates an electrical signal and the SMART implant completely takes over the external load (Figure 1).

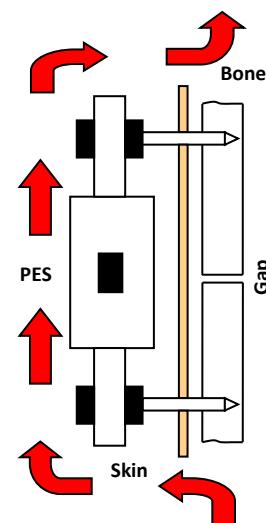


Figure 1. SMART implant takes electrical signal over external load

As the bone heals, a partial callus forms, reducing the gap between the bottom and top of the broken bone. Leaning back on the injured leg reduces the distance, movement of the moving parts of the SMART implant and the signal generated by the piezoelectric sensor. Some of the response from the floor is transmitted over to the bone (Figure 2).

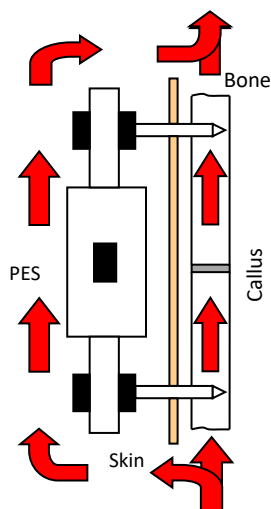


Figure 2. Bone takes partial response from the floor

When the bone is healed, there is no gap between the bottom and top of the bone, there is no movement of the moving parts of the SMART implant, and the signal generated is minimal or disappears (Figure 3). This means that the healed leg completely takes over the reaction from the floor.

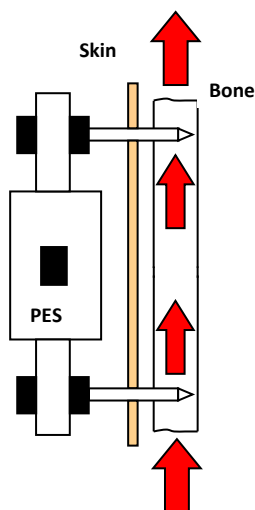


Figure 3. Healed leg takes over the reaction from the floor

Unlike traditional implant treatment, which requires numerous X-rays and other uncomfortable treatments, treatment with SMART implants is based on the parameters generated by the piezoelectric sensors, making treatment more comfortable for patients.

Decision-making criteria and controls are intended to assist surgeons and physicians and provide information relevant to recovering patients and can be a powerful argument for doctors.

2.5 What is smart in SMART?

Implants should be considered “smart” when they not only provide but also analyze data, autonomously recognize normal or abnormal patterns, and proactively alert doctors. It should be noted that even if the data collected is accessible at any time, the resources available to doctors can be limited. Therefore, the pre-assessment and filtering of raw data should be left to the SMART implant system [10].

In the future, SMART implants will likely integrate different measurement parameters to evaluate the mechanical performance of the fracture healing.

3. CONCLUSION

One of the biggest differences between conventional implants and SMART implants is the integration of sensors into SMART implants. Sensors can indicate an implant lose and thus help physicians repair it in a short time.

The SMART implant is equipped with piezoelectrical sensors that can help doctors monitor a patient’s recovery and progress after discharge from the hospital.

The SMART implant has two functions. One is structural support and the other includes monitoring, recording and storing the data during the healing process.

Based on personalized data, physicians can take measures to detect some abnormalities in the fractured area and to provide faster and more effective fracture treatment.

REFERENCES

- [1] A. Sorriento, M. Chiurazzi, L. Fabbri, M. Scaglione, P. Dario, G. Ciuti: A Novel Capacitive Measurement Device for Longitudinal Monitoring of Bone Fracture Healing, *Sensors*, Vol. 21, No. 19, 2021, available at: <https://doi.org/10.3390/s21196694>
- [2] C. O'Connor, A. Kiourti: Wireless sensors for smart orthopedic implants, *J Bio Trib oCorros.*, 2017, pp. 3-20.
- [3] D. D'Lima, B.J. Fregly, C.W. Collwel: Implantable sensor technology: Measuring bone and joint biomechanics of daily life in vivo, *Arthritis Res Theor.*, 15, 203, 2013.
- [4] W.D. Anderson, S.L.M. Wilson, D.W. Holdsworth: Development of a wireless telemetry sensor device to measure load and deformation in orthopaedic applications, *Sensors*, Vol. 20, No. 23, 6772, 2020, available at: <https://doi.org/10.3390/s20236772>
- [5] R. Sun, B. Zhang, L. Yang, W. Zhang, I. Farrow, F. Scarpa, J. Rossiter: Kirigami stretchable strain sensors with enhanced piezoelectricity induced by topological electrodes, *Appl. Phys. Lett.*, 112, 251904, 2018, available at: <https://doi.org/10.1063/1.5025025>
- [6] R. Nagarajan: Wireless RF passive strain sensor: Health and Safety Monitoring, 2014, available at: <https://www.uml.edu/new-venture-initiative/dept-news/wireless-rf-passive-strain-sensor.aspx>
- [7] Umass Lowell: *Wireless RF passive strain sensor: Health and safety monitoring*, 2014, available at: <https://www.uml.edu/new-venture-initiative/dept-news/wireless-rf-passive-strain-sensor.aspx>
- [8] E.H. Ledet, B. Liddle, K. Kradinova, S. Harper: Smart implants in orthopaedic surgery improving patient outcomes: a review, *Innov Enterp Heal.*, 5, 2018.
- [9] W. Borchani, K. Aono, N. Lajnef, S. Chakrabartty: Monitoring of postoperative bone healing using smart trauma-fixation device with integrated self-powered piezo-floating-gate sensors, *IEEE Trans Biomed Eng.*, Vol. 63, No. 7, 2016, pp. 1463-72, available at: <https://doi.org/10.1109/TBME.2015.2496237>
- [10] M. Ernst, R.G. Richcards, M. Windolf: Smart implants in fracture care – only buzzword or real opportunity? *Injury* 52S2, pp. S100-S105, 2021, available at: [https://www.injuryjournal.com/article/S0020-1383\(20\)30766-X/fulltext](https://www.injuryjournal.com/article/S0020-1383(20)30766-X/fulltext)
- [11] Electrical technology. *What is Piezoelectric Sensor – Construction, Working & Application*, 2023, available on: <https://www.electricaltechnology.org/2020/05/piezoelectric-sensor.html>
- [12] D. D'Alessandro, C. Ricci, M. Miazzo, G. Strangis, F. Forli, G. Buda, M. Petrini, S. Berrettini, M.J. Uddin, S. Danti, P. Parchi: Piezoelectric signals in vascularized bone regeneration, *Biomolecules*, Vol. 11, No. 11, 1731, 2021, available at: <https://doi.org/10.3390/biom11111731>
- [13] E.H. Ledet, B. Liddle, K. Kradinova, S. Harper: Smart implants in orthopedic surgery, improving patient outcomes: a review, *Innovation and Entrepreneurship in Health*, 2020, pp. 41-51.
- [14] H. Pelham, D. Benza, P.W. Millhouse, N. Carrington, Md. Ariffuzamann, C.J. Behrend, J.N. Anker, J.D. Des Jardins: Implantable strain sensor to monitor fracture healing with standard radiography, *Scientific Reports* 7, 1489, 2017, available at: <https://doi.org/10.1038/s41598-017-01009-7>
- [15] P. Augat, M. Faschingbauer, K. Seide, K. Tobita, S.A. Callary, L.B. Solomon: Biomechanical method for the assessment of fracture repair, *Injury*, 45, 2014, pp. S32-S38, available at: <https://doi.org/10.1016/j.injury.2014.04.006>
- [16] D.J. Wilson, R.L. Morgan, K.L. Hasselden, J.R. Dodd, S.W. Janna, M.J. Fagan: A single channel telemetric intramedullary nail for in vivo measurement of fracture healing, *J. Orthop. Trauma*, Vol. 23, No. 10, 2009, pp. 702-709.
- [17] K. Seide, M. Aljudaibi, N. Weinrich, B. Kowald, C. Jurgens, J. Muller, M. Faschingbauer: Telemetric assessment of bone healing with an instrumented internal fixator: a preliminary study, *J. Bone Joint Surg. Br.*, Vol. 94, No. 3, 2012, pp. 398-404.



Society of Production
Engineering

SPMS 2023

39. Savetovanje proizvodnog mašinstva Srbije

ICPES 2023

39th International Conference on Production Engineering of
Serbia



Faculty of Technical
Sciences
University of Novi Sad

Novi Sad, Serbia, 26. – 27. October 2023

ANALYSIS OF THE IMPACT OF INDUSTRY 4.0 TECHNOLOGIES ON OCCUPATIONAL SAFETY AND HEALTH

Tijana Lazendić¹, Slobodan Tabaković¹, Miodrag Hadžistević¹

¹ Faculty of Technical Sciences, Novi Sad 21000, Republic of Serbia

Abstract: *The development of technologies intended for the digitalization of activities in industry and their implementation into manufacturing process imply changes that affect access to activities related to the occupational safety and health. The paper analyzes the impact of Industry 4.0 technologies on occupational safety and health. The analysis was realized from the perspective of employees, employers and the appropriate legal framework. The impact on employees was analyzed through the potential hazards that employees may be exposed during the use of these technologies. The impact on employers was analyzed through the need for changes in work organization during the implementation of Industry 4.0 technologies in existing production systems. The legal framework was observed through the need for changes and additions to requirements related to the safety and health of employees who handle machines and devices. In accordance with the previous, the paper presents potential improvements and problems that experts in the field of occupational safety and health may encounter when analyzing the impact, control and prevention of risks to the safety and health of employees in systems where Industry 4.0 technologies are implemented.*

Keywords: *Industry 4.0, Industry Internet of Things, Occupational Safety and Health, Industry 4.0 technologies, Occupational Safety and Health system*

1. INTRODUCTION

The term "Industry 4.0" (the fourth industrial revolution) refers to the digitization activities of the industry, which represents the basic postulate of the project related to the computerized production of the future. This project was managed by the German Ministry of Education and Research, and the term was introduced for the first time in Germany, at the Hanover fair in 2011, to describe a new way of organizing the global value chain. The fourth industrial revolution describes a world in which virtual and physical production systems

cooperate in a flexible way creating "smart factories" [1,2].

Figure 1 shows the historical changes from the first to the fourth industrial revolution. The fourth industrial revolution led to significant changes resulting from the implementation of new technologies such as: additive manufacturing, artificial intelligence, Internet of Things, robotics, digitization, simulation, virtualization technologies and others [3].

The implementation of Industry 4.0 technologies in existing production systems can be a challenge for employees, employers and experts in the field of occupational safety and health, from the hazard identification

procedure to the definition and implementation of measures for safe and healthy work.

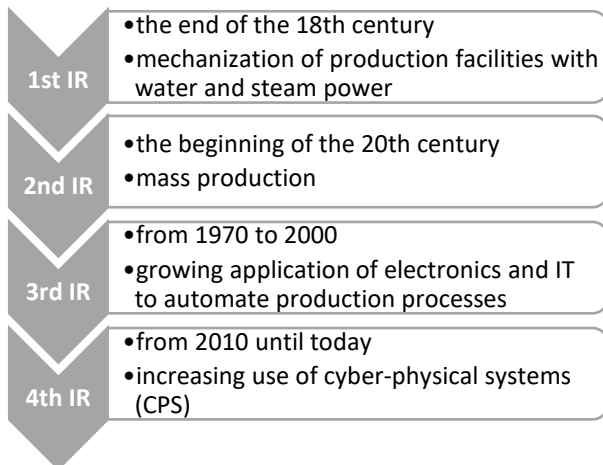


Figure 1. A history of industrial revolutions (IR) [4]

In order to implement prevention measures in the most effective way, it is necessary to analyze the impact of Industry 4.0 technologies on occupational safety and health from the perspective of employees, employers and legal framework.

2. IMPACT OF INDUSTRY 4.0 ON OCCUPATIONAL SAFETY AND HEALTH

The analysis was done from the aspects that represent the essence for the establishment of an appropriate occupational safety and health system in companies. Effective and safe work is possible through cooperation between employees, employers and occupational safety and health experts and implementation requirements contained in the legal framework.

The implementation of additive manufacturing technologies (depending on the type) can help employees to avoid contact with toxic chemicals used in conventional manufacturing processes [5].

Artificial intelligence can contribute to creation an index of well-being and working ability of employees through the analysis of different types of data (acceleration, audio signals, biosignals, etc.). Artificial intelligence technologies can be used to analyze data collected from various sensors in order to monitor and improve the health of employees.

These technologies can be used to analyze stress at work and improve the mental health of employees [5].

Robots and cobots (collaborative robots, adapted to work in the immediate human environment) enable the reduction of the physical load and exposure of employees to dangers because robots can be used to perform various work activities such as the transfer of heavy loads, work in dangerous work environments, etc. [5].

The Internet of Things enables a faster flow of information from employees to occupational health and safety experts. In this way, it is possible to monitor the work activities and working conditions of employees in real time and warn about dangerous situations. This information helps to avoid or reduce the level of risk that employees may be exposed to during the performance of work activities in different working conditions [5].

Technologies based on virtual objects and a virtual environment contribute to increasing efficiency during employee training, especially for work in extraordinary and risk working conditions. The use of these technologies enables employee training without direct exposure to hazards. These technologies generate large amounts of data that can be used to assess the safety and health risks of employees, which contributes to improving the safety of the entire production process [5].

A review of the literature that studies the impact of Industry 4.0 technologies on safety and health at work indicates that it is necessary to analyze this impact from three aspects.

Accordingly, an analysis of the impact from the perspective of employees was carried out, which is an analysis of potential hazards, as well as the improvements that occur through the application of these technologies.

The implementation of Industry 4.0 technologies in existing production systems leads to the need for changes in work organizations, which represents their impact on employers. The changes that occur during the implementation and use of Industry 4.0 technologies require changes in the legal framework related to occupational safety and

health in order to enable responding to potential risks at the right time and their adequate control and elimination.

Figure 2 provides an illustration of the impact of Industry 4.0 technologies on occupational safety and health, considered from the perspective of employees, employers and the legal framework.

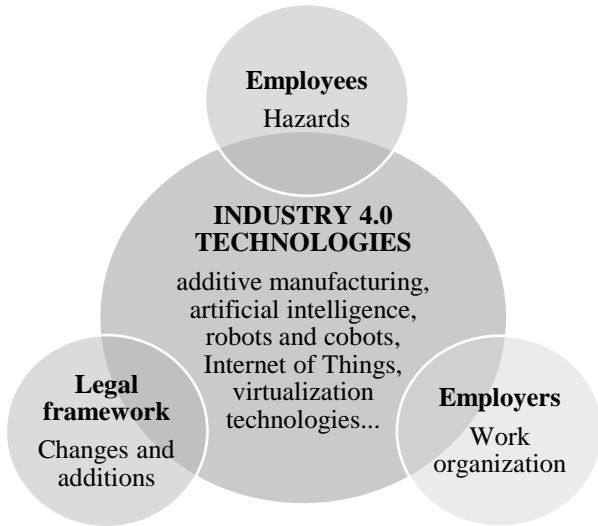


Figure 2. The impact of Industry 4.0 technologies on occupational safety and health

3. RESULTS AND DISCUSSION

Analysis of the impact of Industry 4.0 technologies on the safety and health of employees working in existing production systems in which these technologies are implemented indicate that there are potential problems as well as improvements affecting occupational safety and health. The positive and negative impact of Industry 4.0 technologies on employees and employers from the aspect of occupational safety and health is shown in table 1.

Table 1. The impact of Industry 4.0 technologies on employees and employers (A- advantages and D-disadvantages)

Industry 4.0 technologies		Employees	Employers
Additive manufacturing	A	Avoid contact with parts of the machine that can cause injury, reduced noise level, reduced physical load, comfortable body position during work, without carrying heavy loads, without unphysiological position of the body during work	Enabled simple integration into the manufacturing process
	D	Increased risk of burns, burns on hot work objects or machine parts, inhalation of fine particles and vapors that occur during the production process	Examination and control of chemical hazards
Artificial intelligence	A	Avoiding physical work and repetitive activities, automatic processing of large amounts of information, the ability to perform work activities more easily and efficiently with the help of voice commands and cameras	Efficient and quick identification of hazards, making decisions at the right time, analysis of data and work activities using information gathering software
	D	The possibility of anxiety and stress arising from the feeling that machines and devices have control over employees	A real-time risk assessment of each employee is required
Robotics	A	Avoided carrying heavy loads, avoided non-physiological position of the body during work, avoiding physical work and repetitive activities,	The use of robots to perform risky work activities and facilitate the work of employees

		avoiding contact with dangerous substances, ability to work from a safe distance	
	D	Contact with a robot/cobot and injury to employees, the movement of robots/cobots may lead to the development of new hazards, stress as a consequence of the fear of losing job, difficulties in adapting to a new/different work environment	It is necessary to design workplaces for employees who work with robots/cobots, installation of protective sensors or fences
Internet of Things	A	Quick and easy exchange of information between employees, machines and devices	Continuous and effective detection of potential hazards, easier organization and management of the occupational health and safety system
	D	Stress caused by the pressure associated with the need to quickly acquire new knowledge and skills	Training of employees in the use of new technologies is required
Virtualization technologies	A	Safe training for performing work activities, especially in workplaces with increased risk, reduction of stress caused by mistakes during training	Training of employees to perform work tasks, especially in jobs with increased risk before entering the workplace
	D	Possible physical discomfort while using equipment supported by virtualization technologies, risk of injury if devices are used outside the intended area, possible appearance of anxiety	It requires a period of adaptation of employees to the real environment after using the equipment supported by these technologies

3.1 Employees

Widespread automation in the manufacturing processes of Industry 4.0 contributes to the reduction of manual work and heavy physical work, which also reduces the risk of physical injury to employees. Psychological risks become more dominant in relation to the risks of injuries due to mental overload and workload that occur as a consequence of more flexible and dynamic activities of smart manufacturing. The use of Industry 4.0 technologies in the manufacturing process can lead to mechanical, electrical, chemical and thermal hazards, noise, vibration and radiation [8].

The complexity of the manufacturing process using Industry 4.0 technologies is constantly growing, which is particularly evident in the complex interaction between work activities, organization, management and other organizational factors in companies. This interaction affects the appearance of several

types of workplace hazards, especially those in the psychosocial category [6].

Creating production systems with Industry 4.0 technologies requires an analysis of risks which can be a challenge in terms of work organization and the legal framework related to the occupational safety and health management system.

3.2 Employers

The fourth industrial revolution includes the automation and digitization of production by applying technologies that are based on the possibilities of self-optimization and autonomous decision-making. The implementation of new technologies in existing production systems affects changes in the organizational structure. The key function in work should be retained by employees, including activities of decentralized decision-making and quality control of the production process [8].

Organizational changes resulting from the implementation of Industry 4.0 technology

require a gradual process of reorganization of existing production processes. When it comes to small and medium-sized enterprises, it is recommended that the implementation be done through four stages:

1. digitization: digital representation of the company in real time, automation of data collection to create a digital representation of the company,
2. process control: horizontal integration with automatic assessment of whether the process is correct,
3. visualization: analysis of vertical integration data and process control data,
4. delegation: self-control of production and logistics [10].

Changes in work organization require additional employee training for safe and healthy work adapted to new working conditions. Employers, in cooperation with occupational safety and health experts must recognize new hazards that are characteristic when applying new technologies, assess the risks and apply appropriate prevention measures.

3.3 Legal framework

Requirements in the legal framework oblige employers to assess risks, apply standardized work procedures and provide training of employees with the aim of reducing the frequency of injuries at work and the negative impact on the health of employees. Legislation establishes participation mechanisms whose goal is to eliminate sources of hazards to the health, safety and physical integrity of employees. However, it does not contain standard procedures and does not provide an explicit definition of the integration of occupational safety and health in the production process. Currently, there is no widely accepted and internationally recognized regulatory framework that deals with this issue, which is a consequence of the tripartite approach to prevention [6].

There is a need for revision and changes in the legal framework related to safe and healthy work with Industry 4.0 technologies, which will

enable the establishment of an appropriate occupational safety and health system in organizations.

Badri et al (2018) state that the review should start with standards when it comes to reviewing the legal framework. According to their opinion it is more efficient to review the standards because changing the law takes more time. It is important to note that the absence of a standards or their modification in response to technological progress can have major consequences for occupational safety and health [6].

Lu et al (2015) state that the appropriate definition and use of information is key to enabling adaptive and smart manufacturing systems, which gives standards a fundamental role to:

1. facilitate the delivery of necessary information in real time,
2. enable activities based on appropriate information and
3. reduce the risk of implementation and development of Industry 4.0 technologies [11].

Existing occupational health and safety management systems are designed to meet the requirements of conventional manufacturing processes. Digital transformations of production systems require the definition and consideration of new types of hazards, risks, risk assessment methodologies, new implementation methods, social issues, etc. [12].

The current occupational health and safety strategy in developed countries is based on a quantitative model of risk management and traditional full-time work and is not adequate when it comes to the rapid technological progress resulting from the fourth industrial revolution. Chia et al (2019) proposed a new workplace safety and health strategy WHS 4.0 (Workplace Safety and Health 4.0) that includes adaptive solutions for safe and healthy work, multi-stakeholder dialogue, anticipatory management with a foundation of shared values and professional development of occupational health and safety experts [12].

4. CONCLUSION

The analysis of the impact of Industry 4.0 technologies on occupational health and safety was carried out in the form of extensive research in order to form the basis for theoretical and experimental research in this field for the purposes of the PhD thesis.

During the fourth industrial revolution, there was the development of new technologies whose impact on occupational health and safety is mostly reflected in the emergence of new potential hazards, changes in the organization of work and the need for changes and additions to the legal framework.

Industry 4.0 technologies contributed to the reduction of physical work and the risks related to it. However, new risks have emerged that are related to the psycho-social condition of employees, which must be assessed and examined in order to enable their control and elimination.

The cooperation of employers with occupational health and safety experts is needed in order to implement Industry 4.0 technologies in existing production systems in a way that will not have a negative impact on employees. The revision of the legal framework related to safe and healthy work in such production systems gives guidelines to employers and occupational health and safety experts when forming a safe and healthy production system for employees.

ACKNOWLEDGEMENT

The results presented in this paper are part of the research within the project "Application of advanced production and information technologies in education, research and cooperation with the economy", at the Department of Production Engineering, Faculty of Technical Sciences, University of Novi Sad, Republic of Serbia.

REFERENCES

- [1] A. Moktadir, M.S. Ali, S. Kusi-Sarpong, A. A. Shaikh: Assessing challenges for implementing Industry 4.0: Implications for process safety and environmental protection, *Process Safety and Environmental Protection*, Vol.117, pp.730-741, 2018.
- [2] K. Schwab: *The Fourth Industrial Revolution*, World Economic Forum, Geneva, 2018.
- [3] G. Arana-Ladin, I. Laskurain-Iturbe, M. Iturrate, B. Landeta-Manzano: Assessing the influence of industry 4.0 technologies on occupational health and safety, *Heliyon*, Vol. 9, pp.1-18, 2023.
- [4] B. Sniderman, M. Mahto, M. J. Cotteleer: *Industry 4.0 and manufacturing ecosystems. Exploring the world of connected enterprises*, Delolte University Press, London, 2016.
- [5] R. Zorzenon, L.F. Lizarelli, B. A. D. Moura: What is the potential impact of industry 4.0 on health and safety at work?, *Safety Science*, Vol. 153, pp. 1-18, 2022.
- [6] A. Badri, B. Boudreau-Trudel, A. S. Soussi: Occupational health and safety in the industry 4.0 era: A cause for major concern?, *Safety Science*, Vol. 10, pp. 403-411, 2018.
- [7] Ö. H. Çavuş: Occupational Health and Safety Practises in The Industry 4.0 Proces, *PJESS*, Vol. 9, No. 2, pp. 147-169, 2022.
- [8] V. Leso, L. Fontana, I. Iavicoli: The occupational health and safety dimension of Industry 4.0, *Official journal of the Italian Society of Occupational Medicine*, Vol. 109, No. 5, pp. 327-338, 2018.
- [9] S. Tepe: The Impact of Industry 4.0 on Occupational Health and Safety, *Int. J. Adv. Eng. Pure Sci.*, Vol.33, No.1, pp. 122-130, 2021.
- [10] A. Benešova, J. Tupa: Requirements for Education and qualification of People in Industry 4.0, *Procedia Manufacturing*, Vol. 11, 2195-2202, 2017.
- [11] Y. Lu, K.C. Morris, S. Frechette: Standards Landscape and Directions for Smart Manufacturing System, in: *Proceedings IEEE International Conference on Automation Science and Engineering (CASE)*, 2015, Gothenburg, Sweden, pp. 998-1005.
- [12] G. Chia, M. S. Lim, G. K. J. Sng, Y. J. Hwang, K. S. Chia: Need for a new workplace safety and health (WHS) strategy for the fourth Industrial revolution, *Am. J. Ind. Med.*, Vol. 62, No. 4, pp. 275-281, 2019



Society of Production
Engineering

SPMS 2023

39. Savetovanje proizvodnog mašinstva Srbije

ICPES 2023

39th International Conference on Production Engineering of
Serbia



Faculty of Technical
Sciences
University of Novi Sad

Novi Sad, Serbia, 26. – 27. October 2023

ANALYSIS OF THE SCANNING SPRAY LAYER THICKNESS USING THE FOCUS VARIATION METHOD

Zeljko SANTOSI^{1*}, Milos RANISAVLJEV¹, Mario SOKAC¹, Djordje VUKELIC¹

¹Faculty of Technical Sciences, Novi Sad, Serbia

*Corresponding author: zeljkos@uns.ac.rs

Abstract: *This paper investigates how the thickness of a scanning spray layer may influence the accuracy of 3D scanning processes. The interaction between the scanning spray layer and the object being scanned can introduce errors and distortions that impact the quality and accuracy of the resulting 3D scans. Thick or uneven scanning spray layers can mask or obscure fine details on the object's surface. This can prevent the 3D scanner from accurately capturing intricate features, leading to incomplete or distorted reconstructions. For determining the thickness of the scanning spray layer the focus variation method was used. The obtained results indicate an increase in geometry where the scanning spray was applied, which is above the limits specified by the manufacturer.*

Keywords: *focus variation, scanning spray, 3D scanning.*

1. INTRODUCTION

The reflective and transparent surfaces are the most demanding challenges for optical 3D digitization methods due to the nature of light and the optical properties of these materials [1] [2]. The challenges arise from the fundamental principles of how these scanners operate and how light interacts with shiny materials. Shiny surfaces exhibit a phenomenon known as specular reflection, in which light is reflected off the surface at specific angles, creating intense highlights. These highlights can make it difficult for the 3D scanner to accurately capture the actual surface geometry, leading to potential inaccuracies in data capture [3]. Specular reflections can also result in the 3D scanner picking up reflections from other

objects or even from the scanner itself, introducing unwanted noise and artefacts into the scanned data.

The thickness of the scanning spray layer can have a significant impact on the accuracy and overall quality of 3D scanning results [4]. When the layer is too thin or uneven, it may fail to provide adequate contrast for the 3D scanner to detect surface features accurately, potentially resulting in missing data and reduced accuracy. Conversely, excessively thick layers can obscure fine details and lead to inaccuracies due to an excess of material on the surface. Additionally, they can make it challenging for the 3D scanner to penetrate the layer and capture underlying details. Therefore, maintaining consistency in layer thickness across the entire scanned area is crucial for

preserving accuracy, as variations in layer thickness can result in inconsistent scan data [3], [5]. Researchers in [6] investigated the influence of material surface on the scanning error of a powder-free 3D measuring system. They found that depending on the thickness of the water film, measurement errors in the order of 300-1,600 μm could be observed. Scanning sprays are also applied in dentistry where the influence of scanning-aid materials on the scanning accuracy is evaluated in specially designed metallic models that imitate intraoral dental restorations, such as inlay, on lay, and bridge [7], or for investigating the three-dimensional coating thickness [6], [8], [9].

2. MATERIALS AND METHOD

In some optical methods, such as photogrammetry based on structure from motion, single-colored objects can also be challenging to digitize [10]. Additionally, dark-colored objects can be very difficult to scan. One solution to address this issue is to apply scanning spray to the scanning surface. A scanning spray layer is a thin layer of material, often in a form of a fine powder or a liquid, that is applied to the surface of an object before 3D scanning. This layer enhances the scanning process by improving the visibility of surface details and making it easier for the 3D scanner to capture accurate data. Various scanning spray products are available in today's market.

AESUB blue is a self-vanishing scanning spray developed by scanning experts [11]. The spray evaporates within a few hours, meaning that there is no need for cleaning after 3D scanning. Unlike traditional sprays, AESUB blue does not contain pigments and thus avoids pigment-contamination of sensitive areas, such as laboratories and production sites, equipment and users. Therefore, AESUB blue can be applied directly, on the spot of scanning, without any costly transport to avoid said pigment contamination in sensitive areas [11].

According to manufacturer specification layer thickness is $\sim 8\text{-}15 \mu\text{m}$, and depends on the user-specific application, thus forms a

consistent and very homogeneous coating on the surface of the object to be scanned [11].

2.1 Focus variation method

Focus variation is one of the passive methods of 3D digitization. It relies on the reconstruction of shapes and surfaces in space using a series of photos of the same scene taken with different focus settings. Due to the optical properties of the photography acquisition device (system of lenses) which is characterized by a shallow depth of field, it is possible to capture suitable photos for the application of this method [12], [13]. The typical schematic operating principle is shown on Fig 1.

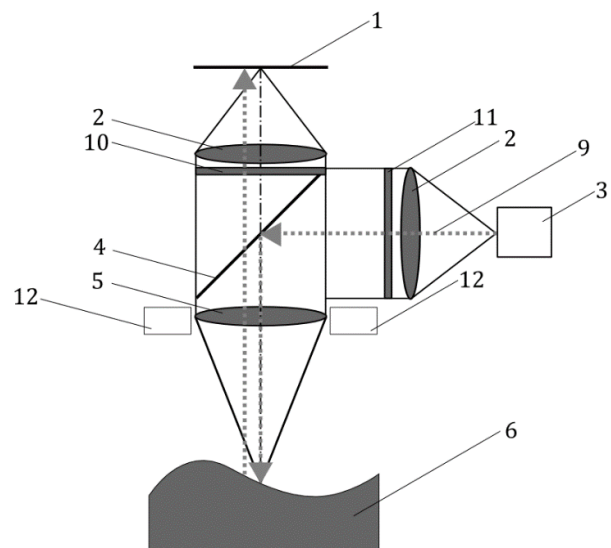


Figure 1. Schematic diagram of a typical measurement device based on focus variation [14].

The white light source (3) produces a light beam (9) which passes through lenses (2) and polarizer (11), then is reflected from the beam splitter (4) toward an objective (5) and travel further to the specimen (6). The specimen is illuminated with ring light (12). Reflected light beam (9) from specimen (6) passes back through objective (5), beam splitter (4), analyser (10), lenses (2) and is detected on array detector (1).

Due to the small depth of field of the optics only small regions of the object are sharply imaged. To perform a complete detection of the surface with full depth of field, the precision optic is moved vertically along the optical axis,

while continuously capturing data from the surface [14].

3. RESULTS AND DISCUSSION

The layer thickness was measured on the Infinite Focus SL measuring device (Fig 2). It is a cost-efficient optical 3D measurement system for easy, fast and traceable measurement of shape and finish on micro structured surfaces. It measures both shape and roughness of components with only one system [15].



Figure 2. Infinite Focus SL focus variation measuring device [15].

Vertical resolution was set on 650 nm, while Lateral resolution was 8,51 μm per manufacturers recommendation.

Fig. 3 shows the applied scanning spray AESUB blue on the plastic sheet. Before applying the spray, an adhesive tape was applied on one half, which was removed after the application of the spray. A clear boundary of the applied spray can be observed at the place of the removed tape.



Figure 3. AESUB blue scanning spray layer applied on plastic card.

Obtained results are shown on Fig 4 in form of Computer aided inspection (CAI). Size of measuring field is square shape of 5x5mm. Maximum measuring deviation was +0.076 mm while minimum was -0,017mm thus range is 0.093 mm.

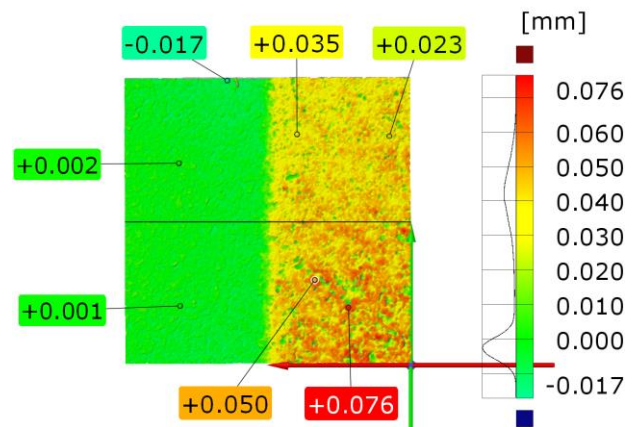


Figure 4. CAI with min, max and characteristic distance deviations.

Figure 5. presents measurements in three cross-sections in the middle and 1mm from the end of sample.

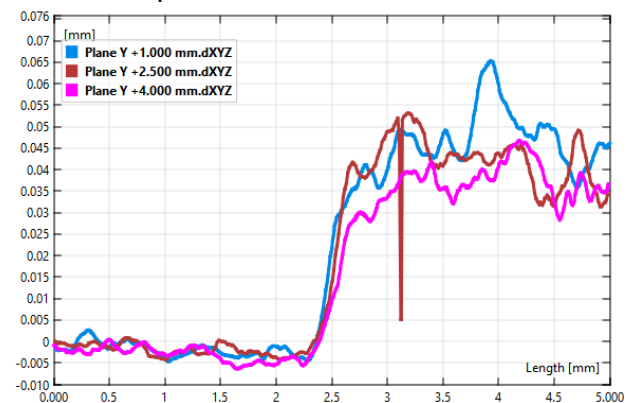


Figure 5. Cross section profile on middle and 1 mm from the end of specimen.

The mean value measured in the middle of the specimen was +0.041 mm, on the 1mm from the bottom is +0.046 and 1mm from above is +0.036mm.

4. CONCLUSION

The study analysed the influence of scanning spray layer thickness on the accuracy of 3D scanning process. This research leads that the interaction between the scanning spray layer and the object being sprayed can introduce errors and distortions, thereby affecting the quality and accuracy of the 3D scans results. Specifically, uneven scanning spray layers were found to may have influence as well, for example covering fine surface details on the object. Consequently, this can impact the 3D scanners ability to faithfully capture intricate features, resulting in small distorted reconstructions. To quantify the thickness of the scanning spray layer, the focus variation method was used, revealing that the geometry of the scanned area increased beyond the manufacturer's specified limits when the scanning spray was applied. These findings emphasize the importance of careful control and measurement of scanning spray layer thickness in order to achieve accurate and reliable 3D scans in various applications.

ACKNOWLEDGEMENT

This research was supported by the company EMUS d.o.o, which temporarily assigned the measuring device Infiniti Focus SL (Bruker Alicona) to the Department for Production Engineering.

REFERENCES

- [1] Ž. Santoši, I. Budak, V. Stojaković, M. Šokac, and Đ. Vukelić, "Evaluation of synthetically generated patterns for image-based 3D reconstruction of texture-less objects," *Measurement*, vol. 147, no. 106883, 2019.
- [2] J. R. M. Pereira, I. de Lima e Silva Penz, and F. P. da Silva, "Effects of different coating materials on three-dimensional optical scanning accuracy," *Advances in Mechanical Engineering*, vol. 11, no. 4, pp. 1–6, 2019.
- [3] B. Valinasab, M. Rukosuyev, J. Lee, J. Ko, and M. B. G. Jun, "Improvement of Optical 3D Scanner Performance Using Atomization-Based Spray Coating," *Journal of The Korean Society of Manufacturing Technology Engineers*, vol. 24, no. 1, pp. 23–30, 2015.
- [4] J. Franke, T. Koutecký, and D. Koutný, "Comparison of Sublimation 3D Scanning Sprays in Terms of Their Effect on the Resulting 3D Scan, Thickness, and Sublimation Time," *Materials*, vol. 16, no. 18, p. 6165, 2023.
- [5] J. Franke, T. Koutecký, M. Malý, M. Kalina, and D. Koutný, "Study of process parameters of the atomizer-based spray gun for the application of a temporary matte coating for 3D scanning purposes," *Materials Chemistry and Physics*, vol. 282, 2022.
- [6] M. Kurz, T. Attin, and A. Mehl, "Influence of material surface on the scanning error of a powder-free 3D measuring system," *Clinical Oral Investigations*, vol. 19, no. 8, pp. 2035–2043, 2015.
- [7] H. S. Oh, Y. J. Lim, B. Kim, M. J. Kim, H. B. Kwon, and Y. W. Baek, "Effect of scanning-aid agents on the scanning accuracy in specially designed metallic models: A laboratory study," *PLoS ONE*, vol. 17, no. 5 2022.
- [8] A. V. Burde, D. Dudea, S. Cuc, M. Moldovan, and R. S. Campian, "Three - Dimensional evaluations of the coating thickness of two optical conditioning scanning sprays," *Materiale Plastice*, vol. 53, no. 1, pp. 65–67, 2016.
- [9] A. Edelmann, J. D. English, S. J. Chen, and F. K. Kasper, "Analysis of the thickness of 3-dimensional-printed orthodontic aligners," *American Journal of Orthodontics and Dentofacial Orthopedics*, vol. 158, no. 5, pp. 91–98, 2020.
- [10] A. Bugeja, M. Bonanno, and L. Garg, "3D scanning in the art & design industry," *Materials Today: Proceedings*, vol. 63, pp. 718–725, 2022.
- [11] Technical Datasheet, "AESUB blue – vanishing scanning spray," 2022.
- [12] Shree K. Nayar, "Shape from Focus," no. 1. Carnegie Mellon University, 1989.
- [13] S. Pertuz, D. Puig, and M. A. Garcia, "Analysis of focus measure operators for shape-from-focus," *Pattern Recognition*, vol. 46, no. 5, pp. 1415–1432, 2013.

- [14] R. Danzl *et al.*, "Focus Variation – a Robust Technology for High Resolution Optical 3D Surface Metrology," *Strojniški vestnik – Journal of Mechanical Engineering*, vol. 2011, no. 1, pp. 245–256, 2015.
- [15] "Optical 3D Measurement System for Shape & Finish - Alicona." Accessed: Oct. 03, 2023. [Online]. Available: <https://www.alicon.com/en/products/infinitefocusl>



SPMS 2023
39. Savetovanje Proizvodnog mašinstva Srbije
ICPE-S 2023
39th International Conference on Production
Engineering -Serbia



Novi Sad, Serbia, 26. – 27. October 2023

ANALYSIS OF THE POSSIBILITY OF USING DIFFERENT MEASURING SYSTEMS FOR TESTING THE ACCURACY OF MACHINE TOOLS

Saša TEŠIĆ^{1*}, Goran JOTIĆ¹, Đorđe ČIČA¹, Branislav SREDANOVIĆ¹, Branko ŠTRBAC², Miloš RANISAVLJEV²

¹ Faculty of Mechanical Engineering, University of Banja Luka, Banja Luka, Bosnia and Herzegovina

² Faculty of Technical Sciences, University of Novi Sad, Novi Sad, Serbia

*Corresponding author: sasa.tesic@mf.unibl.org

Abstract: Today, machine tools are subject to high requirements for machining parts with strict requirements for deviations from the nominal geometry. Satisfying these requirements, i.e. achieving high precision and accuracy in the machining of parts, becomes an increasing challenge with the increase in the number of working hours of the machine tool. For these reasons, it is necessary to periodically check the accuracy of the machine tool. In this paper, the accuracy of the three-axis milling center was examined and the possibility of different measuring systems for testing the accuracy of the machine tool was analyzed. The main goal of the analysis is to determine the possibilities of using faster and cheaper tests and measuring systems for testing the accuracy of machine tools, without impairing the reliability of the test. This research includes two measuring systems for collecting data on machine tool accuracy, namely a coordinate measuring machine with a contact sensor and a 3D laser scanner.

Keywords: machine tools, accuracy, CMM, 3D laser scanner

1. INTRODUCTION

The requests placed on machine tools today in terms of accuracy and precision have reached an unexpectedly high level, and therefore accuracy and precision can be singled out as one of the primary goals for designers, manufacturers, and users of machine tools. Achieving high accuracy and precision leads to an increase in the cost of machining parts, which on the other hand leads manufacturers to become uncompetitive on the market. To minimize the aforementioned problem of competition,

manufacturers generally strove for the concept of meeting the minimum requirements of customers so that price of the product could be as low as possible.

However, as already emphasized, today even the minimum requirements of customers regarding the accuracy and precision of parts produced by cutting have reached a high level, and for these reasons, it is necessary to constantly monitor the accuracy of machine tools. When purchasing or commissioning a machine tool after installation in a new production system, it is necessary to carry out a geometric validation test, as well as a

performance test of the machine tool in the machining process from the point of view of accuracy and precision of the machine tool [1]. For these tests, standard procedures have been developed [2-4] that are applied in cases of purchase and installation of machine tools, but they are time-consuming and expensive for subsequent monitoring of machine tool performance. To find faster and cheaper ways of testing machine tool accuracy, some researchers apply other procedures of machine tool performance analysis with the application of different measurement systems [5].

Machine tool users have a great need for the excellent performance that comes from machining. Therefore, for them, checking the accuracy of a machine tool includes checking it on a "test workpiece". This is especially pronounced for testing machining centres. After machining, the "test workpiece" is analysed on various measuring devices, most often on coordinate measuring machines (CMM) due to their high accuracy. Apart from CMM, the analysis of the deviation of the machining workpiece from the nominal geometry can also be performed with 3D optical scanners [6, 7]. 3D optical scanners have an advantage in terms of data acquisition speed compared to coordinate measuring machines, but their use is not dominant due to lower accuracy.

Kortaberria et al. [8] evaluated the measurement uncertainty of 3D optical scanners based on comparative results obtained by measuring a "test workpiece" using a coordinate measuring machine and a 3D optical scanner. Mendricky in his research [9] highlights speed as an advantage of 3D optical scanners, but also mentions precision and accuracy as a possible disadvantage, and performs an analysis when scanning prismatic parts with an emphasis on edges and small diameter holes. Giganto et al. [10] examined the advantages and limitations of five different optical measuring systems for dimensional and tolerance deviations of parts made by additive

technology, where reference parameter values were obtained using a coordinate measuring machine.

In this work, the goal is to analyse the possibilities of applying optical measuring systems for analysing the accuracy of machine tools, and in that way, to use their speed of data collection from the machined workpiece. The characteristic of optical measuring systems is the possibility of faster data collection compared to contact measuring systems. For this purpose, a "test workpiece" was created in which the verification of dimensional and geometric characteristics was performed with the contact method using a coordinate measuring machine and the non-contact method using a 3D laser scanner. By further comparing the results of these two methods, a conclusion was drawn about the suitability of the 3D laser scanner for testing the accuracy of machine tools.

2. MATERIALS AND METHODS

Given that the goal of this work is to test the accuracy of the machining center for milling, the "test workpiece" was a prismatic part with characteristic shapes that are made on three-axis machining centers. The model of the "test workpiece" is adopted on the model of the test model from the ISO 10791-7 standard, but simplified to speed up the test performance. The test model with the indicated characteristic dimensional and geometrical characteristics is shown in Fig. 1.

The part was machined on a vertical machining center EMCO ConceptMill450, for which the accuracy was tested. The main spindle of the machining center has a power of 11kW, and the maximum spindle speed is 12,000 rpm. The machining center has a work area of 600x500x500 mm. Three different cutting tools were used for the machining of the workpiece, namely a 50 mm diameter face mill, a 10 mm diameter end mill, and a 10 mm diameter drill. The material of the workpiece is aluminium alloy AW 6060.

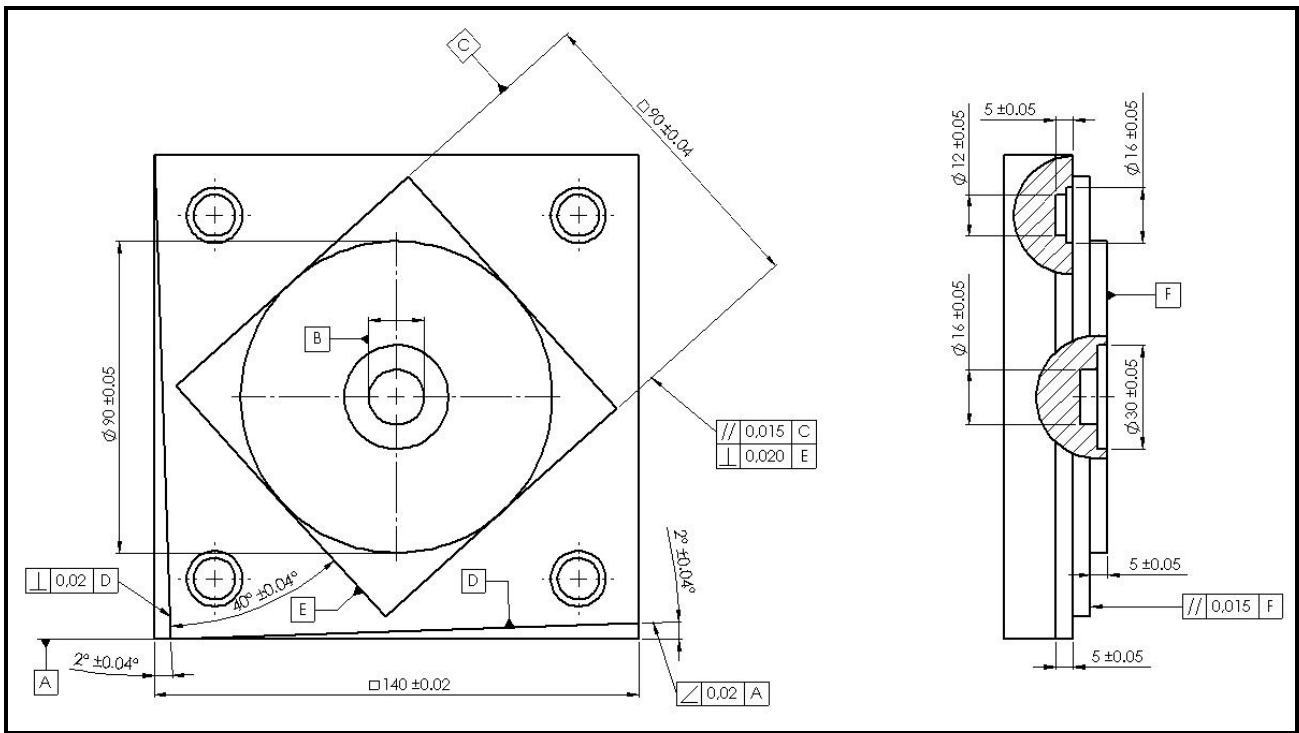


Figure 1. Machine tool part



Figure 2. Coordinate measuring machine Carl Zeiss Contura G2 RDS

Tabela 2. Characteristics CMM

CMM Carl Zeiss Contura G2 RDS	
Maximum allowable length measurement error	MPEE=(1,8+L/300) μm
Maximum allowable sensor error	MPEP=1,8 μm
Maximum allowable error in scan mode	MPETHP=3,5 μm

Table 2. Characteristics of the 3D laser scanner

MMDx100	
Accuracy	10 μm
Min. point resolution	65 μm
Max. frame rate	150 Hz
Stripe width	100 mm
Max. points per stripe	1000
Accuracy comb. with MCAx arm	48 μm
Light source	1 laser crosses



Figure 3. MMDx100 laser scanner integrated with Nikon MCAx+2.0 measuring arm

The geometrical inspection of the test object was realized using the CMM Carl Zeiss Contura G2 RDS with a contact measuring sensor, Figure 2. The metrological performance of the CMM is listed in Table 1. Its maximum permissible error for dimensional measurements in point-by-point measurement

mode is $1.8+L/300 \mu\text{m}$, while the maximum allowed error in scanning mode is $3.5 \mu\text{m}$. The maximum permissible error of the sensor is $1.8 \mu\text{m}$. In addition to the CMM, to digitize the test object, a 3D laser scanner MMDx100 integrated into the Nikon MCAX+2.0 measuring arm was used, Figure 3. The metrological performance of the laser scanner is shown in Table 2. Its accuracy is $10 \mu\text{m}$, while its accuracy in combination with articulated measuring arm by hand is $48 \mu\text{m}$. It has a resolution of $65 \mu\text{m}$ and a maximum sampling frequency of 150 Hz.

3. RESULTS AND DISCUSSION

The results of the analysis of the dimensional and geometric characteristics of the "test workpiece", generated by the application of the specified coordinate measurement systems, are shown in Table 3. The analysis of the obtained results aims to examine the justification of the application of optical coordinate measuring systems to test the accuracy of machine tools. Other factors were not considered in this analysis.

Table 6. Results of the analysis of variance

No	Characteristic	Nom. value [mm]	\pm Tol.	CMM [mm]	Dev. CMM +/- [mm]	In toler. yes/no	LS [mm]	Dev. LS +/- [mm]	In toler. yes/no
1	Perpendicular	0	0.02	0.0065	0.0065	Yes	0.044	0.044	No
2	Tilt	0	0.04	0.039	0.039	Yes	0.055	0.055	No
3.1	perpendicular	0	0.02	0.0085	0.0085	Yes	0.087	0.087	No
3.2	Parallelism	0	0.015	0.0092	0.0092	Yes	0.091	0.091	No
4	Parallelism	0	0.015	0.0082	0.0082	Yes	0.091	0.091	No
5	Cylinder diameter	90	0.05	90.041	0.041	Yes	90.009	0.009	Yes
6	Angle	2	0.04	1.962	-0.038	Yes	1.974	-0.026	Yes
7	Length	140	0.02	139.993	-0.007	Yes	139.933	-0.067	No
8	Angle	40	0.04	40.0056	0.0056	Yes	40.017	0.017	Yes
9	Length	90	0.04	90.04	0.04	Yes	90.03	0.03	Yes
10	High	5	0.05	4.994	-0.006	Yes	4.975	-0.025	Yes
11	High	5	0.05	5.0082	0.0082	Yes	4.975	-0.025	Yes
12	Diameter of hole	30	0.05	29.9619	-0.0381	Yes	29.94	-0.06	No
13	Diameter of hole	16	0.05	15.9612	-0.0388	Yes	15.956	-0.044	Yes
14	Diameter of hole	16	0.05	15.9562	-0.0438	Yes	15.93	-0.07	No
15	Diameter of hole	12	0.05	11.9637	-0.0363	Yes	11.967	-0.033	Yes
16	Diameter of hole	5	0.05	5.008	0.008	Yes	4.96	-0.04	Yes

The set tolerances and their differences were adopted based on the recommendations

of the ISO 10791-7:2014 standard. In addition, when defining the tolerances, the needs that

the observed machine tool should satisfy were taken into account. For positions and shapes for which more complex interpolations are required during production, slightly higher tolerance values have been adopted.

Using the set accuracy test of the machine tool, and based on the results of the experiment (Table 1), it is clearly observed that the machine tool meets all the analyzed accuracy parameters by measuring the "test workpiece" by the contact method using the coordinate measuring machine. However, by measuring the "test workpiece" with a non-contact method using a laser scanner, a significant number of the observed characteristics do not meet the set specifications and enter the tolerance limits, which leads to the conclusion that the machine tool is not satisfactory in terms of accuracy. Given that the coordinate measuring machine has significantly higher accuracy, as indicated by the metrological performance of the measurements obtained by the contact method, they were taken as reference measurements. Deviations of the analyzed parameters generated by the difference in the results of the used coordinate measuring systems are a consequence of the unreliability of the laser measuring systems regarding the analysis of the characteristics with the associated specifications. A representation of deviations for orientation tolerances and dimensional characteristics obtained with the observed systems are shown in the graphs of Figure 4 and Figure 5, respectively. The unreliability of laser measurement systems comes from their methodology of use and system limitations in terms of accuracy. Deviations that occurred, among other things, are a consequence of the necessary application of powder on the workpiece during scanning, which is necessary to eliminate reflection. Based on the deviations that the laser measurement system gives concerning the coordinate measuring machine, and based on the need to analyze the high requirements that are reflected in strict specifications through small deviations and narrow tolerances in machine tools, the laser scanner

is not reliable and sufficient for use in testing working accuracy machine tools using a "test workpiece".

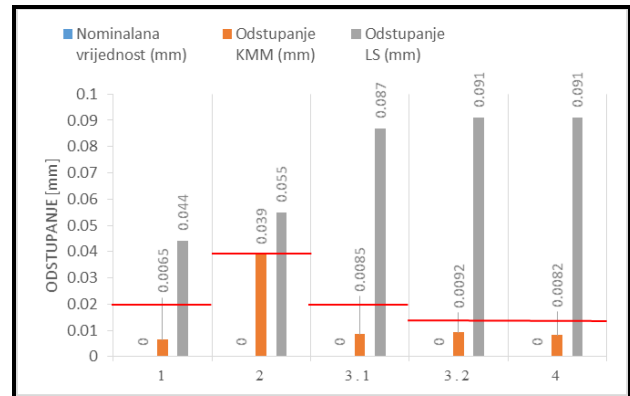


Figure 4. Deviations for orientation tolerances

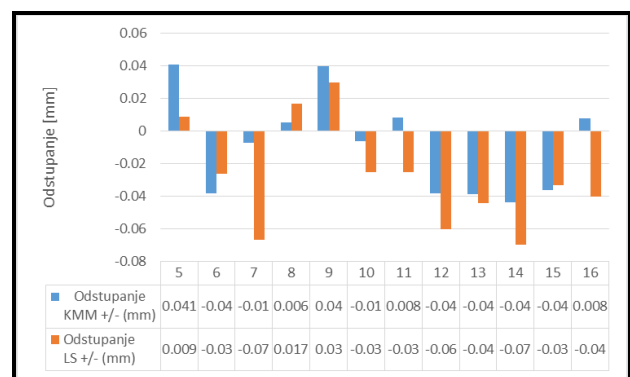


Figure 5. Deviations for dimensional characteristics

4. CONCLUSIONS

Given that high goals are set for machine tools in terms of accuracy and precision for machining, it is necessary to periodically check whether these machines meet the accuracy and precision during the use period. In this study, an analysis of the possibility of using two different measuring systems for testing the accuracy of the machine tool using a "test workpiece" was performed. Based on the conducted analysis, it can be concluded that the observed machine tool meets the set accuracy conditions. Non-contact measuring systems have advantages in the speed of collecting the required data, however, due to certain limitations in application as well as the specified accuracy, they are not suitable for analysing parameters with strict specifications, in contrast to KMM with a contact measuring sensor. The non-contact measuring system considered in this analysis, the MMDx100 laser scanner, is not suitable for use when testing

the accuracy of a machine tool by measuring a "test workpiece".

In the further analysis of this issue, it is necessary to examine the possibilities of using other non-contact measuring systems, newer generation and higher accuracy, and determine whether they meet the characteristics required for testing the accuracy of machine tools.

REFERENCES

- [1] Lopez, L.N.L., Lamikiz, A. Machine Tools for High Performance Machining. British Library Cataloguing in Publication Data, Springer, 2009. doi: 10.1007/978-1-84800-380-4
- [2] ISO 230-2:2014. Test code for machine tools – Part 2: Determination of accuracy and repeatability of positioning of numerically controlled axes.
- [3] JIS B 6201, 93rd Edition, 2012. MACHINE TOOLS – RUNNING TESTS AND RIGIDITY TESTS – GENERAL REQUIREMENTS
- [4] ASME B5.54 – 2005 (R2020). Methods for Performance Evaluation of Computer Numerically Controlled Machining Centres.
- [5] Barnfather, J.D., Goodfellow, M.J., Abram, T. Photogrammetric measurement process capability for metrology assisted robotic machining. *Measurement*, 78, 29 – 41, 2016. <http://dx.doi.org/10.1016/j.measurement.2015.09.045>
- [6] Ramos, B.B., Santos, E.U. Comparative study of different digitization techniques and their accuracy. *Computer – Aided Design*, 43, 188 – 206, 2011. 10.1016/j.cad.2010.11.005
- [7] Radomir, M. Aspect Affecting Accuracy of Optical 3D Digitalization, *MM Science Journal*, March 2267, 2018. 10.17973/MMSJ.2018_03_2017106
- [8] Kortaberria, G., Mutilba, U., Gomez, S., Ahmed, B. Three-Dimensional Point Cloud Task-Specific Uncertainty Assessment Based on ISO 15530-3 and ISO 15530-4 Technical Specifications and Model-Based Definition Strategy. *Metrology*, 2, 394 – 413, 2022. <https://doi.org/10.3390/metrology2040024>
- [9] Radomir, M. Analysis of Measurement Accuracy of Contactless 3D Optical Scanners. *MM Science Journal*, October 711, 2015. 10.17973/MMSJ.2015_10_201541
- [10] Giganto, S., Martinez-Pellitero, S., Cuesta, E., Meana, V.M., Barreiro, J. Analysis of Modern Optical Inspection Systems for Parts Manufactured by Selective Laser Melting. *Sensors*, 20, 3202, 2020. 10.3390/s20113202



Society of Production
Engineering

SPMS 2023

39. Savetovanje proizvodnog mašinstva Srbije

ICPES 2023

39th International Conference on Production Engineering of
Serbia



Faculty of Technical
Sciences
University of Novi Sad

Novi Sad, Serbia, 26. – 27. October 2023

THE INFLUENCE OF THE TECHNOLOGICAL PARAMETERS OF THE PRODUCTION PROCESS AND THE MATERIAL QUALITY ON THE MICROGEOMETRIC PRODUCT SPECIFICATIONS

Dejan BOŽIĆ¹, Miloš RANISAVLJEV¹, Mijodrag MILOŠEVIĆ¹, Borislav SAVKOVIĆ¹, Dejan LUKIĆ^{1*}

¹University of Novi Sad, Faculty of Technical Sciences, Department of Production Engineering,
Novi Sad, Serbia

bozic997dejan@uns.ac.rs, mranisavljev97@uns.ac.rs, mido@uns.ac.rs, savkovic@uns.ac.rs,
lukicd@uns.ac.rs

*Corresponding author: lukicd@uns.ac.rs

Abstract: *The microgeometric specifications of the product are key factors that ensure the correct functioning of the final product. They usually mean the values of the observed roughness parameters of the treated surface, which can be linear (2D) or surface (3D). The values of the roughness parameters depend on many factors, including the applied manufacturing procedure, tool geometry, fixtures, and others. In addition to the mentioned factors, the quality of the processed surface of the preparation called the input quality in the paper, can have a significant impact on the results of the roughness parameters, that is, on the quality of the final product. In this paper, the influence of processing parameters (feed and depth of cut) and input material quality of pipes from renowned manufacturers from three different countries (China, Germany, and Russia) on the quality of the processed surface was analyzed. The preparation material used in the study is 100Cr6. The observed quality characteristic is the arithmetic mean roughness Ra. The measured results were analyzed using the response surface methodology (RSM) with prior analysis of equality of variances and t-test.*

Keywords: *Roughness of treated surface, processing parameters, input quality, response surface methodology*

1. INTRODUCTION

Surface roughness is one of the most important quality characteristics in the machining. However, surface roughness is also affected by the cutter path strategies. For minimizing the surface roughness, the proper selection of cutter path strategies is very important. Machining with optimum parameters and path strategies will contribute to lower energy consumption and hence, will lead to lower production costs [1].

In the aviation industry, Gilge et al. [2] highlighted the importance of analyzing the distribution of surface roughness on the surface of a jet engine blade. This analysis has proven to be crucial for understanding and modeling the effects of real-world surface roughness values and forming predictive models for evaluating the performance and durability of jet engine components.

Assessment of roughness parameters plays a significant role in production processes. Vukman et al. [3] optimized the parameters of high-speed machining of thin-walled aluminum structures as a function of the quality of the machined surface, where, by analyzing the results, they concluded that the processing strategy, depth of cut, and number of revolutions have the most influence on the roughness of the machined surface, and the wall thickness has the lowest influence.

Machining process parameters such as cutting speed, radius of the cutting tool, feed, and workpiece material have a significant impact on the value of surface roughness in machining processes with chip removal [4]. By processing ALSI 1019, it was determined that the cutting speed, feed, and radius of the cutting tool have a significant

influence on the value of the surface roughness parameters [5].

Similarly, by processing a cobalt-based alloy (Cobalt-Based Stellite 6), Ying-Fei et al. [6] found that feed and cutting speed are primary influencing factors on surface roughness. In addition to the process parameters, they included in their study the geometry of the cutting tool, and they processed the aluminum alloy on a numerically controlled milling machine. To analyze the obtained results, they used the response surface method - RSM. The parameters that have a significant influence on the turning process are the cutting parameters (cutting speed, feed, depth of cut), the geometry of the tool, the type and quality of the preparation, the coolant, and the rigidity of the machining system [7].

Several different studies have shown that the quality of the material has a significant impact on the quality of the final product. Paris et al. [8] focused on the influence of material variability on the quality of the final product. Shih & Wang [9] also emphasized that the quality of the final product depends not only on the quality of the production process but also on the quality of the used material, i.e. raw material. One way to maintain the high quality of components and products is to choose reliable suppliers of raw materials [10].

In this paper, the influence of technological parameters, in the turning process, on the size of the linear parameter of the surface roughness R_a was analyzed. The technological factors included in the study are feed, radius tip of the cutting tool, and depth of cut. To include the variability of the material, the roughness of the machined surface was analyzed on pipes from three different manufacturers China, Russia, and Germany. The design of the experiment and data analysis was performed in the Minitab

17 software package, and the methodology used for data analysis is the response surface methodology. Before analyzing the response surface diagrams, the basic assumptions about the collected data were checked. Normality tests and tests of equal variances were analyzed. To determine a statistically significant difference in the mean values of the roughness parameter Ra, for different workpiece materials, a t-test was used.

2. EXPERIMENTAL RESEARCH

The measurement of the roughness parameter Ra was performed on processed pipes of manufacturers from three different countries: China, Germany, and Russia. The pipes have the same chemical composition as 100Cr6, but they are made using different methods, so their microstructure and hardness are different. Components made of this type of steel are characterized by high hardness and tensile strength in the hardened state, and for this reason, it is widely used in the production of elements with rolling contact and components that are exposed to high material fatigue. This was also the case with the observed pipes, which are used for the production of bearing rings in a domestic company.

Manufacturing was performed with a constant number of revolutions $n=266$ rpm, on a universal lathe. The tool used in the experiment was a cutting tool ISO 3 with a soldered insert made of tungsten carbide of quality P10. During machining, three values of feed, cutting depth, and tool tip radius values were varied.

Table 1 shows the factors and levels used in the experimental setup.

Table 1. Factors and levels

Level	Feed	Radius of the tool tip	Depth of cut
Upper	0,4	1,6	1,2
Middle	0,2	0,9	0,69
Lower	0,1	0,5	0,4

During the implementation of the experiment, the examined pipes were divided into twelve equal segments, where each segment represented one combination of processing parameters. Figure 1 shows the manufactured pipe with divided segments of the realized experimental tests.

The device used to measure the roughness of the machined surface is a profilometer Mitutoyo SJ-210, Figure 2. The observed roughness parameter is the arithmetic mean roughness Ra. The processing of the obtained roughness profile was performed according to ISO 4287. The relevant parameters for the processing of the roughness profile are given in Table 2.



Figure 1. Manufactured pipe with divided segments of the realized experimental tests



Figure 2. Mitutoyo SJ-210 profilometer

Table 2. Parameters for processing the roughness profile Ra

Noise Filter Cut-Off, λ_s :	2,5 μm
Cut-Off Wavelength, λ_c :	0,8 mm
No. of Cut-Offs:	5
Evaluation length:	4 mm

3. RESULTS AND DISCUSSION

To analyze and optimize the level of individual factors, the response surface methodology (RSM) was used, and the software package that was used to create the experiment plan was Minitab 17. The response surface method models the dependence between a pair of independent variables and one dependent variable. Based on these dependencies, spatial diagrams or surface diagrams are constructed. Before modeling the response surface plot, it is necessary to perform a test of equal variances for the surface roughness results. The measured roughness data is grouped into three different columns for easier comparison of results. The columns are named as follows: Ra K, which indicates the measured roughness parameter for the pipe manufactured in China, and Ra N and Ra R, the measured roughness parameter for the pipe manufactured in Germany and Russia, respectively.

Based on the p-value of Levin's test (0.336) and multiple comparisons test (0.665), it can be concluded that the variances are equal, that is, they do not differ significantly with a probability of 95% and a significance threshold of $\alpha=0.05$.

Based on the Anderson-Darling normality test, it was determined that the data sets Ra K, Ra N and Ra R do not fall under the normal distribution with a confidence level of 95%. In addition to variance analysis and the normality test, it is necessary to analyze the mean values of individual groups of results, in order to determine whether the differences for individual producers are statistically significant. A two sample t-test was used for this purpose. T-test was performed for each combination of observed sets, ie. Ra K-Ra N, Ra K-Ra R and Ra N-Ra R. Based on the t-test analysis, statistically significant differences in the mean values for each combination of the examined data sets were determined. Table 3 shows pairs of examined data with associated p-values and two-sided confidence intervals.

Table 3. T-test results

Pairs of analyzed data	p-values	confidence intervals
Ra K, Ra N	0,024	(0.106, 1.455)
Ra K, Ra R	0.000	(0.911, 2.267)
Ra N, Ra R	0.013	(0.179, 1.438)

Analysis of variance (ANOVA) was used to determine the statistical significance of the observed parameters and obtain the regression equation. According to the analysis of variance, the linear model adequately describes the dependency between the independent and dependent variables, since the adequacy of the model (R-sq) is 96%, and the p-value is close to zero. However, it should be noted that the model error (lack of fit) is statistically significant.

In the linear model, the significant parameters are the feed and the depth of cut, while the tool tip radius was found to be insignificant (with a p-value of 0.468) with a confidence interval of 95%. All interactions of the observed parameters are also significant in the model with 2-way interactions, i.e. the p-value for interactions is less than the significance threshold of 0.05.

The diagrams of the response surface were obtained, which are shown in Figure 3. Based on the diagram and the collected data, it is possible to optimize the input parameters of the response. Due to limited space, part of the available diagrams is shown in Figure 3, i.e. dependence diagram of the roughness parameter Ra for a pipe of a) Russian, b) Chinese, and c) German manufacturer.

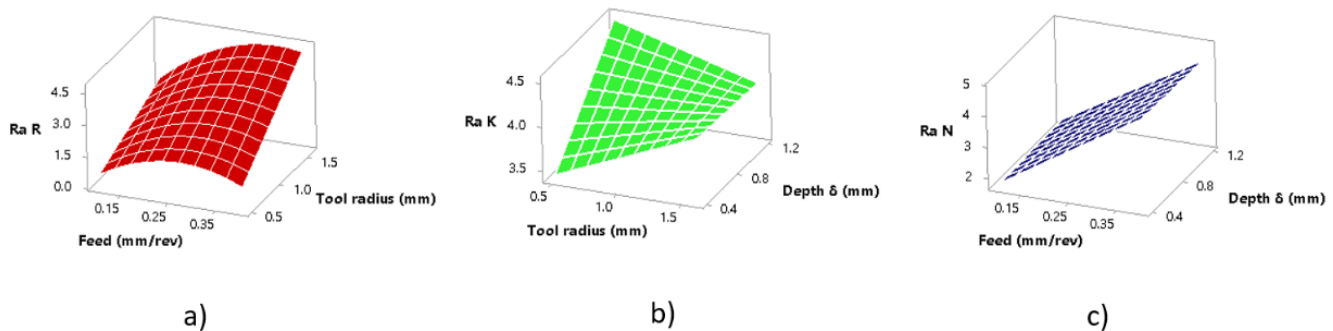


Figure 3. Response surface diagrams of the roughness parameter Ra

4. CONCLUSION

Significant differences in the quality of the treated surface, ie. in the values of the parameter Ra were observed when manufacturing the pipes from three different manufacturers. At the same time, the technological parameters during pipe manufacturing were kept at a constant level. This fact shows that the variability of the material can have a significant impact on the processing quality of the final product, as stated in the literature analysis. Since in this study, only the arithmetic mean roughness Ra was observed, the direction of future research would be to include more influential factors from the machining process as well as to observe more complex roughness parameters such as surface (3D) parameters.

The creation of a general model and the possibility of predicting the results of the surface roughness, with a certain probability, based on the obtained model, is the basis of the optimization of every production process.

ACKNOWLEDGEMENT

This paper is part of a study in the project “Collaborative systems in the digital industrial environment” No. 142-451-3178/2022-01/01, supported by the Provincial Secretariat for Higher Education and Scientific Research of the Autonomous Province of Vojvodina and "Innovative scientific and artistic research from the FTS domain", No. 451-03-47/2023-01/200156, supported by the Ministry of Education, Science and Technological Development of the Republic of Serbia.

REFERENCES

- [1] Z. Grešová, P. Ižol, I. Maňková, and M. Vrabe: The Effect of Cutter Path Strategies on Surface Roughness When Machining Titanium Alloy, *Journal of Production Engineering*, Vol. 24, No. 2, pp. 9–12, 2021.
- [2] Gilge, P., Kellersmann, A., Friedrichs, J., & Seume, J. Surface roughness of real operationally used compressor blade and blisk. *Proceedings of the Institution of Mechanical Engineers Part G Journal of Aerospace Engineering*, Vol. 233, No. 14, pp. 5321-5330, 2019.
- [3] Vukman, J., Milošević, M., Antić, A., Božić, D., Todić, V., Lukić D.: Optimization of high-speed machining parameters of thin-walled aluminium structures in the function of surface roughness, *Proceedings of the 16th International Conference on Accomplishments in Mechanical and Industrial Engineering, Banja Luka*, 2023.
- [4] K. Palanikumar: *Modeling and analysis for surface roughness in machining glass fibre reinforced plastics using response surface methodology*. *Materials & Design (1980-2015)*, Vol. 28, No. 10, pp. 2611-2618. 2007.
- [5] Bhardwaj, B., Kumar, R., & Singh, P: Effect of machining parameters on surface roughness in end milling of aisi 1019 steel. *Proceedings of the Institution of Mechanical Engineers Part B Journal of Engineering Manufacture*, Vol. 228, No. 5, pp. 704-714, 2013.
- [6] Ying-fei, G., Escalona, P., & Galloway, A.: Influence of cutting parameters and tool wear on the surface integrity of cobalt-based stellite 6 alloy when machined under a dry cutting environment. *Journal of Materials Engineering and Performance*, vol. 26, No. 1, pp. 312-326. 2016.
- [7] Trung, D., Quang, N., Hoang, T., Linh, N., Kien, H., Tam, D., ... & Tuan, N: Optimization study on turning process by using taguchi-copras method. *E3s Web of Conferences*, 309, 01010. 2021.
- [8] Paris, A., Duchesne, C., & Poulin, E.: Establishing multivariate specification regions for incoming raw materials using projection to latent structure models: comparison between direct mapping and model inversion. *Frontiers in Analytical Science*, 1. 2021.
- [9] Shih, N. and Wang, C.: An inspection model of products and their input materials. *Systems Science & Control Engineering*, Vol. 2, No. 1, pp. 297-307. 2014.
- [10] Gonzalez, M., Quesada, G., & Monge, C.: Determining the importance of the supplier selection process in manufacturing: a case study. *International Journal of Physical Distribution & Logistics Management*, Vol. 34, No. 6, pp. 492-504. 2004.

SPMS/ICPES 2023

**39TH INTERNATIONAL CONFERENCE ON
PRODUCTION ENGINEERING OF SERBIA**

SPONZORI KONFERENCIJE

Novi Sad, 26 – 27 October 2023

Ministry of Science, Technological Development, and Innovation



 **LOLA INSTITUT**



”MIREN” d.o.o.

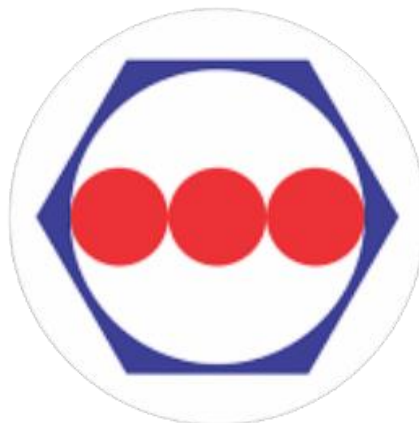




ASIP PREVENT

Mislimo preventivno,
živimo i radimo
bezbedno!

www.asipprevent.rs



 **ALING-CONEL**



ESCO ELIOS

GM-CNC DOO

INGEN *INŽENJERING*

 **Mecafor** 
products

FKL[®] 



1963
2023

